

CARBOXYLIC ACIDS AS DIRECTING GROUPS FOR
INTRAMOLECULAR CATALYTIC OXIDATION OF
UNACTIVATED C(SP₃)-H BONDS WITH
BIOINSPIRED CATALYSTS

Marco Cianfanelli

Per citar o enllaçar aquest document:
Para citar o enlazar este documento:
Use this url to cite or link to this publication:
<http://hdl.handle.net/10803/675382>



<http://creativecommons.org/licenses/by-nc-nd/4.0/deed.ca>

Aquesta obra està subjecta a una llicència Creative Commons Reconeixement-
NoComercial-SenseObraDerivada

Esta obra está bajo una licencia Creative Commons Reconocimiento-NoComercial-
SinObraDerivada

This work is licensed under a Creative Commons Attribution-NonCommercial-
NoDerivatives licence



Doctoral Thesis

**“Carboxylic Acids as Directing Groups for
Intramolecular Catalytic Oxidation of Unactivated
C(sp³)-H bonds with Bioinspired Catalysts”**

Marco Cianfanelli

2021

Doctoral Programme in Chemistry

Supervised by: Dr. Miquel Costas Salgueiro and

Dr. Xavi Ribas Salamaña

Tutor: Miquel Costas Salgueiro

Presented in partial fulfilment of the requirements for a doctoral degree from
the University of Girona



Dr. Miquel Costas Salgueiro and Dr. Xavi Ribas Salamaña of Universitat de Girona,

WE DECLARE:

That the thesis “Carboxylic Acids as Directing Groups for Intramolecular Catalytic Oxidation of Unactivated C(sp³)-H bonds with Bioinspired Catalysts”, presented by Marco Cianfanelli to obtain a doctoral degree, has been completed under our supervision.

For all intents and purposes, we hereby sign this document.

Dr. Miquel Costas Salgueiro

Dr. Xavi Ribas Salamaña

Marco Cianfanelli

Girona, 28th September 2021

*“Max Planck really didn't understand physics,
because during the eclipse of 1919 he stayed up all night
to see if it would confirm the bending of light by the gravitational field.
If he had really understood the theory, he would have gone to bed the way I did.”*

Albert Einstein

To my Family

List of publications

Chapter III, Chapter V

Manuscript in preparation derived from the results obtained from the primary C-H bond oxidation.

“Stereoselective Primary C-H Bond Oxidation Catalyzed by Mn Complexes”

Marco Cianfanelli, Arnau Call, Pau Besalù, Giorgio Olivo, Andrea Palone, Laia Vicens, Josep M. Luis, Massimo Bietti*, and Miquel Costas*

Chapter IV

“Enantioselective C-H Lactonization of Unactivated Methylenes Directed by Carboxylic Acids”

Marco Cianfanelli, Giorgio Olivo, Michela Milan, Robertus J. M. Klein Gebbink, Xavi Ribas, Massimo Bietti*, and Miquel Costas*
J. Am. Chem. Soc. **2020**, *142*, 3, 1584–1593

Publications not included in this thesis

“Iron Catalyzed Highly Enantioselective Epoxidation of Cyclic Aliphatic Enones with Aqueous H₂O₂”

Olaf Cussó, Marco Cianfanelli, Xavi Ribas, Robertus J. M. Klein Gebbink*, and Miquel Costas*

J. Am. Chem. Soc. **2016**, *138*, 8, 2732–2738

“Highly enantioselective epoxidation of olefins by H₂O₂ catalyzed by a non-heme Fe(II) catalyst of a chiral tetradentate ligand”

Mainak Mitra, Olaf Cussó, Satish S. Bhat, Mingzhe Sun, Marco Cianfanelli, Miquel Costas* and Ebbe Nordlander*

Dalton Trans., **2019**, *48*, 6123–6131

List of abbreviations

API	Active pharmaceutical ingredient
°C	Celsius degrees
δ	Chemical Shift
AcOH	Acetic acid
Ar	Aryl
BDE	Bond dissociation energy
CA	Carboxylic acid
Cat	Catalyst
CF ₃ SO ₃ , OTf	Trifluoromethanesulfonate anion
CH ₂ Cl ₂	Dichloromethane
CH ₃ CN	Acetonitrile
CI	Chemical ionization
Conv	Conversion
Cyt P450	Cytochrome P450
DCM	Dichloromethane
DMF	Dimethyl formamide
dMM	Dimethylmethoxide
e ⁻	Electron
ee	Enantiomeric excess
Equiv	Equivalents
EtOH	Ethanol
Et ₂ O	Diethyl ether
ESI-MS	Electrospray ionization Mass Spectrometry
EDG	Electron donating group
EWG	Electron withdrawing group
FT-IR	Fourier transform infrared spectroscopy

GC	Gas chromatography
GC-FID	Gas chromatography-flame ionization detector
GC-MS	Gas chromatography-mass spectrometry
h	Hour
HAT	Hydrogen atom transfer
H ₂ O ₂	Hydrogen peroxide
HBA	Hydrogen bond acceptor
HBD	Hydrogen bond donor
HBF ₄	Tetrafluoroboric acid
HFIP	1,1,1,3,3,3-Hexafluoro-2-propanol
HRMS	High-resolution mass spectrometry
<i>i</i> Pr	<i>Iso</i> -propyl
L	Ligand
K	Kelvin
KIE	Kinetic isotopic effect
kcal	Kilocalories
KIE	Kinetic isotope effect
m	Multiplet
M	Metal
mcp	<i>N,N'</i> -dimethyl- <i>N,N'</i> -bis(2-pyridylmethyl)-cyclohexane-1,2-diamine
Me	Methyl
MeOH	Methanol
min	Minutes
mL	Milliliter
mM	Millimolar
MW	Molecular weight

N ₂	Molecular nitrogen
NMe ₂	Dimethylamino group
NMR	Nuclear Magnetic Resonance
O ₂	Molecular oxygen
OAc	Acetate group
OPiv	Pivalate group
OsO ₄	Osmium tetroxide
Ox	Oxidant
<i>p</i>	<i>para</i>
p.	Page
pdp	<i>N,N'</i> -bis(2-pyridylmethyl)-2,2'-bipyrrolidine
Ph	Phenyl
PhIO	Isodosylbenzene
Py	Pyridine
q	Quadruplet
QTOF	Quadrupole Time-of-flight
R•	Carbon radical
RT	Room temperature
s	Singlet
SiO ₂	Silica
t	Triplet
T	Temperature
<i>t</i> Bu	<i>Tert</i> -butyl group
TfOH	Trifluoromethanesulfonic acid
TFE	2,2,2-Trifluoroethanol
THF	Tetrahydrofuran
TIBS	<i>Tris</i> -(triisobutyl)silyl group
TIPS	<i>Tris</i> -(triisopropyl)silyl group

TMS	<i>Tris</i> -(trimethyl)silyl group
TS	Transition state

Agradecimientos

En primer lugar, me gustaría agradecer mi primer director de tesis Dr. Miquel Costas por haberme dado confianza y la posibilidad de trabajar en su grupo por 7 años...si 7...prácticamente un padre. Aun vívidamente recuerdo mi primera estancia aquí en Girona en el 2014 donde tu pasión y dedicación en encontrar química excitante me capturaron y desde entonces siempre me empujaste a hacer nada mas que no fuera lo mejor. Gracias por tu apoyo y paciencia infinita. De la misma manera, quiero dar las gracias a mi segundo director de tesis, Xavi Ribas, por el apoyo, la química, las ideas y las charlas. Tambien quiero agradecer muchísimo Anna por animarme siempre antes de los group meeting y por los buenos momentos pasados juntos. Quiero agradecer Raquel, "La Reina", por su infinida disponibilidad y su dedicación al trabajo.

Podría contar un montón de fantásticas experiencias que he tenido en el QBIS desde obtener cristales de nuevos complejos, el primer exceso enantiomérico por encima del 90% hasta pagar 90 euros en chupitos en un karaoke de Tokio o pasear por el red light district de Ámsterdam. Sin embargo, estos recuerdos no hubieran sido los mismos sin todas las fantásticas personas que he conocido aquí en el Qbis. Personas que permiten que el trabajo de laboratorio sea apasionante también a las 1am. Gracias.

Grazie mamma e papà per l'infinito sostegno, per la guida e l'amore. Grazie ai miei fratelloni, Marcello e Stefano, per i vostri preziosissimi insegnamenti e per i 100€ ad ogni 30 preso agli esami ;).

Finally, gracias a ti Muriel, luz de mis ojos. Sin tu fuerza, tu paciencia y tu amor esta historia no hubiera sido posible. Ciao Rebecca! Papà ti ama perché da due anni gli dai tanta tanta forza.

Acknowledgements

This work would not have been possible without the following collaborations:

- Serveis tècnics de Recerca (STR) from Universitat de Girona for technical support, with special remark to Dr. Laura Gómez.
- Dr. Antoni Riera from Institute for Research in Biomedicine of Barcelona for the access to the polarimeter.
- Prof. Dr. Massimo Bietti and Prof. Bert Klein Gebbink for the collaboration in the development of the C-H lactonization reaction
- Prof. Dr. Bert Klein Gebbink for hosting and supervision during my scientific stay in University of Utrecht
- Prof. Dr. Shigeyoshi Inoue for hosting and supervision during my scientific stay in Technical University of Munich
- Dr. Shengfa Ye for hosting and supervision during my scientific stay in Max-Planck Institut für Kohlenforschung
- Dr. Kevin Mahoney for hosting and supervision during my scientific stay in AbbVie Ireland Sligo.
- Financial support by:

Marie Curie fellowship: 675020-MSCA-ITN-2015-ETN (NoNoMeCat project).

Spanish Ministry of Science: CTQ2015-70795-P, CTQ2016-77989-P, CTQ2018-101737-B-I00.

Generalitat de Catalunya: 2014 SGR 862, 2017 SGR 00264.

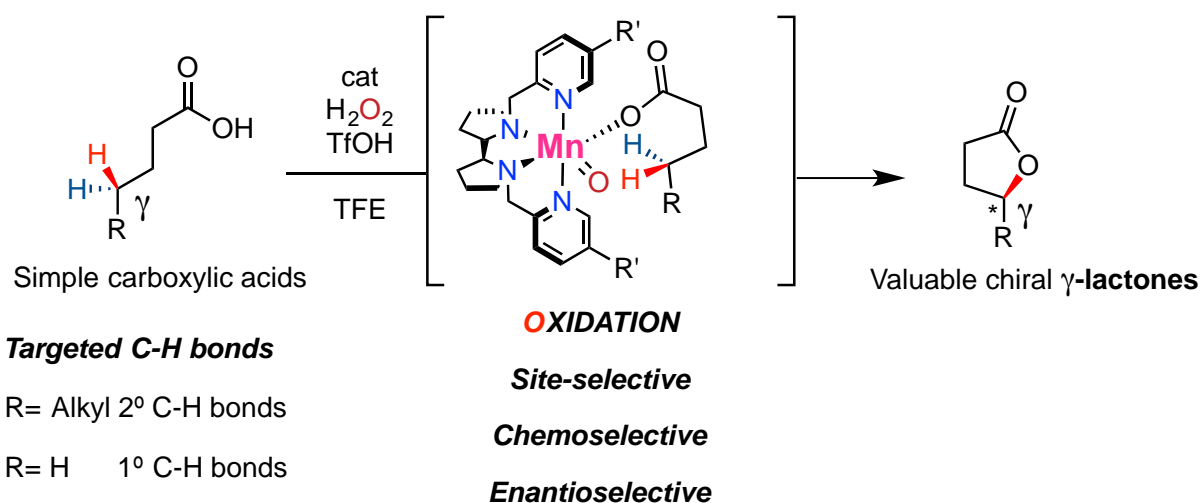
Graphical abstract

Summary (p. 1)

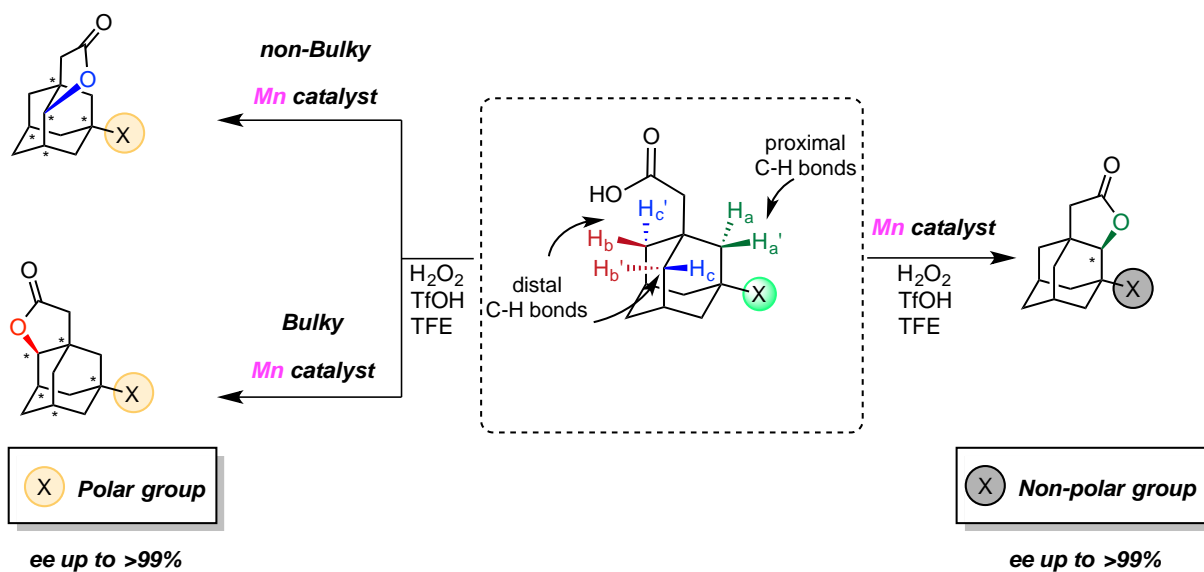
Chapter I. General Introduction (p. 11)

Chapter II. Objectives (p. 53)

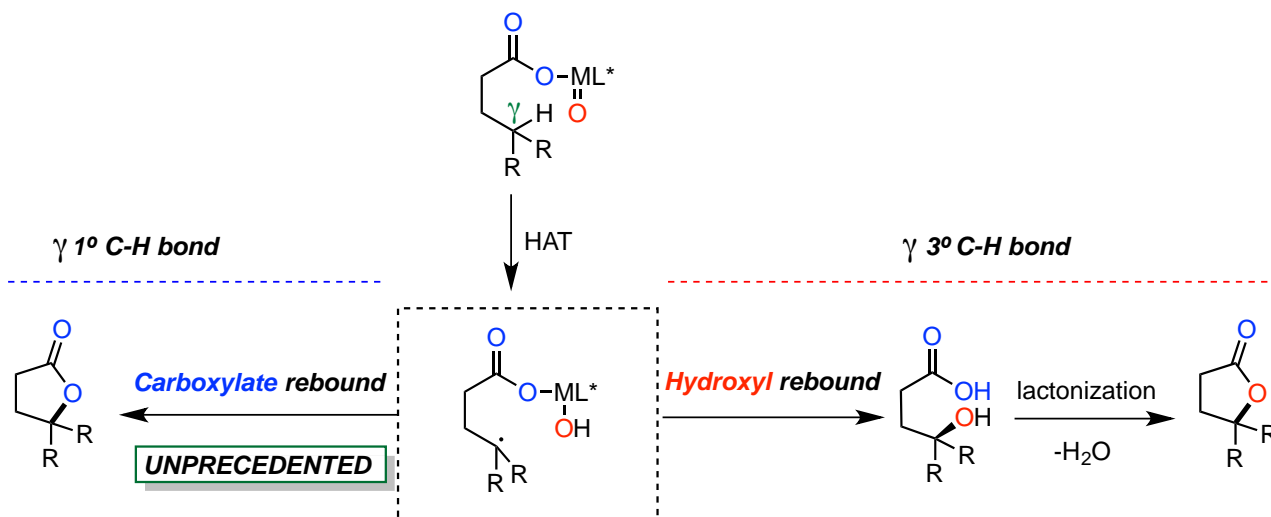
Chapter III. Selective Formation of γ -Lactones via Mn-catalyzed Oxidation of Unactivated C-H Bonds Directed by Carboxylic Acids (p. 57)



Chapter IV. Intramolecular Highly Enantioselective γ -C-H Lactonization of Unactivated Methylenes in Adamantaneacetic Acids (p. 77)



Chapter V. Mechanistic insights into the γ -C-H lactonization catalyzed by bioinspired Fe and Mn complexes (p. 95)



Chapter VI. General Conclusions (p. 113)

Table of Contents

List of Figures	1
List of Tables	6
Summary.....	7
Resumen	8
Resum	10
Chapter I: General Introduction	11
1.1. C(sp ³)-H functionalization: Opportunities and challenges	12
1.2. The mechanisms of C-H functionalization	13
1.3. Innate and guided selectivity.....	14
1.3.1. Catalyst-controlled selectivity	15
1.3.2. Directing group-controlled selectivity	16
1.3.3. Carboxylic acids as DG	17
1.4. The key role of oxygenated functionalities	18
1.5. Bioinspired C(sp ³)-H oxidations	19
1.6. Predicting selectivity in C-H oxidation.....	23
1.6.1. Bond Dissociation Energy (BDE)	23
1.6.2. Polar effects.....	23
<i>Polarity reversal strategy</i>	25
1.6.3. Steric effects	25
1.6.4. Stereoelectronic effects	26
1.6.5. Directed oxidations	27
1.6.6. Enantioselective oxidations.....	29
1.7. Carboxylic acid directed C(sp ³)-H functionalization	30
1.7.1. Carboxylic acid directed organometallic C-H functionalization	30
1.7.2. Carboxylic acid directed C(sp ³)-H lactonization	30
<i>Platinum</i>	30
<i>Palladium</i>	32
1.7.3. Carboxylic acid directed C(sp ³)-H arylation	34
<i>Enantioselective C-H arylation</i>	40
1.7.4. Carboxylic acid directed C(sp ³)-H olefination	42
1.7.5. Carboxylic acid directed C(sp ³)-H acyloxylation	43
1.8. Carboxylic acid directed bioinspired C(sp ³)-H oxidation	44
1.8.1. Limitation and challenges in carboxylic acid directed C(sp ³)-H oxidation	50
1.8.2. Carboxylic acid directed C(sp ³)-H oxidation in total synthesis	51
Chapter II: Objectives	53
Chapter III: Selective formation of γ -Lactones via Mn-catalyzed Oxidation of Unactivated C-H Bonds Directed by Carboxylic Acids	57
III.1. Design of the project	59
III.2. Results and discussion.....	61
III.2.1 Enantioselective γ -C-H Lactonization of Unactivated Methylens	61
III.2.2. Selective γ -C-H Lactonization of Linear Carboxylic Acid.....	69
III.2.3. Adding Primary C-H Bond to the Field of Bioinspired Oxidations.....	71
III.3. Summary	75

Chapter IV: Intramolecular Highly Enantioselective γ-C-H Lactonization of Unactivated Methylenes in Adamantaneacetic Acids	77
IV.1. Design of the project	79
IV.2. Results and discussion	80
IV.3. Summary	92
Chapter V: Mechanistic Insights into the γ-C-H Lactonization Catalyzed by Bioinspired Fe and Mn Complexes	95
V.1. Design of the project	97
V.2. Result and discussion	98
V.2.1. Elucidating the role of directing group, solvent and additive in γ -C-H lactonization.	98
V.2.2. Diverting bioinspired C-H hydroxylation towards acetoxylation: Evidence for an unprecedented carboxylate rebound mechanism.	101
V.3. Summary	111
Chapter VI: General Conclusion	113
Experimental Section	119
Experimental Section: Methodologies	121
Experimental section Chapter III	123
Experimental section Chapter IV	140
Experimental section Chapter V	168
Annex.....	173
Annex Chapter III	175
Annex Chapter IV	176
Annex Chapter V	186
References	187

Supplementary digital material

The material listed below can be found in the attached CD-ROM:

- PDF file of the PhD dissertation.
- PDF files containing the full spectroscopic characterization of the substrates and products reported in Chapters III, IV, V, GC traces of the catalysis experiments and the chiral GC traces of the asymmetric compounds. This pdf file is called *Digital Annex* and can be found in the folder named *Characterization*.
- CIF files for each crystal structure presented in Chapter IV and they are named as they are labelled in the PhD dissertation. They can be found in the folder named *CIF files*

List of Figures

Figure I.1. The evolution of logic disconnections in organic synthesis.	12
Figure I.2. Mechanistic scenario of metal-catalyzed C-H functionalizations.	14
Figure I.3. Challenges of carboxylic acid as directing group in Pd-catalyzed C-H functionalizations.	17
Figure I.4. Biosynthesis of Taxol.	18
Figure I.5. A) Example of non-heme iron enzyme active site and reactivity upon oxygen activation. B) Replication of the non-heme iron enzyme reactivity with an artificial complex. C) State of the art for synthetically useful bioinspired oxidations.	21
Figure I.6. A) General HAT/hydroxyl rebound mechanism in biological and artificial C-H oxidation. B) Mechanism for the generation of the metal-oxo species in bioinspired system.	22
Figure I.7. BDE values of different type of C-H bond within a small model organic molecule.	23
Figure I.8. Electronically controlled site-divergent C-H oxidation of amide and phthalimides.	24
Figure I.9. Polarity inversion promotes remote oxidation of an amine group by covalent protonation or hydrogen bonding with fluorinated solvents.	25
Figure I. 10. Modulation of the selectivity by rational catalyst design.	26
Figure I.11. Mechanism of carboxylic acid-directed C-H γ -lactonization and comparison between intermolecular and intramolecular selectivities in presence of B) competitive C-H bonds or C) deactivating EWG.	28
Figure I.12. Overview of the strategies for enantioselective oxidation of unactivated C-H bonds. A) State of the art for enantioselective oxidative desymmetrization of unactivated C-H bond with artificial catalysts. B) State of the art for enantioselective C-H oxidation of enantiotopic C-H bonds.	29
Figure I.13. Directed γ -C-H oxidations of carboxylic acids <i>via</i> formation of organometallic platinacycle. A) First directed γ -C-H lactonization of aliphatic carboxylic acids (Sen 1991). ⁴⁹ B) γ -Lactonization of aminoacids (Sames 2001). ⁵⁰ C) γ -Lactonization of <i>ortho</i> -methylbenzoic acid (Chang 2006). ⁵¹ D) γ -C-H hydroxylation of butanoic acid (De Vos 2019). ⁵²	32

Figure I.14. Palladium catalyzed γ -C-H lactonization of carboxylic acids. A) γ -Lactonization of ortho-methylbenzoic acid derivatives (Martin 2011). ⁵³ B) β -Lactonization of aliphatic carboxylic acids (Yu 2019). ⁵⁴	34
Figure I.15. First examples of palladium catalyzed β -C-H arylation of carboxylic acids	35
Figure I.16. A) Equilibrium between the conformers in κ^1 -carboxylate Pd complexes. B) Side reaction enabled by β -C-H cleavage of α -non quaternary CAs.	36
Figure I.17. β -C-H arylation of <i>N</i> -protected alanine and preliminary results for aliphatic carboxylic acid by A) Yu and coworkers (2017) ⁵⁹ and B) Zhao and coworkers (2017) ⁶¹ . C) β -C-H arylation of simple aliphatic carboxylic acids (van Gemmeren 2017). ¹⁷	38
Figure I.18. A) The first example of Pd-catalyzed γ -C-H arylation directed by CAs. B) Iterative γ -arylation protocol.	39
Figure I.19. The first example of enantioselective C-H arylation by using CAs as directing group: A) Chiral Arylation of cyclopropanoic acids and B) amino acids.	41
Figure I.20 Extension of the enantioselective C-H arylation protocol towards cyclobutanoic acids.....	41
Figure I.21. Palladium-catalyzed β -C-H olefination of carboxylic acids with A) benzyl acrylate and B) various electron-poor alkenes.	43
Figure I.22 Palladium-catalyzed β -C-H A) acetoxylation of various carboxylic acids and B) acyloxylation of pivalic acid.	44
Figure I.23. The first examples of Fe(pdp) catalyzed carboxylic acid-directed C-H oxidations.	46
Figure I.24. The ability of carboxylic acid as DG in overriding A) electronic, B) steric and C) stereoelectronic effects.....	47
Figure I.25. A) Hydroxyl rebound/lactonization pathway confirmed by isotopic labeling experiment. B) Proposed mechanistic scenario for carboxylic acid-directed C-H oxidation with Fe(pdp).	49
Figure I.26. Challenges of the current state of the art in carboxylic acid directed C-H oxidations: A) low enantioselectivity, B) and C) low chemoselectivity and efficiency in secondary C-H lactonization.	50
Figure I.27. Late-stage C-H oxidations of carboxylic acids with bioinspired Fe catalysts to streamline the synthesis of biologically relevant products: A) gracilioether F (Brown 2014), ⁷¹ B) Scaparvins (Snyder 2017) ⁷² and C) various <i>Illicium</i> sesquiterpenes (Maimone 2019). ⁷³ .52	52

Figure III.1. Representative example of γ -lactone moiety biosynthesis.	59
Figure III.2. Design of the project.....	61
Figure III.3. Fe and Mn catalysts involved in this project.	62
Figure III.4. Overview of the enantioselectivity and diastereoselectivity of the reaction. ..	64
Figure III.5. Substrate scope for the enantioselective γ -C-H lactonization of cycloalkylacetic acids. The major product is depicted along with the conversion, total lactone yield and ee which were determined by chiral GC analysis. Diastereomeric ratio (d.r.) is reported as <i>trans:cis</i> ratio. n.d. not determined. ^a 1 equiv. of H ₂ O ₂ was employed.....	66
Figure III.6. A, Origin of the Thorpe-Ingold effect. B, Proposed transition state of the HAT process in 4- and 5-membered cycloalkaneacetic acid.	68
Figure III.7. Direct comparison of the γ -C-H lactonization with traditional methodologies in affording chiral lactone 2a	69
Figure III.8. γ -C-H lactonization of linear carboxylic acids. A, Remarkable γ -selectivity in the oxidation of nonanoic acid 12 to yield valuable γ -nonalactone 12a . B, Substrate scope for the enantioselective γ -C-H lactonization of linear carboxylic acids. Conversion, yields and ee were determined by chiral GC analysis.....	70
Figure III.9. Substrate scope for the γ -C-H lactonization of primary C-H bonds. A, Scope of butanoic acid derivatives for the rationalization of structural effects. B, Intramolecular competitive experiments of 1° against 2° C-H bonds in γ -lactonization reaction. Conversions, yields and ee's were determined by chiral GC analysis. ^a Isolated yield. The regioisomeric ratio is expressed as γ -2°/ γ -1° ratio.....	74
Figure IV.1. A) Fe and Mn catalysts used in this work. The catalyst steric bulk is modulated by inserting substituents on position 5 of the pyridines (highlighted in red). B) ORTEP diagram of the solid state structure of (<i>S,S</i>)-(Mn ^{TIBS} pdp). Note the restricted cone trajectories imposed by the bulky silyl groups. Triflate groups are omitted for clarity, except for the Mn bound oxygen atoms).	81
Figure IV.2. Oxidation of 2,2-dimethyladamantaneacetic acid 3 (ee was determined by chiral GC analysis while absolute configuration was determined by single crystal X-ray diffraction, see Annex IV for details).....	84

Figure IV.3. Depiction of all possible lactone products of 3'-substituted adamantane acids.	85
Figure IV.4. Oxidation of 3'-hydroxyadamantaneacetic acid (4) and the impact of catalyst steric bulk on selectivity. Diastereomeric ratio (d.r.) corresponds to <i>exo:endo</i> (4b:4c) ratio while regioisomeric ratio (r.r.) refers to the ratio of proximal over distal oxidation products (4a):(4b + 4c). For conversions, yields and ee's of minor products see Annex Chapter IV (Table S6). ^a Cone angle value obtained from the topologically similar Fe(^{TMS} pdp) (i.e. cone of Mn(pdp)=146°, Fe(pdp)=145°). ^{41,95} Absolute chirality of 4b was assigned by its X-ray structure; taking into account that the oxidation does not occur on the same carbon, absolute configuration of 4c can also be assigned, while that of 4a is proposed for similarity to 2a .	86
Figure IV.5. Substrate scope for enantioselective lactonization of bridgehead substituted adamantaneacetic acids.....	88
Figure IV.6. The impact of solvent coordination with polar substituents on diastereoselectivity.....	89
Figure IV.7. Synthesis of chiral, densely hydroxylated bicyclo[3.3.1]nonane (+)- 22 . Absolute configuration of (+)- 22 could not be unequivocally assigned by X-ray diffraction. Results for Mn(pdp) catalyzed oxidation of 20 are shown in Figure S5 (Annex Chapter IV)	91
Figure V.1. Fe and Mn catalysts involved in this study.....	98
Figure V.2. Divergent reactivity and selectivity between directed (1 to 1a) and non-directed oxidations (2 to 2a).	99
Figure V.3. Proposed rebound mechanisms for the carbon radical generated after the HAT. Note that the oxygen atoms can be differentiated by isotopic labelling (i.e. blue ¹⁶ O and red ¹⁸ O, with the latter coming from isotopically enriched H ₂ ¹⁸ O ₂).	102
Figure V.4. Isotope labelling experiments to ascertain the origin of the O-atom incorporated into the lactones (GC-MS analysis via chemical ionization with NH ₃ /CH ₄). The reported ¹⁸ O incorporations are obtained after correction for the isotopic purity of the labelled reactants. A) ¹⁸ O-incorporation in the lactone product 3a from ¹⁸ O-labelled hydrogen peroxide and B) from doubly ¹⁸ O-labelled carboxylic acid 1 . C) ¹⁸ O-incorporation from ¹⁸ O-labelled water was not observed. D) The impact of the Thorpe-Ingold effect in the rebound step.	103
Figure V.5. Estimation of the carboxylate rebound mechanism in a set of substrates containing different types of γ-C-H bonds. The percentage of carboxylate rebound corresponds to the percentage of the doubly ¹⁸ O-labelled lactone. ¹⁸ O incorporations are	

obtained after correction for the isotopic purity of the labelled substrates. Conversions and yields are reported in Figure S1 (Annex Chapter V).	105
Figure V.6. Proposed mechanism for the bioinspired Mn-catalyzed α -C-H lactonization of primary C-H bonds (IV is a Mn ^{III} -OH species).	110

List of Tables

Table III.1. Reaction development using 1 as model substrate. ^a	63
Table III.2. Optimization of the directed oxidation of <i>tert</i> -butylacetic acid (16) ^a	72
Table IV.1. Optimization of adamantaneacetic acid (1) directed oxidation. ^a	83
Table V. 1. The effect of solvent and external acid on the intermolecular oxidation of 3 ..	100
Table V. 2. The effect of solvent and TfOH on the rebound step to generate 3a	104
Table V.3. The effect of catalyst, solvent and TfOH on the rebound step to yield 12a	108
Table V.4. Intramolecular deuterium Kinetic Isotope Effects (k_H/k_D) in the oxidations of deuterated 13-<i>d</i>₁₀ (at different reaction time and temperatures), 13-<i>d</i>₅ and 14-<i>d</i>₅	109

Summary

The lack of reactivity of largely abundant hydrocarbons makes the few practical processes capable of converting them in more valuable compounds, highly desired. This aspect confers to catalytic Carbon-Hydrogen (C-H) bond oxidation a privileged place in modern organic chemistry, since this powerful reaction installs oxygen atoms into ubiquitous and notoriously poorly-reactive C-H bonds thus, enabling straightforward product diversification. After intense investigation of the catalytic action of enzymatic C-H bonds oxidations, the scientific community has turned its attention towards bioinspired Fe and Mn coordination complexes as promising candidates to reproduce such naturally occurring oxidations, in presence of H₂O₂ and carboxylic acids as co-ligands. Despite some progresses on oxidation-site predictability and chemoselectivity have been achieved with these artificial systems, enantioselective oxidation of aliphatic C-H bonds, capable to produce chirality at the forged C(sp³)-O bond, remains limited to enzymatic transformations. Realization of this goal would require conceptual innovations in order to address the chemo-, site- and stereo-selectivity challenges associated with the formation of chiral C(sp³)-O bond from a specific non-activated alkyl C-H bond. In this scenario, the aim of this thesis is the discovery of innovative methodologies precisely designed for this challenging task.

Therefore, in **Chapter III** we developed a protocol for the intramolecular oxidation of prochiral secondary C-H bonds in which carboxylic acids, acting as directing groups for the oxidant species, promoted a highly site-selective and lactone product chemoselective oxidation. The versatility and general applicability of the reaction is witnessed by the successful oxidation of 25 substrates involved in this study, of note, even at strong primary C-H bonds. The data collected concerning the reaction stereoselectivity acquired in this chapter were fundamental for the development of the highly enantioselective C-H lactonization described in **Chapter IV**. Here, rational catalyst design and judicious choice of the substrates enabled the first example of non-enzymatic, chiral C(sp³)-O bond-forming catalytic reaction from an unactivated C-H bond. Mechanistic considerations are collected in **Chapter V**, where rationally designed experiments unveiled the single contribution of reagents and solvents to the reaction efficiency. More interestingly, isotopic labelling experiments bring to light a carboxylate rebound pathway, unprecedented in the mechanistic landscape of Fe and Mn bioinspired oxidations.

Resumen

La falta de reactividad de los hidrocarburos, moléculas muy abundantes, hace que los pocos procesos prácticos capaces de convertirlos en compuestos más valiosos sean extremadamente deseables. Este aspecto confiere a la oxidación catalítica de enlaces carbono-hidrógeno (C-H) un lugar privilegiado en la química orgánica moderna, ya que esta poderosa reacción es capaz de instalar un átomo de oxígeno en enlaces C-H ubicuos y notoriamente poco reactivos, lo que permite una diversificación directa del producto. Después de una intensa investigación de la acción catalítica de las oxidaciones enzimáticas de enlaces C-H, la comunidad científica ha dirigido su atención hacia complejos de coordinación de Fe y Mn bioinspirados como candidatos prometedores para reproducir estas oxidaciones naturales, en presencia de H₂O₂ y ácidos carboxílicos como co-ligandos. A pesar de que se han logrado algunos avances en la predictibilidad del sitio de oxidación y la quimioselectividad con estos sistemas artificiales, la oxidación enantioselectiva del enlace C-H alifático, capaz de producir quiralidad en el enlace C(sp³)-O forjado, permanece limitada a transformaciones enzimáticas. La realización de este objetivo requeriría innovaciones conceptuales con el fin de abordar los desafíos de quimio-, sitio- y estereoselectividad asociados con la formación del enlace quiral C(sp³)-O a partir de un específico enlace alquílico C-H no activado. En este escenario, el objetivo de esta tesis es el descubrimiento de metodologías innovadoras diseñadas precisamente para esta desafiante tarea.

Por lo tanto, en el **Capítulo III** hemos desarrollado un protocolo para la oxidación intramolecular de enlaces C-H secundarios proquirales en los que los ácidos carboxílicos, actuando como grupos directores para las especies oxidantes, promovieron una oxidación quimioselectiva altamente selectiva de sitio y producto de lactona. La versatilidad y aplicabilidad general de la reacción es atestiguada por la oxidación exitosa de 25 sustratos involucrados en este estudio, y es de destacar, incluso la oxidación de enlaces C-H primarios fuertes. Los datos recopilados sobre la estereoselectividad de reacción adquiridos en este capítulo fueron fundamentales para el desarrollo de la lactonización C-H altamente enantioselectiva descrita en el **Capítulo IV**. Aquí, el diseño racional del catalizador y la elección juiciosa de los sustratos permitieron descubrir el primer ejemplo de reacción catalítica formadora de enlaces C(sp³)-O quiral, no enzimática. Las consideraciones mecanísticas se recogen en el **Capítulo V**, donde experimentos diseñados racionalmente

revelaron la contribución singular de los reactivos y solventes en la eficiencia de la reacción. Más interesante aún, los experimentos de marcaje isotópico sacan a la luz un mecanismo de rebote del grupo carboxilato, sin precedentes en el panorama mecanístico de oxidaciones bioinspiradas de Fe y Mn.

Resum

La manca de reactivitat dels hidrocarburs, molècules abundants, fa que els pocs processos pràctics capaços de convertir-los en compostos més valuosos siguin extremadament desitjats. Aquest aspecte confereix a l'oxidació catalítica d'un enllaç carboni-hidrogen (C-H) un espai privilegiat en la química orgànica moderna, ja que aquesta poderosa reacció és competent per instal·lar l'àtom d'oxigen en enllaços C-H omnipresents i notòriament poc reactius, permetent així una ràpida diversificació de productes senzills. Després d'una intensa investigació en l'acció catalítica de les oxidacions enzimàtiques d'enllaços C-H, la comunitat científica ha dirigit la seva atenció a complexos de coordinació de Fe i Mn bioinspirats com a candidats prometedors per reproduir aquestes oxidacions naturals, en presència d'H₂O₂ i àcids carboxílics com a co-lligands. Malgrat s'han aconseguit alguns progressos en la previsibilitat del lloc d'oxidació i la quimioselectivitat amb aquests sistemes artificials, l'oxidació enantioselectiva de l'enllaç C-H alifàtic, capaç de produir quiralitat a l'enllaç C(sp³)-O forjat, es limita a les transformacions enzimàtiques. La realització d'aquest objectiu requeriria innovacions conceptuals per tal d'abordar els desafiaments quimio i estereo-selectius associats a la formació d'un enllaç quiral C(sp³)-O a partir d'un enllaç C-H alquil no activat específic. En aquest escenari, l'objectiu d'aquesta tesi és el descobriment de metodologies innovadores dissenyades amb precisió per a aquesta tasca desafiant.

Per tant, al capítol III es desenvolupa un protocol per a l'oxidació intramolecular d'enllaços C-H secundaris proquirals en què els àcids carboxílics, que actuen com a grups directors per a les espècies oxidants, promouen una oxidació quimioselectiva de d'enllaços C-H per produir lactones. La versatilitat i l'aplicabilitat general de la reacció són testimonis de l'oxidació reeixida de 25 substrats implicats en aquest estudi, destacant fins i tot en forts enllaços C-H primaris. Les dades sobre la estereoselectivitat de la reacció recollides en aquest capítol són fonamentals pel desenvolupament de la lactonització C-H altament enantioselectiva descrita al capítol IV. Aquí, el disseny racional del catalitzador i l'elecció dels substrats van permetre el primer exemple de reacció catalítica que forma enllaços C(sp³)-O quirals no enzimàtics. Les consideracions mecanístiques es recullen al capítol V, on experiments dissenyats racionalment van revelar la contribució única de reactius i dissolvents a l'eficiència de la reacció. Més interessant, els experiments de marcatge isotòpic posen de manifest una via de rebot del carboxilat, sense precedents en el panorama mecanístic de les oxidacions bioinspirades de Fe i Mn.

Chapter I

General Introduction

I.1. C(sp³)-H functionalization: Opportunities and challenges

Synthetic organic chemists are daily challenged with developing more efficient, versatile and fast synthetic routes for making the molecules that we need in our everyday life. Traditional synthetic methodologies rely on pre-functionalized starting building blocks to prepare functional organic molecules. In direct contrast, the ability to directly handle ubiquitous C(sp³)-H bonds, traditionally regarded as inert, is a long-standing goal in modern organic chemistry (Figure I.1). Potentially, C-H functionalization reactions are those transformations capable to convert strong and unactivated C(sp³)-H bonds into C-X linkages (X = O, N, C, Halide) paving the way not only to straighter transformations of feedstock materials into final products but also to the introduction of new concepts in the organic synthesis logic such as the late-stage functionalization.¹

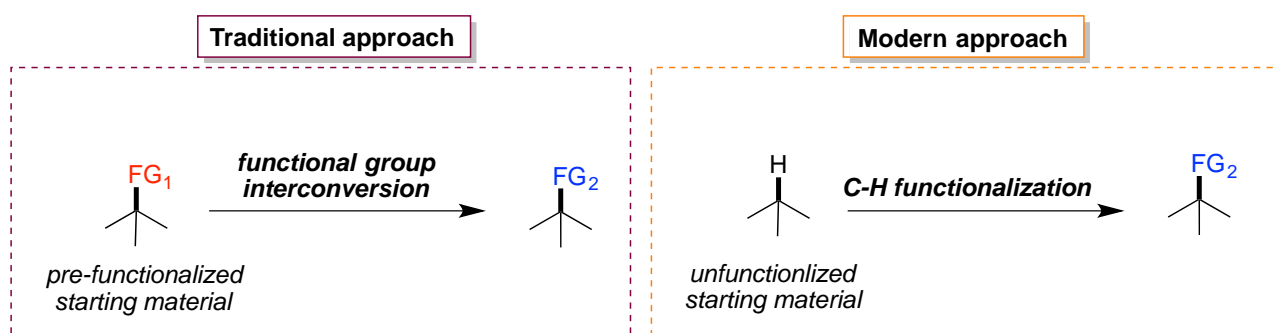


Figure I.1. The evolution of logic disconnections in organic synthesis.

In this particular case, selective C(sp³)-H functionalization can be exploited to the rational diversification of complex molecules providing a straightforward entry to new derivatives, without the *de novo* synthesis with considerable savings in terms of cost and time. Despite many advantages, the high thermodynamic stability and the relative non-polar character of this linkage pose fundamental *selectivity challenges* that hamper the widespread implementation of C-H functionalization in organic synthesis. To overcome the low reactivity of the C(sp³)-H bond a highly reactive species is required and consequently the selective functionalization of *only one* C-H bond among many similar ones within the same molecule (chemoselectivity and site selectivity) becomes very challenging. In the case of stereoselective C-H functionalization the challenges are even harder. Efforts have to be devoted to design a reaction capable to cleave poorly reactive C-H bonds with precision and under mild conditions, addressing the previously described site selectivity and

chemoselectivity issues, while retaining the essential sensitivity to efficiently discriminate the prochiral faces of a molecule.²⁻⁴

Nevertheless, novel strategies based on *transition metal catalysts* have emerged as valuable tools to address these challenges and perform synthetic manipulations directly onto strong C(sp³)-H bonds under mild reaction conditions, redefining this linkage from a silent spectator to a functional group in its own right.⁵ The community has recognized the tremendous potential associated to this class of transformations capable to revolutionize the logic of organic synthesis and therefore, in the last decades experimental and computational studies have been focused on the deep understanding of the key concepts inherent to these processes, in the mechanistic pathways *via* which C-H bonds are functionalized and the intrinsic factors that govern the reactivity of each C-H bond, with the particular aim of overcoming the aforementioned selectivity limitations.

I.2. The mechanisms of C-H functionalization

C-H functionalization processes can be mechanistically classified into two main classes (Figure I.2). One class involves an inner-sphere mechanism in which the reactive C-H bond directly coordinates to the metal center of the catalyst generating, after the bond cleavage event, a discrete organometallic species.⁶ Afterwards, the hydrocarbyl species present in the “inner-sphere” of the metal affords the functionalized product by reacting with a second ligand or with an external reagent. The second class of C-H functionalization collects those “outer-sphere” mechanisms in which the carbon-hydrogen bond is cleaved by an activated ligand of a high-valent metal complex, mimicking the reactivity displayed in nature by a variety of metalloenzymes.⁷⁻⁹ A further subclassification can be also established depending on the nature of the active species and consequently on their C-H bond breaking mechanism. In the case of metal-carbene ($X = CR_2$) and metal-nitrene ($X = NR$) the strong C-H linkage is broken by a direct insertion mechanism characterized by the simultaneous formation of X-H and X-C bonds and the X-metal dissociation. Contrarily, metal-oxo species promote the cleavage of the strong C-H bond by a hydrogen atom transfer (HAT) process generating a carbon center radical. In the most common scenario, this radical is then trapped by a M-X ($X = \text{halide or OH}$) unit in the so-called rebound mechanism, although other reactions are also possible.

The profound difference between “inner-sphere” and “outer-sphere” mechanisms is consequently reflected on the differences in selectivity imparted by these methodologies. Generally speaking, to achieve the organometallic pathway the metal center has to be in close proximity to the carbon-hydrogen bond. Thus, inner-sphere reactions are more sensitive to the steric environment of the targeted C-H bond than the “outer-sphere” processes where the selectivity expressed is usually directed by the most reactive, often the weakest, C-H bond.

Therefore, to clearly distinguish between the organometallic mechanism (“inner-sphere”) from the C-H functionalization reactions performed *via* coordinated ligands to the metal (“outer-sphere”), the community coined the definition of “C-H activation” to strictly refer to the former.

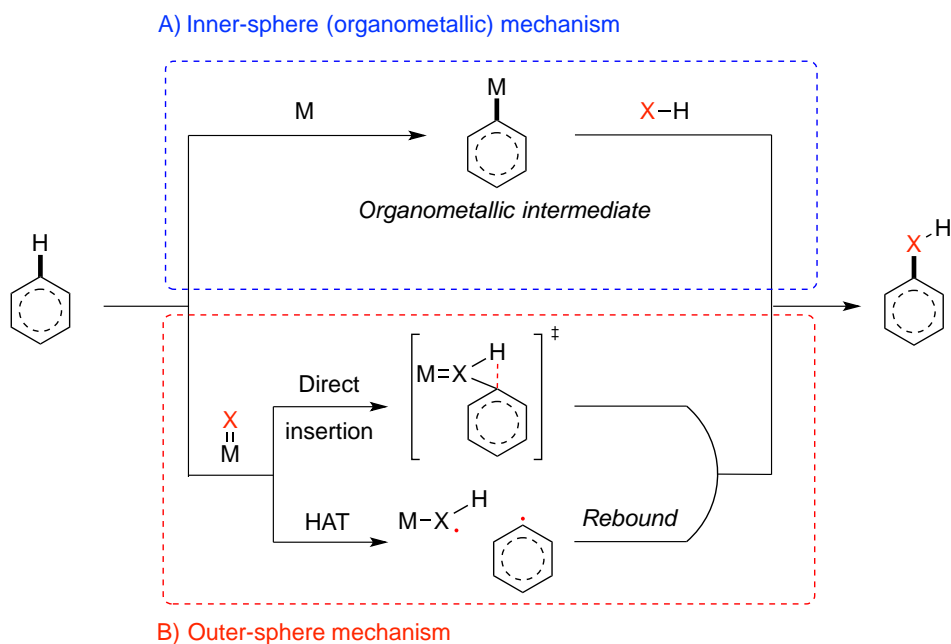


Figure I.2. Mechanistic scenario of metal-catalyzed C-H functionalizations.

I.3. Innate and guided selectivity

Irrespective of the category of mechanism involved in a C-H functionalization reaction, two conceptually different ways of site selection can be defined: substrate-controlled (or innate) and reagent/catalyst or directing group-controlled (or guided) selectivity.¹⁰ In the first type, more classical, the constructive combination of inherent substrate features (i.e. bond strength, acidity, steric environment, electronics, etc.) directs the functionalization toward a selected C-H bond. While excellent levels of site-selectivity can be achieved when these

inherent properties synergistically differentiate among the C-H bonds that constitute an organic molecule, when the individual factors contrast to each other, multiple sites become functionalizable, thereby producing multiple reaction products.¹¹ As a result, the substrate-controlled reactivity provides a good approach to be undertaken in the case of relative small molecules, where the relative reactivity of the different C-H bonds can be identified and predicted. On the other hand, substrate-controlled selectivity suffers in the case of structurally complex molecules or when one aims at diverging the desired functionalization towards alternative aliphatic sites. These great limitations can be mitigated by the second approach in which the site-selectivity is dictated by the specific properties of the reagent/catalyst or by the presence of directing groups that can enhance or completely override the natural reactivity of the substrate. Notably, this approach may allow the functionalization of aliphatic sites that bear unfavorable properties to be reactive, often providing orthogonal selectivities to the reactions that only rely on natural reactivity patterns, thereby broadening the scope of a specific C-H functionalization transformation. In the field of metal catalyzed C-H functionalizations, this concept can be further split in two different strategies: catalyst-controlled selectivity and directing group-controlled selectivity.

I.3.1. Catalyst-controlled selectivity

The structural and electronic properties of a catalyst can amplify or even overturn the natural relative reactivity of the C-H bonds of a substrate. Enzymatic transformations for example can occur at sites inaccessible for conventional reagents.^{12,13} The shape and the presence of recognition elements inside the active site pocket, which orientate the substrate in a specific manner toward the reactive center, are critical features to afford the outstanding C-H functionalization selectivities observed in Nature. However, successful strategies to reproduce such selectivities by introducing recognition motifs into the ligand of a synthetic catalyst have been described only in few reports and often with a very narrow substrate scope.¹⁴ Although with different relevance, both outer-sphere and inner-sphere C-H functionalization are influenced by the steric environment of the targeted C-H bond. Different C-H bonds can display a different reactivity depending on the steric bulk of the catalysts. Therefore, synthetic manipulation of the steric properties of the catalysts, to alter the accessibility of particular type of C-H bonds toward the active center of the metal complex, has represented a powerful strategy to modulate and reverse site selectivity.⁸

I.3.2. Directing group-controlled selectivity

The most popular approach to achieve *guided* C-H functionalizations is based on the use of directing groups (DG) covalently incorporated into the substrate and capable to reversibly bind to the metal center of the catalyst. DG-assisted C-H functionalization gained momentum especially in C-H activation processes where the transition metal insertion into the poor reactive C-H bond requires the close proximity between the metal and the targeted aliphatic site. Therefore, the pre-coordination of the directing group to the metal is often required to favor reactivity. In addition, this effect, called complexation-induced proximity effect (CIPE), not only accelerates the C-H bond cleavage (often the rate determining step) but also dictates the site-selectivity.¹⁵ The pre-organization delivered by the directing group places the metal center close to geometrically defined C-H bonds. A clear example of that is the C-H functionalization reactions of DG-containing substrates catalyzed by palladium(II), where the C-H bond cleavage event occurs at the specific site to afford the highly favored 5-membered cyclopalladated intermediate. Subsequently, this metallacycle can undergo functionalization with a vast array of reagents to forge new C-O, C-N, C-C, C-halogen bonds.¹⁶ Remarkably, the high degree of control exerted on the transition state by the coordination of the substrate to the metal enabled the development of challenging enantioselective C(sp³)-H functionalizations.⁴

However, two main drawbacks are associated with the directing group approach; firstly, despite the exquisite level of site-selectivity reached, the reactivity cannot be easily displaced to other sites of the molecule and variation of the transition state geometry, which determines the selectivity, can be hopefully obtained only after extensive catalyst design, directing group screening or by the use of non-straightforward devised additives. In second place, the directing groups usually involved are not general for the entire array of C-H functionalization reactions and very often a specifically designed directing group has to be synthetically installed into the substrate to the sole purpose to promote the reaction. Furthermore, in many cases the removal or modification of the DG is not trivial and, in some cases, even not possible. All things considered, the introducing-removal extra steps of the directing group is synthetic and atom-economy costly. In this context, the use of natural abundant and ubiquitous functionality as DGs, such as carboxylic acids, is remarkably beneficial.

I.3.3. Carboxylic acids as DG

Carboxylic acids (CAs) are ubiquitous in Nature as well as in multiple fields of chemistry. This functionality characterizes a huge number of essential molecules such as fatty acids, amino acids, keto-acids crucial for life. Because of that, the carboxylic acid moiety regularly features in artificial biologically active compound like pharmaceuticals and agrochemicals. Thanks to the abundancy and readily availability, the low cost and the rich chemical transformations that distinguish this functional group, free carboxylic acids are of paramount importance in organic chemistry as solvents, additives, building blocks, products and ligands for transition metals. Accordingly, these highly desirable features make this functionality a privileged DG to assist metal-catalyzed C-H functionalization. Remarkably, they can be easily introduced by oxidation of alcohols and alkenes, and after functionalization, cleaved or transformed *via* decarboxylative coupling reactions. However, when compared with more electron rich functional groups like carbenes, N- and P-based ligands, carboxylic acids display a weaker coordination ability to transition metals.¹⁷ Therefore, they can be easily replaced by other anions present in the reaction mixture causing an equilibrium that decrease the concentration of the reactive adduct and consequently the overall efficiency of the C-H functionalization. The inherent capability of the carboxylate moiety to engage in metal-binding with one or two oxygen atoms simultaneously to the metal further complicates the scenario. For instance, upon binding with a palladium catalyst, an equilibrium is usually established between the bidentate κ^2 -coordination and the monodentate κ^1 -coordination complexes (Figure I.3).¹⁷ Although the κ^2 -coordination is thermodynamically more stable, the palladium center cannot conformationally approach to the aliphatic C-H, while in the less favored κ^1 -coordination, palladium and the β -C-H are located in a strict proximity.¹⁸

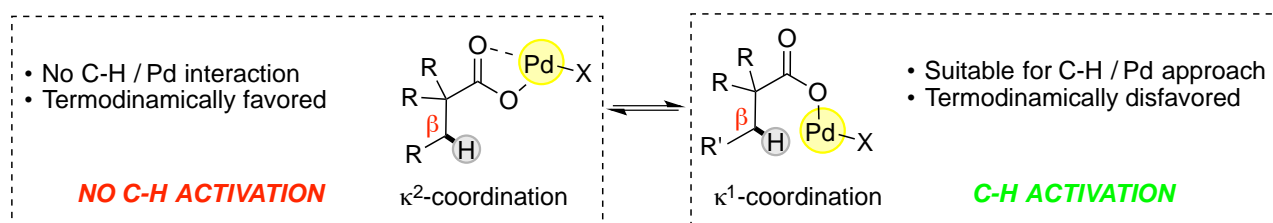


Figure I.3. Challenges of carboxylic acid as directing group in Pd-catalyzed C-H functionalizations.

As a consequence, stronger DGs are usually the preferred choice while the fully implementation of carboxylic acids as native DGs in C-H functionalization methodologies is still in its infancy.

I.4. The key role of oxygenated functionalities

Carbon-oxygen represents a fundamental linkage in chemistry. In organic synthesis, this bond can be converted into other functional groups (C-N, C-S, C-C) or be further derivatized (e.g. esters, ethers, silyl ethers, phosphates). Furthermore, the physical properties of a molecule, such as solubility and polarity, are directly related with the presence of hydrogen bond donors and acceptors like alcohols and ketones. Therefore, oxygenated moieties are ubiquitous in drug design, conferring to the active pharmaceutical ingredient (API) the proper water solubility as well as the interaction sites with the bio-target. Nevertheless, the desired physiological response to an API treatment depends in the optimal positions and orientations of these oxidized motifs. On the other hand, oxidation reactions are also fundamental in nature in which oxygen-activating heme or non-heme metalloenzymes perform hydroxylation reactions in both metabolic processes and biosynthesis. For instance, P450-containing systems are crucial in metabolism for the detoxification of our bodies from potentially hazardous hydrophobic compounds by installing polar OH groups. However, is in the biosynthesis of natural product that nature shows its incredible synthetic skills. A selected example of the ability of nature to build up densely oxidized motifs from relatively simple hydrocarbons is the biosynthesis of the anti-cancer Taxol in *Taxus brevifolia* (Figure I.4). Initially, the polycyclic Taxadiene core is assembled *via* enzymatic cyclization from geranylgeranyl diphosphate. Subsequently, 8 different heme-based Cytochrome P450 tailoring enzymes decor with oxygen functionality the periphery of the hydrocarbon with incredible levels of site-, chemo-, and stereoselectivity.¹⁹

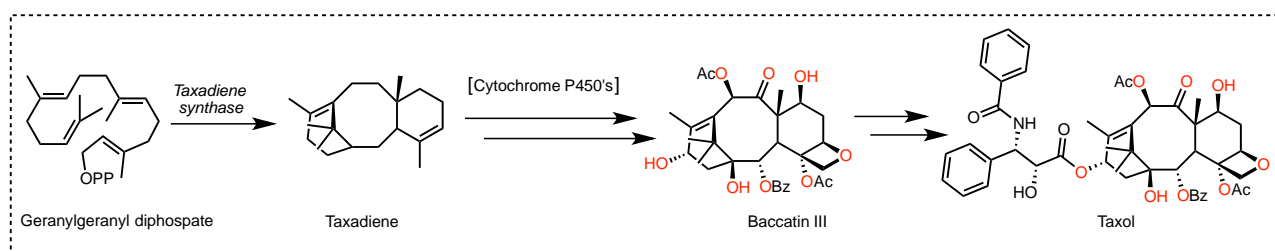


Figure I.4. Biosynthesis of Taxol.

Due to the scarcity of *Taxus brevifolia*, their slow growth, as well as the low concentration of Taxol in the trees, this compound became a molecular target in the 1990s. Nevertheless, traditional organic methods for the introduction of oxygen within a carbon skeleton rely on the elaboration of pre-existing groups with the corresponding limitations. For instance, oxidation reactions are generally carried out under harsh reaction conditions (acid-base reactions, high temperatures) which may lead to wasteful protection-deprotection sequences and complex mixture of oxidized products. Consequently, the shortest sequence for obtaining the intermediate Baccatin III is 43 steps²⁰ in very low yield and moreover the oxidation reactions relied on hazardous and toxic reagents (*e.g.* Ozone, OsO₄). Therefore, the development of efficient and selective oxidation protocols capable to reproduce the enzymes selectivity in a synthetic lab is highly desirable but still challenging in modern organic chemistry.

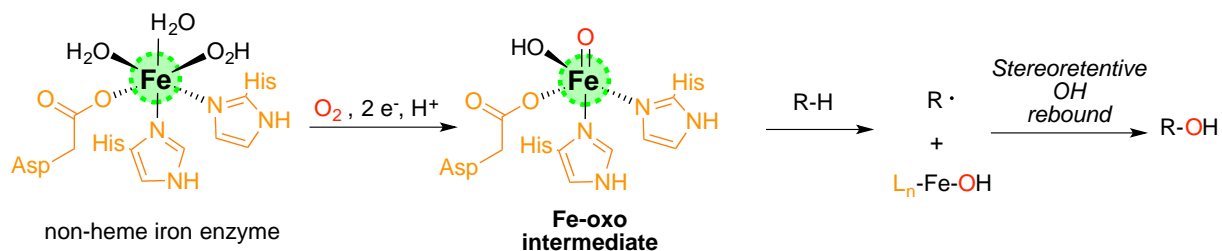
I.5. Bioinspired C(sp³)-H oxidations

Like a painter with a blank canvas, Nature has recognized the omnipresent “masked functional group” C-H as the opportunity to modulate and diversify the biological activity of hydrocarbon skeletons. In this way, a common and readily accessible starting material can be elaborated through site-, chemo- and stereoselective C-H oxidations to generate analogs with different properties. Thousands of years of evolution have conceived heme or non-heme metalloenzymes with active sites capable to incorporate earth-abundant redox active metals, such as iron and manganese, and fine-tune their redox properties by ligation with the N and O atoms of amino acid residues. Reductive O₂ activation at the metal center leads to the generation of reactive high-valent metal-oxo species responsible of directly oxygenating organic compounds thereby drastically altering their physicochemical properties (Figure I.5, A).^{21,22} The outstanding control over selectivities expressed by these metalloenzymes is generally attributed to the second coordination sphere of the active site, which is decorated with recognition sites for binding and dispose of the substrate in well-defined orientation toward the metal center where the reaction takes place. In this way, among the multitude of C-H bonds present in the molecule, only the C-H of interest approaches the reactive metal-oxygen center.

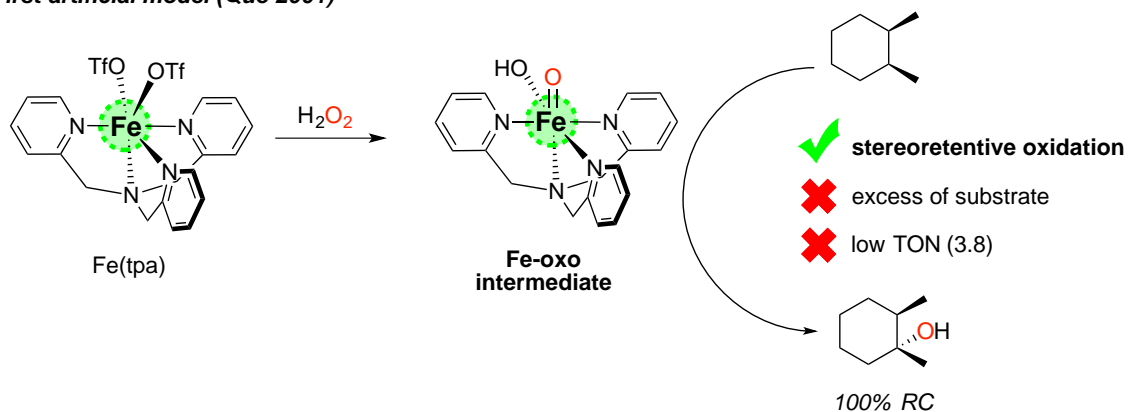
The ability to reproduce such selective oxidations in the laboratory has attracted the interest of the synthetic community in the last century. However, direct C(sp³)-H hydroxylation has

been considered the less selective C-H functionalization and for this reason not suitable for synthetic purpose. Basically, the high reactivity required to break very strong and ubiquitous C-H bonds, usually performed in Fenton chemistry by one of the most reactive radical HO^\bullet ,^{23,24} unfit with a selective process. Among the strategies undertaken, the bioinspired approach that leads to mimic the first coordination sphere of mononuclear non-heme metalloenzyme designing artificial small-molecule catalysts represents a valuable strategy.²⁵⁻²⁷ The field started once recognized that most of these enzyme shared an Fe(II) center in the active site with a recurrent facial coordination geometry composed by two histidine and one carboxylate ligands (Figure I.5, A). Consequently, efforts have been devoted to synthetically reproduce the structural and reactive aspects of this active site. In 2001, Que and coworkers clearly demonstrated that the replication of the enzymatic reactivity was more efficiently attained with N4-ligands, with the Fe(tpa) (tpa = tris(2-methylpyridyl)amine) complex as a catalyst of reference and hydrogen peroxide as terminal oxidant ($2 e^-$ surrogate of O_2) (Figure I.5, B). Since this milestone, the bioinspired oxidation field has been evolving with the aim of furnishing viable oxidation methods in organic synthesis. The impetuous redox-activity of iron complexes in presence of H_2O_2 has been more efficiently controlled and stabilized by linear bis-alkylamine-bis-pyridine (N2Py2) tetradentate ligands⁸ while carboxylic acid co-ligands were discovered to be crucial for significant enhancement of catalytic activity²⁷ (see below) (Figure I.5, C). The corresponding manganese complexes, based on the same class of ligands, display very similar reactivity in presence of H_2O_2 and carboxylic acids and therefore, they are supposed to operate under analogous catalytic cycle.²⁸

A) Enzymatic C-H oxidation



B) First artificial model (Que 2001)



C) Progressed bioinspired C-H oxidation

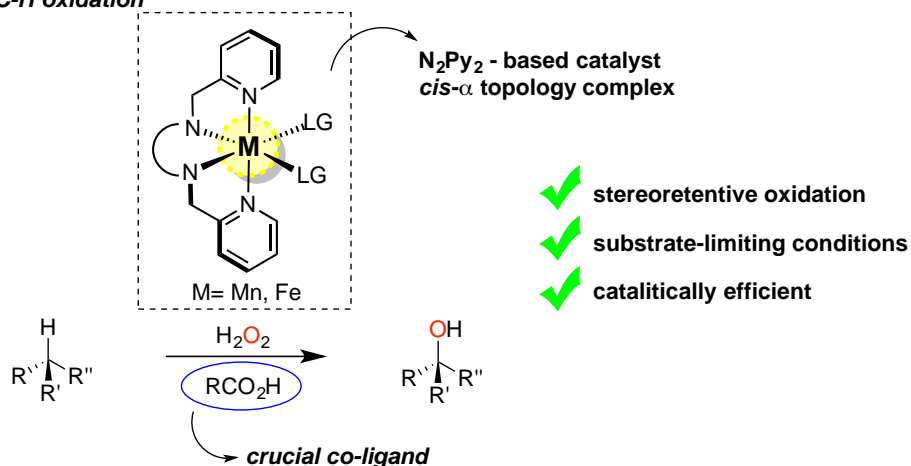


Figure I.5. A) Example of non-heme iron enzyme active site and reactivity upon oxygen activation. B) Replication of the non-heme iron enzyme reactivity with an artificial complex. C) State of the art for synthetically useful bioinspired oxidations.

Mechanistically, these catalytic oxidations are thought to proceed in accordance to the heme system (Figure I.6, A).²⁶ The aliphatic C-H bond is cleaved *via* a hydrogen atom abstraction (HAT) from the high valent metal-oxo to generate a short-lived carbon-centered radical and a metal-hydroxo complex. Then, fast hydroxyl rebound from this latter metal intermediate to the alkyl radical provide the hydroxylated product in a stereoretentive manner.

Controlled activation of the H_2O_2 oxidant by O-O bond heterolysis at the metal center is crucial for the generation of the powerful, yet selective, metal-oxo (Figure I.6, B).^{7,29} Homolytic O-O cleavage would lead to unmanageable O-centered radical triggering Fenton-like processes and consequently must be avoided. Polarization of the O-O bond and subsequent heterolysis is accomplished successfully *via* the so-called *push-pull effect* also operating in heme systems.²¹ Electronically rich N-donor ligand “push” electron density towards the metal center while an ancillary ligand, such as water or more effective carboxylic acids, engage hydrogen bonding with the O-O bond (*pull effect*). Carboxylic acid-assisted pathway has been proved to facilitate the heterolytic cleavage of the O-O by a more efficient protonation of the distal oxygen to form a water molecule.

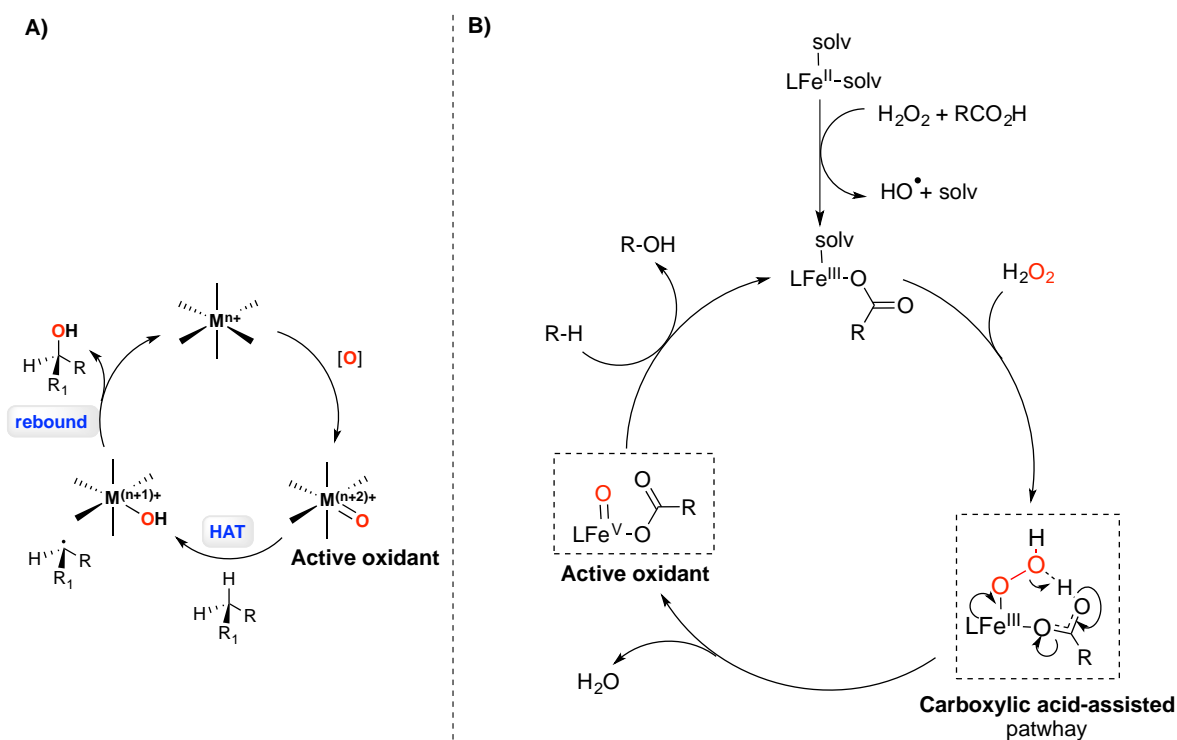


Figure I.6. A) General HAT/hydroxyl rebound mechanism in biological and artificial C-H oxidation. B) Mechanism for the generation of the metal-oxo species in bioinspired system.

I.6. Predicting selectivity in C-H oxidation

I.6.1. Bond Dissociation Energy (BDE)

The straightest way to correlate different C-H bonds and their relative reactivity in C-H functionalization is evaluating their relative bond strength. In this context, the homolytic bond dissociation energy (BDE), which expresses the energy required to cleave a generic R-X bond to the corresponding radicals R• and X•, is the pertinent thermodynamic parameter to establish a scale of reactivity. The prior knowledge of the C-H bond BDE values can, albeit in an approximate manner, allow the prediction of the potential reactive sites. For example, although the model target molecule depicted in Figure I.7 bears 22 functionalizable C(sp³)-H bonds, the cleavage of activated C-H bonds (benzylic, allylic and α-to-heteroatoms) are energetically favored as suggested by their low BDE values.³⁰ On the other hand, simple aliphatic C-H bonds are characterized by higher BDEs and consequently are far less reactive, displaying the general trend tertiary > secondary > primary, which reflects the stability of the corresponding radical.

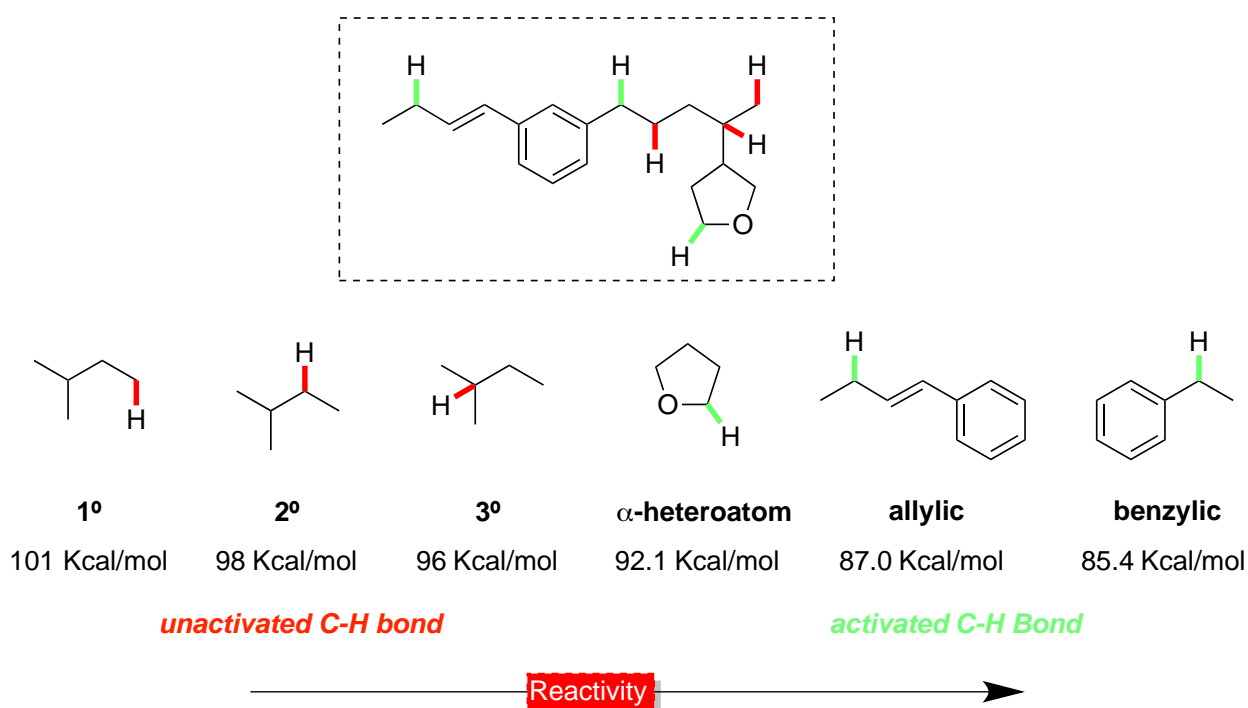


Figure I.7. BDE values of different type of C-H bond within a small model organic molecule.

I.6.2. Polar effects

The general electrophilic character displayed by most of the HAT oxidants is reflected on their sensitivity to react toward the most electron rich C-H bonds of a molecule.²⁷ Therefore, the carbon center radical, generated after the HAT event, is properly stabilized when the

carbon bears substituents capable to release electron density by inductive effects. As a consequence, electronically rich tertiary C-H bonds show an improved susceptibility to be oxidized when compared with methylenic sites, while primary C-H bonds are much less reactive. This manageable interpretation of selectivity is drastically changed by the presence of electro withdrawing groups (EWGs) or electro donating groups (EDGs) within the molecule which deeply overturn the reactivity of the corresponding unfunctionalized hydrocarbon skeleton. Since inductive effects is a distance-dependent phenomenon, by removing e-density from the carbon framework, an EWG moves the oxidation site-selectivity toward remote positions where the negative inductive effects expressed by the functionality are less pronounced. Contrarily, EDGs favor the oxidation of proximal C-H bonds. N-based functionalities have been demonstrated as superior functional groups to modulate the site selectivity in the oxidation of aliphatic C-H bonds.^{2,31-33} Amines are typically critical functional groups in metal catalyzed C-H oxidation due to their propensity to strongly coordinate the metal, thereby killing its catalytic activity. However, this functional group strongly activates proximal α -C-H bonds.³⁴⁻³⁷ Amides as well can be considered as protected amines where the acyl group decreases the nucleophilicity of the N-lone pair. In this context, Milan *and coworkers*,³³ by playing with the electron-withdrawing ability of the N-protecting groups, have described the tunable site selective oxidation of amides and phthalimides using bioinspired Mn catalyst and H₂O₂ as terminal oxidant (Figure I.8).

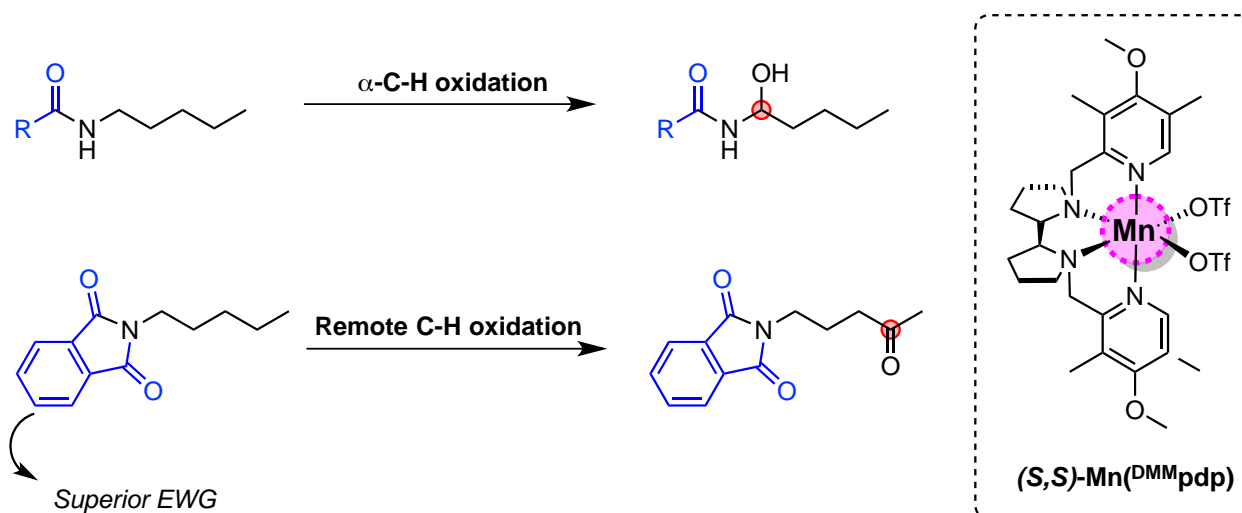


Figure I.8. Electronically controlled site-divergent C-H oxidation of amide and phthalimides.

Polarity reversal strategy

The covalent or fleeting modification of a specific functional group may alter its polarity and consequently its inductive effect allowing secondary site-selectivity orientations. For instance, a common strategy to generalize the oxidation of amines relies in the complexation (with Lewis acid) or protonation of the strongly coordinating *N*-lone pair.³¹ At this point, the positive charge located on the nitrogen diverges the oxidation site-selectivity towards remote positions, in accordance with the aforementioned inductive effect (Figure I.9). Similarly, highly fluorinated alcohols, such as 2,2,2-trifluoroethanol (TFE) or 1,1,1,3,3,3-hexafluoroisopropanol (HFIP), are strong hydrogen bond donor (HBD) solvents and exert a polarity reversal by fleetingly coordinating to alcohol, amine, amide³⁸ and, most recently, 1,2-diol³⁹ functionalities. Upon strong hydrogen bond coordination of these solvents, a partial positive charge is generated at the heteroatom of the functional group which in turn alters the electronic distribution of the carbon chain promoting the remote oxidation of unactivated C-H bonds without covalent manipulation (Figure I.9).

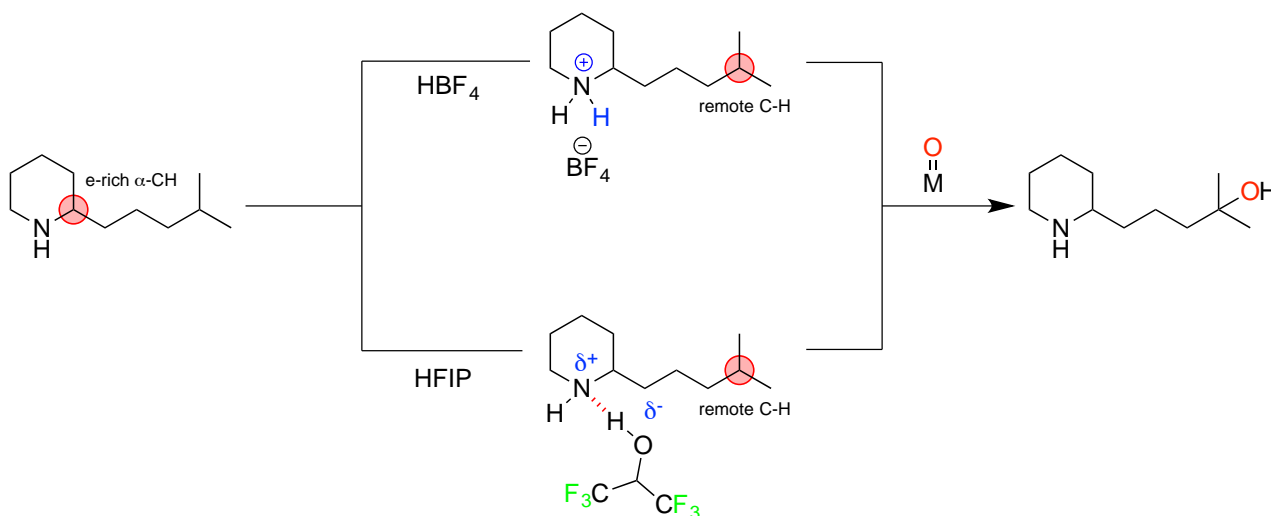


Figure I.9. Polarity inversion promotes remote oxidation of an amine group by covalent protonation or hydrogen bonding with fluorinated solvents.

I.6.3. Steric effects

Despite bioinspired metal-catalysts are commonly defined as “small-molecule catalysts”, the active metal center is not completely exposed to the external environment but actually contained inside a cavity generated by the ligand envelopment. Thus, these species can be sensitive to the steric features of the substrate and discriminate C-H bonds on the basis of

their different steric properties.²⁷ As a consequence, exposed C-H bonds can be oxidized more efficiently when compared to sterically hindered ones. Interestingly, this behavior also explains the competitive oxidation of more accessible methylenic units in presence of more electronically favored but difficult to reach tertiary C-H bonds. The preference for secondary C-H bonds can be further enhanced by the rational design of the sterically elaborated catalyst leading, as previously discussed, to catalyst-controlled selectivity.⁴⁰⁻⁴² In a recent example of this concept (Figure I.10),⁴² the model substrate *trans*-1,2-dimethylcyclohexane was exposed to the oxidation protocol with two sterically different iron catalysts. While the first-generation White's catalyst Fe(pdp) provides a mixture 1:1 of secondary oxidized products over tertiary C-H oxidation, the analogue bulky *tris*-isopropylsilyl (TIPS) functionalized catalyst Fe(^{TIPS}pdp), not only showed an improved activity due to the suppression of detrimental catalyst dimerization, but also an improved selectivity for the more exposed methylenic sites.

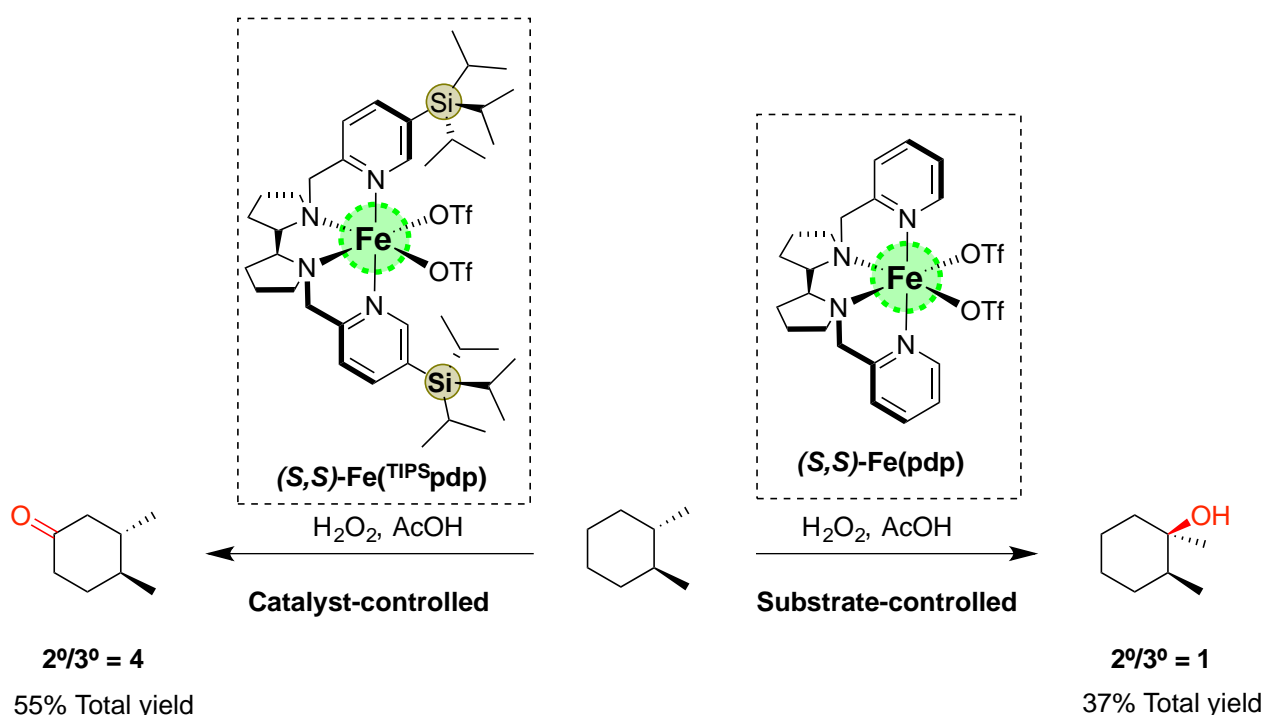


Figure I. 10. Modulation of the selectivity by rational catalyst design.

I.6.4. Stereoelectronic effects

Stabilizing or destabilizing interactions between molecular orbitals and/or atoms can affect the reactivity of geometrically defined C-H bonds. These effects are often invoked to explain counterintuitive selectivity observed in substrate that contain donor-acceptor stabilizing interactions or donor-donor destabilizing interactions not associable with simple steric

repulsions. The two principal stereoelectronic effects invoked in C-H oxidation are hyperconjugation effects and strain release effects.⁴³ The first one rises when a group is capable to donate e-density from its filled orbital to the empty antibonding orbital of the proximal C-H bonds, thereby activating them toward oxidation. For instance, heteroatoms with available lone pairs, such as oxygen and nitrogen in ethers and amines respectively, can weaken the C-H bonds located in alpha position, although the negative inductive effects exerted by these electronegative atoms. The destabilization effect arises when the available lone pairs of the heteroatoms can release electron density by overlapping the σ^* orbitals of the adjacent C-H bonds. Similarly, hyperconjugative activation can be also achieved by the cyclopropane ring. The very strain geometry of this cycle confers C-C bond orbitals with p-character which, if favorably oriented, can release electron density to the antibonding orbitals of the alpha C-H bonds.

The release of torsional strain in the transition state of the HAT process has been recognized as an important factor to be considered in the site selectivity observed in cyclic hydrocarbon oxidations. A clear example of this effect can be found in the oxidation of substituted cyclohexanes where the selective functionalization of equatorial C-H bonds is explained by the relief of unfavorable 1,3 diaxial strain.^{11,44,45}

I.6.5. Directed oxidations

The use of directing groups to bind the substrate directly into the first coordination sphere of the metal catalyst has the potential to direct the oxidation with high degree of selectivity, overriding the inherent substrate bias. In this regard, the carboxylic acid functionality represents a privileged DG due to its crucial role as co-ligand on the catalytic activity of iron-catalyzed oxidation and the weak metal coordination ability of this group. On the basis of these concepts, White and co-workers found that the oxidation of carboxylic acids enables highly γ -selective lactone-forming C-H oxidation (Figure I.11, A).^{27,46,47} Key to development of such selective transformation was the involvement of non-heme tetracoordinated system and its peculiar topology. Contrarily to heme-based catalyst, where the two open axial coordination sites are in *trans*, in non-heme tetracoordinated Fe(pdp) the two available *cis* coordination sites support the terminal oxo unit and the DG of the substrate in close proximity. Remarkably, the oxo-carboxylate species (I) (Figure I.11, A) are capable of outcompeting the intermolecular background reactivity and overcoming the electronic, steric and stereoelectronic effects within the substrate, paving the way to orthogonal

selectivities.⁴⁶ The directed oxidation of the hexanoic acid derivative (Scheme I.10, B) occurred with exquisite selectivity for the γ position and in relatively high yield of the corresponding butyrolactone, while the potentially competitive remote secondary site remained untouched.²⁷ In direct contrast, the oxidation of corresponding methyl hexanoate took place mostly on the methylenic site. The example C (Figure I.11, C) depicts the ability of the carboxylic acid moieties to efficiently direct the oxidation toward electronically deactivated tertiary C-H bond, overriding the unfavorable electronic effect exerted by an EWG. On the other hand, the corresponding methyl esters oxidation, which should undergo through the intermolecular pathway, regularly provides half of the lactone yield irrespective of the proximity of the EWG.

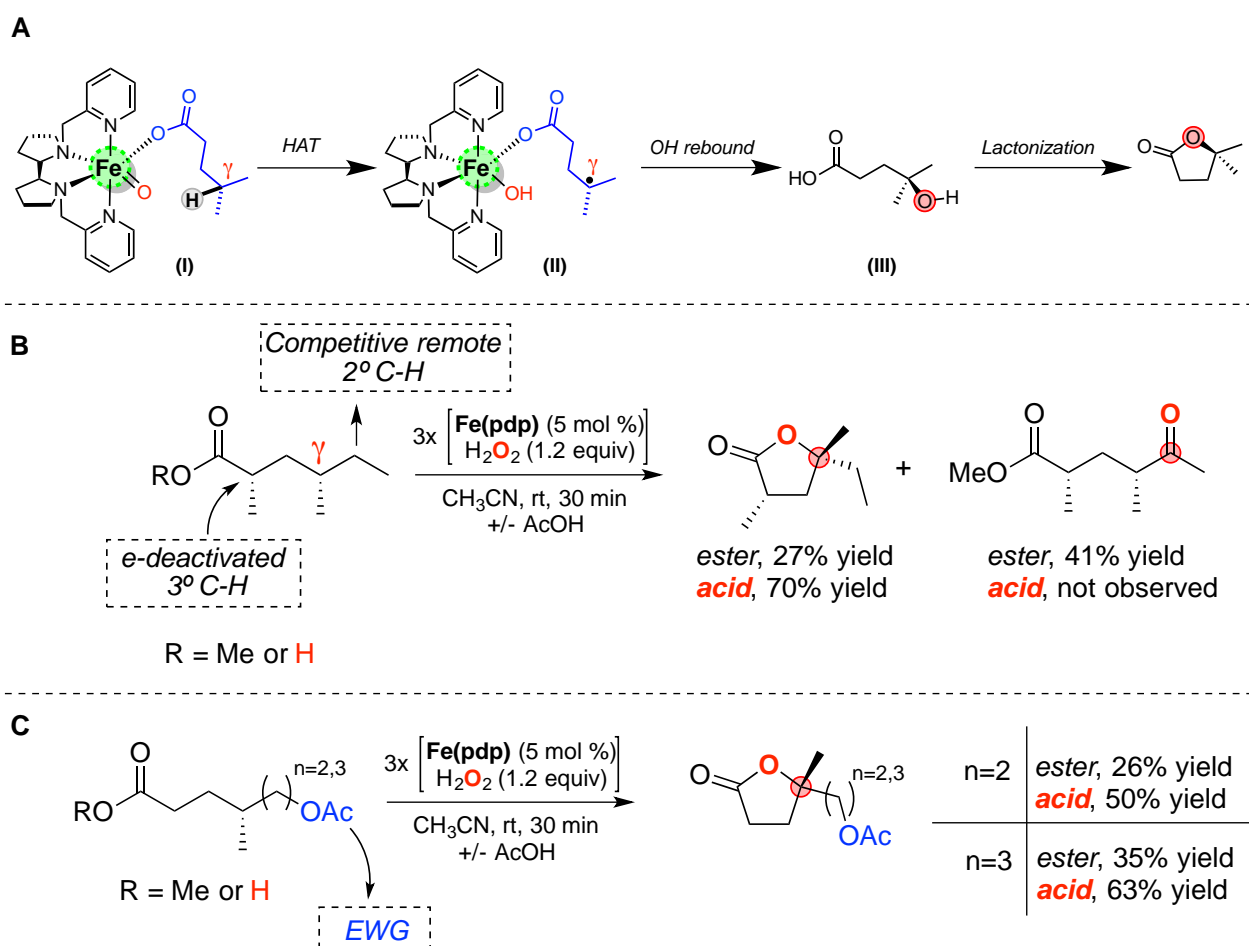


Figure I.11. Mechanism of carboxylic acid-directed C-H γ -lactonization and comparison between intermolecular and intramolecular selectivities in presence of **B)** competitive C-H bonds or **C)** deactivating EWG.

I.6.6. Enantioselective oxidations

Chiral oxygenated motifs are of paramount importance both in Nature and organic synthesis. A clear demonstration of that is the fact that Sharpless was awarded with the Nobel Prize in 2001 for the development of chiral catalytic oxidations of alkenes. Therefore, enantioselective C(sp³)-H oxidations with artificial systems are particularly attractive in this respect. However, the achievement of such reactivity is highly challenging because it would require a strong oxidizing reagent capable to cleave C-H bonds while maintaining a refined control over the site-, chemo- and enantioselectivity of the reaction. Chirality can be introduced within an aliphatic substrate by two strategies²: the enantioselective oxidative desymmetrization of prochiral molecule (Figure I.12, A) or by the more challenging enantioselective oxidation of enantiotopic C-H bonds (Figure I.12, B).

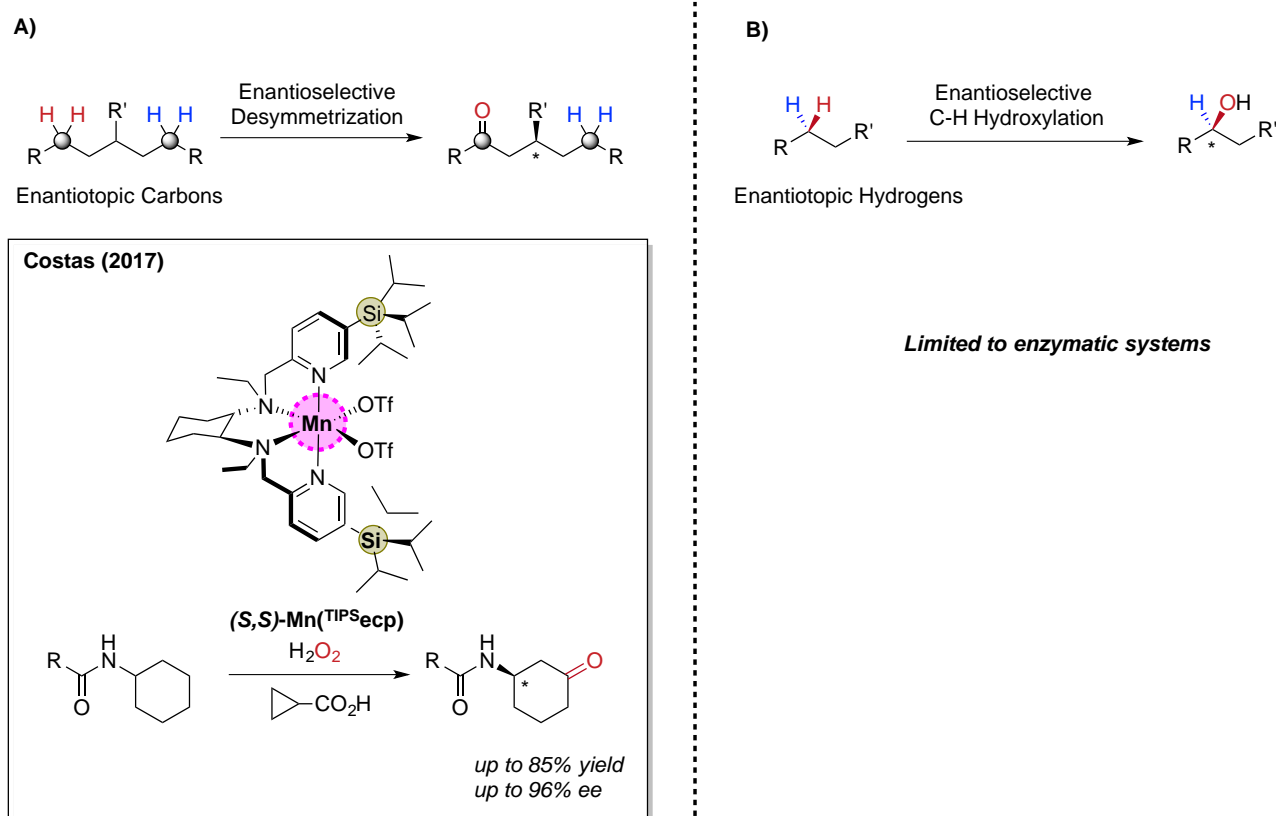


Figure I.12. Overview of the strategies for enantioselective oxidation of unactivated C-H bonds. **A)** State of the art for enantioselective oxidative desymmetrization of unactivated C-H bond with artificial catalysts. **B)** State of the art for enantioselective C-H oxidation of enantiotopic C-H bonds.

In 2017, Milan *and coworkers* reported for the first time the asymmetric oxidative desymmetrization of unactivated methylenes in monosubstituted cyclohexanes.⁴⁵ The authors described that the enantiotopic C3 carbons could be differentiated by ketonization in excellent yield and enantioselectivity when the bulky Mn catalyst Mn(^{TIPS}ecp), oxidative robust cyclopropanoic acid and H₂O₂ as oxidant were involved in the oxidation protocol (Figure I.12, A). Since in Mn catalyzed bioinspired oxidations the HAT process is followed by a stereoretentive rebound of the hydroxyl moiety, the authors comment that the enantio-discriminative pathway must be the C-H bond cleavage at the HAT stage. On the other hand, the enantioselective oxidative discrimination of unactivated enantiotopic C-H bonds is still an unsolved problem for artificial systems. Besides exerting site-selectivity, the catalytic system should selectively oxidize one of the two nearly identical enantiotopic secondary C-H bonds and simultaneously prevents the facile overoxidation of the first formed chiral secondary alcohol product to an achiral ketone.

I.7. Carboxylic acid directed C(sp³)-H functionalization

I.7.1. Carboxylic acid directed organometallic C-H functionalization

While the carboxylic acid directed activation of C(sp²)-H bonds is a long-established reaction,⁴⁸ the directed C-H activation of simple aliphatic carboxylic acids is still underdeveloped. The challenges related to the coordination issues are usually faced by the synthetic conversion of the carboxylate moiety into stronger N- and P-based directing groups. However, in the last decades, prompted by the inherent benefits related to the use of this native DG, a number of protocols for the directed C-H activation of carboxylic acids have been reported. In these works, tailor-made ligands and specialized catalyst conditions balanced the weak coordination properties of this directing group thereby enabling its incorporation in reactions previously described only with stronger DGs.

I.7.2. Carboxylic acid directed C(sp³)-H lactonization

Platinum

The debut of aliphatic carboxylic acids as directing group in C-H activation was in lactonization reactions. In 1991 Sen *and coworkers* found that the Shilov conditions (PtCl₄²⁻ in combination with PtCl₆²⁻) catalyzed the directed oxidation of unactivated C-H bonds of linear and branched aliphatic carboxylic acids in water with the following reactivity order:

$\alpha\text{-C-H} \ll \beta\text{-C-H} < \gamma\text{-C-H} \geq \delta\text{-C-H} \approx \varepsilon\text{-C-H}$ (Figure I.13, A).⁴⁹ The observation of thermodynamically unstable β -lactones strongly supports the directing effect of the carboxylic acid moieties while the selectivity for the γ -site was justified by the strain-free 6-membered platinacycle formed after the C-H activation step. Under the reaction conditions, butanoic acid (**1**) affords a mixture of γ -butyrolactone (**2**) and β -butyrolactone (**3**), obtained after C-H activation of the γ -C-H bond and the β -C-H bond respectively, together with the ring-opening product of γ -hydroxybutyric acid **2** with an overall site selectivity of 12:1 for the γ -oxidation. However, the low turnover numbers (TON, < 1) and the stoichiometric amount of platinum required both as a catalyst and co-oxidant (indispensable for Pt(II) regeneration) heavily reduce the large-scale synthetic appeal of this process. Ten years later, Sames *and coworkers* developed an improved platinum(II) catalytic system for the γ -lactonization of amino acids in which the platinum(IV) co-oxidant was replaced by more sustainable CuCl_2 (Figure I.13, B).⁵⁰ In this study, the corresponding γ -lactone (**7**) of the model substrate L-valine was obtained after oxidation and protection of the amino group in an overall 35% yield and moderate diastereoselectivity. In 2006 Chang *and coworkers* described the *ortho*-methyl lactonization of benzoic acids based on a related catalytic protocol (Figure I.13, C).⁵¹ Under the optimized reaction conditions, the lactonization of the model substrate 2,4,6-trimethylbenzoic acid affords the corresponding lactone **9** in 56% yield. In addition, De Vos group developed in 2019 a catalytic system based on PtCl_4^{2-} catalyst and inexpensive and environmentally benign oxygen (20 atm) as co-oxidant capable to oxidize butanoic acid (**1**) to form γ -hydroxybutyric acid (GHB) (**4**) (Figure I.13, D).⁵² The kinetic limitation imposed by the O_2 activation was overcome by the employment of an inexpensive redox mediator, FeCl_2 , as co-catalyst. Thus, while the chelate-directing effect guaranteed the site selective oxidation of **1** on the primary γ position, the addition of boronic acid or 2-pyridone as stabilizing additives, improved both catalytic efficiency and chemoselectivity, stopping the oxidation at the alcohol stage.

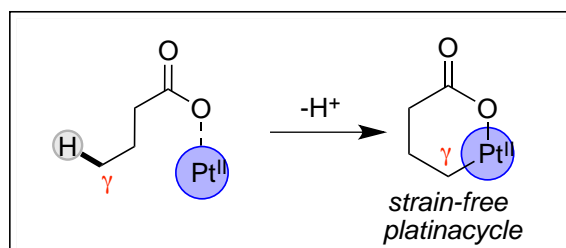
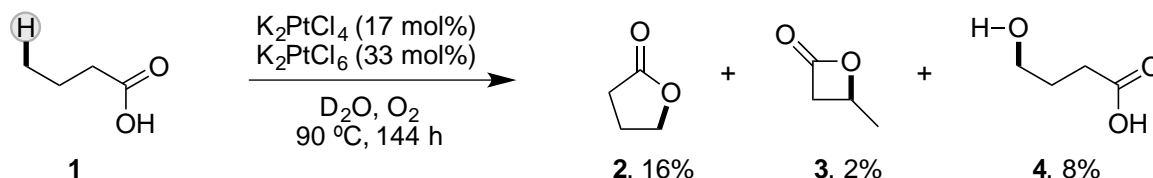
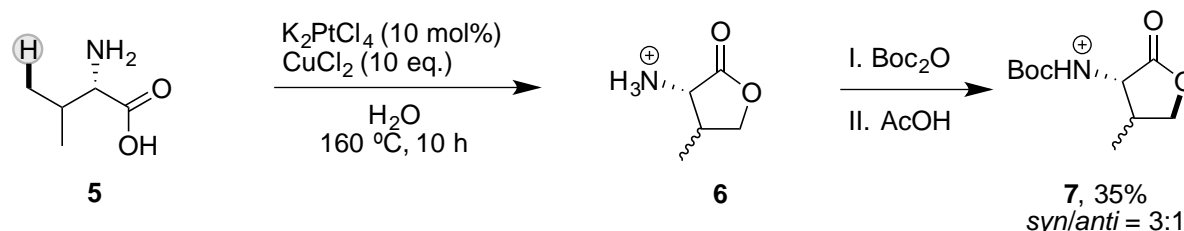
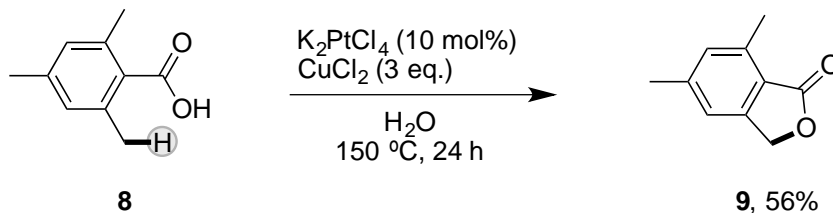
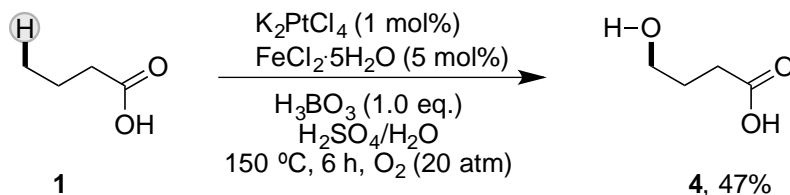
**A) Sen 1991****B) Sames 2001****C) Chang 2006****D) De Vos 2019**

Figure I.13. Directed γ -C-H oxidations of carboxylic acids *via* formation of organometallic platinumacycle. **A)** First directed γ -C-H lactonization of aliphatic carboxylic acids (Sen 1991).⁴⁹ **B)** γ -Lactonization of amino acids (Sames 2001).⁵⁰ **C)** γ -Lactonization of *ortho*-methylbenzoic acid (Chang 2006).⁵¹ **D)** γ -C-H hydroxylation of butanoic acid (De Vos 2019).⁵²

Palladium

Contrarily to platinum, palladium has found a widespread application in the field of C-H functionalization because of the versatile reactivity of Pd-C bond intermediates. Furthermore, palladium complexes display a faster ligand exchange and consequently

enables the development of more efficient catalytic transformations usually accomplished under milder reaction conditions. In the field of lactonization reactions, in 2011 Martin developed a Pd-based catalytic system capable to reproduce the platinum reactivity,⁵³ reported five years earlier by Chang and co-workers, in the directed lactonization of *ortho*-methyl-substituted benzoic acids (Figure I.14, A). Crucial for the success of this methodology was the employment of *N*-acetyl-leucine (**L1**) as ligand, and silver (Ag_2CO_3) and potassium (K_2HPO_4) salt as additives. Therefore, the lactonization of the reference substrate **8** proceeded almost quantitatively while moderate to good yields have been obtained with electronically different benzoic acids demonstrating the versatility and tolerability of the systems toward several types of functionalities. Although benzylic C-H lactonization using palladium catalyst was accomplished successfully, the corresponding reaction for the more challenging unactivated C-H bonds was developed only in 2019 by Yu and co-workers (Figure I.14, B).⁵⁴ In this report, β -C-H activation of a wide scope of simple aliphatic carboxylic acids furnished highly strained 4-membered lactones with moderate to excellent yields (**13a-13f**). The authors demonstrated that the undesired reductive elimination pathways, those that favors non-cyclic oxidized products, could be suppressed by employing sterically bulky tert-butyl hydrogen peroxide (TBHP) and PdCl_2 -derived catalyst. Moreover, *N*-protected β -amino acid ligand **L2**, by providing a six-membered chelate complex, increase the bite angle which in turns favors the desired reductive elimination for the strained β -lactonization.

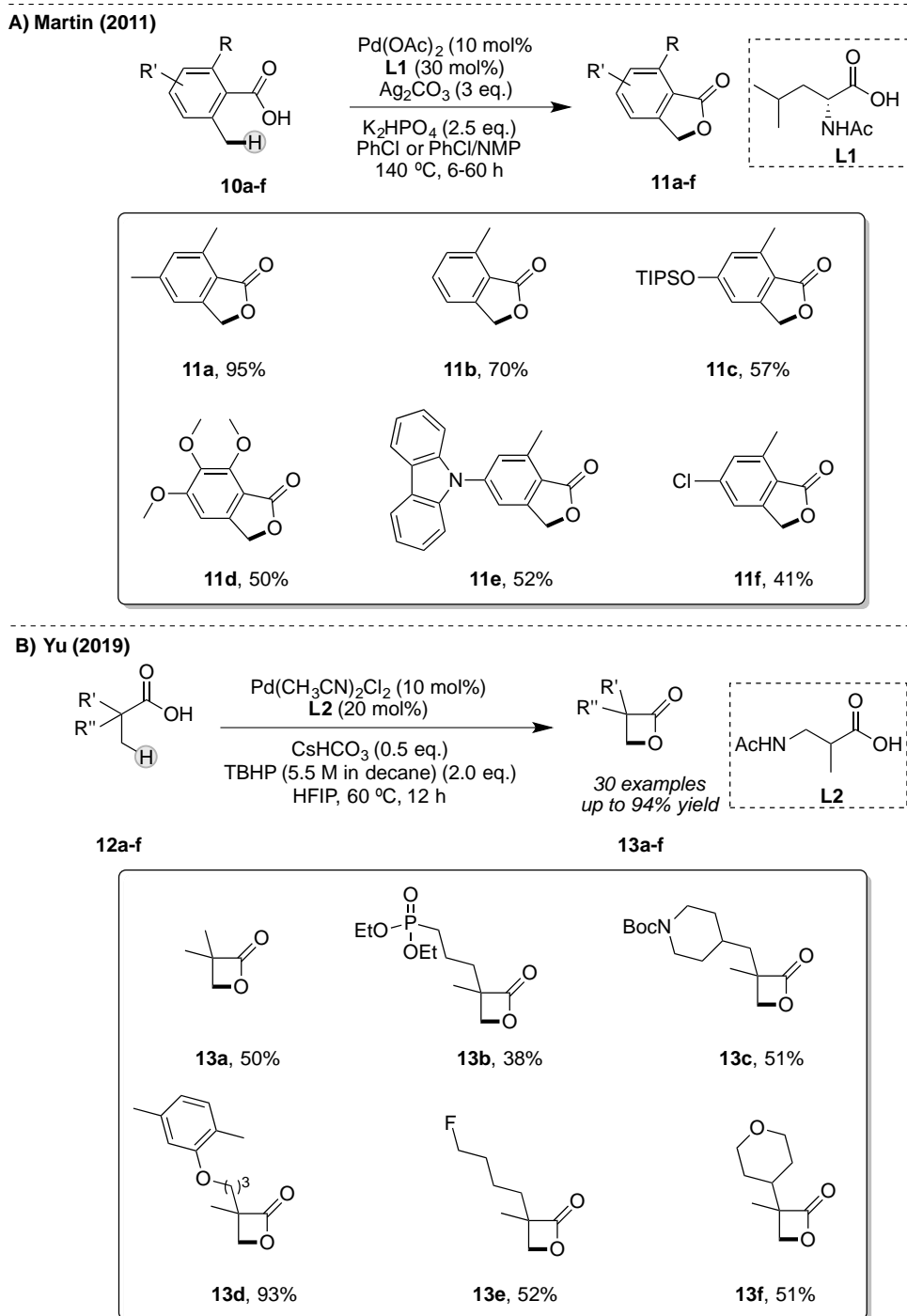


Figure I.14. Palladium catalyzed γ -C-H lactonization of carboxylic acids. **A)** γ -Lactonization of ortho-methylbenzoic acid derivatives (Martin 2011).⁵³ **B)** β -Lactonization of aliphatic carboxylic acids (Yu 2019).⁵⁴

I.7.3. Carboxylic acid directed C(sp³)-H arylation

The first application of carboxylic acids as DG in Pd catalyzed C-H functionalization, was described in 2007 by Yu and co-workers (Figure I.15).⁵⁵ In this seminal work, α -quaternary carboxylic acids were successfully arylated at the β -C-H bonds by Pd(0)/Pd(II) catalytic

cycle in presence of aryl boronic esters or by Pd(II)/Pd(IV) cycle with aryl iodides as arylating reagents. Remarkably, the authors solved the inherent coordinating issues of carboxylic acids by adding potassium and silver salts as additives. The beneficial effect of cations was attributed to the shift of the κ^1 - κ^2 -coordination equilibrium towards the monodentate κ^1 -complex upon its coordination with one oxygen of the carboxylate while the silver salt abstracts I⁻ from the palladium coordination sphere by anion-exchange at the end of the catalytic cycle thereby restoring the active Pd(II) species. However, the effective role of silver metal is still not completely understood and its active implication in the C-H activation step is possible.⁵⁶ The application of the two methodologies to the model substrate pivalic acid (**14**) is reported in Figure I.14. The reaction with the aryl boronic ester (**15**) as arylating agent gave the desired **16** in 38% yield as a single product while the aryl iodides-involving protocol afforded 50% of yield for **16**, albeit in concomitant formation of 20% of the diarylated **17** as side product.

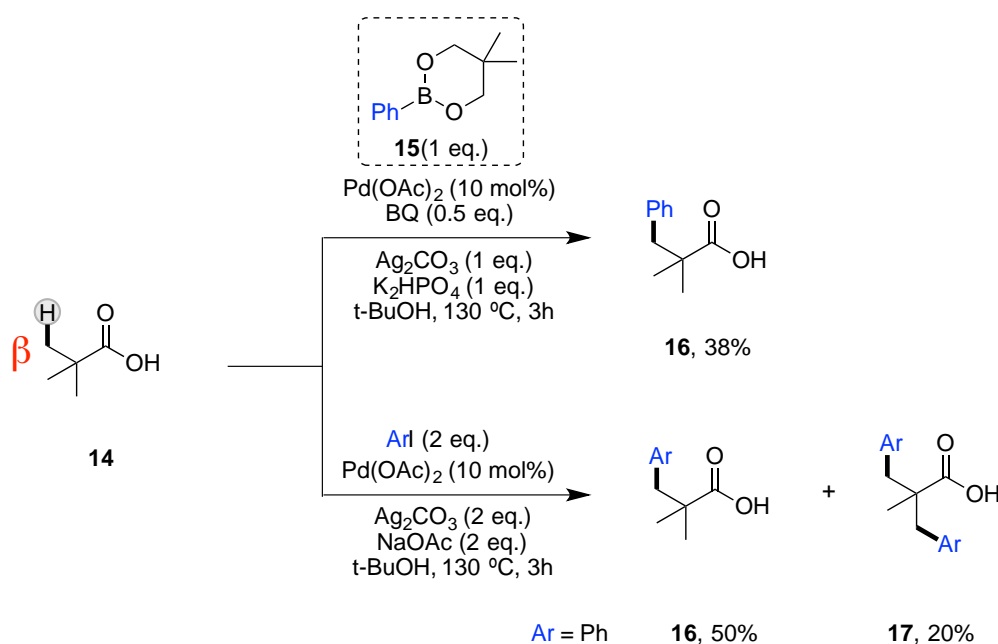


Figure I.15. First examples of palladium catalyzed β -C-H arylation of carboxylic acids

However, the reaction was not extensible to α -non-quaternary carboxylic acids due to the lack of Thorpe-Ingold effect that accelerates the C-H activation step.^{57,58} Indeed, sterically α -substituted substrates conformationally direct the Pd center towards the C-H bond (Figure I.16, A), in. In addition, the presence of α - (and γ) C-H bonds can potentially lead to the undesired β -hydride elimination product after the C-H cleavage (Figure I.16, B).¹⁸

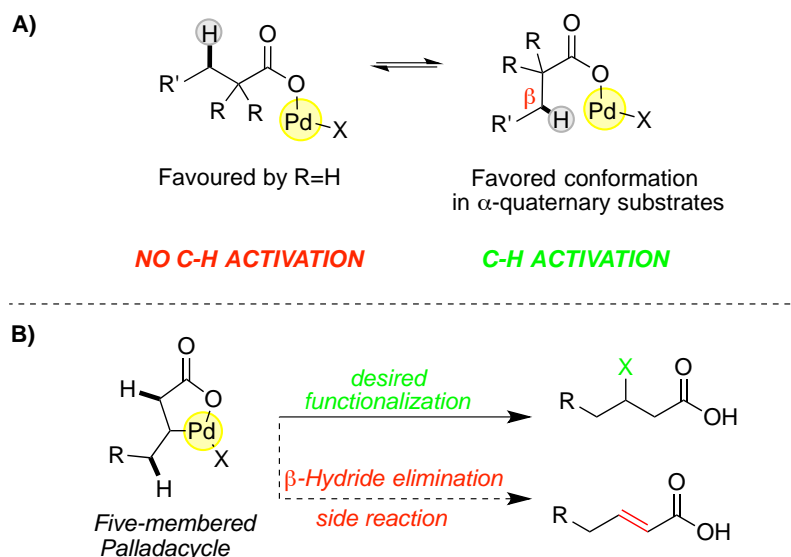


Figure I.16. A) Equilibrium between the conformers in κ^1 -carboxylate Pd complexes. B) Side reaction enabled by β -C-H cleavage of α -non quaternary CAs.

This great limitation of the methodology remained unsolved until 2017 when three independent groups successfully addressed this challenge by undertaking a ligand strategy. The protocol reported by Yu⁵⁹ (Figure I.17, A.I) focused on the arylation of *N*-phthalimido alanine to yield several non-natural phenylalanine derivatives. Key to this step forward was the implementation of pyridine-based ligands and polar, highly fluorinated HFIP as solvent. A broad aryl iodide scope was used to demonstrate the versatility of the reaction. Several functionalities were well tolerated affording the desired products in high yield especially for *e*-rich aryl iodides (**18b-c**) which can undergo a faster oxidative addition to the palladium catalyst when compared to the electronically poor counterparts (**18d**).⁶⁰ Interestingly, the authors also provide preliminary results for α -unsubstituted carboxylic acids, albeit with moderate yield (up to 34%) (Figure I.17, A.II). In parallel, Zhao and co-workers developed a similar protocol demonstrating that also *N*-protected amino acids were suitable ligands for this transformation (Figure I.17, B.I).⁶¹ In particular, *N*-acetyl glycine (**L5**) was selected as efficient ligand for the arylation of **17** providing similar product yields to the ones reported by Yu few months earlier. To demonstrate the generality of this amino acid-assisted C(sp³)-H arylation reaction, the authors investigated the scope of simple aliphatic acids under the optimal conditions (Figure I.17, B.II). Although, even the challenging propionic acid has been shown to be compatible with this transformation, reasonable results have been obtained by using the arylating agent as limiting reagent. Nevertheless, an improved β -C-H arylation methodology for simple α -non-quaternary

carboxylic acids was described by the van Gemmeren group along the same year (Figure I.17, C).⁶² The key finding for the realization of such challenging reaction was the use of *N*-acetyl- β -alanine ligand (**L6**) which delivered better results presumably by establishing a 6-membered chelate with the Pd metal center. Furthermore, the silver source Ag₂O maximizes the concentration of the active Pd species due to the fewer competitive anions in the catalytic mixture when compared to protocols based on acetate or carbonate silver salts. With the optimized conditions and ligand, the authors reported the arylation of α -di-, α -mono-, and α -non-substituted substrates with good to excellent yields irrespective of the electronic nature of the aryl iodides used.

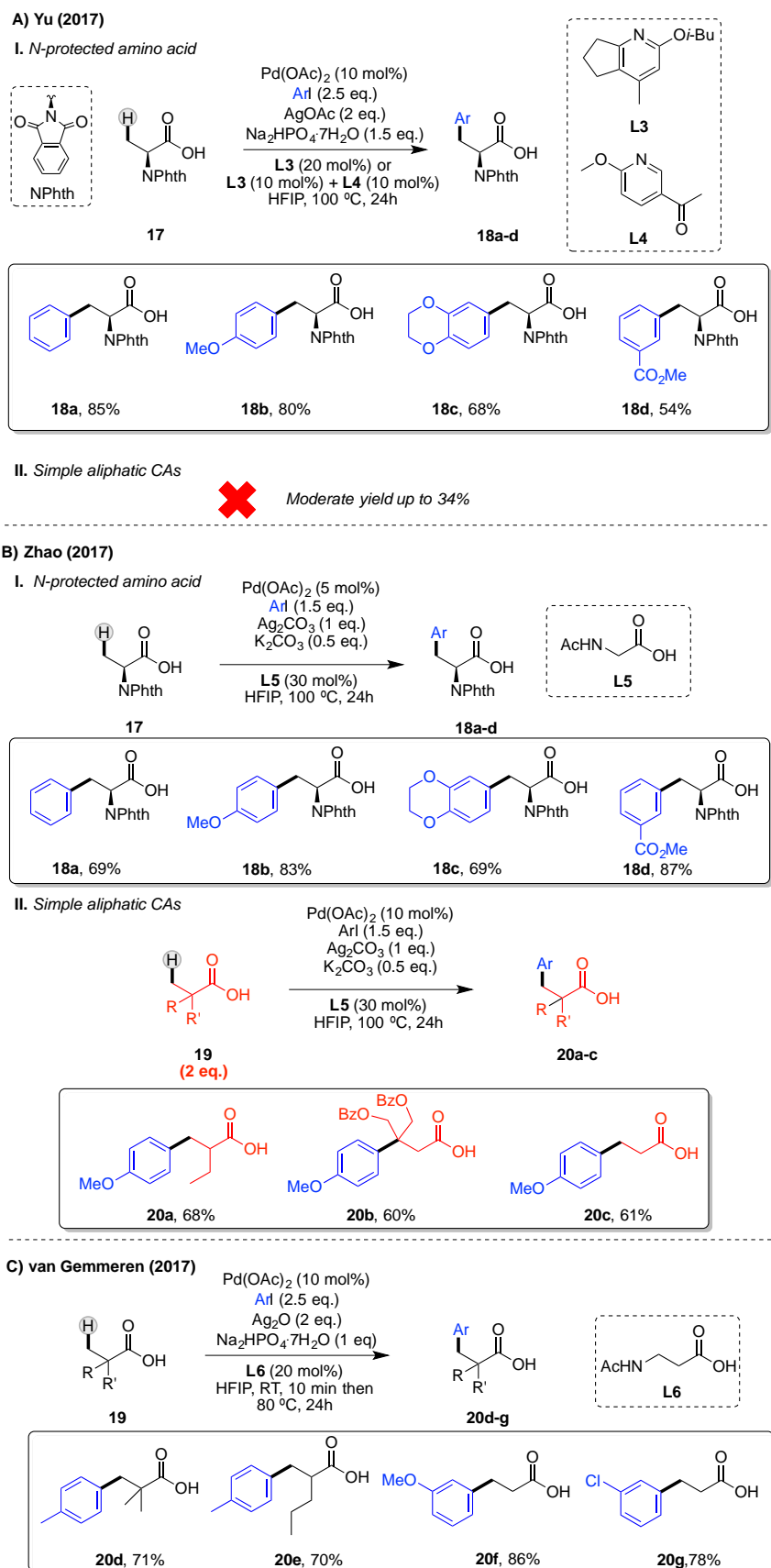


Figure I.17. β -C-H arylation of *N*-protected alanine and preliminary results for aliphatic carboxylic acid by **A)** Yu and coworkers (2017)⁵⁹ and **B)** Zhao and coworkers (2017)⁶¹. **C)** β -C-H arylation of simple aliphatic carboxylic acids (van Gemmeren 2017).¹⁷

Very recently, Maiti and co-workers faced one of the main challenges in the field by designing a methodology to expand the palladium catalyzed C-H arylation to a more distal site from the carboxylate moiety (Figure I.18, A).⁶³ This novel reactivity was possible due to the precise selection of β -quaternary-substrates. Interestingly, in this particular class of carboxylic acids, C-H arylation took place in γ position *via* an unusual 6-membered palladacycle intermediate. Good yields were obtained by complexation of the palladium center with the previously described **L5** for both electron-poor and electron-donating aryl iodides (**22a-22c**). The authors also described an iterative protocol to obtain non-equivalent diarylated compounds by developing a sequential stepwise γ -C-H arylation methodology (Figure I.18, B).

Maiti (2019)

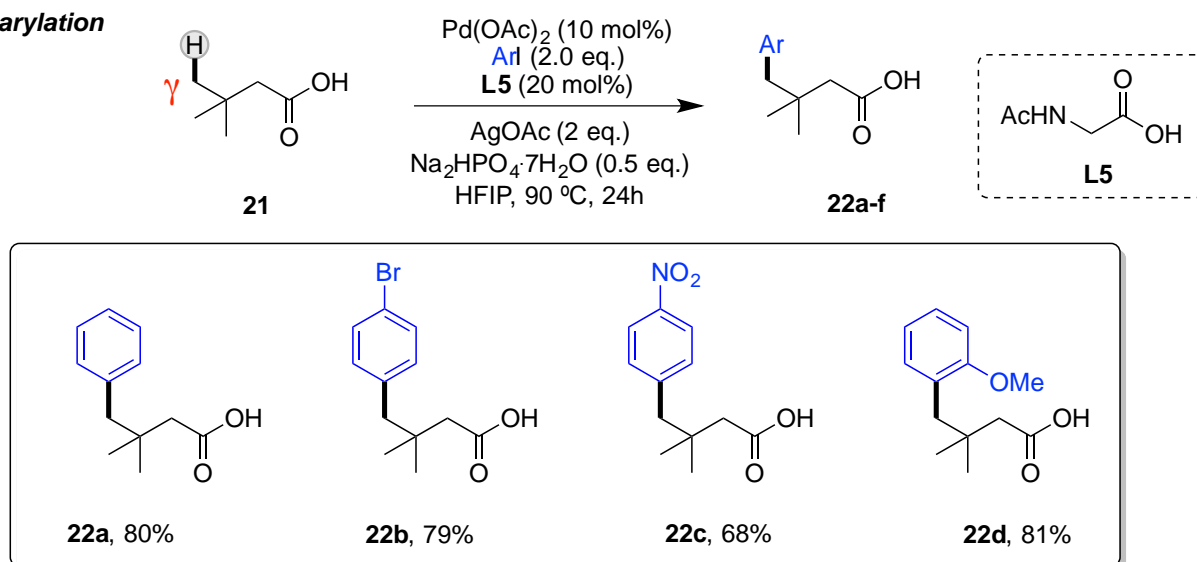
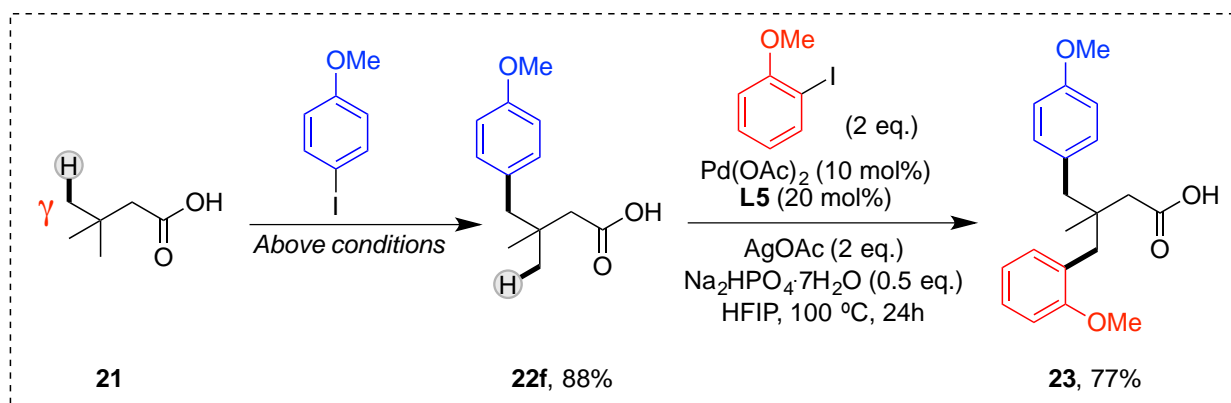
A) γ -arylationB) Iterative γ -arylation

Figure I.18. A) The first example of Pd-catalyzed γ -C-H arylation directed by CAs. B) Iterative γ -arylation protocol.

Enantioselective C-H arylation

The contemporary installation of functionality and chirality onto prochiral substrates constitutes a highly attractive goal in the development of novel synthetic methods. In this context, the high degree of control required in the transition state of an enantioselective C-H transformation is usually reached by the employment of strong directing groups incorporated directly in the substrate.⁴ In this rapidly evolving field, the first report that involves the use of carboxylic acid substrates, described in 2018 by Yu *and coworkers* (Figure I.19, A),⁶⁴ focused on the asymmetric desymmetrization of cyclopropane carboxylic acids by C-H arylation of β -methylenes. Generally, C-H activation of methylene units is considered much more challenging compared to the methylic C-H bond cleavage depicted until now. However, the strain and rigidity of cyclopropane and cyclobutane structures lead to a sp^2 -like character of the methylenic carbons atoms, thereby facilitating their C-H activation step. Therefore, this powerful reaction introduced simultaneously two stereocenters by differentiating the two previously symmetrical methylene sites into one methylene and one methine groups. An extensive ligand design and screening led to the *N,N*-donor ligand catalyst (**L7**) constituted by *N*-acetyl amide and a tertiary amine group. The chiral backbone that gave access to the highest level of enantioselectivity was the one that supported a benzyl moiety adjacent to the amide functionality. A broad aryl iodide scope (**25a-g**) functionalized with halides, electron-withdrawing and electron-donating groups and even hetero arenes were successfully employed under the catalytic conditions. Good to excellent yields were in all the cases matched with exquisite enantiomeric ratios up to 98:2 (**25b**, **25g**). Notably, to further demonstrate the utility of this new methodology the authors extended the carboxylic acid scope to less rigid acyclic 2-aminoisobutyric acid as prochiral substrate (Figure I.19, B). Remarkably, enantioselectivity was only slightly eroded remaining excellent independently from the nature of the arylating agent. In 2019, the same group tackled also the more demanding enantioselective C-H arylation of cyclobutanecarboxylic acids (Figure I.20).⁶⁵ However, to obtain satisfactory results for this class of substrates drastic changes of the previously described catalytic conditions were necessary. Arylboronic acid pinacol esters were used as arylating reagents instead of aryl iodides and consequently a Pd(0)/Pd(II) cycle was postulated for this reaction. Moreover, HFIP solvent was replaced by a mixture of *t*-BuOH/H₂O. To obtain the desired enantioselectivity the authors sterically manipulate the ligand **L5** by introducing two phenyl groups in the ortho position of the benzene ring on the side chain (**L8**). Under these optimal conditions, α -substituted and

unsubstituted carboxylic acids functionalization was attained successfully in terms of both yields and enantioselectivity (**29a-29d**).

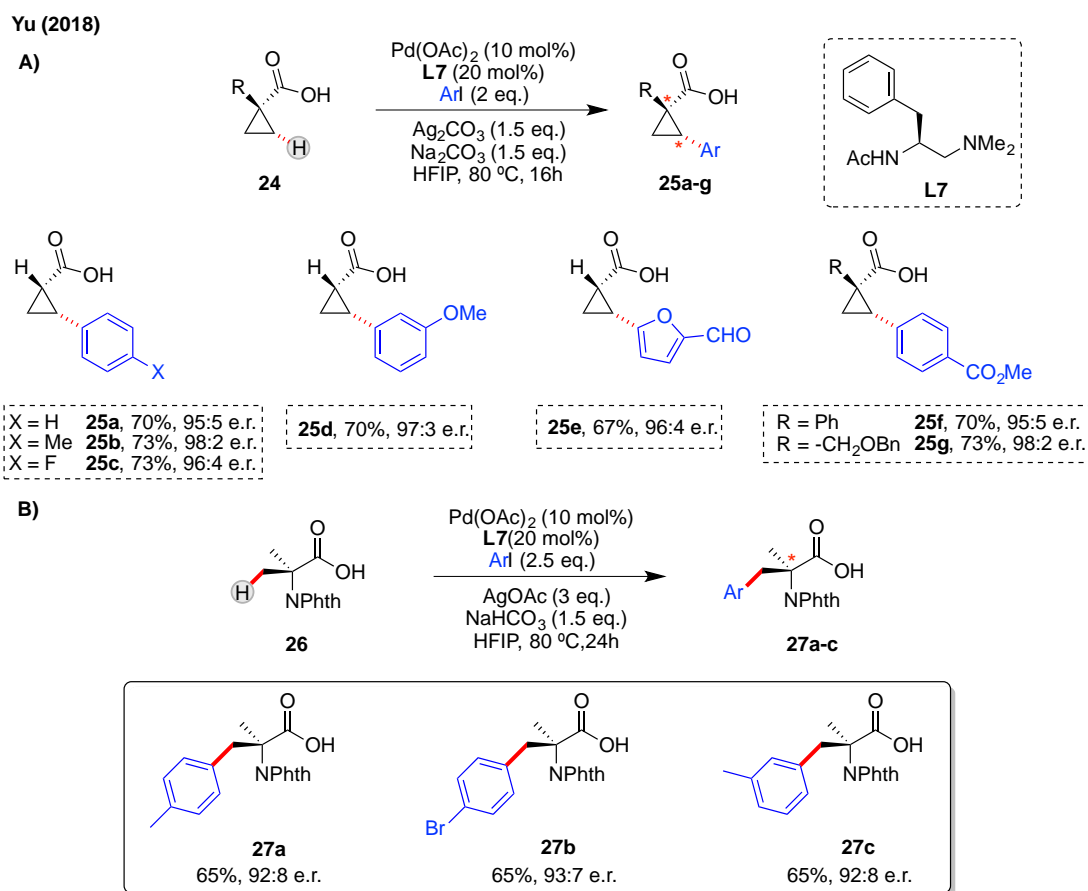


Figure I.19. The first example of enantioselective C-H arylation by using CAs as directing group: **A)** Chiral arylation of cyclopropanoic acids and **B)** amino acids.

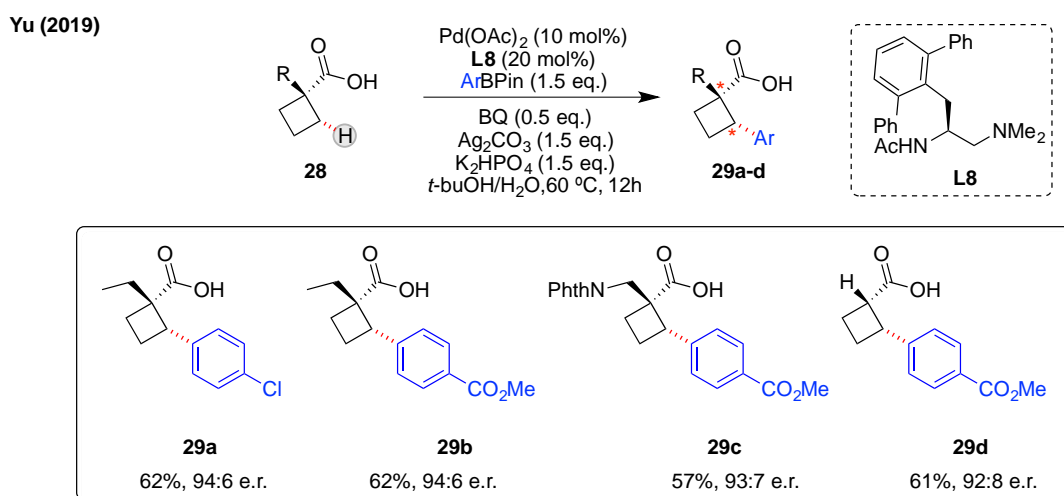


Figure I.20 Extension of the enantioselective C-H arylation protocol towards cyclobutanoic acids.

I.7.4. Carboxylic acid directed C(sp³)-H olefination

In 2018, the Yu group was capable, for the first time, to extend the protocol of palladium-catalyzed C-H arylation to another C-C bond forming C-H functionalization reaction using free carboxylic acid substrates.⁶⁶ The authors succeeded in developing a Pd(II)-catalyzed β -C-H olefination reaction without synthetic manipulation of the carboxylic functionality (Figure I.21, A). Benzyl acrylate was used as model olefin coupling reagent to investigate the catalyst conditions and the carboxylic acid scope. The olefinated products underwent intermolecular 1,4-addition providing valuable γ -lactones as single product. Extensive ligand design led to the discovery of the N,S-bidentate ligand N-acetylaminoethyl phenyl thioether (**L9**) as superior ligand for this reaction by drastically increasing the initial reaction rate and stabilizing the Pd much more efficiently than the commonly used N,O-ligands (higher turnovers numbers). During the evaluation of the CA scope, the authors found that systematic substitution on the α -position strongly increased the lactone product yield. Consequently, α -unsubstituted propanoic acid provided a moderate 40% of the corresponding γ -lactone while the α -pivalic acid afforded nearly quantitative yield. Remarkably, this protocol was highly efficient also for strained cyclopropane substrates. Next, the authors expanded the scope of the olefinating agent with excellent results by using strong electron deficient alkenes and pivalic acid as model substrate (**33a-33d**) (Figure I.21, B).

Yu (2018)

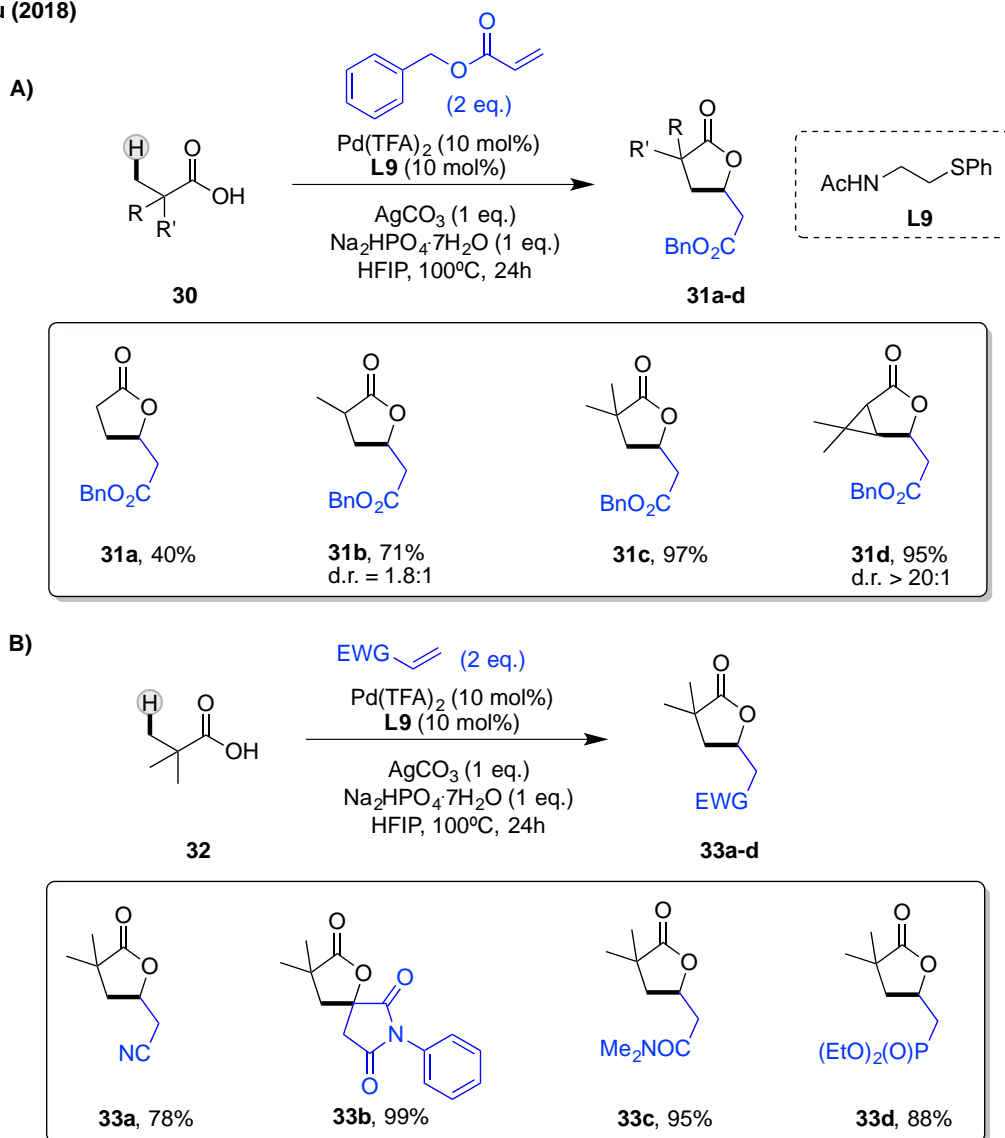


Figure I.21. Palladium-catalyzed β -C-H olefination of carboxylic acids with **A)** benzyl acrylate and **B)** various electron-poor alkenes.

I.7.5. Carboxylic acid directed C(sp³)-H acyloxylation

In 2019, van Gemmeren *and coworkers* reported the first intermolecular C-O bond forming C-H activation reaction by performing palladium-catalyzed C(sp³)-H acyloxylation of free carboxylic acids (Figure I.22, A).⁶⁷ Besides the substrate and Pd catalyst, the reaction conditions involved (diacetoxyiodo)benzene as oxidant and a mixture HFIP/acetic anhydride as solvent. Concerning the base additive necessary for the *in situ* generation of the carboxylate anion, the author found that the counter anions deriving from the typical alkali bases used in the previously described C-H activation reactions of carboxylic acid were not suitable for this transformation. This critical issue was solved by employing the sodium salt of the HFIP solvent (NaHFIP) as traceless base. However, to obtain satisfactory

product yields, an excess of the carboxylic acid was required. With the optimized conditions in hand, various α -quaternary carboxylic acids underwent acetoxylation with moderate to good product yield (**35a-c**). After that, the pilot substrate pivalic acid was functionalized in good yield with various ester partners demonstrating the versatility of the reaction (Figure I.22, B).

van Gemmeren (2019)

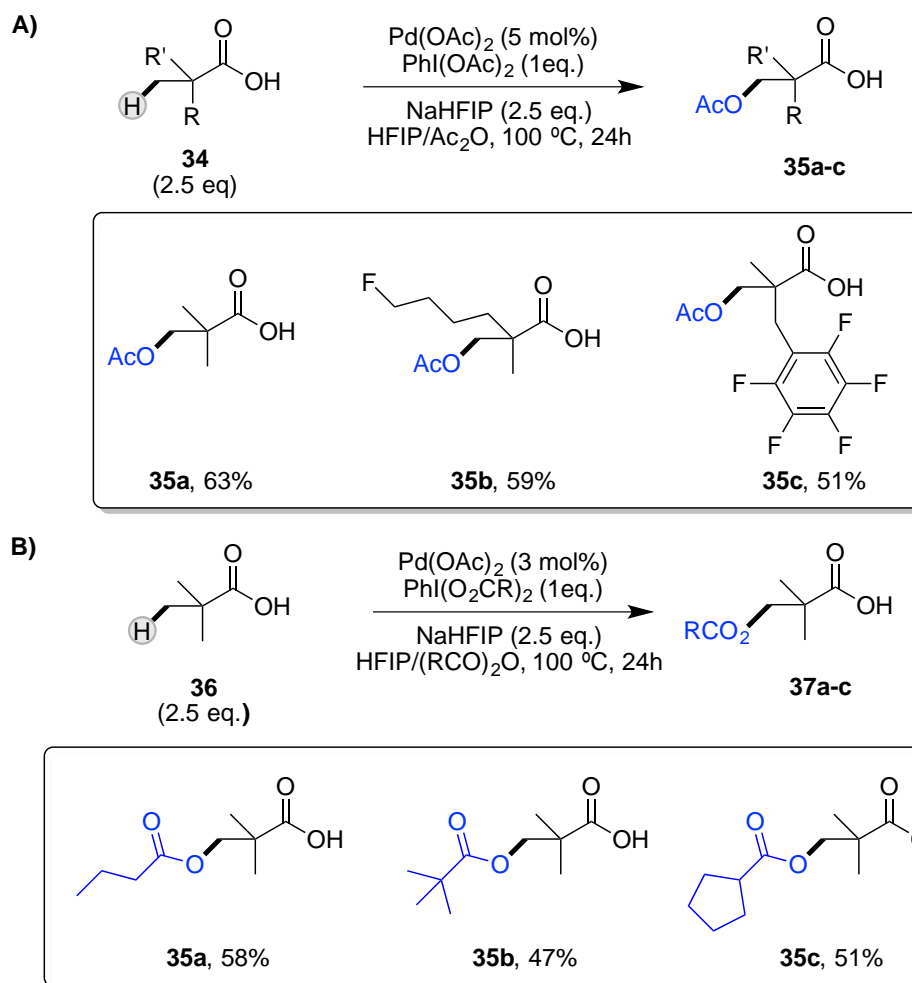


Figure I.22 Palladium-catalyzed β -C-H **A)** acetoxylation of various carboxylic acids and **B)** acyloxylation of pivalic acid.

I.8. Carboxylic acid directed bioinspired C(sp³)-H oxidation

In 2007, the seminal work of White and co-worker described a non-heme iron(II) catalyst Fe(pdp) that used environmentally benign H₂O₂ to effect predictably site-selective aliphatic C-H oxidations of secondary and tertiary sites in preparative yields.²⁷ Previous to this methodology, bioinspired iron catalysts were mostly considered as mechanistic probes to

investigate the chemistry behind metalloenzymes. These reactions employed large excesses of substrate and provided low product yields, which overall hampered their use as synthetic tools. In White's breakthrough work, the key discovery was the employment of acetic acid as co-ligand for increasing the catalytic activity of the iron catalyst towards intermolecular C-H oxidation, analogously as in epoxidation reaction with non-heme iron catalysts.⁶⁸ Structurally, the *cis*- α topology of linear tetra-aminopyridine-based complexes, such as Fe(pdp) locates the ancillary ligand and the terminal oxidant H₂O₂ in *cis* relative proximity.⁶⁹ Therefore, the carboxylic acid establishes hydrogen bond interactions with the hydrogen peroxide and consequently assists the heterolysis of the polarized O-O bond by protonating the distal oxygen.⁷⁰ As a consequence, the resultant putative high valent iron-oxo(-carboxylate) species is more efficiently generated when compared to the so-called water-assisted pathway, where a water molecule assists the O-O cleavage. Since this step controls the catalytic performance, any gain of efficiency at this stage will translate into improved turnover numbers and selectivities. Collectively, these inherent features of the catalytic system, strongly suggest that carboxylic acids could be suitable DGs to be involved in directed, intramolecular C-H oxidations. Indeed, along with the same work, the authors reported the oxidation of tertiary C-H bonds in carboxylic acid substrates in absence of external AcOH co-ligand. Remarkably, highly site-selective oxidation of the γ -C-H bond followed by ring-closure lactonization was observed in the case of an hexanoic acid derivative (Figure I.23, A). Despite the presence of multiple competitive sites, the resultant 5-membered γ -lactone was obtained in 70% yield as single product. More interestingly, structurally more complex tetra-hydrogibberellic acid analog was exposed to the same catalytic conditions affording 52% of the corresponding γ -lactone and, presumably due to the inherent substrate rigidity, it was obtained as a single diastereomer (Figure I.23, B). With these results, the authors demonstrated the potential of carboxylic acid-directed C-H oxidation to strictly favor the oxidation in γ position, no matter the inherent substrate bias.

White (2007)

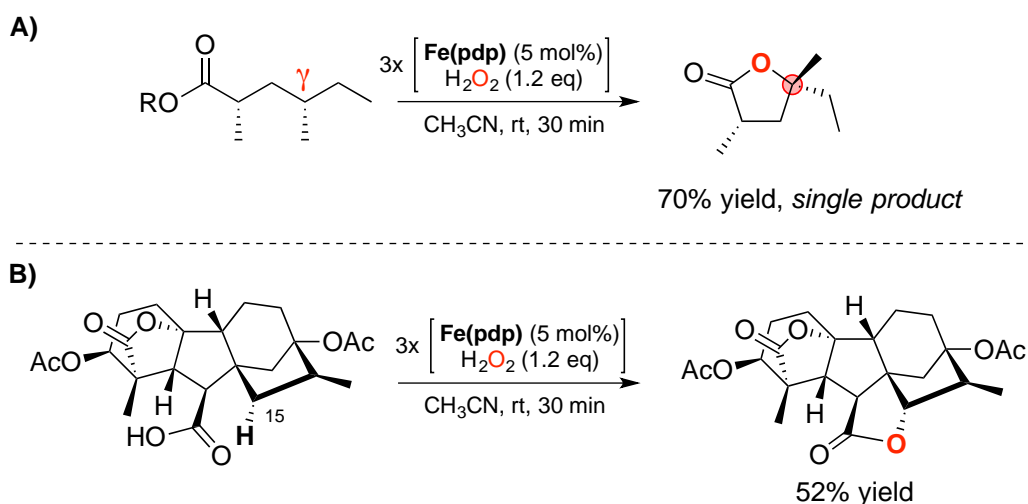
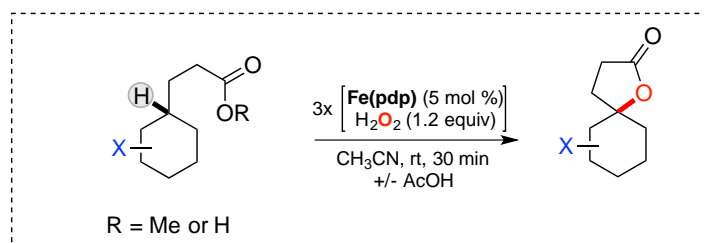


Figure I.23. The first examples of Fe(pdp) catalyzed carboxylic acid-directed C-H oxidations.

A more detailed study about the capability of the carboxylate moiety to override unfavorable electronic, steric and stereoelectronic effects within the substrate was reported by the same group in 2012.⁴⁶ Each effect was evaluated independently by applying the previously described protocol over an array of rationalized carboxylic acids that intrinsically bear such properties (Figure I.24). Thus, the obtained outcomes were compared with the ones achieved by the oxidation of the corresponding methyl esters (in presence of AcOH to promote the formation of the oxidant species), which lack of coordination ability while retaining near identical electronic character. Example **A** shows the ability of carboxylic acid to overcome the unfavorable electro-withdrawing effect exerted by the ketonic function into the cyclohexane carbon skeleton (Figure I.24, A). Thus, the carboxylic acid substrate underwent C-H oxidation/lactonization reaction in 46% of product yield, while the same reaction carried out in presence of the methyl ester derivative, only afforded 10% of the lactone yield since it cannot act as co-ligand for the catalyst. Afterwards, the authors demonstrated that carboxylate ligation could overcome unfavorable steric features. To this end, the carboxylic acid and corresponding ester featuring a conformationally locked cyclohexane, depicted in example **B**, were prepared and exposed to the oxidation protocol (Figure I.24, B). It should be noted that intermolecular abstraction of tertiary axial C-H bond has been demonstrated to be less readily accomplished by the bulky Fe(pdp) catalyst due to steric congestion at this site in comparison with the more exposed equatorial C-H counterpart. Nevertheless, in direct contrast with previous results, carboxylic acid directed

oxidation took place exclusively at the less accessible axial γ -C-H in synthetically useful 50% lactone yield. Contrarily, its methyl ester derivative only furnished 9% of this compound while the major product ketone (36% yield) arose from the oxidation of the less sterically hindered methylenic site.



	Starting Material	Directed Products	Non-Directed Products
A) Electronics		 <i>ester, 10% yield</i> <i>acid, 46% yield</i>	
B) Sterics		 <i>ester, 9% yield</i> <i>acid, 50% yield</i>	 <i>ester, 36% yield</i> <i>acid, -</i>
C) Stereoelectronics		 <i>ester, 2% yield</i> <i>acid, 58% yield</i>	 <i>ester, 22% yield</i> <i>acid, -</i>

Figure I.24. The ability of carboxylic acid as DG in overriding **A)** electronic, **B)** steric and **C)** stereoelectronic effects.

Taken together these reactions indicate that the intramolecular nature of the carboxylic acid oxidation is strongly characterized by a well-defined relative orientation of the oxo unit and the γ -C-H, irrespective from the steric environment.

To complete the set of guidelines for predicting C-H oxidation site, the authors evaluated the ability of the carboxylate to perform directed γ -C-H oxidation/lactonization in presence of competitive stereoelectronically activated sites (Figure I.24, C). In example C, although the carboxylic acid featured two sites activated through hyperconjugative donation from an

oxygen atom, the oxidation occurred in a selective manner in favor of the γ position, furnishing the desired lactone product in 58% yield. In stark contrast, the methyl ester derivative underwent unselective oxidation affording only traces of the γ -lactone product (2% yield) while the major product was the oxidation at the 2° C-H bond adjacent to the ethereal functionality. Cooperatively, all these experiments shed light on the intermolecular nature of the reaction and the strong impact of carboxylic acid moieties in imparting orthogonal selectivities to the one observed in non-directed oxidations. Successively, the authors were interested in depicting a mechanistic scenario for this transformation. Previous studies⁴⁷ on directed oxidation of carboxylic acids demonstrated that the carbon-centered radical, formed after the HAT process, is short-lived and the radical rebound step occurs in a stereoretentive fashion, analogously to the intermolecular oxidation with heme and non-heme iron systems. However, the real nature of the rebound process was unknown and lactone product could arise from two potential pathways: the commonly described hydroxyl rebound followed by lactonization of the hydroxyacid intermediate or the direct lactone formation by a non-canonical carboxylate rebound. To shed light over this mechanistic enigma, ¹⁸O-enriched acid (88% doubly labeled) was prepared and oxidized under the standard reaction conditions to furnish singly labeled lactone (87% singly labeled) (Figure I.25, A). Thus, the outcome evidenced that hydroxyl rebound/lactonization is the active mechanism taking place in this transformation and carboxylate rebound, if operative, provided only a minor contribution. Consequently, the mechanism for the C-H lactonization depicted in Figure I.25, B was proposed.

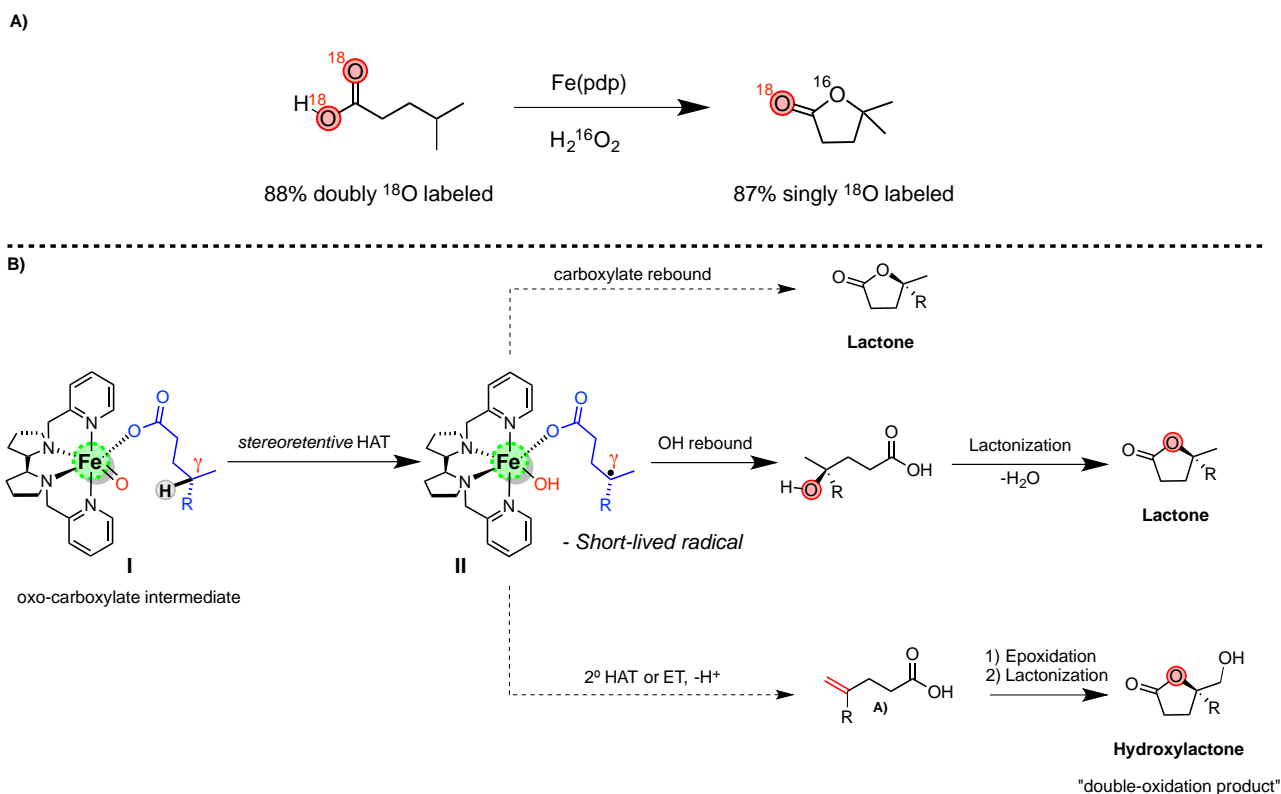


Figure I.25. A) Hydroxyl rebound/lactonization pathway confirmed by isotopic labeling experiment. B) Proposed mechanistic scenario for carboxylic acid-directed C-H oxidation with Fe(pdp).

Interestingly, the authors found that under Fe(pdp)/H₂O₂ standard conditions, 10-20% of unexpected hydroxylactone product was obtained besides the desired γ -lactones.⁴⁷ They demonstrated that the tertiary carbon-centered radical **II** (Figure I.25, B) can undergo desaturation instead of lactonization and oxidation of the *in situ* generated olefin accounts for the formation of this “double-oxidation” product. However, the mechanism of formation of the alkene intermediate could not be defined unequivocally. Indeed, the formation of the C=C bond can be attributed either to the generation of the tertiary carbocation (via single electron transfer from the carbon-centered radical to the Fe(IV)-OH) followed by a proton transfer from an adjacent C-H bond to the resultant complex, or to a second HAT process from those C-H bonds that are in α to the radical.^{71,72} In the current reaction, the strong directing effect conferred by carboxylate ligation to the iron-oxo has been invoked to rationalize the desaturation reactivity observed. In particular, the authors postulated that the intramolecular nature of the oxidation with carboxylic acid substrates

may strongly impact the orientation of the radical during the rebound step and promote a second HAT step to furnish the dehydrogenation products.

I.8.1. Limitation and challenges in carboxylic acid directed C(sp³)-H oxidation

Despite the tremendous potential of this type of oxidation in solving site selectivity challenges, three main limitations have emerged from these works.^{46,47} Firstly, taking in consideration the chiral nature of the Fe(pdp), only modest enantioenrichment (up to 35% ee) could be obtained by kinetic resolution of the racemic mixture of an α -substituted pentanoic acid derivative (Figure I.26, A).

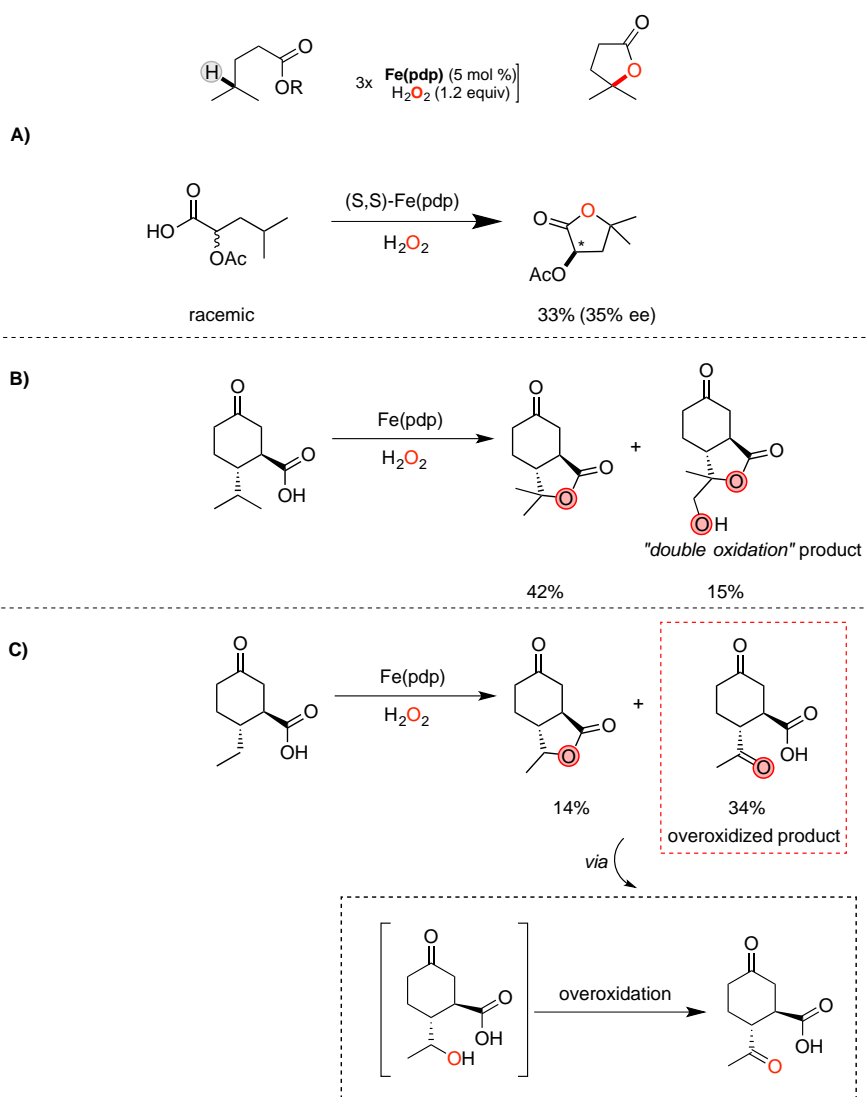


Figure I.26. Challenges of the current state of the art in carboxylic acid directed C-H oxidations: **A)** low enantioselectivity, **B)** and **C)** low chemoselectivity and efficiency in secondary C-H lactonization.

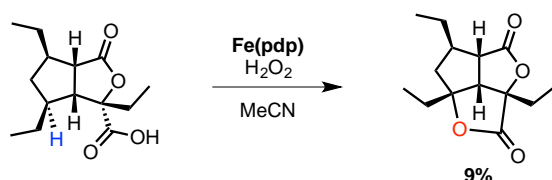
Second, besides the formation of the lactone product, the so-called “double-oxidation” product is also observed in the oxidation of tertiary C-H bonds, thereby eroding the overall chemoselectivity of the reaction (Figure I.26, B). Third, the extension of the carboxylic acid directed-oxidation protocol to secondary γ -C-H bonds is not general and in most of the cases the overoxidation product prevails (Figure I.26, C). Indeed, bearing 2 adjacent C-H bonds, the methylenic group can suffer overoxidation of the hydroxyacid intermediate, which is more susceptible to undergo a second round of oxidation instead of lactonization, to yield the corresponding γ -ketoacid.

I.8.2. Carboxylic acid directed C(sp³)-H oxidation in total synthesis

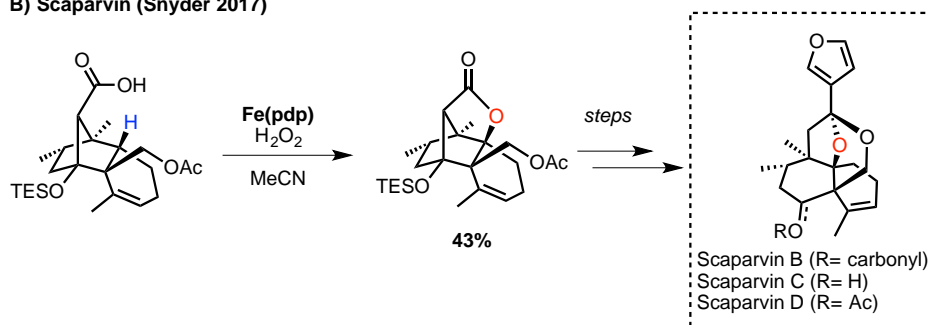
With the advent of the rapid evolving C-H functionalization science, novel and convenient reactions are enriching the toolbox of methodologies for the synthesis of complex molecules. Previously unconceivable disconnections are now not only feasible but truly reliable in streamlining synthesis. Remarkably, the general mild reaction conditions required for transition-metal catalyzed C-H functionalization enable the advantageous late-stage installation of the desired functionality into already densely functionalized synthons. For example, the direct C-H bond oxidation in the final phase of a synthetic sequence prevents worthless manipulations such as protection/deprotection steps. However, to be maximally implemented, a catalytic system should provide predictable and controlled site-selectivity avoiding complex mixture of oxidized products. In this context, carboxylic acids proved to provide excellent level of predictable γ -selectivity by acting as directing groups for the iron-oxo species. In addition, the lactone product is usually a highly desired motif due to the ubiquitous presence of this functionality in both natural and unnatural compounds. Consequently, iron-catalyzed carboxylic acid directed C-H oxidation debuted in the total synthesis of Gracilioether F reported by Brown in 2014 (Figure I.27, A).⁷³ Non-heme Fe(pdp) catalyst was used in the final step to oxidize the 3^o C-H bond in γ -position relative to the acid residue. Although modest yield of the desired lactone was obtained (9%), it represented the only oxidized product in the reaction mixture, albeit the presence of 4 tertiary C-H bonds. The authors attributed the low mass balance and yield to a putative, yet unproven, detrimental decarboxylation pathway. In 2017, Snyder implemented the same transformation in the total synthesis of Scaparvins (Figure I.27, B).⁷⁴ In this case, useful 43% yield of the lactone could be directly obtained. Nevertheless, the overall yield was increased up to 63% upon restoring the olefin moiety from the double oxidized epoxy lactone product.

Most recently, Maimone made use of the Fe-catalyzed lactonization to afford a versatile synthon for the preparation of various *illicium* sesquiterpenes (Figure I.27, C).⁷⁵ However, in this case the Fe(pdp) was replaced by the Fe(mep) catalyst featuring a ligand with an achiral less rigid diamine backbone. This variation from the standard conditions enables an improved 52% of lactone yield from the 25% observed with Fe(pdp).

A) Gracilioether F (Brow 2014)



B) Scaparvin (Snyder 2017)



C). *Illicium* sesquiterpenes (Maimone 2019)

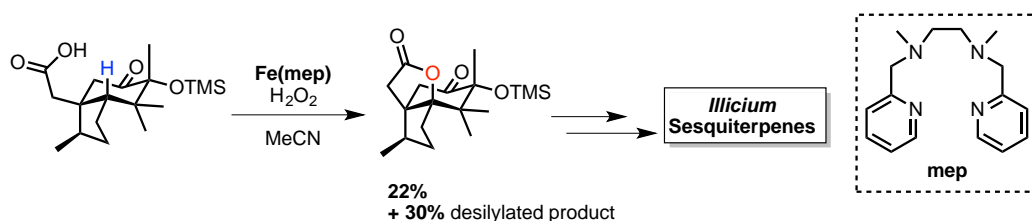


Figure I.27. Late-stage C-H oxidations of carboxylic acids with bioinspired Fe catalysts to streamline the synthesis of biologically relevant products: **A)** gracilioether F (Brown 2014),⁷³ **B)** Scaparvins (Snyder 2017)⁷⁴ and **C)** various *Illicium* sesquiterpenes (Maimone 2019).⁷⁵

Chapter II

Objectives

To advance the frontier of chemical synthesis, novel and efficient catalytic oxidations based on the direct functionalization of the poorly reactive but ubiquitous C-H bonds are becoming necessary. Moreover, the asymmetric nature of the majority of bioactive compounds demands for the development of enantioselective C-H oxidation reactions, which enable the simultaneous installation of oxygen atoms and chirality onto traditionally unreactive hydrocarbon frameworks. The modelling of metalloenzymes reactivity with small molecule catalysts is becoming a reliable strategy to pursue this ambitious goal. Prompted by the impressive results obtained with biologically inspired manganese and iron tetradentate complexes in asymmetric epoxidation, *cis*-dihydroxylation and oxidative desymmetrization *via* ketonization of methylenes, **this thesis aims at developing novel enantioselective C-H oxidation reactions and their application to the synthesis and diversification of organic molecules** (Figure II.1).

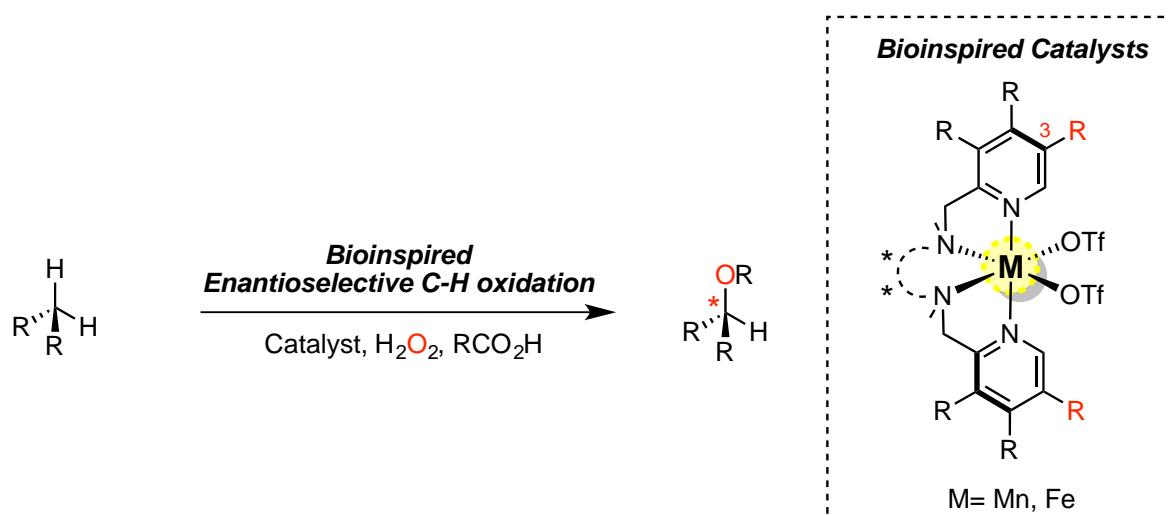


Figure II.1. General example of enantioselective C-H oxidation catalyzed by bioinspired complexes.

The research performed in this thesis addresses 3 key points:

- **The exploration of a directing group approach**

In particular, our attention is focused on the oxidation of carboxylic acids with the aim of using the carboxylic acid group as a ligand, supplying an auxiliary **directing element to the**

chiral metal-oxo species which should translate into some degree of control on the site and enantioselectivity of the reaction.

- **The design of the catalysts required for the reactions**

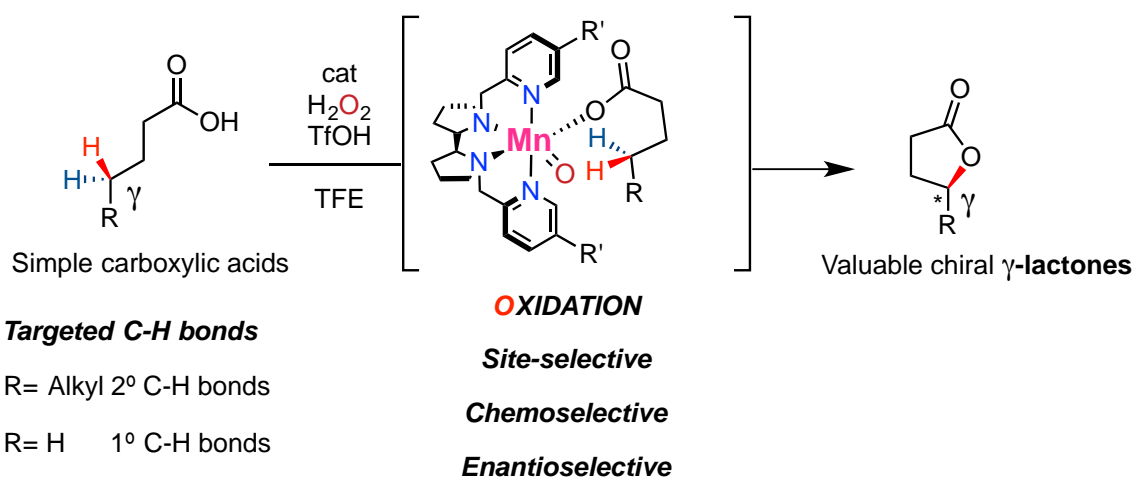
In addition, we envisioned that structural manipulation at the key position 3 of the pyridines moiety (highlighted in red in Figure II.1) of the complexes would lead to the **development of new catalysts** with improved performance in the stereoinduction of intramolecular oxidations.

- **The study of the mechanism by which the reactions operate**

In the framework of this thesis, **mechanistic investigations** will be also undertaken in response to the question raised by the experimental outcomes with the ultimate goal of elucidating the nature of the active oxidant species at the origin of the observed selectivities.

Chapter III

Selective Formation of γ -Lactones via Mn-catalyzed Oxidation of Unactivated C-H Bonds Directed by Carboxylic Acids



III.1. Design of the project

γ -Lactone rings have been recognized as a common and widespread core in many fine chemicals, natural products, and pharmaceuticals. Additionally, their rich chemical reactivity makes this class of compounds valuable synthons for the construction of more elaborated molecules. Therefore, due to their versatile chemical and biological activity, saturated five-membered lactones are usually key molecules in many chemistry fields. Classical approach to γ -lactones, such as halolactonization or intramolecular substitutions, mostly rely on laborious γ -derivatizations with either electrophilic or nucleophilic functionalities.^{76,77} On the other hand, naturally occurring lactones are usually result of selective C-H oxidations of simple hydrocarbon skeletons carried out by powerful heme and non-heme iron oxygenases (**Figure III.1**)⁷⁸.

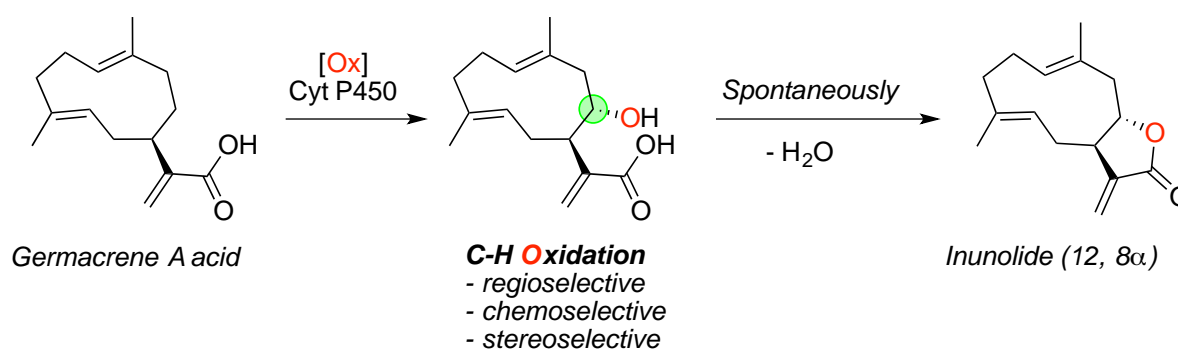


Figure III.1. Representative example of γ -lactone moiety biosynthesis.

In the past decades, bioinspired non-heme Fe and Mn complexes have emerged as catalysts competent for challenging C(sp³)-H oxidations.⁷⁹⁻⁸¹ These complexes activate H₂O₂ to generate electrophilic high-valent metal-oxo species capable to perform site and stereoselective C(sp³)-H hydroxylation via hydrogen atom transfer (HAT) followed by stereoretentive hydroxyl rebound mechanism.⁸⁰ Despite selectivity rules for C-H oxidation with these systems have been established,²⁷ the development of C-H oxidations with high control over site selectivity, chemoselectivity and stereoselectivity is still a main goal in modern organic chemistry. In the broader context of transition-metal catalyzed C-H functionalization, a common strategy to pursuit such selectivity entails the use of directing groups which can support and guide the species responsible for the C-H bond cleavage toward a specific position.⁸²

Carboxylic acids are known to bind the metal center in Fe and Mn catalyzed C–H oxidations where they have been shown to assist the cleavage of H₂O₂ to generate a high-valent metal-oxo carboxylate species.⁸⁰ Furthermore, in Fe catalyzed C–H oxidations, carboxylic acids have been shown to act as directing groups, enabling highly selective intramolecular hydroxylation of bonds to provide valuable γ -lactones with a selectivity orthogonal to the generally β -directed Pd-catalyzed C-H functionalization.^{4,46,82} Notably, such a predictable γ -lactonization reaction accounts for most of the few Fe-catalyzed C-H oxidations that have found application in total synthesis.^{75,79} Nevertheless, the directed oxidation of secondary γ -C(sp³)-H bonds is in general less efficient, with overoxidation to the corresponding γ -ketoacid that strongly limits the applicability of this powerful reaction.^{46,47} As a result, a general catalytic methodology for the γ -lactonization of secondary and also the notoriously strong primary C(sp³)-H bonds is highly desired but still not available to date. Within this framework, we hypothesized that the use of fluorinated alcohols as strong hydrogen bond donor (HBD) solvents may reduce or prevent such overoxidation enabling the development of a versatile γ -lactonization protocol.³⁸ Interestingly, by preserving the chirality of the first formed γ -hydroxyacid, the subsequent spontaneous cyclization would afford precious enantioenriched γ -lactones.

Following this design (Figure III.2), in this chapter we describe the first example of Mn catalyzed oxidation of non-activated secondary and primary C(sp³)-H bonds directed by simple carboxylic acids. The reaction takes place under mild reaction conditions and short reaction time with exquisite γ -selectivity and chemoselectivity, with the desired lactone as only detectable oxidation product. Remarkably, pioneering examples of enantioselective C-H lactonization of secondary sites were also disclosed, delivering preliminary basic concepts key for the design of highly enantioselective C-H lactonizations.

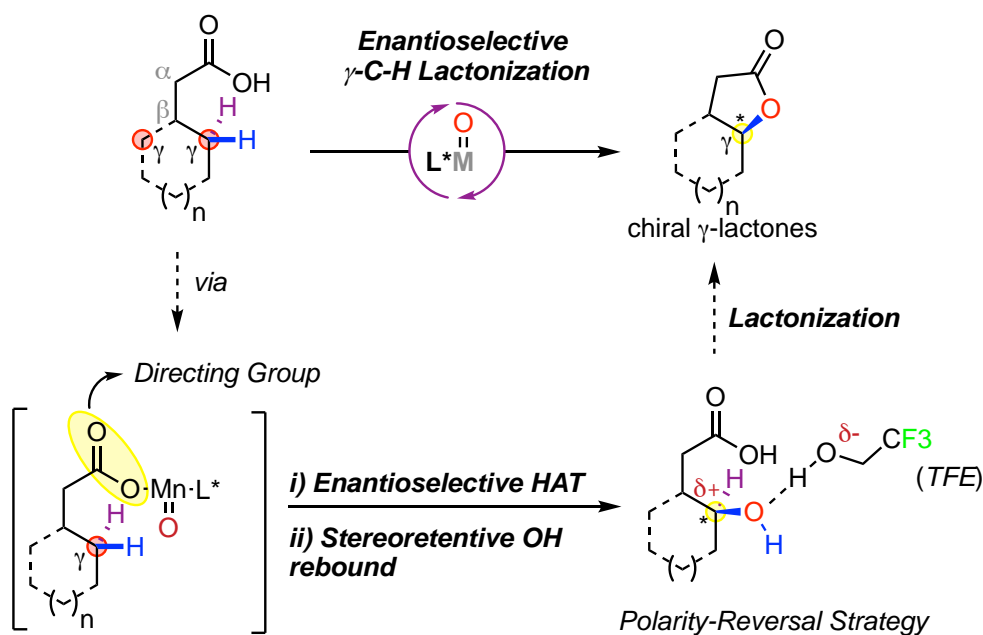


Figure III.2. Design of the project.

III.2. Results and discussion

III.2.1 Enantioselective γ -C-H Lactonization of Unactivated Methylenes

To test our hypothesis we firstly focused on the asymmetric desymmetrization of the (4,4-dimethylcyclohexyl)acetic acid (**1**) as model substrate because of the presence of two accessible γ -enantiotopic secondary sites located in a structurally defined cyclohexyl core (**Figure III.4.A**). Therefore, functionalization of any one of the four γ -CH₂ hydrogen atoms creates two consecutive chiral centers at once. Moreover, each γ -carbon bears, in turn, two diastereotopic C-H bonds and consequently, two couples of enantiomers can be formed upon lactonization. Analysis of the diastereomeric ratio (d.r.), quantified by the product γ -lactone diastereoisomers ratio (*trans:cis*), might provide helpful structural information of the metal-oxo carboxylate active complex.

Catalysts used are chiral Fe and Mn complexes with tetradentate ligands of general formula (*S,S*)-[M(L)(OTf)₂] (L = (*S,S*)-pdp and (*S,S*)-mcp, pdp = *N,N'*-bis(2-pyridylmethyl)-2,2'-bipyrrolidine, mcp = *N,N'*-dimethyl *N,N'*-bis(2-pyridylmethyl)-1,2-*trans*-diamino cyclohexane, OTf = CF₃SO₃, **Figure III.3**).⁸³

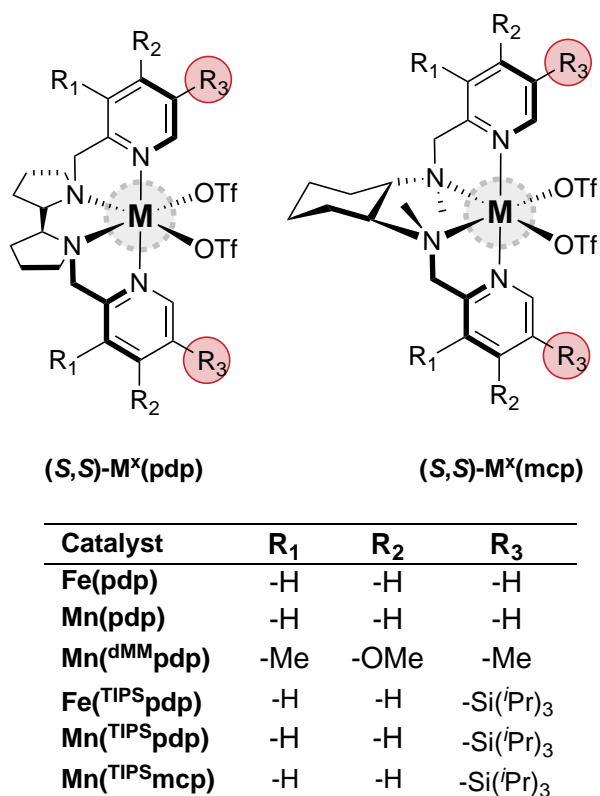
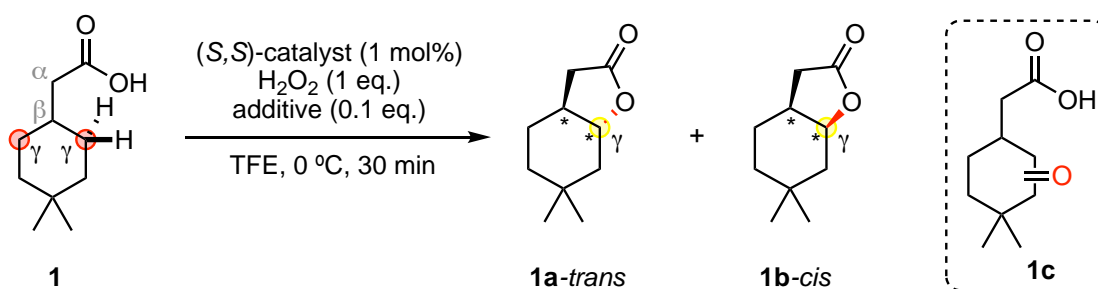
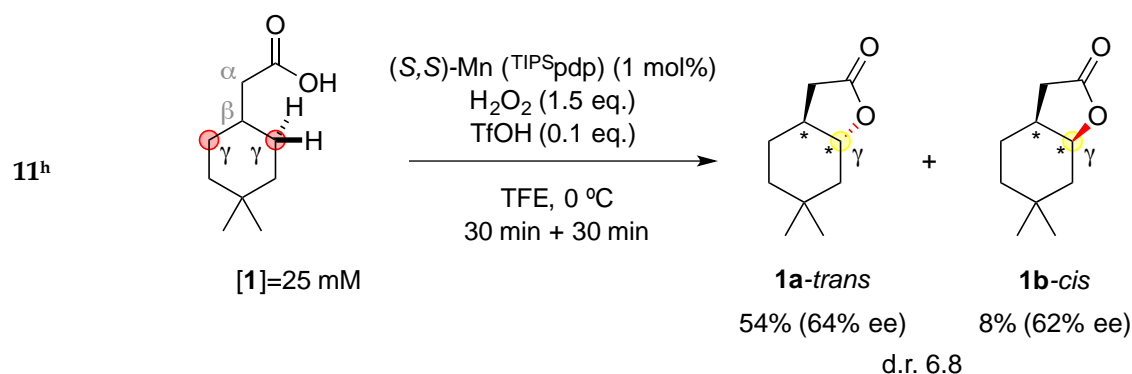


Figure III.3. Fe and Mn catalysts involved in this project.

Oxidation of **1** with 1 equivalent of H₂O₂, delivered over 30 minutes by syringe pump, was performed in 2,2,2-trifluoroethanol (TFE), employing 1 mol% of catalyst, at 0 °C, in the absence of an external carboxylic acid co-ligand (**Table 1**). Since Fe(pdp) catalysts have been previously shown to promote tertiary C-H lactonization on a number of carboxylic acids⁴⁶ we started the development of this reaction with Fe(pdp) and bulkier Fe(^{TIPS}pdp) complexes (entries 1-2).

Table III.1. Reaction development using **1** as model substrate.^a

Entry	Catalyst	Solvent (0.1 M)	Conv. (%)	Tot. Lactone Yield ^b (1c , %)	Chemo. ^c	d.r. ^d	ee <i>trans</i> (%)	ee <i>cis</i> (%)
1	Fe(pdp)	TFE	53	11 (8.5)	1.3	8.1	11	21
2	Fe(TIPSpdp)	"	64	16 (13)	1.2	7.3	19	23
3	Mn(pdp)	"	71	31 (3.7)	8.4	9.8	15	26
4	Mn(TIPSpdp)	"	81	39 (7.5)	5.2	8.2	62	68
5	Mn(TIPSmcp)	"	76	37(7.2)	5.1	2.2	28	42
6	Mn(dMMpdp)	"	78	32 (4.3)	7.4	7.8	8	32
7 ^e	Mn(TIPSpdp)	(25mM)	81	44 (-)	only lact.	8.3	58	50
8	"	HFIP	79	35 (11)	3.2	11	33	57
9 ^f	"	MeCN	42	20 (1.5)	byproducts	6.6	49	56
10 ^{e,g}	"	TFE	83	59 (-)	only lact.	6.4	62	54

Optimized conditions

^a Reaction conditions: substrate 0.1 M in TFE, cat. 1 mol%, H₂O₂ added as 0.9 M TFE solution (and, whenever indicated, a 0.09 M of TfOH in TFE, 0.1 eq., delivered independently) over 30 minutes by syringe pump, 0°C. Workup described in the Experimental section. Conversions, yields and ee's were determined by chiral GC analysis with biphenyl as internal standard. ^b Yields correspond to the sum of the *trans* and *cis* lactone yield. ^c Chemoselectivity of the reaction expressed as the product ratio [lactone **1a** + lactone **1b**]/[ketoacid **1c**]. ^d Diastereomeric ratio (d.r.) correspond to (**1a trans**:**1b cis**) ratio. ^e Substrate 0.25 M in TFE. ^f Multiple unidentified byproducts detected. ^g TfOH, 0.1 eq., delivered independently. ^h Optimized conditions.

We were pleased to observe the formation of the desired γ -lactones (**1a trans** and **1b cis**) as major oxidation products (*Chemoselectivity* = [lactone **1a** + lactone **1b**]/[ketoacid **1c**] = 1.3, entry 1), albeit with poor overall lactone yield and enantioselectivity. The increased steric

bulkiness of the Fe(^{TIPS}pdp) catalyst provided slightly higher lactone product yield (up to 16%, entry 2) and enantioselectivity (up to 19% ee for the *trans* lactone, while 23% for the *cis* diastereoisomer). The relatively good diastereoselectivity in favor of *trans* product, which is consistently observed for all the catalysts, deserves a discussion. As depicted in **Figure III.4.B**, the *trans* lactone diastereoisomer formation is associated with the HAT process coming from the less sterically hindered equatorial γ -C-H bonds (C-H_{eq}) while the *cis* isomer from the congested axial ones (γ -C-H_{ax}). In addition, in terms of torsional strain, the HAT transition state of the equatorial C-H bond could benefit from the relief of the unfavorable 1,3-diaxial strain between the axial methyl in position 4 and the γ -C-H_{ax}.

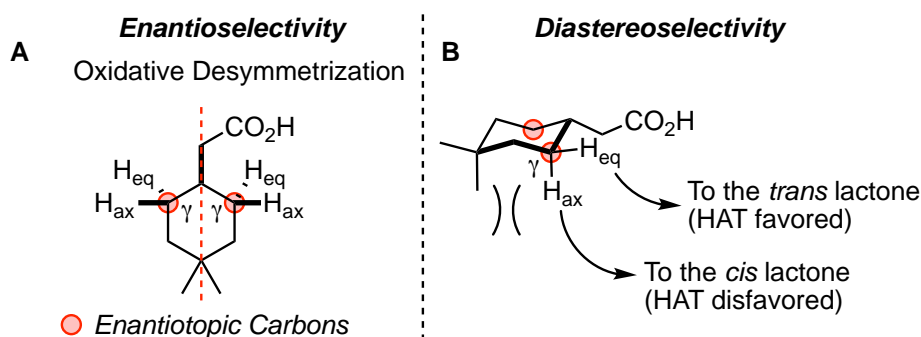


Figure III.4. Overview of the enantioselectivity and diastereoselectivity of the reaction.

Taking in consideration that Fe and Mn may operate *via* similar mechanisms,⁸⁴ we decided to explore also the corresponding (*S,S*)-Mn(pdp) complexes (entry 3). Very interestingly, this Mn catalyst not only exhibited the same γ -lactonization reactivity observed with Fe, but also a remarkably increased chemoselectivity (lactones/ketoacid= 8.3). Furthermore, when compared with the Fe(pdp), a significant improvement was observed in terms of yield (up to 31%), diastereoselectivity (d.r. 9.8) and slightly better ee (up to 15%). In agreement to what is observed with Fe, the increase of steric hindrance around the Mn center of the Mn(^{TIPS}pdp) catalyst allowed a further increment of yield (up to 39%) and a remarkable leap of enantioselectivity (up to 62% for **1a** and 68% for **1b**). Variation on the nature of the chiral diamine backbone from bipyrrrolidine to 1,2-cyclohexanediamine (entry 5) led to a general lower selectivity outcome of the reaction especially in terms of diastereoselectivity and enantioselectivity. Replacement of the sterically bulky pyridines by electronically rich ones (entry 6) negatively affects the enantioselectivity further pointing out the relevance of steric hindrance in proximity of the metal center where the reactive metal-oxo is presumably

formed. Once we identified Mn(^{TIPS}pdp) as the optimal catalyst for this reaction, we optimized the catalytic conditions to increase the product yield and address the issue related to the low mass balance, also observed in previously described Fe catalyzed C-H lactonization reactions. To further deplete intermolecular processes, which may favor the formation of the undesired ketoacid byproduct, we envisioned that reduction of the global concentration of the catalytic system may have a beneficial effect on the reaction outcomes. Remarkably, by increasing the amount of solvent four times ([substrate]=25 mM), the formation of the oxidized byproduct was completely suppressed together with an increment of the lactones yield (up to 44%, Entry 7, see Annex III for the GC traces) without altering the stereo induction of the process. Other solvent media such as HFIP or MeCN (c=1 M, entries 8-9) led to worse results, with the latter that promoted also the formation of unidentified multiple oxidation products. Fe and Mn-catalyzed intermolecular C-H oxidations are in general performed with a large excess of a carboxylic acid as a proton-source co-ligand to ensure the efficient activation of H₂O₂. However, due to the intrinsic design of the γ -C-H lactonization reaction, where the carboxylic acid is part of the substrate, a large excess is discarded. Therefore, we reasoned that the addition of a Brønsted acid, as a source of proton, could facilitate the heterolytic O-O cleavage⁸⁵⁻⁸⁷, thereby increasing the overall efficiency of the reaction. We were pleased to observe that the slow addition of 0.1 equiv of trifluoromethanesulfonic acid (triflic acid, TfOH, entry 10), while retaining the similar substrate conversion and enantioselectivity, increased the lactone yield (up to 59%) and consequently improving the reaction mass balance. Finally, fine tune of the H₂O₂ equiv (entry 11) and extra stirring time after the H₂O₂/TfOH addition (additional 30 minutes, to ensure complete lactonization of the hydroxyacid) allowed to reach 62% of overall lactones yield with a good 64% ee in the case of the major product **1a**.

With these optimized conditions, we next extended the substrate scope to other cyclohexaneacetic acids (**Figure III.5**). Previously reported studies have shown that monosubstituted cyclohexanes with bulky or EWG, when exposed to HAT-based reactions, undergoes selective functionalization at positions C3 and C4, while C1 and C2 are deactivated by steric and torsional effect.^{11,45} Nevertheless, the carboxylic acid directing group enabled in all cases exquisite γ -site selectivity and lactone chemoselectivity providing, by facilitating oxygen installation at C2, orthogonal selectivities to those previously described. The directed C-H oxidation of cyclohexaneacetic acid (**2**) afforded the corresponding γ -lactones in a 50% combined yield and a very good 75% of ee for the major

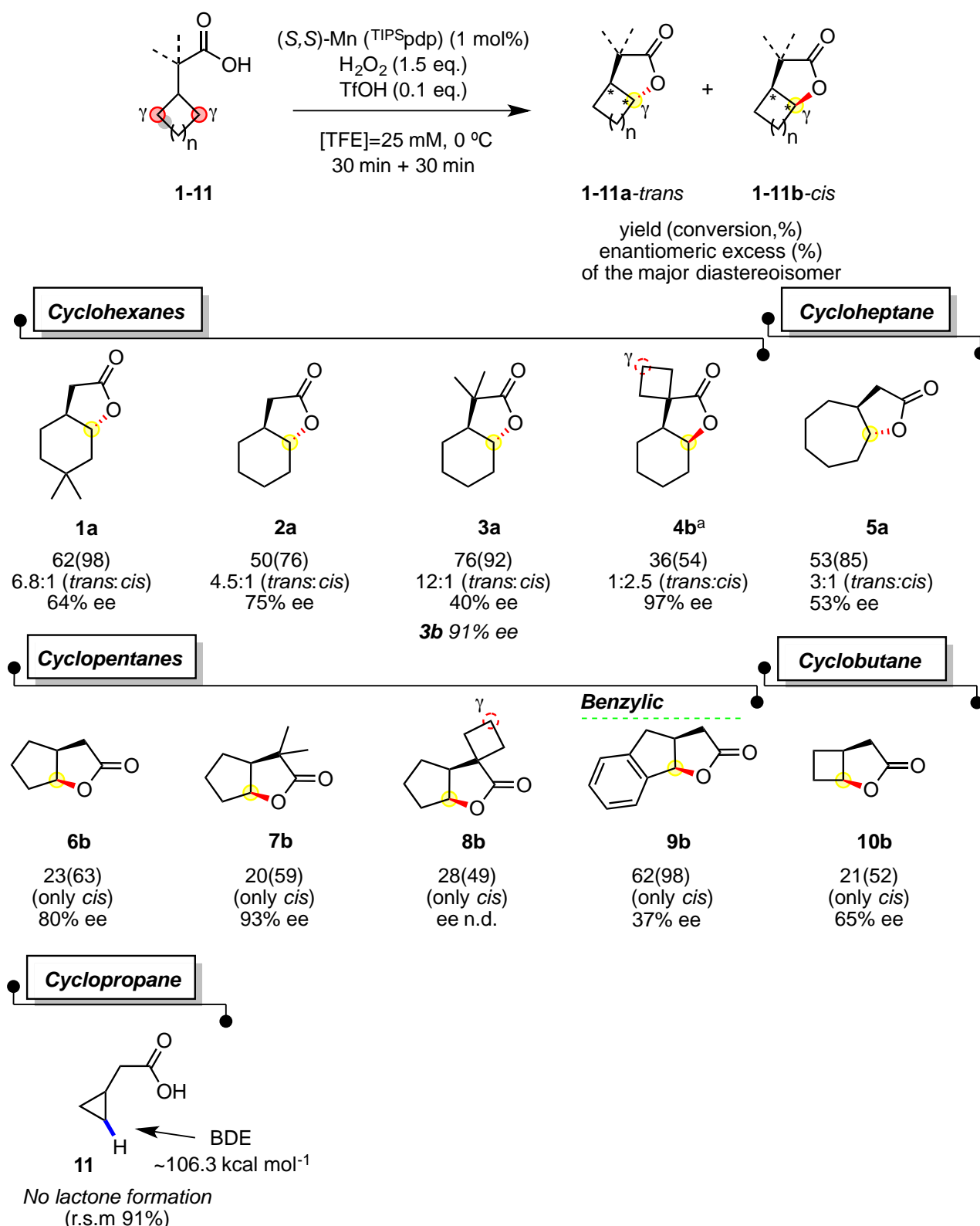


Figure III.5. Substrate scope for the enantioselective γ -C-H lactonization of cycloalkylacetic acids. The major product is depicted along with the conversion, total lactone yield and ee which were determined by chiral GC analysis. Diastereomeric ratio (d.r.) is reported as *trans:cis* ratio. n.d. not determined. ^a 1 equiv. of H₂O₂ was employed.

trans diastereomer (**2a**) product. The lower diastereoselectivity observed, when compared to substrate **1**, further supports the assumption of steric and stereoelectronic factors as major contribution in diastereo-determining HAT step. In details, this can be attributed to the reduced steric hinderance (at position 4) and 1,3-diaxial strain (replacement of a -CH₃ for -H), which in turn translated into less selective equatorial HAT process. Very good product yield was observed in the lactonization of **3**, which took place in sharp favor of the *trans* lactone **3a** (d.r.=12:1), albeit in a moderate 40% ee. It is well established that gem-dimethyl substitution can favor ring closure and intramolecular reactions.⁵⁸ This effect, known as Thorpe-Ingold effect, reasonably rises from the increased size of the substituents (Me instead of -H) and consequently from the increased bond angle between them (**Figure III.6.A, red angle**). This distortion of the geometry is directly reflected in a compressed angle between the other two groups which bear the cyclization reaction partners (**Figure III.6.A, blue angle**). As a result of the increased proximity, the reaction between them is accelerated. Along this line, we functionalized the α position of the cyclohexaneacetic acid with a cyclobutane moiety (**4**). Surprisingly, in sharp contrast to what was observed with **3**, we found an inversion of diastereoselectivity in favor of the *cis* isomer **4b** (d.r.= 1: 2.5) with an outstanding 97% of ee. Of note, the γ -methylene located in the cyclobutyl moiety keep untouched, most probably due to conformational reasons. Collectively, the controversial enantio- and diastereoselectivity exhibited in the oxidation of **3** and **4** may suggest that steric manipulation of the proximal position of the directing group -CO₂H strongly influences its binding with the Mn center and therefore the substrate/metal-oxo relative orientation.

We then set out to study the oxidation of different cycloalkaneacetic acid derivatives. Thus, the directed oxidation of the cycloheptaneacetic acid provides the desired γ -lactones in good combined yield (53%), with preferential formation of the *trans* isomer **5b** (d.r. = 3:1). Most probably, the less conformationally defined nature of this cycle leads to a decreased diastereoselectivity and enantioselectivity when directly compared with the more conformationally rigid cyclohexane analog (**2**). Contrarily, when the ring size was decreased to cyclopentane (**6-9**) and cyclobutane (**10**) the corresponding γ -lactonization reaction took place with exquisite diastereoselectivity affording the *cis* lactones as only detectable products. The drastic change in diastereoselectivity may suggest that the increased rigidity of 4- and 5-membered rings is reflected in a more fixed orientation of the metal-oxo toward the γ -methylene during the HAT transition state, enabling the selective abstraction of one of the two diastereotopic hydrogen atoms. In the general context of condensed bicyclic systems,

although for larger rings (>5 carbons) both *cis*- and *trans*-fused isomers are possible (with *trans*-fused ones more stable because the 1,3-diaxial interactions are minimized), when the rings are smaller only *cis* fusion is often observed because *trans* junction introduces too much ring strain.⁸⁸ As a consequence of this general concept, we hypothesize that the selective formation of the *cis*-lactone would be promoted by the more favorable *cis*-bicyclic HAT Transition State (TS) depicted in **Figure III.6.B**.

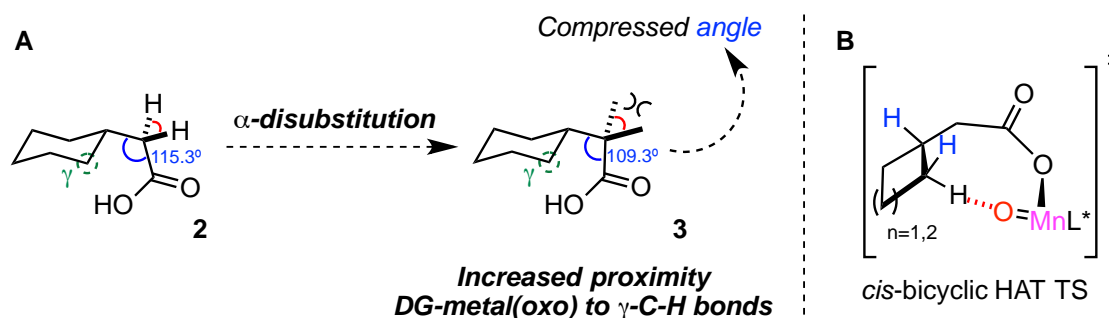


Figure III.6. A, Origin of the Thorpe-Ingold effect. B, Proposed transition state of the HAT process in 4- and 5-membered cycloalkaneacetic acid.

In general, the reaction of cyclopentaneacetic acid derivatives suffered of low product yield paired with loss of mass balance, even in the case of α -gem-dimethyl substituted analog (**7b**). Nevertheless, the desired lactones were obtained with good to excellent enantioselectivity (80-93% of ee), thereby reinforcing the hypothesis in which the reaction of these substrates takes place with a more structurally defined TS. In stark contrast, the C-H lactonization of indanylacetic acid (**9**), in which the γ -methylene bears activated benzylic C-H bonds, proceeded smoothly (62% of yield) but with moderate 37% ee. However, due to the relatively low BDE of this type of C-H bonds, contamination of the reaction outcomes by competitive, (less) enantioselective non-directed benzylic C-H hydroxylation cannot be excluded. Analogously to cyclopentanes, oxidation of cyclobutaneacetic acid (**10**) showed 21% of lactone yield (**10b**) with remarkable 65% of ee. Although in modest yield, the formation of the very strained **10b** further supports the hypothesis formulated in the oxidation of **4**, underlining the importance of conformationally favorable orientation between the directing group and the γ -C-H bonds in directed oxidative lactonization. On the other hand, the absence of lactone product in the oxidation of **11** can be rationalized on the basis of the high strength of the cyclopropane C-H bonds. Finally, the potential of

enantioselective C-H lactonization is depicted in **Figure III.7**, where the efficiency of the methodology developed in this project was directly compared with a traditional organic procedure in achieving lactones **2a** and **2b**.⁸⁹ While the traditional approach is afflicted by multi-step sequences, most of them performed at high temperatures, long reaction times, hazardous solvents and reagents and the use of precious noble metal, our approach affords the desired product starting from commercially available carboxylic acid in short time and mild reaction conditions, involving the use of an abundant and non-toxic metal as Mn. Furthermore, we demonstrated the versatility of the protocol with an array of structurally different carboxylic acids whereas, in the case of conventional organic chemistry, if an analogue is desired a *de novo* synthesis should be re-designed accordingly. However, despite the gap in enantioselectivity is not too demanding, it is significant and therefore, future efforts should be aimed in the optimization of the reaction conditions and catalyst development.

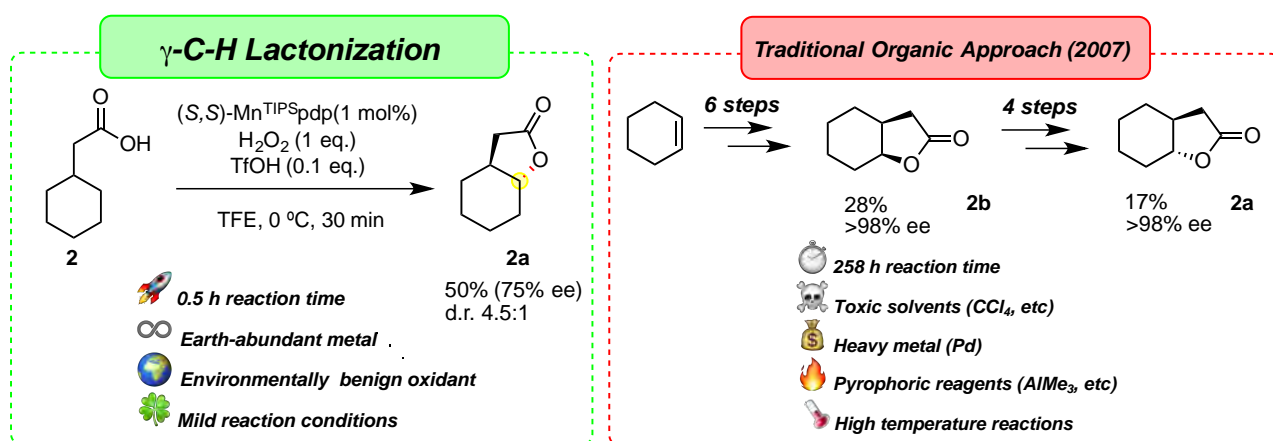


Figure III.7. Direct comparison of the γ -C-H lactonization with traditional methodologies in affording chiral lactone **2a**.

III.2.2. Selective γ -C-H Lactonization of Linear Carboxylic Acid

Branched γ -lactones are essential compounds in food and cosmetic industry because they significantly contribute to the smell and taste of fruit, flowers, vegetables, meat, mushrooms and alcoholic beverages.⁹⁰ However, due to the high costs of isolation from natural feedstocks, many of these valuable compounds are prepared in large scale by chemical synthesis, more often as a racemic mixture. Therefore, due to the particular interest toward this class of lactones, we wondered if the Mn-catalyzed γ -C-H lactonization of simple, linear carboxylic acids would be a valuable tool to afford such relevant compounds.

In addition, long-chain carboxylic acids with multiple and almost equivalent methylenic sites, like nonanoic acid (**12**, **Figure III.8.B**), would represent a suitable model substrate to challenge the exquisite site selectivity previously observed for more structurally defined cycloalkanoic acid. Very remarkably, when **12** was exposed to the optimized conditions, only the formation of γ -nonalactone (**12a**) in 74% isolated yield was observed, despite the presence of 8 electronically richer C-H bonds (δ - η) in principle more reactive under electrophilic oxidation.

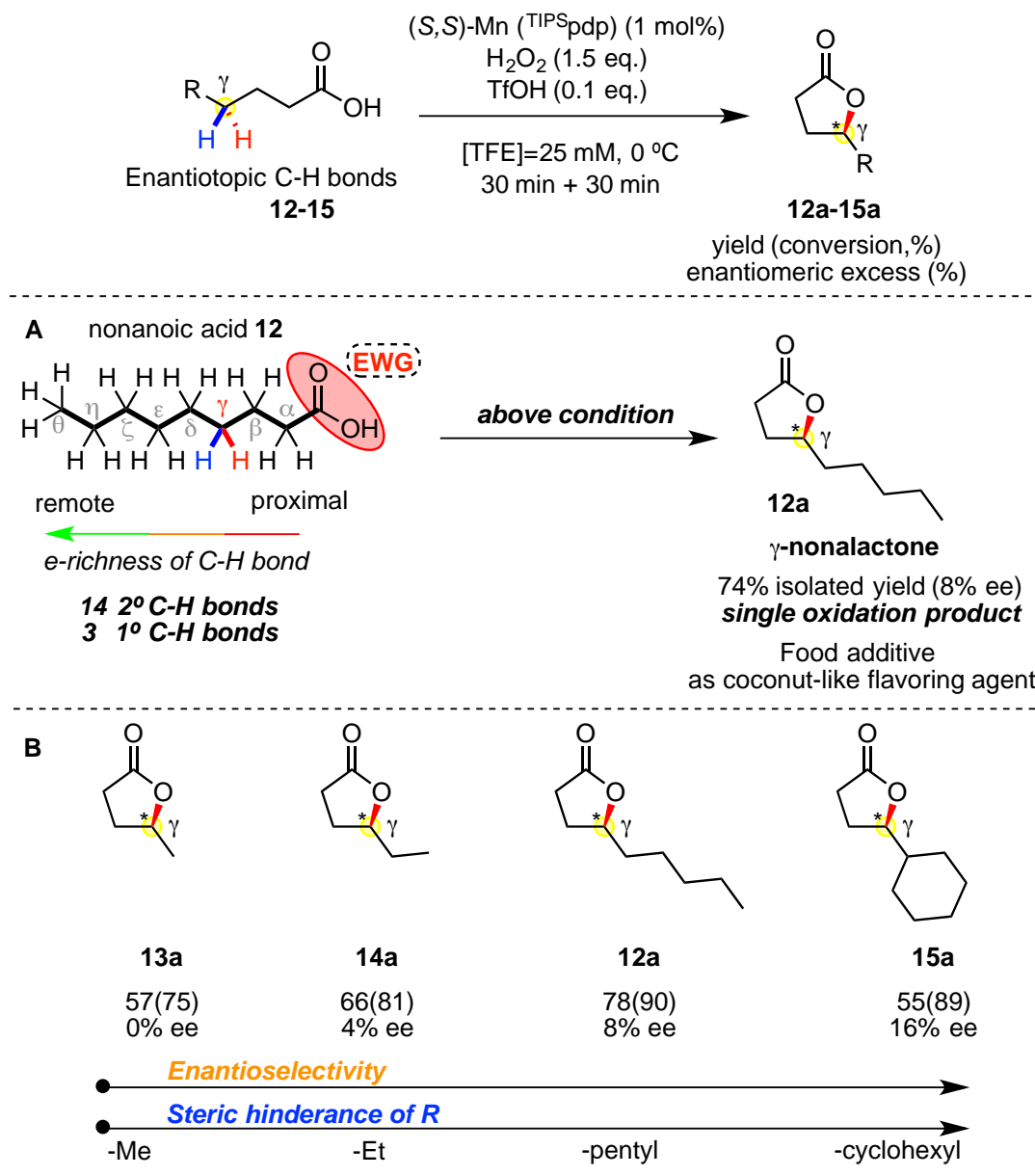


Figure III.8. γ -C-H lactonization of linear carboxylic acids. **A**, Remarkable γ -selectivity in the oxidation of nonanoic acid **12** to yield valuable γ -nonalactone **12a**. **B**, Substrate scope for the enantioselective γ -C-H lactonization of linear carboxylic acids. Conversion, yields and ee were determined by chiral GC analysis.

The low enantioselectivity (8% ee) observed deserves some discussion. Reasonably, the challenges associated with the discrimination of enantiotopic C-H bonds, located in the same methylenic unit instead of into enantiotopic carbons (oxidative desymmetrization), requires a much higher degree of control exerted by the catalyst to be addressed.² Additionally, the low steric hinderance and the inherent flexibility of the linear carbon chains make the achievement of this task even more difficult. In agreement, when the shorter pentanoic and hexanoic acids were processed under the same conditions (**Figure III.8.B**), even lower enantioselectivity was observed with the former affording the lactone **13a** as racemic mixture. On the other hand, by increasing the steric hinderance adjacent to the reacting γ -C-H bond with a cyclohexyl group, an appreciable increasing of the enantioselectivity (up to 16%) was recorded. Of note, δ -lactone, deriving from the oxidation of the more electron rich 3° C-H bond in δ position, was not formed, showcasing again the outstanding γ -site selectivity of the reaction.

Collectively, these results stand out the formidable challenges related to the asymmetric C-H oxidation of enantiotopic C-H bonds, with ee that are far from being satisfactory. Nevertheless, the preliminary series of substrates tested point toward a direct relation between the size of the alkyl γ -substituent (-R) with the enantioselectivity of the reaction, therefore providing valuable starting point for the development of highly enantioselective C-H lactonization.

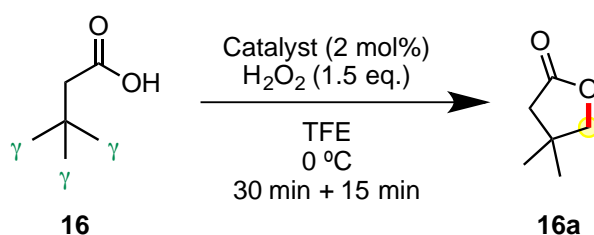
III.2.3. Adding Primary C-H Bond to the Field of Bioinspired Oxidations

Although primary C-H bond functionalization is quite common with processes that involve organometallic intermediates, when the HAT mechanism is operating the C-H bond relative reactivity should decrease in the following order: 3° C-H > 2° C-H >> 1° C-H. This sequence arises from the substantial bond dissociation energy (BDE) increment in the progression from tertiary to secondary to primary C-H bonds. Only very few exceptions to this general rule have been reported with only one making use of a bioinspired system and precisely designed amino acids as directing group.⁹¹

With the methodology for the secondary C-H γ -lactonization established, we wondered if simple carboxylic acids could also facilitate the challenging oxidation of strong primary γ -C-H bonds (> 100 kcal/mol). Thus, taking as reference the protocol developed for the

secondary C-H lactonization, *tert*-butylacetic acid (**16**) was selected as model substrate, where the presence of 9 equivalents primary γ -C-H bonds would maximize the promotion of the reaction (**Table 2**). To our delight, under these conditions, we observed the formation of the desired lactone (**16a**) as a single product in 54% yield (**Table S1, Annex Chapter III**). After a first screening of the reaction conditions (**Table S1, Annex Chapter III**), we found that the increase of the catalyst loading (up to 2 mol%) provided the best results in terms of lactone yield. As previously observed in the lactonization of 2° C-H bonds, the Fe(pdp) catalyst (**Table 2**, entry 1) delivered lower yields than the corresponding Mn-based counterpart (entry 2). Again, while the electronically rich Mn^{dMM}(pdp) (entry 3) failed in affording higher product yield, the sterically bulky Mn^{TIPS}(pdp) resulted as the most efficient catalyst of the series providing 64% of isolated lactone yield (entry 4).

Table III.2. Optimization of the directed oxidation of *tert*-butylacetic acid (**16**)^a.



Entry	Catalyst	Solvent	Additive	Conv. (%)	Yield (%)
1	Fe(pdp)	"		82	25
2	Mn(pdp)	TFE	-	92	54
3	Mn(^{dMM} pdp)		-	81	28
4	Mn(^{TIPS} pdp)		-	96	66(64) ^b
5	"		TfOH (0.1 eq)	97	62
6	"	HFIP	-	98	64
7	"	MeCN	-	57	11
8	Mn(^{TIPS} mcp)		-	71	41

^a Reaction conditions: substrate 25 mM in TFE, cat. 2 mol%, H₂O₂ added as 0.9 M TFE solution (and, whenever indicated, a 0.09 M of TfOH, 0.1 eq., delivered independently) over 30 minutes by syringe pump, 0°C. Workup described in the Experimental section. Conversion and yields were determined by chiral GC analysis with biphenyl as internal standard. ^b Isolated yield.

Changing the nature of the chiral diamine backbone led, also in this case, to worse lactone yield (entry 8). Surprisingly, the beneficial effect of triflic acid exhibited in the secondary C-

H bond lactonization was not shown for this substrate (entry 5) suggesting that, under similar conditions, the limiting factor(s) of the yields for the catalytic oxidation of the two types of C-H bonds diverge. Solvent variation to HFIP did not alter the fate of the reaction (entry 6), while a significant drop in the reaction efficiency was recorded by using MeCN as medium (entry 7). We subsequently explored the general applicability of this methodology to various types of substrates containing 1° γ -C-H bonds. Therefore, a systematic study was undertaken by investigating the reactivity of a series of butanoic acid derivatives bearing different structural features (**Figure III.9.A**). At first, we were interested in expanding the substrate scope toward those analogues that bear a reduced number of equivalent primary C-H bonds. Interestingly, we found that sequential removal of methyl substituents on the β -carbon from **16**, isovaleric acid (3-methylbutanoic acid, **17**) and butanoic acid (**18**) respectively, drastically decreased the corresponding lactonization product yield. At first sight, these results may suggest a strong dependency of the reaction efficiency with the number of primary C-H bonds available in γ position. Nevertheless, when the α -positions of the butanoic acid backbone were transformed in a quaternary carbon the desired reactivity was restored (**20-22**), indicating that, besides the number of equivalent primary C-H bonds, the Thorpe-Ingold effect, by angle compression, is paramount for the lactonization of primary C-H bonds. Reconsidering the oxidation of **16** from a closer look, this beneficial structural effect may also be implied in the case of this substrate where it could be exerted by the β -quaternary carbon. Thus, inspired by this finding, a series of α,α -disubstituted butanoic acids were examined. An outstanding very high yield was obtained for lactone **21a** (91%), as a result of the synergy between the Thorpe-Ingold effect with the statistically favored 9 identical primary γ -C-H bonds. In analogy, an α,α -cyclopropyl substituent showed the same beneficial effect allowing the formation of highly strained spiro lactone **22a** in a good 56% yield. Along this line, sequential expansion of the flanking cycle to 4-, 5- and 6-membered rings introduced within the substrates a competitive, and by far more reactive, γ -methylenic site (**Figure III.9.B, 23-25**). Thus, they represented suitable platforms to perform intramolecular competitive experiments providing information about the relative reactivity of primary against secondary C-H bonds under oxidative lactonization conditions. In analogy to the results previously collected, the cyclobutyl framework keep untouched, with the oxidation taking place exclusively at the strongest primary C-H bond to afford **23a** in a 54% yield. However, the less strained architecture of

cyclopentyl (**24**) and cyclohexyl (**25**) derivatives allowed a more favorable orientation of the methylenic C-H bonds toward directed oxidation (**24b**, **25b**), thereby strongly attenuating the selectivity for the primary site. In support of this structural hypothesis, the different geometry of these cycles was directly reflected on the oxidation site-selectivity (quantified with the product ratio ($\gamma_{-2^{\circ}}/\gamma_{-1^{\circ}}$)).

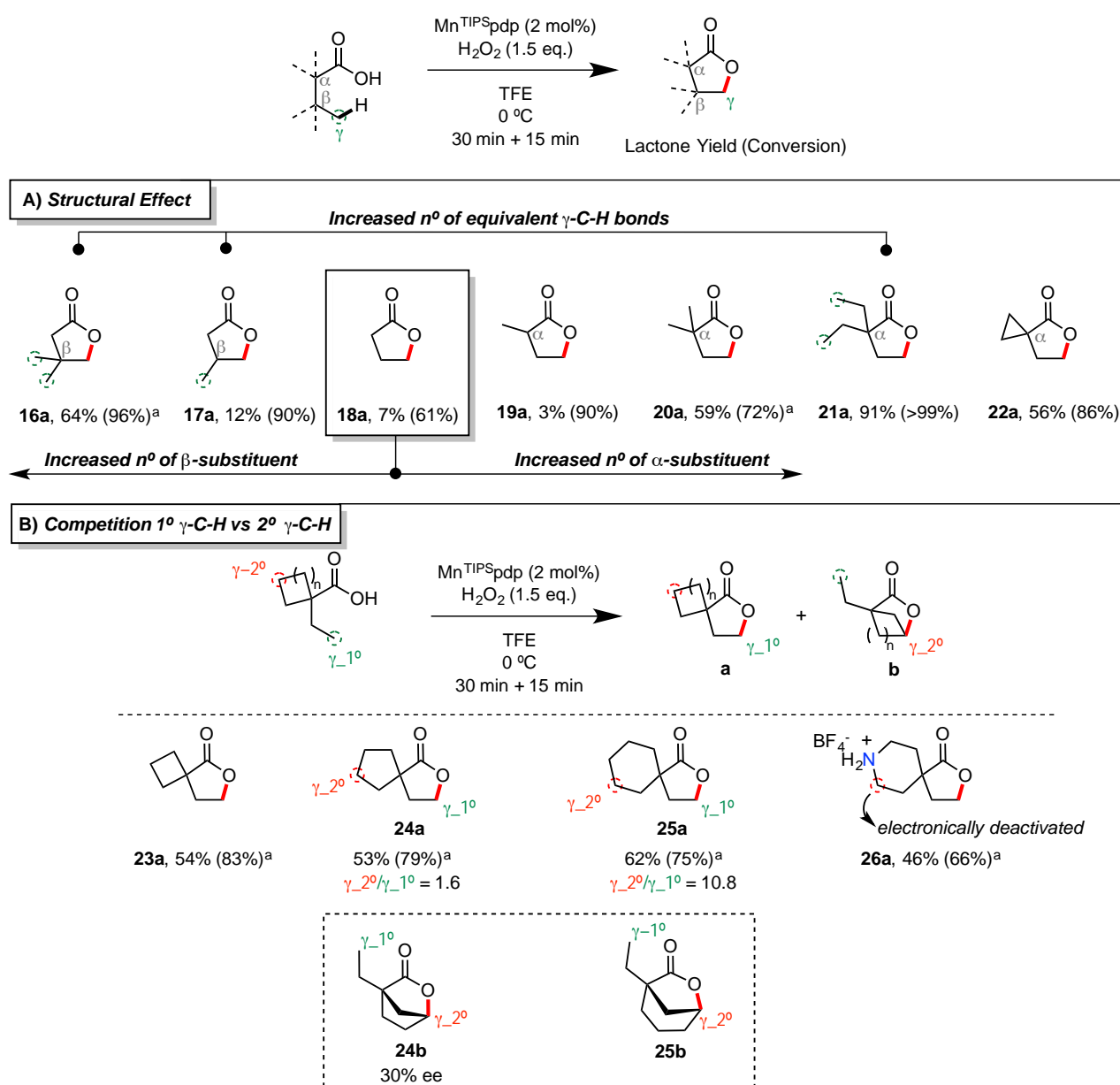


Figure III.9. Substrate scope for the γ -C-H lactonization of primary C-H bonds. **A**, Scope of butanoic acid derivatives for the rationalization of structural effects. **B**, Intramolecular competitive experiments of 1° against 2° C-H bonds in γ -lactonization reaction. Conversions, yields and ee's were determined by chiral GC analysis. ^a Isolated yield. The regioisomeric ratio is expressed as $\gamma_{-2^{\circ}}/\gamma_{-1^{\circ}}$ ratio.

Reasonably, the secondary γ -C-H bonds located in the conformationally more rigid and flat cyclopentane ring of **24**, upon carboxylic acid coordination, are not entirely directed toward the metal-oxo unit, thus affording a mixture of 1° and 2° C-H lactonization products (**24a** and **24b**) in a ratio $\gamma_{2^\circ}/\gamma_{1^\circ}=1.6$. On the other hand, after coordination of **25**, the secondary γ -C-H bonds situated on the cyclohexane ring are more properly oriented facing the oxidant species and consequentially, drastically increasing their effective reactivity ($\gamma_{2^\circ}/\gamma_{1^\circ}=11$). On the basis of these results, we next wondered whether changes in the electronics of substrate **25** might be used to alter the reaction site-selectivity toward the energetically disfavored primary C-H bond, in the presence of a priori more reactive secondary sites because of their weaker C-H bonds. Protonation of basic amines by Brønsted acids deactivate adjacent C-H bonds toward HAT process with electrophilic oxidants.³¹ Inspired by this concept, we considered the incorporation of a nitrogen atom within the cyclohexane scaffold (**26**). Remarkably, upon protonation with HBF₄, the oxidation reaction occurred exclusively at the primary C-H bond (**26a**) leaving the electronically deactivated γ -methylenes on the piperidine ring untouched. Albeit preliminary, this strategy provides a first evidence that selective primary C-H bond oxidation can occur even in presence of a priori more reactive sites, as long as the latter are electronically deactivated.

Overall, the catalytic carboxylic acid-directed γ -C-H lactonization of strong primary C-H bonds was successfully accomplished by using bioinspired Mn-based complexes. The basic reactivity principles were rationalized on the basis of structural effects of the carboxylic acid substrate which, by precisely orienting the targeted γ -C-H toward the metal-oxo unit, can overcome the high BDE associated with these bonds. Furthermore, judicious tuning of the substrate electronics allowed the selective oxidation of primary C-H bonds in presence of weaker secondary ones.

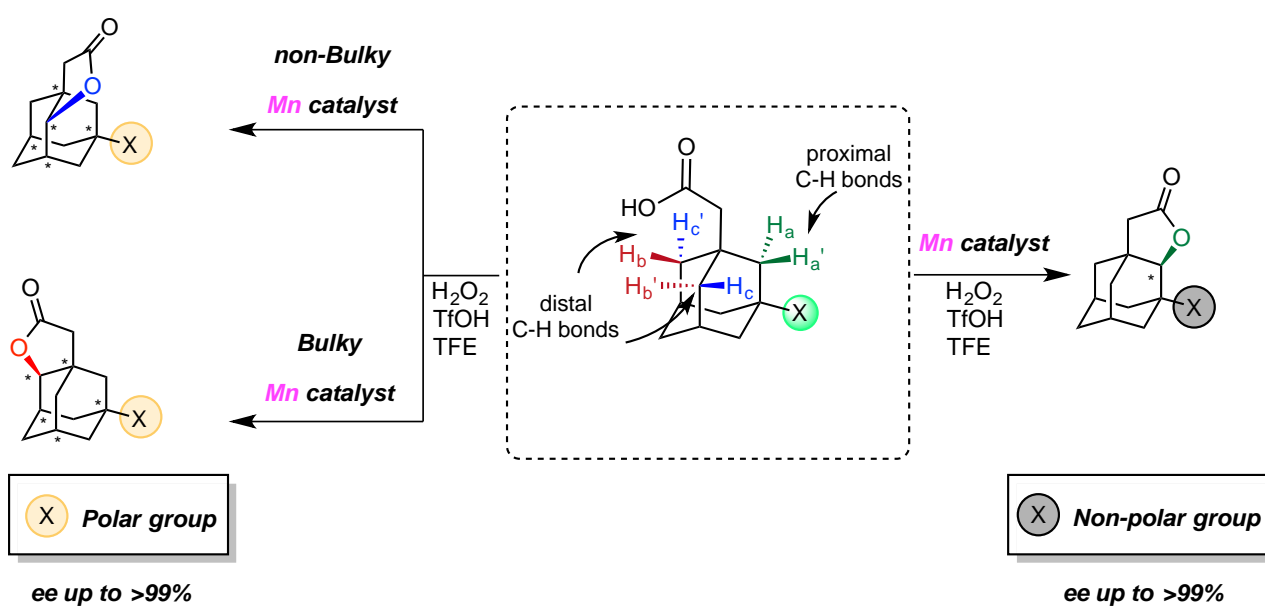
III.3. Summary

In this chapter, we described catalytic C-H oxidation of unactivated methylenic sites to afford γ -lactones as a result of the development of a novel catalytic system capable to address the selectivity challenges associated with this transformation. Key to the high efficiency is the combination of a bulky chiral Mn catalyst with carboxylic acid directing group, which act synergistically to yield exquisite site-selective, chemoselective, and often, diastereo- and enantioselective oxidations. Remarkably, the fluorinated alcohol solvent (i.e.

TFE) and the Mn-catalyst combo successfully prevents collateral oxidations, while efficient activation of the H₂O₂ oxidant is ensured by the addition of a catalytic amount of triflic acid. The robustness and the general applicability of the reaction was demonstrated over an array of carboxylic acids featuring structurally different γ -methylene groups affording the desired chiral lactones as single product. Examples of very high enantioselective lactonization were accomplished. In addition, the reaction was successfully applied in the oxidation of strong 1° C-H bonds located in γ -position. In general, after rational choice of the substrates, the principles for effective lactonization were found to be related to structural features such as the number of equivalent γ -C-H bonds but in particular, to the presence of the Thorpe-Ingold effect.

Chapter IV

Intramolecular Highly Enantioselective γ -C-H Lactonization of Unactivated Methylenes in Adamantaneacetic Acids



IV.1. Design of the project

Since chirality is crucial in determining the functionality of biologically active compounds, such as pharmaceuticals and natural products, the development of catalytic enantioselective transformations is particularly desired. In this context, highly enantioselective C-H functionalization reactions promise to reshape the synthetic logic to achieve chiral molecular targets. However, enantioselective C-H oxidation of secondary aliphatic C(sp³)-H bonds, designed to forge *chiral* C(sp³)-O bonds with promising manganese and iron catalysts, are still scarce and limited to activated benzylic, allylic and α -to-heteroatom C-H bonds.⁹² Extension of the scope towards unactivated methylenic sites is extremely demanding because it would require the design of highly reactive chiral species capable i) to cleave a specific strong secondary C(sp³)-H bond among many others with similar electronic and steric properties (site-selectivity), ii) to functionalize only one of the two enantiotopic C-H bond (enantioselectivity), and iii) to prevent the facile overoxidation of the 2° alcohol to achiral ketone. Collectively, these three key challenging features make asymmetric C-H oxidation still an unsolved problem for artificial systems. Nevertheless, on the basis of the remarkable results obtained in asymmetric epoxidation,⁸ *syn*-dihydroxylation⁹³ and, more recently, in the oxidative desymmetrization of enantiotopic carbons in monosubstituted cyclohexanes with bioinspired Mn and Fe catalysts,⁴⁵ we envisioned that this class of complexes were suitable to pursue high enantioselectivity even for the more challenging asymmetric oxidation of enantiotopic hydrogens, so far exclusively observed in enzymatic reactions. Following previously reported Fe-catalyzed, carboxylic acid directed C-H lactonization of tertiary C-H bonds,^{27,46} we developed in **Chapter III** an efficient methodology to successfully target also γ -secondary and even strong primary C-H bonds with outstanding site selectivity and chemoselectivity for the lactone product. Very interestingly, the catalyst-substrate proximity ensured by the directing effect of the carboxylic acid moiety, allowed the design of promising diastereo- and enantioselective C(sp³)-H oxidations. A relevant aspect to ensure stereocontrol on the reaction emerged to be the combination of sterically bulky Mn catalyst with structurally and conformationally defined carboxylic acids. Inspired by these early findings, we reasoned that this new methodology could pave the way towards highly enantioselective C-H lactonization provided that a higher structural control over the stereo-determining HAT transition state is exerted. The adamantane core is a particularly recurrent motif in drug discovery, catalyst

design and materials due its peculiar properties, such as the defined shape and rigidity.^{94,95} These same features make this structural motif an ideal platform in the quest for enantioselective C-H oxidations. Parallely, from a catalyst design prospective, rationalization of the key structural modifications on the pyridine moiety, to generate a more structured second coordination sphere around the active metal center, may amplify the enantioinduction during the HAT process. Following these hypotheses, in this chapter we describe the first example of Mn catalyzed highly enantioselective directed oxidation of non-activated C(sp³)-H bonds of adamantaneacetic acids.

IV.2. Results and discussion

The rigidity and the presence of three γ -CH₂ units, available for directed oxidation, make adamantaneacetic acid **1** a suitable substrate to test our hypotheses. Furthermore, the γ -C-H lactonization of **1** would enable the challenging functionalization of adamantane methylenes, with a selectivity orthogonal to common bridgehead derivatizations which target the more reactive tertiary C-H bonds. The catalysts involved in this study, depicted in **Figure IV.1.A**, are chiral Fe and Mn complexes with tetradentate ligands of general formula (S,S)-[M(L)(OTf)₂] (L = (S,S)-pdp and (S,S)-mcp, pdp = *N,N'*-bis(2-pyridylmethyl)-2,2'-bipyrrolidine, mcp = *N,N'*-dimethyl *N,N'*-bis(2-pyridylmethyl)-1,2-*trans*-diamino cyclohexane, OTf = CF₃SO₃).⁸³

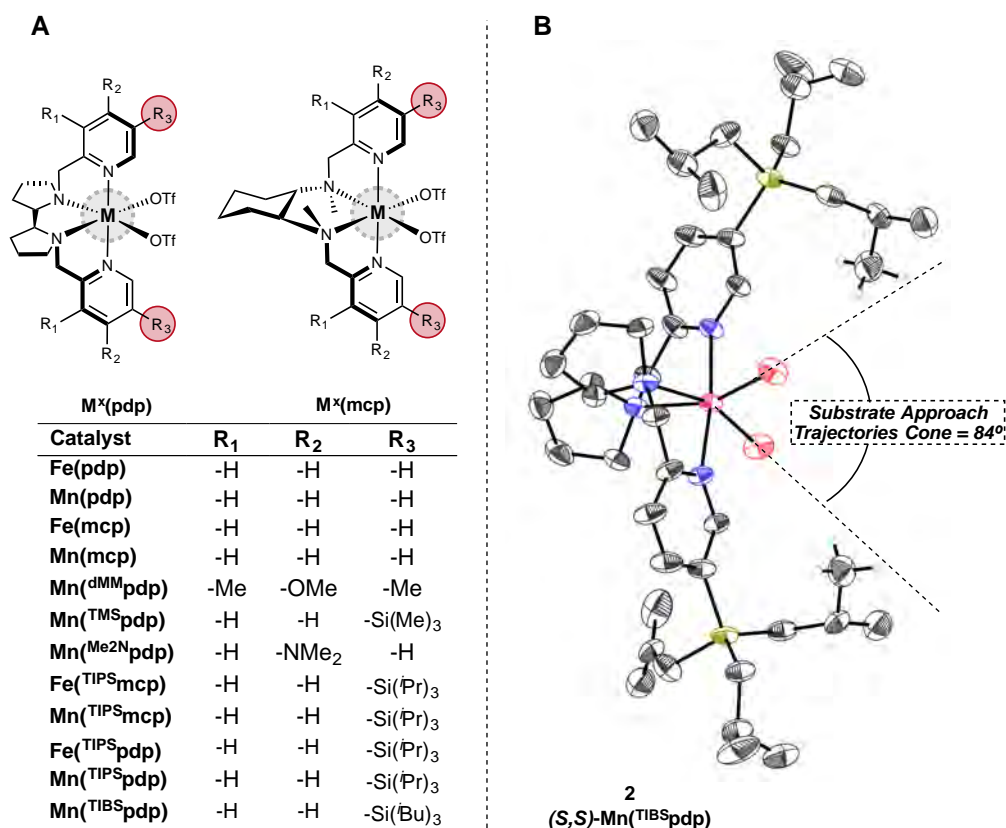
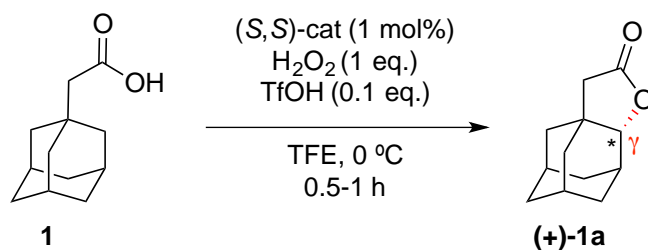


Figure IV.1. A) Fe and Mn catalysts used in this work. The catalyst steric bulk is modulated by inserting substituents on position 5 of the pyridines (highlighted in red). **B)** ORTEP diagram of the solid state structure of (*S,S*)-Mn(^{TIBS}pdp). Note the restricted cone trajectories imposed by the bulky silyl groups. Triflate groups are omitted for clarity, except for the Mn bound oxygen atoms).

Thus, we started the optimization of the oxidation of **1** (25 mM) by using Fe complexes (1 mol%), 1 equivalent of H₂O₂ delivered over 30 minutes by syringe pump, and TFE as solvent at 0 °C. In line to what observed in **Chapter III**, Fe complexes (entries 1-3), albeit behaving as catalysts for the directed γ -lactonization of **1**, struggled in affording satisfactory yield of the desired chiral lactone **1a**. However, we were pleased to find consolidation on key points previously disclosed in **Chapter III**: i) chiral bipyrrolidine-based Fe(pdp) (entry 1), delivered better enantioselectivity (75% ee) than the 1,2-cyclohexanediamine-based Fe(mcp) (67% ee, entry 2) and ii) the more structured environment around the metal of Fe(^{TIPS}pdp) (entry 3) provided **1a** with higher product yield (12%) and enantioselectivity (84% ee) when compared with unsubstituted Fe catalysts.

Thus, we turned our attention to the corresponding Mn catalysts which, in agreement to our previous observations, led to a sharp increment in both yield and ee (Mn(pdp), entry 4,

26% and 89%, respectively). Again, bulky Mn(^{TIPS}pdp) improved the reaction outcomes up to 28% yield and remarkable 94% ee (entry 5). Therefore, we decided to further pursue this structural effect by designing a novel catalyst, Mn(^{TIBS}pdp) (**2**, **Figure IV.1.B**), with a greater steric hindrance. The solid-state geometry of **2** is very similar to previously reported Mn(pdp)-based catalysts, but the larger triisobutylsilyl substituents, acting as blocking elements, define the narrowest cone (84°) of possible approach trajectories of a substrate to the Mn-oxo moiety among the catalysts investigated (see also **Figure IV.4**). Thus, by employing our new Mn(^{TIBS}pdp), the desired lactone **1a** was obtained in slightly improved yield and ee (entry 6, 29% and 95%, respectively). When the absolute configuration of the chirality of the catalyst was inverted the catalytic system delivered the opposite enantiomer (**Table S1, Annex Chapter IV**). Changing the reaction medium to CH₃CN or HFIP led to worse or similar outcomes respectively (entries 7 and 8), while the modification of the chiral backbone from pdp to mcp (entry 9) or ecp⁴⁵ has a negative effect like in the case of Fe catalysts (**Table S1, Annex Chapter IV**). Differently from the results disclosed in **Chapter III**, electron rich catalysts considerably increase the formation of the lactone product up to 43% yield with Mn(^{NMe₂}pdp) (entries 10 and 11). This improvement can be rationalized with a beneficial interplay between electron-rich catalysts with **1** in increasing the efficiency of hydrogen peroxide activation, generating the putative metal-oxo species via the push-pull mechanism, previously proposed to operate also in bioinspired epoxidation catalyzed by these complexes.⁹⁶ Along this line, the addition of catalytic amounts of triflic acid (0.1 equiv.), proved to be key in the γ -lactonization of 2° C-H bonds, generally improving the reaction product yield and, to a lower extent, reaction enantioselectivity (entries 12–20 and **Table S1, Annex Chapter IV**). Now, the efficient H₂O₂ activation was ensured by the positive effect of TfOH, thus not requiring the use of electron-rich catalysts (entries 14 and 15). Systematic increase of the catalyst bulkiness, from Mn(^{TMS}pdp) (TMS: trimethylsilyl group) to Mn(^{TIBS}pdp) (entries 16–18), enhanced product yield and enantioselectivity up to a 68% isolated yield and an outstanding 98% ee for the latter catalyst (entry 18 and **Table S1, Annex Chapter IV**). Appreciably, the reaction proceeded smoothly also when **1** was scaled up to 0.8 g (4.5 mmol), with retention of efficiency and selectivity (entry 13)).

Table IV.1. Optimization of adamantaneacetic acid (**1**) directed oxidation.^a

Entry	Catalyst	Additive	Conversion (%)	Yield (%)	ee (%)
1	Fe(pdp)	-	59	6	75
2	Fe(mcp)	-	53	5	67
3	Fe(^{TIPS} pdp)	-	75	12	84
4	Mn(pdp)	-	72	26	89
5	Mn(^{TIPS} pdp)	-	81	28	94
6	Mn(^{TIBS} pdp)	-	74	29	95
7 ^b	"	-	54	14	93
8 ^c	"	-	89	28	95
9	Mn(^{TIPS} mcp)	-	38	8	65
10	Mn(^{dMM} pdp)	-	85	38	90
11	Mn(^{NMe2} pdp)	-	86	43	90
12 ^d	Fe(^{TIPS} pdp)	TfOH	97	36	94
13 ^d	Mn(pdp)	TfOH	80	56 (64) ^{e,f}	96
14	Mn(^{NMe2} pdp)	TfOH	60	35	91
15 ^d	Mn(^{dMM} pdp)	TfOH	>99	63	93
16	Mn(^{TMS} pdp)	TfOH	89	51	96
17	Mn(^{TIPS} pdp)	TfOH	88	52	97
18 ^d	Mn(^{TIBS} pdp)	TfOH	85	70 (68) ^e	98

^aReaction conditions: substrate (25 mM) and (*S,S*)-cat. 1 mol% were dissolved in TFE, 1.0 eq. of H₂O₂ (and, when indicated, a 0.09 M TfOH solution (0.1 eq.), delivered independently) was added as a 0.9 M TFE solution over 30 minutes by syringe pump, at 0°C. Workup as described in the Experimental Section. Conversion, yield and ee were determined by chiral GC analysis of two or three different runs with biphenyl as internal standard. Traces (<5%) of hydroxyacids have been detected in the oxidations. ^bCH₃CN solvent. ^cHFIP solvent. ^dAdditional 30 minutes of stirring to promote lactonization. ^eIsolated yield. ^f0.8 g (4.5 mmol) scale.

Then, the oxidation protocol was applied to 2,2-dimethyladamantaneacetic acid **3** (Figure IV.2), where the two α -methyls should trigger the beneficial Thorpe-Ingold effect. Delightfully, the corresponding γ -lactone **1a** was delivered in a very high isolated yield (88%) and outstanding ee (97% ee).

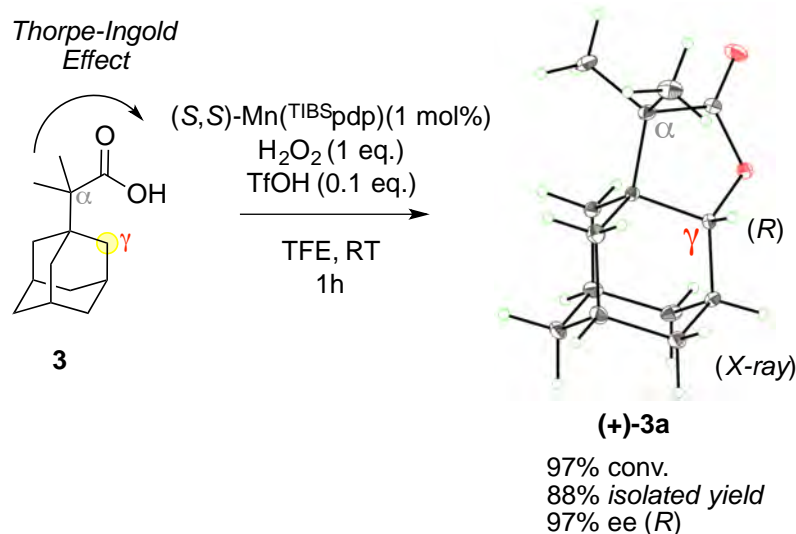


Figure IV.2. Oxidation of 2,2-dimethyladamantaneacetic acid **3** (ee was determined by chiral GC analysis while absolute configuration was determined by single crystal X-ray diffraction, see **Annex IV** for details).

Then we extended the substrate scope of the reaction towards substituted adamantaneacetic acids. Interestingly, when the position 3' is substituted, the C₃-symmetry of the adamantane cage is lost, differentiating the three γ -methylenes into one *proximal* and two *distals* sites (**Figure IV.3**). Each of the *distal* secondary sites bear, in turn, two diastereotopic C-H bonds pointing towards (*endo*, H_c and H_{c'}) or away (*exo*, H_b and H_{b'}) from the 3'-substituent. Collectively, three possible lactones, coupled with the corresponding enantiomers, can be generated after exposure of general substrate **X** to the C-H lactonization protocol: one proximal, **Xa**, and two diastereomeric distal *exo* and *endo* lactones, **Xb** and **Xc**, respectively, with the simultaneous formation of up to five stereogenic centers in the latter cases. Therefore, 3'-substituted adamantaneacetic acids, with their unique set of six nonequivalent C-H bonds, represent an ideal platform to investigate the catalyst/substrate interplay on dictating enantio-, diastereo-, and site-selectivity in a single experiment.

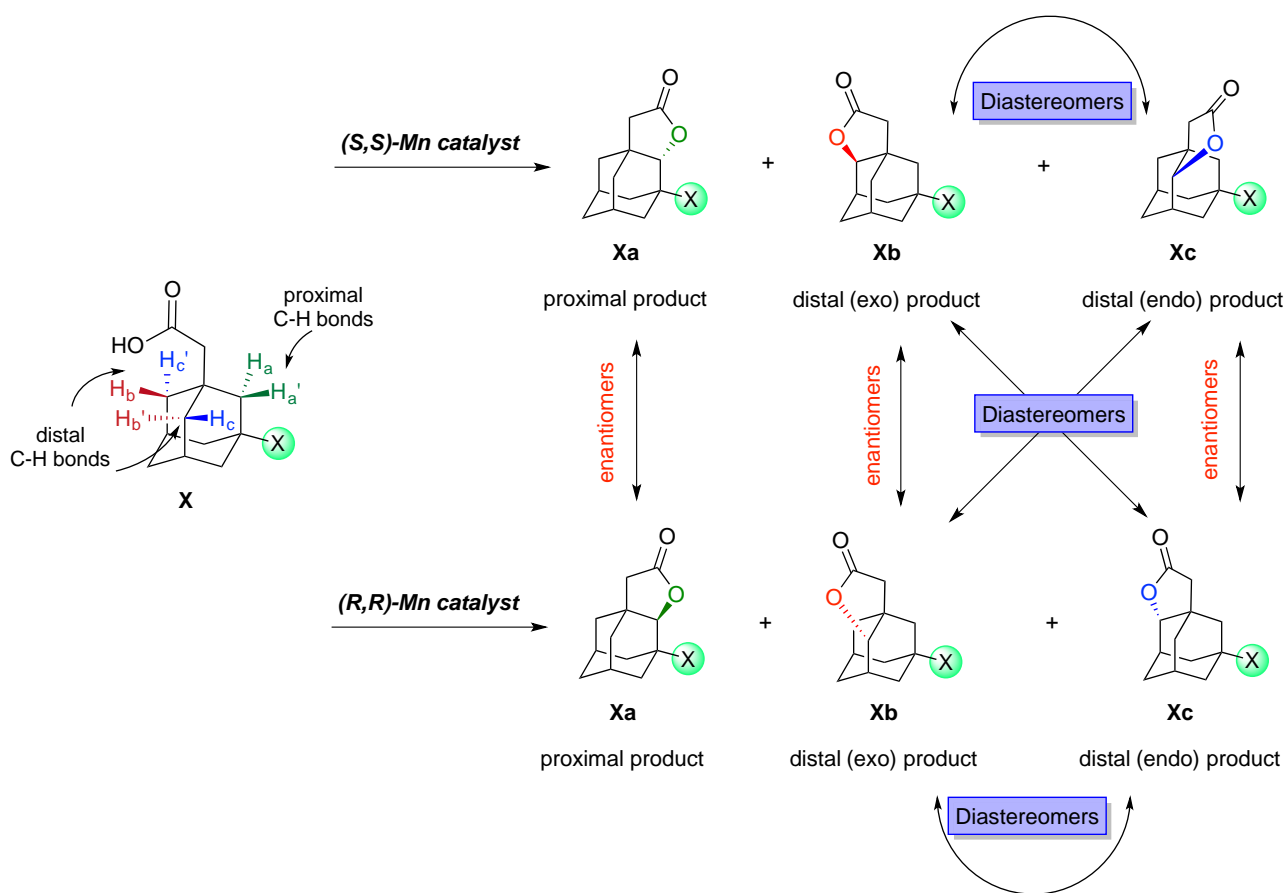


Figure IV.3. Depiction of all possible lactone products of 3'-substituted adamantane acids.

To this end, 3'-hydroxyadamantane (**4**) was employed as model substrate providing, under the optimized conditions with complex $\text{Mn}(\text{TIBS})\text{pdp}$ (**Figure IV.4**, entry 1), the three lactones **4a**, **4b**, and **4c** in a 1:2.7:1 ratio, and with 91, 99 and 67% ee, respectively. Distal lactonization (**4b** + **4c**) is favored over proximal (**4a**), giving a regioisomeric ratio (r.r.) of 1:3.7, reasonably due to deactivation of the proximal methylene via polarity reversal exerted by hydrogen bonding of the solvent to the hydroxyl group and, to a lesser extent, by steric effects.³⁸ The *exo*-lactone **4b**, with 32% of yield and exquisite 99% ee, is the major product of the reaction most probably due to the more steric accessibility of this site when compared with the endo counterpart **4c**. We also demonstrate that the diastereomers **4b** and **4c** formation is the result of the oxidation at two different distal methylene groups (**Figure S2**, Annex Chapter IV). Very remarkably, we found a correlation between the systematic decrease of the steric hindrance on the β positions of the pyridine rings, which could be interestingly parameterized with the increment of the substrate approaching trajectory cone angle to the Mn center, and the regular decrease of the *exo:endo* ratio from 2.7:1 with $\text{Mn}(\text{TIBS})\text{pdp}$ (**Figure IV.4**, entry 1) up to complete inversion with the 1:2.5, observed for the unsubstituted $\text{Mn}(\text{pdp})$ (**Figure IV.4**, entry 5). In the latter case, we showcased a rare example of catalyst-

controlled selectivity, since **4c** became the major product while retaining high enantioselectivity (89% ee).

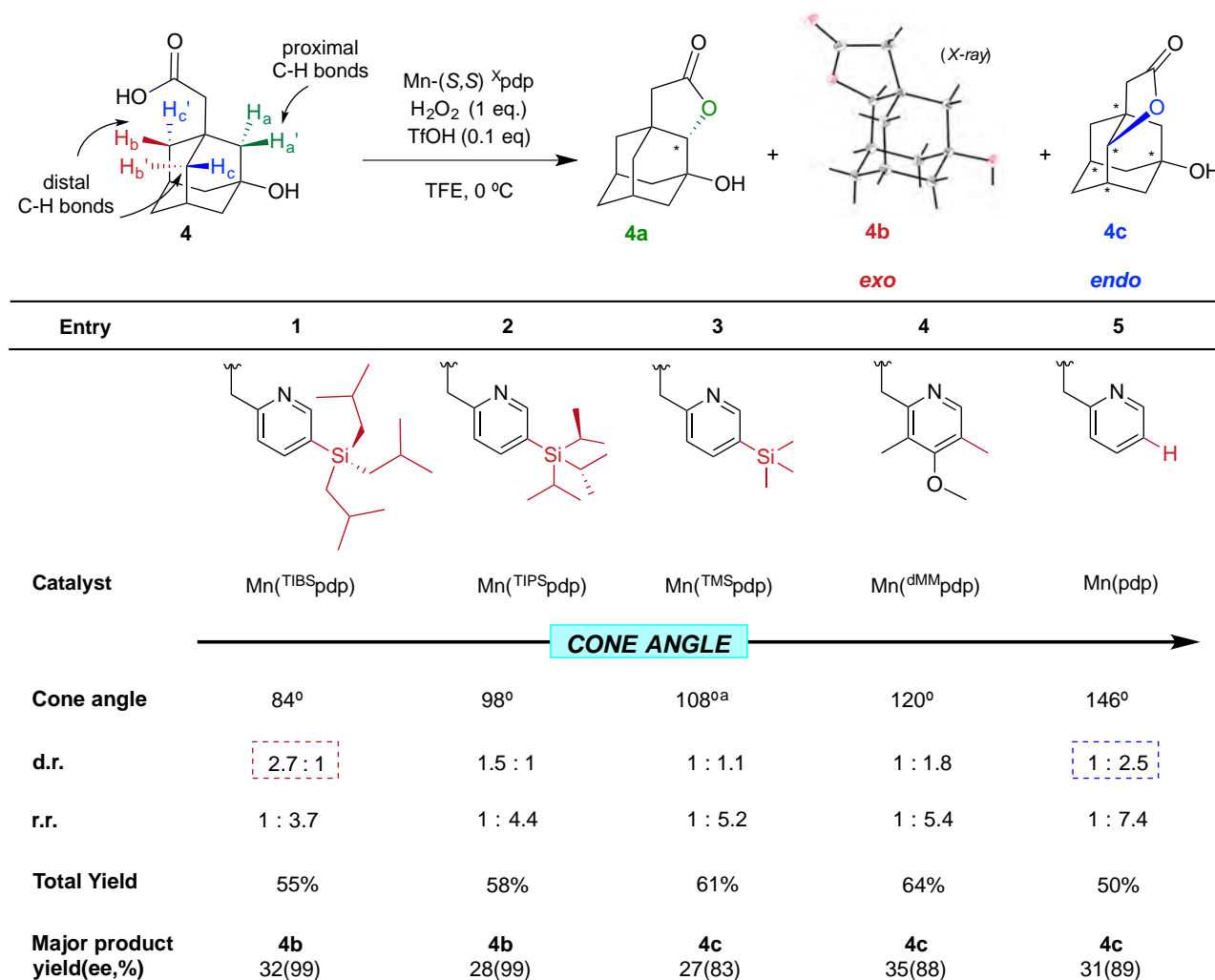
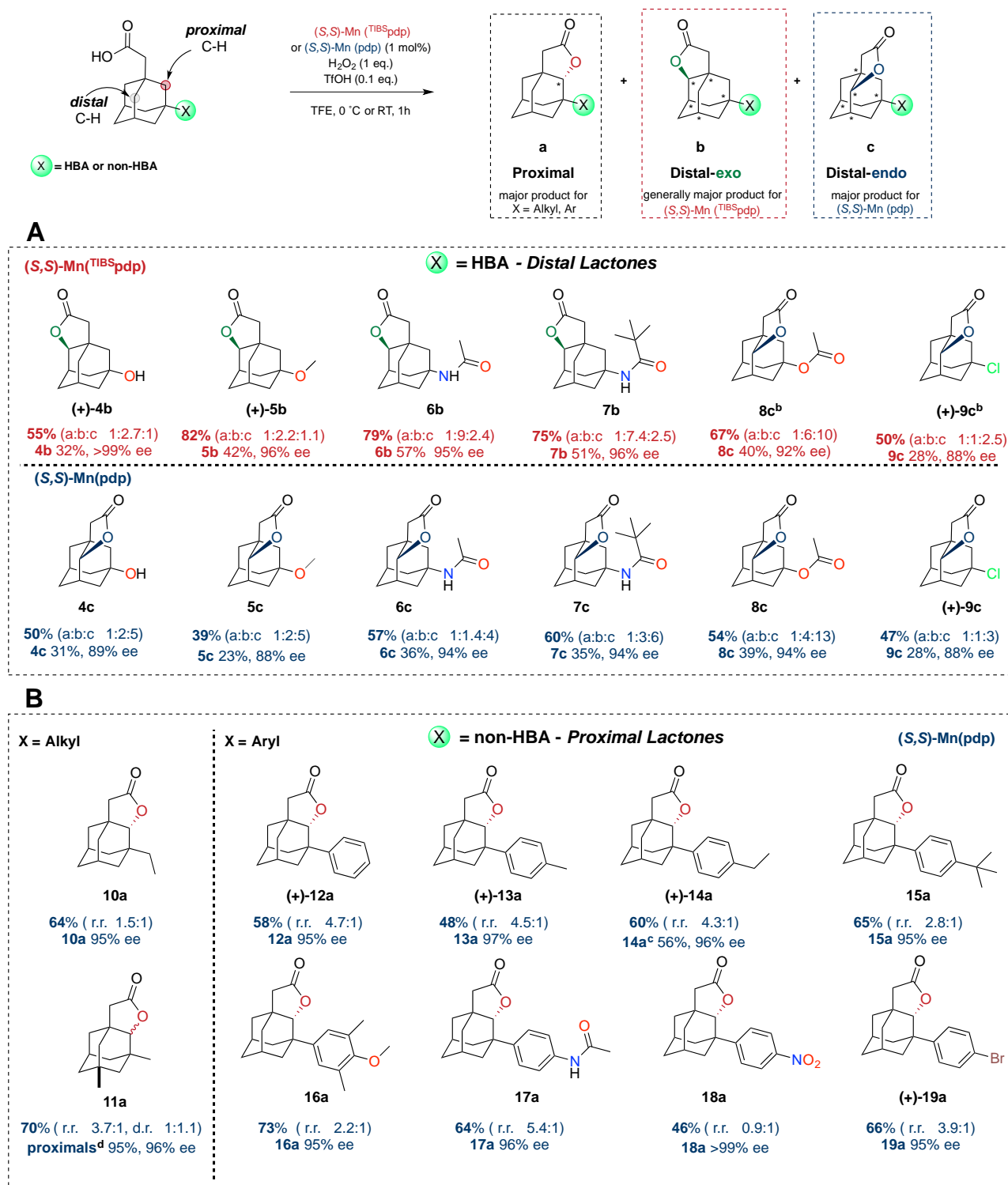


Figure IV.4. Oxidation of 3'-hydroxyadamantaneacetic acid (**4**) and the impact of catalyst steric bulk on selectivity. Diastereomeric ratio (d.r.) corresponds to *exo:endo* (**4b:4c**) ratio while regioisomeric ratio (r.r.) refers to the ratio of proximal over distal oxidation products (**4a**):(**4b** + **4c**). For conversions, yields and ee's of minor products see Annex Chapter IV (**Table S6**). ^a Cone angle value obtained from the topologically similar Fe(TMSPdp) (i.e. cone of Mn(pdp)=146°, Fe(pdp)=145°).^{41,97} Absolute chirality of **4b** was assigned by its X-ray structure; taking into account that the oxidation does not occur on the same carbon, absolute configuration of **4c** can also be assigned, while that of **4a** is proposed for similarity to **3a**.

With these results in hand, we extended the study to various 3'-substituted adamantaneacetic acids (**Figure IV.5**), with the aim of elucidating the role of the substituent's electronic and structural properties on the reaction selectivity. Substitution

with an heteroatomic linkage at this position (**Figure IV.5, A**) such as ether (**5**), amide (**6-7**), ester (**8**) and halogen (**9**) was well tolerated, providing always distal lactones as major products in modest to good yields and exquisite ee's, especially when the new catalyst $\text{Mn}^{\text{(TIBS)pdp}}$ was employed. In agreement with the oxidation of **4**, also for these substrates, the resultant *exo:endo* ratio was found to be related with the catalyst bulkiness as emerged from the direct comparison between $\text{Mn}^{\text{(TIBS)pdp}}$ catalyst (blue) and $\text{Mn}(\text{pdp})$ (red).

Amide substituents, as previously observed in other C-H oxidation reactions,⁴⁵ gave the highest yields and stereoselectivities, up to 79% yield and a d.r. of 3.7:1, with 95-96% ee. Remarkably, the reaction is also highly selective for distal sites, with a r.r. < 1:9.9 for **6** (X=NHCOCH₃) and **7** (X=NHCOC(CH₃)₃). The tuning of the catalyst structure allowed complete inversion of the *exo:endo* ratio for hydroxyl (**4**), methoxy (**5**) and amido (**6** and **7**) substituents. No inversion for acetoxy (**8**) and chlorine (**9**) substituents was observed, although also with these substrates the diastereomeric ratio (d.r.) decreased upon catalyst switch. Since groups with similar sterics, such as hydroxyl **4** and chlorine **9** or acetamido **6** and acetoxy **8**, influenced the d.r. in a remarkably different degree, we hypothesize that in addition to electronics, solvent coordination to the substituent can affect its size, therefore influencing diastereoselectivity in an extent that depends from the hydrogen bond acceptor ability (HBA) of the functional group (**Figure IV.6**). A further evidence for this hypothesis was found in the lack of *exo:endo* selectivity when the oxidation of **4** was carried out in non-HBD solvent like MeCN, while similar diastereoselectivity observed in TFE was restored by using HFIP as reaction medium (**Table S6**, entries 6 and 7, **Annex Chapter IV**).



For each reaction, the major product is drawn (with its ee displayed in the second row, along with its GC yield for section A), and the total yield of the three lactones is displayed in the first row (GC yield for section A, isolated yield for section B), together with the distribution of products in the crude mixture (a:b:c ratio or rr ratio). Further details, such as conversions, yields, and ee of minor products, whenever determined, and results with Mn(TIBSpdp) catalyst are reported in **Table S7** and **Figure S3 (Annex Chapter IV)**. ^bWith substituents OAc and Cl the main product is the endo lactone c with both catalysts. ^cIsolated single lactone yield. ^dTwo diastereomeric proximal lactones are formed.

Figure IV.5. Substrate scope for enantioselective lactonization of bridgehead substituted adamantaneacetic acids.

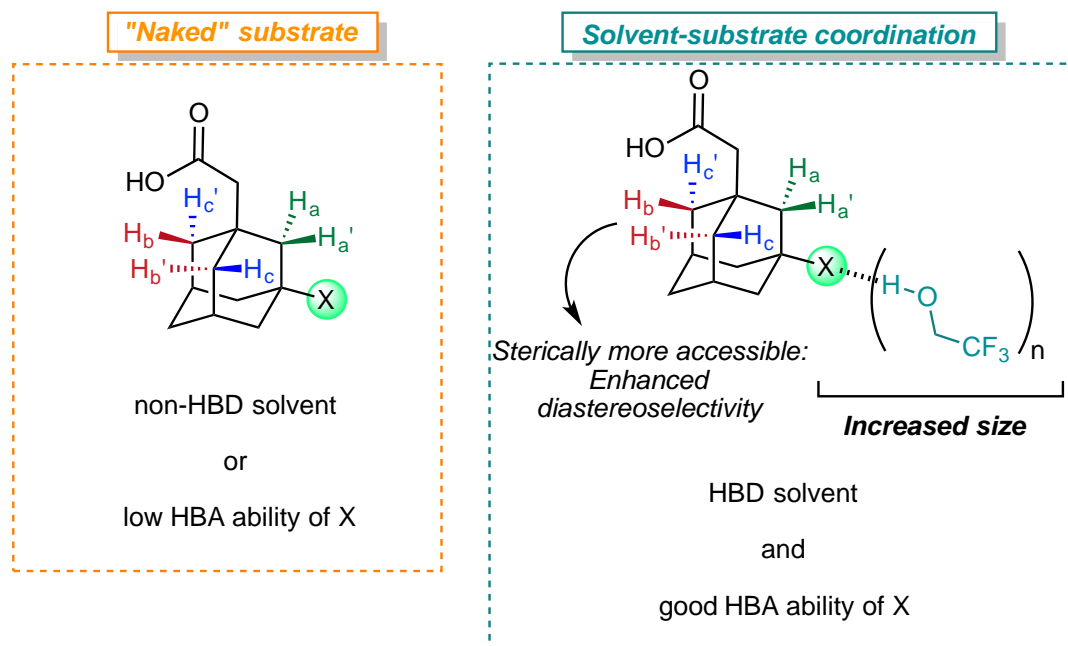


Figure IV.6. The impact of solvent coordination with polar substituents on diastereoselectivity.

Collectively, the results obtained so far suggest that the preference for distal oxidation is mainly dictated by the polar nature of the substituents, accentuated upon solvent coordination, which deplete proximal site of electron density hampering its reactivity towards HAT process.

Intrigued by this concept, we were interested in exploring the selectivity exerted by non-polar alkyl substitutions, which display a weak electron-donating character via inductive effects and moreover, not able of engaging hydrogen bonding with TFE. In sharp contrast to the previous results, when an ethyl substituent was located at 3' (**10**) proximal oxidation prevails, with a r.r. of 1.4:1 and an excellent enantioselectivity for the proximal lactone product **9a** (95% ee). Additionally, the lack of solvent coordination suppressed the diastereoselectivity of the distal lactones, which were afforded in nearly equal amounts, no matter the catalyst used, resembling the reactivity of **4** in MeCN.

Unsubstituted Mn(pdp) was selected as the catalyst of choice for proximal lactonization because, although Mn(^{TIBS}pdp) displayed the same preference, their bulky silyl groups may unfavorably interact with the 3'-substituent, thus, moderating the oxidation at this site (the results for Mn(^{TIBS}pdp) are reported in **Figure S3 in Annex Chapter IV**). The presence of a

second alkyl substituent (**11**) did not influence the reaction selectivity, with the two diastereomeric proximal lactones **11a** obtained as major products with excellent ee's. Remarkably, when the ethyl substituent was replaced with a phenyl ring, we observed a significant increase of selectivity for the proximal product (r.r. 4.7:1) without altering the enantioselectivity of the process. This observation could be rationalized on the basis of the slightly reduced BDE of these bonds due to homobenzylic stabilization of the resulting radical via stereoelectronic effect exerted by the aromatic ring.³⁰ These results remark the robustness of the enantioinduction of the reaction, that is not affected to any significant extent by the size and the electronics of the substituent. To further explore this effect, we extended the scope of aryl substituted adamantaneacetic acids (**12-19**). For all the substrate investigated, proximal γ -lactone is the major product obtained in good yield (33-61%) and outstanding enantioselectivity (95-99% ee). Of note, no traces of aromatic oxidations were observed, even in the case of electron rich arenes, which typically represent unsuitable moieties in bioinspired C-H oxidations. At first, we focused on a series of electron rich, *para*-alkyl substituted aryls (**13-15**). Very remarkably, despite the relatively low BDE associated to benzylic C-H bonds, undesired oxidation at these sites was not detected neither on primary (**13**) nor secondary (**14**) C-H bonds, thus showcasing one of the few chemoselective systems in which oxidation of unactivated C-H bonds is preferred over potentially more reactive sites. A high selectivity for proximal C-H lactonization is retained in the case of toluene (**13**) and ethylbenzene (**14**) derivatives (r.r. 4.5 and 5.2, respectively), while the bulkier 4-*tert*-butyl group (**15**) erodes to some extent the proximal selectivity (r.r. = 2.8). Along a similar line, oxidation of **16**, bearing a *para* electron-donating OMe and two *meta*-methyl groups, gives a comparable proximal selectivity (r.r. = 4.4), highlighting the sensitivity of the proximal/distal selectivity to steric perturbation both on the substrate and on the catalyst (see **Figure S3** for results with Mn(^{TiBS}pdp)). Electron donating acetanilide group (**17**) furnishes the highest proximal selectivity of the series (r.r = 5.4), while the strong electron-withdrawing nitro group (**18**) the lowest one (r.r. = 0.9), in accordance with a proximal C-H activation/deactivation scenario determined by an increase/decrease in electron density from the aryl substituent. 4-bromophenyl (**19**) falls in between, with a good proximal selectivity (r.r. = 3.9) close to that of the unsubstituted phenyl. Interestingly, the corresponding lactone **19a** is a potential chiral synthon suitable for further transformation (i.e. cross-coupling). Summarizing, these reactions disclose a rational impact of substrate and catalyst structure over site selectivity and diastereoselectivity in asymmetric Mn-

catalyzed γ -lactonization of carboxylic acids, setting the stage for the rational prediction of the lactonization selectivity.

Besides being crucial for the bioactivity of natural and artificial compounds, the synthetic versatility of γ -lactones to form chiral derivatives, such as 1,4-diols, hydroxyacids, hydroxyamides and hydroxyesters, makes this class of molecules particularly attractive as chiral building blocks in organic chemistry. As an illustration, we could remarkably transform the lactone **2a** into the corresponding 1,4-diol in exquisite 95% yield and 97% ee (**Figure S4, Annex Chapter IV**). The synthetic potential of our methodology was further exhibited in the preparation of ketoacid **20**, previously prepared by seven-step synthesis.⁹⁸ Exposure of **1** to the lactonization protocol afforded **1a** which, after ring-opening reduction and reoxidation, yielded the desired **20** in a combined 53% yield over three steps.

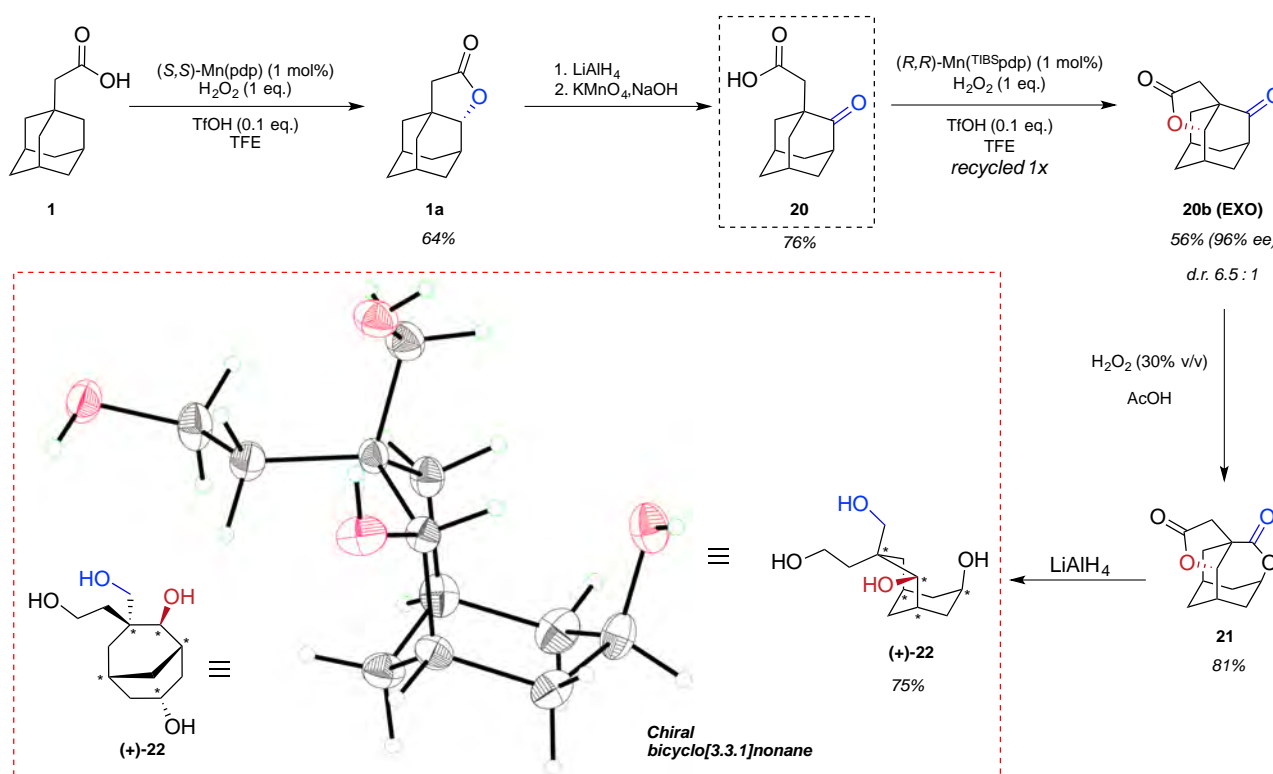


Figure IV.7. Synthesis of chiral, densely hydroxylated bicyclo[3.3.1]nonane (+)-22. Absolute configuration of (+)-22 could not be unequivocally assigned by X-ray diffraction. Results for Mn(pdp) catalyzed oxidation of **20** are shown in **Figure S5 (Annex Chapter IV)**.

Interestingly, the carboxylic acid function, now restored, can be considered as a handle to consecutively install oxygen atoms onto multiple γ -methylenes with high enantioselectivity,

increasing molecular complexity in a stepwise fashion. Indeed, 2-oxo-1-adamantaneacetic acid **20** was ready for a second round of lactonization to sequentially forge a novel, chiral γ -C-O bond on a different methylenic group. This time, the presence of the ketone limits the oxidation to two sites, with formation of two diastereomeric lactones *exo* **20b** or *endo* **20c**. The highest diastereoselectivity was observed with bulky Mn(^{TiBS}pdp) (results for Mn(pdp) are shown in **Figure S6, Annex Chapter IV**), affording the tetracyclic lactones **20b** and **20c** in a combined 56% yield, a 6.8:1 d.r and excellent 96% ee for the major diastereoisomer **20b**, with 5 chiral center generated at once. The higher degree of diastereoselectivity observed in this case, in comparison with the bridgehead-substituted adamantane discussed so far, reasonably originates from the increased proximity of the ketone function to the carboxylic acid moiety.

From an organic synthesis perspective, the appeal for this chiral adamantane core can be even greater after realizing that the oxo group offers a useful handle to deconstruct the robust adamantane cage. In fact, judicious C-C bond cleavage pathways, would furnish an easy entry into chiral, densely functionalized bicyclic [3.3.1] nonane, a carbon skeleton found in several biologically active products/metabolites as well as considered a simplified analogue of Taxol.⁹⁹⁻¹⁰² Thus, Baeyer-Villiger oxidation of **20b**, by selectively inserting the oxygen atom at the e-richest C-C bond, afforded the bis-lactone **21** with retention of configuration at all the chiral centers. Reduction of the lactone functionalities opened the tetracycle affording tetrahydroxylated chiral bicyclo[3.3.1]nonane (+)-**22** in a combined 75% yield over three steps.

Summarizing, the potential of directed Mn-catalyzed lactonization was illustrated in the concise synthesis of a tetrahydroxylated bicyclo[3.3.1]nonane enabled by two key, sequential γ -C-H lactonizations, with the latter fixing the chirality of five stereogenic centers in one step with 96% ee.

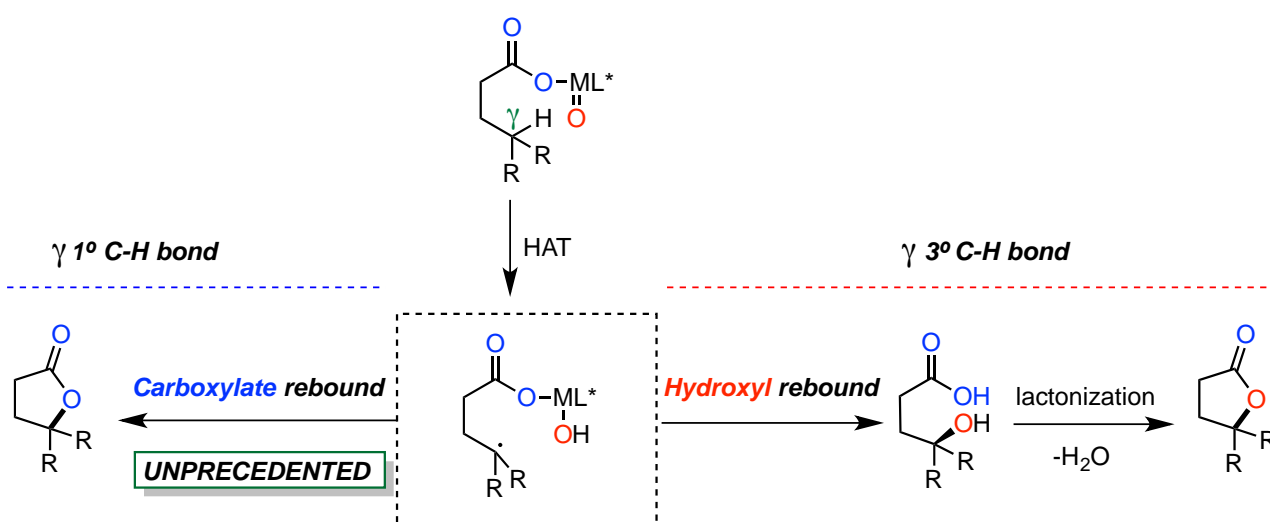
IV.3. Summary

In this chapter, we describe the first example of non-enzymatic, highly enantioselective C-H oxidation of unactivated methylenes by employing the novel catalytic approach developed in **Chapter III**, based on chiral Mn catalyst, a carboxylic acid directing group in combination with hydrogen peroxide, a fluorinated alcohol solvent and triflic acid in catalytic amount. Our strategy allows to address the long-standing challenges associated

with enantioselective C-H oxidation, affording valuable chiral γ -lactones in high enantiomeric excesses. Site-selectivity is directed towards the γ -position as a result of the interaction of the carboxylic acid with the Mn catalyst, in spite of the presence of weaker and conventionally more reactive benzylic or tertiary C-H bonds as well as oxidizable aryl substituents. At the basis of the outstanding enantioselectivity there is the synergistic interplay of a carboxylic acid directing group and a rigid adamantane core to define the spatial orientation of the γ -methylene C-H bonds towards the chiral catalytic center. The reaction is robust, tolerates several functional groups and does not necessarily require elaborated Mn catalysts. Site-selectivity in the oxidation of the three non-equivalent methylenic sites of monosubstituted adamantanes can be predicted by considering polarity effects exerted by fluorinated alcohols in polar groups, as well as inductive and homoconjugation effects induced by alkyl and aryl substituents. In addition, rational choice of the catalyst architecture can be employed to modulate the diastereoselectivity of the reaction in a predictable manner, while retaining high enantiomeric excess, enabling a straightforward differentiation of a single compound into different products. Finally, the power of this methodology was showcased in the streamlined synthesis of chiral, densely hydroxylated bicyclo[3.3.1]nonane enabled by two enantioselective C-H lactonization followed by oxidative deconstruction of the adamantane core. The principles disclosed in this work are envisioned to be rapidly incorporated into synthetic planning and to strongly impact in the field of enantioselective C-H functionalization, opening alternative paths, orthogonal to those currently undertaken with noble metals (Ir, Pd, Rh, Ru).

Chapter V

Mechanistic Insights into the γ -C-H Lactonization Catalyzed by Bioinspired Fe and Mn Complexes



V.1. Design of the project

The design of highly selective C-H oxidations, naturally catalyzed by powerful oxygenases, represents a main goal in the field of C-H functionalization.⁴³ The current stage of the art is represented by Fe and Mn small-molecule complexes, which have been shown to perform intermolecular oxidation of 3° and 2° C-H bonds with, in some cases, good level of oxidation site predictability even in complex molecules.^{11,33,45,103}

The catalytic mechanism of nonheme Fe mediated C-H oxidations has been extensively investigated and now the basic concepts have been elucidated. In details, the initial Fe(II)-complex evolves, in presence of H₂O₂ and a carboxylic acid as crucial co-ligand, to an Fe-oxo carboxylate which is proposed to be the active species competent to deliver hydroxylated products through a hydrogen-atom abstraction (HAT)/hydroxyl rebound mechanism.²⁶ Contrarily to Fe, the putative Mn-oxo intermediate has not been detected by spectroscopic techniques so far, thus leaving the mechanism of non-porphyrinic Mn-mediated bioinspired C-H oxidations mostly hypothetical. Nevertheless, the limited mechanistic experiments obtained so far, along with the selectivity patterns shown by these systems in intermolecular aliphatic C-H oxidations, suggest that Mn complexes probably undertake similar mechanistic pathways to yield the putative Mn-oxo species, in analogy to Fe-based systems.⁸⁴

In the previous chapters, we demonstrated that oxidation-site predictability could be maximized by incorporating, within the substrate, a carboxylic acid functionality as directing group for the metal-oxo species. This approach enabled the development of a highly γ -selective, lactone-forming oxidation reaction of unactivated secondary and primary C-H bonds, even in presence of *a priori* more reactive sites. Key for the reaction efficiency was the combination of TFE solvent and triflic acid (TfOH) as additive, and Mn complexes consistently delivered higher yield of the desired lactones than the related Fe-catalyzed oxidations. On the basis of ¹⁸O-isotopic labelling experiments, previously reported C-H lactonizations of 3° C-H bond catalyzed by Fe complexes have been proposed to proceed in accordance to the well-established HAT/OH rebound sequence operative in intermolecular oxidations.⁴⁶ On the other hand, no mechanistic data regarding the C-H lactonization of other type of bonds (1° and 2° C-H bonds) or about the use of Mn in this reaction, are reported to date. Consequently, having optimized the reaction conditions and delineated the scope of the carboxylic acid-directed C-H lactonization reaction in the previous chapters,

we are now interested in gaining insight into this oxidation mechanism, addressing the following opened questions: *i) What is the actual role of carboxylic acid functionality, fluorinated alcohol solvent and TfOH additive? ii) How does the lactone-forming cyclization step of tertiary, secondary and primary C-H bonds take place in presence of Mn catalyst?* Intrigued by these open issues, we disclose below systematic mechanistic experiments judiciously designed to shed some light on the catalytic action of bioinspired C-H lactonizations. Very remarkably, isotopic labelling experiments allow to propose an unprecedented¹⁰⁴ carboxylic acid rebound path that competes or, in some cases, completely prevails over the well-established hydroxyl rebound in affording the γ -oxidized product.

V.2. Result and discussion

V.2.1. Elucidating the role of directing group, solvent and additive in γ -C-H lactonization.

All the oxidation experiments discussed in this chapter were performed with the Fe and Mn complexes depicted in **Figure V.1.**, with tetradentate ligands of general formula (S,S)-[M(L)(OTf)₂] (L = (S,S)-pdp and (S,S)-mcp, pdp = *N,N'*-bis(2-pyridylmethyl)-2,2'-bipyrrolidine, mcp = *N,N'*-dimethyl *N,N'*-bis(2-pyridylmethyl)-1,2-*trans*-diamino cyclohexane, OTf = CF₃SO₃).

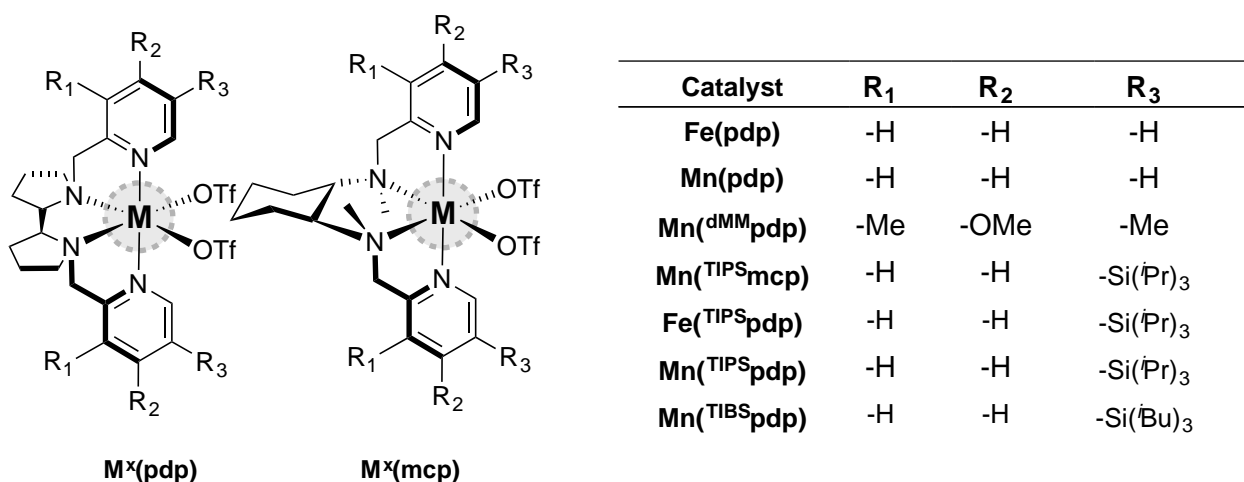


Figure V.1. Fe and Mn catalysts involved in this study.

At first, we were interested in gathering further details on the influence of the carboxylic acid as directing group in overriding the innate reactivity pattern, affording the exclusive

oxidation at γ -C-H bonds. To this end, the intramolecular nature of the C-H lactonization reaction, at the basis of the outstanding site-selectivity and chemoselectivity showcased so far, was demonstrated by directly comparing the oxidation products obtained from the oxidation of 2,2-dimethyladamantaneacetic acid **1** with the related methyl ester derivative **2**, as non-coordinating analogue (**Figure V.2**). In the case of the latter, acetic acid as external carboxylic acid was added to ensure the efficient activation of the H_2O_2 ,⁸ as well as the intermolecularity of the reaction. While the oxidation of **1** took place at the γ -methylene delivering the lactone **1a** as single product (as previously observed in **Chapter IV**), the ester **2** underwent intermolecular hydroxylation selectively at the weakest 3° C-H bonds providing 76% yield of the non-directed oxidation product **2a**.

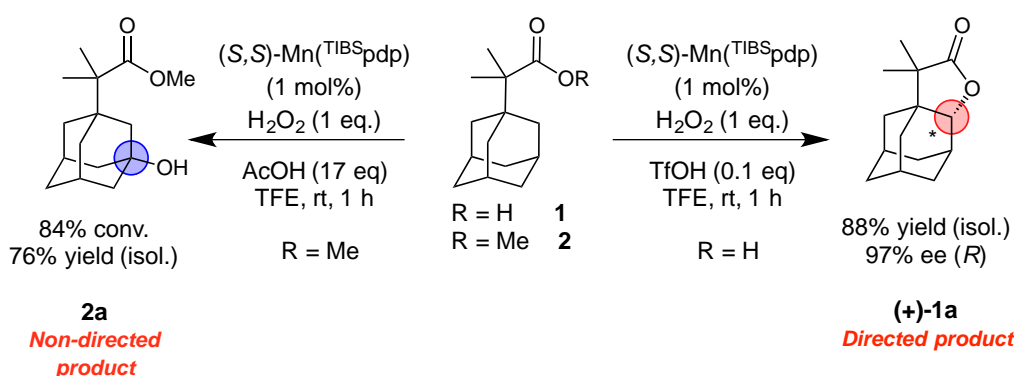
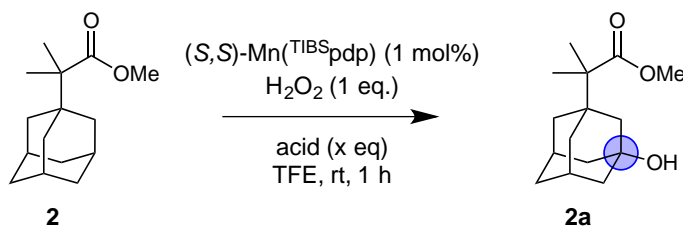


Figure V.2. Divergent reactivity and selectivity between directed (**1** to **1a**) and non-directed oxidations (**2** to **2a**).

We next focused our attention on clarifying the role of the triflic acid additive and solvent in the reaction efficiency. It is well established that an acidic environment facilitates the ring-closure lactonization of γ -hydroxyacids, even in CH_3CN .⁴⁶ Nevertheless, we carried out a set of experiments to ascertain if, besides providing this favorable acidic conditions, triflic acid and TFE are also mechanistically implicated in the activation of the H_2O_2 by assisting the Mn-carboxylate complex in the effective O-O heterolysis. To this end, tailored intermolecular oxidation experiments of **2** were performed avoiding the interference of the carboxylic acid moiety in promoting lactone-forming reaction, and consequently restricting the plausible contribution of TFE and TfOH to their involvement in the H_2O_2 activation.

Table V. 1. The effect of solvent and external acid on the intermolecular oxidation of **3**.


Entry	Acid Additive	Solvent	Conv. (%)	Yield 2a (%)
		CH₃CN		
1	none	"	5	4
2	TfOH (0.1 eq)	"	51	43
3	AcOH (1 eq)	"	22	21
4	AcOH (1 eq) + TfOH (0.1 eq)	"	37	33
5	AcOH (17 eq)	"	54	49
		TFE		
6	none	"	37	36
7	TfOH (0.1 eq)	"	42	41
8	AcOH (1 eq)	"	81	79
9	AcOH (1 eq) + TfOH (0.1 eq)	"	87	85
10	AcOH (17 eq)	"	81	76 (isol.)

In the absence of an external acid, the oxidation of the ester **2** (Table V.1, entry 1 and 6) in CH₃CN, a solvent commonly employed in bioinspired oxidations, provided only modest conversion and yield of **2a** (4% yield, entry 1) while, the same reaction in TFE yielded 36% of product **2a** (entry 6), highlighting a solvent assistance in the activation of the H₂O₂.¹⁰⁵ Very remarkably, addition of 0.1 equiv. of TfOH increased the hydroxylated product **2a** in both solvents (entry 2 and 7), supporting the hypothesis that Brønsted acids facilitate the O-O cleavage.⁸⁷

This beneficial effect is particularly significant in CH₃CN, where the yield increases from 4% to 43% upon addition of TfOH. In TFE, the total yield is similar (41%), but the improvement is lower, likely because the reaction is already efficient even with no acid additives as a result of the TFE involvement in the H₂O₂ activation process.

Replacement of TfOH for AcOH (1 eq), known to trigger O-O cleavage via the carboxylic acid assisted pathway, afforded the oxidized product **2a** in 21% or 79% yield in CH₃CN or TFE, respectively. In accordance with previous studies, higher carboxylic acid loadings are required in CH₃CN for efficient oxidations,^{28,45} while the operating role of TFE in H₂O₂ activation makes the reaction to proceed smoothly even at low AcOH loadings (entry 8). Importantly, TfOH, TFE and an external carboxylic acid can act synergistically in intermolecular oxidations furnishing the highest yield of the series (85% yield, entry 9).

These findings could be directly translated to intramolecular lactonization since this optimal combination is consistent with the best combination found in intramolecular oxidations and our hypothesis.

In this latter case, oxidation of the bound substrate outcompetes any intermolecular oxidation, given the entropic advantage of intramolecular processes to promote the functionalization of the γ -methylene group.

V.2.2. Diverting bioinspired C-H hydroxylation towards acetoxylation: Evidence for an unprecedented carboxylate rebound mechanism.

Mechanistically, non-heme Fe catalyzed oxidations have been previously demonstrated to proceed according to the HAT/hydroxyl rebound mechanism. Nevertheless, in the presence of a ligated substrate via a carboxylic acid moiety, the iron-radical carboxylate intermediate generated upon hydrogen abstraction could be envisioned to provide the lactone product via two distinct pathways: 1) the hydroxyl rebound to deliver a γ -hydroxyacid which spontaneously undergoes nucleophilic lactonization or 2) carboxylate rebound to directly generate the lactone (the two possible rebounds for adamantaneacetic acid **3** are depicted in **Figure V.3**). To differentiate between these two alternatives, White and co-workers, made use of 88% doubly ^{18}O -labelled carboxylic acid as mechanistic probe for Fe(pdp)-mediated C-H lactonization of 3° γ -C-H bonds. The predominant formation of singly labelled ^{18}O -lactone (87% singly labelled) suggested that hydroxyl rebound is, by far, the main pathway to the formation of the lactone product.⁴⁶ In this context, we wondered if also the C-H lactonization of methylenic site in adamantaneacetic acid **3**, under our conditions (Mn catalyst, fluorinated solvent and TfOH), follow the same mechanistic scenario.

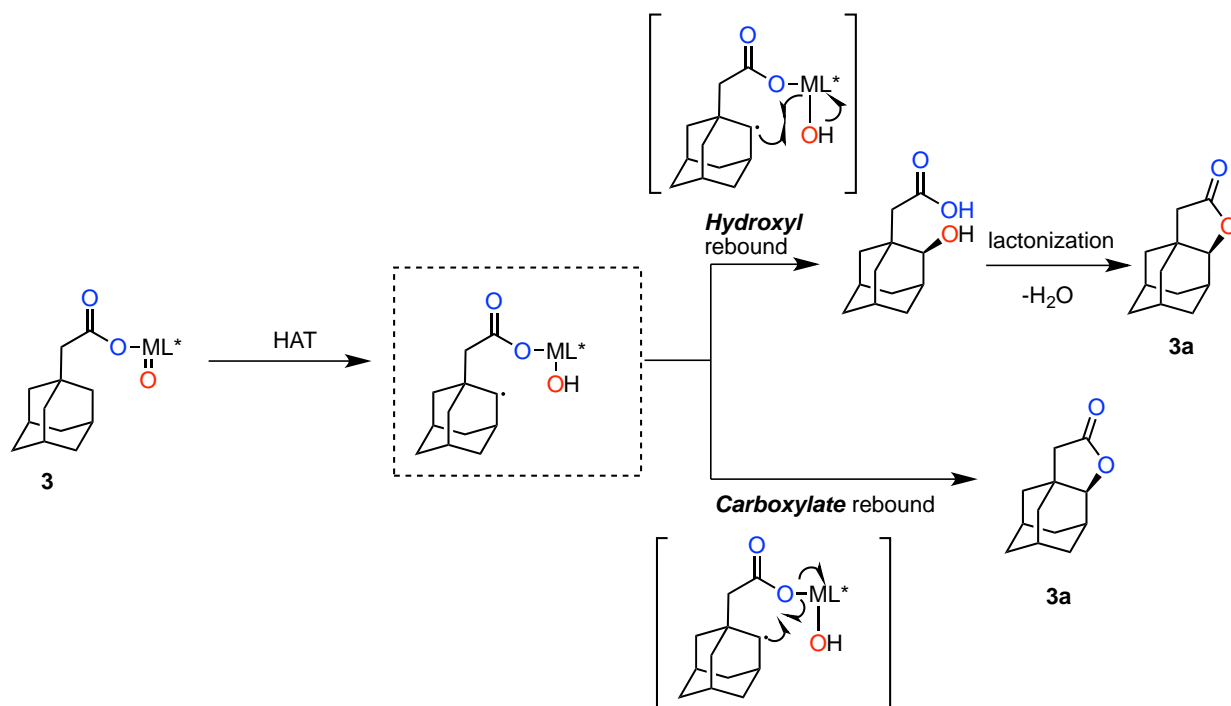


Figure V.3. Proposed rebound mechanisms for the carbon radical generated after the HAT. Note that the oxygen atoms can be differentiated by isotopic labelling (i.e. blue ¹⁶O and red ¹⁸O, with the latter coming from isotopically enriched H₂¹⁸O₂).

The most straightforward way to prove this scenario was the exposure of **3** to our methodology using labelled H₂¹⁸O₂ as oxidant. Surprisingly, only 50% of ¹⁸O-atom incorporation was observed in the C-H lactonization of **3** catalyzed by Mn(^{Ti}BS)pdp) (**Figure V.4, A**), indicating that a competitive carboxylate rebound mechanism is operative under our conditions. In full agreement with this hypothesis, the complementary oxidation experiment with the doubly ¹⁸O-labelled **3**, with non-labelled H₂O₂, provided 55% of doubly ¹⁸O-labelled lactone **3a** (**Figure V.4, B**). Intrigued by these findings, unprecedented in the field of Fe and Mn bioinspired oxidation chemistry, we asked ourselves an additional question: *can we define conditions to control this alternative rebound in order to make predictions on the fate of the carbon centered radical?* Remarkably, even if in a lower extent, this alternative carboxylate rebound path was also found to be active when complex Fe(pdp) was employed as catalyst for the C-H lactonization of doubly ¹⁸O-labelled **3**, as witnessed by the formation of 17% of doubly ¹⁸O-labelled lactone **3a** (**Figure V.4, B**). The O-incorporation from water into the final product was excluded by performing the standard C-H lactonization protocol in presence of ¹⁸O-labelled water (**Figure V.4, C**). Interestingly, the Thorpe-Ingold effect exerted by the α -dimethyl substitution in carboxylic acid **1** considerably reduced (ca. by half, down to a 27%) the entity of hydroxyl rebound (**Figure V.4, D**), reasonably favoring

the carboxylate one as result of the closer proximity between the carbon radical with the carboxylate moiety. Thus, this result strongly suggests that also structural features of the radical substrate are relevant in defining the concluding part of the mechanism, responsible to yield the lactone product.

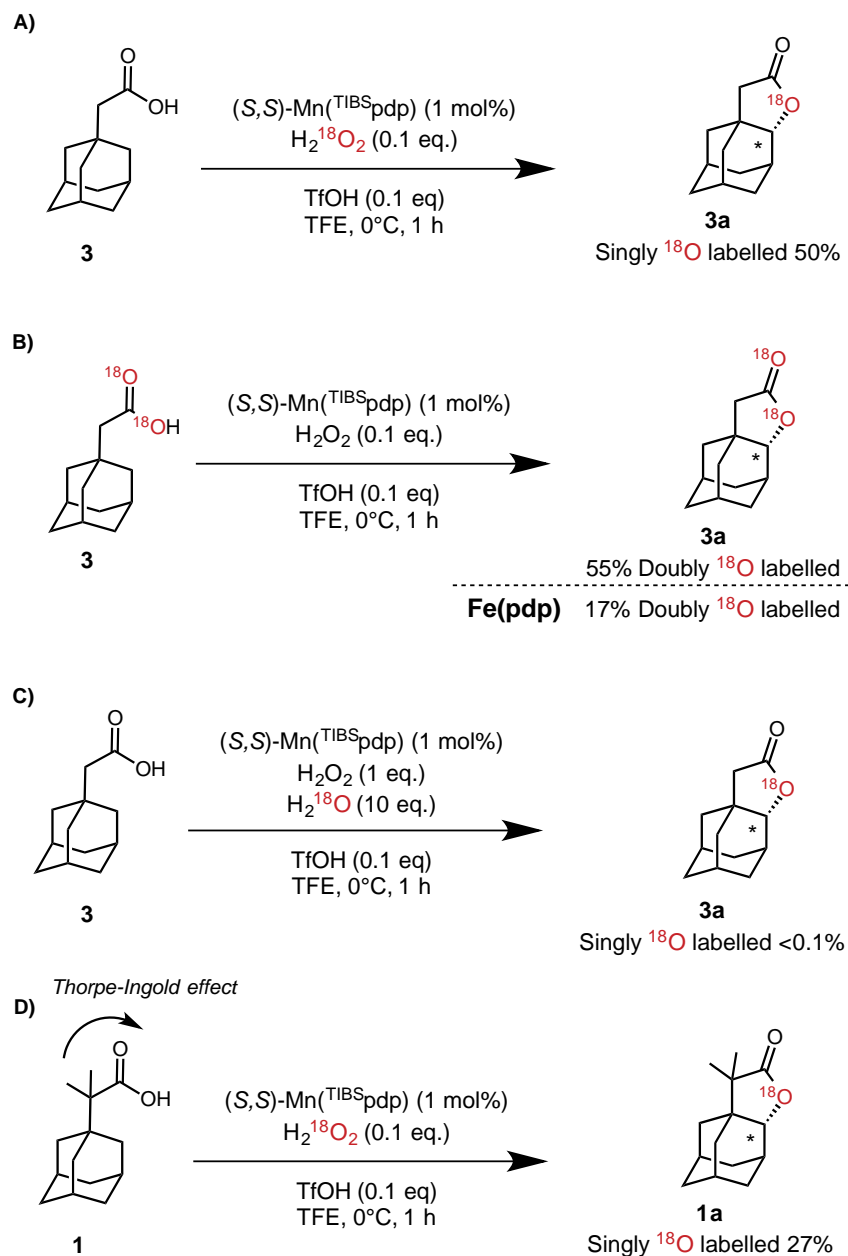
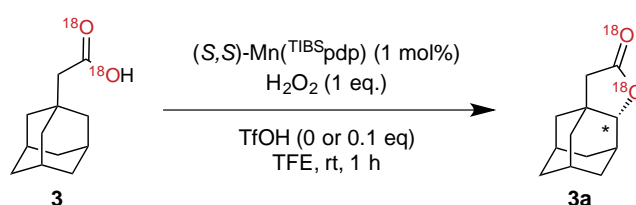


Figure V.4. Isotope labelling experiments to ascertain the origin of the O-atom incorporated into the lactones (GC-MS analysis via chemical ionization with NH₃/CH₄). The reported ¹⁸O incorporations are obtained after correction for the isotopic purity of the labelled reactants. A) ¹⁸O-incorporation in the lactone product **3a** from ¹⁸O-labelled hydrogen peroxide and B) from doubly ¹⁸O-labelled carboxylic acid **1**. C) ¹⁸O-incorporation from ¹⁸O-labelled water was not observed. D) The impact of the Thorpe-Ingold effect in the rebound step.

Next, we evaluated the extent of the carboxylate rebound coming from the oxidation of the doubly labelled ^{18}O **3** in different solvents, with or in absence of TfOH additive. Notably, we regularly observed that when TfOH was not added into the catalysis mixture (**Table V.2**, entries 2, 4, 6), a strongly enhanced doubly incorporation of ^{18}O into the final product **3a** was observed, correlated with an improved carboxylate rebound mechanism.

Table V. 2. The effect of solvent and TfOH on the rebound step to generate **3a**.



Entry	Solvent	TfOH (eq.)	3a (%) (Carboxylate rebound)
1	MeCN	0.1	60
2		-	84
3	TFE	0.1	54
4		-	86
5	HFIP	0.1	56
6		-	87

^{18}O -atom incorporated into the lactones was calculated on the basis of GC-MS analysis (via chemical ionization with NH_3/CH_4). The percentage of carboxylate rebound corresponds to the percentage of the doubly ^{18}O -labelled lactone. The reported ^{18}O incorporations are obtained after correction for the isotopic purity of the labelled **3**.

Unfortunately, this peculiar behavior of the triflic acid in favoring the hydroxyl rebound path could not be explained rigorously and its full role on the catalytic mechanism should be further clarified in future experiments. Overall, these experiments provided preliminary indications that multiple factors may be operative in defining the post-HAT mechanism, with the new proposed carboxylate rebound particularly favored by Mn-based complexes and the structural Thorpe-Ingold effect. Nevertheless, this enhanced effect was preserved both in fluorinated solvents and in MeCN and interestingly, the extent of the carboxylate rebound, under equal conditions, was independent from the solvent used as witnessed by

the almost identical ^{18}O incorporation detected along the oxidation experiments. Once investigated the impact of metal, solvent and additive on the rebound mechanism of **3**, we focused our attention towards the nature of the carboxylic acid substrate, with particular emphasis on the class of the targeted γ -C-H. To this end, a set of doubly ^{18}O -labelled carboxylic acids featuring tertiary, secondary and primary γ -C-H bonds were tested under C-H lactonization conditions (TfOH was not added in order to maximize the carboxylate rebound) (**Figure V.5**). In line with the isotopic labelling experiments reported by White with $\text{Fe}(\text{pdp})$, carboxylic acids bearing tertiary γ -C-H bonds yielded the corresponding lactones (**4a-6a**) mostly following the well-established hydroxyl rebound path even with $\text{Mn}(\text{TIBS}\text{pdp})$. The amount of carboxylate rebound slightly increased up to 22% with the rigid adamantane **6**, which may indicate that also the steric features, around the reactive tertiary γ site are probably a relevant aspect to be considered in the radical rebound competition.

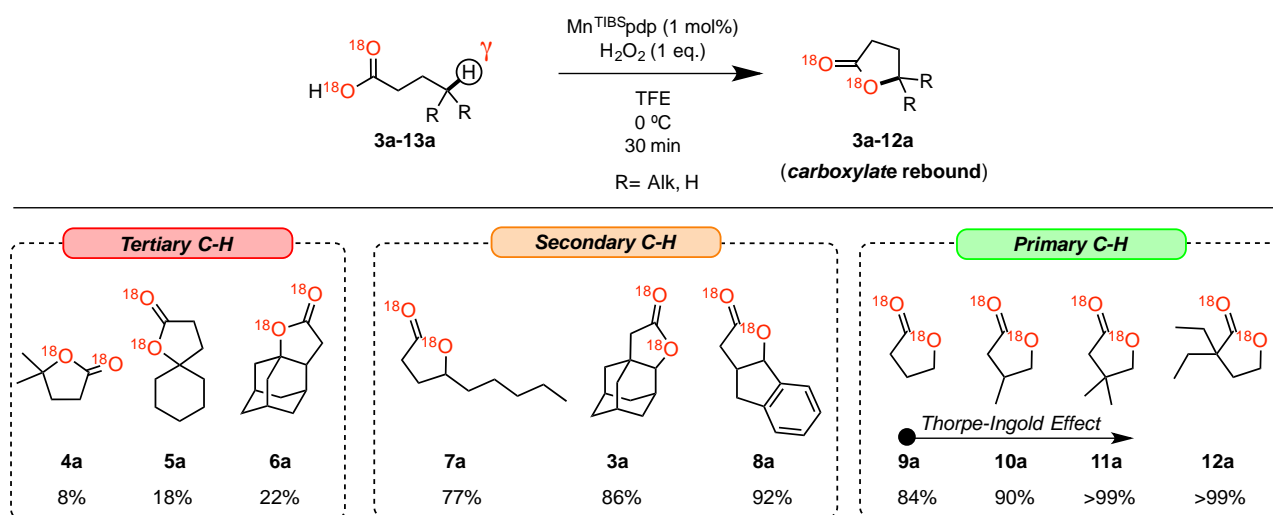


Figure V.5. Estimation of the carboxylate rebound mechanism in a set of substrates containing different types of γ -C-H bonds. The percentage of carboxylate rebound corresponds to the percentage of the doubly ^{18}O -labelled lactone. ^{18}O incorporations are obtained after correction for the isotopic purity of the labelled substrates. Conversions and yields are reported in Figure S1 (Annex Chapter V).

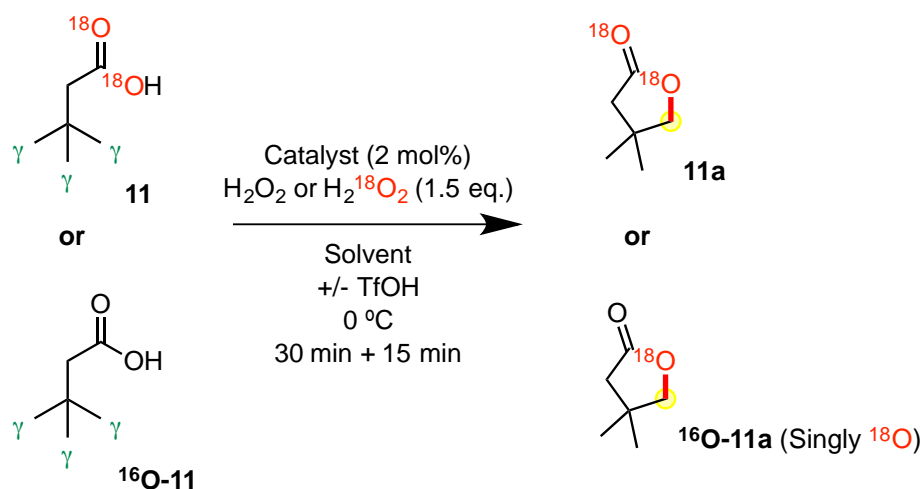
More interestingly, the stark different ^{18}O -incorporation exhibited by lactone **6a** and **3a**, which are structurally very similar but diverse in the alkyl substitution of the γ -C-H bond, clearly demonstrated that the nature of the γ -site (tertiary or secondary C-H bond) is a fundamental factor for the resultant radical when choosing a rebound instead of another.

Indeed, the selectivity for the carboxylate rebound sharply improved in the case of lactones stemmed from the oxidation of γ -methylene site, where the level of the doubly ^{18}O -incorporation goes from 77% of the nonanoic lactone (**7a**) up to 92% for the indanyl lactone derivative (**8a**). However, since benzylic C-H bonds generally display a substantially lower dissociation energy than 3° C-H bonds (~ 85 and ~ 96 kcal/mol, respectively), the latter result makes a possible correlation between the rebound selectivity with the BDE of the C-H bond oxidized (or the stability of the resulting carbon center radical) difficult to set. Nevertheless, to further study this effect, we also included in the scope carboxylic acids containing highly strong primary γ -C-H bonds (>100 kcal/mol) (**9a-12a**). Interestingly, for these substrates, the amount of double ^{18}O -incorporations persistently reached a value higher than 90%, supporting again the hypothesis of a relation between the bond dissociation energy of the reacting C-H bond with the selectivity for the rebound step. In agreement with the experiment of **1**, the Thorpe-Ingold effect, triggered by the α or β quaternary carbon of **11** and **12** respectively, enhanced the carboxylate rebound mechanism up to complete double ^{18}O -incorporation into the final lactone products **11a** and **12a**. These results may suggest that the unstable primary radical, generated upon hydrogen abstraction, is rapidly captured by the carboxylate ligand (carboxylate rebound) to furnish the lactone rather than the OH one (hydroxyl rebound). The reasons for this preference are still unclear, as the factors that define the post-HAT selectivity are still elusive and difficult to interrogate experimentally. This high preference for the carboxylate rebound may be due to a peculiar reaction disclosed by the high reactivity of the primary radical (which would favor the kinetic rebound product) and the proximity of the carboxylate ligand, in turn favored by Thorpe-Ingold effect.

On the other hand, a more elaborated theory would suggest that in the case of primary C-H bonds, generally too robust for metal-oxo based oxidations,¹⁰⁶ the HAT step could be performed by the carboxylate radical bound to the metal via an 1,5-HAT process, instead of a 1,7-HAT executed by the oxo moiety. This latter hypothesis can also account for the exquisite γ -selectivity of the reaction, typically found in 1,5-HAT based transformations.¹⁰⁷ In this scenario, the rebound via carboxylate should be facilitated. However, the complexity of the reaction intermediates and the factor manifold that regulates the reactivity make the complete comprehension of the mechanism a tremendously challenging task.

To further explore the oxidation mechanism of primary C-H bonds, we set out a study that involved the screening of different catalysts, solvents and additive by employing the

optimized conditions for primary C-H bond lactonization found in **Chapter III**. The results reported in **Table V.3** revealed that all the Mn catalysts investigated, irrespective from their steric (entries 1-4 and 8) and electronic properties (entries 9-10), regularly promoted the formation of the lactone **11a** exclusively via a carboxylate rebound. These results are also well-supported by the complementary experiment based on the oxidation of non-labelled **11** in presence of labelled $\text{H}_2^{18}\text{O}_2$ as terminal oxidant (entry 4). Changing the solvent to MeCN or HFIP (entries 5-6, respectively) did not affect the selectivity observed in TFE for the carboxylate rebound path. In contrast to the oxidation of **3**, triflic acid is now irrelevant in terms of reaction efficiency and mechanism, since no improvement in the lactone yield neither change in the rebound selectivity was observed upon addition of 0.1 equiv (entry 7). Notably, these results showcased that Mn-catalyzed lactonization for 1° C-H bonds, irrespective of the reaction conditions (ligand, solvent and additive), follow a well-defined mechanism in which the lactone product arose from the carboxylate rebound, without the intermediacy of a hydroxyacid. On the other hand, although with Fe complexes the selectivity for the carboxylate rebound remains high (up to 73-86%, entries 11-12), the competitive hydroxyl rebound was found to be again an accessible channel towards the lactone product (entry 12), further enhanced by the addition of 0.1 equiv. of TfOH. Collectively, all the isotopic labelling experiments support the hypothesis that the rebound step in non-heme bioinspired C-H lactonization is mainly substrate-dependent, since the selectivity for one of the two competitive rebound paths remarkably change if the hydrogen abstraction is executed from 3° , 2° or 1° C-H bond. Albeit to a lesser extent, the metal and the additive were also found to affect the preference of the radical rebound path, with the use of iron complexes and triflic acid slightly fostering the hydroxyl rebound.

Table V.3. The effect of catalyst, solvent and TfOH on the rebound step to yield **11a**.

Entry	Catalyst	Solvent	TfOH (eq.)	Lactone Yield (%)	$^{18}\text{O}^{18}\text{O}$ incorporation (%)
1	Mn(pdp)	TFE	-	54	>99
2	Mn(^{TIBS} pdp)	“	-	54	>99
3	Mn(^{TIPS} pdp)	“	-	65	>99
4	“ (with H ₂ ¹⁸ O ₂)	“	-	64	0 (0% singly ¹⁸ O)
5	“	MeCN	-	11	>99
6	“	HFIP	-	64	>99
7	“	TFE	0.1	62	>99
8	Mn(^{TIPS} mcp)	“	-	41	>99
9	Mn(^{DMM} mcp)	“	-	29	>99
10	Mn(^{NMe2} mcp)	“	-	17	98
11	Fe(pdp)	“	-	25	73
12	Fe(^{TIPS} pdp)	“	-	6	86
13	“ (with H ₂ ¹⁸ O ₂)	“	-	10	0 (15% singly ¹⁸ O)
14	“	“	0.1	6	72

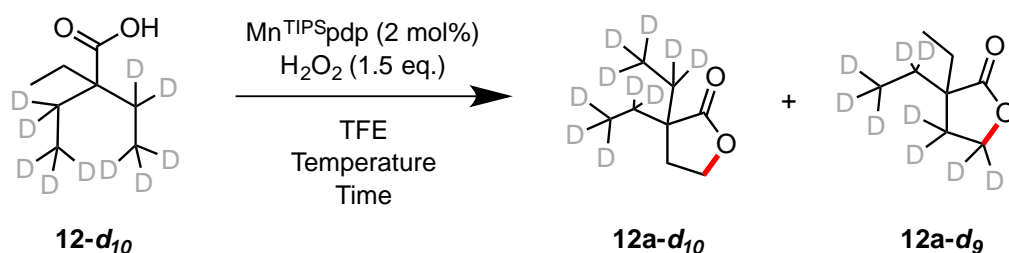
¹⁸O-atom incorporated into the lactones was calculated on the basis of GC-MS analysis (via chemical ionization with NH₃/CH₄). The percentage of Carboxylate Rebound corresponds to the percentage of the doubly ¹⁸O-labelled lactone. The reported ¹⁸O incorporations are obtained after correction for the isotopic purity of the labelled reactants. In the experiments with labelled H₂¹⁸O₂, non-labelled **11** was used.

To further elucidate the mechanistic details, we performed intramolecular kinetic isotopic effect studies. KIE values for intermolecular oxidations of secondary and tertiary sites with Mn complexes have been already reported to fall in the range of 3.8-4.7,⁸⁴ thus indicating that the C-H bond cleavage during the HAT path represents the rate-determining step of the oxidation process. The observed $k_{\text{H}}/k_{\text{D}}$ values in **Table V.4** are comparable with the ones documented for the H abstraction with Fe/H₂O₂ catalytic systems (3.2-5)^{26,108-110} and tBuO•

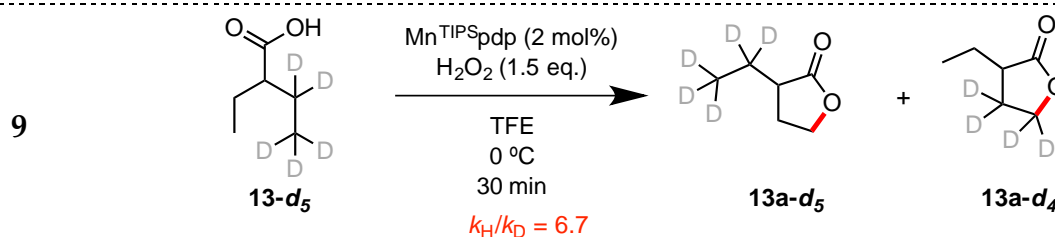
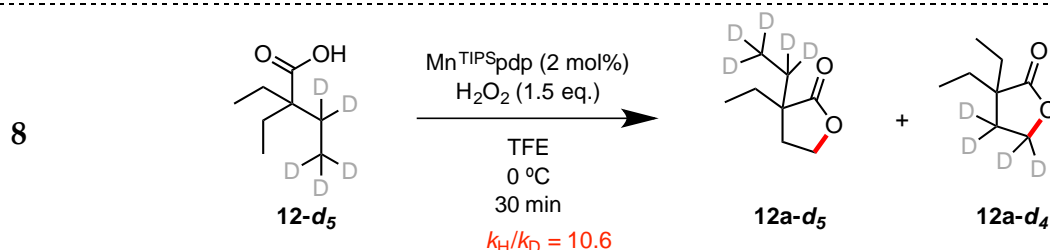
radical (~ 4),¹¹¹ but higher than those observed with $\bullet\text{OH}$ radical (1-2)¹¹² and substantially lower than the ones reported for benzotriazole-*N*-oxyl radical (11-27).¹¹³⁻¹¹⁶

In this regard, we synthesized γ -isotopically enriched **12-*d*₁₀**, **12-*d*₅** and **12-*d*₅** and exposed them under the lactonization conditions in presence of Mn(^{TIPS}pdp).

Table V.4. Intramolecular deuterium Kinetic Isotope Effects ($k_{\text{H}}/k_{\text{D}}$) in the oxidations of deuterated **12-*d*₁₀** (at different reaction time and temperatures), **12-*d*₅** and **13-*d*₅**.



Entry	Time (min)	Temperature (°C)	Corrected 13a- <i>d</i> ₁₀ : 13a- <i>d</i> ₉	$k_{\text{H}}/k_{\text{D}}$
1	30	0	84 : 16	10.5
2	30	-35	83 : 17	9.8
3	1	0	82 : 18	9.1
4	2	0	83 : 17	9.8
5	5	0	83 : 17	9.8
6	10	0	82 : 18	9.1
7	20	0	83.5 : 16.5	10.1



KIE ($k_{\text{H}}/k_{\text{D}}$) values were obtained from the d_5/d_4 or d_{10}/d_9 lactone ratios, which in turn come from HRMS or GC-MS (CI source) and are corrected for the isotopic purity of the deuterated acid substrate.

Intramolecular competitive oxidation of **13-d₁₀**, under standard conditions (entry 1), revealed an intramolecular KIE value of 10.5. This sizeable value is consistent with a rate-determining hydrogen abstraction step for which, quantum mechanical tunneling contributions are involved. Lowering of the temperature (-35 °C) did not alter the k_H/k_D (entries 2). Time-dependence analysis demonstrated that the operative mechanism is retained along the oxidation experiment, as witnessed by the similar KIE values recorded at different reaction time (entries 3-7). These results were well-supported by the equally large KIE values also observed in the intramolecular competitive oxidation of **13-d₅** and **14-d₅**, 10.6 and 7 respectively (entries 8-9).

Overall, the data collected so far allows to propose a mechanism for the γ -C-H lactonization of primary C-H bonds mediated by Mn catalysts (**Figure V.6**).

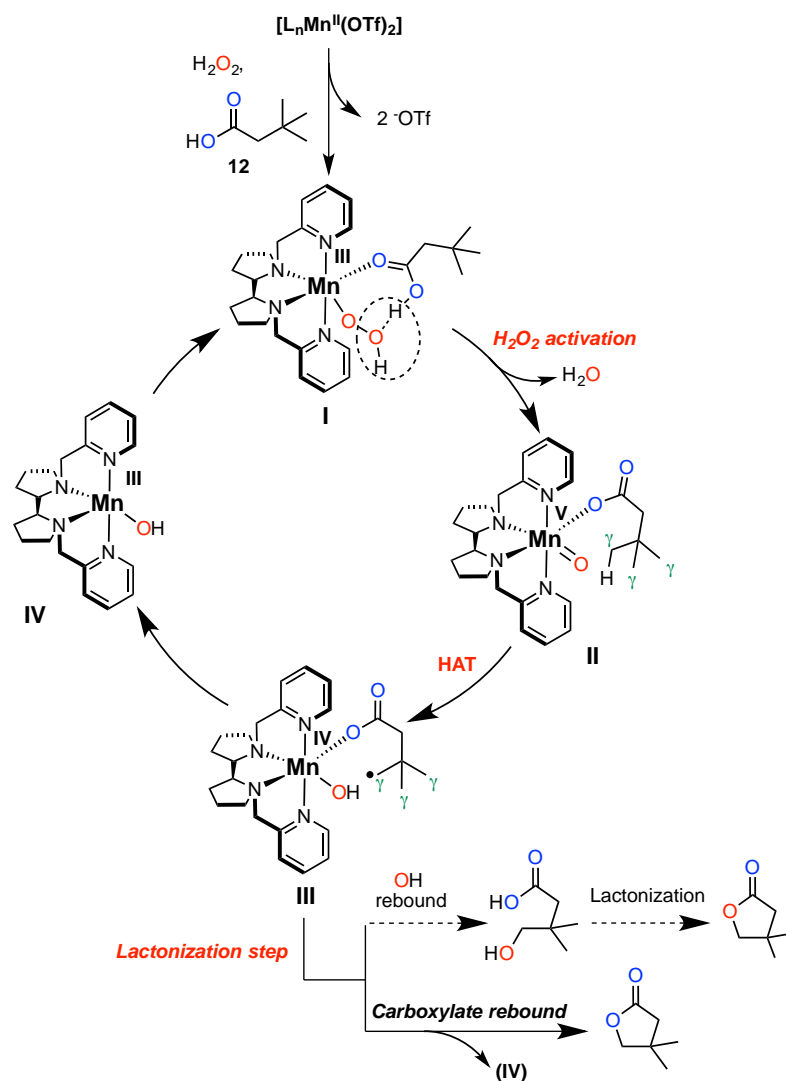


Figure V.6. Proposed mechanism for the bioinspired Mn-catalyzed γ -C-H lactonization of primary C-H bonds (IV is a Mn^{III}-OH species).

In presence of excess hydrogen peroxide and carboxylic acid (i.e. **12**), the initial Mn^{II} complex evolve to the Mn^{III}-peroxo carboxylate species **I**. Then, the carboxylic acid assists the heterolytic cleavage of the O-O bond to yield the final oxidant species **II**, a putative high valent Mn^V-oxo-carboxylate intermediate, competent for the highly selective intramolecular HAT at the γ -C-H bond of the ligated **12**. Presumably, triflic acid and the hydrogen donor ability of the fluorinated alcohol solvents facilitate the cleavage of the O-O bond. On the basis of the large kinetic isotopic effect found, C-H cleavage was confirmed to be the rate-determining step of the catalytic cycle. On the basis of ¹⁸O-isotopic labelling experiments, we also demonstrated that the primary carbon radical generated collapsed rapidly with the carboxylate moiety, instead of the hydroxyl group, affording the desired lactone product and releasing a Mn^{III}-OH (**IV**).

V.3. Summary

In this chapter mechanistic details of bioinspired Fe and Mn-catalyzed γ -C-H lactonization developed in the previous chapters have been investigated. The open questions regarding the effective role of TfOH as key additive and TFE as optimal solvent found reasonable explanation in their directed involvement into the H₂O₂ activation process. Furthermore, ¹⁸O-isotopic labelling experiments witnessed that two different rebound pathways, the well-established hydroxyl rebound and the unprecedented carboxylate rebound, are actually in competition for the short-lived carbon radical, generated upon HAT process, in affording the final lactone product. However, the fact that multiple factors simultaneously operate in tuning the preference for a specific rebound makes the set of prediction rules still not completely reliable. Nevertheless, we could observe that the carboxylic acids reacting at the tertiary C-H bonds mainly follow the hydroxyl rebound, while lactonization at primary C-H bonds is mostly achieved by a rebound via carboxylate. Depending on the reaction conditions (primarily, metal and additive), secondary C-H lactonization falls somehow in the middle, where the competition of the two rebound paths is observed. The Thorpe-Ingold effect, so far exclusively disclosed as favorable structural effect by accelerating the HAT process, was found to be relevant also at the rebound stage, where it fosters carboxylate rebound presumably by increasing the proximity of the substrate radical and the metal-carboxylate species. Thus, these findings, in combination with the large KIE observed (>7),

have put forward an alternative oxidative mechanism to the classical rebound mechanism, unprecedented in the landscape of bioinspired oxidations.

Chapter VI

General Conclusions

Since the first examples, reported more than 20 years ago, the field of C-H oxidation catalyzed by bioinspired Fe and Mn complexes has grown exponentially. Nevertheless, although the progress in oxidation site-predictability and the first examples of enantioselective oxidations have been documented, the tremendous potential of this reaction is far from being completely unlocked. General and synthetically reliable methodologies struggle to emerge since the interpretation of the complex selectivity patterns behind the reaction delays the investigation of a wide substrate scope. In this thesis, by making use of the carboxylic acid functionality as a native directing group, we have developed an exceptionally versatile, γ -selective, chemoselective (**Chapter III**) and enantioselective (**Chapter IV**) lactone-forming intramolecular oxidation. The knowledge acquired from these studies, together with the mechanistic findings reported in (**Chapter V**), provide a global perspective of the sizable contribution of γ -C-H lactonization to the field of C-H oxidation.

In particular, in **Chapter III** we demonstrated that this new methodology, based on bioinspired Mn catalysts, H_2O_2 as a green oxidant, a polyfluorinated alcohol solvent and triflic acid additive, enabled the intramolecular oxidation of carboxylic acids with outstanding γ -selectivity and lactone product chemoselectivity. The reaction was proved to be extraordinarily general since several types of γ -C-H bonds (benzylic, tertiary, secondary and even strong primary sites) could be successfully targeted in synthetically useful yields. Importantly, when the $\text{C}(\text{sp}^3)\text{-O}$ bond is forged on a secondary carbon, a stereogenic center is generated thus, allowing the design of powerful asymmetric C-H lactonizations for which preliminary basic principles have been established.

Following these basic concepts, in **Chapter IV**, we reported the first example of non-enzymatic, highly enantioselective C-H oxidation of unactivated methylenic C-H bonds enabled by Mn-catalyzed C-H lactonizations. Particularly, the new bulky $\text{Mn}(\text{TIBS})\text{pdp}$ catalyst, tailor-made to synergistically operate with structurally defined adamantaneacetic acids in delivering the corresponding γ -lactones in high ee (up to >99%) and good to moderate yields. In the case of 3'-substituted adamantanes, where the three γ -methylenic sites are non-equivalent, site selectivity could be rationally predicted on the basis of activating/deactivating effects exerted by the substituents or from their interaction

with the HBD solvent (polarity reversal). Additionally, the diastereoselectivity of the reaction could be controlled in a predictable manner by judicious choice of the catalyst structure. Finally, we showcased the potential of this reaction in the synthesis of a chiral polyoxygenated bicycle nonane enabled by two key consecutive asymmetric C-H lactonizations.

In **Chapter V**, we were interested in elucidating the mechanistic details of the C-H lactonization reaction. In particular, it has been verified that the carboxylic acid moiety truly acts as directing group for the metal-oxo, while TFE and TfOH assist the O-O cleavage promoting the hydrogen peroxide activation. On the basis of ¹⁸O-labelling experiments we discovered that the reaction follows a “bifurcated” rebound mechanism: the well-established hydroxyl rebound and the carboxylate rebound, unprecedented in the panorama of bioinspired C-H oxidations. The latter is mostly observed in the case of primary γ -C-H lactonization, where is further increased by using Mn catalysts, while the selectivity for the hydroxyl rebound is favored by oxidation at 3° C-H bonds, Fe-based catalysts and by using triflic acid. Large intramolecular kinetic isotopic effects were observed in the case of γ -deuterated substrates, demonstrating that the HAT process is the rate-determining step of the catalytic cycle.

Experimental Section

Experimental Section: Methodologies

Materials

2,2,2-Trifluoroethanol (TFE) and 1,1,1,3,3,3-Hexafluoro-2-propanol (HFIP) were purchased from Fluorochem while the other solvents were purchased from SDS and Scharlab. Anhydrous solvents were purified and dried by passing through an activated alumina purification system (M-Braun SPS800). Hydrogen peroxide solutions employed in the oxidation reactions were prepared by diluting commercially available hydrogen peroxide (50% H₂O₂ solution in water, Aldrich). Commercially available trifluoromethanesulfonic acid (TfOH, 99%) was purchased from Fluorochem and used as received.

Instrumentations

Oxidation products were identified by comparison of their GC retention times and GC/MS with those of authentic compounds, and/or by ¹H and ¹³C-NMR analyses. IR spectra were taken in a Mattson-Galaxy Satellite FT-IR spectrophotometer using a MKII Golden Gate single reflection ATR system. Elemental analyses were performed using a CHNS-O EA-1108 elemental analyzer from Fisons. X-ray diffraction analysis were carried out on a BRUKER SMART APEX CCD diffractometer using graphite-monochromated MoK α radiation ($\lambda = 0.71073 \text{ \AA}$) from an X-ray Tube. NMR spectra were taken on BrukerDPX300 and DPX400 spectrometers using standard conditions. Electrospray ionization mass spectrometry (ESI-MS) experiments were performed on a Bruker Daltonics Esquire 3000 Spectrometer using a 1 mM solution of the analyzed compound. High resolution mass spectra (HRMS) were recorded on a Bruker MicroTOF-Q^{II} (Q-TOF) instrument with a ESI source at Serveis Tècnics of the University of Girona. Samples were introduced into the mass spectrometer ion source by direct infusion through a syringe pump and were externally calibrated using sodium formate. Chromatographic analyses were performed on an AgilentGC-7820-A chromatograph using a HP5 column (30 m) while enantiomer resolution using HP-Chiral-20B column and HPLC 1200 series Agilent technologies using CHIRALPAK-IA and CHIRALPAK-IC columns.

Experimental section Chapter III

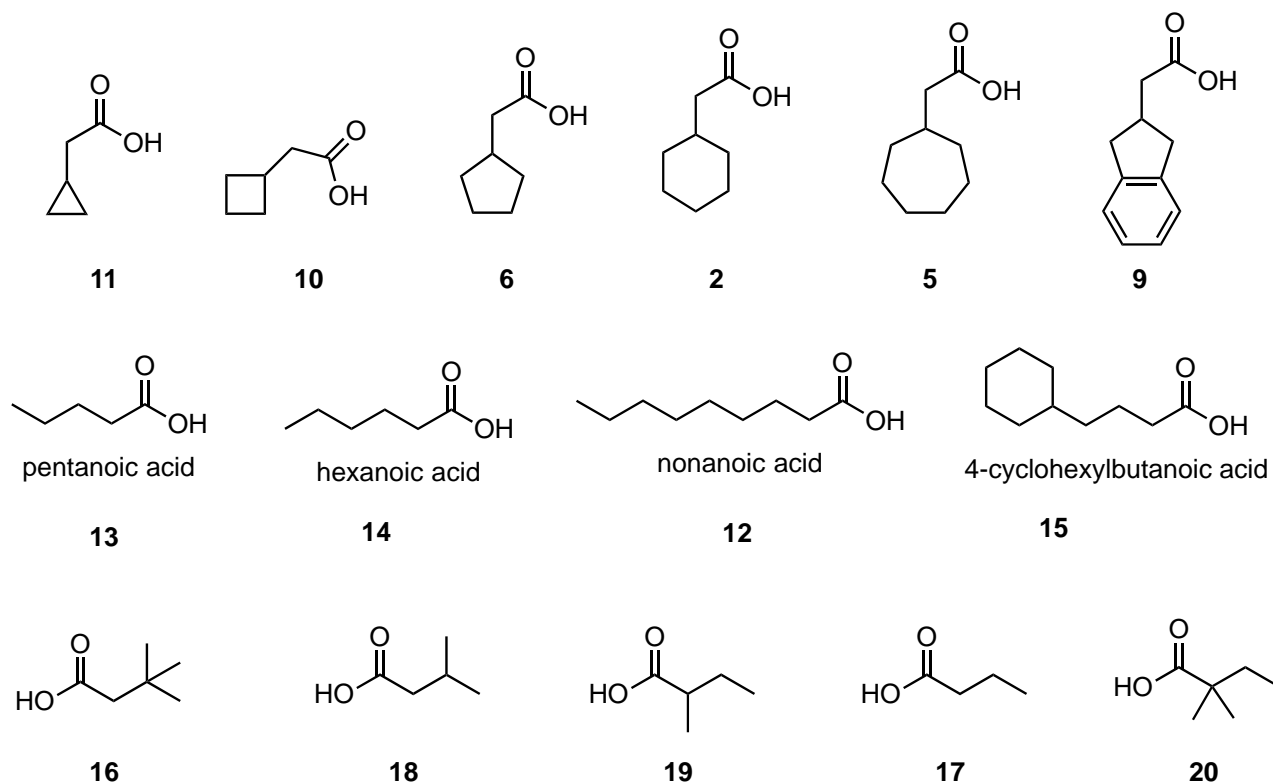
3.1. Synthesis of catalysts and substrates

3.1.1. Synthesis of the complexes

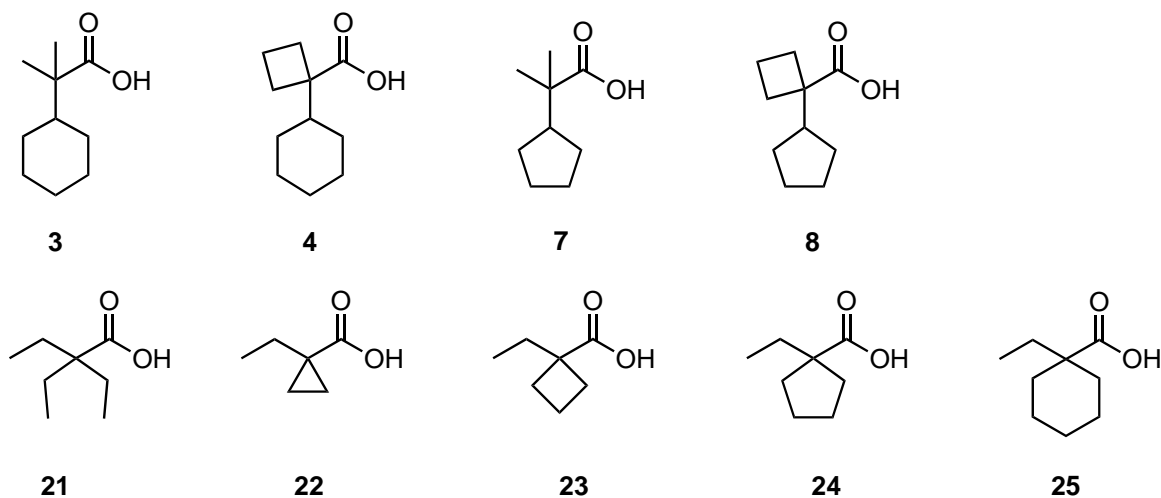
Triflate complexes (S,S) -Fe(pdp),²⁷ (S,S) -Fe(TIPSPdp),¹⁰³ (S,S) -Mn(pdp),²⁸ (S,S) -Mn(TIPSPdp),⁴⁵ (rac) - or (S,S) -Mn(TIPSMcp)⁴⁵ and (S,S) -Mn(dMMpdp)¹¹⁷ were synthesized according to reported procedures.

3.1.2. Synthesis of the substrates

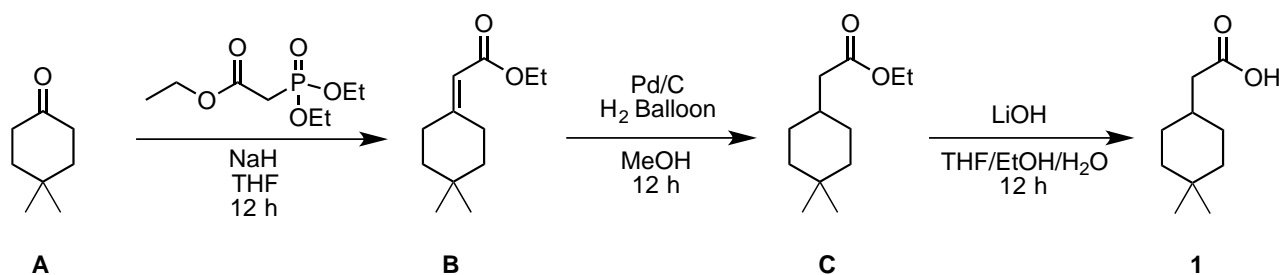
The following substrates were commercially available and purchased by Fluorochem and Sigma-Aldrich and used as received.



The following substrates were synthesized following the **General Procedure A** (see below).



Synthesis of 1



Triethyl phosphonoacetate (5 mmol) was added to a suspension of NaH (5 mmol) in THF (25 mL) cooled at 0 °C. After 30 minutes, the corresponding ketone **A** (4 mmol) is added and the mixture was left warm up to room temperature and stirred overnight. At this point, the reaction was quenched by adding 25 mL of water. The organic phase was separated while the aqueous one was extracted three times with Et₂O (3 x 25 mL). The combined organic layers were dried over anhydrous MgSO₄ and concentrated. The resultant compound **B** was used directly in the next step without further purification.

In a two-neck round bottom flask, a 0.1 M solution of **B** in MeOH was purged with nitrogen for 2 minutes. Palladium on carbon (10% by weight solid) was added under a flow of nitrogen. Then, the flask was then evacuated and back-filled with hydrogen three times before leaving to stir under an atmosphere of hydrogen (balloon). The reaction was monitored by TLC and after the consumption of the corresponding alkene the balloon of hydrogen was removed, and the flask was evacuated and back-filled with nitrogen three

times before opening the reaction to air. The reaction mixture was filtered over a pad of Celite, rinsing with ethyl acetate. The filtrate was concentrated under reduced pressure to obtain C which was used in the next step without further purification.

To a solution of C (2.75 mmol) in 15 mL of THF, 15 mL of EtOH, and 1 mL of H₂O was added LiOH·H₂O (3.29 mmol). The reaction mixture was heated to reflux 12 hours. The reaction was cooled to room temperature and quenched with 0.1 N aqueous HCl. The reaction volume was reduced to ~ 2 mL by rotary evaporation under reduced pressure and the aqueous phase was extracted five times with DCM. The combined organic layers were then washed once with brine, dried over magnesium sulfate, filtered and concentrated. Purification by column chromatography (SiO₂, hexane:EtOAc 15:1) provided the pure carboxylic acid **1** as a pale yellow solid (47% overall yield, 3 steps). ¹H NMR (CDCl₃, 400 MHz) δ: 11.88 (b, 1H), 2.26 (d, J = 7.0 Hz, 2H), 1.79 – 1.67 (m, 1H), 1.65 – 1.53 (m, 2H), 1.44 – 1.31 (m, 2H), 1.27 – 1.14 (m, 4H), 0.89 (d, J = 8.0 Hz, 6H).

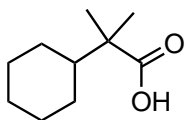
¹³C NMR δ: 180.1, 41.6, 38.7, 34.6, 32.6, 32.6, 29.7, 28.7, 24.4.

General Procedure A



R= cyclohexane, cyclopentane, ethyl

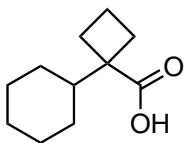
A solution of the corresponding carboxylic acid (5.0 mmol, 1.0 equiv) in THF (2 mL) was added dropwise to a lithium diisopropylamide (1 M in THF, 11 mmol, 2.2 equiv) at -80 °C (AcOEt/N₂ bath). The resulting solution was allowed to warm to room temperature and stirred for 1 h. After the addition of alkyl iodide (5.0 mmol, 1.0 equiv) in THF (2 mL) at -80 °C, the reaction mixture was stirred for 12 h at room temperature, then poured into 2 N HCl (10 mL) and extracted with EtOAc. The combined organic layers were washed with brine, dried over anhydrous MgSO₄, filtered and concentrated. Purification by silica gel flash chromatography with ethyl acetate:hexane eluent mixture provided the pure carboxylic acid.



3: Following the general procedure A, the crude mixture was purified by column chromatography (SiO₂, hexane:EtOAc 15:1) affording the desired product as a white solid (65% yield).

¹H NMR (CDCl₃, 400 MHz) δ: 12.39 (b, 1H), 1.78 (dt, J = 12.8, 3.1 Hz, 2H), 1.64 (s, 4H), 1.36 – 1.15 (m, 3H), 1.13 (s, 6H), 1.08 – 0.96 (m, 2H).

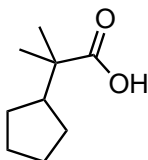
¹³C NMR δ: 185.6, 45.6, 45.1, 27.7, 26.8, 26.5, 21.7.



4: Following the general procedure A, the crude mixture was purified by column chromatography (SiO₂, hexane:EtOAc 15:1) affording the desired product as a white solid (34% yield).

¹H NMR (CDCl₃, 400 MHz) δ: 2.41 (m, 2H), 2.09 (m, 2H), 1.97 – 1.55 (m, 8H), 1.39 – 0.88 (m, 6H).

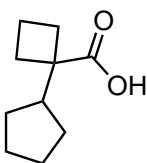
¹³C NMR δ: 184.2, 51.8, 44.4, 28.1, 27.4, 26.6, 26.4, 15.6.



7: Following the general procedure A, the crude mixture was purified by column chromatography (SiO₂, hexane:EtOAc 15:1) affording the desired product as a colorless liquid (45% yield).

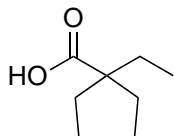
¹H-NMR (CDCl₃, 400 MHz) δ: 2.25 – 2.10 (m, 1H), 1.78 – 1.48 (m, 6H), 1.34 (m, 2H), 1.19 (s, 6H).

¹³C-NMR δ: 183.4, 47.6, 29.7, 27.4, 25.6, 22.5.



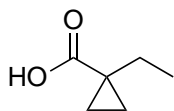
8: Following the general procedure A, the crude mixture was purified by column chromatography (SiO₂, hexane:EtOAc 20:1) affording the desired product as a yellowish solid (49% yield).

^1H NMR (CDCl_3 , 400 MHz) δ : 11.70 (b, 1H), 2.48 – 2.37 (m, 2H), 2.37 – 2.28 (m, 1H), 2.12 – 2.01 (m, 2H), 1.99 – 1.82 (m, 2H), 1.82 – 1.71 (m, 2H), 1.70 – 1.51 (m, 4H), 1.44 – 1.31 (m, 2H).
 ^{13}C NMR δ : 184.6, 49.9, 45.2, 27.7, 27.5, 25.5, 15.4.



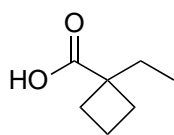
21: Following the general procedure A, the crude mixture was purified by column chromatography (SiO_2 , hexane:EtOAc 20:1) affording the desired product as a white solid (58% yield).

^1H NMR (400 MHz, CDCl_3) δ : 11.37 (b, 1H), 1.60 (q, $J = 7.5$ Hz, 6H), 0.81 (t, $J = 7.5$ Hz, 9H).
 ^{13}C NMR δ : 183.4, 49.8, 26.0, 8.28.



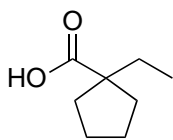
22 Following the general procedure A, the crude mixture was purified by column chromatography (SiO_2 , hexane:EtOAc 20:1) affording the desired product as a yellowish semi solid (16% yield).

^1H NMR (400 MHz, CDCl_3) δ : 11.86 (b, 1H), 1.56 (q, $J = 7.3$ Hz, 2H), 1.26 (q, $J = 3.9$ Hz, 2H), 1.01 (t, $J = 7.3$ Hz, 3H), 0.78 – 0.72 (q, 2H).
 ^{13}C NMR δ : 182.1, 26.5, 24.3, 16.2, 11.7.



23: Following the general procedure A, the crude mixture was purified by column chromatography (SiO_2 , hexane:EtOAc 20:1) affording the desired product as a yellowish semi solid (32% yield).

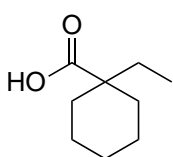
^1H NMR (400 MHz, CDCl_3) δ : 11.39 (b, 1H), 2.54 – 2.35 (m, 2H), 1.97 – 1.86 (m, 4H), 1.83 (q, $J = 7.4$ Hz, 2H), 0.88 (t, $J = 7.4$ Hz, 3H).
 ^{13}C NMR δ : 183.84, 48.12, 30.54, 29.51, 15.41, 9.04.



24: Following the general procedure A, the crude mixture was purified by column chromatography (SiO₂, hexane:EtOAc 20:1) affording the desired product was obtained as a white solid (51% yield).

¹H NMR (400 MHz, CDCl₃) δ 11.71 (b, 1H), 2.20 – 2.05 (m, 2H), 1.74 – 1.58 (m, 6H), 1.50 (m, 2H), 0.90 (t, J = 7.4 Hz, 3H).

¹³C NMR δ: 184.67, 184.61, 54.46, 35.61, 31.74, 25.11, 10.20.

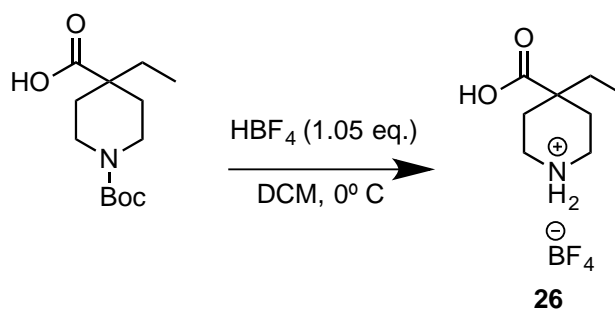


25: Following the general procedure A, the crude mixture was purified by column chromatography (SiO₂, hexane:EtOAc 20:1) affording the desired product was obtained as a white solid (68% yield).

¹H NMR (400 MHz, CDCl₃) δ: 11.26 (b, 1H), 2.12 – 2.00 (m, 2H), 1.58 (m, 5H), 1.41 (m, 2H), 1.30 – 1.15 (m, 3H), 0.86 (t, J = 7.5 Hz, 3H).

¹³C NMR δ: 183.05, 47.18, 33.52, 33.04, 25.97, 23.22, 8.49.

Synthesis of 26



1-(*tert*-butoxycarbonyl)-4-ethylpiperidine-4-carboxylic acid (103 mg, 0.4 mmol) was dissolved in anhydrous CH₂Cl₂ (4 mL) under nitrogen atmosphere at 0 °C. Then, a solution of HBF₄·Et₂O (0.42 mmol, 1.05 eq.) in anhydrous CH₂Cl₂ (1 mL) was added dropwise. After 5 minutes, the solvent was evacuated under reduced pressure. The off-white solid was washed with Et₂O (4 mL) multiple times and then dried under high vacuum for 2 hours.

Recrystallization from hot MeCN afforded **26** as white solid (95% yield), which was used directly in the oxidation reaction.

3.2. Oxidation reaction

3.2.1 General oxidation protocol A (methylenic C-H lactonization of carboxylic acids)

Substrate (100 μmol , 1 molar equivalent) and catalyst (1.0 μmol , 1 mol%) were dissolved in 4.0 mL of TFE inside a 12-mL vial equipped with a magnetic stirring bar. A 0.9 M solution of H_2O_2 in TFE (1.5 molar equivalent) diluted from commercially available H_2O_2 water solution (50% w/w, Sigma Aldrich) and 0.09 M solution of triflic acid (0.1 molar equivalents) were delivered independently over 30 minutes by syringe pump into the solution under air. At the end of the addition, the mixture was left under stirring for additional 30 minutes to ensure complete lactonization. *Workup for GC analysis:* 50 μmol of the internal standard (biphenyl) were added and the mixture was quickly filtered through a short plug of silica gel, which was subsequently rinsed with EtOAc. GC analysis of the filtrate provided substrate conversion and product yields relative to the internal standard integration (calibration constant of the substrate was used for the yield determination of those products which were not isolated). *Ee's* were determined by GC equipped with a chiral column. *Workup for isolation or $^1\text{H-NMR}$ analysis:* The solvent was removed under reduced pressure and the resultant crude was dissolved in EtOAc and washed with a saturated Na_2CO_3 aqueous solution. The organic phases were collected, dried over MgSO_4 and the solvent removed by rotatory evaporation, to yield the lactone (or mixture of lactones) along with minor impurities mainly coming from the ligand. Afterward, the products were analyzed by GC to determinate the enantiomeric excess and the product distribution. ^1H NMR, ^{13}C NMR, HSQC, COSY and Selective TOCSY experiments were employed for the characterization of the lactones while selective NOESY experiments were performed for the diastereoisomers identification.

3.2.2. General oxidation protocol B (Primary C-H lactonization of carboxylic acids)

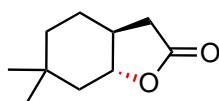
Substrate (100 μmol , 1 molar equivalent) and catalyst (2.0 μmol , 2 mol%) were dissolved in 4.0 mL of TFE inside a 12-mL vial equipped with a magnetic stirring bar. A 0.9 M solution of H_2O_2 in TFE (1.5 molar equivalent) diluted from commercially available H_2O_2 water

solution (50% w/w, Sigma Aldrich) was delivered over 30 minutes by syringe pump into the solution under air. At the end of the addition, the mixture was left under stirring for additional 15 minutes to ensure complete lactonization. *Workup for GC analysis:* 50 μmol of the internal standard (biphenyl) were added and the mixture was quickly filtered through a short plug of silica gel, which was subsequently rinsed with EtOAc. GC analysis of the filtrate provided substrate conversion and product yields relative to the internal standard integration. *Ee's* were determined by GC equipped with a chiral column. *0.3-0.5 mmol catalysis scale for isolation:* The solvent was removed under reduced pressure and the resultant crude was dissolved in EtOAc and washed with a saturated Na_2CO_3 aqueous solution. The organic phases were collected, dried over MgSO_4 and the solvent removed by rotatory evaporation, to yield the crude lactone (or mixture of lactones) along with minor impurities mainly coming from the ligand. After purification by column chromatography, ^1H NMR and ^{13}C NMR (eventually HSQC, COSY and Selective TOCSY) analyses were employed for the characterization of the lactones.

3.3. Characterization of the lactone products

Oxidation of 1

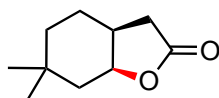
General oxidation protocol A. The lactone products, obtained as a mixture of diastereoisomers, were identified by spectroscopic analyses which were in agreement to those previously reported.¹¹⁸



1a (major product)

^1H NMR (CDCl_3 , 400 MHz) δ : ^1H NMR (400 MHz, CDCl_3) δ 3.98 (ddd, $J = 12.1, 10.4, 3.9$ Hz, 1H), 2.57 – 2.47 (m, 1H), 2.24 (dd, $J = 16.2, 13.1$ Hz, 1H), 1.97 (m, 1H), 1.88 – 1.76 (m, 2H), 1.50 (m, 1H), 1.46 – 1.38 (m, 1H), 1.32 (dd, $J = 12.8, 4.0$ Hz, 1H), 1.28 – 1.23 (m, 1H), 1.04 (s, 3H), 1.00 (s, 3H).

^{13}C NMR δ : 176.9, 82.6, 45.3, 42.6, 38.9, 35.8, 33.1, 32.9, 26.0, 24.7.

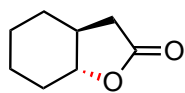
**1b (minor product)**

$^1\text{H NMR}$ (CDCl_3 , 400 MHz) δ : $^1\text{H NMR}$ (400 MHz, CDCl_3) δ 4.60 (m, 1H), 2.62– 2.51 (dd, J = 16 Hz, 1H), 2.46 (m, 1H), 2.36-2.30 (dd, J = 16.0 and 5.1 Hz, 1H) 1.71 (dd, J = 14.7, 5.8 Hz, 1H), 1.65 – 1.55 (m, 1H), 1.53 (dd, J = 15.0 and 5.3 Hz, 1H), 1.47 (m, 1H), 1.42 (m, 1H), 1.27 (m, 1H), 0.98 (s, 3H), 0.93 (s, 3H).

$^{13}\text{C NMR}$ δ : 177.7, 79.3, 40.0, 35.4, 35.0, 34.2, 29.4, 28.5, 28.4, 22.9.

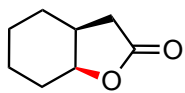
Oxidation of 2

General oxidation protocol A. The lactone products, obtained as a mixture of diastereoisomers, were identified by spectroscopic analyses which were in agreement to those previously reported.⁸⁹

**2a (major product)**

$^1\text{H NMR}$ (CDCl_3 , 400 MHz) δ : 3.79 (ddd, J = 11.4, 10.3, 3.8 Hz, 1H), 2.51 (dd, J = 16.2, 6.4 Hz, 1H), 2.24-2.26 (dd, J = 16.2, 13.0, 1 H), 2.00–1.20 (m, 9 H)

$^{13}\text{C NMR}$ δ : 176.6, 85.2, 44.8, 35.9, 30.2, 28.4, 25.3, 24.1.

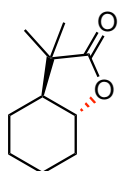
**2b (minor product)**

$^1\text{H NMR}$ (CDCl_3 , 400 MHz) δ : 4.53 (ddd, J = 4.2 Hz, 1H), 2.63 (dd, J = 16.7, 6.9 Hz, 1H), 2.44 – 2.18 (m, 2H), 2.10 (dd, J = 14.7, 4.3 Hz, 1H), 1.81 – 1.58 (m, 3H), 1.56 – 1.38 (m, 2H), 1.29 (m, 2H).

$^{13}\text{C NMR}$ δ : 177.6, 79.1, 37.5, 34.9, 27.8, 27.1, 22.8, 19.9.

Oxidation of 3

General oxidation protocol A. The lactone products, obtained as a mixture of diastereoisomers, were identified by spectroscopic analyses which were in agreement to those previously reported.¹¹⁹ **3b** could not be fully characterized due to the low yield.

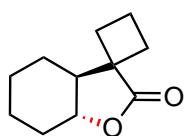
**3a (main product)**

$^1\text{H NMR}$ (CDCl_3 , 400 MHz) δ : 3.90 (td, $J = 10.6, 3.9$ Hz, 1H), 2.32 – 2.19 (m, 1H), 1.99 – 1.89 (m, 1H), 1.88 – 1.81 (m, 1H), 1.78 – 1.70 (m, 1H), 1.69 – 1.56 (m, 1H), 1.54 – 1.45 (m, 1H), 1.45 – 1.26 (m, 3H), 1.23 (d, $J = 1.4$ Hz, 3H), 1.09 (d, $J = 1.3$ Hz, 3H).

$^{13}\text{C NMR}$ δ : 182.3, 80.4, 54.3, 42.2, 30.7, 25.3, 24.4, 23.7, 23.4, 17.3.

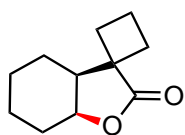
Oxidation of 4

General oxidation protocol A. The lactone products, obtained as a mixture of diastereoisomers, were identified and characterized by spectroscopic analyses.

**4a (minor product)**

$^1\text{H NMR}$ (CDCl_3 , 400 MHz) δ : 3.69 (td, $J = 10.9, 4.0$ Hz, 1H), 2.44 – 2.29 (m, 2H), 2.24–1.87 (m, 8H), 1.69 (m, 1H), 1.56 – 1.32 (m, 4H).

$^{13}\text{C NMR}$ δ : 181.1, 80.3, 51.0, 47.4, 30.4, 25.6, 25.1, 24.4, 24.2, 24.0, 16.6

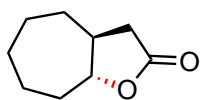
**4b (major product)**

$^1\text{H NMR}$ (CDCl_3 , 400 MHz) δ : 4.45 (m, 1H), 2.60 – 2.48 (m, 2H), 2.27 – 2.07 (m, 5H), 2.02 – 1.68 (m, 3H), 1.56 (m, 2H), 1.38 (m, 1H), 1.20 (m, 1H), 0.97 – 0.83 (m, 1H).

$^{13}\text{C NMR}$ δ : 181.4, 75.2, 51.8, 44.2, 30.8, 27.5, 23.4, 23.3, 23.1, 19.5, 16.2

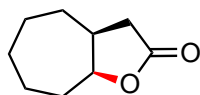
Oxidation of 5

General oxidation protocol A. The lactone products, obtained as a mixture of diastereoisomers, were identified by spectroscopic analyses which were in agreement to those previously reported.¹²⁰

**5a (major product):**

^1H NMR (CDCl_3 , 400 MHz) δ : 4.20 (td, $J = 10.0, 4.9$ Hz, 1H), 2.67 – 2.60 (m, 1H), 2.39 – 2.20 (m, 3H), 1.77 – 1.70 (m, 2H), 1.69 – 1.46 (m, 7H).

^{13}C NMR δ : 176.6, 85.8, 42.3, 37.4, 32.9, 30.1, 27.7, 25.2, 24.8.

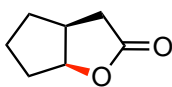
**5b (minor product):**

^1H NMR (CDCl_3 , 400 MHz) δ : 4.67 (m, 1H), 2.83 – 2.68 (m, 2H), 2.25 – 2.20 (m, 1H), 2.13 – 2.05 (m, 1H), 1.45 – 1.17 (m, 9H).

^{13}C NMR δ : 176.9, 84.4, 39.0, 36.5, 31.0, 30.9, 30.7, 27.8, 24.0.

Oxidation of 6

General oxidation protocol A. The lactone product **6b** was identified by spectroscopic analyses which were in agreement to those previously reported.¹²¹

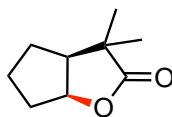


6b: ^1H NMR (CDCl_3 , 400 MHz) δ : 5.01 (m, 1H), 2.91 – 2.78 (m, 2H), 2.33 – 2.26 (m, 1H), 2.08 – 2.02 (m, 1H), 1.90 – 1.84 (m, 1H), 1.76 – 1.68 (m, 3H), 1.58 – 1.49 (m, 1H).

^{13}C NMR δ : 178.0, 86.5, 38.0, 36.1, 33.6, 33.5, 23.4.

Oxidation of 7

General oxidation protocol A. The lactone product **7b** was identified by spectroscopic analyses which were in agreement to those previously reported.¹¹⁹

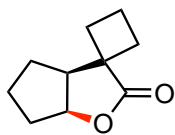


7b: ^1H NMR (CDCl_3 , 400 MHz) δ : 4.94 (td, $J = 5.8, 1.9$ Hz, 1H), 2.41 (m, 1H), 1.85 – 1.69 (m, 6H), 1.26 (s, 3H), 1.20 (s, 3H).

^{13}C NMR δ : 181.9, 82.9, 51.7, 42.9, 32.7, 27.3, 24.5, 21.1, 20.4.

Oxidation of 8

General oxidation protocol A. The lactone product **8b** was identified and characterized by spectroscopic analyses.

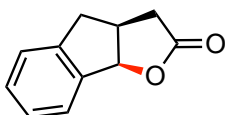


8b: ^1H NMR (CDCl_3 , 400 MHz) δ : δ 4.86 (td, $J = 5.4, 1.5$ Hz, 1H), 2.74 (dt, $J = 9.4, 5.8$ Hz, 1H), 2.50 – 2.35 (m, 2H), 2.28 – 1.90 (m, 5H), 1.88 – 1.75 (m, 2H), 1.69 – 1.60 (m, 2H), 1.49 (dt, $J = 12.7, 6.2$ Hz, 1H).

^{13}C NMR δ : 181.5, 83.3, 50.5, 48.2, 34.0, 33.4, 27.5, 25.8, 23.8, 16.3.

Oxidation of 9

General oxidation protocol A. The lactone product **9b** was identified by spectroscopic analyses which were in agreement to those previously reported.¹²²

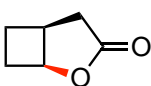


9b: ^1H NMR (CDCl_3 , 400 MHz) δ : 7.49 (d, $J = 7.3$ Hz, 1H), 7.39 – 7.26 (m, 3H), 5.90 (d, $J = 7.0$ Hz, 1H), 3.44 – 3.26 (m, 2H), 2.97 – 2.85 (m, 2H), 2.45 – 2.34 (m, 1H).

^{13}C NMR δ : 176.9, 142.5, 138.8, 130.0, 127.6, 126.4, 125.3, 87.7, 37.9, 37.4, 35.7.

Oxidation of 10

General oxidation protocol A. The lactone product **10b** was identified and characterized by spectroscopic analysis.



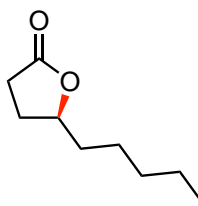
10b: ^1H NMR (CDCl_3 , 400 MHz) δ : 4.99 (ddt, $J = 6.0, 4.0, 2.0$ Hz, 1H), 3.20 (m, 1H), 2.78 – 2.66 (m, 1H), 2.56 – 2.44 (m, 2H), 2.35 (m, $J = 15.5, 10.0, 8.2, 3.8$ Hz, 1H), 2.24 – 2.17 (m, 1H), 1.94 – 1.86 (m, 1H).

^{13}C NMR δ : 178.7, 80.3, 35.8, 34.1, 28.3, 24.4.

Oxidation of 12

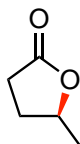
General oxidation protocol A. The lactone product **12a** was identified by spectroscopic analysis which were in agreement to those previously reported.

Purification by column chromatography (SiO_2 , hexane:EtOAc 10:1) afforded pure **12a** (74% yield).



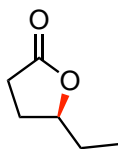
12a: ^1H NMR (400 MHz, CDCl_3) δ : 4.55 - 4.42 (m, 1H), 2.53 (d, J = 6.6 Hz, 1H), 2.52 (d, J = 7.0 Hz, 1H), 2.34-2.33 (m, 1H), 1.86-1.33 (m, 9H), 0.90 (t, J = 7.0 Hz, 3H).

Oxidation of 13



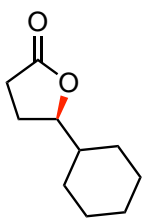
13a: *General oxidation protocol A*. The lactone product was identified by spectroscopic analyses which were in agreement to those previously reported.¹²³

Oxidation of 14



14a: *General oxidation protocol A*. The lactone product was identified by spectroscopic analyses which were in agreement to those previously reported.¹²⁴

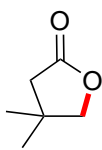
Oxidation of 15



15a: *General oxidation protocol A*. The lactone product was identified by spectroscopic analyses which were in agreement to those previously reported.¹²¹

Oxidation of 16

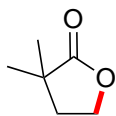
General oxidation protocol B. The desired product **16a** was obtained after column chromatography (SiO_2 , hexane:EtOAc 15:1) as a colorless oil (64% yield).



16a: ^1H NMR (400 MHz, CDCl_3) δ : 4.00 (s, 2H), 2.35 (s, 2H), 1.22 (s, 6H), 0.96 (t, 6H).
 ^{13}C NMR δ : 177.1, 79.6, 43.1, 36.7, 25.9.

Oxidation of 20

General oxidation protocol B. The desired product **20a** was obtained after column chromatography (SiO₂, hexane:EtOAc 15:1) as a colorless oil (59% yield).

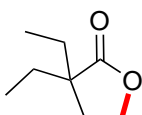


20a: ¹H NMR (400 MHz, CDCl₃) δ: 4.26 (t, J = 7.2 Hz, 2 H), 2.11 (t, J = 7.2 Hz, 2 H), 1.26 (s, 6 H).

¹³C NMR δ: 182.3, 64.7, 37.1, 24.2.

Oxidation of 21

General oxidation protocol B. Pure sample of the desired product **21a** was obtained after column chromatography (SiO₂, hexane:EtOAc 5:1) as a colorless oil.

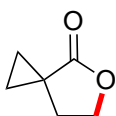


21a: ¹H NMR (400 MHz, CDCl₃) δ: 4.26 (t, J = 7.4 Hz, 2H), 2.14 (t, J = 7.4 Hz, 2H), 1.66 (q, J = 7.5, 1.5 Hz, 4H), 0.96 (t, J = 7.5 Hz, 6H).

¹³C NMR δ: 181.3, 65.2, 46.8, 31.2, 28.5, 8.7.

Oxidation of 22

General oxidation protocol B. Pure sample of the desired product **22a** was obtained after column chromatography (SiO₂, hexane:EtOAc 15:1) as a pale yellow oil.

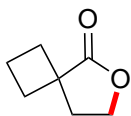


22a: ¹H NMR (400 MHz, CDCl₃) δ: 4.43 (t, J = 7.4 Hz, 2H), 2.32 (t, J = 7.5 Hz, 2H), 1.26 (m, 2H), 1.01 - 0.96 (m, 2H).

¹³C NMR δ: 180.2, 65.7, 29.7, 19.7, 15.1.

Oxidation of 23

General oxidation protocol B. The desired product **23a** was obtained after column chromatography (SiO₂, hexane:EtOAc 15:1) as a colorless oil (54% yield).

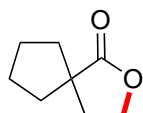


23a: ¹H NMR (400 MHz, CDCl₃) δ: 4.20 (t, J = 6.9 Hz, 2H), 2.56 - 2.44 (m, 2H), 2.35 (t, J = 6.9 Hz, 2H), 2.20 - 1.99 (m, 4H).

^{13}C NMR δ : 181.3, 65.1, 43.1, 36.0, 30.1, 16.4

Oxidation of 24

General oxidation protocol B. The lactone products were obtained, after column chromatography (SiO_2 , hexane:EtOAc 10:1), as a mixture of isomers. Colorless oil (53% yield).

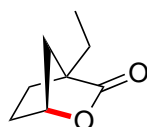


24a

minor product **24a**: ^1H NMR (400 MHz, CDCl_3) δ : 4.25 (t, $J=6.9$ Hz, 2H), 2.14 (t, $J=6.9$ Hz, 2H), 1.95-2.10 (m, 2H), 1.8-1.9 (m, 2H), 1.65-1.72 (m, 4H).

^{13}C NMR δ : 182.9, 65.5, 48.6, 36.9, 36.6, 25.5.

HRMS(ESI+) m/z calculated for $\text{C}_{10}\text{H}_{18}\text{O}_2$ $[\text{M}+\text{Na}]^+$



24b

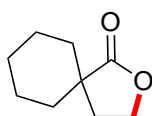
major product **24b**: ^1H NMR (400 MHz, CDCl_3) δ : 4.86 (d, $J = 2.4$ Hz, 1H), 2.06 (dd, $J = 10.2, 2.3$ Hz, 1H), 1.98 - 1.92 (m, 1H), 1.94-1.85 (m, 1H), 1.80 - 1.67 (m, 1H), 1.03 (t, $J = 7.5$ Hz, 3H), 1.81 (ddd, $J = 12.6, 9.5, 6.4$ Hz, 0H), 1.65 - 1.53 (m, 2H).

^{13}C NMR δ : 179.6, 79.2, 52.3, 42.6, 29.5, 27.8, 21.6, 9.8.

HRMS(ESI+) m/z calculated for $\text{C}_{10}\text{H}_{18}\text{O}_2$ $[\text{M}+\text{Na}]^+$

Oxidation of 25

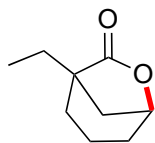
General oxidation protocol B. The lactone products were obtained, after column chromatography (SiO_2 , hexane:EtOAc 10:1), as a mixture of isomers. Colorless semisolid (62% yield).



25a

minor product **25a**: ^1H NMR (400 MHz, CDCl_3) δ : 4.27 (t, $J = 7.1$ Hz, 2H), 2.17 (d, $J = 7.1$ Hz, 2H), 1.79 - 1.64 (m, 5H), 1.54 - 1.53 (m, 2H), 1.44 - 1.31 (m, 3H).

^{13}C NMR δ : 182.0, 65.1, 43.1, 33.1, 32.4, 25.3, 22.2.



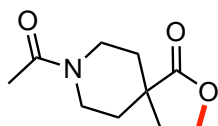
25b

major product **25b**: ^1H NMR (400 MHz, CDCl_3) δ : 4.78 (m, 1H), 2.31 (m, 1H), 2.06 – 1.95 (m, 1H), 1.87 – 1.72 (m, 2H), 1.67 – 1.50 (m, 6H), 0.92 (t, $J = 7.5$ Hz, 3H).

^{13}C NMR δ : 180.1, 75.7, 46.7, 40.2, 32.5, 27.8, 27.0, 18.7, 8.6.

Oxidation of 26

General oxidation protocol B. The desired product was obtained as the acetyl derivate **26aAc**. After column chromatography (SiO_2 , hexane:EtOAc 5:1), the product was obtained as a white solid (46% yield).



26aAc: ^1H NMR (400 MHz, CDCl_3) δ : δ 4.33 (t, $J = 7.3$ Hz, 2H), 4.09 (m, 1H), 3.84 (m, 1H), 3.35 (m, 2H), 2.28 – 2.17 (m, 2H), 2.11 (s, 3H), 2.00 – 1.83 (m, 2H), 1.65 – 1.54 (m, 2H).

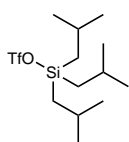
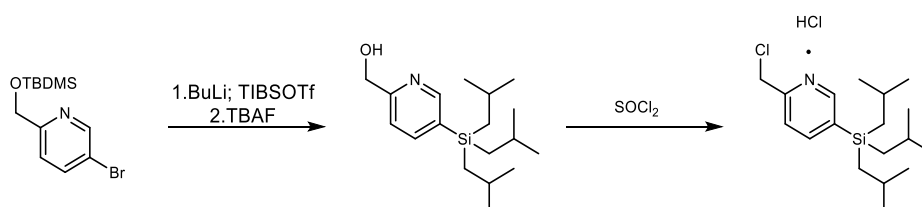
^{13}C NMR δ : 179.9, 168.9, 64.9, 42.8, 41.0, 37.8, 33.9, 32.8, 31.7, 21.4.

Experimental section Chapter IV

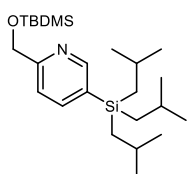
4.1. Synthesis of the complexes

4.1.1 Synthesis of the pyridine synthons

5-bromo-2-(((*tert*-butyldimethylsilyl)oxy)methyl)pyridine was synthesized following a previously reported procedure.⁴¹

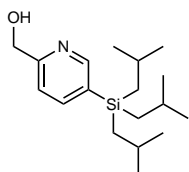


Generation in situ of triisobutylsilyl trifluoromethanesulfonate: A flame-dried schlenk tube, equipped with a magnetic stir bar, was charged with triisobutylsilane (1.2 mL, 1 eq) under nitrogen atmosphere and cooled down in an ice bath. Triflic acid (0.95 eq, 0.384 mL) was added dropwise in 10 minutes (*Caution! H₂ is formed in situ*) and the mixture was left warming up to room temperature and then left under stirring overnight. Afterwards, the schlenk tube was cooled down again in an ice bath and the colorless solution was used directly in the further step.



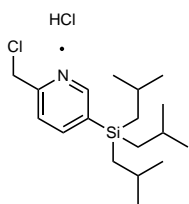
TIBS-Py-CH₂-OTBDMS: 5-bromo-2-(((*tert*-butyldimethylsilyl)oxy)methyl)pyridine⁴¹ (1.2 g, 3.97 mmol) was dissolved in 11 mL of anhydrous diethyl ether under inert atmosphere and cooled to -80 °C in an ethyl acetate/liquid N₂ bath. Then 1 eq. of *n*-BuLi (1.6 M in hexanes, 2.5 mL) were added dropwise over 10 min, and the reaction mixture was let stir for 45 min. After this time, 1 eq. of freshly prepared triisobutylsilyl trifluoromethanesulfonate (1.1 eq., 4.35 mmol) was added all at once at -80 °C under N₂, and left stirring for another hour. The temperature was left warming up to -15 °C, and the reaction was carefully quenched with 10 mL of H₂O. The mixture was extracted with diethyl ether (3 x 10 mL), the combined organic layers were washed with 10 mL of brine, dried over MgSO₄, concentrated on a rotatory evaporator. The crude product was purified by flash column chromatography (petroleum ether/EtOAc 10:1) to obtain the desired compound as a slight yellow oil (1.1 g, 66%). ¹H NMR (400 MHz, CDCl₃): δ 8.55 (s, 1H), 7.80 (d, J = 7.7 Hz, 1H), 7.45 (d, J = 7.7 Hz, 1H), 4.81 (s, 2H), 1.74 (ddd, J = 13.3, 6.7, 1.6 Hz, 3H), 0.95 (s, 9H), 0.87 (dd, J = 6.6, 1.7 Hz, 24H), 0.10 (s, 6H). ¹³C NMR (75

MHz, CDCl₃) δ 162.0, 154.2, 143.3, 132.4, 120.0, 66.8, 27.2, 27.2, 26.7, 25.5, 24.7, 19.1, -4.6.
 HRMS (ESI-MS) *m/z* calculated for C₂₄H₄₇NOSi₂ [M+H]⁺ 422.3269, found 422.3265.



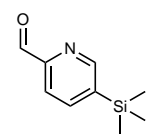
TIBSPyCH₂OH: TIBSPyCH₂OTBDMS (591 mg, 1.4 mmol) was dissolved in THF (7 mL) and cooled down at 0 °C. Then 1.68 mL of TBAF in THF (1.0 M, 1.2 eq) was added dropwise to the solution and the reaction mixture was left stirring for 1 hour at the same temperature. The reaction was quenched with

5 ml of water and extracted with 3 × 10 ml of CH₂Cl₂. The combined organic phases were dried with anhydrous MgSO₄ and the solvent was removed under reduced pressure to yield the crude alcohol which was purified by column chromatography (SiO₂, Hex:EtOAc 5:1→3:1) to yield 410 mg (1.33 mmol, 95%) of the pure product as a yellow solid. ¹H NMR (400 MHz, CDCl₃): δ 8.64 (s, 1H), 7.80 (dd, *J* = 7.7, 1.8 Hz, 1H), 7.22 (d, *J* = 7.7, 0.9 Hz, 1H), 4.77 (s, 2H), 1.78 (hept, *J* = 13.3, 6.7 Hz, 3H), 0.89 (dd, *J* = 6.8, 5.2 Hz, 24H). ¹³C NMR (CDCl₃, 100 MHz): δ 159.6, 154.0, 143.2, 133.3, 120.6, 64.7, 27.2, 25.5, 24.6. HRMS (ESI-MS) *m/z* calculated for C₁₈H₃₃NOSi [M+H]⁺ 308.2404, found 308.2395.



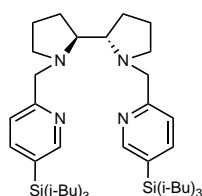
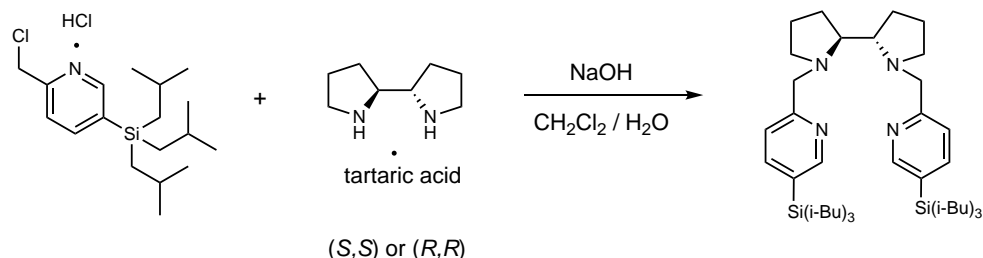
TIBSPyCH₂Cl · HCl: TIBSPyCH₂OH (557 mg, 1.81 mmol) was dissolved in 9 ml of anhydrous CH₂Cl₂ and a solution of SOCl₂ (5 equiv., 9.1 mmol) in anhydrous CH₂Cl₂ (1 ml) was added dropwise at 0°C. The reaction mixture was left stirring overnight at room temperature and then the solvent and the

excess of thionyl chloride was removed under vacuum to yield the desired product as a white solid (638 mg, 1.76 mmol, 97% yield). ¹H NMR (400 MHz, CDCl₃): δ 8.52 (s, 1H), 8.45 (dd, *J* = 7.9, 1.6 Hz, 1H), 8.03 (d, *J* = 7.9 Hz, 1H), 5.13 (s, 2H), 1.65 (hept, *J* = 13.3, 6.7 Hz, 3H), 0.85 (d, *J* = 7.0 Hz, 6H), 0.81 (d, *J* = 6.6 Hz, 18H). ¹³C NMR (CDCl₃, 100 MHz): δ 157.0, 154.8, 143.8, 134.6, 122.7, 47.4, 27.2, 25.5, 24.69. HRMS (ESI-MS) *m/z* calculated for C₁₈H₃₂ClNSi [M+H]⁺ 326.2065, found 326.2059.



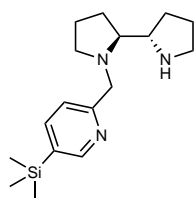
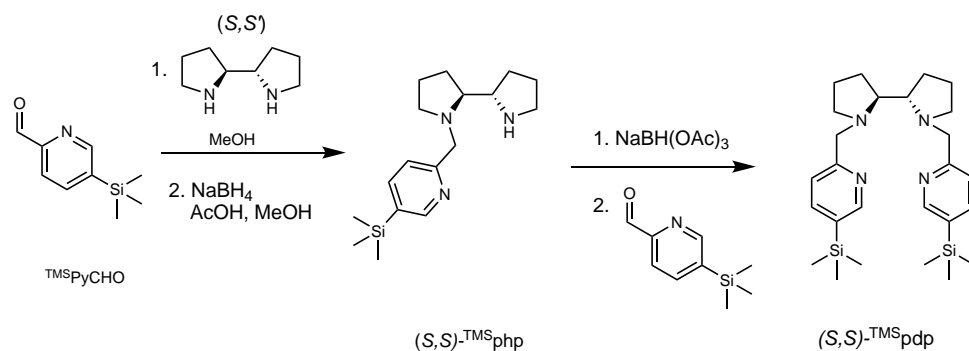
TMS³PyCHO:⁹⁷ 2,5-dibromopyridine (2.4 g, 10 mmol) were dissolved in 30 mL of anhydrous diethyl ether under inert atmosphere and cooled to -80°C in an ethyl acetate/liquid N₂ bath. Then 1 equiv of *n*-BuLi (1.6 M in hexanes, 6.2 mL, 10 mmol) was slowly added over 10 min, and the reaction mixture was let stir for 45 min. At that point, 1.1 equiv of trimethylsilyl chloride (1.4 mL, 11 mmol) were added all at once at -80°C, and the mixture was left stirring for an additional hour. 1.1 equivalents of *n*-BuLi (1.6 M in hexanes, 6.8 mL, 11 mmol) were added over 10 min to the mixture at -80 °C. After additional 45 minutes, 1.6 equivalents of anhydrous DMF (1.3 mL, 16 mmol) were slowly added. The reaction was left stirring for 2h, and the temperature was raised up to -15 °C after that time. At this point, the reaction was quenched with 10 mL of H₂O and extracted with diethyl ether (3 x 30 mL). The combined organic layers were washed with 30 mL of brine, dried over MgSO₄, concentrated on a rotatory evaporator and purified by column chromatography (SiO₂, hexane:EtOAc 10:1) to yield 1.13 g (6.29 mmol, 63%) of the pure product as a yellow oil. ¹H NMR (CDCl₃, 400 MHz): δ, ppm: 10.06 (s, 1H), 8.83 (s, 1H), 7.96 (ddd, J = 7.6, 1.6, 0.8 Hz, 1H), 7.88 (dd, J = 7.6, 1.0 Hz, 1H), 0.33 (s, 9H). ¹³C NMR (CDCl₃, 100 MHz): δ, ppm: 193.8, 154.1, 152.7, 142.1, 141.5, 120.6, 1.53. HRMS (ESI-MS): *m/z* calculated for C₉H₁₄NOSi [M + Na]⁺ 180.0845, found 180.0853.

4.1.2. Synthesis of the ligands



(S,S)-TIBSpdp: A solution containing (S,S)-2,2'-bipyrrrolidine D-tartrate (0.23 g, 0.8 mmol) and NaOH (0.25 g) in H₂O (2 mL) was added to a 10 mL round bottom flask charged with a stir bar and TIBSPyCH₂Cl · HCl (0.4 g, 1.7

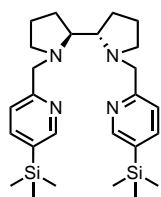
mmol) dissolved in CH_2Cl_2 (5 mL). The combined mixture was left stirring for 24 hours. At this point, the aqueous phase was extracted with CH_2Cl_2 (3 x 5 mL). The organic fractions were combined, dried over MgSO_4 and the solvent was removed under vacuum. The residue was purified by column chromatography (SiO_2 , CH_2Cl_2 : MeOH : NH_3 96:3:1) to provide 272 mg (0.62 mmol, yield 78%) of a yellow oil. ^1H NMR (400 MHz, CDCl_3): δ 8.52 (m, 2H), 7.65 (dd, $J = 7.7, 1.9$ Hz, 2H), 7.28 (dd, $J = 7.7, 0.9$ Hz, 2H), 4.04 (d, $J = 14.1$ Hz, 2H), 3.41 (d, $J = 14.1$ Hz, 2H), 2.97 – 2.85 (m, 2H), 2.73 – 2.62 (m, 2H), 2.21 – 2.08 (m, 2H), 1.77 – 1.56 (m, 14H), 0.80 (dd, $J = 12.7, 6.7$ Hz, 48H). ^{13}C NMR (CDCl_3 , 100 MHz): δ 160.2, 153.7, 142.2, 131.6, 122.2, 65.3, 61.2, 55.5, 26.8, 26.5, 25.7, 24.8, 23.9, 23.5. HRMS (ESI-MS) m/z calculated for $\text{C}_{44}\text{H}_{78}\text{N}_4\text{Si}_2$ $[\text{M}+\text{H}]^+$ 719.5838, found 719.5836.



(S,S)-TMSphp:⁹⁷ To an anhydrous methanol (15 mL) solution of (2*S*,2*S*)-2,2'-bipyrrolide (420 mg, 3.0 mmol), 3 Å molecular sieves (500 mg) were added. TMSPyCHO (540 mg, 3.0 mmol) was then added to this mixture and the reaction was left stirring overnight under N_2 atmosphere. Afterwards, the

solution was cooled to 0 °C and NaBH_4 (1.5 eq., 170 mg, 4.5 mmol) was added portion-wise. At this point, AcOH (4 eq., 0.7 mL, 12 mmol) was added over 15 min and the mixture was left stirring for 2 h at the same temperature. Then the mixture was diluted with EtOAc (50 mL) and hydrolyzed with 15 mL of NaOH 2 M. The aqueous layer was extracted with EtOAc (2 x 30 mL) and CH_2Cl_2 (2 x 30 mL). Finally, the combined organic layers were dried over MgSO_4 and brought to dryness. The desired product was obtained as a white solid (810 mg, 2.7 mmol, 90%). ^1H MR (CDCl_3 , 400 MHz): δ 8.53 (s, 1H), 7.67 (dd, $J = 7.6, 1.5$ Hz, 1H), 7.30 (d, $J = 7.7$ Hz, 1H), 4.23 (d, $J = 14.4$ Hz, 1H), 3.57 (d, $J = 14.4$ Hz, 1H), 3.04-2.67 (m, 5H), 2.35-2.29 (m, 1H), 1.90-1.33 (m, 8H), 0.21 (s, 9H). ^{13}C NMR (CDCl_3 , 100 MHz): δ 160.6, 153.2, 141.6,

132.7, 122.1, 67.9, 63.9, 62.5, 55.1, 46.3, 28.4, 24.8, 34.0, -1.3. HRMS (ESI-MS): m/z calculated for $C_{17}H_{30}N_3Si$ $[M+H]^+$ 304.2209, found 304.2208.

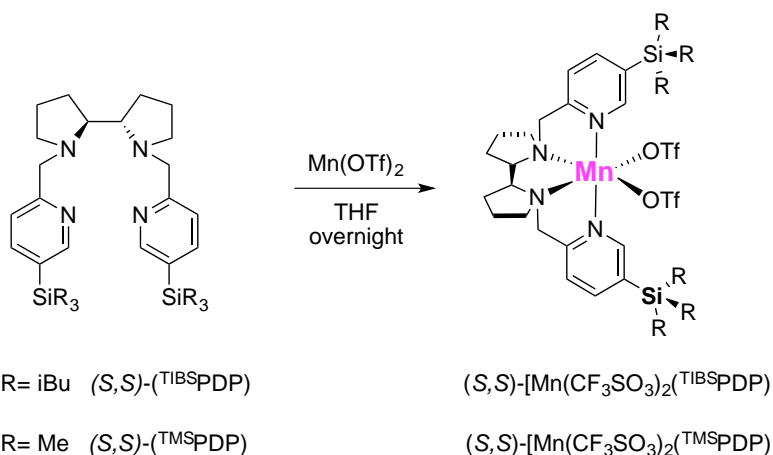


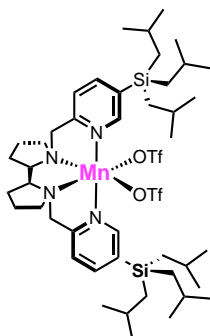
(*S,S*)-TMSpdp:⁹⁷ TMSPyCHO (540 mg, 3.0 mmol) was added to a solution of (*S,S*)-TMSphp (810 mg, 3 mmol) in CH_2Cl_2 (50 mL) at 0 °C. The mixture was left stirring for 30 min at this temperature, and then 1.3 equiv of $NaBH(OAc)_3$ (827 mg, 3.9 mmol) were added, and the reaction was left stirring at room

temperature overnight. 40 mL of a $NaHCO_3$ aqueous saturated solution were added, the mixture was extracted with CH_2Cl_2 (3x40 mL). The combined organic layers were dried over $MgSO_4$ and concentrated under rotatory evaporation. The product was purified by column chromatography (Al_2O_3 , hexane:EtOAc 1:9) to afford 720 mg of a white solid (1.55 mmol, 52%). 1H NMR (CD_3OD , 300 MHz): δ 8.45 (dd, $J = 7.7, 1.7$ Hz, 2H), 7.88 (dd, $J = 7.6, 1.7$ Hz, 2H), 7.49 (d, $J = 7.6$ Hz, 2H), 4.25 (d, $J = 14.4$ Hz, 2H), 3.51 (d, $J = 14.4$ Hz, 2H), 3.00-2.98 (m, 2H), 2.81-2.77 (m, 2H), 2.27-2.24 (m, 2H), 1.97-1.74 (m, 8H), 0.31 (s, 18H). ^{13}C NMR (101 MHz, $CDCl_3$) δ 160.5, 152.9, 141.4, 132.4, 122.0, 65.3, 60.9, 55.2, 25.8, 23.5, -1.3. HRMS (ESI-MS), $[M+H]^+$: m/z calculated for $C_{26}H_{42}N_4Si_2$ 467.3021, found 467.3022.

4.1.3. Synthesis of the complexes

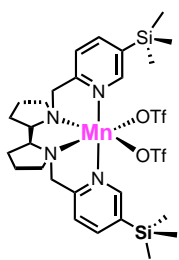
Triflate complexes (*S,S*)-Fe(pdp),²⁷ (*S,S*)-Fe(mcp),⁴⁵ (*S,S*)-Fe(TIPSpdp),¹⁰³ (*S,S*)-Fe(TIPSmcp),¹⁰³ (*S,S*)-Mn(pdp),¹²⁵ (*S,S*)-Mn(mcp),¹²⁶ (*rac*)- or (*S,S*)-Mn(TIPSpdp),⁴⁵ (*S,S*)-Mn(TIPSmcp),⁴⁵ (*S,S*)-Mn(TIPSecp),⁴⁵ (*S,S*)-Mn(dMMpdp)¹¹⁷ and (*S,S*)-Mn(NMe₂pdp)¹¹⁷ were synthesized according to reported procedures.





(*S,S*)-Mn(^{TIBS}pdp): Under N₂ atmosphere, solid Mn(OTf)₂ (46 mg, 0.13 mmol) was added to a vigorously left stirring solution of (*S,S*)-^{TIBS}pdp in anhydrous THF (1 mL) (94 mg, 0.25 mmol). The reaction mixture was left under stirring overnight at room temperature. At this point, the solvent

was removed under reduced pressure and the resulted solid was dissolved in CH₂Cl₂, filtered over a plug of Celite[®] and crystallized under N₂ atmosphere by layering this solution with hexane to obtain, after few days, colorless crystals (100 mg, 0.09 mmol, 71%). Elemental analysis for C₄₆H₇₈F₆MnN₄O₆S₂Si₂: calculated C, 51.52; H, 7.33; N, 5.22. Found C, 51.54; H, 7.42; N, 5.56. HRMS (ESI-MS) for C₄₆H₇₈F₃MnN₄O₆SSi₂: *m/z* calculated [M-OTf]⁺: 922.4660. Found 922.4644. FT-IR (ATR) ν , cm⁻¹: 2953-2867 (C-H sp³) 1594, 1463, 1299, 1215, 1186, 1032, 833, 761, 637, 512.

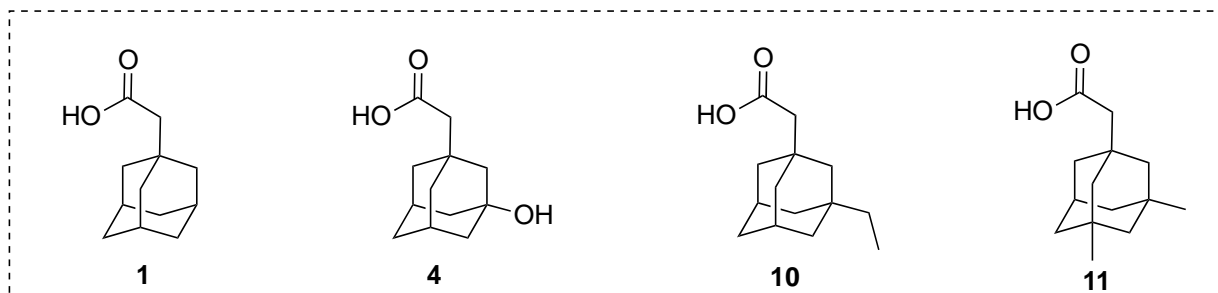


(*S,S*)-Mn(^{TMS}pdp): Under N₂ atmosphere, solid Mn(OTf)₂ (86.5 mg, 0.25 mmol) was added to a vigorously left stirring solution of (*S,S*)-^{TMS}pdp in anhydrous THF (1 mL) (117 mg, 0.25 mmol). The reaction mixture was left under stirring overnight at room temperature. At this point, the solvent was removed under reduced pressure and the resulted solid residue was

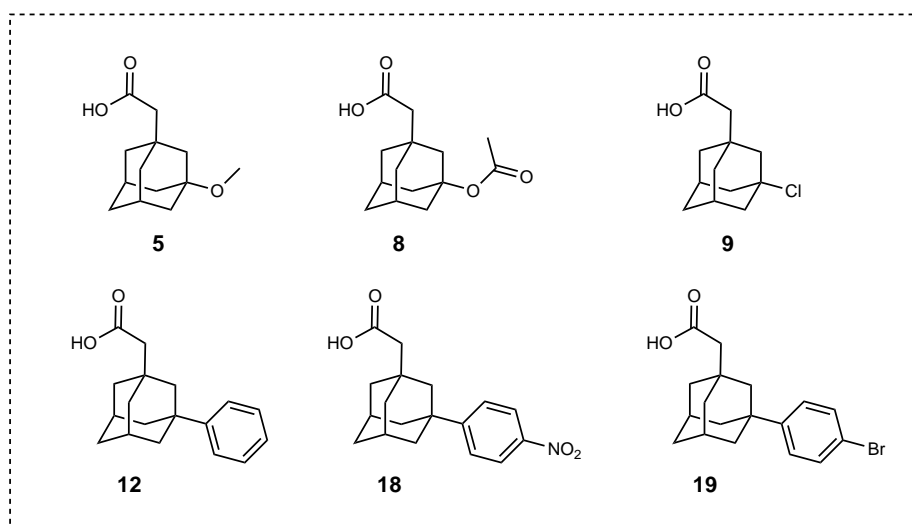
dissolved in CH₂Cl₂, filtered over a plug of Celite[®] and crystallized under N₂ atmosphere by layering this solution with hexane to obtain, after few days, pale brown crystals (81%). Elemental analysis: calculated C₂₈H₄₂F₆MnN₄O₆S₂Si₂: C, 41.02; H, 5.16; N, 6.83. Found C, 41.18; H, 5.12; N, 7.08. HRMS (ESI-MS): calculated *m/z* C₂₈H₄₂F₆MnN₄O₆S₂Si₂ [M-OTf]⁺: 670.1843. Found 670.1859. FT-IR (ATR) ν , cm⁻¹: 2959-2897 (C-H sp³), 1596, 1312, 1236, 1211, 1164, 1024, 833, 758, 634, 514.

4.2. Synthesis of the substrates

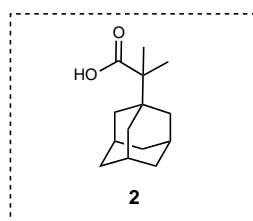
The following substrates are commercially available (Sigma Aldrich, Fluorochem) and were used as received.



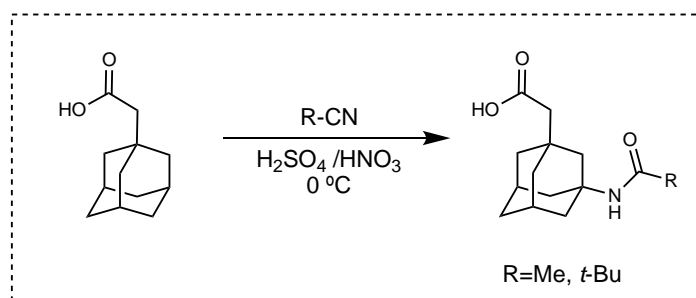
The following substrates were synthesized following reported literature procedures.¹²⁷



The following substrates were synthesized following another reported procedure.¹²⁸

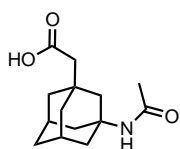


4.2.1. General Procedure A (Synthesis of acids 6, 7)

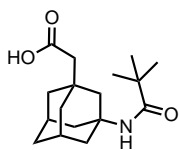


A round-bottom flask equipped with a stirring bar was charged with conc. H₂SO₄ (16 mL) and conc. HNO₃ (4 mL) at 0 °C. 1-Adamantaneacetic acid (1 g, 0.78 mmol) was added

portion-wise into this mixture in 1 hour and stirring was continued for an additional hour. Then, the pertinent nitrile (18 or 23 mL for CH₃CN or *t*-BuCN, respectively) was added dropwise into the reaction mixture and left under stirring for additional 4 hours. At this point, the solution was poured onto ice and extracted with CH₂Cl₂ (3 x 50 mL). The combined organic layers were dried over MgSO₄ and the solvent was evaporated under reduced pressure to give a yellowish solid which was further purified by flash column chromatography (SiO₂, CH₂Cl₂:MeOH 98:2).

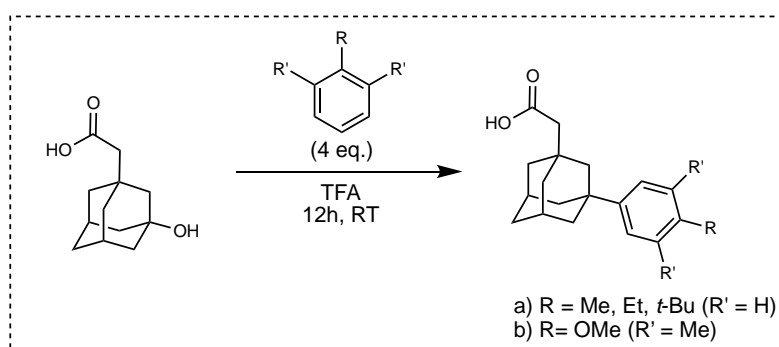


[3-(acetamido)-1-adamantyl]acetic acid (6): Following general procedure A, the product was isolated as a white solid (68%). ¹H NMR (300 MHz, CDCl₃) δ 11.88 (s, 1H), 6.40 (s, 1H), 2.18 – 2.09 (m, 4H), 1.98 (s, 3H), 1.96 – 1.87 (m, 6H), 1.65 – 1.50 (m, 6H). ¹³C NMR δ 176.2, 171.4, 53.2, 47.9, 45.3, 41.0, 40.4, 35.3, 34.3, 29.4, 23.7. HRMS (ESI-MS) *m/z* calculated for C₁₄H₂₁NO₃, [M+Na]⁺ 274.1414, found 274.1412.



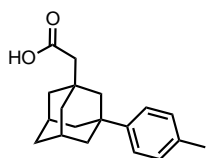
[3-(pivalamido)-1-adamantyl]acetic acid (7): Following general procedure A, the product was isolated as a white solid (56%). ¹H NMR (300 MHz, CDCl₃) δ 5.31 (s, 1H), 2.18 (s, 2H), 2.18 – 2.13 (m, 2H), 2.04 – 1.85 (m, 6H), 1.71 – 1.53 (m, 6H), 1.16 (s, 9H). ¹³C NMR δ 178.8, 177.4, 52.9, 48.4, 46.8, 41.9, 41.5, 39.9, 36.3, 35.3, 30.3, 28.6. HRMS (ESI-MS) *m/z* calculated for C₁₇H₂₇NO₃ [M+Na]⁺ 316.1883, found 316.1875.

4.2.2 General procedure B (Synthesis of acids 13, 14, 15, 16)

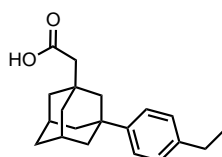


A round-bottom flask equipped with a stirring bar was charged with 3-hydroxyadamantane-1-acetic acid **4** (1 mmol), the corresponding aromatic hydrocarbon (4 mmol) and trifluoroacetic acid (3 mL). The resulting solution was left under stirring

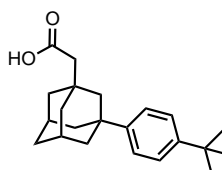
overnight. At this point, water (10 ml) is cautiously added to the reaction mixture and the resulting white suspension is extracted with CH₂Cl₂ (3 x 5ml). The collected organic phases were dried over anhydrous MgSO₄ and then under reduced pressure to give the crude solid which was purified by flash column chromatography or by crystallization with hexane/EtOAc mixtures.



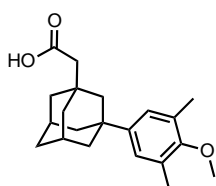
[3-(4-Methylphenyl)-1-adamantyl]acetic acid (12): Following general procedure B, the product was purified by crystallization with hexane/EtOAc mixtures to yield a white solid (67%). Spectral data in agreement with those reported in literature.¹²⁷ ¹H NMR (300 MHz, CDCl₃) δ 7.28 (d, J = 7.9 Hz, 2H), 7.16 (d, J = 7.9 Hz, 2H), 2.35 (s, 3H), 2.22 (m, 4H), 1.94 – 1.63 (m, 12H). ¹³C NMR (75 MHz, CDCl₃) δ 177.7, 147.4, 135.2, 128.9, 124.7, 48.4, 48.0, 42.3, 41.4, 36.7, 35.8, 33.7, 29.2, 20.9.



[3-(4-Ethylphenyl)-1-adamantyl]acetic acid (13): Following general procedure B, the product was purified by flash column chromatography (SiO₂, hexane:EtOAc 2:1) White solid (87%). ¹H NMR (300 MHz, CDCl₃): δ 7.27 (d, J = 8.3 Hz, 2H), 7.15 (d, J = 8.2 Hz, 2H), 2.62 (q, J = 7.6 Hz, 2H), 2.23 – 2.14 (m, 4H), 1.92 – 1.82 (m, 4H), 1.78 (s, 2H), 1.72 – 1.59 (m, 6H), 1.23 (t, J = 7.6 Hz, 3H). ¹³C NMR (300 MHz, CDCl₃): δ 178.1, 148.4, 142.2, 128.3, 125.5, 49.0, 48.7, 43.0, 42.1, 37.4, 36.5, 34.4, 29.9, 29.0, 16.2. HRMS (ESI-MS) *m/z* calculated for C₂₀H₂₆O₂ [M+Na]⁺ 321.1825, found 321.1821.

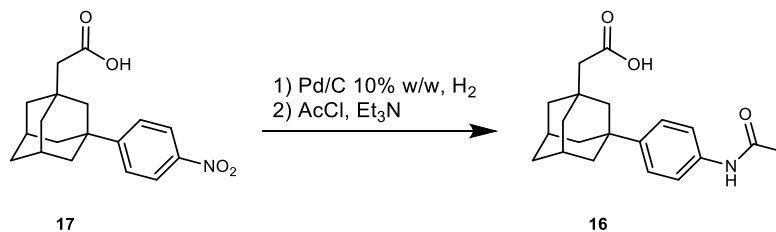


[3-(4-(*tert*-butyl)phenyl)-1-adamantyl]acetic acid (14): Following general procedure A, the product was purified by flash column chromatography (SiO₂, hexane:EtOAc 2:1) to yield a white solid (71%). ¹H NMR (300 MHz, CDCl₃) δ 7.45 – 7.25 (m, 4H), 2.22 (s, 4H), 1.93 – 1.85 (m, 4H), 1.81 (s, 2H), 1.72 (s, 6H), 1.34 (s, 9H). ¹³C NMR (75 MHz, CDCl₃) δ 154.8, 145.6, 130.1, 125.2, 59.6, 48.2, 48.1, 42.3, 41.4, 36.4, 35.8, 33.7, 29.2, 16.4. HRMS (ESI-MS) *m/z* calculated for C₂₂H₃₀O₂ [M+Na]⁺ 349.2138, found 349.2134.



3-(4-methoxy-3,5-dimethylphenyl)adamantan-1-yl)acetic acid (15): Following general procedure A, the product was purified by recrystallization with hexane/EtOAc mixtures as a white solid (51%). ¹H NMR (300 MHz, CDCl₃) δ 6.99 (s, 2H), 3.72 (s, 3H), 2.30 (s, 6H), 2.20 (d, J =

6.6 Hz, 4H), 1.96 – 1.52 (m, 12H). ^{13}C NMR (101 MHz, CDCl_3) δ 154.8, 145.7, 130.1, 125.2, 59.6, 48.3, 48.1, 42.3, 41.4, 36.5, 35.8, 33.7, 29.2, 16.4. HRMS (ESI-MS) m/z calculated for $\text{C}_{21}\text{H}_{28}\text{O}_3$ $[\text{M}+\text{Na}]^+$ 351.1931, found 351.1934.



3-(4-acetamidophenyl)adamantan-1-yl)acetic acid (16): In a two-neck round bottom flask equipped with a magnetic stir bar, a solution of **17** (114 g, 0.361 mmol) in 4 mL of anhydrous MeOH was purged with nitrogen for 2 minutes. Palladium on carbon (12 mg of a 10% by weight solid, 10% w/w) was added under nitrogen. The flask was then evacuated and back-filled with hydrogen gas three times before leaving to stir under an atmosphere of hydrogen (balloon) overnight. The solution was filtered over a pad of Celite, rinsing with ethyl acetate. The filtrate was concentrated to obtain a white solid. To an anhydrous THF (3 mL) solution of this solid (81 mg, 0.284 mmol) under nitrogen acetyl chloride (1.5 eq.) and triethylamine (1 eq.) were added dropwise at 0 °C, and the mixture was left warming up to room temperature and stirring overnight. At this point, saturated aqueous Na_2CO_3 was added until pH ~ 10-11 was reached and the resulting mixture was extracted with EtOAc (3x). The combined organic layers were washed with 1N HCl (1x) and dried over Na_2SO_4 . The solvent was removed under rotatory evaporation to give a solid which was recrystallized with a hexane/ CHCl_3 mixture to yield 60.3 mg of a white crystalline solid (0.184 mmol, 51%, two steps). ^1H NMR (300 MHz, CDCl_3) δ 7.44 (d, J = 8.2 Hz, 2H), 7.31 (d, J = 8.2 Hz, 2H), 2.21 (m, 2H), 2.19 (s, 3H), 1.99 (m, 1H), 1.78 (m, 13H). ^{13}C NMR (101 MHz, CDCl_3) δ 175.9, 168.3, 135.4, 125.4, 119.9, 48.0, 47.7, 42.2, 41.5, 36.7, 35.8, 33.6, 29.2, 28.6, 24.5. HRMS (ESI-MS) m/z calculated for $\text{C}_{20}\text{H}_{25}\text{NO}_3$ $[\text{M}+\text{Na}]^+$ 350.1727, found 350.1716.

4.3. Oxidation Reactions

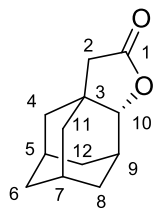
Hydrogen peroxide solutions employed in the oxidation reactions were prepared by diluting commercially available hydrogen peroxide (50% w/w H_2O_2 solution in water, Aldrich) in the corresponding solvent to achieve a concentration of 0.9 M. Commercially

available trifluoromethanesulfonic acid (TfOH, 99%) purchased from Fluorochem was employed and used as received.

4.3.1. General oxidation protocol A (enantioselective lactonization of carboxylic acids)

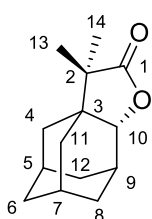
Substrate (100 μmol , 1 molar equivalent) and catalyst (1.0 μmol , 1 mol%) were dissolved in 4.0 mL of TFE inside a 12-mL vial equipped with a magnetic stirring bar (if the substrate is poorly soluble the reaction was performed at room temperature and CH_2Cl_2 was added dropwise until a clear solution is obtained). A 0.9 M solution of H_2O_2 in TFE (1 molar equivalent) diluted from commercially available H_2O_2 water solution and 0.09 M solution of triflic acid (0.1 molar equivalents) were delivered independently over 30 minutes by syringe pump into the solution under air. At the end of the addition, the mixture was left under stirring for additional 30 minutes to ensure complete lactonization. *Workup for GC analysis:* 50 μmol of the internal standard (biphenyl) were added and the mixture was quickly filtered through a short plug of silica gel, which was subsequently rinsed with 2×1 mL of EtOAc. GC analysis of the filtrate provided substrate conversion and product yields relative to the internal standard integration. *Ee's* were determined by GC or HPLC equipped with a chiral column. *Workup for isolation:* The solvent was removed under reduced pressure and the resultant crude was dissolved in EtOAc and washed with a saturated Na_2CO_3 aqueous solution. The organic phases were collected, dried over MgSO_4 and the solvent removed by rotatory evaporation, to yield the lactone (or mixture of lactones) along with minor impurities. Afterward, the reaction was analyzed by GC to determinate product distribution and enantiomeric excess. Purification by flash column chromatography gave the pure lactone (or mixture of lactones). The unreacted acid substrate was recovered by acidification of the aqueous phase (with HCl 1M) and extraction with dichloromethane. *For larger scale reaction the quantities of the reagents were scaled accordingly.*

4.4. Characterization of lactone products



1a: Lactone **1a** was obtained following general oxidation protocol A using (*S,S*)-Mn(^{TiBS}pdp) as catalyst. Purification by flash chromatography (SiO₂; hexane:AcOEt 5:1) gave the product as a glassy solid (68% yield, 98% ee).

¹H NMR (400 MHz, CDCl₃) δ 4.11 (d, *J* = 3.0 Hz, 1H, C₁₀ [1H]), 2.35 (m, 1H; C₉ [1H]), 2.24 (d, *J* = 16.0 Hz, 1H; C₂ [1H]), 2.13 (d, *J* = 16.0 Hz, 1H; C₂ [1H]), 2.03 (m, 1H; C₁₂ [1H]), 1.99 - 1.81 (m, 4H; C₅ [1H] + C₇ [1H] + C₄ [2H]), 1.80 - 1.59 (m, 6H; C₁₁ [2H] + C₆ [2H] + C₈ [2H]), 1.53 (dt, *J* = 12.9, 2.8 Hz, 1H; C₈ [1H]). ¹³C NMR (101 MHz, CDCl₃) δ 182.7 (C₁), 82.5 (C₁₀), 47.42 (C₂), 42.4 (C₃), 36.9 (C₄ or C₁₂), 36.4 (C₄ or C₁₂), 35.3 (C₈ or C₁₁), 34.2 (C₈ or C₁₁), 29.7 (C₉), 29.4 (C₆), 28.3 (C₅ or C₇), 27.2 (C₅ or C₇), 17.8 (C₁₄), 17.7 (C₁₃). HRMS (ESI-MS) *m/z* calculated for C₁₂H₁₆O₂ [M+Na]⁺ 215.1044, found 215.1043. [α]_D²⁴ +13.78 (CHCl₃, *c* 0.075). Chiral GC analysis with HP-Chiral-20B (isothermal method at 130 °C).



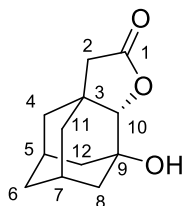
(R)-3a: Lactone **(R)-3a** was obtained following general oxidation protocol A using (*S,S*)-Mn(^{TiBS}pdp) as catalyst. Purification by flash chromatography (SiO₂; hexane:AcOEt 5:1) gave the product as a white solid (88% yield, 97% ee).

¹H NMR (300 MHz, CDCl₃) δ 4.30 (d, *J* = 3.3 Hz, 1H; C₁₀ [1H]), 2.36 (h, *J* = 3.2 Hz, 1H; C₉ [1H]), 2.07 (hept, *J* = 3.2 Hz, 1H; C₁₂ [1H]), 2.02 - 1.50 (m, 11H; C₁₁ [2H] + C₆ [2H] + C₄ [2H] + C₈ [2H] + C₁₂[1H] + C₅[1H] + C₇[1H]), 1.11 (s, 3H; C₁₄ [3H]), 1.04 (s, 3H; C₁₃ [3H]). ¹³C NMR (75 MHz, CDCl₃) δ 182.7 (C₁), 82.5 (C₁₀), 47.42 (C₂), 42.4 (C₃), 36.9 (C₄), 36.4 (C₁₂), 35.3 (C₈ or C₁₁), 34.2 (C₈ or C₁₁), 29.7 (C₉), 29.4 (C₆), 28.3 (C₅ or C₇), 27.2 (C₅ or C₇), 17.8 (C₁₄), 17.7 (C₁₃). HRMS (ESI-MS) *m/z* calculated for C₁₄H₂₀O₂ [M+Na]⁺ 243.1356, found 243.1356. [α]_D²⁴ +66.25 (CHCl₃, *c* 0.805). Single crystals were obtained by slow evaporation of a CHCl₃ solution of **3a**, and the absolute configuration was determined by x-ray analysis. The enantiomeric excess was calculated from the corresponding acetylated 1,4-diol (**3b**) by Chiral GC analysis with HP-Chiral-20B (isothermal method at 200 °C).

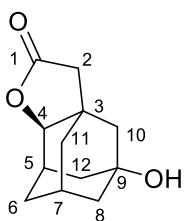
Oxidation of 4

Lactones **4a**, **4b** and **4c** were obtained following the general oxidation protocol A using (*S,S*)-Mn(^{TiBS}pdp) as catalyst. Purification by flash chromatography (SiO₂; hexane:AcOEt

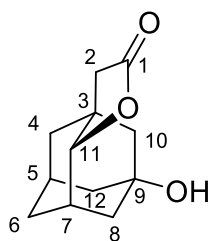
5:1) gave analytical samples of the three essentially pure products as crystalline colorless solids. Chiral GC analysis with HP-Chiral-20B isothermal method at 150 °C.



4a: (91% ee). ^1H NMR (400 MHz, CDCl_3) δ 3.96 (s, 1H; C_{10} [1H]), 2.39 - 2.17 (m; C_2 [2H] + C_5 [1H] + C_7 [1H]), 2.00-1.91 (m, 1H; C_4 [1H]), 1.89-1.72 (m, 3H; C_{12} [2H] + C_{11} [1H]), 1.72-1.56 (m, 5H; C_6 [2H] + C_4 [1H] + C_8 [1H] + C_{11} [1H]), 1.50-1.40 (m, 1H; C_8 [1H]). ^{13}C NMR (101 MHz, CDCl_3) δ 176.1 (C_1), 89.8 (C_{10}), 68.4 (C_9), 44.4 (C_2), 43.2 (C_{12}), 42.3 (C_3), 38.1 (C_4), 37.3 (C_{11}), 35.9 (C_8), 35.1 (C_6), 31.2 (C_5 or C_7), 30.0 (C_5 or C_7). HRMS (ESI-MS) m/z calculated for $\text{C}_{12}\text{H}_{16}\text{O}_3$ [$\text{M}+\text{Na}$] $^+$ 231.0992, found 231.0998.



(R)-4b: (>99 % ee). ^1H NMR (400 MHz, CDCl_3) δ 3.96 (s, 1H; C_{10} [1H]), 2.39 - 2.17 (m; C_2 [2H] + C_5 [1H] + C_7 [1H]), 2.00-1.91 (m, 1H; C_4 [1H]), 1.89-1.72 (m, 3H; C_{12} [2H] + C_8 [1H]), 1.72-1.56 (m, 5H; C_6 [2H] + C_4 [1H] + C_8 [1H] + C_{11} [1H]), 1.50-1.40 (m, 1H; C_{11} [1H]). ^{13}C NMR (101 MHz, CDCl_3) δ 176.1 (C_1), 89.8 (C_{10}), 68.4 (C_9), 44.4 (C_2), 43.2 (C_{12}), 42.3 (C_3), 38.1 (C_4), 37.3 (C_8), 35.9 (C_{11}), 35.1 (C_6), 31.2 (C_5 or C_7), 30.0 (C_5 or C_7). HRMS (ESI-MS) m/z calculated for $\text{C}_{12}\text{H}_{16}\text{O}_3$ [$\text{M}+\text{Na}$] $^+$ 231.0992, found 231.0998. $[\alpha]_{\text{D}}^{24} +78.28$ (CHCl_3 , c 0.290). X-ray quality crystals were obtained by slow evaporation of a solution of **4b** in CHCl_3 .

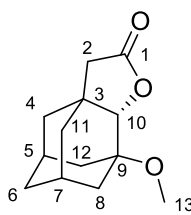


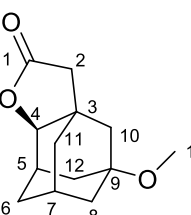
4c: (67 % ee). ^1H NMR (400 MHz, CDCl_3) δ 4.07 (s, 1H; C_4 [1H]), 2.50 (s, 1H; C_5 [1H]), 2.29 (d, J = 16.0 Hz, 1H; C_2 [1H]), 2.22 - 2.14 (m, 2H; C_2 [1H] + C_7 [1H]), 1.81 (m, 4H; C_6 [2H] + C_{10} [1H] + C_8 [1H]), 1.74 (m, 3H; C_{12} [2H] + C_8 [1H]), 1.63 (d, J = 13.1 Hz, 1H; C_8 [1H]), 1.50 (d, J = 13.2 Hz, 1H; C_4 [1H]), 1.43 (d, J = 13.1 Hz, 1H; C_8 [1H]). ^{13}C NMR (75 MHz, CDCl_3) δ 177.1 (C_1), 85.7 (C_{11}), 68.8 (C_9), 46.1 (C_{10}), 44.5 (C_{12}), 43.9 (C_2), 43.4 (C_6), 40.7 (C_3), 35.58 (C_4), 31.0 (C_7), 28.4 (C_5), 27.8 (C_8). HRMS (ESI-MS) m/z calculated for $\text{C}_{12}\text{H}_{16}\text{O}_3$ [$\text{M}+\text{Na}$] $^+$ 231.0992, found 231.0998.

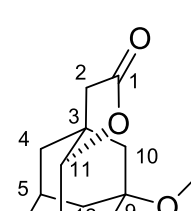
Oxidation of 5

Lactones **5a**, **5b** and **5c** were obtained following the general oxidation protocol A using (*S,S*)- $\text{Mn}(\text{TIBS})\text{pdp}$ as catalyst. Extensive purification by flash chromatography (SiO_2 ;

hexane:AcOEt 5:1) gave analytical samples of the three essentially pure products as crystalline colorless solids. Chiral GC analysis with HP-Chiral-20B isothermal method at 170 °C.

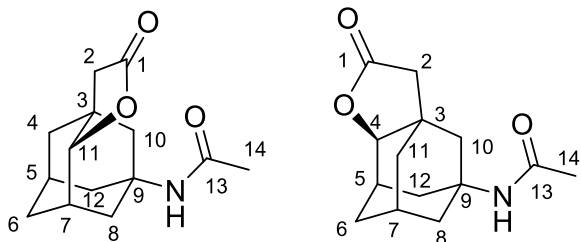
 **(+)-5a** (96% ee). ^1H NMR (400 MHz, CDCl_3) δ 4.04 (s, 1H; C_{10} [1H]), 3.36 (s, 3H; C_{13} [3H]), 2.27 (d, $J = 16.0$ Hz, 3H; C_2 [1H] + C_5 [1H] + C_7 [1H]), 2.20 (d, $J = 16.0$ Hz, 1H; C_2 [1H]), 2.10 (d, $J = 11.0$ Hz, 1H; C_{12} [1H]), 1.86 – 1.78 (m, 2H; C_4 [1H] + C_{11} [1H]), 1.75 (m, $J = 7.4$ Hz, 1H; C_8 [1H]), 1.65 (m, $J = 15.4$ Hz, 5H; C_6 [2H] + C_{12} [1H] + C_8 [1H] + C_{11} [1H]), 1.44 (d, $J = 13.3$ Hz, 1H; C_4 [1H]). ^{13}C NMR (101 MHz, CDCl_3) δ 176.4 (C_1), 88.4 (C_{10}), 72.2 (C_9), 50.1 (C_{13}), 43.7 (C_2), 42.6 (C_3), 40.9 (C_8), 38.21 (C_4 or C_{11}), 36.3 (C_4 or C_{11}), 35.4 (C_6), 33.0 (C_{12}), 31.0 (C_5 or C_7), 29.6 (C_5 or C_7). HRMS (ESI-MS) m/z calculated for $\text{C}_{13}\text{H}_{23}\text{NO}_2$ [$\text{M}+\text{Na}$] $^+$ 245.1148, found 245.1150. $[\alpha]_{\text{D}}^{24} +30.93$ (CHCl_3 , c 0.250).

 **(+)-5b** (96% ee). ^1H NMR (400 MHz, CDCl_3) δ 3.98 (s, 1H; C_4 [1H]), 3.22 (s, 3H; C_{13} [1H]), 2.61 (s, 1H; C_5 [1H]), 2.37 (d, $J = 16.1$ Hz, 1H; C_2 [1H]), 2.28 (s, 1H; C_7 [1H]), 2.21 (d, $J = 16.1$ Hz, 1H; C_2 [1H]), 1.94 (dq, $J = 12.2, 2.5$ Hz, 1H; C_{12} [1H]), 1.86 – 1.76 (m, 3H; C_6 [1H] + C_8 [1H] + C_{11} [1H]), 1.76 – 1.61 (m, 5H; C_{10} [2H] + C_8 [1H] + C_{11} [1H] + C_{12} [1H]), 1.47 (dd, $J = 12.1, 2.7$ Hz, 1H; C_8 [1H]). ^{13}C NMR (101 MHz, CDCl_3) δ 176.0 (C_1), 85.2 (C_4), 70.7 (C_9), 47.9 (C_{13}), 43.3 (C_2), 42.1 (C_3), 40.1 (C_8 or C_{10}), 39.9 (C_8 or C_{10}), 37.9 (C_{11}), 34.8 (C_6), 32.5 (C_{12}), 32.07 (C_5), 30.0 (C_7). HRMS (ESI-MS) m/z calculated for $\text{C}_{13}\text{H}_{18}\text{O}_3$ [$\text{M}+\text{Na}$] $^+$ 245.1148, found 245.1150. $[\alpha]_{\text{D}}^{24} +46.60$ (CHCl_3 , c 0.186).

 **(+)-5c** (65% ee). ^1H NMR (400 MHz, CDCl_3) δ 4.07 (s, 1H; C_{11} [1H] of **5c**), 3.98 (s, 1H; C_4 [1H] of **5b**), 3.24 (s, 3H; C_{13} [3H] of **5c**), 3.22 (s, 3H; C_{13} [3H] of **5b**), 2.61 (s, 1H; C_5 [1H] of **5b**), 2.54 (s, 1H; C_7 [1H] of **5c**), 2.44 – 2.17 (m, 8H), 1.97 – 1.86 (m, 3H), 1.86 – 1.60 (m, 17H), 1.60 – 1.41 (m, 6H). ^{13}C NMR (101 MHz, CDCl_3) δ 177.2 (C_1 of **5c**), 176.6 (C_1 of **5b**), 85.8 (C_{11} of **5c**), 85.5 (C_4 of **5b**), 72.6 (C_{13} of **5b**), 71.0 (C_{13} of **5c**), 48.6, 48.3, 44.0, 43.6, 41.9, 40.5, 39.9, 39.4, 38.0, 35.9, 34.9, 32.6, 32.2, 30.8, 30.1, 28.1. HRMS (ESI-MS) m/z calculated for $\text{C}_{13}\text{H}_{23}\text{NO}_2$ [$\text{M}+\text{Na}$] $^+$ 245.1148, found 245.1150. $[\alpha]_{\text{D}}^{24} +7.89$ (CHCl_3 , c 0.245).

Oxidation of 6

Lactones were isolated as a mixture following the general oxidation protocol A using (*S,S*)-Mn(pdp) as catalyst. Purification by flash chromatography (SiO₂; hexane:AcOEt 5:1) gave the product as a colorless oil. **6a** was obtained in to low yield to be analyzed spectroscopically. Chiral GC analysis with HP-Chiral-20B (isothermal methods at 200 °C for **6c** and 175 °C for **6b**). **6a**

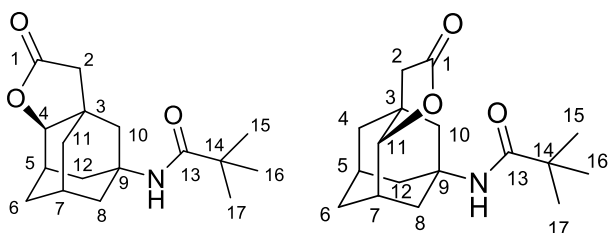


6b+6c (main product 6c): (95% ee). ¹H NMR (400 MHz, CDCl₃) δ 5.17 (s, 1H, NH), 4.03 (d, J = 2.8 Hz, 1H, C₁₁ [1H] *endo*), 2.51 (d, J = 25.1 Hz, 1H, C₇ [1H]), 2.34 (d, J = 16.1 Hz, 1H; C₂ [1H]), 2.25 – 2.00 (m, 5H; C₂ [1H] + C₅ [1H] + C₈ [1H] +

C₁₀ [2H]), 1.92 (d, J = 5.3 Hz, 7H, C₁₄ [3H] + C₄ [1H] + C₆ [1H] + C₁₂ [2H]), 1.76 – 1.63 (m, 3H; C₄ [1H] + C₆ [1H] + C₈ [1H]). ¹³C NMR (101 MHz, CDCl₃) δ 176.9 (C₁ *exo*), 176.3 (C₁ *endo*), 169.6 (C₁₃), 85.5 (C₁₁ *endo*), 85.0 (C₄ *exo*), 52.3, 50.9, 43.9, 43.6, 42.2, 41.3, 41.0, 40.5, 39.8, 39.7, 38.1, 37.8, 36.1, 35.8, 35.2, 34.8, 34.1, 31.2, 30.2, 29.9, 29.6, 29.3, 28.5, 28.2, 27.5, 24.4. HRMS (ESI-MS) *m/z* calculated for C₁₄H₁₉NO₃ [M+Na]⁺ 272.1257, found 272.1256. [α]_D²⁴ -12.0 (CHCl₃, c 0.366).

Oxidation of 7

Lactones **7a**, **7b** and **7c** were isolated as a mixture following the general oxidation protocol A using (*S,S*)-Mn(pdp) as catalyst. Purification by flash chromatography (SiO₂; hexane:AcOEt 5:1) gave the product as a colorless oil. **7a** was obtained in to low yield to be analyzed spectroscopically Chiral GC analysis with HP-Chiral-20B isothermal methods at 200 °C for **7c** and 175 °C for **7b**.



7b+7c (main product): (**7c** 94% ee). ¹H NMR (400 MHz, CDCl₃) δ 5.32 (s, 1H, NH), 4.13 (s, 1H, C₄[H] *exo*), 4.02 (s, 0.34H, C₁₁[H] *endo*), 2.56 – 2.50 (m, 0.5H, C₇ [1H] *endo*), 2.47 (s, 1H; C₅ [1H] *exo*), 2.44 –

2.28 (m, 3H), 2.25 (s, 1H), 2.16 (m, 3H), 2.04 (m, 2H), 1.95 (m, 3H), 1.90 – 1.79 (m, 5H), 1.66 (m, 3H), 1.58 (m, 1H), 1.49 (m, 1H), 1.14 (s, 9H, *tBu* *exo*), 1.13 (s, 3H, *tBu* *endo*). ¹³C NMR (101 MHz, CDCl₃) δ 178.1, 176.9, 85.5 (C₄ *exo*), 85.5

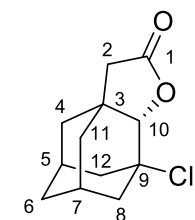
(C_4 *endo*), 51.9, 50.6, 43.9, 43.6, 42.1, 41.3, 41.1, 40.4, 39.7, 39.6, 39.0, 37.8, 35.9, 34.9, 34.2, 31.3, 30.3, 29.4, 28.4, 27.6, 27.6, 26.4, 24.7 ($C_{15} + C_{16} + C_{17}$ *endo*), 23.8 ($C_{15} + C_{16} + C_{17}$ *exo*). HRMS (ESI-MS) m/z calculated for $C_{17}H_{25}NO_3$ $[M+Na]^+$ 314.1727, found 314.1734.

Oxidation of 8

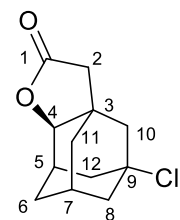
Products of acetate-adamantane acetic acid **8** oxidation (**8a**, **8b** and **8c**) have been identified by comparison of their GC retention times with samples of **8a**, **8b** and **8c** obtained by acetylation of **4a**, **4b** and **4c** (in turn obtained by separation of the products derived by **4** oxidation). Chiral GC analysis with HP-Chiral-20B (isothermal methods at 200 °C).

Oxidation of 9

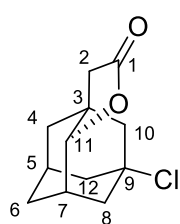
Lactones (+)-**9a**, (+)-**9b** and (+)-**9c** were obtained following the oxidation protocol A using (*S,S*)-Mn(pdp) as catalyst. Extensive purification by flash chromatography (SiO₂; hexane:AcOEt 5:1) gave analytical samples of the three essentially pure products as crystalline colorless solids. Chiral GC analysis with HP-Chiral-20B isothermal method at 200 °C.



(+)-9a: (91% ee). ¹H NMR (400 MHz, CDCl₃) δ 4.13 (s, 1H, C_{10} [1H]), 2.40 – 2.05 (m, 7H; C_2 [2H] + C_5 [1H] + C_7 [1H] + C_4 [2H] + C_{12} [1H]), 2.00 (d, $J = 14.2$ Hz, 1H; C_{12} [1H]), 1.87 (s, 1H, C_8 [1H]), 1.79 – 1.60 (m, 4H; C_{11} [1H] + C_8 [1H] + C_6 [2H]), 1.49 (d, $J = 13.2$ Hz, 1H; C_{11} [1H]). ¹³C NMR (101 MHz, CDCl₃) δ 175.0 (C_1), 89.4 (C_{10}), 64.3 (C_9), 46.9 (C_4), 44.3 (C_2), 43.0 (C_3), 39.3 (C_8 or C_{12}), 38.0 (C_8 or C_{12}), 35.5 (C_{11}), 34.6 (C_6), 31.9 (C_5 or C_7), 30.5 (C_5 or C_7). HRMS (ESI-MS) m/z calculated for $C_{12}H_{15}ClO_2$ $[M+Na]^+$ 249.0653, found 249.0650. $[\alpha]_D^{24} +46.67$ (CHCl₃, c 0.220).



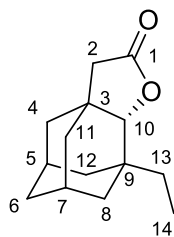
(+)-9b: (96% ee). ¹H NMR (400 MHz, CDCl₃) δ: 4.12 (s, 1H; C_4 [1H]), 2.53 (s, 1H, C_5 [1H]), 2.37 – 2.07 (m, 9H; C_2 [2H] + C_7 [1H] + C_{10} [2H] + C_{12} [2H] + C_8 [2H]), 1.84 (d, $J = 13$ Hz, 1H; C_6 [1H]), 1.70 (d, $J = 13$ Hz, 1H; C_{11} [1H]), 1.61 (d, $J = 13$ Hz, 1H; C_6 [1H]), 1.51 (d, $J = 13$ Hz, 1H; C_{11} [1H]). ¹³C NMR (101 MHz, CDCl₃) δ: 176.2 (C_1), 84.8 (C_4), 65.5 (C_9), 48.7 (C_{12}), 46.7 (C_{10}), 45.8 (C_8), 43.7 (C_2), 41.4 (C_3), 35.1 (C_{11}), 32.2 (C_5), 29.5 (C_7), 27.5 (C_6). HRMS (ESI-MS) m/z calculated for $C_{13}H_{23}NO_2$ $[M+Na]^+$ 249.0653, found 249.0650. $[\alpha]_D^{24} +114.48$ (CHCl₃, c 0.610).



(+)-9c: (88% ee). ^1H NMR (400 MHz, CDCl_3) δ 4.00 (s, 1H; $\text{C}_{11}[1\text{H}]$), 2.58 (s, 1H; $\text{C}_7[1\text{H}]$), 2.36 (d, $J = 16.2$ Hz, 1H; $\text{C}_2[1\text{H}]$), 2.26 (m, 2H; $\text{C}_5[1\text{H}] + \text{C}_8[1\text{H}]$), 2.21 (d, $J = 16.1$ Hz, 1H; $\text{C}_2[1\text{H}]$), 2.17 – 2.01 (m, 5H; $\text{C}_{12}[2\text{H}] + \text{C}_{10}[1\text{H}] + \text{C}_8[1\text{H}]$), 1.86 (m, $J = 15.1$ Hz, 3H; $\text{C}_6[1\text{H}] + \text{C}_4[1\text{H}] + \text{C}_{10}[1\text{H}]$), 1.72 (m, 2H; $\text{C}_6[1\text{H}] + \text{C}_4[1\text{H}]$). ^{13}C NMR (101 MHz, CDCl_3) δ 175.7 (C_1), 84.4 (C_{11}), 64.7 (C_9), 46.4 (C_{10} or C_{12}), 46.3 (C_{10} or C_{12}), 43.3 (C_2), 43.1 (C_3), 39.3 (C_8), 37.4 (C_4), 34.2 (C_6), 33.1 (C_7), 31.3 (C_5). HRMS (ESI-MS) m/z calculated for $\text{C}_{13}\text{H}_{23}\text{NO}_2$ $[\text{M}+\text{Na}]^+$ 249.0653, found 249.0650. $[\alpha]_{\text{D}}^{24} +51.80$ (CHCl_3 , c 0.195).

Oxidation of 10

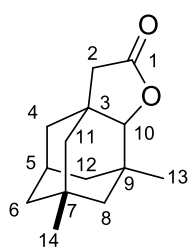
Lactones were obtained as a mixture following the general oxidation protocol A using (*S,S*)-Mn(pdp) as catalyst. Purification by flash chromatography (SiO_2 ; hexane:AcOEt 5:1) gave the product as a colorless oil. Chiral GC analysis with HP-Chiral-20B isothermal method at 150 °C.



10a (main product): (95% ee). ^1H NMR (300 MHz, CDCl_3) δ 4.06-4.04 (m, 1H, $\text{C}_4\text{-H}$ and $\text{C}_{11}\text{-H}$ of distal **10b** and **10c**), 3.83 (s, 1H, $\text{C}_{10}\text{-H}$ of **10a**), 2.32 – 2.10 (m, 2H), 2.08 (d, $J = 4.2$ Hz, 1H), 2.02 (s, 1H), 1.90 – 1.79 (m, 1H), 1.75 (d, $J = 18.2$ Hz, 1H), 1.69 – 1.31 (m, 9H), 1.27 – 1.08 (m, 1H), 0.91 – 0.73 (m, 3H). ^{13}C NMR (75 MHz, CDCl_3) δ 177.4, 177.2, 177.1, 89.6, 87.1, 86.7, 44.4, 44.2, 43.1, 41.5, 40.7, 40.6, 40.1, 39.8, 39.6, 39.2, 39.1, 36.7, 36.5, 36.1, 35.7, 35.4, 35.3, 35.1, 34.5, 34.2, 33.7, 32.1, 31.5, 30.5, 29.7, 29.0, 28.9, 28.9, 27.7, 27.2, 7.1, 6.8, 6.8. HRMS (ESI-MS) m/z calculated for $\text{C}_{14}\text{H}_{20}\text{O}_2$ $[\text{M}+\text{Na}]^+$ 243.1356, found 243.1360.

Oxidation of 11

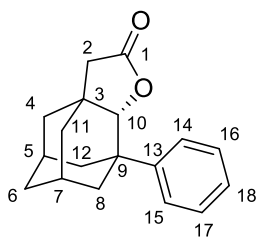
Lactones were obtained as mixture following the general oxidation protocol A using (*S,S*)-Mn(pdp) as catalyst. Purification by flash chromatography (SiO_2 ; hexane:AcOEt 5:1) gave the product as a colorless oil. Chiral GC analysis with HP-Chiral-20B isothermal method at 160 °C.



^1H NMR (400 MHz, CDCl_3) δ 3.98 (s, 0.2H, $\text{C}_4[1\text{H}]$ **11a**), 3.70 (d, $J = 3.0$ Hz, 1H; C_{10} [1H], **11b** + **11c**), 2.32 – 2.12 (m, 3H, $\text{C}_2[2\text{H}]$ + $\text{C}_5[1\text{H}]$ **11a**), 2.07 (d, $J = 6.2$ Hz, 1H), 1.79 – 1.06 (m, 16H), 0.98 (d, $J = 5.5$ Hz, 3H, $\text{C}_{13}[3\text{H}]$ or $\text{C}_{14}[3\text{H}]$), 0.89 – 0.81 (m, 5H, $\text{C}_{13}[3\text{H}]$ or $\text{C}_{14}[3\text{H}]$). ^{13}C NMR (101 MHz, CDCl_3) δ 177.0 (C_1), 91.2 (C_{10} ; distal), 90.7 (C_{10} , distal), 86.2 (C_4 , proximal), 51.2, 50.8, 48.5, 45.7, 45.2, 44.4, 44.2, 44.0, 43.0, 42.9, 42.3, 40.5, 40.1, 38.3, 35.6, 35.6, 35.5, 33.6, 32.8, 32.4, 30.6, 29.7, 29.6, 29.6, 28.2, 25.8, 25.6. HRMS (ESI-MS) m/z calculated for $\text{C}_{14}\text{H}_{20}\text{O}_2$ $[\text{M}+\text{Na}]^+$ 243.1356, found 243.1359. $[\alpha]_{\text{D}}^{24}$ -12.0 (CHCl_3 , c 0.366).

Oxidation of 12

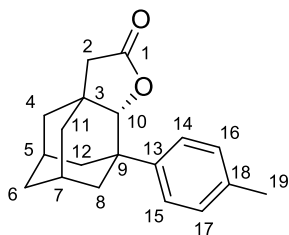
Lactone products were obtained as a mixture following general oxidation protocol A using (*S,S*)-Mn(pdp) as catalyst. Purification by flash chromatography (SiO_2 ; hexane:AcOEt 5:1) afforded the product as a white solid. Chiral GC analysis with HP-Chiral-20B (isothermal method at 220 °C).



12a (main product): (95% ee); ^1H NMR (400 MHz, CDCl_3 ; **12a** signals assigned. Small peaks are the signals of **12b** and **12c**) δ 7.33 (s, 2H; C_{14} [1H] + C_{15} [1H]), 7.25 (s, 3H; C_{16} [1H] + C_{17} [1H] + CHCl_3), 7.14 (s, 1H; C_{18} [1H]), 4.16 (s, 1H; C_{10} [1H]), 2.15 (s, 5H; C_2 [2H] + C_5 [1H] + C_7 [1H] + C_8 [1H]), 1.90 (s, 4H; C_4 [1H] + C_{12} [2H] + C_8 [1H]), 1.68 (s, 4H; C_6 [2H] + C_4 [1H] + C_{11} [1H]), 1.51 (m, 1H; C_{11} [1H]). ^{13}C NMR (101 MHz, CDCl_3 , **12a** signals assigned. Small peaks are the signals of **12b** and **12c**) δ 176.5 (C_1), 145.0 (C_{13}), 128.3 (C_{14} + C_{15}), 126.5 (C_{18}), 125.6 (C_{14} + C_{15}), 89.2 (C_{10}), 44.2 (C_2), 43.0 (C_{12}), 40.1 (C_3), 39.1 (C_9), 38.9 (C_4), 36.2 (C_{11}), 35.6 (C_6), 34.7 (C_8), 29.3 (C_5 or C_7), 27.9 (C_5 or C_7). HRMS (ESI-MS) m/z calculated for $\text{C}_{18}\text{H}_{20}\text{O}_2$ $[\text{M}+\text{Na}]^+$ 291.1356, found 291.1351. $[\alpha]_{\text{D}}^{24}$ +91.5 (CHCl_3 , c 0.660).

Oxidation of 13

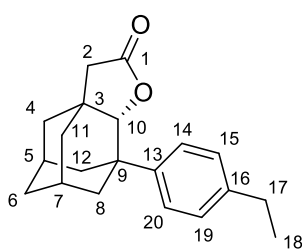
Lactones were obtained as mixture following general oxidation protocol A using (*S,S*)-Mn(pdp) as catalyst. Purification by flash chromatography (SiO_2 ; hexane:AcOEt 5:1) gave the product as a colorless oil. Chiral GC analysis with HP-Chiral-20B (isothermal method at 220 °C).



13a (main product): (97% ee); ^1H NMR (400 MHz, CDCl_3) δ 7.33 (d, $J = 8.3$ Hz, 2H; C_{16} [1H] + C_{17} [1H]), 7.15 (d, $J = 8.0$ Hz, 2H; C_{14} [2H] + C_{15} [1H]), 4.22 (s, 1H; C_{10} [1H]), 2.33 (s, 1H; C_{19} [3H]), 2.20 (m, $J = 15.9$ Hz, 4H; C_2 [2H] + C_5 [1H] + C_7 [1H]), 1.97-1.59 (m, 9H; C_{11} [2H] + C_{12} [1H] + C_8 [2H] + C_6 [2H] + C_4 [1H] + C_{12} [1H]), 1.56 (m, $J = 12.7$ Hz, 1H; C_4 [1H]). ^{13}C NMR (101 MHz, CDCl_3) δ 176.5 (C_1), 142.1 (C_{13}), 136.0 (C_{18}), 128.9 (C_{16} + C_{17}), 125.4 (C_{14} + C_{15}), 89.4 (C_{10}), 44.3 (C_2), 43.1 (C_4), 40.1 (C_3), 39.0 (C_{12}), 38.8 (C_9), 36.2 (C_{11}), 35.6 (C_6), 34.8 (C_8), 29.4 (C_5 or C_7), 27.9 (C_5 or C_7), 20.8 (C_{19}). HRMS (ESI-MS) m/z calculated for $\text{C}_{19}\text{H}_{22}\text{O}_2$ [$\text{M}+\text{Na}$] $^+$ 305.1512, found 305.1508. $[\alpha]_{\text{D}}^{24} +85.3$ (CHCl_3 , c 0.788).

Oxidation of 14

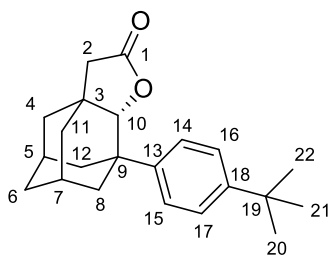
Pure lactone **14a** was obtained following general oxidation protocol A using (*S,S*)-Mn(pdp) as catalyst. Purification by flash chromatography (SiO_2 ; hexane:AcOEt 5:1) gave the pure product (+)-**14a** as a white solid. Chiral GC analysis with HP-Chiral-20B isothermal method at 220 $^\circ\text{C}$.



(+)-14a (56% yield, 96% ee) ^1H NMR (400 MHz, CDCl_3) δ 7.34 (d, $J = 8.3$ Hz, 2H; C_{14} [1H] + C_{15} [1H]), 7.17 (d, $J = 8.3$ Hz, 2H; C_{16} [1H] + C_{17} [1H]), 4.22 (s, 1H; C_{10} [1H]), 2.62 (q, $J = 7.6$ Hz, 2H; C_{19} [2H]), 2.34 - 2.16 (m, 5H; C_2 [2H] + C_5 [1H] + C_7 [1H] + C_{12} [1H]), 2.08-1.94 (m, 3H; C_8 [2H] + C_4 [1H]), 1.89 (d, $J = 11.7$ Hz, 1H; C_{12} [1H]), 1.86-1.69 (m, 4H; C_6 [2H] + C_4 [1H] + C_{11} [1H]), 1.57 (d, $J = 14.3$ Hz, 1H; C_{11} [1H] + H_2O), 1.23 (t, $J = 7.6$ Hz, 3H; C_{20} [3H]). ^{13}C NMR (101 MHz, CDCl_3) δ 176.5 (C_1), 142.4 (C_{13}), 142.3 (C_{18}), 127.8 (C_{14} + C_{15}), 125.5 (C_{16} + C_{17}), 89.5 (C_{10}), 44.4 (C_2), 43.1 (C_8), 40.2 (C_3), 39.1 (C_4), 38.8 (C_9), 36.3 (C_{12}), 35.7 (C_6), 34.9 (C_{12}), 29.5 (C_5), 28.3 (C_{19}), 28.0 (C_7), 15.4 (C_{20}). HRMS (ESI-MS) m/z calculated for $\text{C}_{20}\text{H}_{24}\text{O}_2$ [$\text{M}+\text{Na}$] $^+$ 319.1669, found 319.1661. $[\alpha]_{\text{D}}^{24} +105.379$ (CHCl_3 , c 1.08).

Oxidation of 15

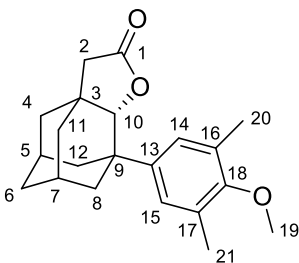
Lactones were obtained as mixture following general oxidation protocol A using (*S,S*)-Mn(pdp) as catalyst. Purification by flash chromatography (SiO_2 ; hexane:AcOEt 5:1) gave the product as a white solid. Chiral GC analysis with HP-Chiral-20B (isothermal method at 220 $^\circ\text{C}$).



15a (main product): (95% ee); ^1H NMR (400 MHz, CDCl_3) δ 7.34 (s, 4H; C_{14} [1H] + C_{15} [1H] + C_{16} [1H] + C_{17} [1H]), 4.21 (s, 1H; C_{10} [1H]), 2.22 (m, 5H; C_2 [2H] + C_5 [1H] + C_7 [1H] + C_8 [1H]), 1.95 (m, 4H; C_{12} [2H] + C_8 [1H] + C_4 [1H]), 1.77 (m, 4H; C_6 [2H] + C_4 [1H] + C_{11} [1H]), 1.58 (m, 1H; C_{11} [1H]), 1.30 (s, 9H; C_{20} [3H] + C_{21} [3H] + C_{22} [3H]). ^{13}C NMR (101 MHz, CDCl_3) δ 176.5 (C_1), 149.1 (C_{18}), 141.9 (C_{13}), 125.1 (C_{14} + C_{15}), 125.1 (C_{16} + C_{17}), 89.4 (C_{10}), 44.3 (C_2), 43.0 (C_{12}), 40.1 (C_3), 39.0 (C_4), 38.7 (C_9), 36.2 (C_{11}), 35.7 (C_6), 34.7 (C_8), 34.2 (C_{19}), 31.3 (C_{20} + C_{21} + C_{22}), 29.4 (C_5 or C_7), 27.9 (C_5 or C_7). HRMS (ESI-MS) m/z calculated for $\text{C}_{22}\text{H}_{28}\text{O}_2$ [$\text{M}+\text{Na}$] $^+$ 347.1980, found 347.1982.

Oxidation of 16

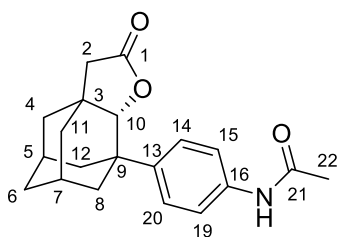
Lactones were obtained as mixture following general oxidation protocol A using (*S,S*)-Mn(pdp) as catalyst. Purification by flash chromatography (SiO_2 ; hexane:AcOEt 5:1) gave the product as a white solid. Chiral GC analysis with HP-Chiral-20B (isothermal method at 240 °C).



16a (main product): (95% ee). ^1H NMR (300 MHz, CDCl_3) δ 7.04 (s, 1H; C_{15} [1H]), 6.95 (d, $J = 9.5$ Hz 1H; C_{14} [1H]), 4.18 (s, 1H; C_{10} [1H]), 3.70 (m, 3H; C_{19} [3H]), 2.28 (s, 6H, C_{20} [3H] + C_{21} [3H]), 2.24 (m, 3H; C_2 [2H] + C_8 [1H]), 2.08 - 1.62 (m, 10H; C_{12} [2H] + C_8 [1H] + C_4 [2H] + C_6 [2H] + C_5 [1H] + C_7 [1H] + C_{11} [1H]), 1.81-1.69 (m, 4H; C_6 [2H] + C_4 [1H] + C_{11} [1H]), 1.62-1.54 (m, 1H; C_{11} [1H]). ^{13}C NMR (101 MHz, CDCl_3) δ 176.6 (C_1), 155.4 (C_{18}), 140.2 (C_{13}), 130.2 (C_{16} or C_{17}), 125.9 (C_{14} + C_{15}), 125.2 (C_{16} or C_{17}), 89.5 (C_{10}), 59.55 (C_{19}), 44.4 (C_2), 43.4 (C_{12}), 40.1 (C_3), 39.0 (C_4), 38.5 (C_9), 36.2 (C_{11}), 35.6 (C_6), 34.6 (C_8), 29.4 (C_5 or C_7), 27.9 (C_5 or C_7), 16.3 (C_{20} + C_{21}). HRMS (ESI-MS) m/z calculated for $\text{C}_{21}\text{H}_{26}\text{O}_3$ [$\text{M}+\text{Na}$] $^+$ 349.1774, found 349.1779.

Oxidation of 17

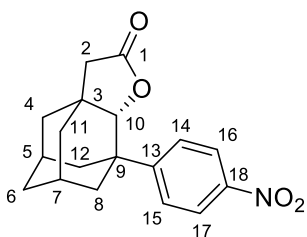
Lactones were obtained as mixture following general oxidation protocol A using (*S,S*)-Mn(pdp) as catalyst. Purification by flash chromatography (SiO_2 ; hexane:AcOEt 5:1) gave the product as a white solid. Chiral HPLC analysis with CHIRALPAK-IA column eluted with isocratic hexane:isopropanol 95:5 (signal at 280 nm).



17a (main product): (97% ee). ^1H NMR (400 MHz, CDCl_3) δ 7.45 (m, 2H; C_{14} [1H] + C_{15} [1H]), 7.36 (m, 2H; C_{16} [1H] + C_{17} [1H]), 4.20 (s, 1H; C_{10} [1H]), 2.30 (d, $J = 16.1$ Hz, 1H; C_2 [1H]), 2.20 (d, $J = 33.8$ Hz, 4H), 1.97 (m, 3H), 1.80 (d, $J = 39.5$ Hz, 5H), 1.57 (d, $J = 12.9$ Hz, 1H), 1.25 (s, 3H; C_{20} [3H]). ^{13}C NMR (101 MHz, CDCl_3) δ 176.5 (C_1), 173.5 (C_1), 141.1 (C_{19}), 136.3 (C_{13}), 126.2 (C_{14} + C_{15}), 119.8 (C_{16} + C_{17}), 89.3 (C_{10}), 44.3 (C_2), 43.0, 40.2 (C_3), 39.0, 38.9 (C_9), 36.2, 35.6, 34.9, 29.7 (C_{20}), 29.4 (C_5 or C_7), 27.9 (C_5 or C_7). HRMS (ESI-MS) m/z calculated for $\text{C}_{20}\text{H}_{23}\text{NO}_3$ [$\text{M}+\text{Na}$] $^+$ 348.1570, found 348.1562.

Oxidation of 18

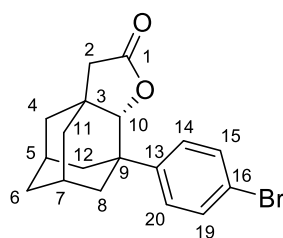
Lactones were obtained as mixture following general oxidation protocol A using (*S,S*)-Mn(pdp) as catalyst. Purification by flash chromatography (SiO_2 ; hexane:AcOEt 5:1) gave the product as a white solid. Chiral GC analysis with HP-Chiral-20B (isothermal method at 240 $^\circ\text{C}$).



18a (main product): (>99% ee). ^1H NMR (400 MHz, CDCl_3) δ 8.18 (d, $J = 8.8$ Hz, 2H; C_{14} [1H] + C_{15} [1H]), 7.49 (d, $J = 8.9$ Hz, 2H; C_{16} [1H] + C_{17} [1H]), 4.23 (s, 1H; C_{10} [1H] **18a**), 4.20 (m, 1H; C_4 [1H] **18b**), 4.16 (s, 1H; C_{11} [1H] **18c**), 2.61 (d, $J = 12.7$ Hz, 0.6H, C_5 [1H] **18b** + C_7 [1H] **18c**), 2.45 – 2.14 (m, 4H, C_2 [2H] + C_5 [1H] **18a** + C_7 [1H] **18a** + C_{11} [1H] **18b**), 2.11 – 1.55 (m, 10H). ^{13}C NMR (101 MHz, CDCl_3) δ 176.5, 176.3, 175.9, 156.0, 155.7, 152.5, 126.8, 125.8, 125.8, 123.6, 123.5, 88.2, 86.0, 85.5, 44.7, 44.1, 44.0, 42.8, 41.9, 41.8, 41.5, 40.1, 38.2, 36.7, 36.1, 35.4, 35.0, 34.9, 34.8, 30.5, 30.0, 29.0, 28.2, 27.3. HRMS (ESI-MS) m/z calculated for $\text{C}_{18}\text{H}_{19}\text{NO}_4$ [$\text{M}+\text{Na}$] $^+$ 336.1206, found 336.1209.

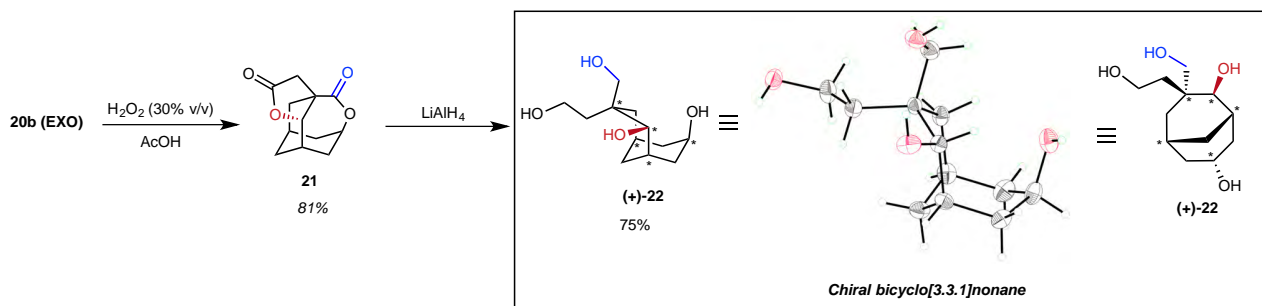
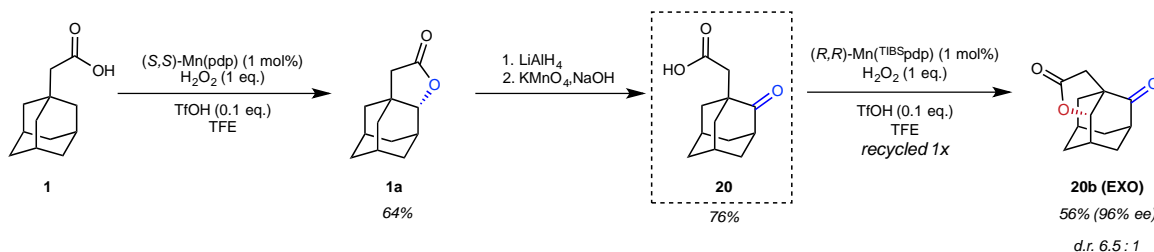
Oxidation of 19

Lactones were obtained as mixture following general oxidation protocol A using (*S,S*)-Mn(pdp) as catalyst. Purification by flash chromatography (SiO_2 ; hexane:AcOEt 5:1) gave the product as a white solid. Chiral GC analysis with HP-Chiral-20B (isothermal method at 240 $^\circ\text{C}$).

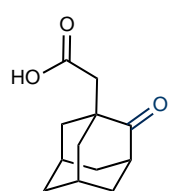


19a (main product): (95% ee). ^1H NMR (400 MHz, CDCl_3) δ 7.44 (d, J = 8.7 Hz, 2H; C_{14} [1H] + C_{15} [1H]), 7.29 (d, J = 8.7 Hz, 2H; C_{16} [1H] + C_{17} [1H]), 4.17 (s, 1H; C_{10} [1H]), 2.32 – 2.16 (m, 5H; C_2 [2H] + C_5 [1H] + C_7 [1H] + C_{12} [1H]), 1.95 (m, 3H; C_8 [2H] + C_4 [1H]), 1.84 – 1.72 (m, 5H; C_6 [2H] + C_4 [1H] + C_{11} [1H] + C_{12} [1H]), 1.58 (d, J = 13.3 Hz, 1H; C_{11} [1H]). ^{13}C NMR (101 MHz, CDCl_3) δ 176.2 (C_1), 144.1 (C_{13}), 131.3 (C_{14} + C_{15}), 127.5 (C_{16} + C_{17}), 120.5 (C_{18}), 88.9 (C_{10}), 44.2 (C_2), 42.8 (C_8), 40.1 (C_3), 39.0 (C_9), 38.9 (C_4), 36.1 (C_{11}), 35.5 (C_6), 34.8 (C_{12}), 29.3 (C_5 or C_7), 27.8 (C_5 or C_7). HRMS (ESI-MS) m/z calculated for $\text{C}_{18}\text{H}_{19}\text{BrO}_2$ $[\text{M}+\text{Na}]^+$ 369.0461, found 369.0459. $[\alpha]_{\text{D}}^{24}$ +93.1 (CHCl_3 , c 0.408).

4.5. Synthesis of (+)-22



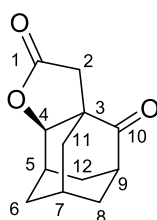
(+)-1a: Lactone **(+)-1a** (3.13 mmol, 70%) was obtained following the general oxidation protocol A using adamantaneacetic acid (868 mg, 4.47 mmol) and (*S,S*)-Mn(pdp) (0.04, 31 mg, 1 mol%). Purification by flash chromatography (SiO_2 ; hexane:AcOEt 5:1) gave the desired compound as a glassy solid (64%). Its characterization has been described above.



(2-oxo-adamantane)acetic acid (20): A THF (10 mL) solution of **(+)-1a** (635mg, 3.3 mmol, 1 eq.) was added dropwise into a 100 mL round-bottom flask containing a solution of LiAlH_4 (280 mg, 7.37 mmol, 2.2 eq.) in THF (33 mL) under nitrogen at room temperature. The reaction was left under stirring

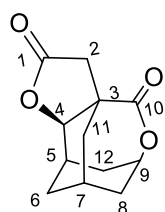
for 3h at the same temperature. Then, the mixture was quenched with NaHCO_3 (15 mL) and extracted with EtOAc (3x25 mL). The collected organic layers were dried over MgSO_4 ,

filtered and the solvent was evaporated under reduced pressure to obtain 615 mg of the 2-hydroxyadamantane-1-ethanol as white solid (3.13 mmol, 95% yield). To a well left stirring suspension of the obtained compound in 10% aqueous sodium hydroxide solution (1.5 mL) was slowly added a solution of 1.68 g of KMnO_4 dissolved in 34 mL of water. Afterward, the mixture was heated to reflux for 3 hours and then left under stirring overnight at room temperature. The precipitated manganese dioxide was filtered off and the filtrate was washed with Et_2O (1x15 mL). The aqueous layer was then acidified with 1 M H_2SO_4 and extracted with Et_2O (3x15 mL). The organic layers were collected and washed with water, dried over Na_2SO_4 and concentrated under vacuum. The resulting solid was recrystallized from Et_2O /hexane mixture to give 520 mg (2.5 mmol, 80%) of the desired product as white crystals (76%, 2 steps). ^1H NMR (400 MHz, CDCl_3) δ 2.67 (t, $J = 3.1$ Hz, 1H; C_9 [1H]), 2.45 (s, 2H; C_2 [2H]), 2.20 – 1.84 (m, 12H). ^{13}C NMR (101 MHz, CDCl_3) δ 217.8 (C_{10}), 175.72 (C_1), 48.7 (C_3), 46.6 (C_2), 44.1 ($\text{C}_4 + \text{C}_{11}$), 41.4 (C_6), 39.1 ($\text{C}_8 + \text{C}_{12}$), 35.5 (C_9), 27.9 ($\text{C}_5 + \text{C}_7$). HRMS (ESI-MS) m/z calculated for $\text{C}_{12}\text{H}_{16}\text{O}_3$ [$\text{M}+\text{Na}$] $^+$ 231.0992, found 231.0995.



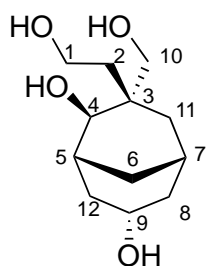
20b: Lactone **20b** was obtained following the general oxidation protocol A using 2-oxo-adamantaneacetic acid **20** as substrate (237 mg, 1.14 mmol) and (*R,R*)- $\text{Mn}(\text{TIBS})\text{pdp}$ as catalyst (12.3 mg, 0.1 molar equivalent). The reaction was treated according to general oxidation procedure A. The crude mixture obtained after solvent rotatory evaporation was dissolved in EtOAc (20 mL) and washed with sat. Na_2CO_3 (3x15 mL). The organic phase, containing the desired lactone, was dried over Na_2SO_4 and concentrated *in vacuo*, while the combined aqueous layers were acidified with diluted HCl up to $\text{pH}=2-3$ and then extracted with EtOAc (3x10 mL) to recover unreacted **20**, which was dried over Na_2SO_4 and concentrated under vacuum to recover **20** as white solid (117 mg, 0.56 mmol, 51% of conversion). The recovered **20** was re-exposed to the general oxidation protocol A using (*R,R*)- $\text{Mn}(\text{TIBS})\text{pdp}$ as catalyst (6.1 mg, 0.1 molar equivalent), the workup was performed as described above and the organic layers containing lactones **20b** and **20c** were united, analyzed by GC, the solvent removed by rotatory evaporation and eventually purified by flash column chromatography (SiO_2 , hexane/ EtOAc 3:2) to give 115 mg of lactone **20b** (*exo*) as white solid (0.56 mmol, 49% yield, 96% ee, over 63% total yield) and an inseparable 1:1 mixture of **20c** (*endo*) and unidentified byproduct (a Baeyer Villiger oxidation product, likely derived by in-situ formation of the peracid of **20**). ^1H NMR (400 MHz, CDCl_3) δ 4.10 (d, $J = 3.0$ Hz, 1H; C_4 [1H]), 2.85 (d, $J = 16.8$

Hz, 1H; C₂ [1H]), 2.64 (s, 1H; C₉ [1H]), 2.53 (s, 1H; C₅ [1H]), 2.15 (d, J = 16.7 Hz, 1H; C₂ [1H]), 2.12 - 2.01 (m, 6H; C₈ [2H] + C₁₁ [1H] + C₇ [1H] + C₆[1H] + C₁₂[1H]), 1.86 (d, J = 13.6 Hz, 1H; C₁₂ [1H]), 1.81 (d, J = 12.2 Hz, 2H, C₆ [1H] + C₁₁[1H]). ¹³C NMR (101 MHz, CDCl₃) δ 209.0 (C₁₀), 174.9 (C₁), 83.6 (C₄), 54.5 (C₃), 46.0 (C₉), 38.2 (C₈), 38.1 (C₁₁), 37.6 (C₂), 34.6 (C₁₂), 28.9 (C₅), 28.0 (C₆), 26.2 (C₇). HRMS (ESI-MS) *m/z* calculated for C₁₂H₁₄O₃ [M+Na]⁺ 229.0835, found 229.0836. Chiral GC analysis with HP-Chiral-20B (isothermal method at 150 °C).



21: 30% aqueous H₂O₂ (0.75 mL, Aldrich) was added dropwise to a cold (0 °C) solution of lactone **20b** (115 mg, 0.56 mmol) in glacial acetic acid (1 mL). The mixture was heated at 80 °C for 5 h. Then, the solvent was evaporated and the residue was dissolved in CHCl₃ (5 mL), washed with saturated

NaHCO₃ solution (2x2 ml), brine (2 ml), dried with anhydrous Na₂SO₄ and solvent was evaporated under vacuum. The residue was purified by flash column chromatography (SiO₂, hexane/EtOAc 4:1) to give 100 mg of the titled compound as white solid (0.45 mmol, 81%). ¹H NMR (400 MHz, CDCl₃) δ 4.63 (s, 1H; C₉ [1H]), 4.40 (s, 1H; C₄[1H]), 3.19 (d, J = 17.4 Hz, 1H; C₂ [1H]), 2.51 (d, J = 17.2 Hz, 2H; C₂ [1H] + C₅[1H]), 2.17 (m, 1H; C₂ [1H]), 2.14-2.05 (m, 4H, C₈ [2H]+ C₁₂ [2H]), 2.05 - 1.96 (m, 1H; C₆ [1H]), 1.93 (m, 1H; C₁₁ [1H]), 1.81 (dd, J = 14.5, 3.9 Hz, 1H; C₁₁ [1H]), 1.69 - 1.62 (m, 1H; C₆[1H]). ¹³C NMR (101 MHz, CDCl₃) δ 174.0 (C₁), 172.7 (C₁₀), 79.2 (C₄), 74.3 (C₉), 48.8 (C₃), 42.5 (C₂), 35.2 (C₈), 33.2 (C₁₂), 33.1 (C₁₁), 28.2 (C₅), 25.9 (C₆), 24.7 (C₇). HRMS (ESI-MS) *m/z* calculated for C₁₂H₁₄O₄ [M+Na]⁺ 245.0789, found 245.0789



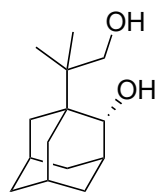
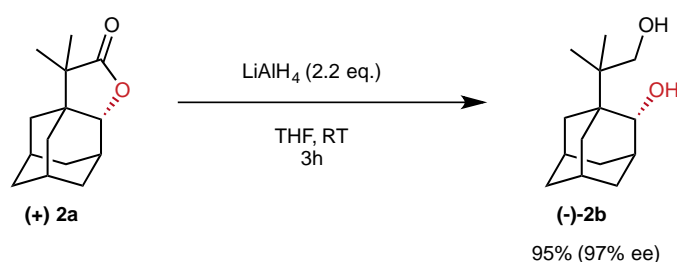
(+)-22: A THF (3 mL) solution of **21** (100 mg, 0.45 mmol, 1 eq.) was added dropwise into a 100 mL round-bottom flask containing a solution of LiAlH₄ (85.5 mg, 2.25 mmol, 5 eq.) in THF (13 ml) under nitrogen at room temperature. The reaction was left under stirring overnight at the same temperature. Then, the mixture was quenched with NaHCO₃ (15 mL) and

extracted with EtOAc (3x25 mL). The combined organic layers were dried over Na₂SO₄, filtered and the solvent was evaporated under reduced pressure. The crude was purified by flash column chromatography (SiO₂, CH₂Cl₂/MeOH 10:1) to obtain 78 mg of colorless oil (0.34 mmol, 75% yield). ¹H NMR (400 MHz, CD₃OD) δ 4.14 (s, 1H; C₄ [1H]), 4.11 - 4.02 (m, 1H; C₉ [1H]), 3.71 - 3.73 (m, 2H; C₁ [2H]), 3.54 (q, 2H, J = 12.2 Hz; C₁₀ [2H]), 2.09 (m, 1H; C₇

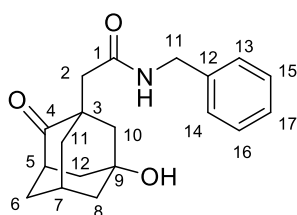
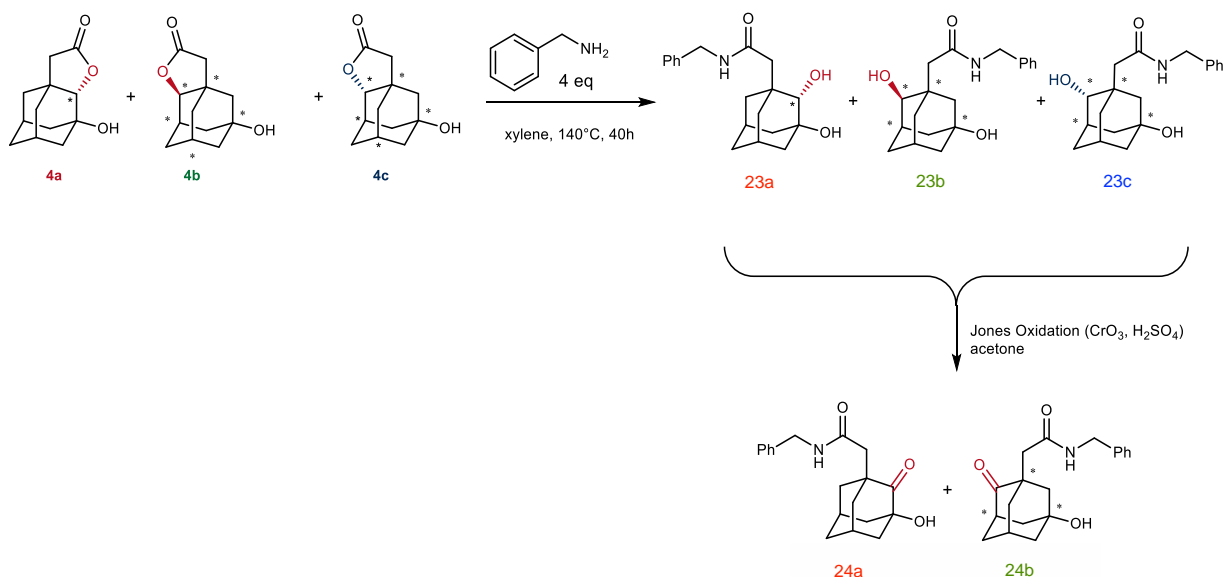
[1H]), 1.99 (d, J = 12.9 Hz, 1H; C₁₂ [1H]), 1.94 – 1.77 (m, 6H; C₂ [2H] + C₅ [1H] + C₆ [2H] + C₈[1H]), 1.72 (d, J = 9.2 Hz, 1H; C₁₁ [1H]), 1.66 (d, J = 14.8 Hz, 2H; C₈ [1H] + C₁₁ [1H]), 1.30 (d, J = 11.3 Hz, 1H; C₁₂ [1H]). ¹³C NMR (101 MHz, CD₃OD) δ 76.7 (C₄), 71.7 (C₁₀), 67.2 (C₉), 59.7 (C₁), 41.9 (C₃), 40.0 (C₈), 38.3 (C₆), 37.1 (C₅), 36.5 (C₂), 33.2 (C₁₁), 27.6 (C₁₂), 26.0 (C₇). HRMS (ESI-MS) *m/z* calculated for C₁₂H₂₂O₄ [M+Na]⁺ 253.1410, found 253.1412. [α]_D²⁴ +7.89 (CHCl₃, c 0.245).

4.6. Lactone derivatizations

Synthesis of 1,4-diol (-)-2b



(-)-2b (97% ee): A THF (2 mL) solution of **(R)-2a** (52 mg, 0.236 mmol) was added dropwise into a 10 mL round-bottom flask containing a solution of LiAlH₄ (19.7 mg, 0.52 mmol, 2.2 eq.) in THF (2.5 ml) under nitrogen at room temperature. The reaction was left under stirring for 3h. Then, the mixture was quenched with NaHCO₃ (5 mL) and extracted with EtOAc (3x15 mL). The collected organic layers were dried over MgSO₄, filtered and the solvent was evaporated under reduced pressure to obtain the desired compound as white solid (95% yield). ¹H NMR (300 MHz, CDCl₃) δ 4.04 (s, 2H), 3.79 (d, J = 3.3 Hz, 1H), 3.62 (d, J = 11.2 Hz, 1H), 3.22 (d, J = 11.3 Hz, 1H), 2.11 – 1.87 (m, 5H), 1.80 (dq, J = 12.5, 2.9 Hz, 1H), 1.68 (ddt, J = 7.9, 4.9, 2.7 Hz, 5H), 1.53 – 1.35 (m, 3H), 0.98 (s, 3H), 0.83 (s, 3H). ¹³C NMR (75 MHz, CDCl₃) δ 74.5, 68.9, 40.9, 40.6, 37.1, 37.1, 36.2, 36.2, 30.9, 30.8, 28.2, 28.1, 22.9, 19.8. HRMS (ESI-MS) *m/z* calculated for C₁₄H₂₄O₂ [M+Na]⁺ 247.1669, found 247.1681. [α]_D²⁴ -9.91 (CHCl₃, c 0.602). The enantiomeric excess was obtained by chiral analysis with HP-Chiral-20B of the acetylated **(-)-2b** (isothermal method at 200 °C).

Synthesis of **24b**

24b (40% ee, 2.38:1 e.r.): The mixture of lactones **4a**, **4b** and **4c** (80 mg, 0.38 mmol, 1:2.4 **4a**:(**4b**+**4c**) ratio, 0.271 mmol of **4b**+**4c**) obtained from oxidation of **4** following general oxidation protocol A was dissolved in anhydrous *p*-xylene and 4 equivalents of benzylamine (163 mg, 1.52 mmol) were added. The reaction was heated to 140°C under N_2 atmosphere for 16 hours. Then, the solvent was removed by rotatory evaporation, the crude was taken up in EtOAc, washed with HCl 1M (2x) and water (1x). The organic layer was dried over MgSO_4 , and the solvent removed by rotatory evaporation, and the mixture was used in the next step without further purification. This mixture was dissolved in acetone (10 mL) and 0.2 mL of Jones reagent were added dropwise at 0°C. After one hour, the mixture was filtered to remove insoluble Cr(III) salts, and the solvent removed by rotatory evaporation. The crude was taken up in Et_2O and washed with water (1x), HCl 1M (1x), NaHCO_3 (3x), water (2x). The organic phase was dried over MgSO_4 , and the solvent removed by rotatory evaporation. The crude was then purified by column chromatography (SiO_2 , EtOAc:Hexane 1:4) to yield 56 mg of **24b** (0.18 mmol, 66% yield over 2 steps). ^1H NMR (400 MHz, CDCl_3) δ 7.36 – 7.28 (m, 2H), 7.25 (d, J = 8.9 Hz, 3H), 6.80 (s, 1H), 4.39 (d, J = 5.8 Hz, 2H), 2.68 (s, 1H), 2.44 – 2.27 (m, 3H), 1.93 (d, J = 13.9 Hz, 8H), 1.85 (d, J = 12.9 Hz, 1H), 1.78 (d, J = 12.2 Hz, 1H). ^{13}C NMR (101 MHz, CDCl_3) δ 217.3, 138.5, 128.6, 127.6, 127.3, 67.5, 50.1, 47.0, 44.8, 43.9, 43.3, 43.0, 38.2, 30.0. HRMS (ESI-MS) m/z calculated for $\text{C}_{19}\text{H}_{24}\text{NO}_3$

[M+H]⁺ 314.1756, found 314.1778. The enantiomeric excess (40% ee) was obtained by chiral HPLC analysis with a chiral IAc column, eluted with isocratic hexane:isopropanol 90:10.

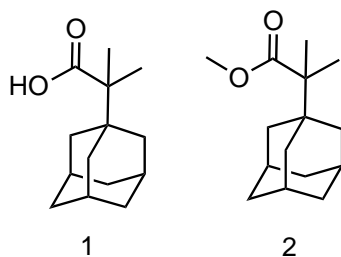
Experimental section Chapter V

5.1. Synthesis of catalysts and substrates

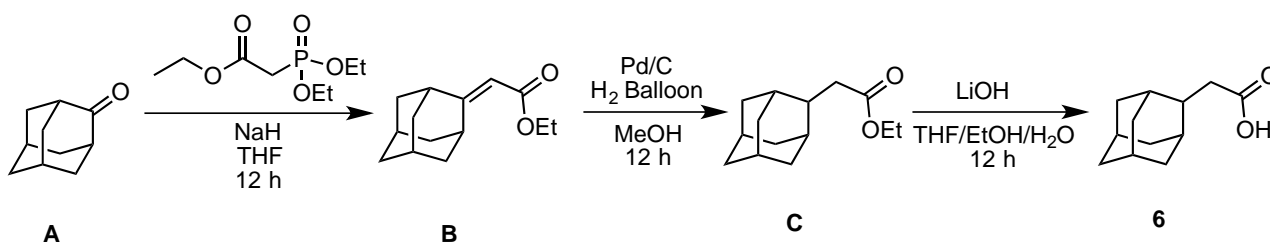
5.1.1 Synthesis of the complexes

Triflate complexes of (*S,S*)-Fe(pdp),²⁷ (*S,S*)-Fe(TIPSpdp),¹⁰³ (*S,S*)-Mn(pdp),¹²⁵ (*S,S*)-Mn(TIPSpdp),⁴⁵ (*S,S*)-Mn(TIPSmcp),⁴⁵ (*S,S*)-Mn(dMMpdp)¹¹⁷ and (*S,S*)-Mn(NMe₂pdp)¹¹⁷ were synthesized according to reported procedures. The synthesis of novel Mn(TIBSpdp) is described in the experimental section of **Chapter IV**.

5.1.2. Synthesis of the substrates



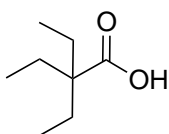
Carboxylic acids **1** and **2** were synthesized according to the reported procedure.¹²⁸



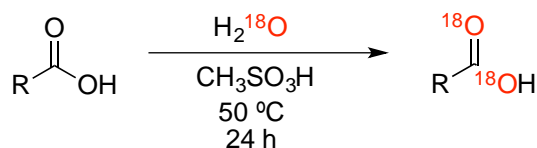
Following the procedure described in the **Chapter III** (preparation of **1**), the desired compound **6** was isolated as a white solid (0.38 g, 79% yield) after column chromatography over silica using hexane:EtOAc 20:1 mixture as eluent.

¹H NMR (CDCl₃, 400 MHz) δ: 11.26 (s, 1H), 2.52 (d, J = 7.5 Hz, 2H), 2.32 - 2.19 (m, 1H), 1.96 - 1.68 (m, 12H), 1.65 - 1.53 (m, 2H).

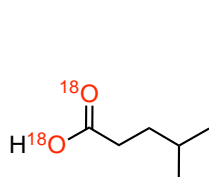
¹³C NMR δ: 180.3, 41.0, 38.8, 38.2, 37.9, 31.5, 27.8.



12: The synthesis of **12** is described in **Chapter III**.

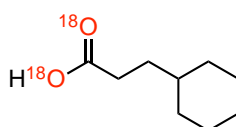
5.1.3 Synthesis of the ^{18}O -labelled substrates

^{18}O -Labelled water (5 eq.) was added dropwise to a stirred suspension of the corresponding carboxylic acid (6 mmol) in MsOH (2 mL) at 50 °C. After 24 h, the clear solution was cooled, treated with ice (3 g), followed by saturated aqueous $(\text{NH}_4)_2\text{SO}_4$ solution (3 mL). The resulting mixture was extracted with CH_2Cl_2 (3 x 4 mL), the combined extracts were washed with saturated aqueous $(\text{NH}_4)_2\text{SO}_4$ (3 x 4 mL), dried over Na_2SO_4 , and concentrated by rotary evaporation. The isotopically enriched carboxylic acids were obtained as a white crystalline solid or colorless oil for which ^{18}O -incorporation was obtained by HRMS analysis.



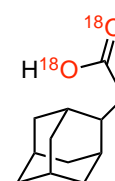
4

79% doubly labelled ^{18}O
18% singly labelled ^{18}O
3% unlabelled



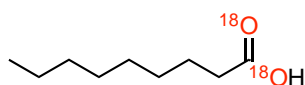
5

62% doubly labelled ^{18}O
34% singly labelled ^{18}O
4% unlabelled



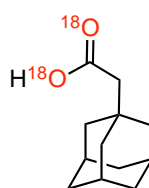
6

68% doubly labelled ^{18}O
30% singly labelled ^{18}O
3% unlabelled



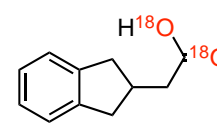
7

56% doubly labelled ^{18}O
38% singly labelled ^{18}O
6% unlabelled



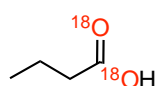
3

70% doubly labelled ^{18}O
28% singly labelled ^{18}O
2% unlabelled



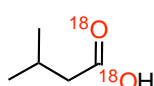
8

73% doubly labelled ^{18}O
24% singly labelled ^{18}O
3% unlabelled



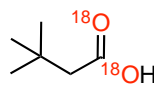
9

48% doubly labelled ^{18}O
43% singly labelled ^{18}O
9% unlabelled



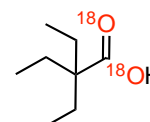
10

50% doubly labelled ^{18}O
42% singly labelled ^{18}O
8% unlabelled



11

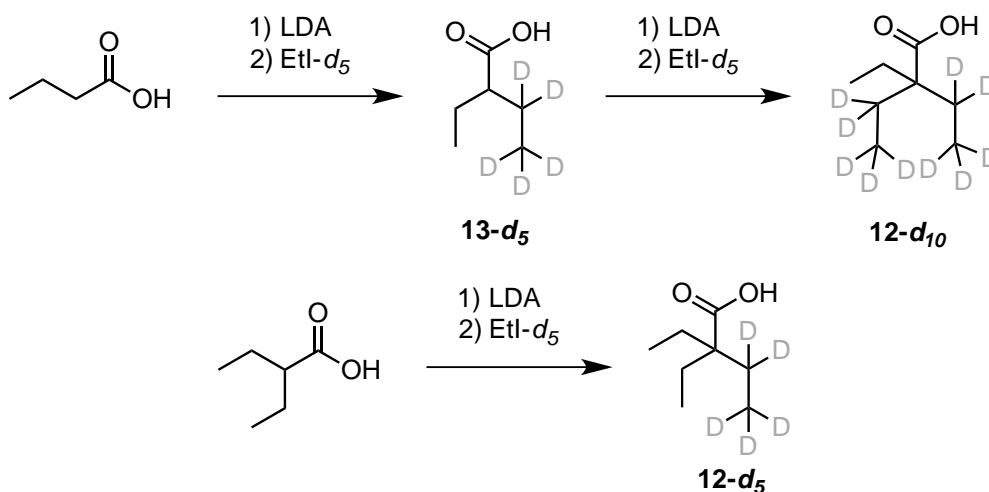
51% doubly labelled ^{18}O
41% singly labelled ^{18}O
8% unlabelled



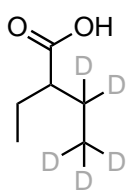
12

58% doubly labelled ^{18}O
37% singly labelled ^{18}O
5% unlabelled

5.1.4. Synthesis of deuterated substrates



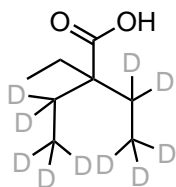
General alkylation protocol: A solution of the corresponding carboxylic acid (1.0 equiv) in THF (0.5 M) was added dropwise to a lithium diisopropylamide (1 M in THF, 2.2 equiv) solution at $-80\text{ }^\circ\text{C}$ (AcOEt/ N_2 bath). The resulting solution was allowed to warm to room temperature and stirred for 1 h. After the addition of Ethyl iodide- d_5 (1.0 equiv) in THF (0.5 mL) at $-80\text{ }^\circ\text{C}$, the reaction mixture was stirred for 12 h at room temperature, then poured into 2 N HCl and extracted with EtOAc. The combined organic layers were washed with brine, dried over anhydrous MgSO_4 , filtered and concentrated. Purification by silica gel flash chromatography with ethyl acetate:hexane eluent mixture provided the pure carboxylic acid.



13- d_5 : Following the *general alkylation protocol* the desired compound was obtained from butanoic acid and isolated after column chromatography (SiO_2 , hexane:EtOAc 20:1) as a pale yellow oil (43% yield).

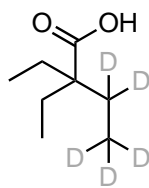
^1H NMR (400 MHz, CDCl_3) δ : 2.22 (dd, $J = 8.4, 5.7$ Hz, 1H), 1.72 – 1.50 (m, 2H), 0.94 (t, $J = 7.4$ Hz, 3H).

^{13}C NMR δ : 182.5, 48.4, 24.7, 11.7.



12-d₁₀: Following the *general alkylation protocol* the desired compound was obtained from **13-d₅** and isolated after column chromatography (SiO₂, hexane:EtOAc 20:1) as a colorless solid (64% yield). ¹H NMR (400 MHz, CDCl₃) δ: 1.60 (q, J = 7.5 Hz, 2H), 0.81 (t, J = 7.5 Hz, 3H).¹

¹³C NMR δ: 183.5, 49.4, 26.0, 8.3.



12-d₅: Following the *general alkylation protocol* the desired compound was obtained from 2-ethylbutyric and isolated after column chromatography (SiO₂, hexane:EtOAc 20:1) as a colorless solid (78% yield).

¹H NMR (400 MHz, CDCl₃) δ: 1.62 (q, J = 7.5 Hz, 4H), 0.92 – 0.78 (t, J = 7.5 Hz, 6H).

¹³C NMR (101 MHz, CDCl₃) δ: 184.1, 49.6, 26.0, 8.3.

5.2. Oxidation Reactions

Hydrogen peroxide solutions employed in the oxidation reactions were prepared by diluting commercially available hydrogen peroxide (50% w/w H₂O₂ solution in water, Aldrich) in the corresponding solvent to achieve a concentration of 0.9 M. Commercially available trifluoromethanesulfonic acid (TfOH, 99%) purchased from Fluorochem was employed and used as received. H₂¹⁸O (99% ¹⁸O) was obtained from Sigma-Aldrich. H₂¹⁸O₂ (80% ¹⁸O) obtained from GiOxCat.

V.4.5.1. General oxidation protocol

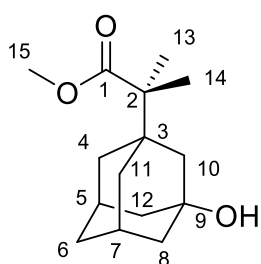
Substrate (100 μmol, 1 molar equivalent) and catalyst (1.0-2.0 μmol, 1-2 mol%) were dissolved in 4.0 mL of the corresponding solvent inside a 12-mL vial equipped with a magnetic stirring bar. A 0.9 M solution of H₂O₂ (or eventually H₂¹⁸O₂) in the same solvent (1 or 1.5 molar equivalent) diluted from commercially available H₂O₂ water solution and (when required) 0.09 M solution of triflic acid (0.1 molar equivalents) were delivered independently over 30 minutes by syringe pump into the solution under air. At the end of

the addition, the mixture was left under stirring for additional 15-30 minutes to ensure complete lactonization. *Workup for GC analysis:* 50 μmol of the internal standard (biphenyl) were added and the mixture was quickly filtered through a short plug of silica gel, which was subsequently rinsed with $2 \times 1 \text{ mL}$ of AcOEt. GC analysis of the filtrate provided substrate conversion and product yields relative to the internal standard integration (calibration constant of the substrate was used for the yield determination of those products which were not isolated). Afterward, the reaction was analyzed by GC-MS (via chemical ionization with NH_3/CH_4) to determinate isotopic distribution.

^{18}O -incorporation in the final product was obtained from the $^{18}\text{O}_2/^{18}\text{O}$ (or $^{16}\text{O}_2/^{18}\text{O}$ in the case of experiments with $\text{H}_2^{18}\text{O}_2$) lactone ratio and corrected for the isotopic purity of the starting material.

IV.4.5. Characterization of oxidized products

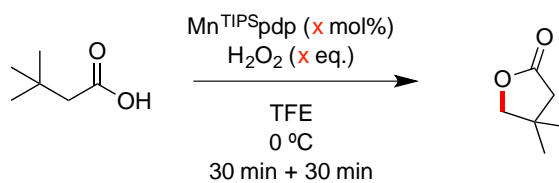
Lactones **5a**, **6a**, **7a** were identified by GC-MS (via chemical ionization with NH_3/CH_4) while the characterization of all the other lactones has been already reported in previous chapters.



2a: **2a** was obtained following the oxidation protocol in TFE and with 15 eq. of AcOH using catalyst (*S,S*)-Mn(^{TIBS}pdp) and isolated in 76% yield as a white solid after column chromatography (SiO_2 , hexane:EtOAc 3:1). ^1H NMR (300 MHz, CDCl_3) δ 3.62 (s, 3H, C_{15} [3H]), 2.19 (s, 2H C_{10} [2H]), 1.61 (m, 5H; C_4 [2H] + C_6 [1H] + C_{11} [2H]), 1.52 (s, 2H; C_5 [1H] + C_7 [1H]), 1.48 (m, 5H; C_6 [1H] + C_8 [2H] + C_{12} [2H]), 1.10 (s, 6H; C_{13} [3H] + C_{14} [3H]). ^{13}C NMR (75 MHz, CDCl_3) δ 177.1 (C_1), 69.1 (C_9), 51.2 (C_{15}), 48.3 (C_{10}), 44.9 (C_2), 44.5 (C_4 + C_{11}), 40.4 (C_3), 35.7 (C_8 + C_{12}), 35.3 (C_6), 30.5 (C_5 + C_7), 20.4 (C_{13} + C_{14}). HRMS (ESI-MS) m/z calculated for $\text{C}_{15}\text{H}_{24}\text{O}_3$ [$\text{M}+\text{Na}$]⁺ 275.1618, found 275.1625

Annex

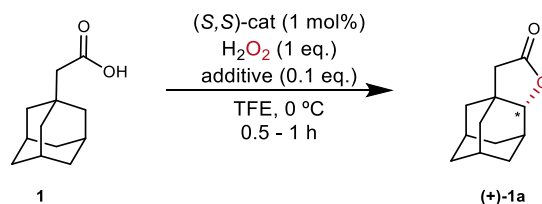
Annex Chapter III

Table S1. Optimization of cat. loading and H₂O₂ equiv. for the oxidation of 16

Entry	H ₂ O ₂ (eq.)	Cat. Loading (mol %)	Conversion (%)	Lactone Yield (%)
1	1	1	75	44
2	1.5	1	94	55
3	1.5	2	96	66
4	2	2	96	61
5	1.5	3	96	65
6	1.5	4	96	65

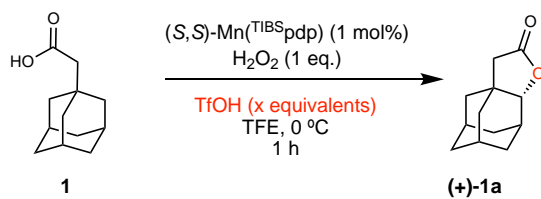
^aReaction conditions and workup as described in General oxidation protocol B. Conversions and yields determined by GC analysis. Ee's determined by chiral GC analysis.

Annex Chapter IV

Table S1. Reaction optimization for oxidation of **1**.

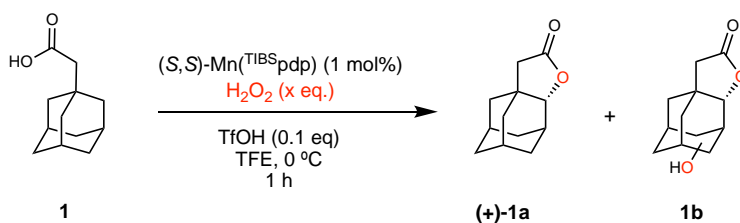
Entry	Catalyst	Additive	Conv. (%)	Lactone yield (%)	ee (%) ^b
1	Fe(pdp)	-	59	6	75
2	Fe(mcp)	-	53	5	67
3	Fe(TIPSpdp)	-	75	12	84
4	Fe(TIPSmcp)	-	92	11	65
5	Mn(pdp)	-	72	26	89
6	Mn(TIPSpdp)	-	81	28	94
7	Mn(TIBSpdp)	-	74	29	95
8 ^c	"	-	54	14	93
9 ^d	"	-	89	28	95
10	Mn(mcp)	-	77	14	10
11	Mn(TIPSmcp)	-	38	8	65
12	Mn(TIPSecp)	-	64	7	89
13	Mn(^d MMpdp)	-	85	38	90
14	Mn(^{NMe} 2pdp)	-	86	43	90
15	Mn(pdp)	TfOH	80	48	96
16	Mn(^{NMe} pdp)	TfOH	60	35	91
17	Mn(^d MMpdp)	TfOH	90	64	93
18	Mn(^{TMS} pdp)	TfOH	89	51	96
19	Mn(^{TIPS} pdp)	TfOH	88	52	97
20	Mn(^{TIBS} pdp)	TfOH	84	60	98
21	(<i>R,R</i>)-Mn(^{TIBS} pdp)	TfOH	82	61	-98
22 ^e	Mn(pdp)	TfOH	80	56	96
23 ^e	Mn(pdp) ^g	TfOH	81	64	96
24 ^e	Mn(^d MMpdp)	TfOH	>99	63	93
25 ^e	Mn(^{TIPS} pdp)	TfOH	88	55	97
26 ^e	Fe(^{TIPS} pdp)	TfOH	97	36	94
27 ^e	Mn(^{TIBS} pdp)	TfOH	85	70(68) ^f	98

^a Reaction conditions as described in general oxidation protocol A with (*S,S*)-catalysts. Conversions and yields determined by GC analysis of two or three different independent runs. ^bee values determined by GC equipped with chiral column. ^cReaction carried out in CH₃CN instead of TFE. ^dReaction carried out in HFIP instead of TFE. ^eReaction left stirring additional 30 minutes to promote lactonization. ^f4.5 mmol (800 mg) scale reaction ^gIsolated yield

Table S2. Optimization of triflic acid (TfOH) loading.

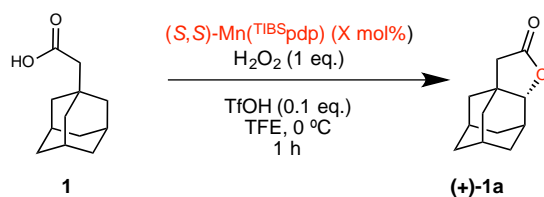
Entry	TfOH (eq.)	Conversion (%)	Yield (%)	ee (%)
1	0.05	90	60	95
2	0.1	85	70	98
3	0.2	92	63	98
4	0.5	77	52	98

^aReaction conditions and workup as described in General oxidation protocol A. Conversions and yields determined by GC analysis. Ee's determined by chiral GC analysis.

Table S3. Effect of increasing H₂O₂ equivalents.^a

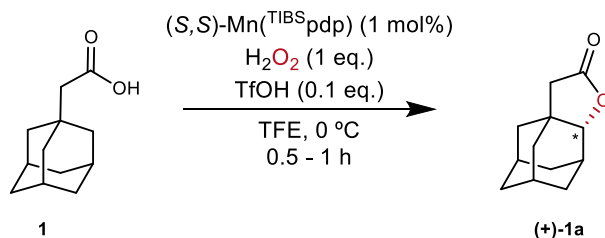
Entry	H ₂ O ₂ (eq.)	Conversion (%)	Yield 1a (%)	Yield 1b (%)
1	0.5	48	31	-
2	1	85	70	-
3	1.3	97	59	5%
4	1.5	>99	57	14%
5	2	>99	41	31%

^aReaction conditions and workup as described in General oxidation protocol A. Conversions and yields determined by GC analysis.

Table S4. Optimization of catalyst loading.^a

Entry	mol%	Conversion (%)	Yield (%)
1	2	95	70
2	1	85	70
3	0.5	83	57
4	0.1	65	29

Reaction conditions and workup as described in General oxidation protocol A. Conversions and yields determined by GC analysis.

Table S5. Optimization of substrate concentration.^a

Entry	[1] (mM)	Conversion (%)	Yield (%)
1	0.7	87	67
2	0.25	85	70
3	0.1	84	56
4	0.07	51	29

Reaction conditions and workup as described in General oxidation protocol A. Conversions and yields determined by GC analysis.

Oxidation of 3'-substituted adamantaneacetic acid

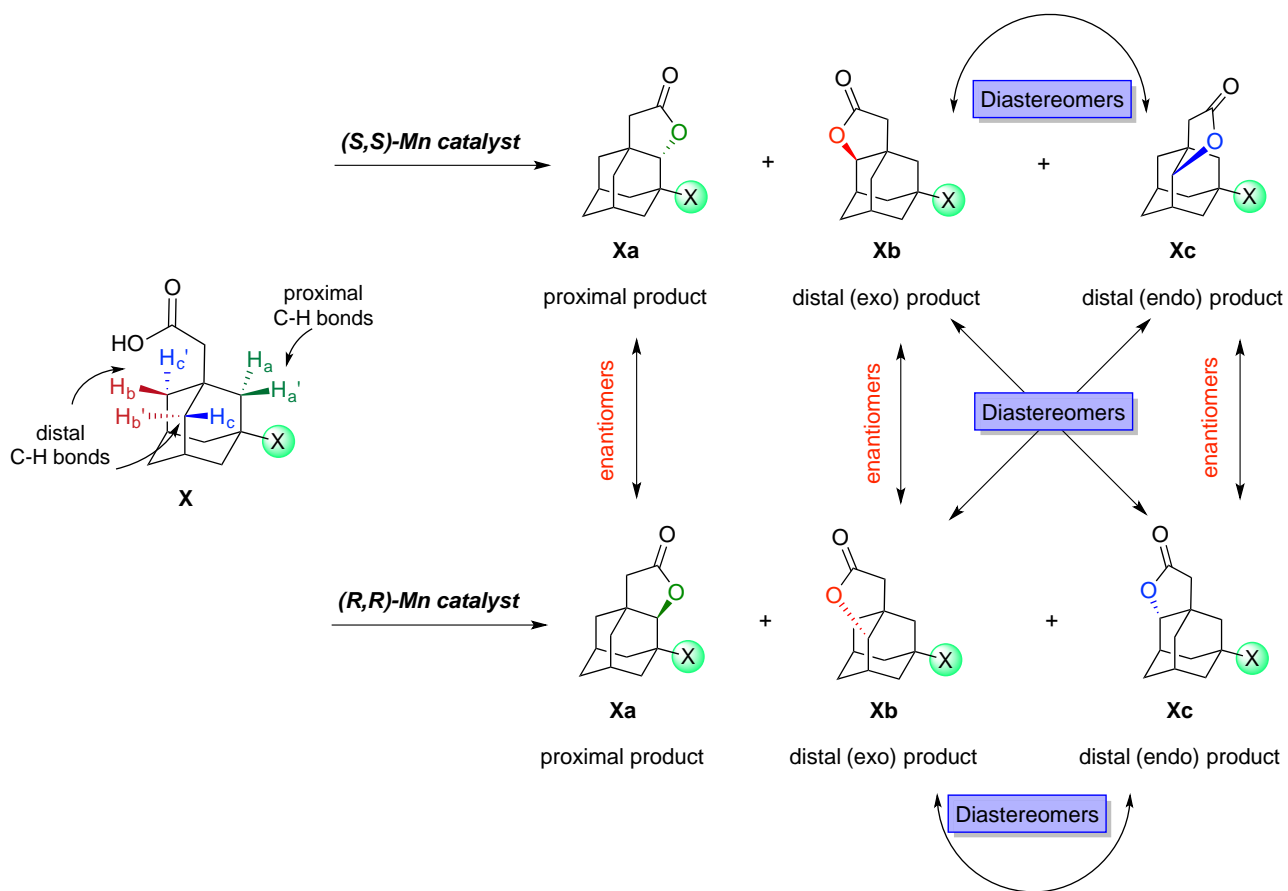
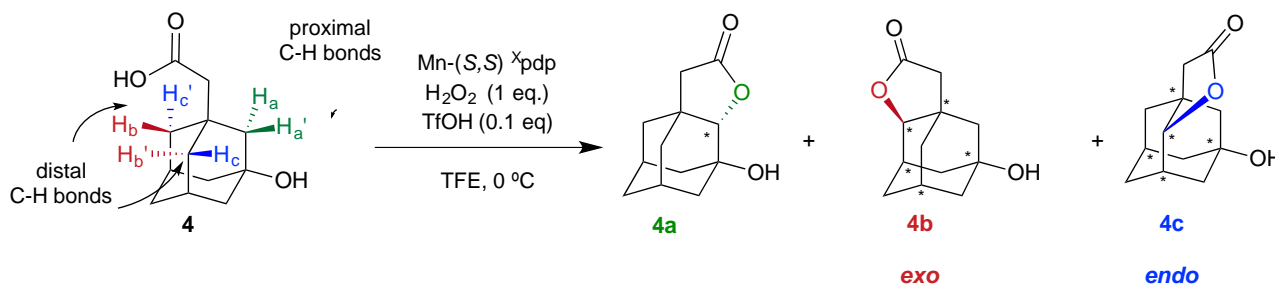


Figure S1 Depiction of all possible lactone products.

Table S6. Oxidation of 3'-hydroxyadamantaneacetic acid (**4**).

Diastereomeric ratio (d.r.) corresponds to *exo:endo* (**4b:4c**) ratio. Regioisomeric ratio (r.r.) refers to the ratio of proximal over distal oxidation products (**4a**):(**4b** + **4c**).



Entry	Catalyst	Total Yield (conv., %)	Yield 4a (ee, %)	Yield 4b (ee, %)	Yield 4c (ee, %)	<i>d.r.</i>	<i>r.r.</i>	4a:4b:4c
1	Mn(^{TIBS} pdp)	55 (77)	11(91)	32(99)	12(67)	2.7 : 1	1:4	1:2.9:1.1
2	Mn(^{TIPS} pdp)	58 (69)	11(88)	28(99)	19(65)	1.5 : 1	1:4.4	1:2.5:1.7
3	Mn(^{TMS} pdp)	61 (78)	10(97)	24(98)	27(83)	1 : 1.1	1:5.2	1:2.4:2.7
4	Mn(^{dMM} pdp)	64 (79)	10(87)	19(99)	35 (88)	1 : 1.8	1:5.4	1:1.9:3.5
5	Mn(pdp)	50 (81)	6(82)	13(99)	31 (89)	1 : 2.5	1:7.4	1:2.2:5.2
6 ^b	Mn(^{TIBS} pdp)	17 (61)	2(n.d.)	7(99)	8(63)	1 : 1.1	1:7.5	1:3.5:4
7 ^c	Mn(^{TIBS} pdp)	25 ^d (83)	11(90)	10(99)	3.5(66)	1.1 : 1	1:1.2	3.1:2.9:1

Reaction conditions as given in the general oxidation protocol A with (*S,S*)-catalysts. Conversions and yields determined by GC analysis of crude reaction mixtures. Ee's determined by GC with chiral stationary phase. ^bReaction performed in CH₃CN instead of TFE. ^cReaction performed in HFIP instead of TFE. ^d10% of another unidentified product.

Determination of site-selectivity in distal lactones

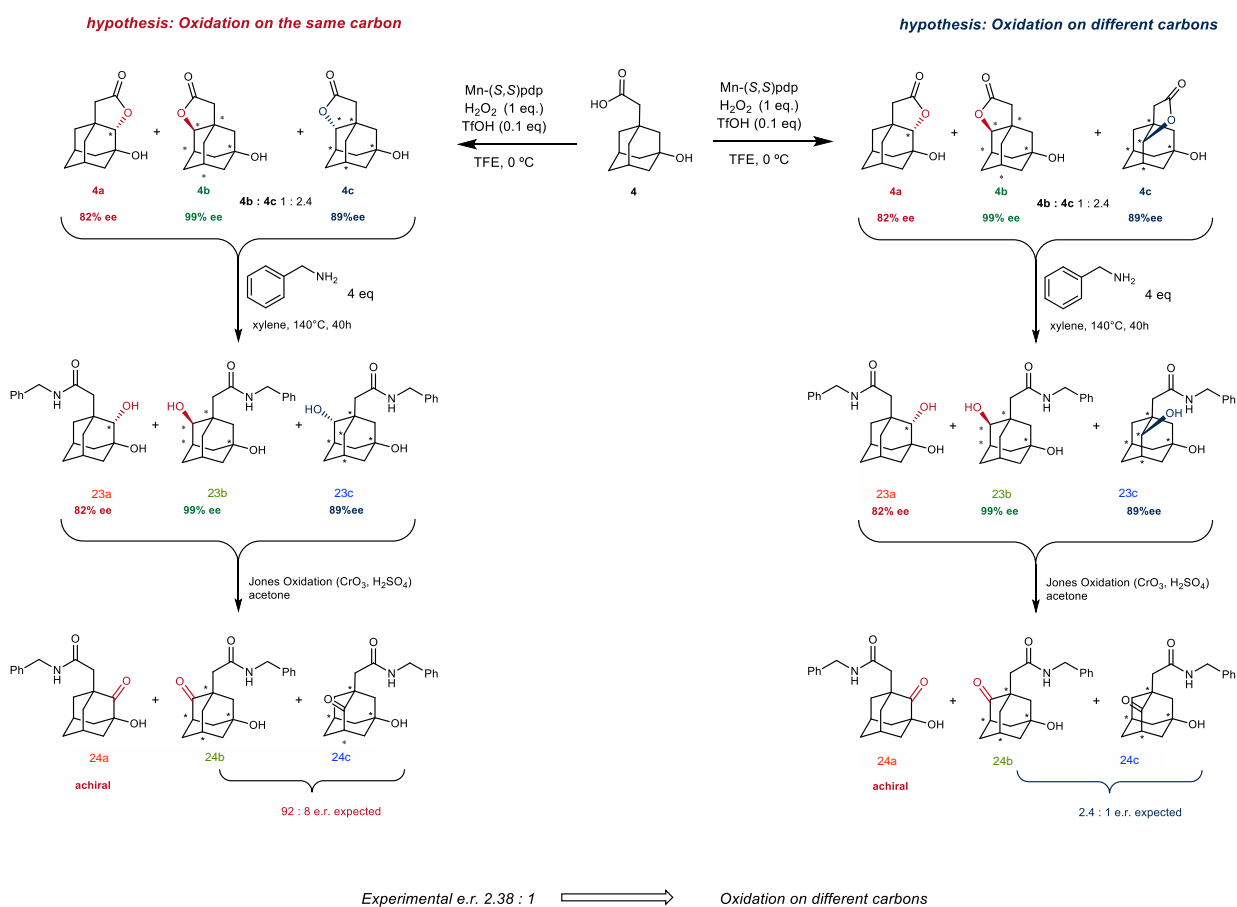
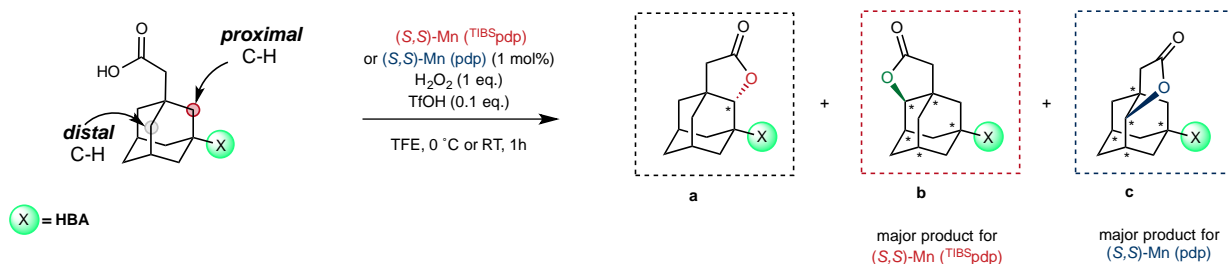


Figure S2: Determination of the connectivity of lactones **4b** and **4c**.

To determine if the directed oxidation on the distal methylenes occurs on the same carbon or on two different carbons (i.e., products **4b** and **4c** differ just from the orientation of the lactone group, with the C-O bond forged on the same methylene) we undertook a three-step derivatization of products **4a**, **4b** and **4c**. These lactones have been subjected to ring opening (aminolysis) and alcohol oxidation to form keto-amide **24**, in which the chirality of the secondary C-O bond is now depleted. If the lactonization of **4** preferentially occurs on the same carbon (i.e., the C-O bond in **4b** and **4c** is forged on the same methylene), **24b** will have a high (>90%) ee, as a weighed sum of the enantiomeric excesses of lactones **4b** and **4c** (Fig. S2, left). On the other hand, if the oxidation occurs on different carbons, the ketone will have an ee that reflects the *exo:endo* ratio **4b:4c** (2.4:1) weighed for their enantiomeric excesses, as **4b** and **4c** will be transformed into the two enantiomers of **24b** (Fig. S2, right). Experimentally, we measured an enantiomeric ratio (e.r.) of 2.38:1, consistent with an oxidation on different carbons. Since the chirality of the lactones **4b** and **4c** is retained upon

catalyst change from (S,S) -Mn(pdp) to (S,S) -Mn(^{TIBS}pdp) or other (S,S) catalysts, this consideration can be applied to every lactone product in this study.

Table S7. Oxidation of 3'-substituted adamantaneacetic acids (Section A, X=HBA)

Entry	Substrate	Catalyst	Tot. yield (Conv., %)	Yield Xa (ee, %)	Yield Xb (ee, %)	Yield Xc (ee, %)	r.r. ^a	d.r. ^b
1		Mn(TIBSpdp)	55 (77)	11(91)	32(99)	12(67)	3.7:1	2.7:1
		Mn(pdp)	50 (81)	6(82)	13(99)	31 (89)	7:1	1:2.5
2		Mn(TIBSpdp)	82 (93)	19 (96)	42(96)	21(65)	3.3:1	2:1
		Mn(pdp)	39 (76)	5(94)	10(93)	24(88)	7:1	1:2.5
3		Mn(TIBSpdp)	79 (82)	6.5(n.d.)	57(95)	15(95)	11.4:1	3.8:1
		Mn(pdp)	57 (74)	8.9(n.d.)	12.5(94)	35.5(94)	5.4:1	1:2.9
4		Mn(TIBSpdp)	75 (>99)	7(n.d.)	51(96)	17(91)	10:1	3:1
		Mn(pdp)	60 (75)	6(n.d.)	19.5(95)	34.5(94)	9:1	2:1
5		Mn(TIBSpdp)	67 (72)	4 (n.d.)	23.5 (n.d.)	39.5 (92)	16:1	1:1.7
		Mn(pdp)	54 (67)	3 (n.d.)	12 (n.d.)	39(94)	17:1	1:3.3
6		Mn(TIBSpdp)	50 (69)	11(90)	11(97)	28(88)	3.5:1	1:2.5
		Mn(pdp)	47 (73)	9.5(91)	9.5(96)	28(88)	4:1	1:3

Reaction conditions as given in the general oxidation protocol A. Conversions, yields and product ratios determined by GC analysis of crude reaction mixtures. Ee's determined by GC with chiral stationary phase. ^ar.r. is defined as regioisomeric ratio, proximal (Xa) over distal (Xb+Xc) ratio. ^bDiastereomeric ratio (d.r.) corresponds to *exo* (Xb)/*endo* (Xc).

Oxidation of 3'-substituted adamantaneacetic acids with $\text{Mn}(\text{TIBS}^{\text{pdp}})$ (section B, X=non-HBA)

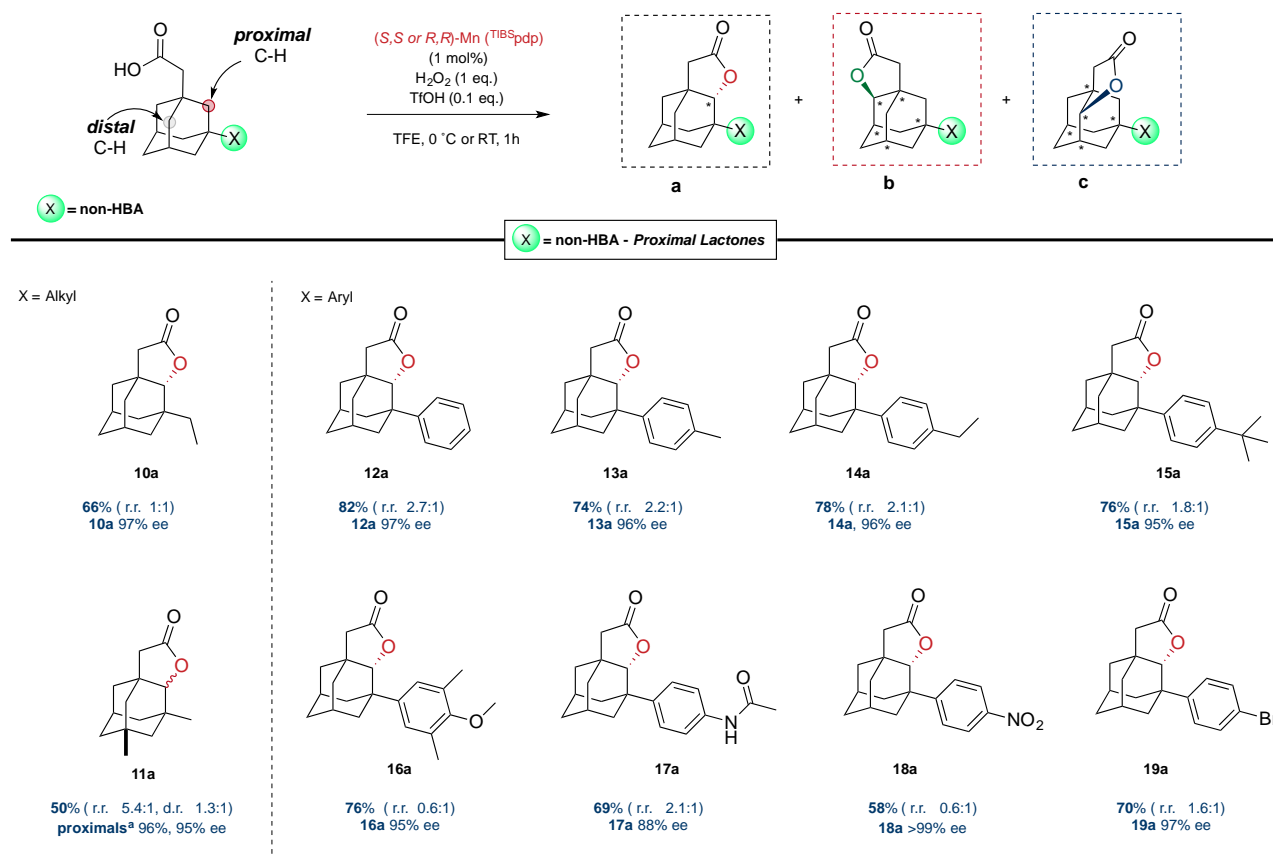


Figure S3. For each reaction, the major product is drawn and the total GC yield of the three lactones is displayed in the first row together with the distribution of products in the crude mixture (r.r. ratio). In the second row is reported the enantioselectivity for the proximal lactone. r.r. is defined as regioisomeric ratio, proximal (a) over distal (b+c) ratio unless for **11** for which the r.r. correspond to proximals/distal lactones. ^aTwo diastereomeric proximal lactones are formed.

Figure S4. Derivatization of lactone (+)-**3a** to form 1,4-diol (-)-**3b**.

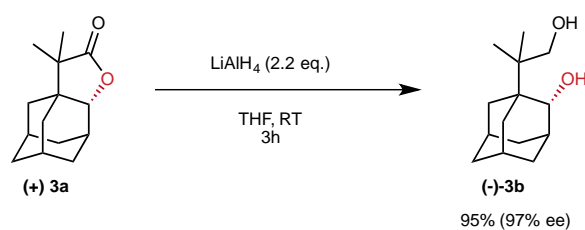
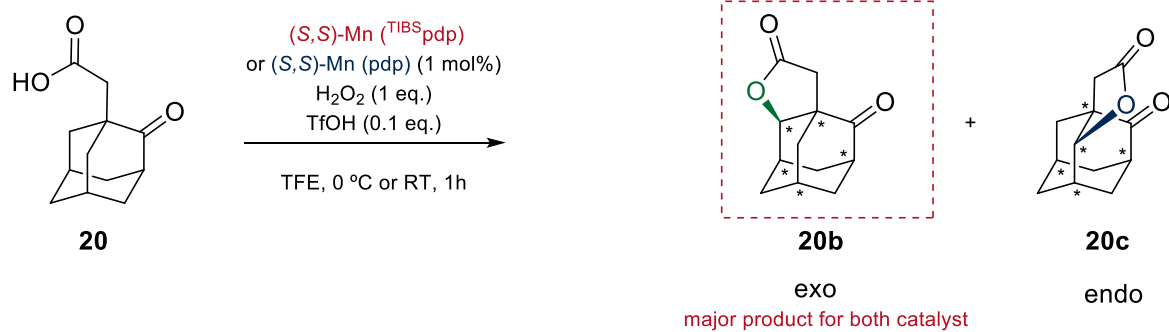


Figure S5. Oxidation of **20** with different catalysts.2x $(S,S)\text{-Mn}(\text{TIBS})_2\text{pdp}$ 49% (96% ee)
d.r. 6.5:1

7.5%

 $(S,S)\text{-Mn}(\text{pdp})$ 38% (90% ee)
d.r. 1.9:1

20%

Annex Chapter V

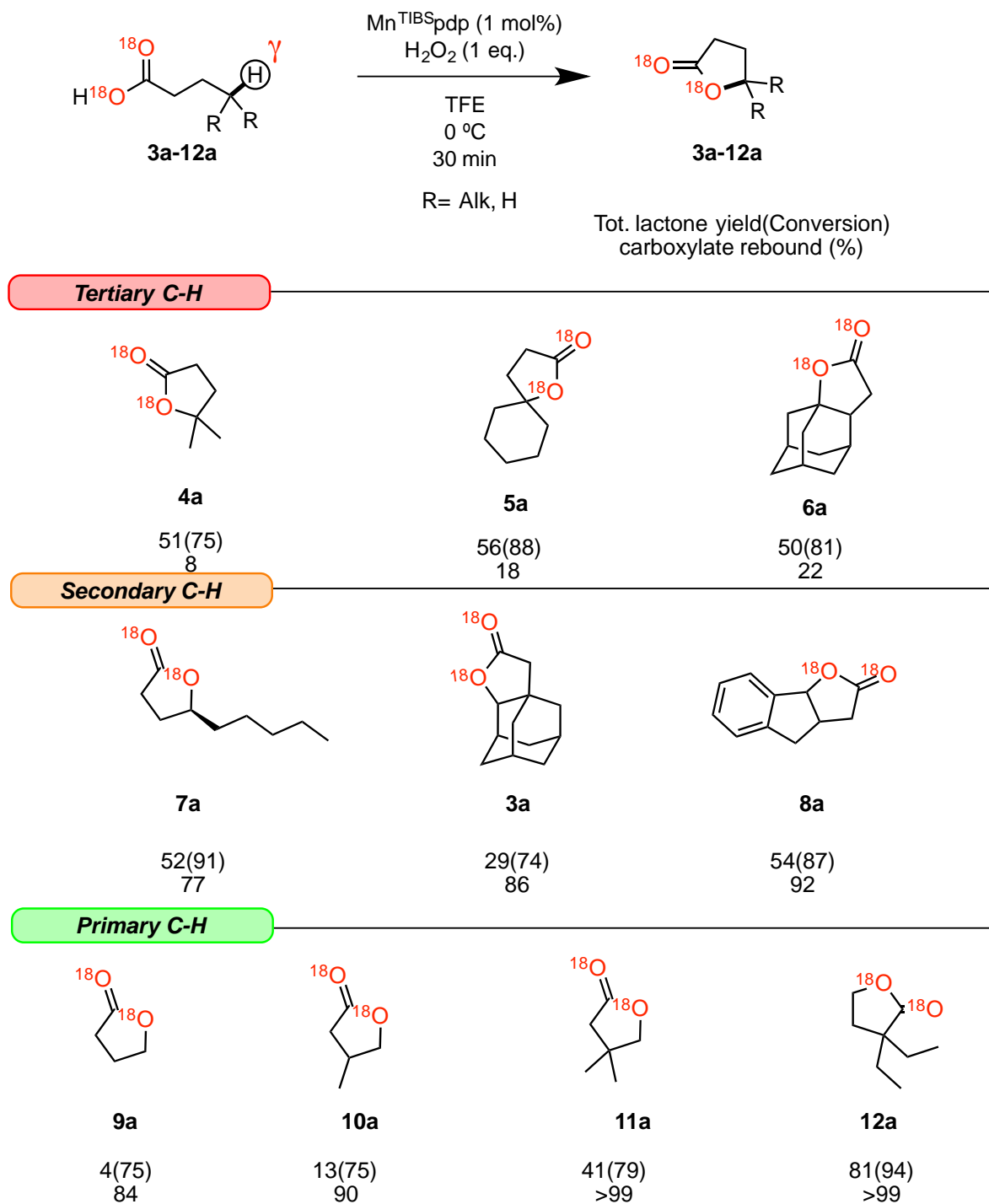


Figure S1. The scope of doubly labelled carboxylic acids involved in the project.

References

- (1) Cernak, T.; Dykstra, K. D.; Tyagarajan, S.; Vachal, P.; Krska, S. W. *Chem. Soc. Rev.* **2015**, *45*, 546-576.
- (2) Milan, M.; Bietti, M.; Costas, M. *Chem. Commun.* **2018**, *54*, 9559-9570.
- (3) Newton, C. G.; Wang, S.-G.; Oliveira, C. C.; Cramer, N. *Chem. Rev.* **2017**, *117*, 8908-8976.
- (4) Saint-Denis, T. G.; Zhu, R. Y.; Chen, G.; Wu, Q. F.; Yu, J. Q. *Science* **2018**, *359*, 759.
- (5) Dyker, G. *Angew. Chem., Int. Ed.* **1999**, *38*, 1698-1712.
- (6) Labinger, J. A.; Bercaw, J. E. *Nature* **2002**, *417*, 507-514.
- (7) Oloo, W. N.; Que Jr., L. *Acc. Chem. Res.* **2015**, *48*, 2612-2621.
- (8) Olivo, G.; Cussò, O.; Costas, M. *Chem. - An Asian J.* **2016**, *11*, 3148-3158.
- (9) Talsi, E. P.; Bryliakov, K. P. *Coord. Chem. Rev.* **2012**, *256*, 1418-1434.
- (10) Brückl, T.; Baxter, R. D.; Ishihara, Y.; Baran, P. S. *Acc. Chem. Res.* **2012**, *45*, 826-839.
- (11) Chen, M. S.; White, M. C. *Science* **2010**, *327*, 566-571.
- (12) Lewis, J. C.; Coelho, P. S.; Arnold, F. H. *Chem. Soc. Rev.* **2011**, *40*, 2003-2021.
- (13) Lichtor, P. A.; Miller, S. J. *Nat. Chem.* **2012**, *4*, 990-995.
- (14) Vidal, D.; Olivo, G.; Costas, M. *Chem. - A Eur. J.* **2018**, *24*, 5042-5054.
- (15) Whisler, M. C.; MacNeil, S.; Snieckus, V.; Beak, P. *Angew. Chem. Int. Ed.* **2004**, *43*, 2206-2225.
- (16) Lyons, T. W.; Sanford, M. S. *Chem. Rev.* **2010**, *110*, 1147-1169.
- (17) Uttry, A.; van Gemmeren, M. *Synlett* **2018**, *29*, 1937-1943.
- (18) He, J.; Wasa, M.; Chan, K. S. L.; Shao, Q.; Yu, J.-Q. *Chem. Rev.* **2017**, *117*, 8754-8786.
- (19) Guo, B. H.; Kai, G. Y.; Jin, H. B.; Tang, K. X. *African J. Biotechnol.* **2006**, *5*, 15-20.
- (20) Wender, P. A.; Badham, N. F.; Conway, S. P.; Floreancig, P. E.; Glass, T. E.; Houze, J. B.; Krauss, N. E.; Lee, D.; Marquess, D. G.; McGrane, P. L.; Meng, W.; Natchus, M. G.; Shuker, A. J.; Sutton, J. C.; Taylor, R. E. *J. Am. Chem. Soc.* **1997**, *119*, 2757-2758.
- (21) Ortiz De Montellano, P. R. *Cytochrome P450: Structure, Mechanism, and Biochemistry*, 3rd ed, 3rd ed.; Ortiz De Montellano, P. R., Ed.; Kluwer Academic/Plenum: New York, 2005.
- (22) Costas, M.; Mehn, M. P.; Jensen, M. P.; Que Jr., L. *Chem. Rev.* **2004**, *104*, 939-986.
- (23) Haber, F.; Weiss, J. J. *Proc. R. Soc. London, Ser. A* **1934**, *147*, 332-351.
- (24) Walling, C. *Acc. Chem. Res.* **1998**, *31*, 155-157.
- (25) MacFaul, P. A.; Ingold, K. U.; Wayner, D. D. M.; Que Jr., L. *J. Am. Chem. Soc.* **1997**, *119*, 10594-10598.

- (26) Chen, K.; Que Jr., L. J. *Am. Chem. Soc.* **2001**, *123*, 6327–6337.
- (27) Chen, M. S.; White, M. C. *Science* **2007**, *318*, 783–787.
- (28) Ottenbacher, R. V.; Samsonenko, D. G.; Talsi, E. P.; Bryliakov, K. P. *Org. Lett.* **2012**, *14*, 4310–4313.
- (29) Oloo, W. N.; Fielding, A. J.; Que Jr., L. J. *Am. Chem. Soc.* **2013**, No. 135, 6438–6441.
- (30) Comprehensive Handbook of Chemical Bond Energies. Luo, Y.-R.; Luo, Y.-R., Ed.; CRC Press: Boca Raton, Florida, USA, 2007.
- (31) Howell, J. M.; Feng, K.; Clark, J. R.; Trzepakowski, L. J.; White, M. C. *J. Am. Chem. Soc.* **2015**, *137*, 14590–14593.
- (32) Milan, M.; Bietti, M.; Costas, M. *Org. Lett.* **2018**, *20*, 2720–2723.
- (33) Milan, M.; Carboni, G.; Salamone, M.; Costas, M.; Bietti, M. *ACS Catal.* **2017**, *7*, 5903–5911.
- (34) Kim, S.; Ginsbach, J. W.; Lee, J. Y.; Peterson, R. L.; Liu, J. J.; Siegler, M. a.; Sarjeant, A. a.; Solomon, E. I.; Karlin, K. D. *J. Am. Chem. Soc.* **2015**, 150223091214009.
- (35) Genovino, J.; Lütz, S.; Sames, D.; Touré, B. B. *J. Am. Chem. Soc.* **2013**, *135*, 12346–12352.
- (36) Ling, Z.; Yun, L.; Liu, L.; Wu, B.; Fu, X. *Chem. Commun.* **2013**, *49*, 4214–4216.
- (37) Park, J.; Morimoto, Y.; Lee, Y.-M.; You, Y.; Nam, W.; Fukuzumi, S. *Inorg. Chem.* **2011**, *50*, 11612–11622.
- (38) Dantignana, V.; Milan, M.; Cussó, O.; Company, A.; Bietti, M.; Costas, M. *ACS Cent. Sci.* **2017**, *3*, 1350–1358.
- (39) Borrell, M.; Gil-Caballero, S.; Bietti, M.; Costas, M. *ACS Catal.* **2020**, *10*, 4702–4709.
- (40) Gómez, L.; Garcia-Bosch, I.; Company, A.; Benet-Buchholz, J.; Polo, A.; Sala, X.; Ribas, X.; Costas, M. *Angew. Chem. Int. Ed.* **2009**, *48*, 5720–5723.
- (41) Gormisky, P. E.; White, M. C. *J. Am. Chem. Soc.* **2013**, *135*, 14052–14055.
- (42) Font, D.; Canta, M.; Milan, M.; Cussò, O.; Ribas, X.; Klein Gebbink, R. J. M.; Costas, M. *Angew. Chem. Int. Ed.* **2016**, *55*, 5776–5779.
- (43) Newhouse, T.; Baran, P. S. *Angew. Chem. Int. Ed.* **2011**, *50*, 3362–3374.
- (44) Eliel, E. L.; Biros, F. J. *J. Am. Chem. Soc.* **1966**, *88*, 3334–3343.
- (45) Milan, M.; Bietti, M.; Costas, M. *ACS Cent. Sci.* **2017**, *3*, 196–204.
- (46) Bigi, M. A.; Reed, S. A.; White, M. C. *J. Am. Chem. Soc.* **2012**, *134*, 9721–9726.
- (47) Bigi, M. A.; Reed, S. A.; White, M. C. *Nat. Chem.* **2011**, *3*, 216–222.
- (48) Pichette Drapeau, M.; Gooßen, L. J. *Chem. – A Eur. J.* **2016**, *22*, 18654–18677.

- (49) Kao, L.-C.; Sen, A. *J. Chem. Soc., Chem. Commun.* **1991**, No. 18, 1242–1243.
- (50) Dangel, B. D.; Johnson, J. A.; Sames, D. *J. Am. Chem. Soc.* **2001**, *123*, 8149–8150.
- (51) Lee, J. M.; Chang, S. *Tetrahedron Lett.* **2006**, *47*, 1375–1379.
- (52) Janssen, M.; De Vos, D. E. *Chem. – A Eur. J.* **2019**, *25*, 10724–10734.
- (53) Novák, P.; Correa, A.; Gallardo-Donaire, J.; Martin, R. *Angew. Chem. Int. Ed.* **2011**, *50*, 12236–12239.
- (54) Zhuang, Z.; Yu, J. *Nature* **2020**, *577*, 1–5.
- (55) Giri, R.; Maugel, N.; Li, J.-J.; Wang, D.-H.; Breazzano, S. P.; Saunders, L. B.; Yu, J.-Q. *J. Am. Chem. Soc.* **2007**, *129*, 3510.
- (56) Feng, W.; Wang, T.; Liu, D.; Wang, X.; Dang, Y. *ACS Catal.* **2019**, *9*, 6672–6680.
- (57) Beesley, R. M.; Ingold, C. K.; Thorpe, J. F. *J. Chem. Soc., Trans.* **1915**, *107*, 1080.
- (58) Jung, M. E.; Piizzi, G. *Chem. Rev.* **2005**, *105*, 1735–1766.
- (59) Chen, G.; Zhuang, Z.; Li, G.-C.; Saint-Denis, T. G.; Hsiao, Y.; Joe, C. L.; Yu, J.-Q. *Angew. Chem. Int. Ed.* **2017**, *56*, 1506–1509.
- (60) Amatore, C.; Pfluger, F. *Organometallics* **1990**, *9*, 2276–2282.
- (61) Zhu, Y.; Chen, X.; Yuan, C.; Li, G.; Zhang, J.; Zhao, Y. *Nat. Commun.* **2017**, *8*, 14904.
- (62) Ghosh, K. K.; van Gemmeren, M. *Chem. – A Eur. J.* **2017**, *23*, 17697–17700.
- (63) Dolui, P.; Das, J.; Chandrashekar, H. B.; Anjana, S. S.; Maiti, D. *Angew. Chem. Int. Ed.* **2019**, *58*, 13773–13777.
- (64) Shen, P.-X.; Hu, L.; Shao, Q.; Hong, K.; Yu, J.-Q. *J. Am. Chem. Soc.* **2018**, *140*, 6545–6549.
- (65) Hu, L.; Shen, P.-X.; Shao, Q.; Hong, K.; Qiao, J. X.; Yu, J.-Q. *Angew. Chem. Int. Ed.* **2019**, *58*, 2134–2138.
- (66) Zhuang, Z.; Yu, C.-B.; Chen, G.; Wu, Q.-F.; Hsiao, Y.; Joe, C. L.; Qiao, J. X.; Poss, M. A.; Yu, J.-Q. *J. Am. Chem. Soc.* **2018**, *140*, 10363–10367.
- (67) Ghosh, K. K.; Utry, A.; Koldemir, A.; Ong, M.; van Gemmeren, M. *Org. Lett.* **2019**, *21*, 7154–7157.
- (68) White, M. C.; Doyle, A. G.; Jacobsen, E. N. *J. Am. Chem. Soc.* **2001**, No. 123, 7194–7195.
- (69) Mas-Ballesté, R.; Costas, M.; van den Berg, T.; Que Jr., L. *Chem. – A Eur. J.* **2006**, *12*, 7489–7500.
- (70) Mas-Ballesté, R.; Que Jr., L. *J. Am. Chem. Soc.* **2007**, *129*, 15964–15972.
- (71) Hull, J. F.; Balcells, D.; Sauer, E. L. O.; Raynaud, C.; Brudvig, G. W.; Crabtree, R. H.;

- Eisenstein, O. *J. Am. Chem. Soc.* **2010**, *132*, 7605–7616.
- (72) Ottenbacher, R. V.; Talsi, E. P.; Bryliakov, K. P. *J. Catal.* **2020**, *390*, 170–177.
- (73) Rasik, C. M.; Brown, M. K. *Angew. Chem. Int. Ed.* **2014**, *53*, 14522–14526.
- (74) Ye, Q.; Qu, P.; Snyder, S. A. *J. Am. Chem. Soc.* **2017**, *139*, 18428–18431.
- (75) Hung, K.; Condakes, M. L.; Novaes, L. F. T.; Harwood, S. J.; Morikawa, T.; Yang, Z.; Maimone, T. J. *J. Am. Chem. Soc.* **2019**, *141*, 3083–3099.
- (76) Gil, S.; Parra, M.; Segura, P. R. and J. *Mini-Reviews in Organic Chemistry*. 2009, pp 345–358.
- (77) Paryzek, Z.; Skiera, I. *Org. Prep. Proced. Int.* **2007**, *39*, 203–296.
- (78) Gou, J.; Hao, F.; Huang, C.; Kwon, M.; Chen, F.; Li, C.; Liu, C.; Ro, D.-K.; Tang, H.; Zhang, Y. *Plant J.* **2018**, *93*, 92–106.
- (79) White, M. C.; Zhao, J. *J. Am. Chem. Soc.* **2018**, *140*, 13988–14009.
- (80) Olivo, G.; Cussó, O.; Borrell, M.; Costas, M. *J. Biol. Inorg. Chem.* **2017**, *22*, 425–452.
- (81) P. Bryliakov, K. *Chem. Rev.* **2017**, *117*, 11406–11459.
- (82) Rej, S.; Das, A.; Chatani, N. *Coord. Chem. Rev.* **2021**, *431*, 213683.
- (83) Vicens, L.; Olivo, G.; Costas, M. *ACS Catal.* **2020**, *10*, 8611–8631.
- (84) Ottenbacher, R. V.; Talsi, E. P.; Bryliakov, K. P. *ACS Catal.* **2015**, No. 5, 39–44.
- (85) Serrano-Plana, J.; Acuña-Parés, F.; Dantignana, V.; Oloo, W. N.; Castillo, E.; Draksharapu, A.; Whiteoak, C. J.; Martin-Diaconescu, V.; Basallote, M. G.; Luis, J. M.; Que Jr., L.; Costas, M.; Company, A. *Chem. – A Eur. J.* **2018**, *24*, 5331–5340.
- (86) Xu, S.; Draksharapu, A.; Rasheed, W.; Que, L. *J. Am. Chem. Soc.* **2019**, *141*, 16093–16107.
- (87) Miao, C.; Wang, B.; Wang, Y.; Xia, C.; Lee, Y.-M.; Nam, W.; Sun, W. *J. Am. Chem. Soc.* **2016**, *138*, 936–943.
- (88) Chang, S. J.; McNally, D.; 2-Tehrany, S.; Mary, S.; Hickey, J.; Boyd, R. H. *J. Am. Chem. Soc.* **1970**, *92*, 3109–3118.
- (89) Fuchs, S.; Berl, V.; Lepoittevin, J. P. *European J. Org. Chem.* **2007**, No. 7, 1145–1152.
- (90) Gawdzik, B.; Kamizela, A.; Szyszkowska, A. *Chemik* **2015**, *69*, 346–349.
- (91) Vicens, L.; Bietti, M.; Costas, M. *Angew. Chem. Int. Ed.* **2021**, *60*, 4740–4746.
- (92) Milan, M.; Bietti, M.; Costas, M. *Chem. Commun.* **2018**, *54*, 9559–9570.
- (93) Zang, C.; Liu, Y.; Xu, Z.-J.; Tse, C.-W.; Guan, X.; Wei, J.; Huang, J.-S.; Che, C.-M. *Angew. Chem. Int. Ed.* **2016**, *55*, 2–7.

- (94) Schwertfeger, H.; Fokin, A. A.; Schreiner, P. R. *Angew. Chem. Int. Ed.* **2008**, *47*, 1022–1036.
- (95) Davies, H. M. L.; Liao, K. *Nat. Rev. Chem.* **2019**, *3*, 347–360.
- (96) Cussó, O.; Ribas, X.; Lloret-Fillol, J.; Costas, M. J. *Am. Chem. Soc.* **2013**, *135*, 14871–14878.
- (97) Canta, M. Development of Highly Structured Non-Heme Iron Catalysts for Selective C-H Group Oxidations, Universitat de Girona, 2014.
- (98) Kolocouris, N.; Zoidis, G.; Fytas, C. *Synlett* **2007**, *2007*, 1063–1066.
- (99) Peters, J. A. *Synthesis (Stuttg.)*. **1979**, *1979*, 321–336.
- (100) Zefirova, O. N.; Nurieva, E. V.; Lemcke, H.; Ivanov, A. A.; Zyk, N. V.; Weiss, D. G.; Kuznetsov, S. A.; Zefirov, N. S. *Mendeleev Commun.* **2008**, *18*, 183–185.
- (101) Kingston, D. G. I.; Snyder, J. P. *Acc. Chem. Res.* **2014**, *47*, 2682–2691.
- (102) Butkus, E. *Synlett* **2001**, *2001*, 1827–1835.
- (103) Font, D.; Canta, M.; Milan, M.; Cussó, O.; Ribas, X.; Klein Gebbink, R. J. M.; Costas, M. *Angew. Chem. Int. Ed.* **2016**, *55*, 5776–5779.
- (104) After our initial results in Mn-catalyzed C-H lactonization (*J. Am. Chem. Soc.* **2020**, *142*, 3, 1584–1593) and during the development of this project, Bryliakov and co-workers observed small percentage of carboxylate rebound product (1–12%) in Mn-catalyzed intermolecular oxidations of tertiary C-H bonds. Ottenbacher, R. V.; Bryliakova, A. A.; Shashkov, M. V.; Talsi, E. P.; Bryliakov, K. P. *ACS Catal.* **2021**, *11*, 5517–5524.
- (105) Berkessel, A.; Adrio, J. A. *J. Am. Chem. Soc.* **2006**, *128*, 13412–13420.
- (106) Dantignana, V.; Company, A.; Costas, M. *Chimia* **2020**, *74*, 470–477.
- (107) Sarkar, S.; Cheung, K. P. S.; Gevorgyan, V. *Chem. Sci.* **2020**, *11*, 12974–12993.
- (108) Costas, M.; Que Jr., L. *Angew. Chem. Int. Ed.* **2002**, *41*, 2179–2181.
- (109) Company, A.; Gómez, L.; Güell, M.; Ribas, X.; Luis, J. M.; Que Jr., L.; Costas, M. J. *Am. Chem. Soc.* **2007**, *129*, 15766–15767.
- (110) Serrano-Plana, J.; Oloo, W. N.; Acosta-Rueda, L.; Meier, K. K.; Verdejo, B.; García-España, E.; Basallote, M. G.; Münck, E.; Que, L.; Company, A.; Costas, M. J. *Am. Chem. Soc.* **2015**, *137*, 15833–15842.
- (111) Kim, J.; Harrison, R. G.; Kim, C.; Que Jr., L. *J. Am. Chem. Soc.* **1996**, *118*, 4373–4379.
- (112) Kopinke, F.-D.; Georgi, A. *J. Phys. Chem. A* **2017**, *121*, 7947–7955.
- (113) Annunziatini, C.; Gerini, M. F.; Lanzalunga, O.; Lucarini, M. J. *Org. Chem.* **2004**, *69*, 3431–3438.

- (114) Koshino, N.; Saha, B.; Espenson, J. H. *J. Org. Chem.* **2003**, *68*, 9364–9370.
- (115) Galli, C.; Gentili, P.; Lanzalunga, O.; Lucarini, M.; Pedulli, G. F. *Chem. Commun.* **2004**, No. 20, 2356–2357.
- (116) Brandi, P.; Galli, C.; Gentili, P. *J. Org. Chem.* **2005**, *70*, 9521–9528.
- (117) Cussó, O.; Garcia-Bosch, I.; Font, D.; Ribas, X.; Lloret-Fillol, J.; Costas, M. *Org. Lett.* **2013**, *15*, 6158–6161.
- (118) Gładkowski, W.; Grabarczyk, M.; Wińska, K.; Bialońska, A.; Ciunik, Z.; Wawrzeńczyk, C. *J. Mol. Catal. B Enzym.* **2006**, *39*, 31–39.
- (119) Fujita, T.; Suga, K.; Watanabe, S.; Yanagi, R. **1977**, No. I, 593–598.
- (120) Trost, B. M.; Rhee, Y. H. *J. Am. Chem. Soc.* **1999**, *121*, 11680–11683.
- (121) Xie, H.; Lu, J.; Gui, Y.; Gao, L.; Song, Z. *Synlett* **2017**, *28*, 2453–2459.
- (122) Bromhead, L. J.; Visser, J.; McErlean, C. S. P. *J. Org. Chem.* **2014**, *79*, 1516–1520.
- (123) Xie, X.; Stahl, S. S. *J. Am. Chem. Soc.* **2015**, *137*, 3767–3770.
- (124) Mebane, R. C.; Grimes, K. D.; Jenkins, S. R.; Deardorff, J. D.; Gross, B. H. *Synth. Commun.* **2002**, *32*, 2049–2054.
- (125) Ottenbacher, R. V.; Bryliakov, K. P.; Talsi, E. P. *Adv. Synth. Catal.* **2011**, *353*, 885–889.
- (126) Murphy, A.; Dubois, G.; Stack, T. D. P. *J. Am. Chem. Soc.* **2003**, *125*, 5250–5251.
- (127) Šilhár, P.; Silvaggi, N. R.; Pellett, S.; Čapková, K.; Johnson, E. A.; Allen, K. N.; Janda, K. D. *Bioorg. Med. Chem.* **2013**, *21*, 1344–1348.
- (128) Mawo, R. Y.; Smoliakova, I. P. *Polyhedron* **2009**, *28*, 77–84.

Digital Annex

NMR SPECTRA, GC TRACES and X-Ray ANALYSIS

**“Carboxylic Acids as Directing Groups for
Intramolecular Catalytic Oxidation of Unactivated
C(sp³)-H bonds with Bioinspired Catalysts”**

Marco Cianfanelli

2021

Table of Contents

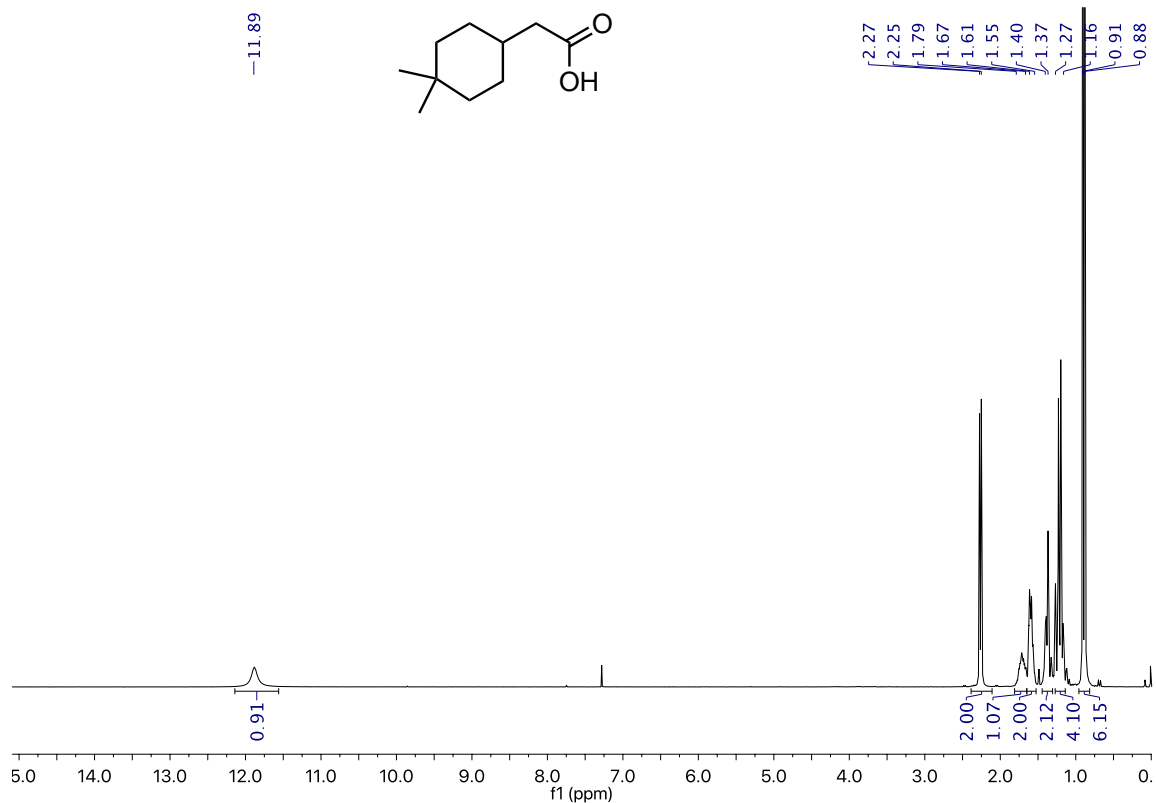
ANNEX CHAPTER III	3
III. NMR characterization of the substrates	4
III. NMR characterization of lactone products	14
III. GC Traces	48
Selected GC traces of the crude mixtures from the oxidation of 1.	48
GC traces for the determination of the enantiomeric excesses	49
ANNEX CHAPTER IV	54
IV. NMR Spectra	55
IV. NMR characterization of the ligand precursors and ligands	55
IV. NMR characterization of the substrates	62
IV. NMR characterization of lactone products	69
IV. NMR characterization of lactone products (Section A, X=HBA)	71
IV. NMR Characterization of lactones (Section B, X=non-HBA)	114
IV. NMR Characterization of the products in the synthesis of (+)-22	157
IV. NMR Characterization of lactone derivatization products	177
IV. HPLC and GC chromatograms of the products	179
IV. GC chromatograms for the determination of the a:b:c ratios (and d.r., r.r.)	180
IV. GC and HPLC traces for the determination of the enantiomeric excesses	196
IV. X-ray analysis	219
IV. Crystal data for (S,S)-[Mn(CF ₃ SO ₃) ₂ (^{TiBS} pdp)	219
IV. Single Crystal structure of (R)-2a:	221
IV. Single crystal structure of (+)-4b:	223
IV. Single crystal structure of (+)-22:	224
ANNEX CHAPTER V	226
V. NMR characterization of 7	227
V. NMR characterization of the deuterated substrates	228
V. NMR characterization of the oxidized product 2a	231

ANNEX CHAPTER III

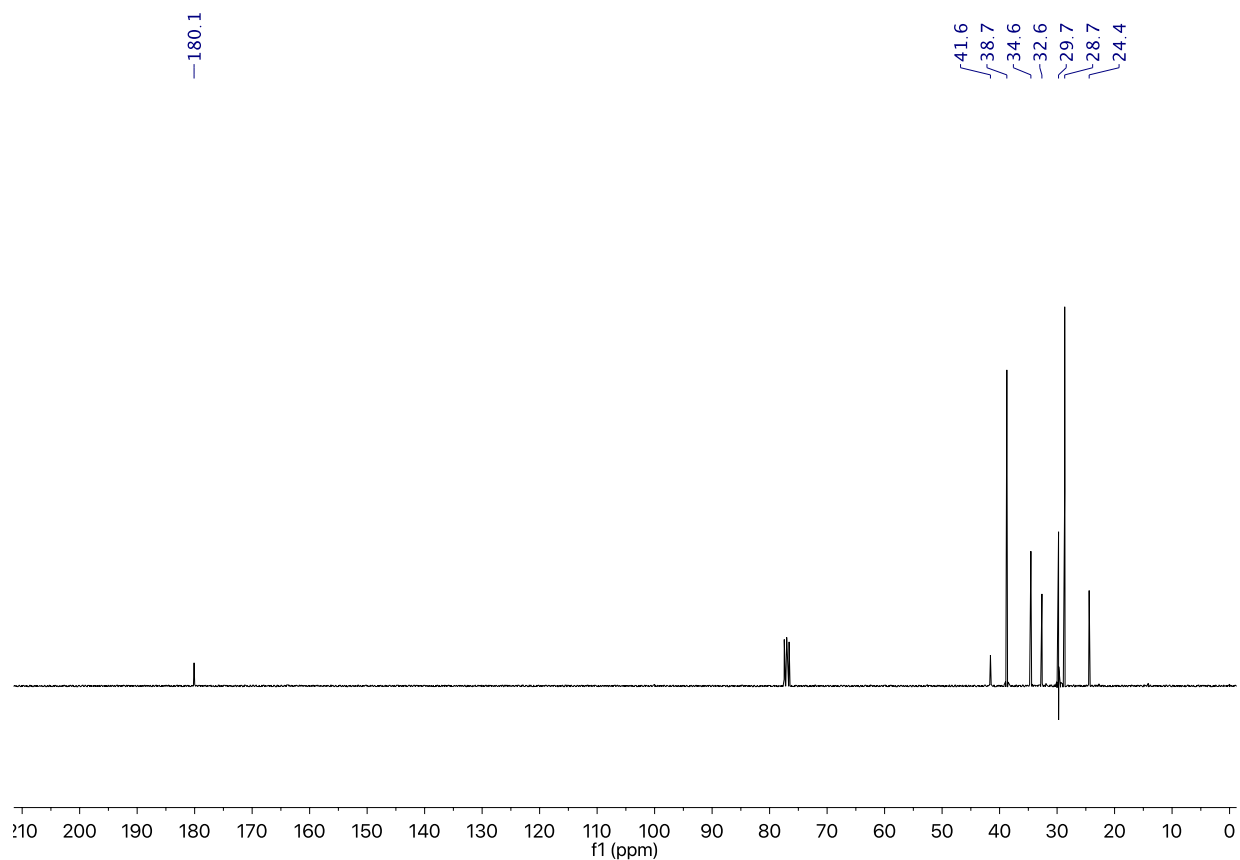
NMR SPECTRA, GC TRACES

III. NMR characterization of the substrates

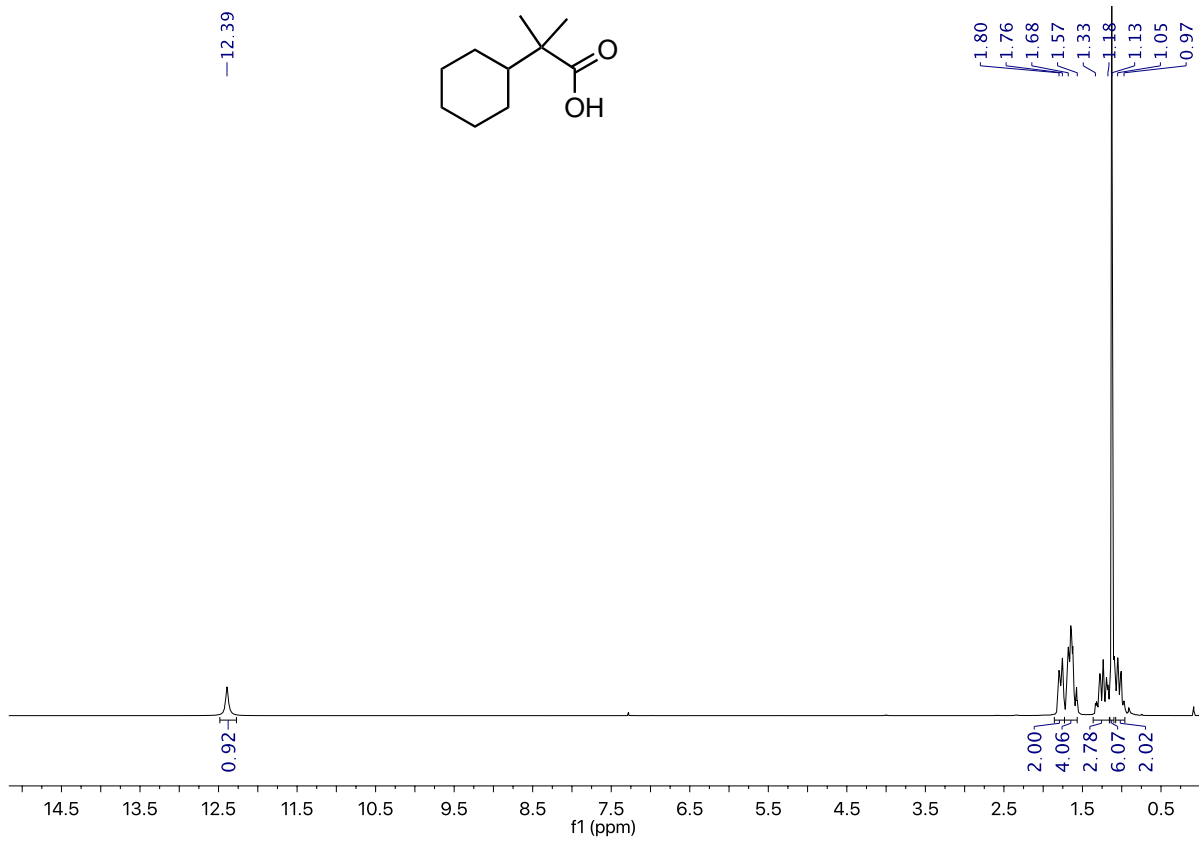
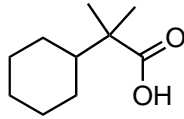
^1H NMR of **1** in CDCl_3



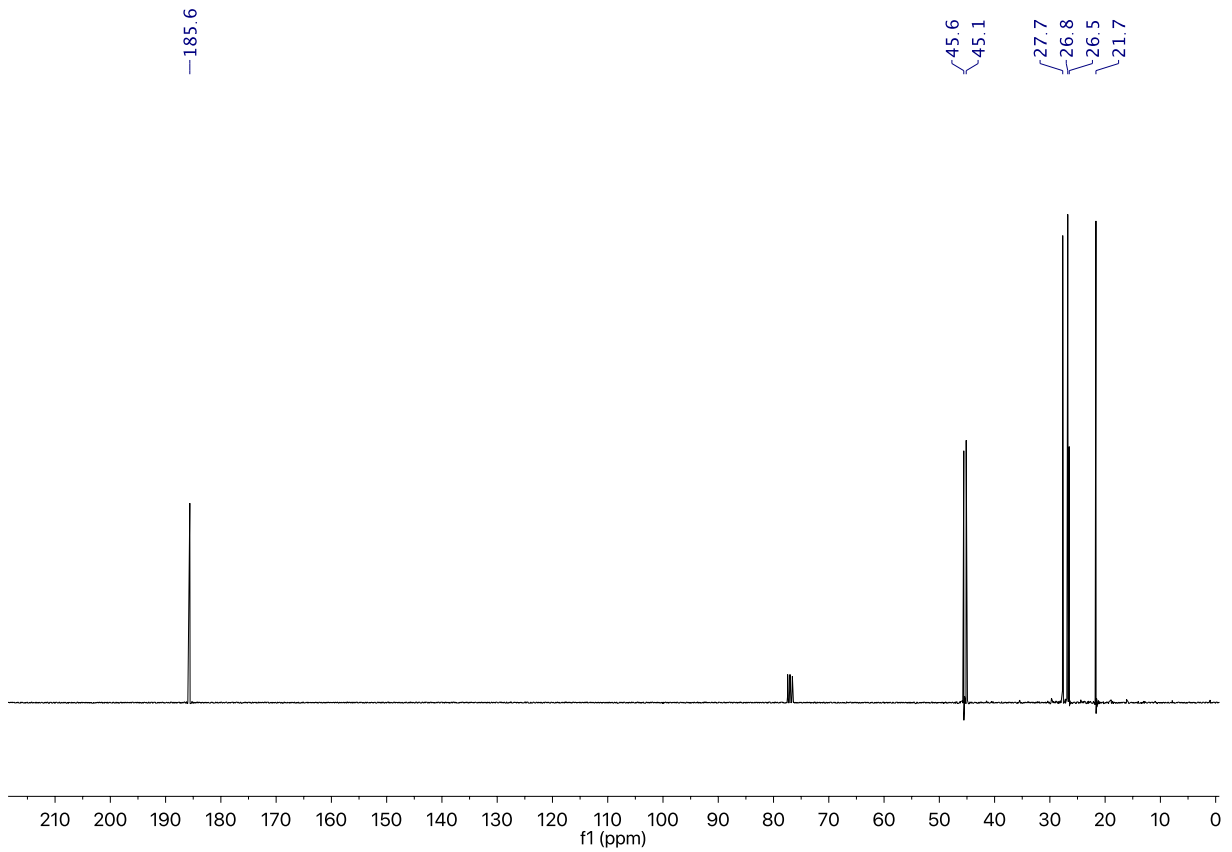
^{13}C NMR of **1** in CDCl_3



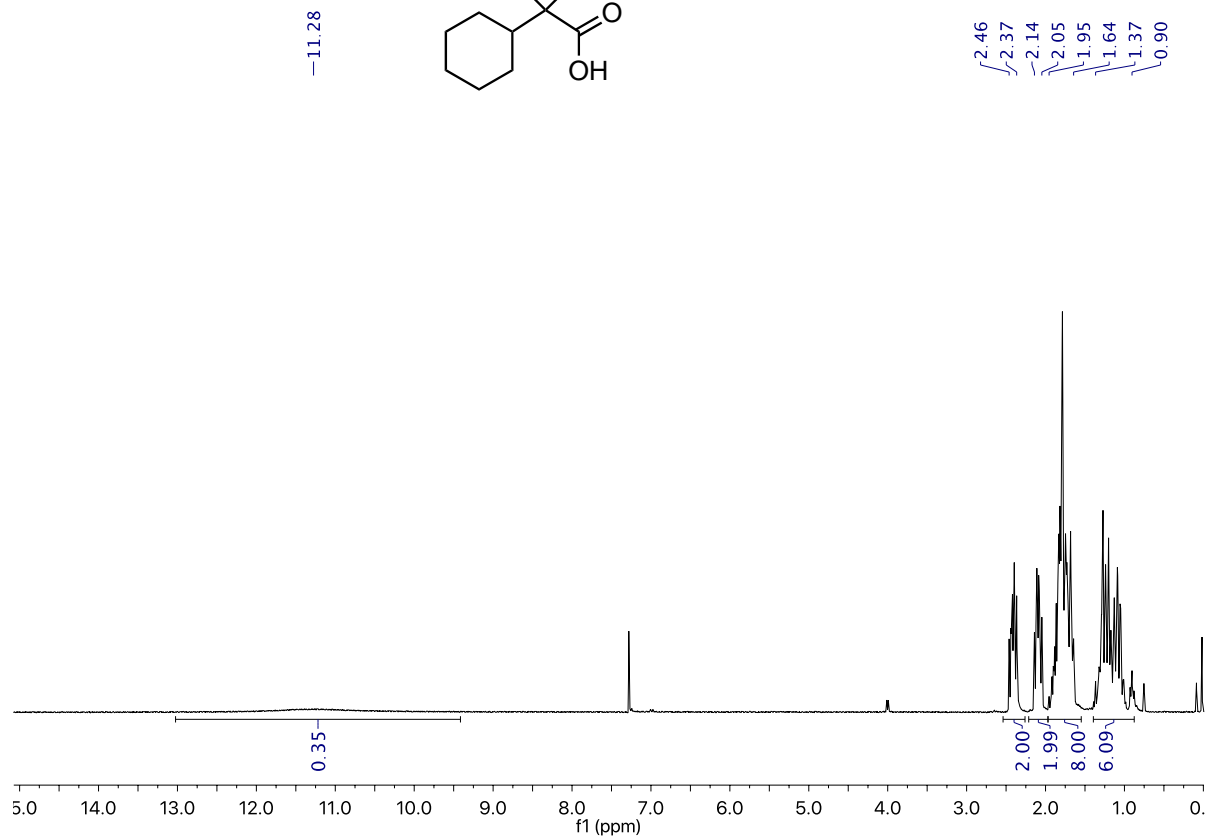
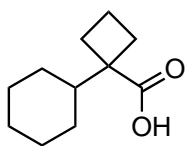
^1H NMR of **3** in CDCl_3



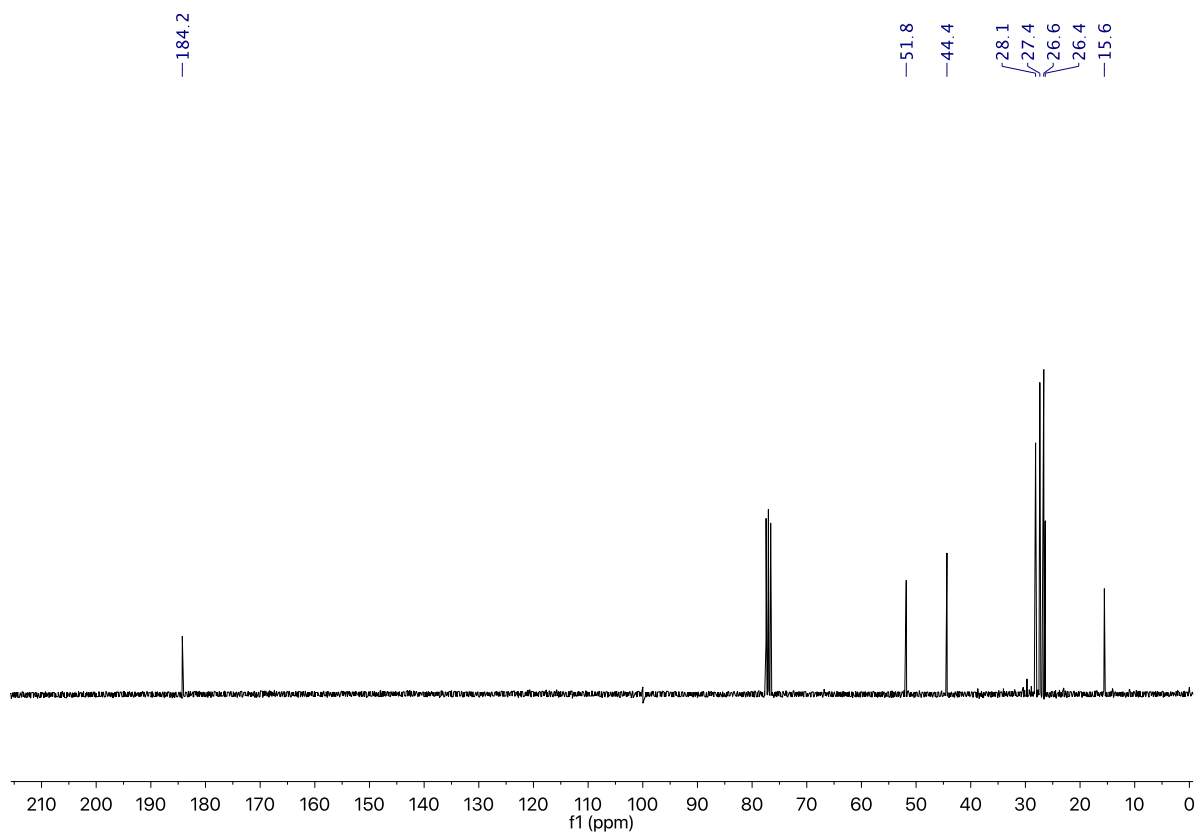
^{13}C NMR of **3** in CDCl_3

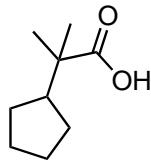


^1H NMR of **4** in CDCl_3

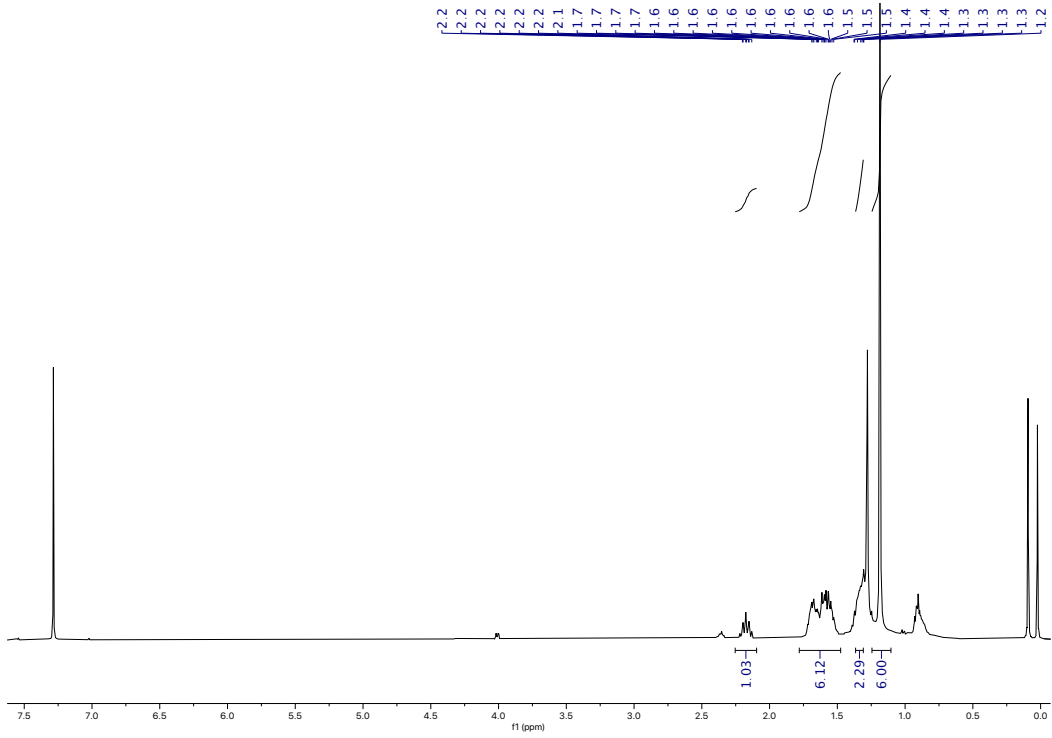


^{13}C NMR of **4** in CDCl_3

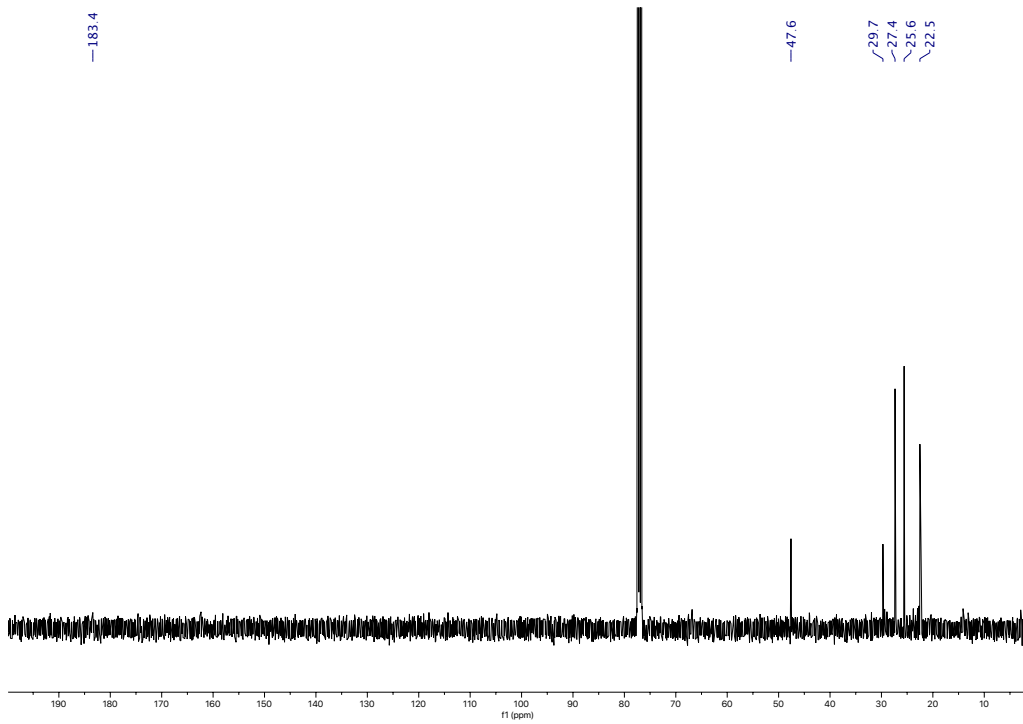


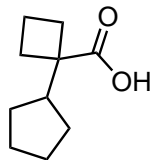


^1H NMR of 7 in CDCl_3

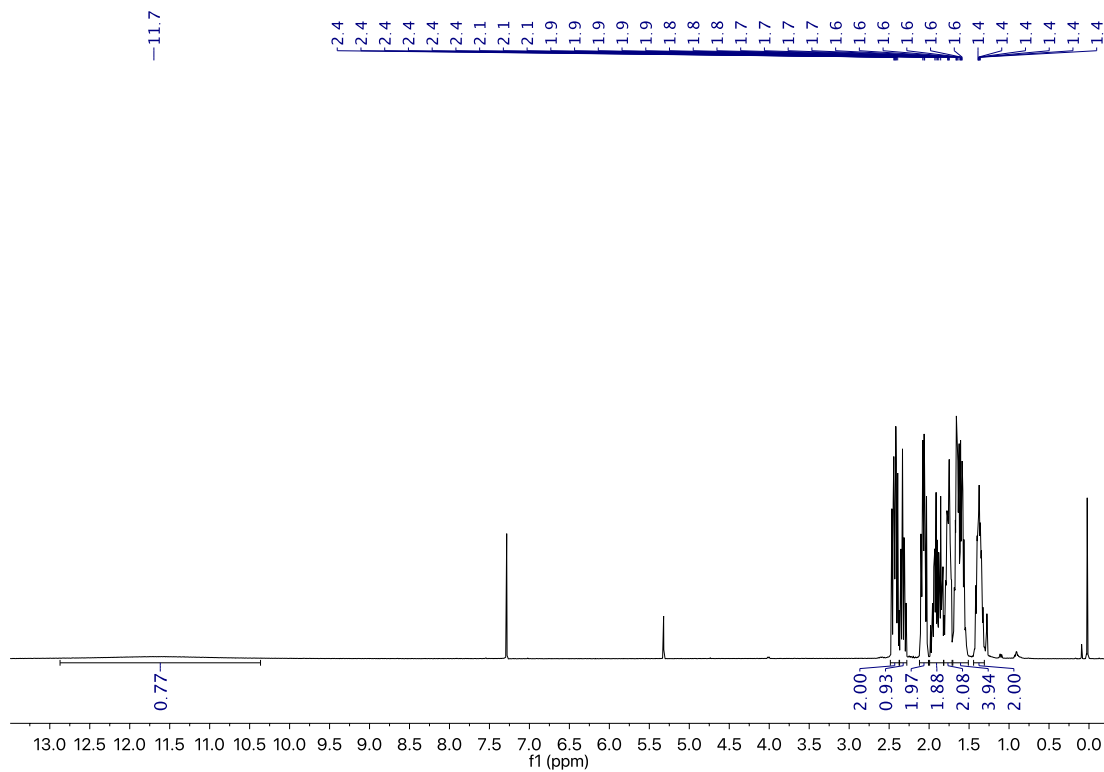


^{13}C NMR of 7 in CDCl_3

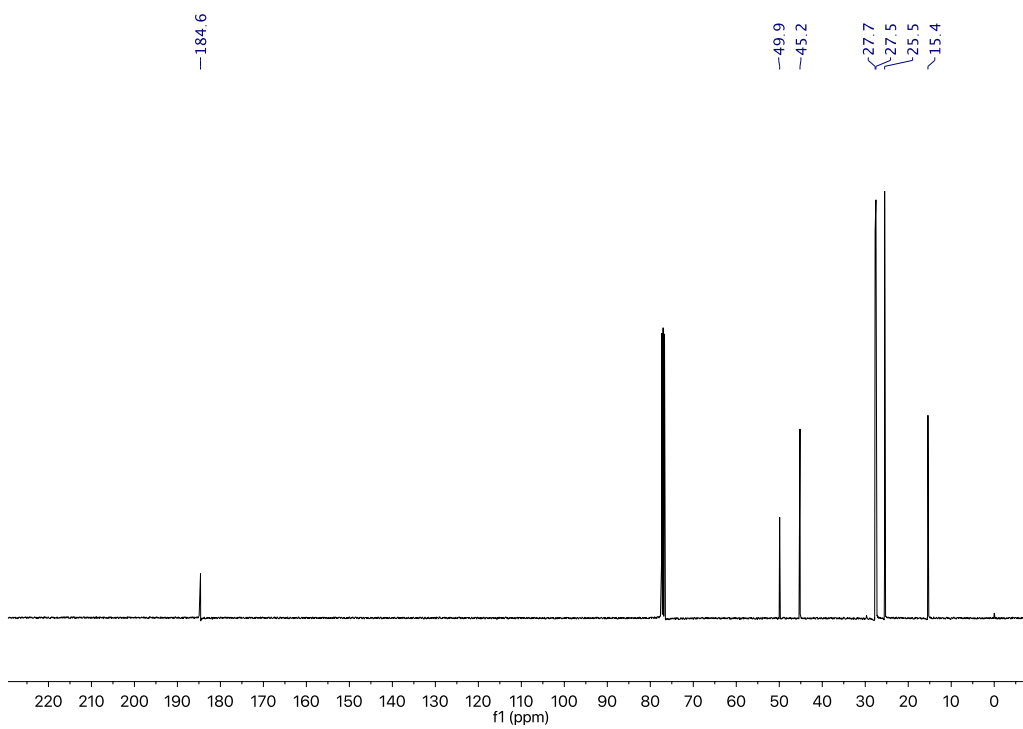




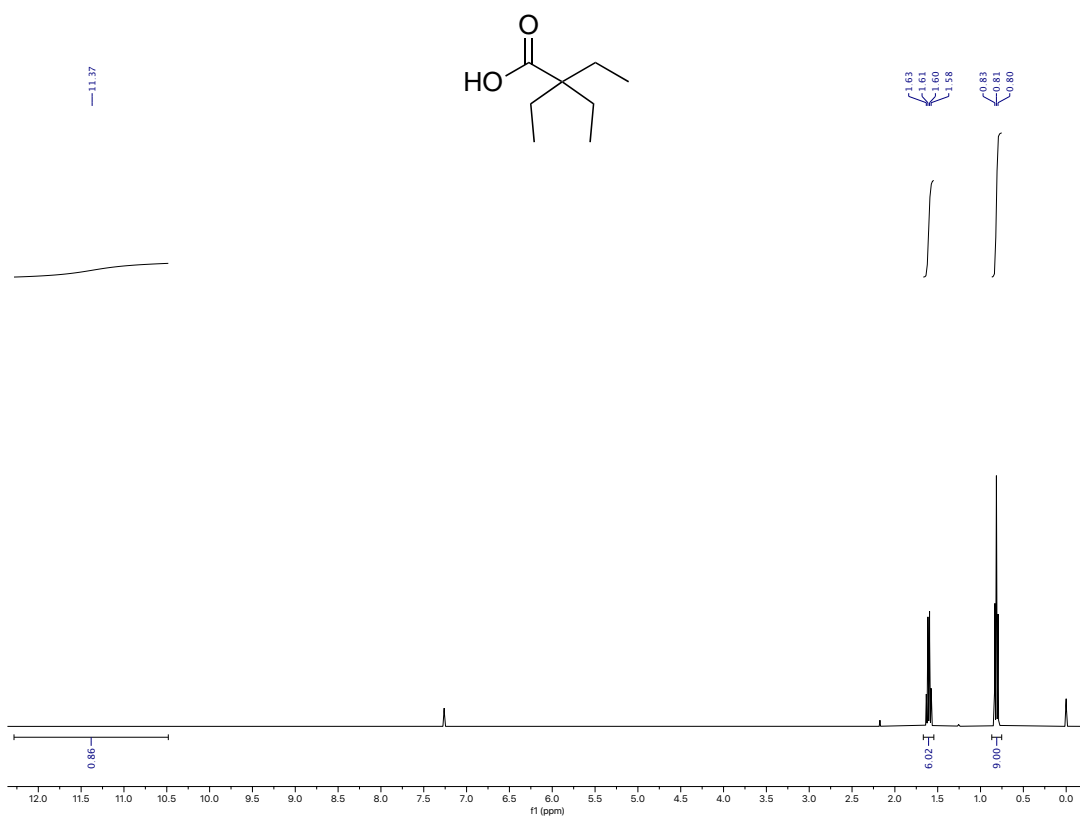
^1H NMR of **8** in CDCl_3



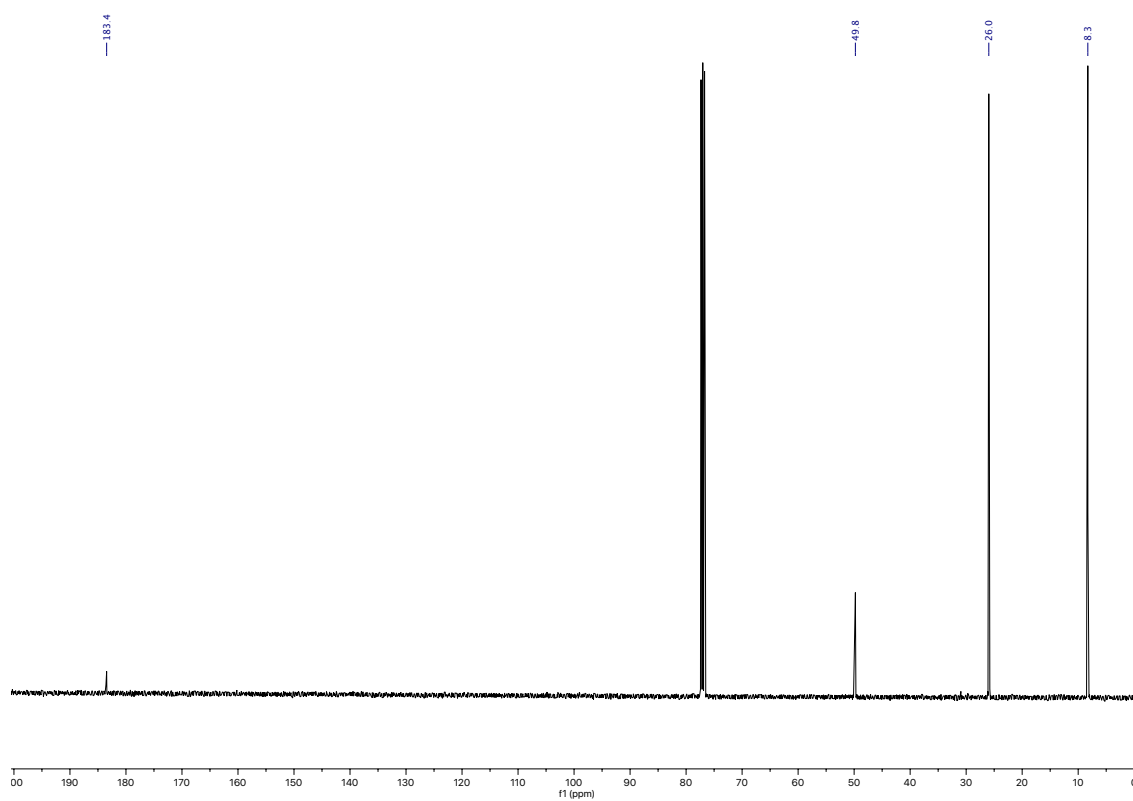
^{13}C NMR of **8** in CDCl_3



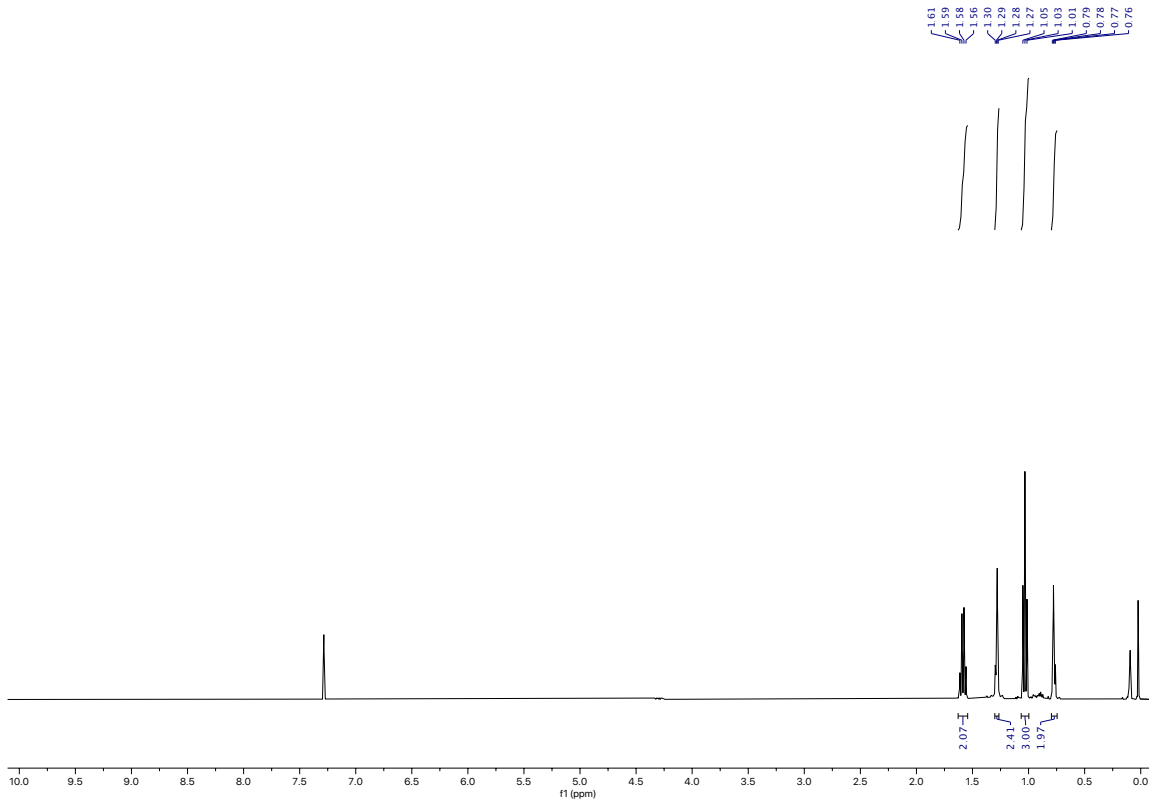
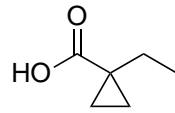
^1H NMR of **21** in CDCl_3



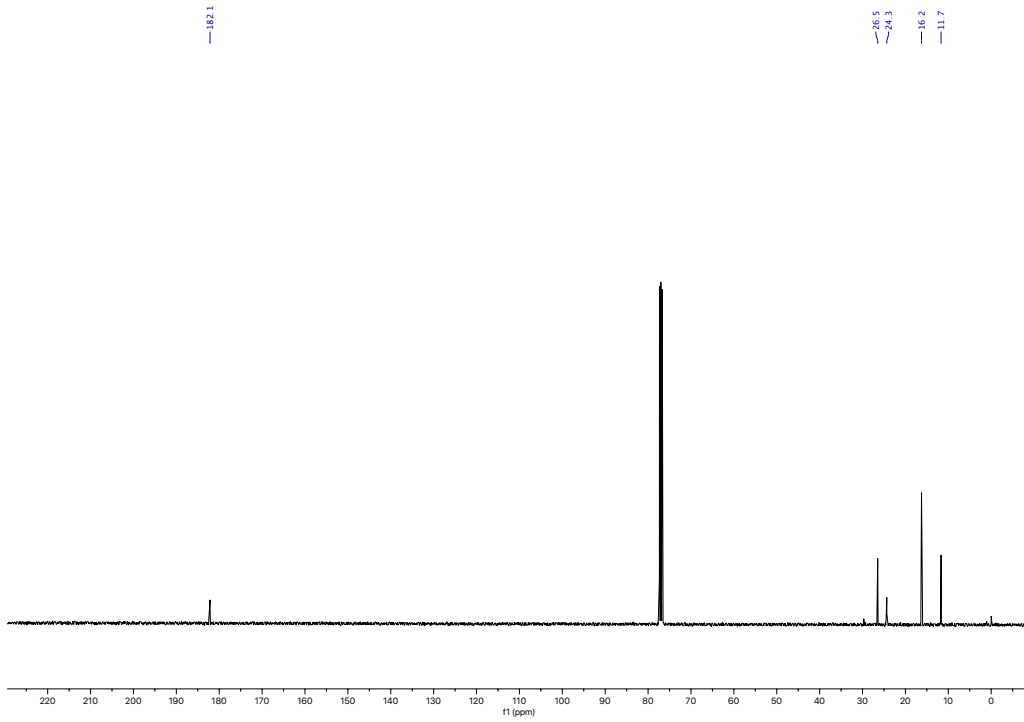
^{13}C NMR of **21** in CDCl_3



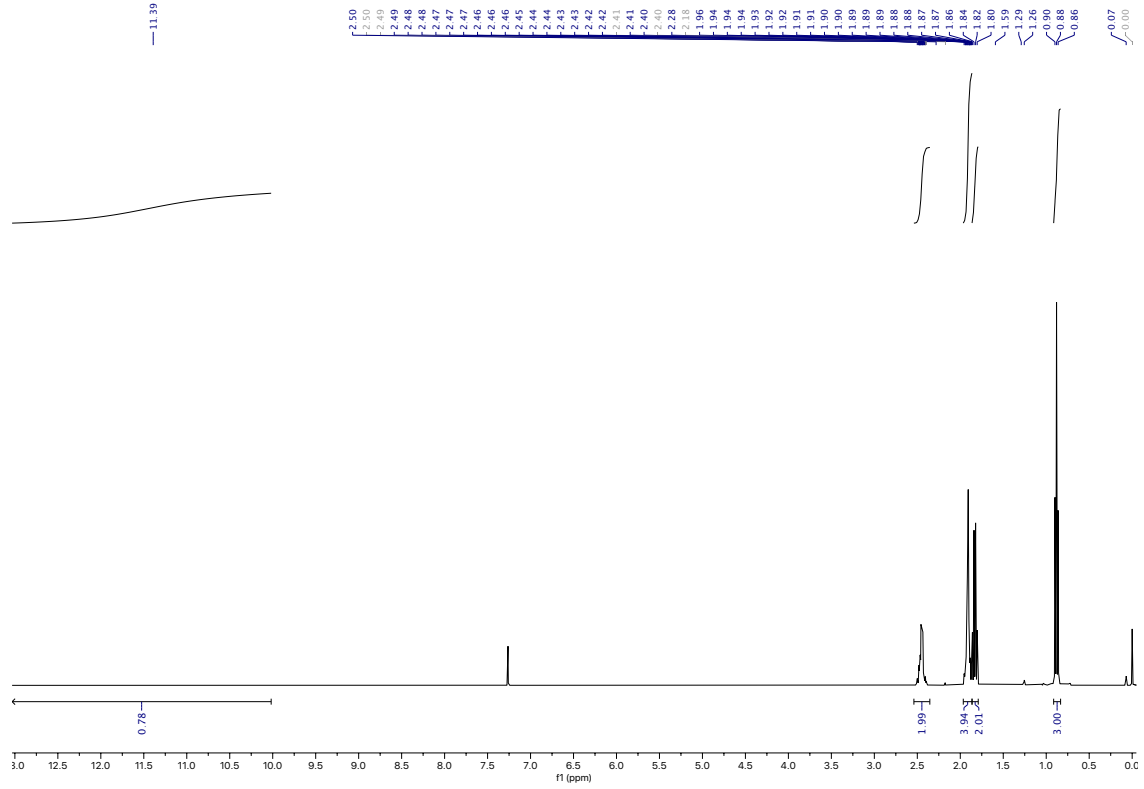
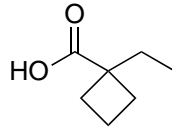
^1H NMR of **22** in CDCl_3



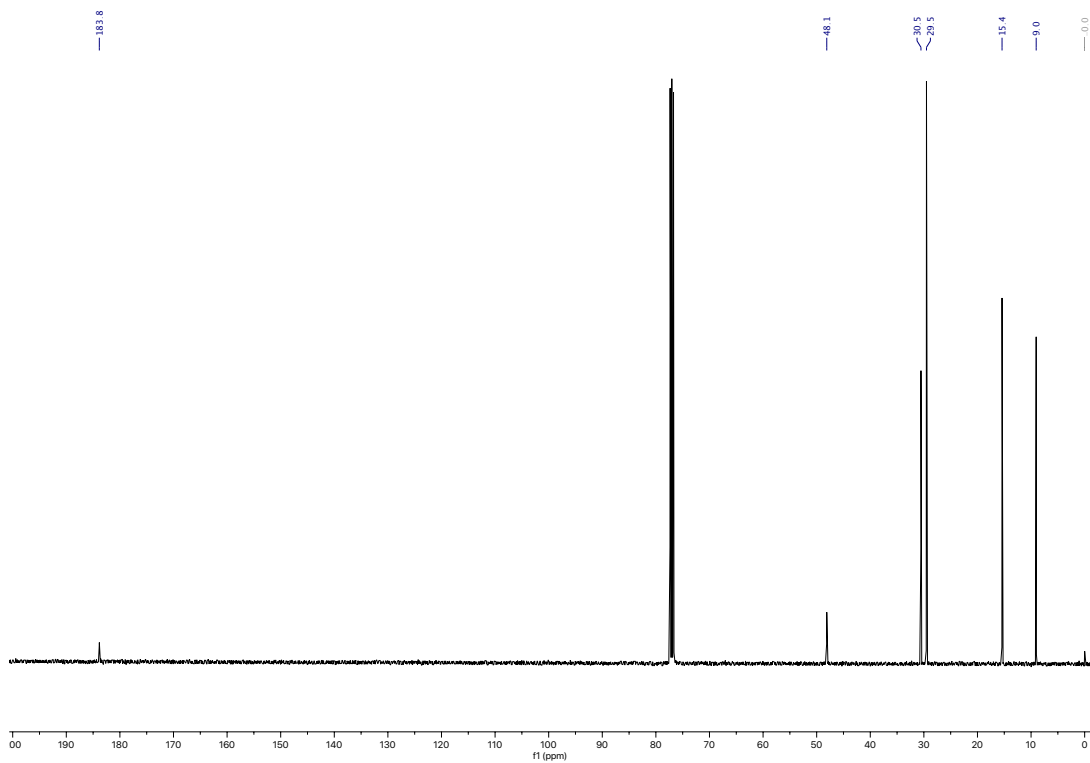
^{13}C NMR of **22** in CDCl_3



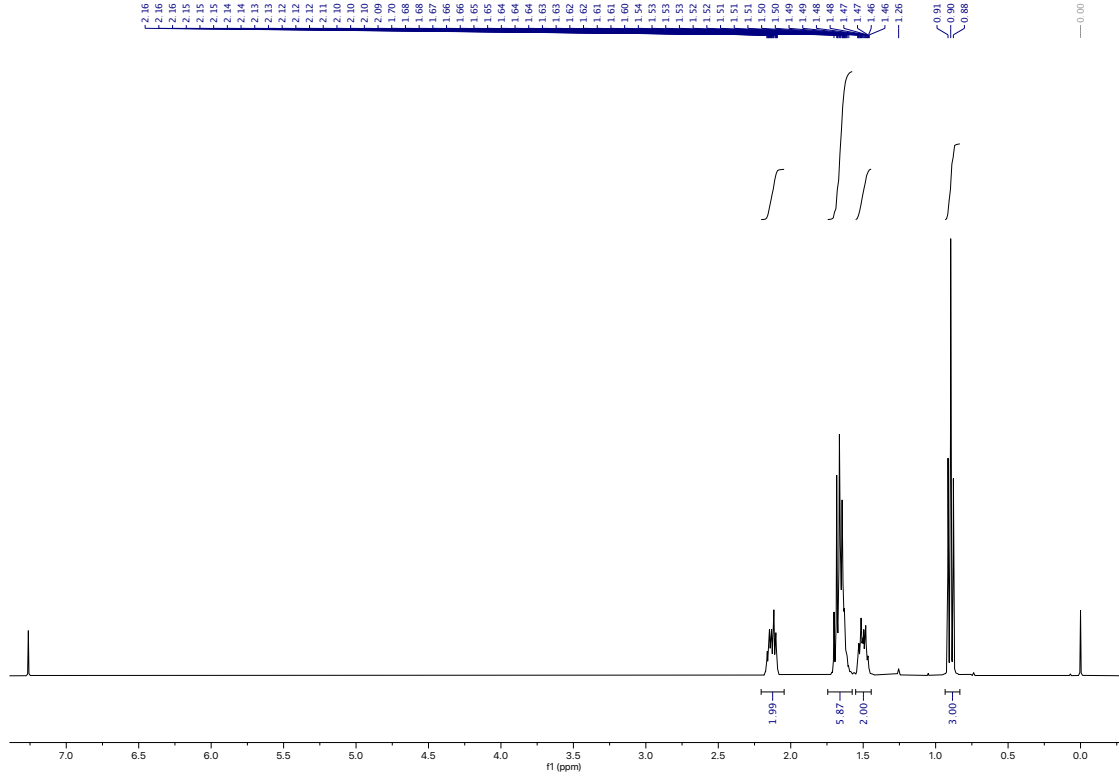
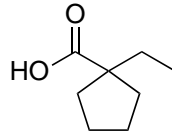
¹H NMR of **23** in CDCl₃



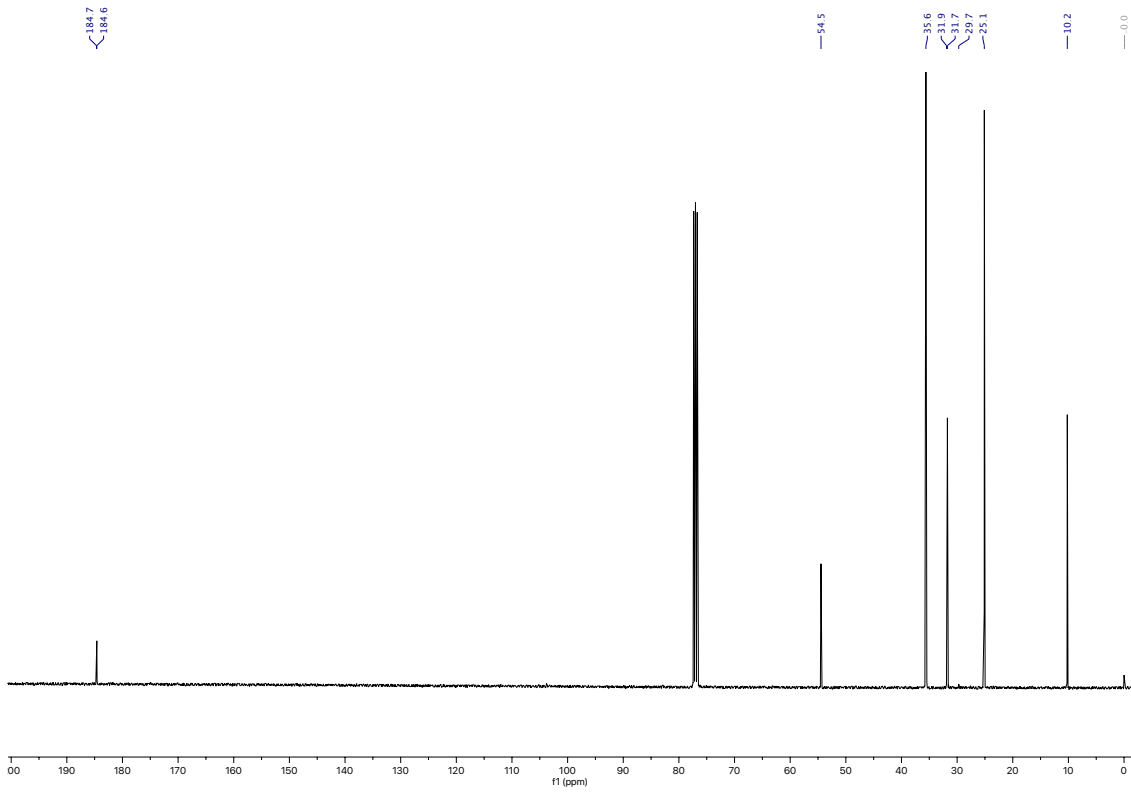
¹³C NMR of **23** in CDCl₃



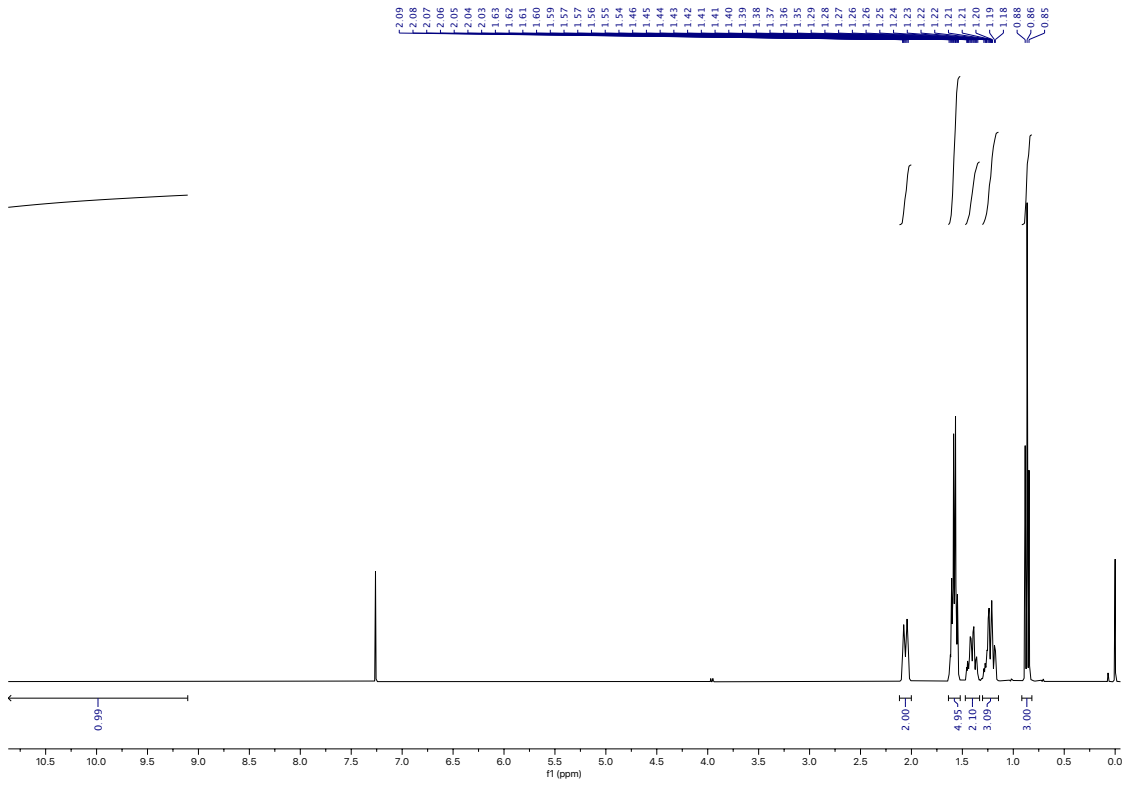
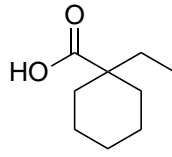
^1H NMR of **24** in CDCl_3



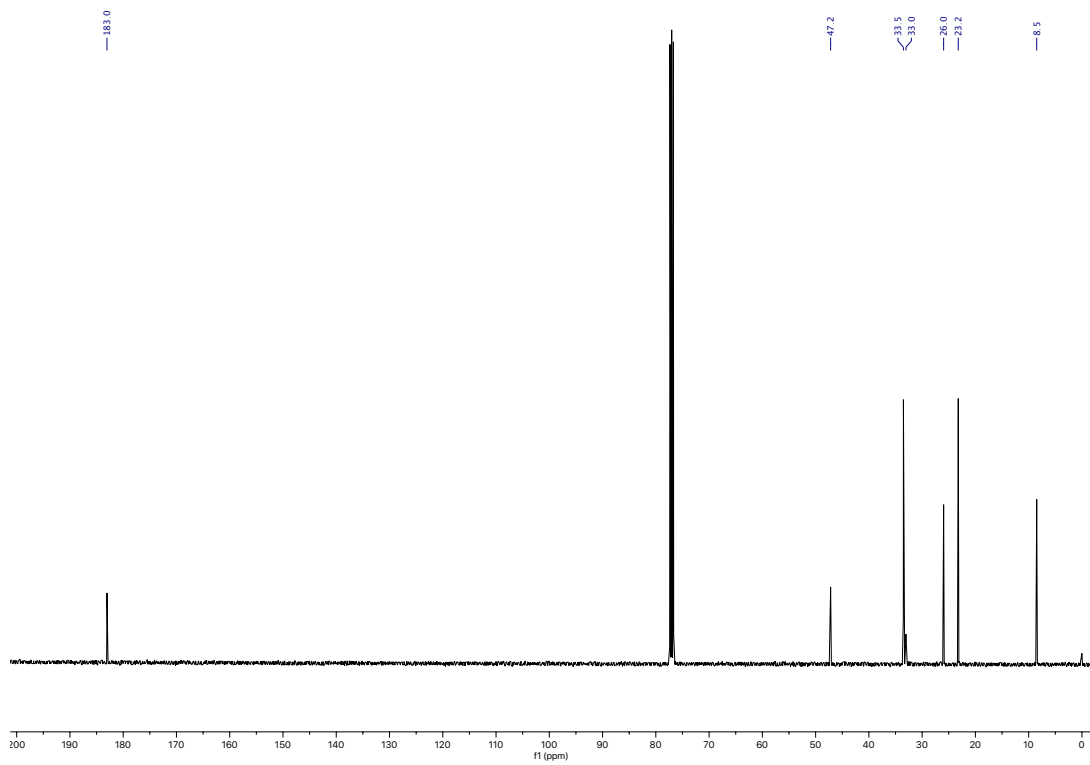
^{13}C NMR of **24** in CDCl_3



^1H NMR of **25** in CDCl_3

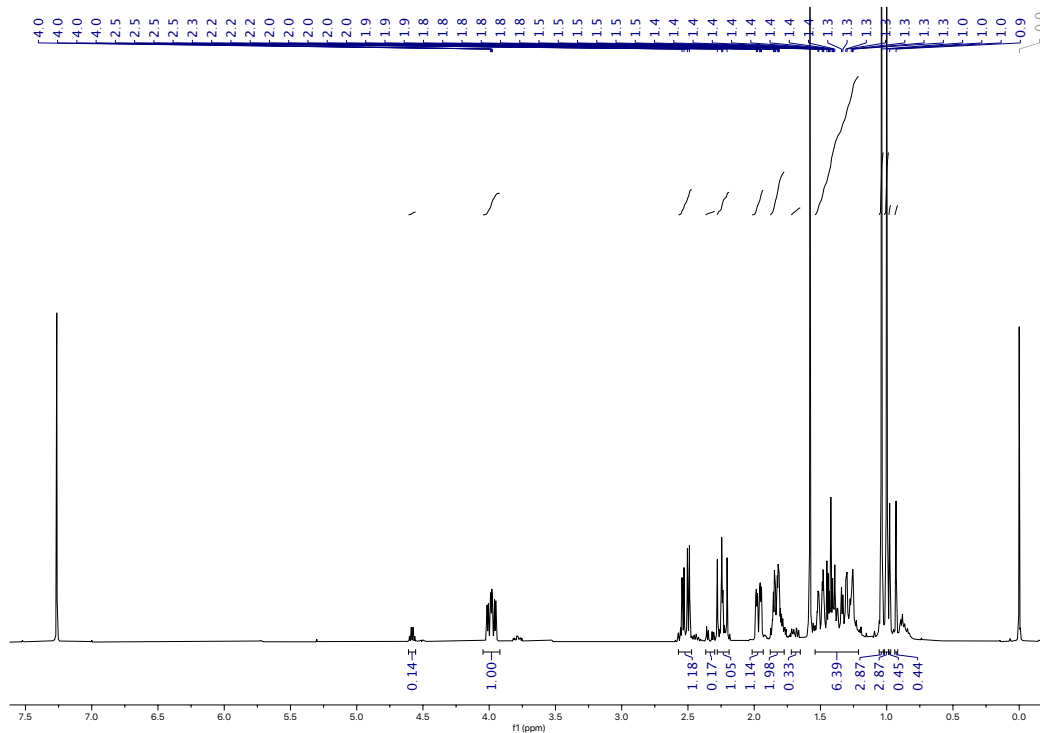
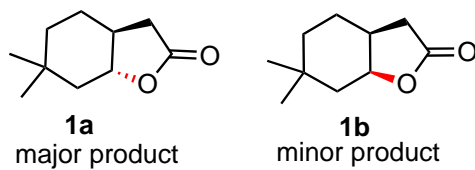


^{13}C NMR of **25** in CDCl_3

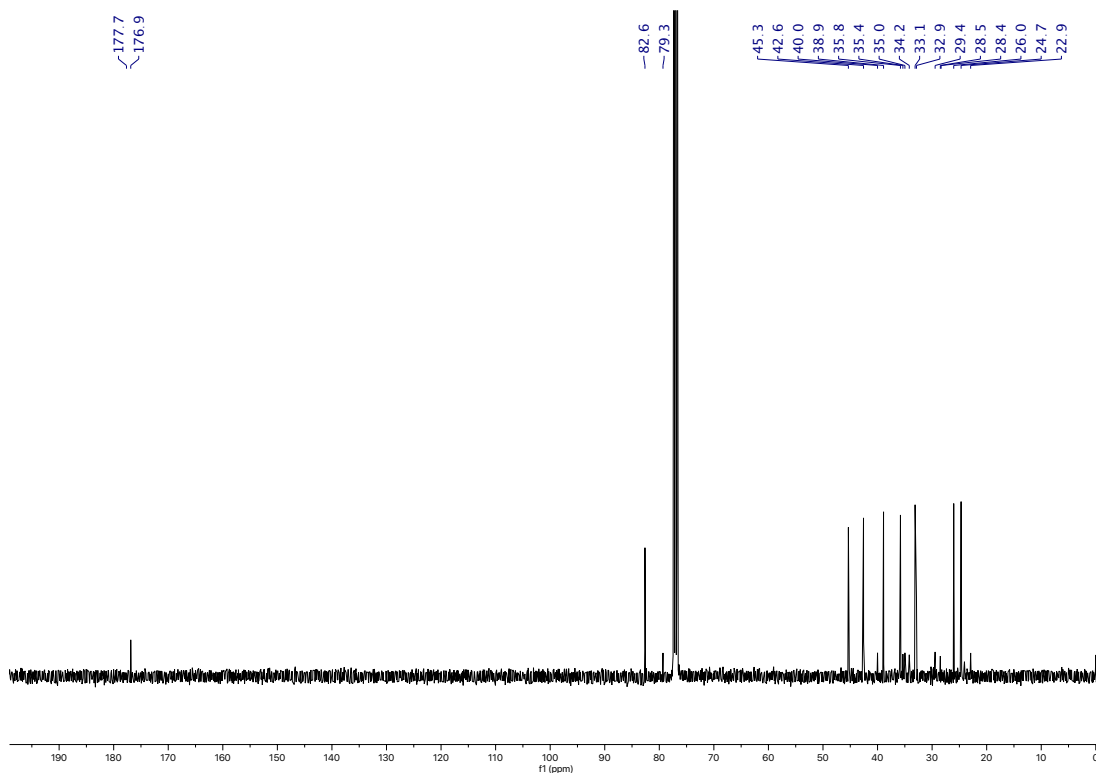


III. NMR characterization of lactone products

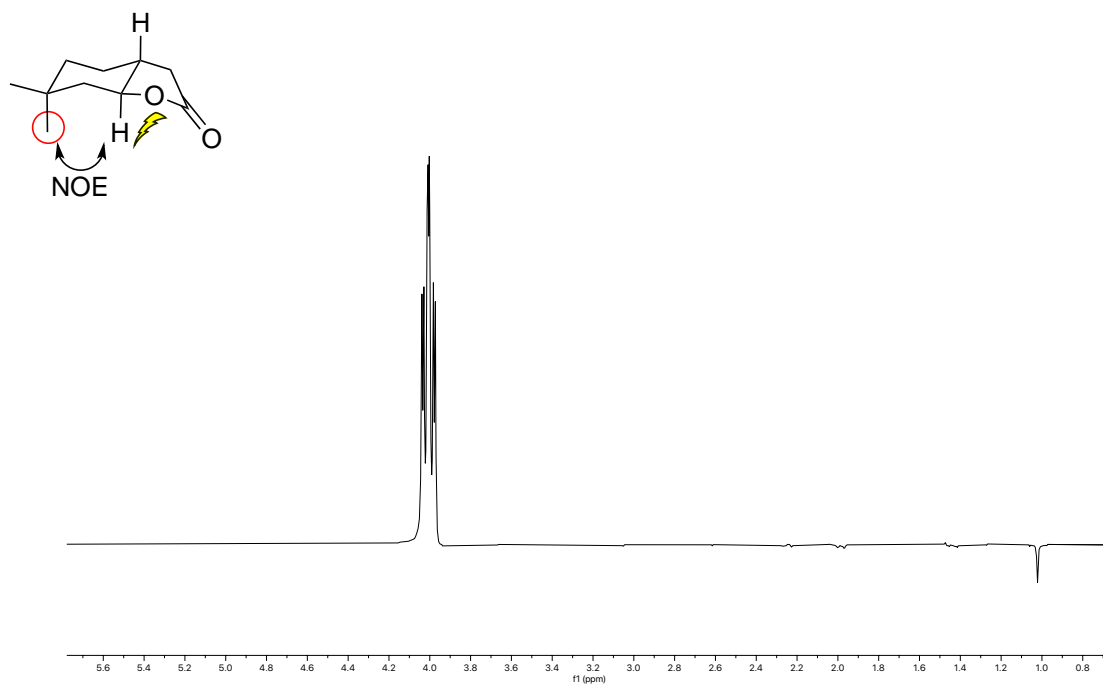
^1H NMR of oxidation of **1** in CDCl_3



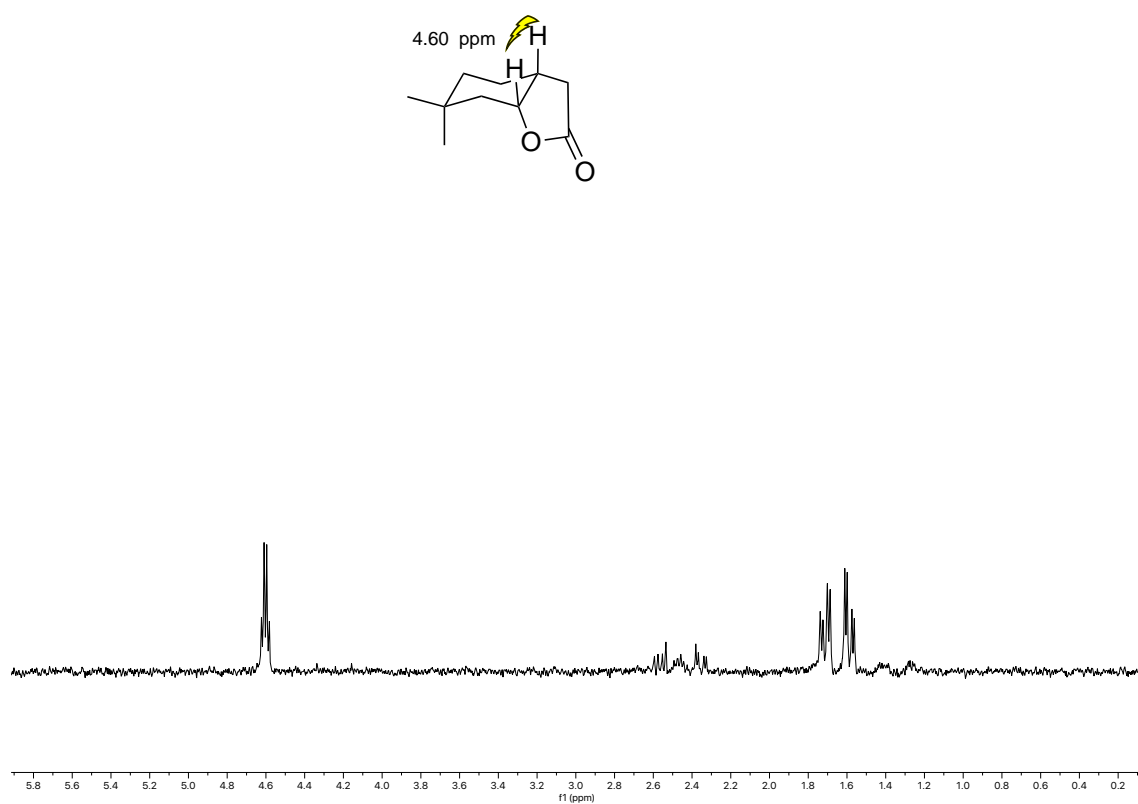
^{13}C NMR of oxidation of **1** in CDCl_3



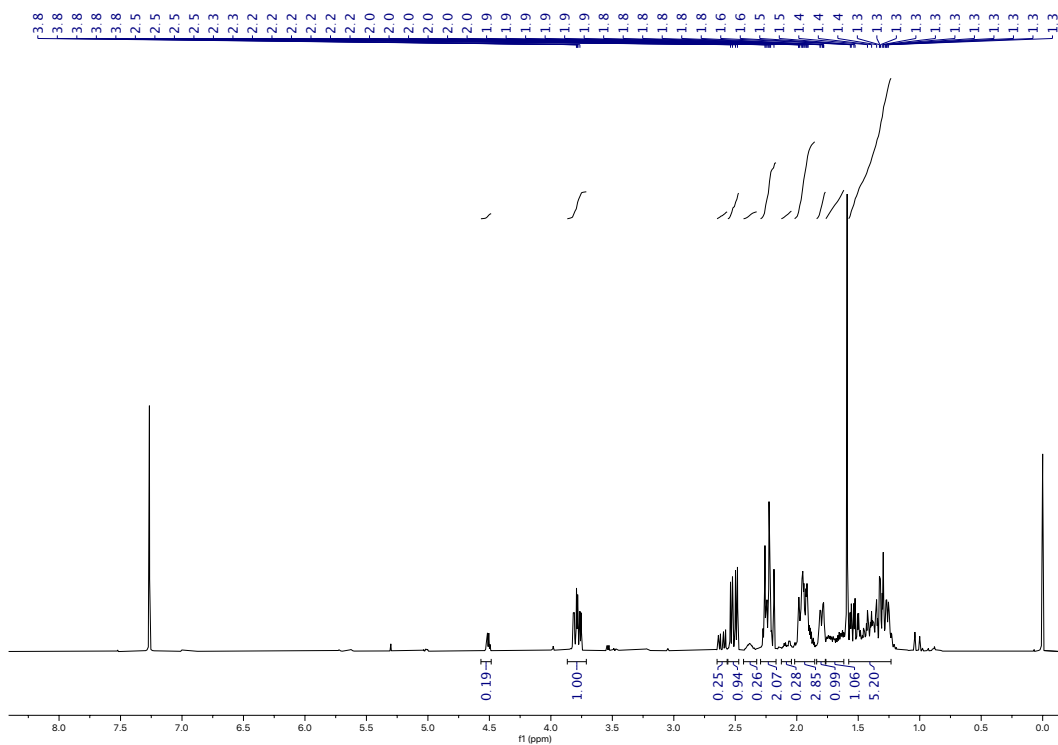
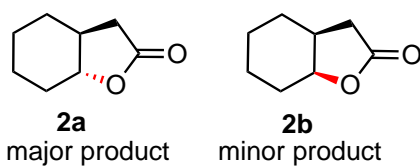
Selective NOESY (at 4.00 ppm) of **1a** in CDCl₃



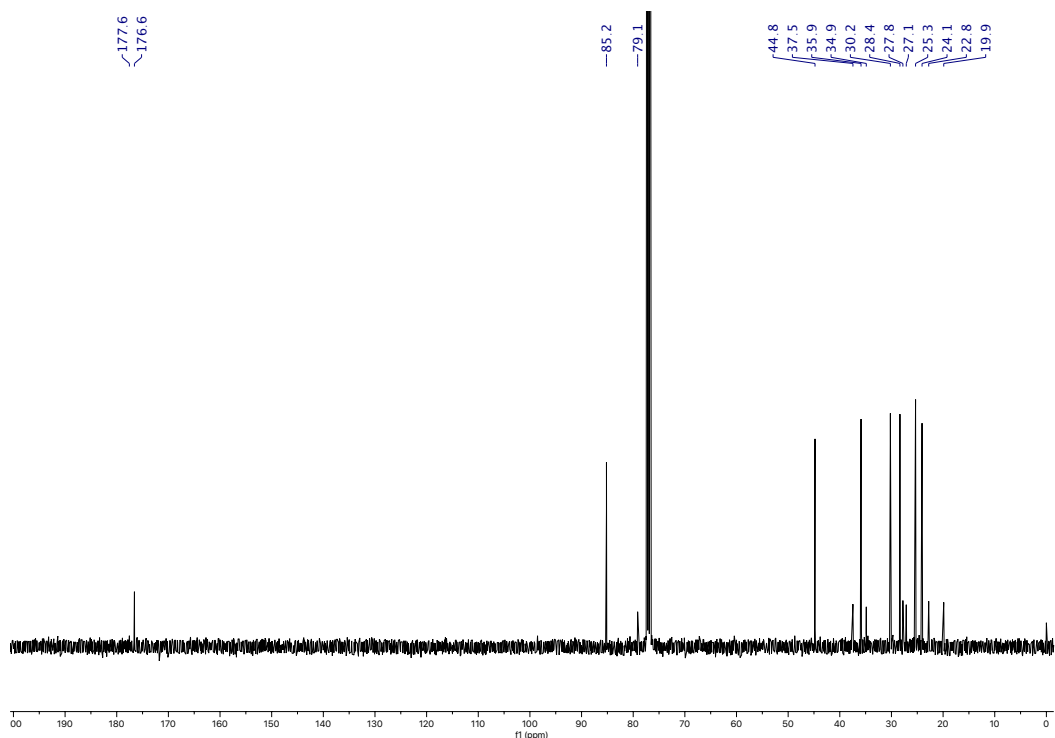
Selective TOCSY (at 4.60 ppm) of **1b** in CDCl₃



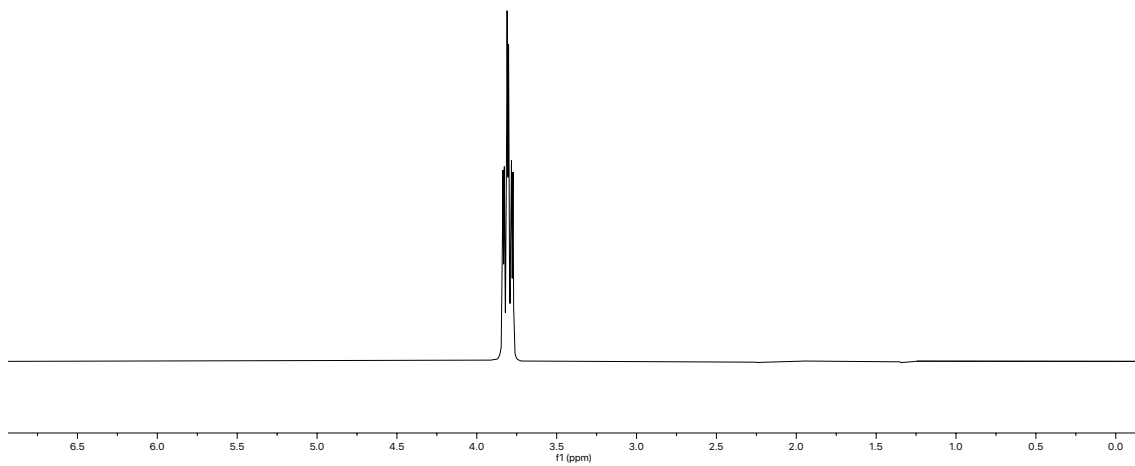
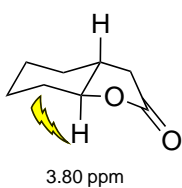
¹H NMR of oxidation of **2** in CDCl₃



¹³C NMR of oxidation of **2** in CDCl₃

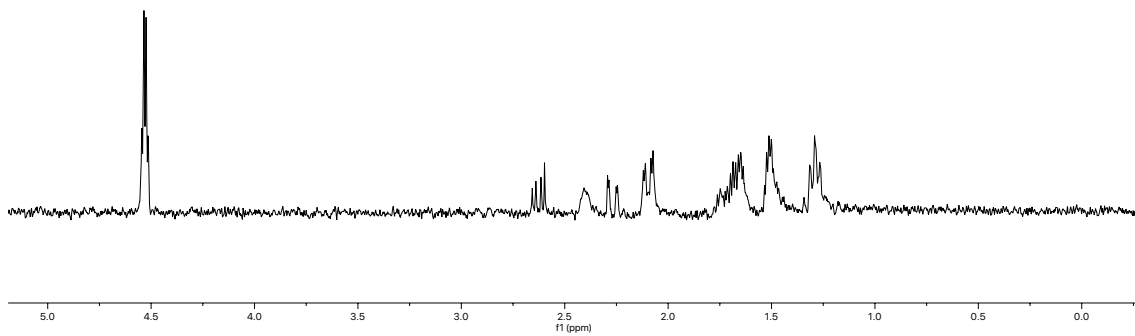
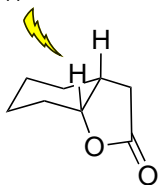


Selective NOESY (at 3.80 ppm) of **2a** in CDCl₃

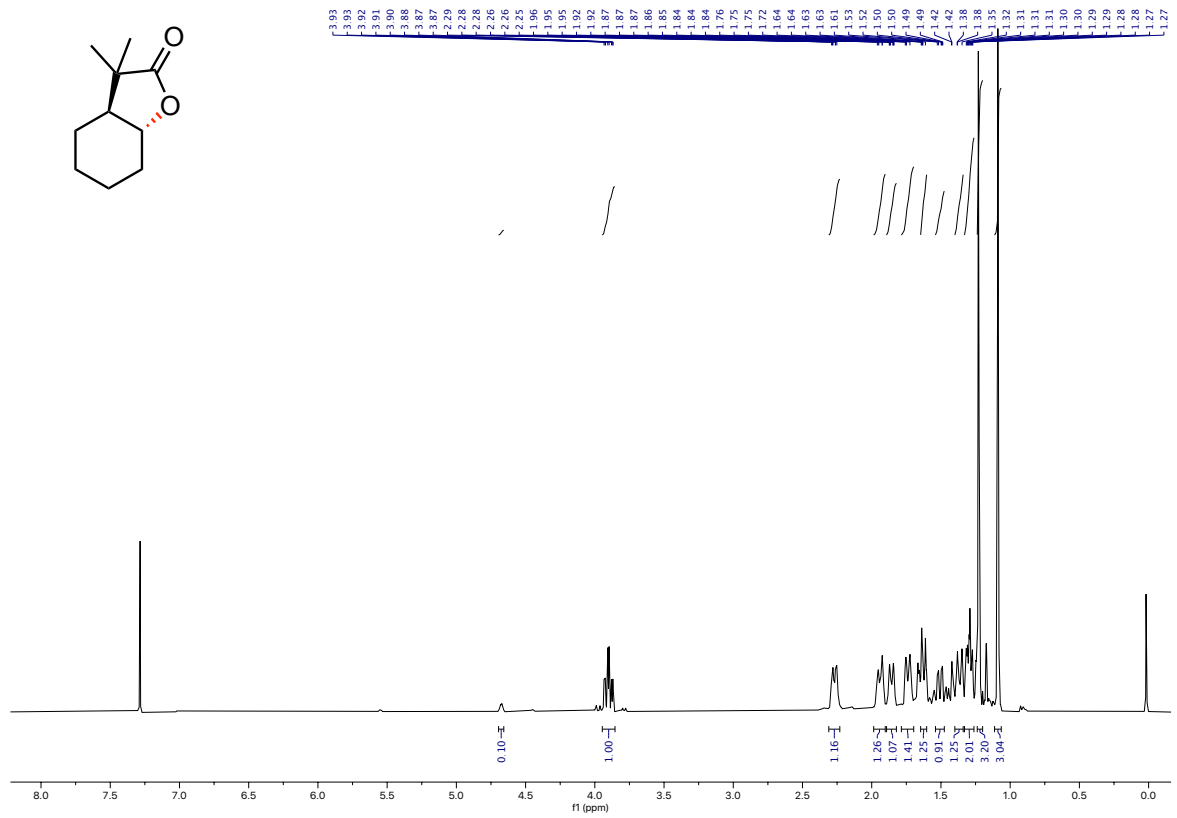


Selective TOCSY (at 4.53 ppm) of **2b** in CDCl₃

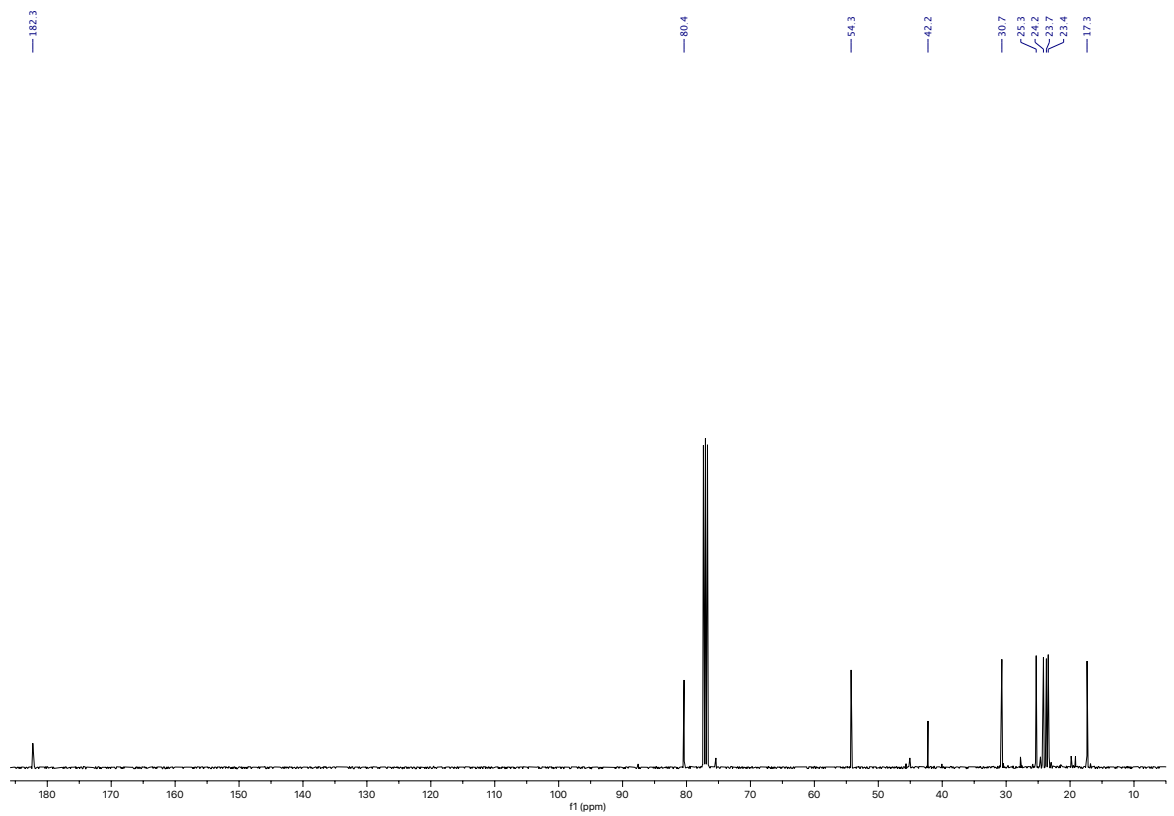
4.53 ppm



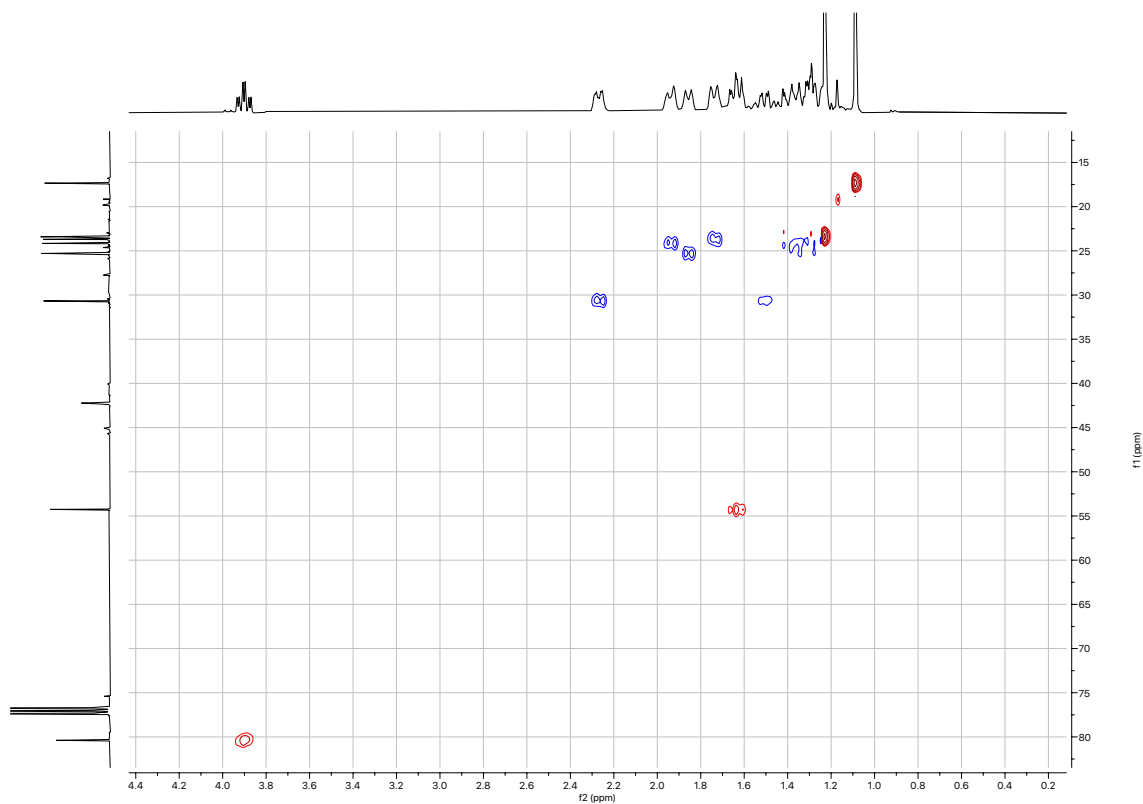
^1H NMR of **3a** in CDCl_3



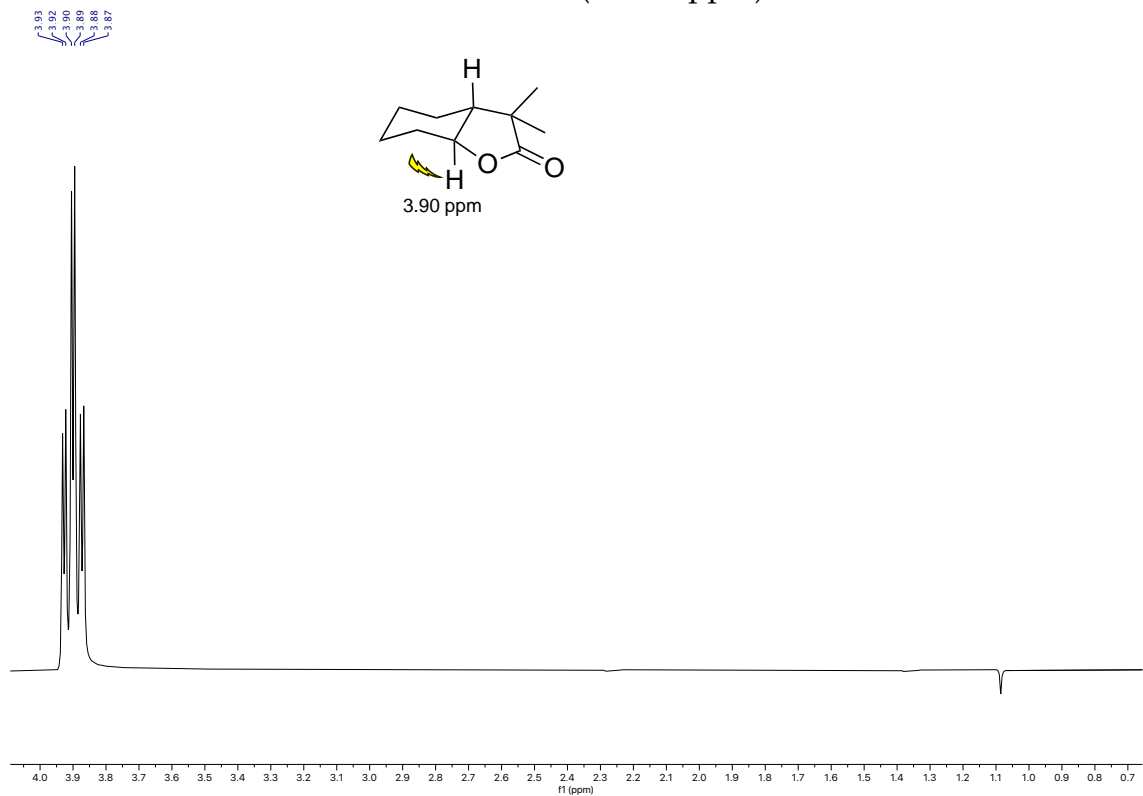
^{13}C NMR of **3a** in CDCl_3

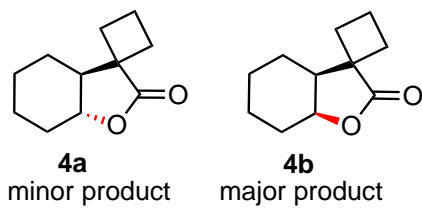


HSQC of **3a** in CDCl₃

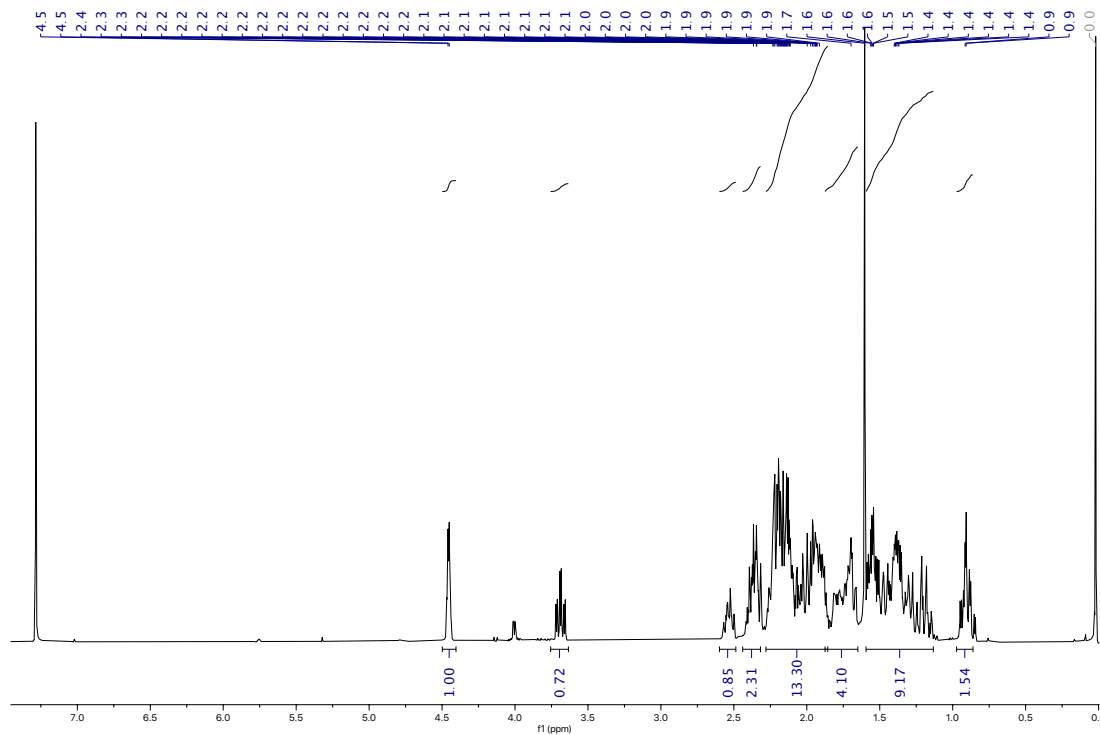


Selective NOESY (at 3.90 ppm) of **3a** in CDCl₃

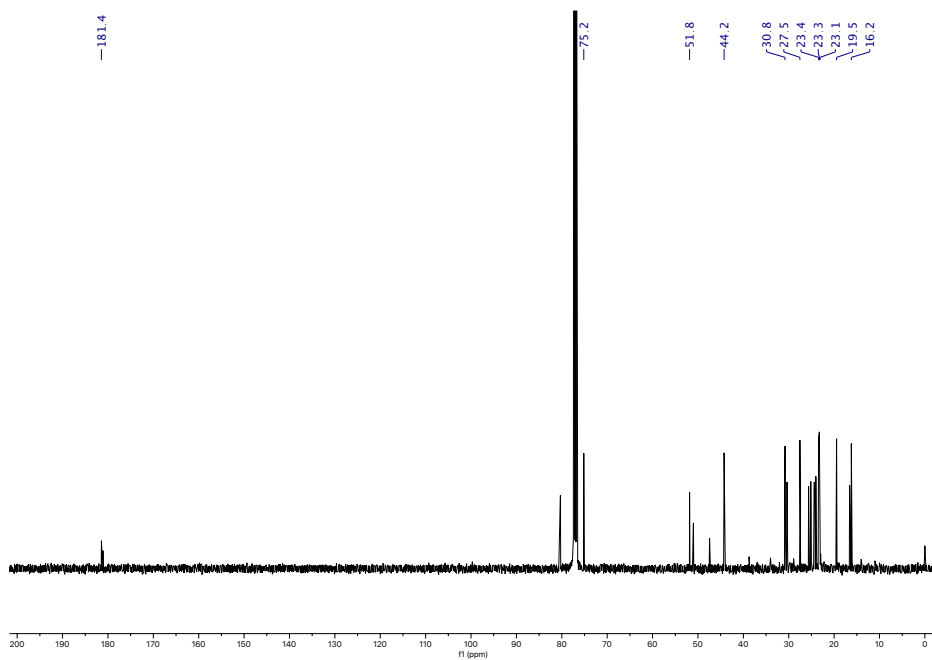




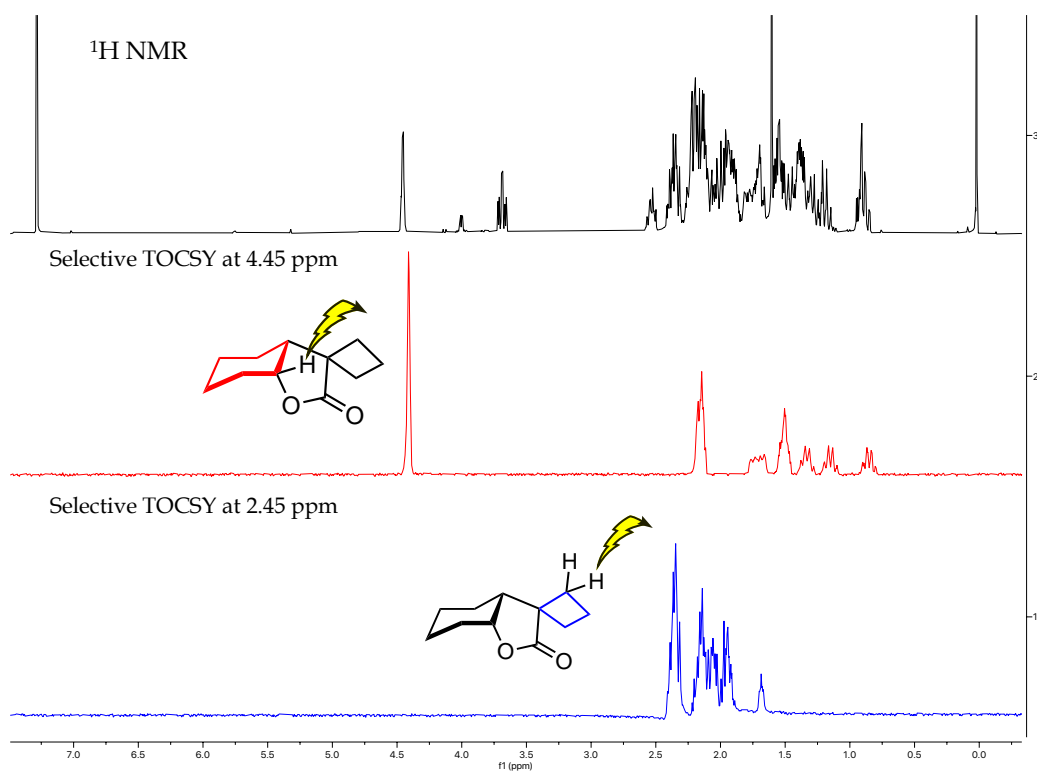
¹H NMR of oxidation of **4b** in CDCl₃



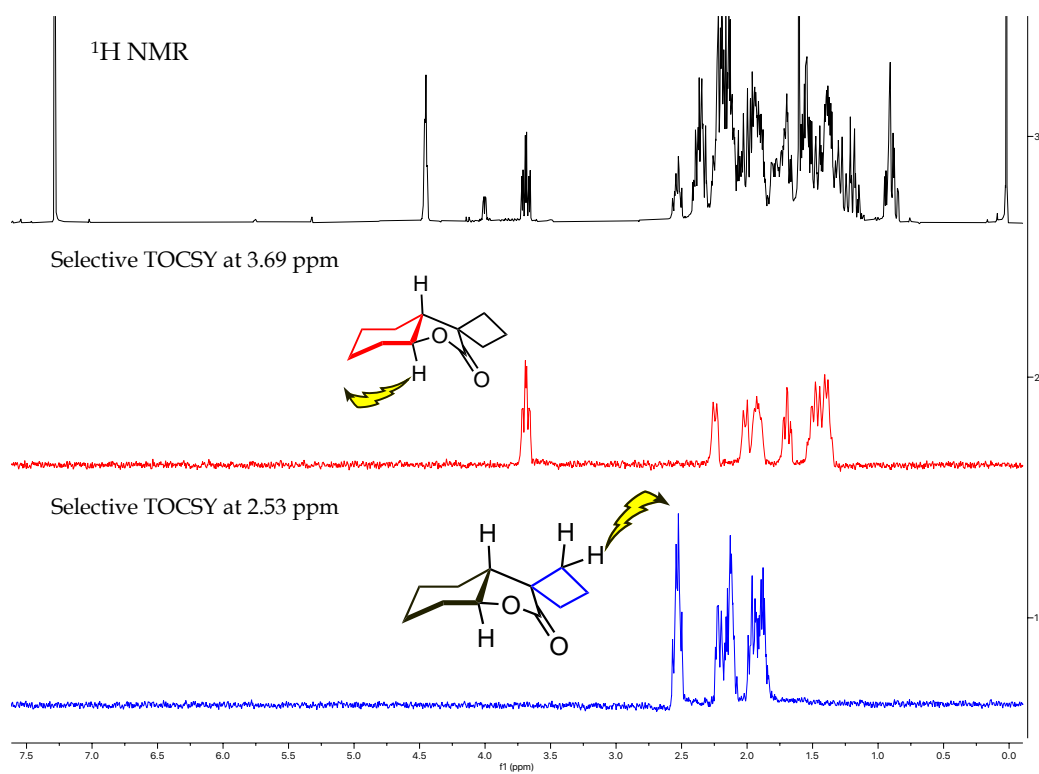
¹³C NMR of oxidation of **4b** in CDCl₃



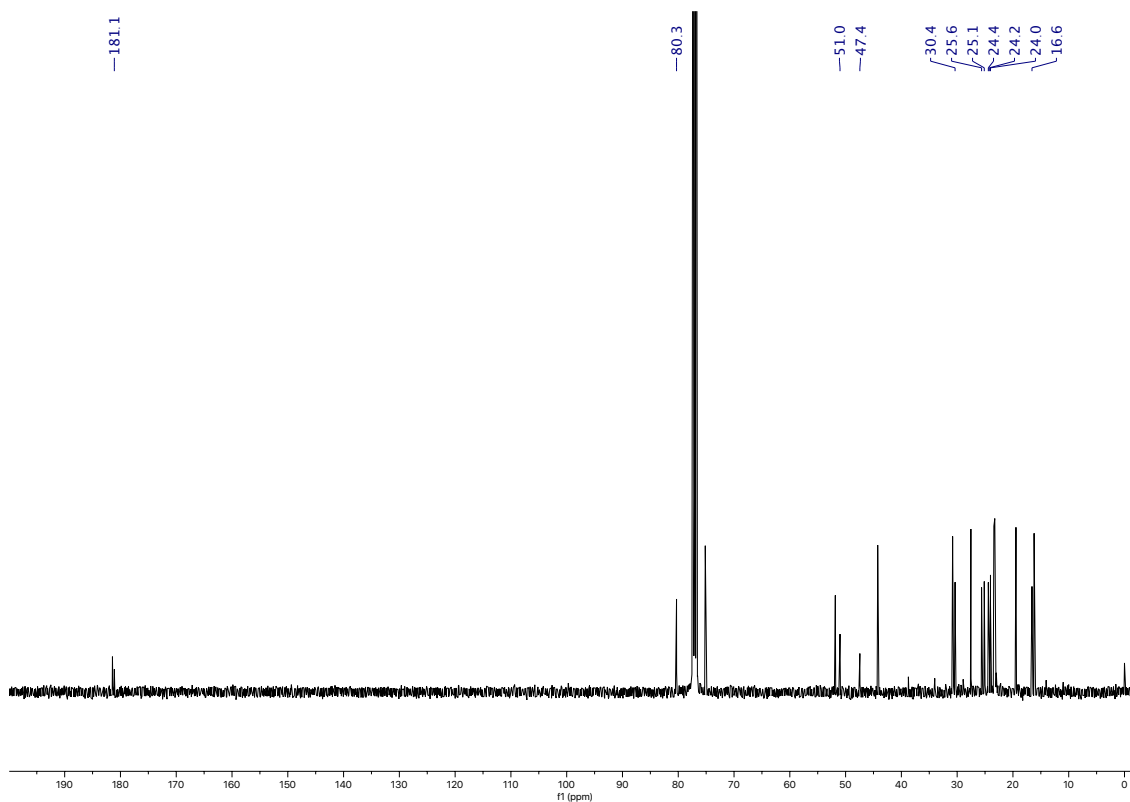
Selective TOCSY experiments of **4b** in CDCl₃



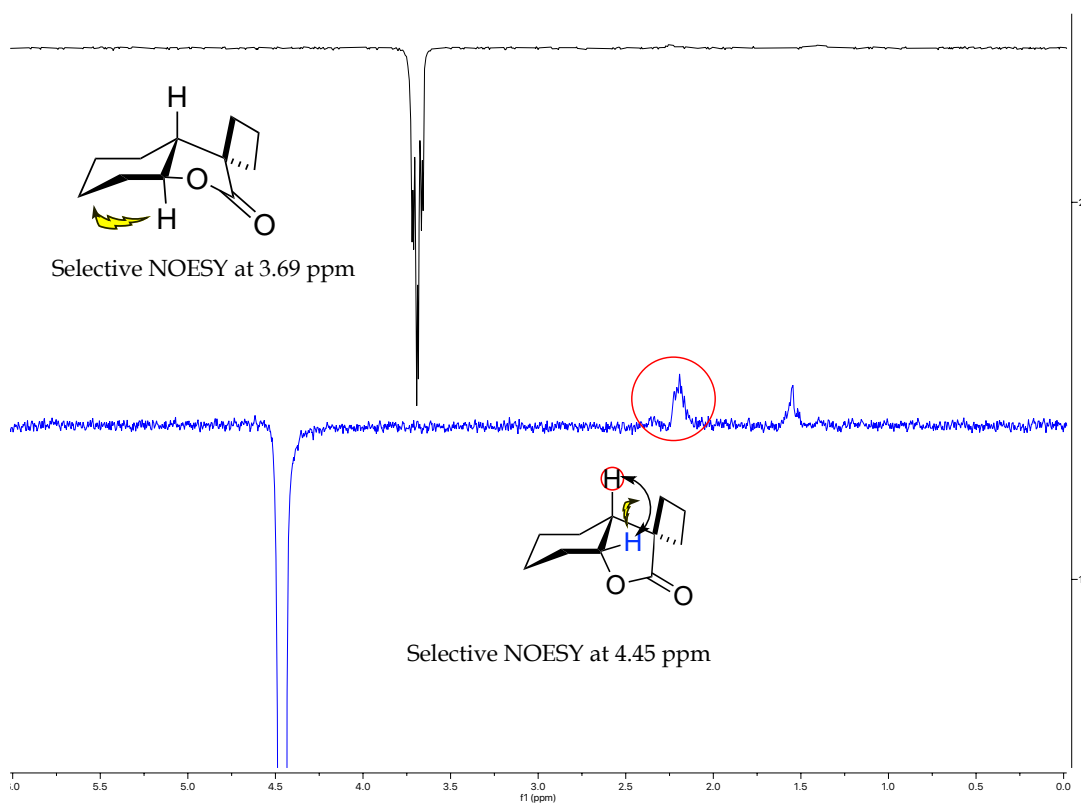
Selective TOCSY experiments of **4a** and **4b** mixture in CDCl₃

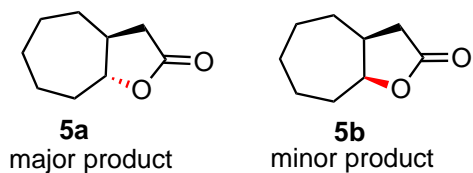


^{13}C NMR of oxidation of **4** in CDCl_3 (**4a** labeled)

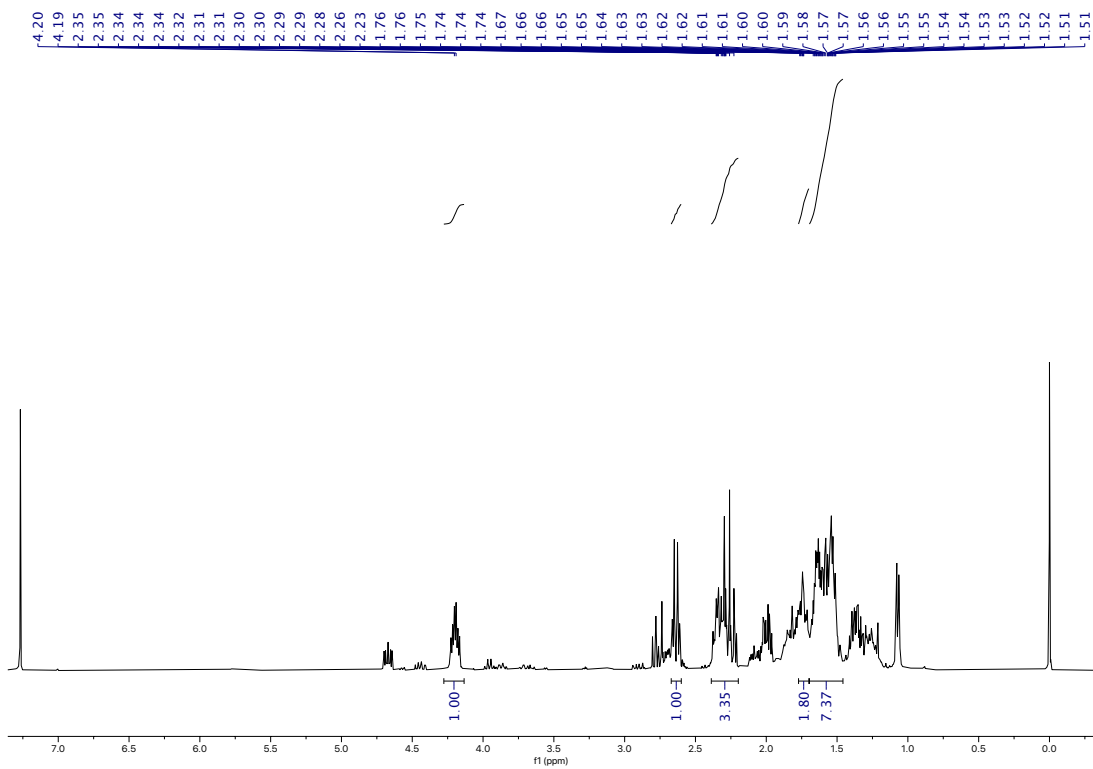


Selective NOESY experiments of **4a** and **4b** mixture in CDCl_3

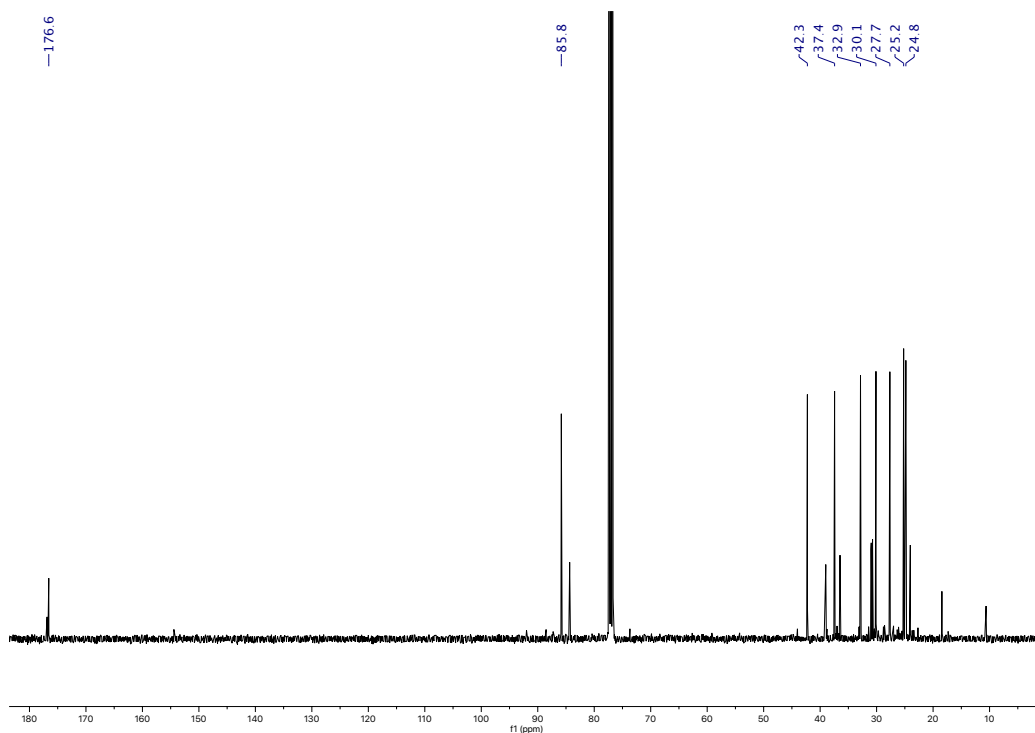




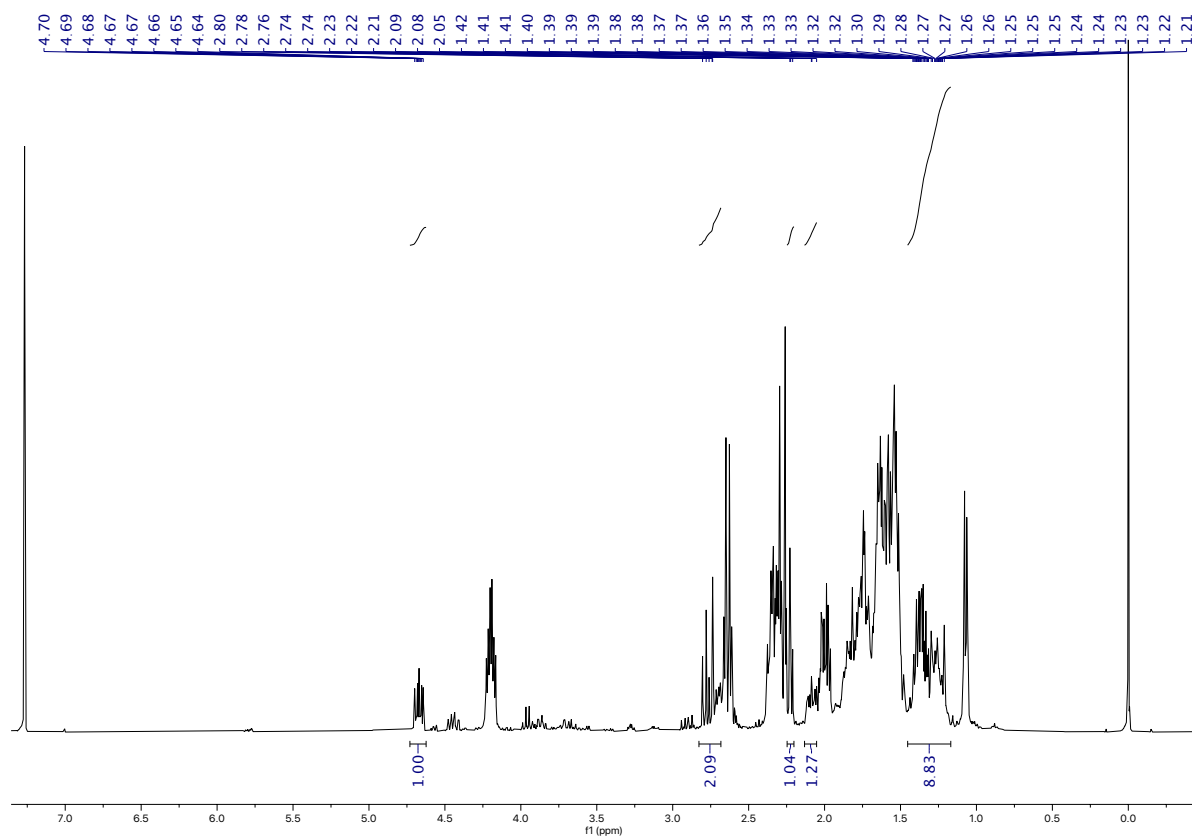
^1H NMR of **5a** in CDCl_3



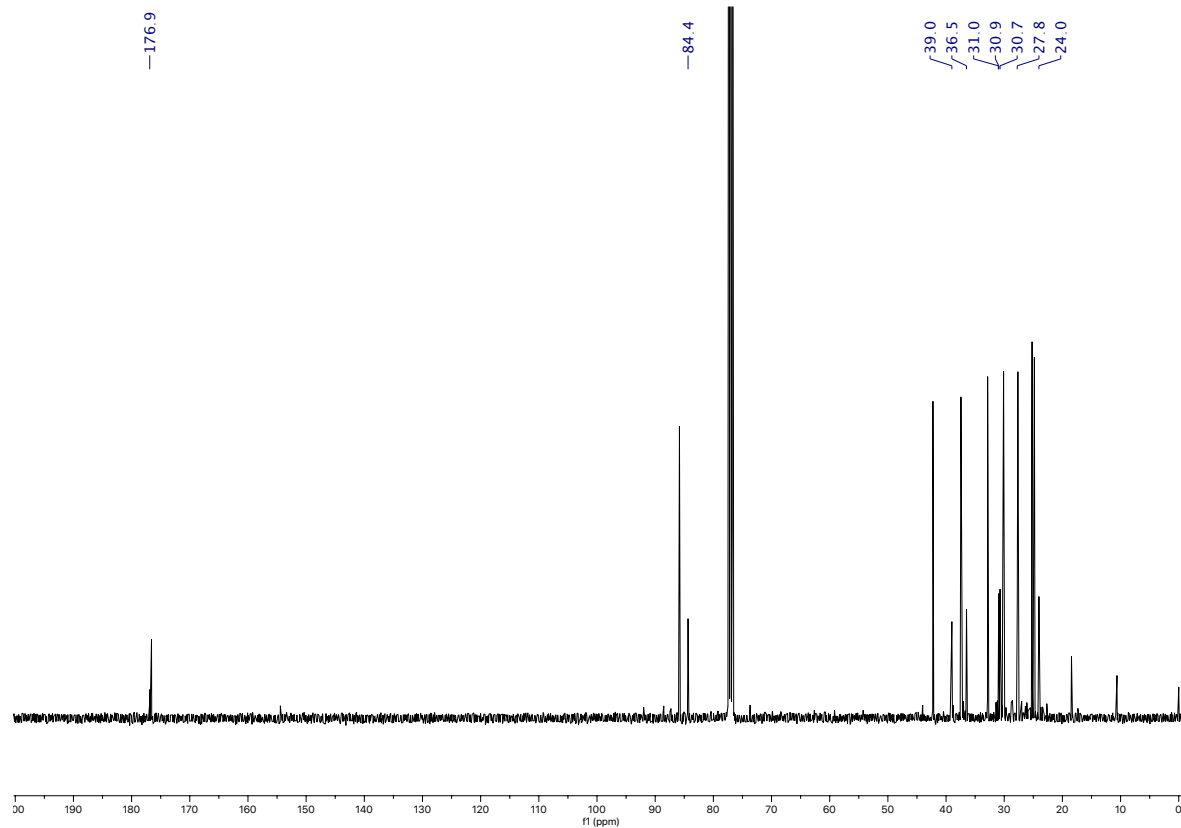
^{13}C NMR of oxidation of **5** in CDCl_3 (**5a** labeled)



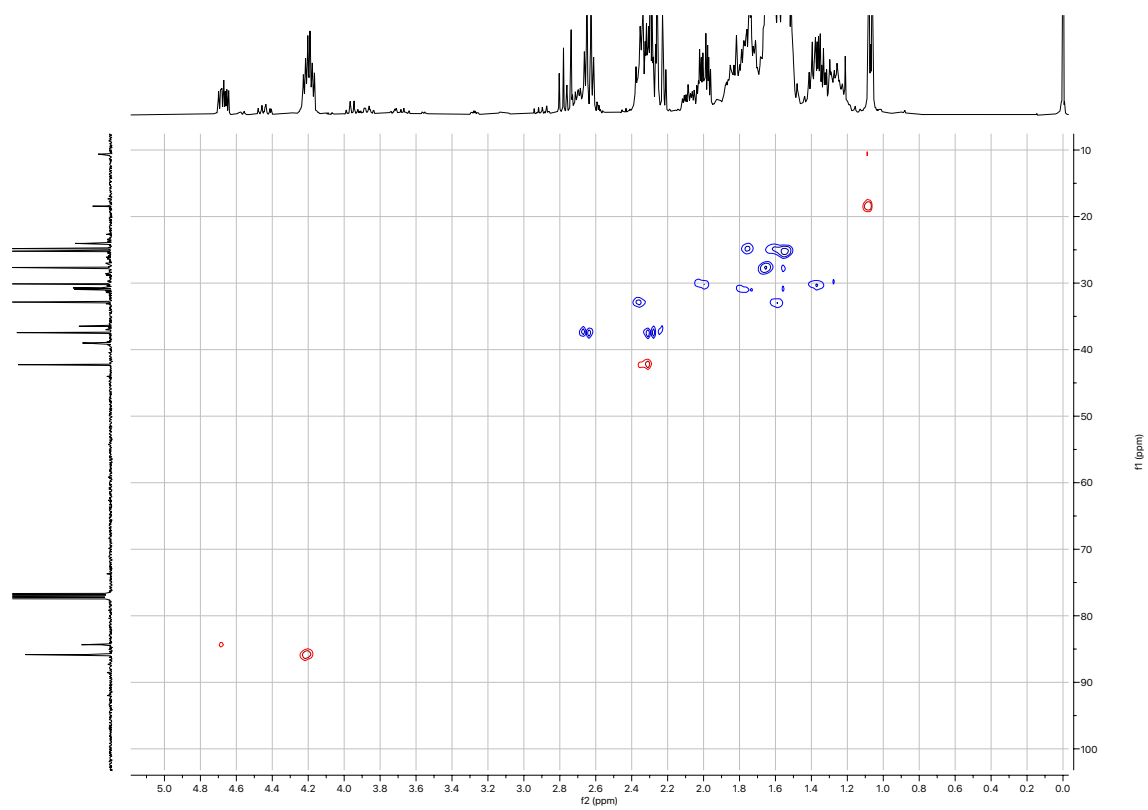
^1H NMR of **5b** in CDCl_3



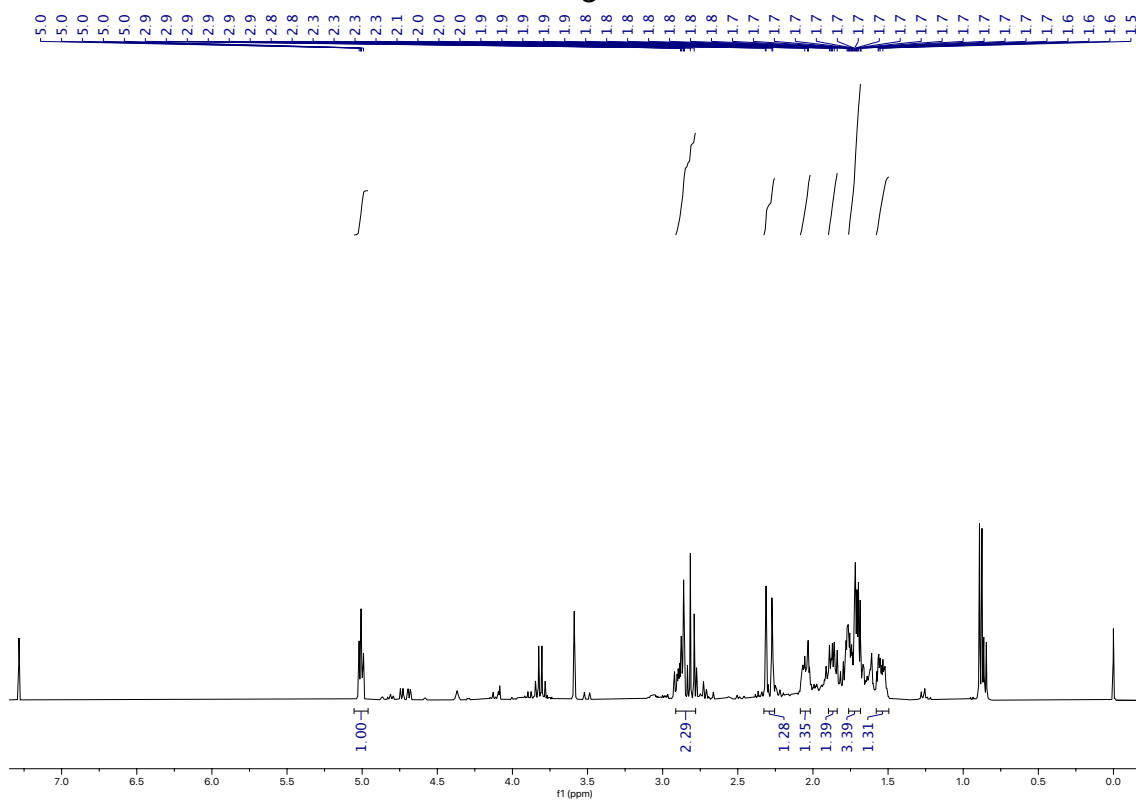
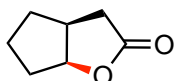
^{13}C NMR of oxidation of **5** in CDCl_3 (**5b** labeled)



HSQC of oxidation of **5** in CDCl₃

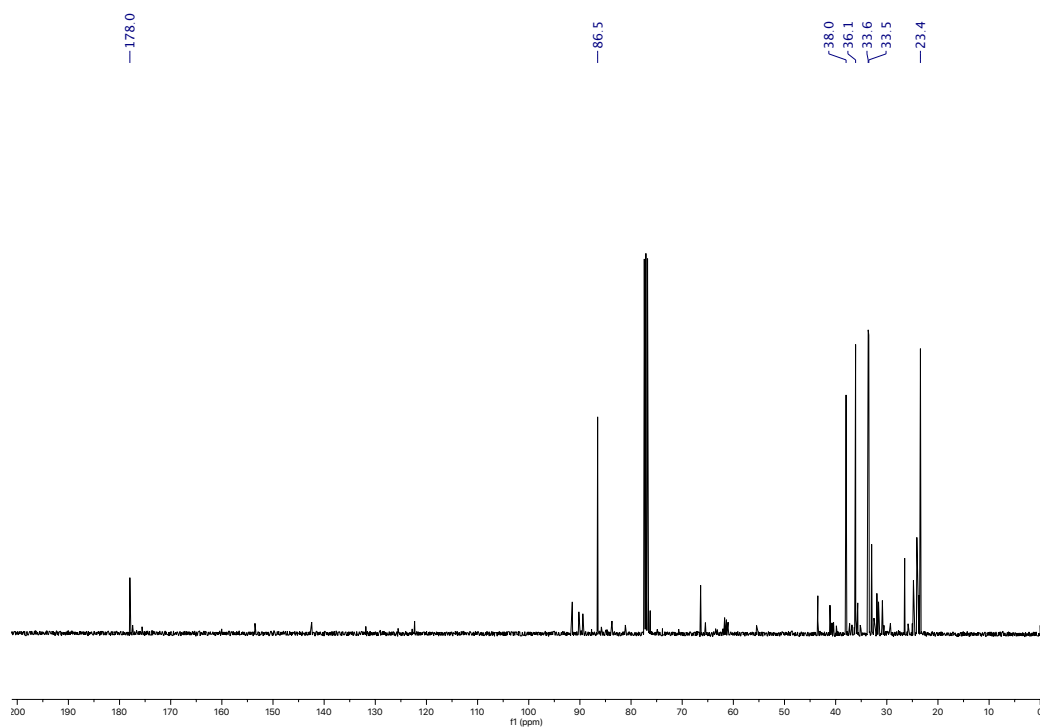


^1H NMR of **6b** in CDCl_3

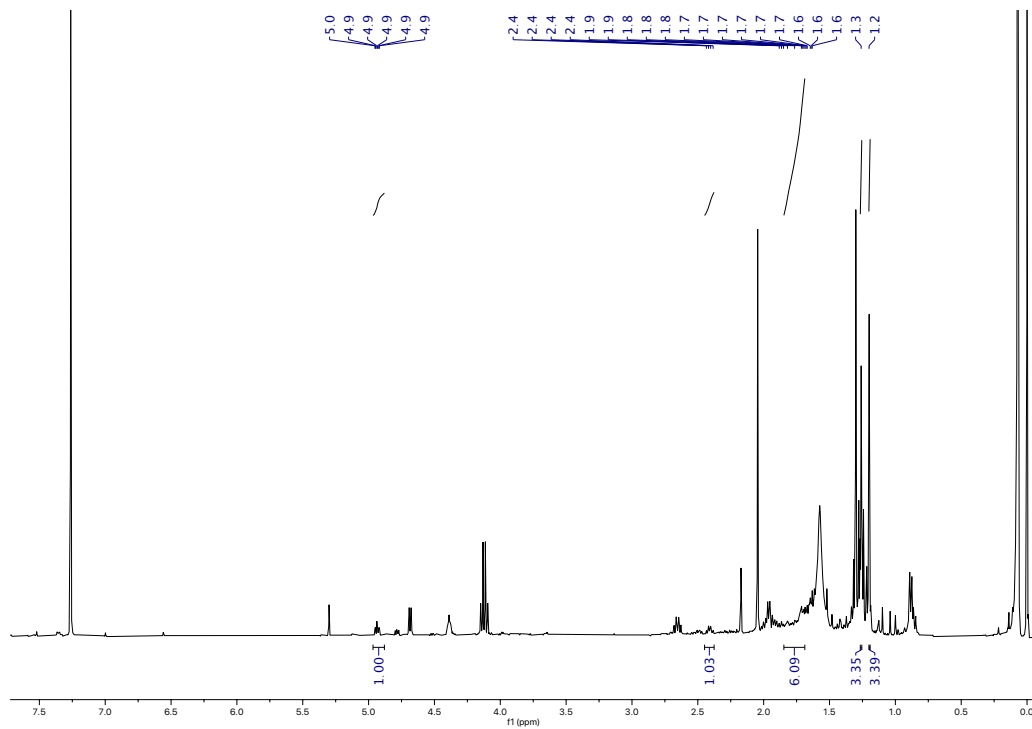
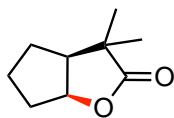


The extra signals mainly come from ligand impurity.

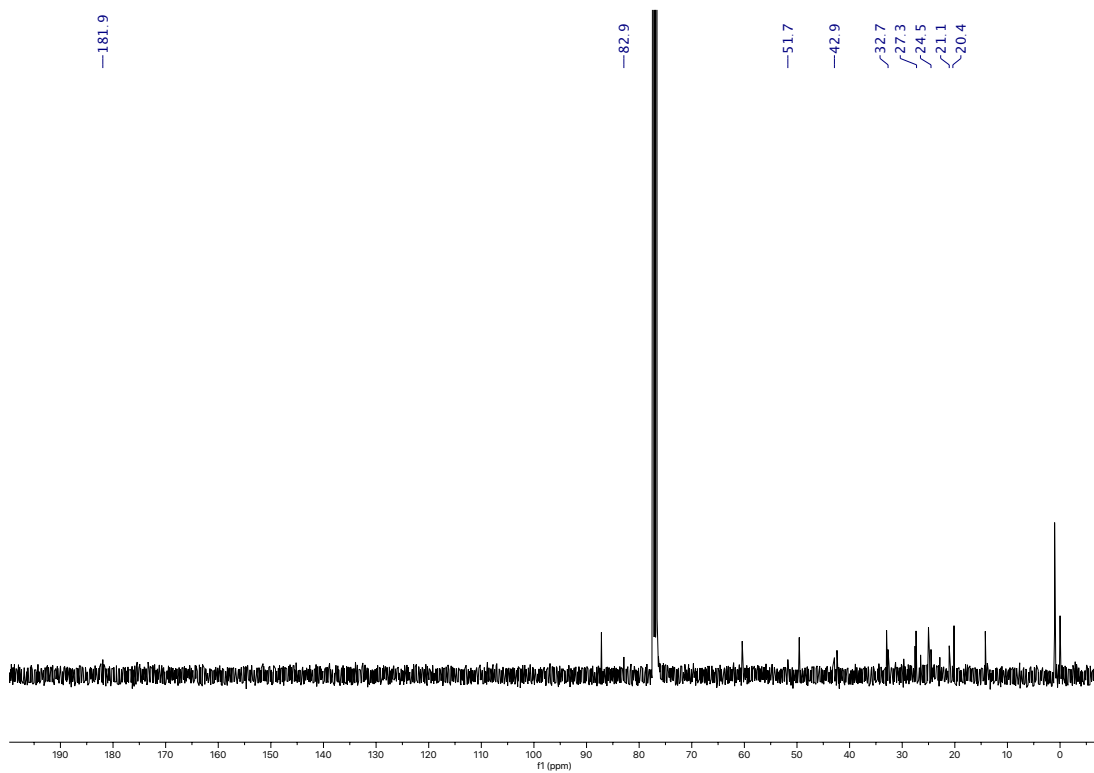
^{13}C NMR of **6b** in CDCl_3



^1H NMR of **7b** in CDCl_3



^{13}C NMR of **7b** in CDCl_3



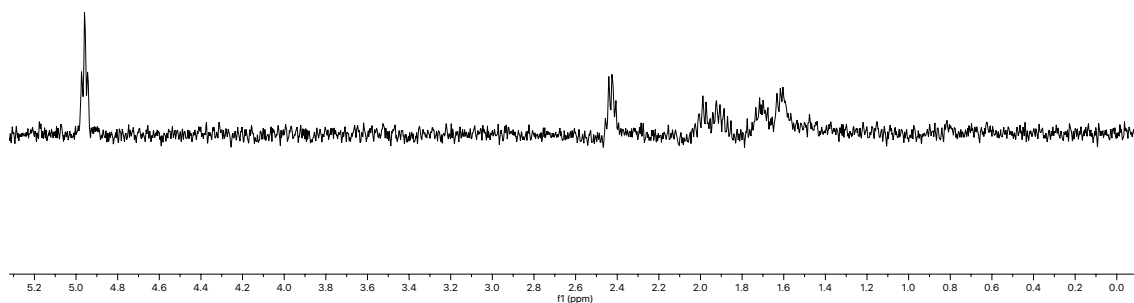
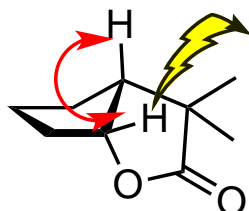
Selective TOCSY (at 4.94 ppm) of **7b** in CDCl₃

5.0
4.9

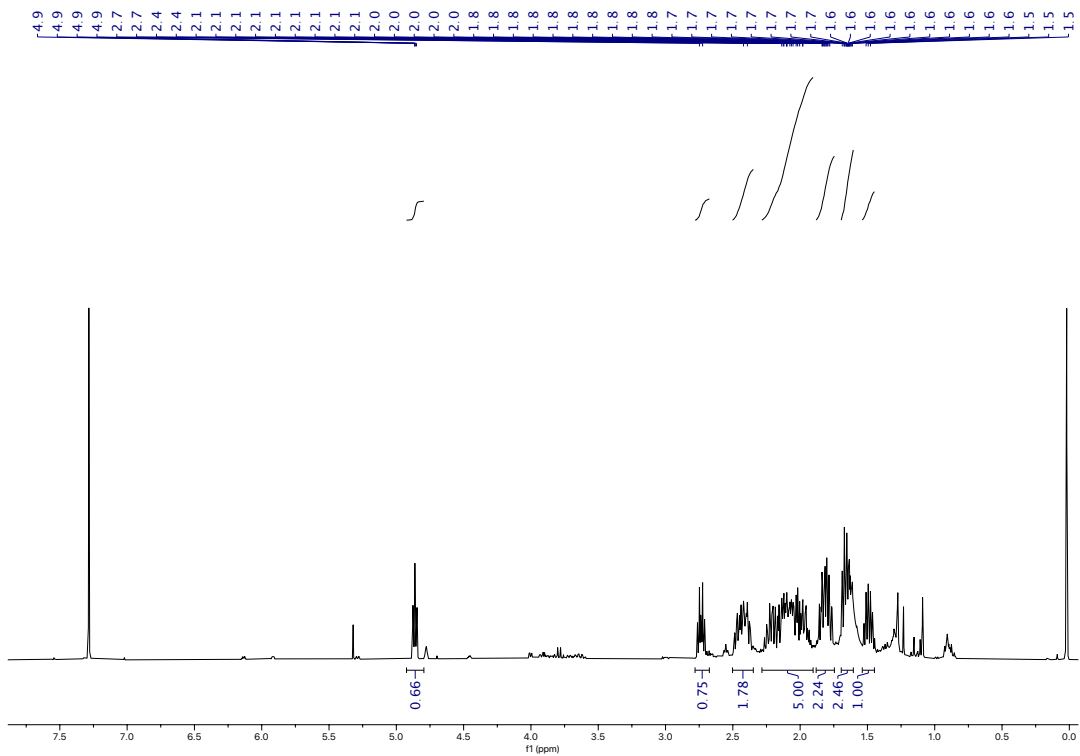
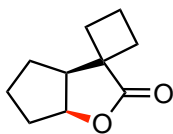
2.4

2.0

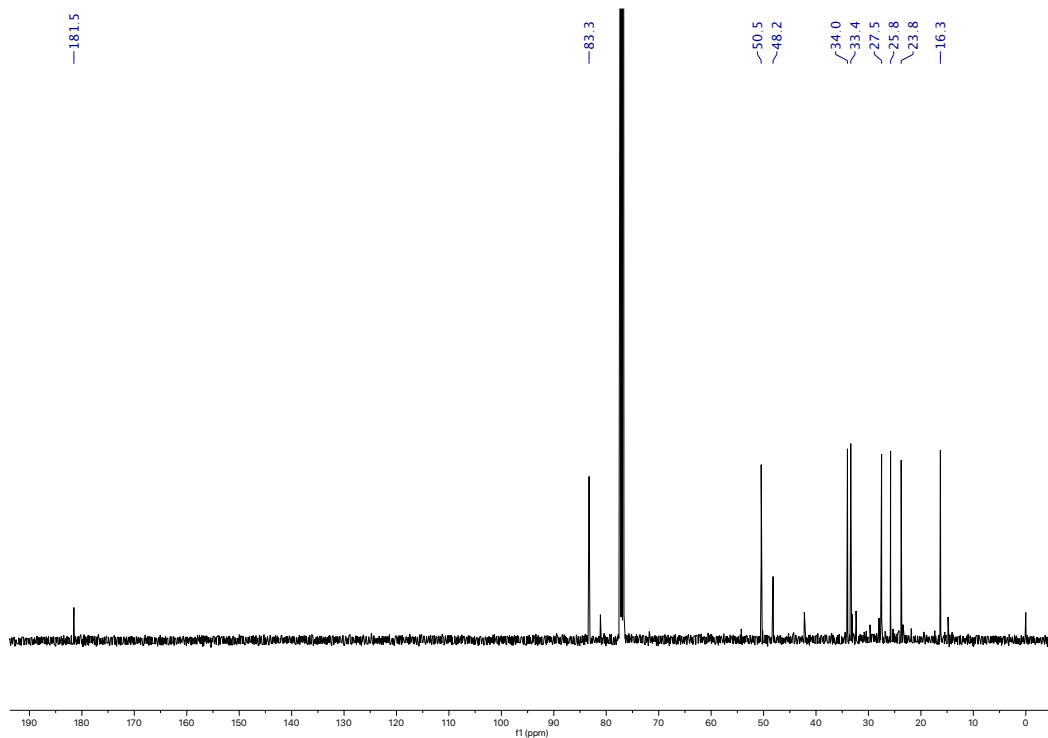
1.6



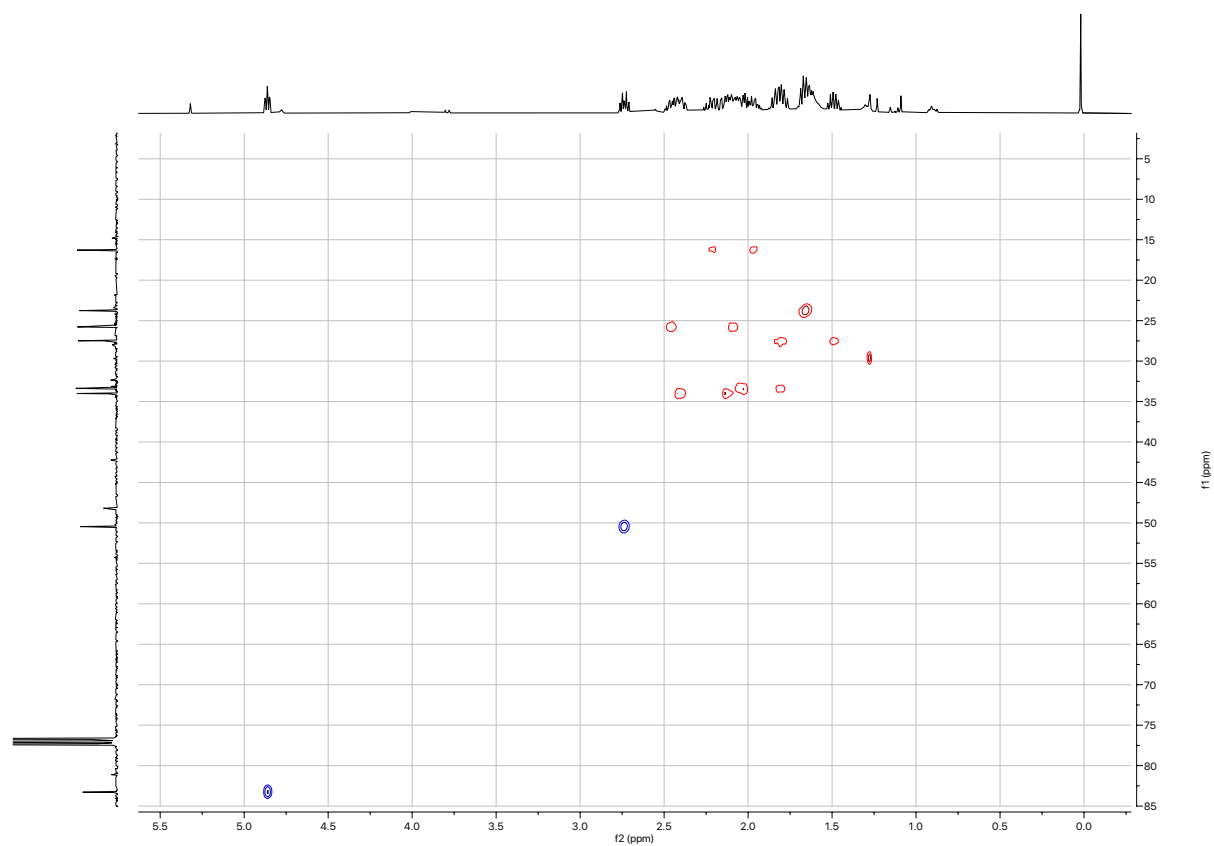
^1H NMR of **8b** in CDCl_3



^{13}C NMR of **8b** in CDCl_3

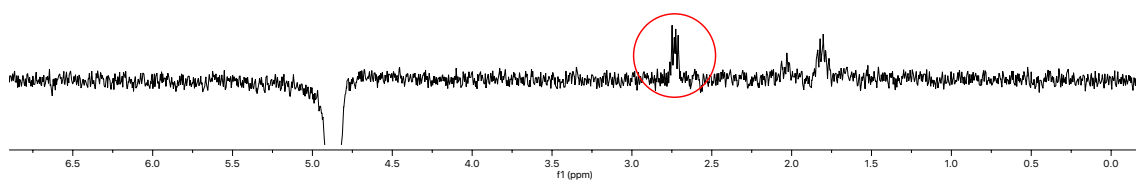
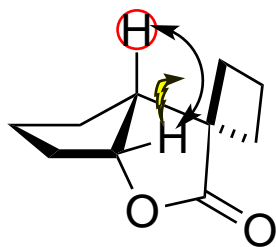


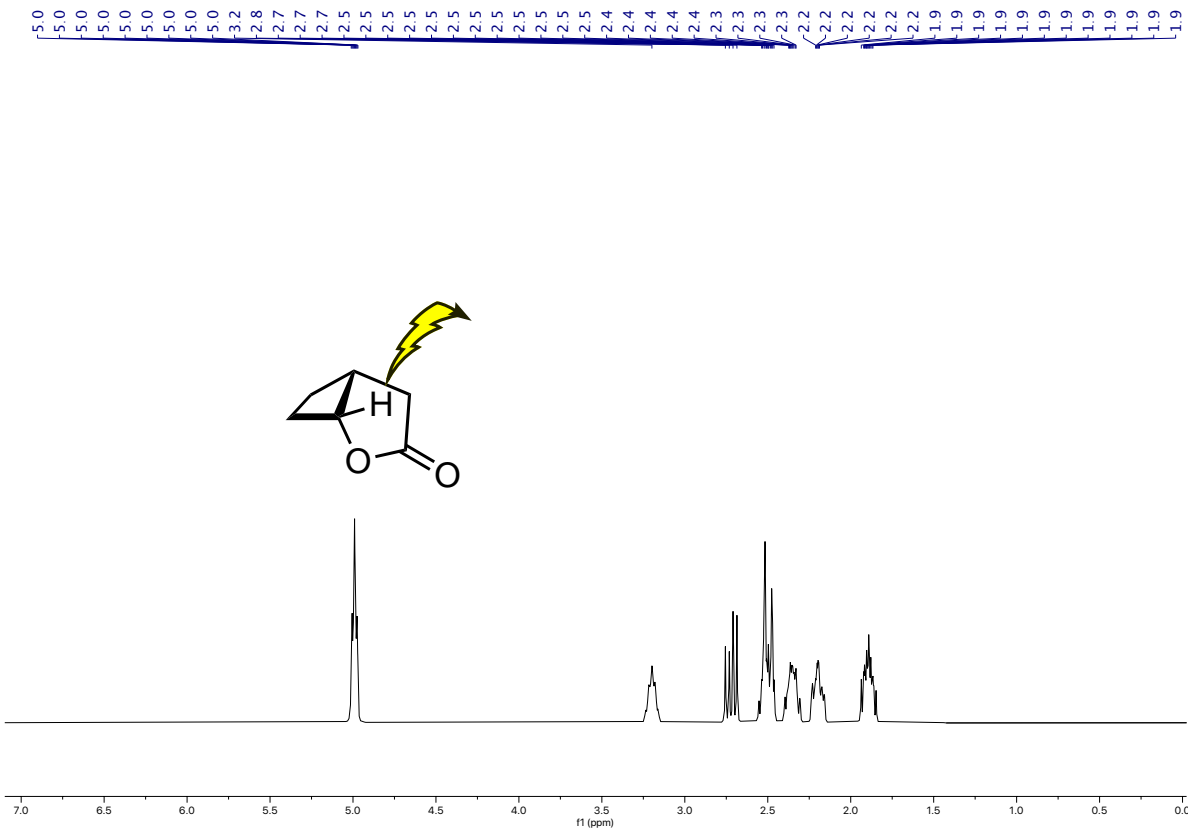
HSQC of **8b** in CDCl₃



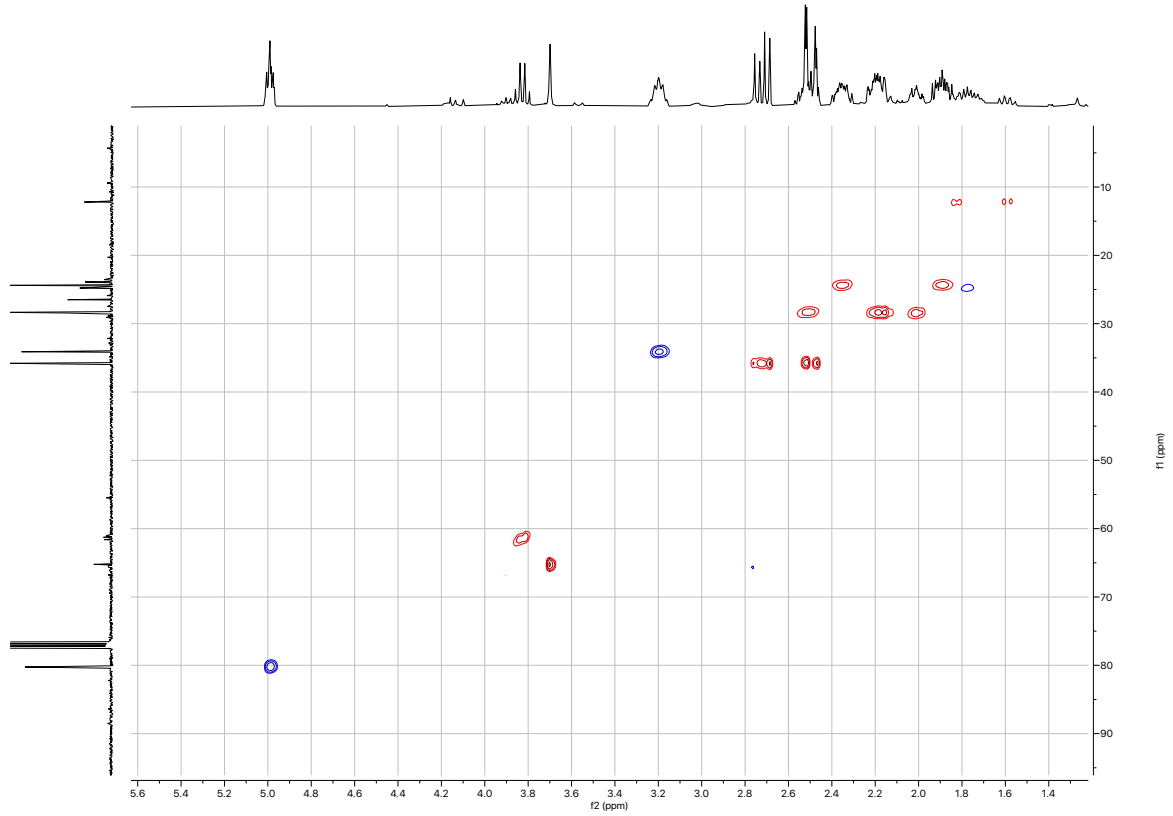
Selective NOESY (at 4.86 ppm) of **8b** in CDCl₃

2.7
2.7
2.7

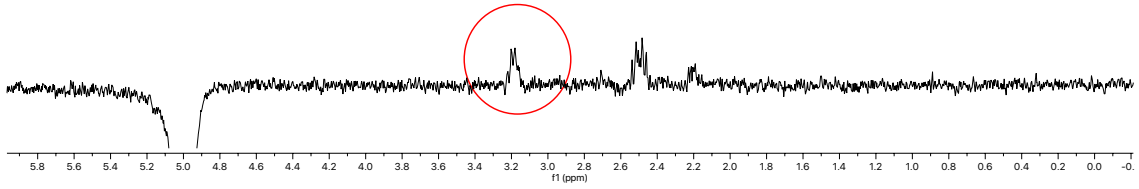
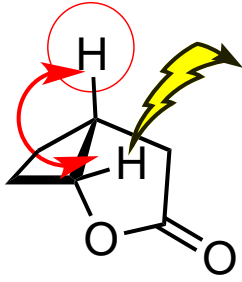




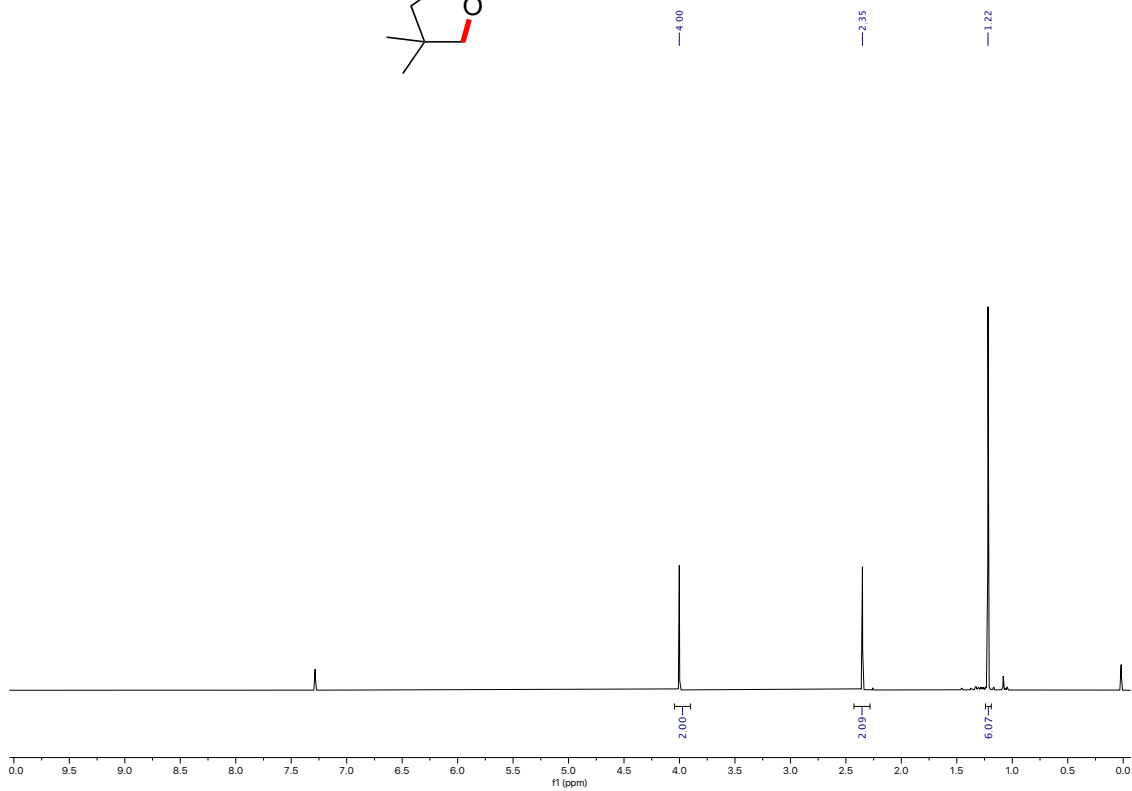
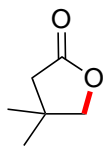
HSQC (at 5.00 ppm) of **10b** in CDCl₃



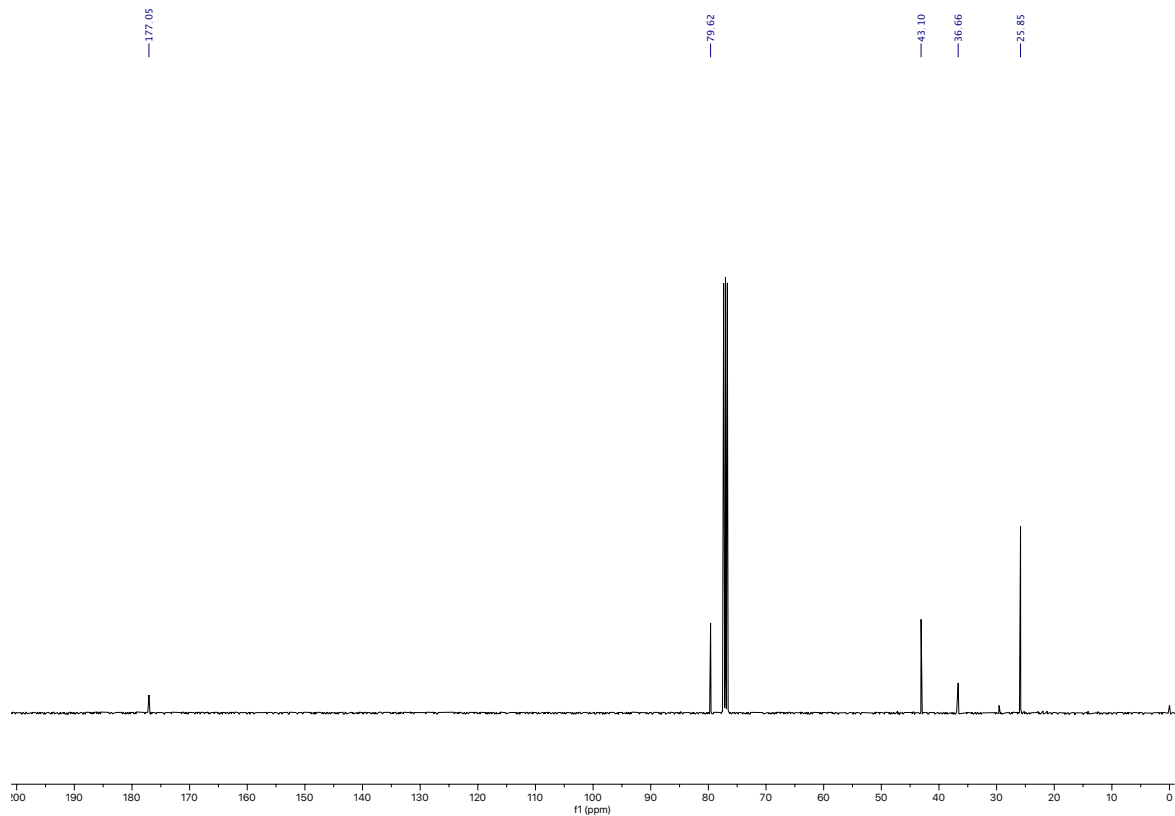
Selective NOESY (at 4.99 ppm) of **10b** in CDCl₃



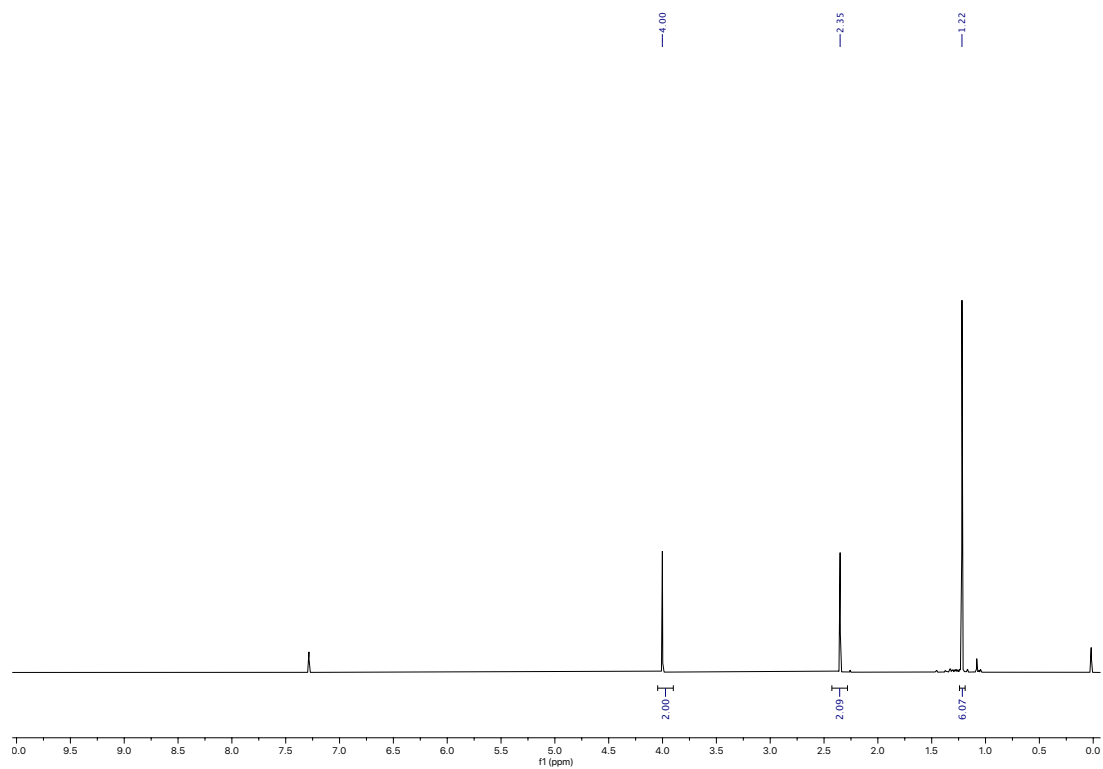
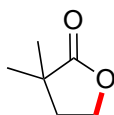
^1H NMR of **16a** in CDCl_3



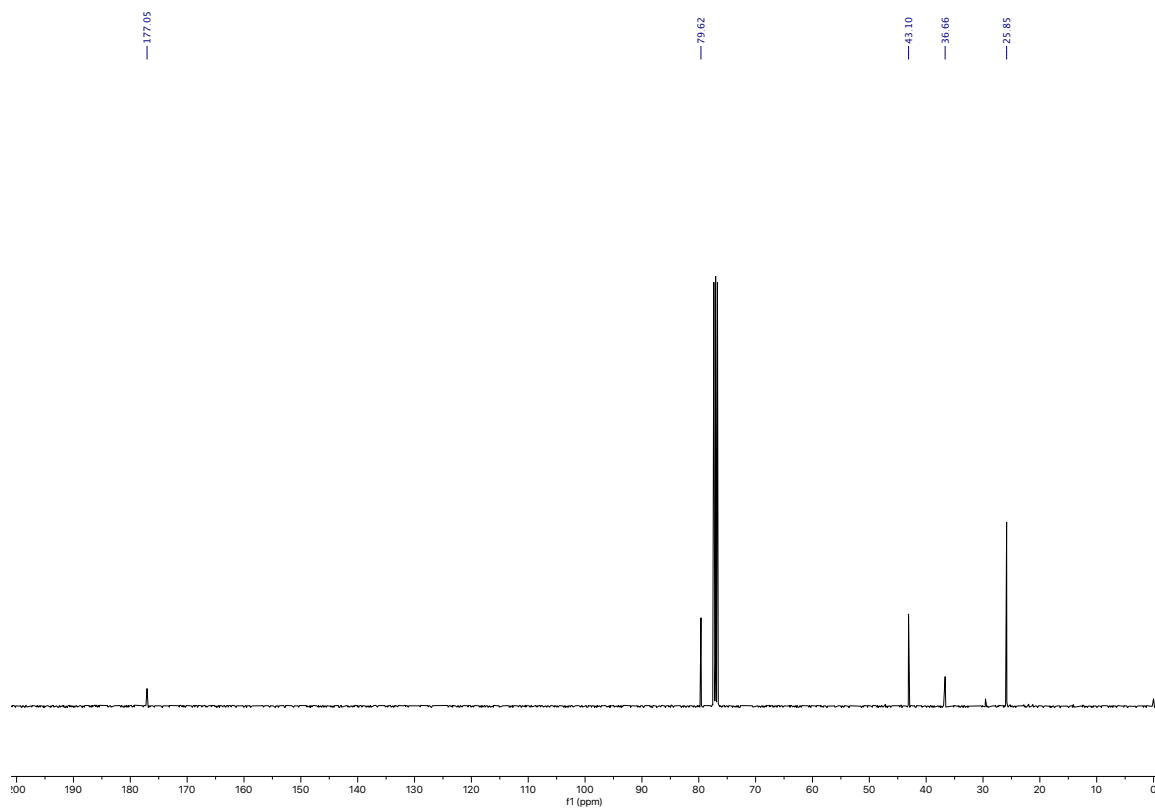
^{13}C NMR of **16a** in CDCl_3



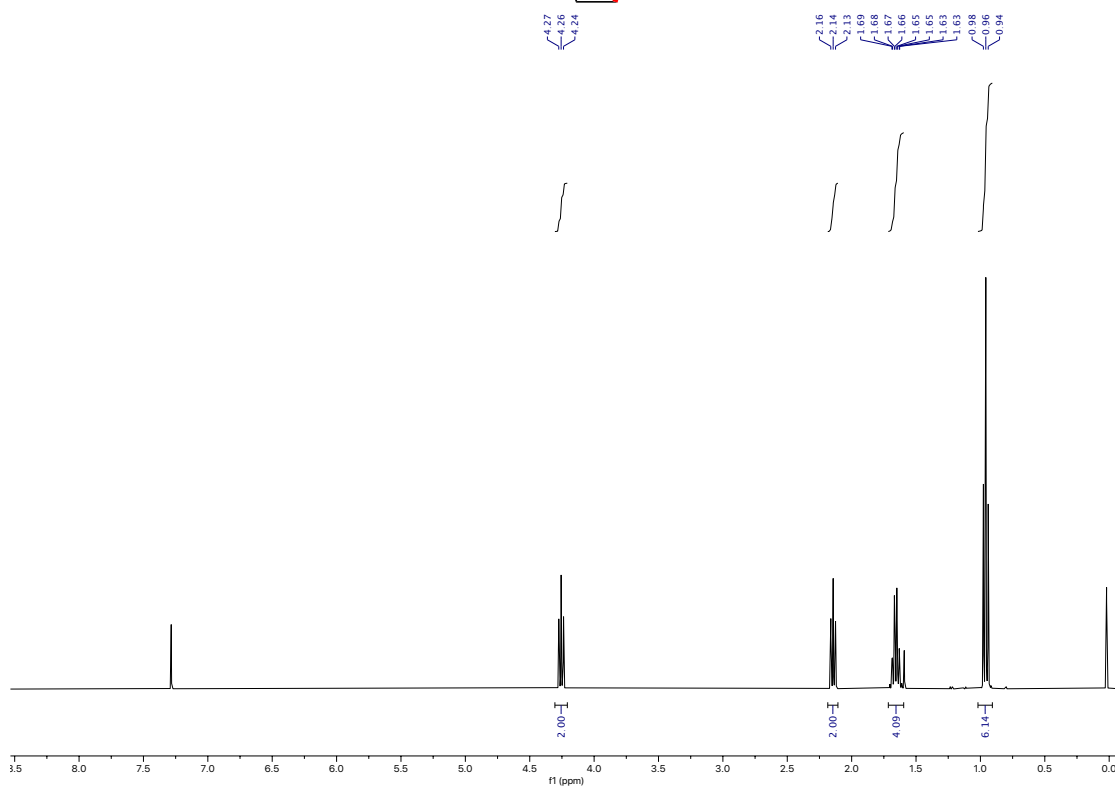
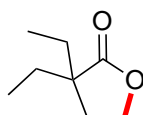
^1H NMR of **20a** in CDCl_3



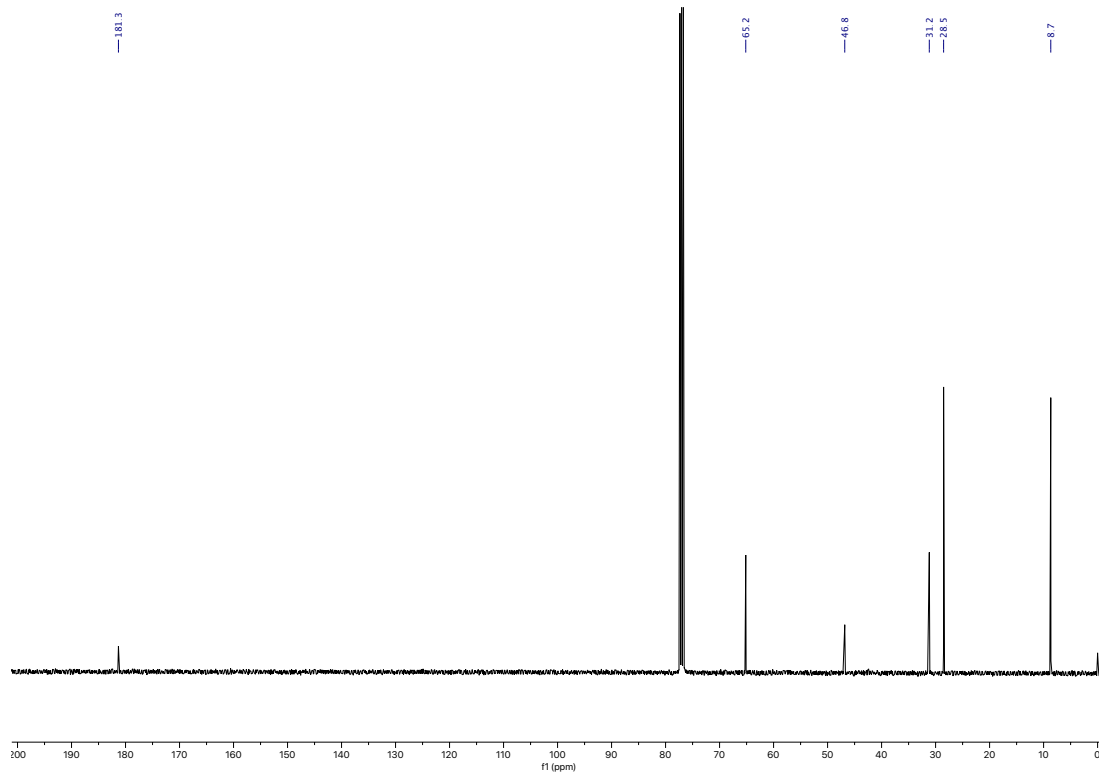
^{13}C NMR of **16a** in CDCl_3



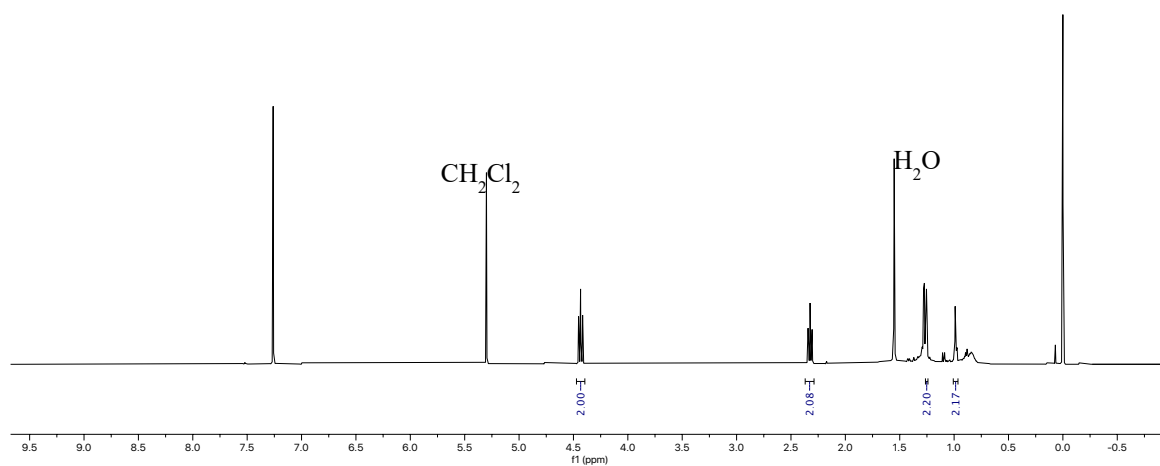
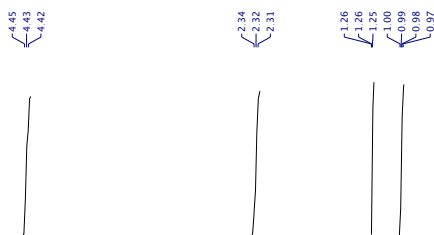
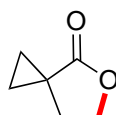
^1H NMR of **21a** in CDCl_3



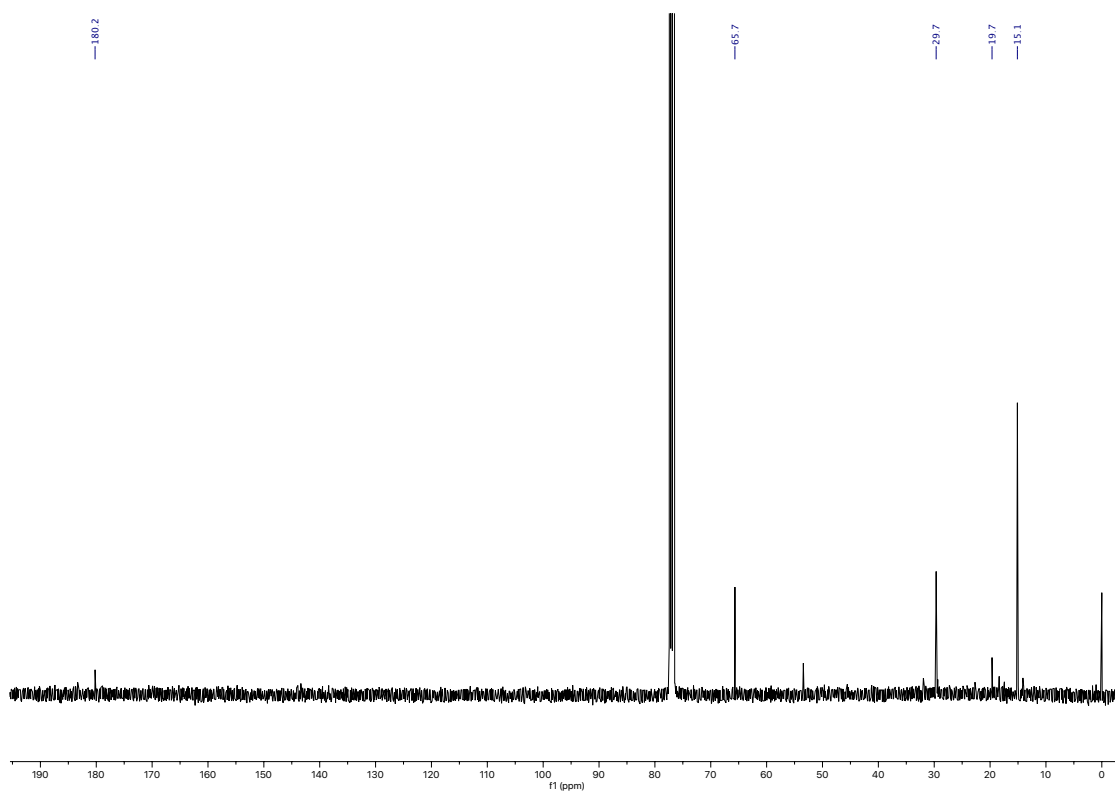
^{13}C NMR of **21a** in CDCl_3



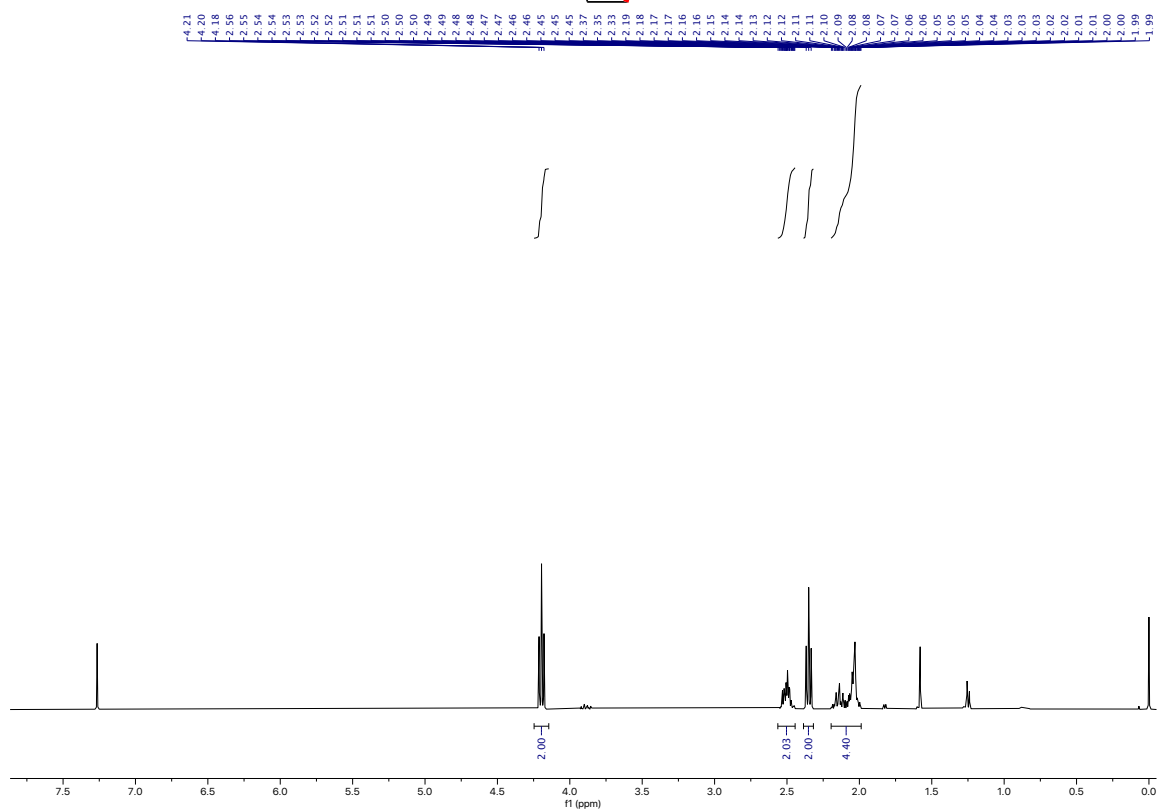
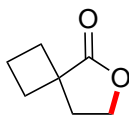
^1H NMR of **22a** in CDCl_3



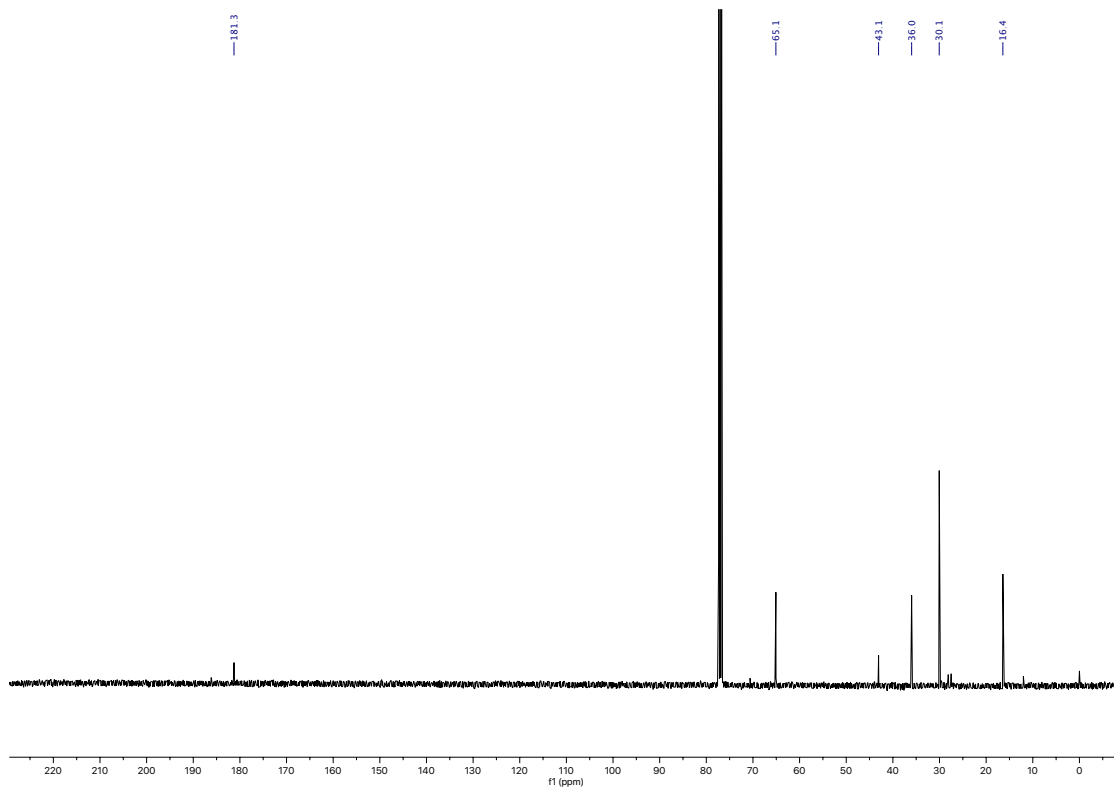
^{13}C NMR of **22a** in CDCl_3



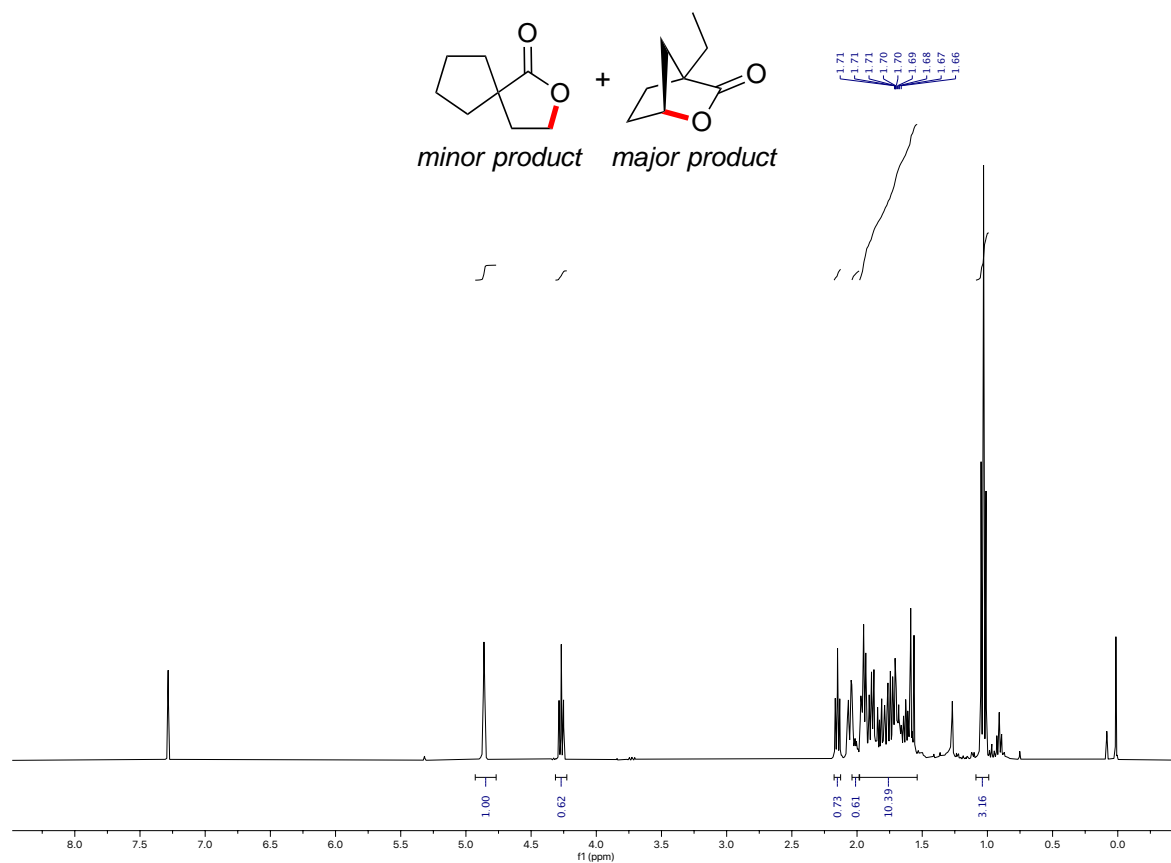
^1H NMR of **23a** in CDCl_3



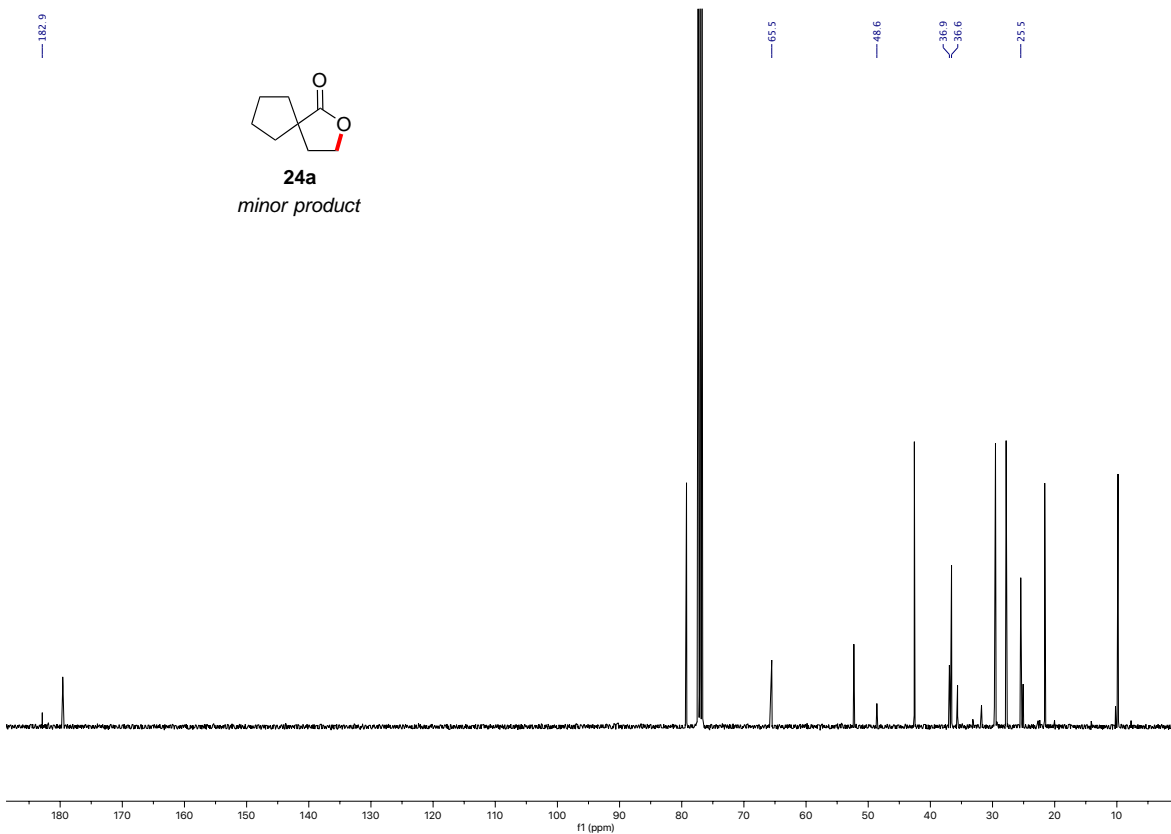
^{13}C NMR of **23a** in CDCl_3



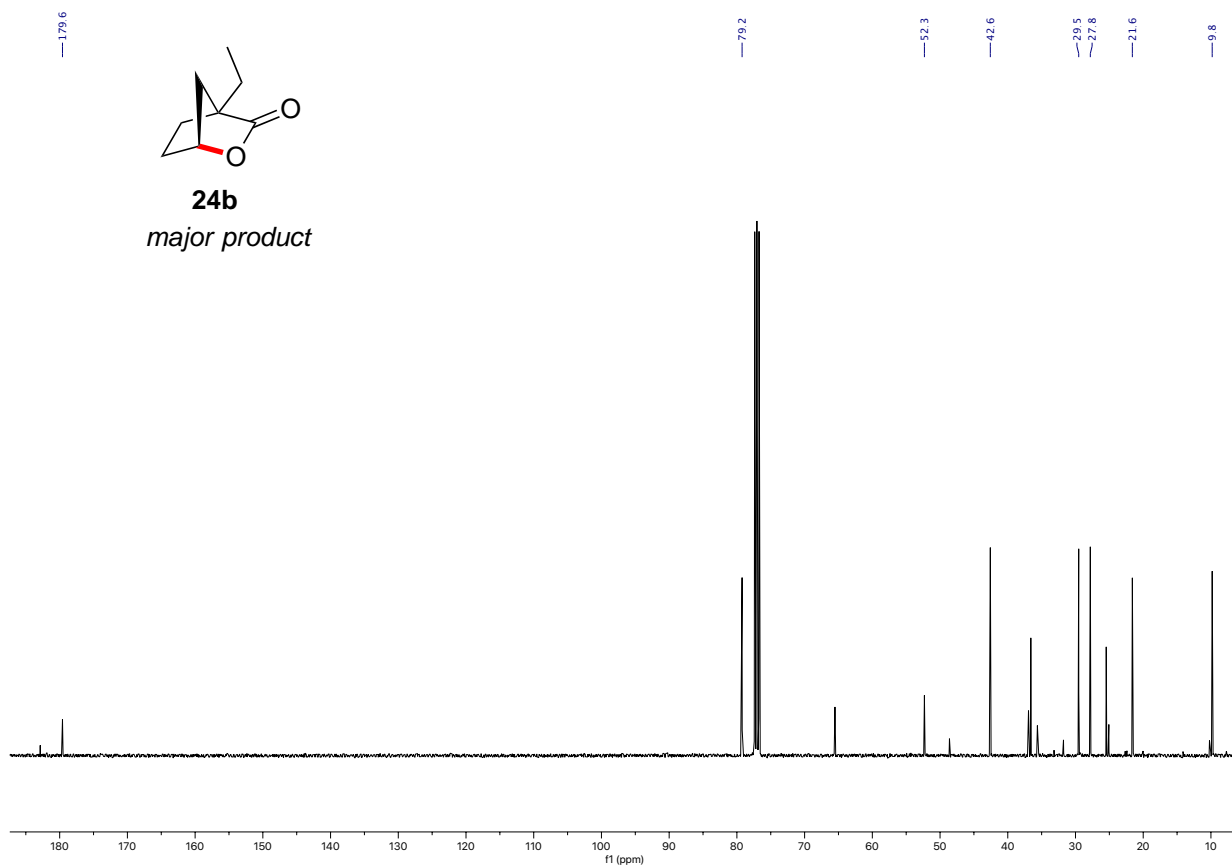
^1H NMR of **24a+24b** in CDCl_3



^{13}C NMR of **24a+24b** in CDCl_3 (signal of **24a** labeled)

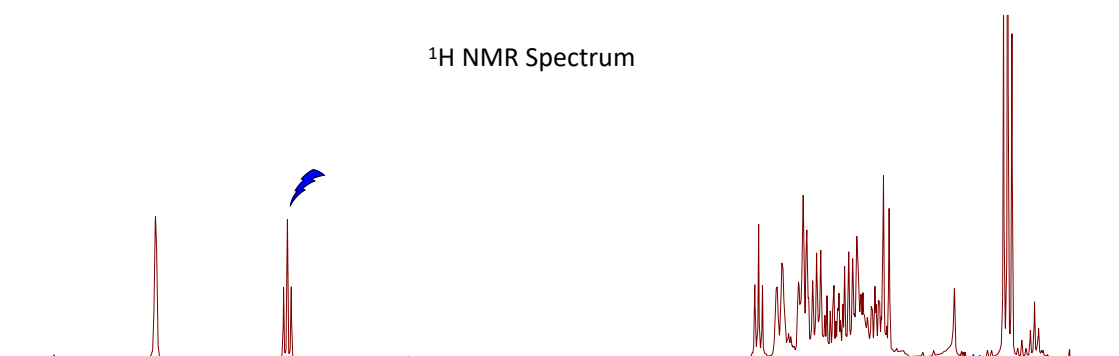


^{13}C NMR of **24a+24b** in CDCl_3 (signal of **24b** labeled)

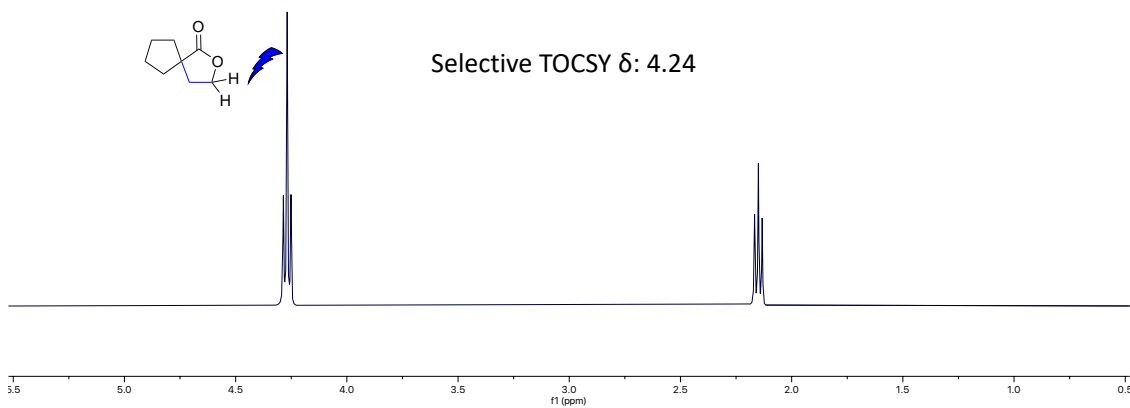


Selective TOCSY experiments of **24a+24b**

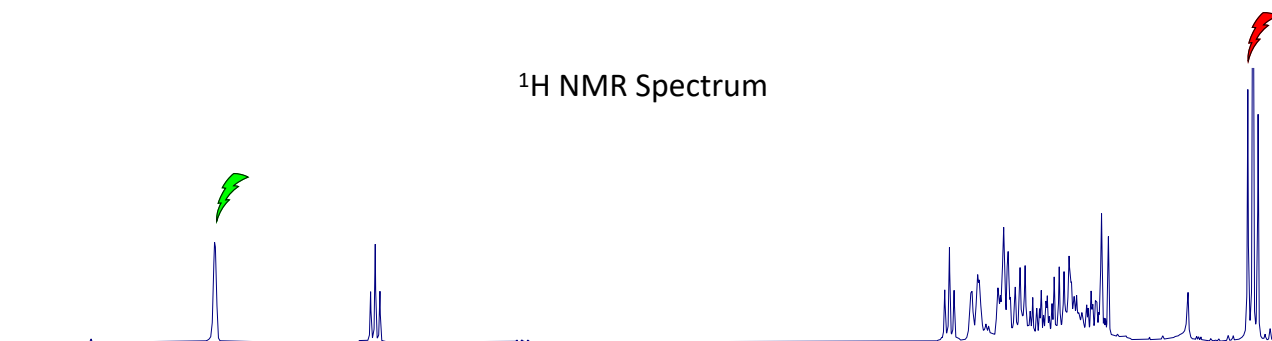
^1H NMR Spectrum



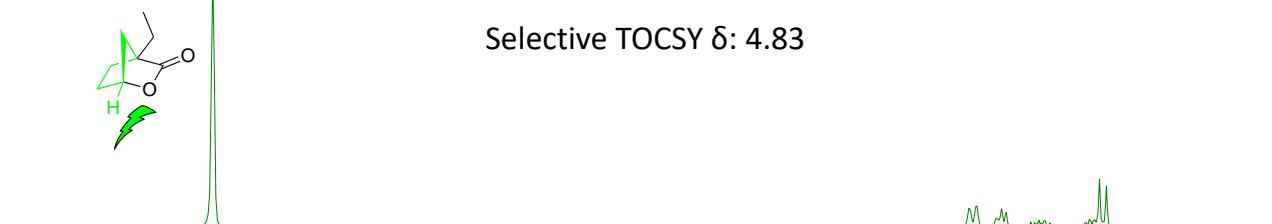
Selective TOCSY δ : 4.24



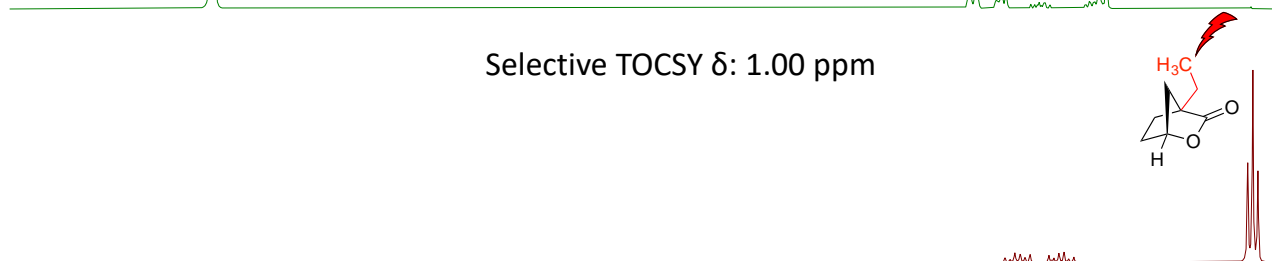
^1H NMR Spectrum



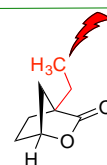
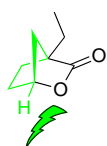
Selective TOCSY δ : 4.83



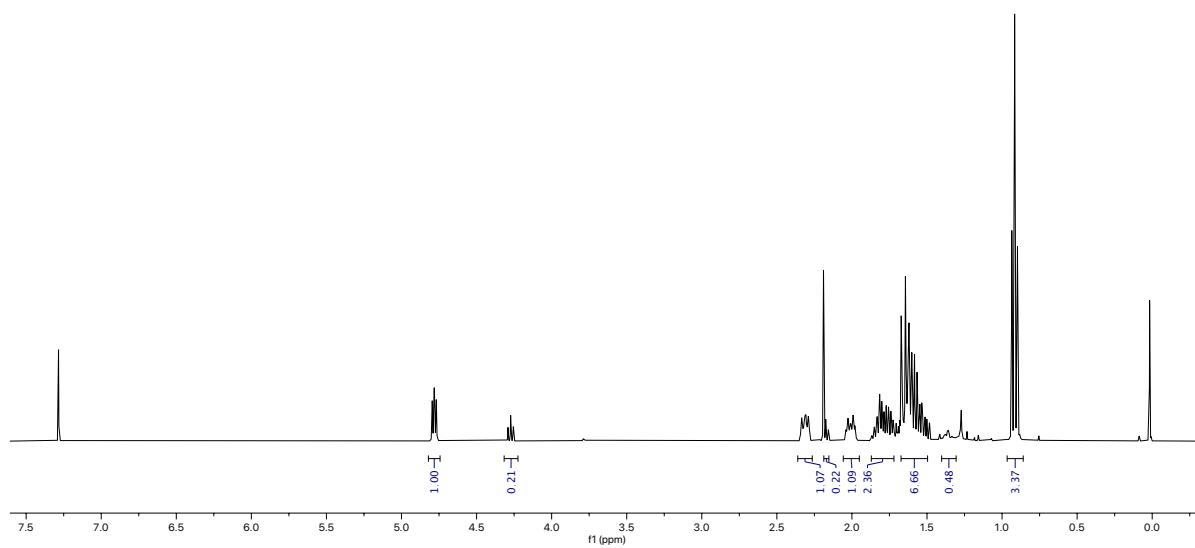
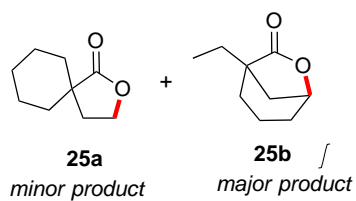
Selective TOCSY δ : 1.00 ppm



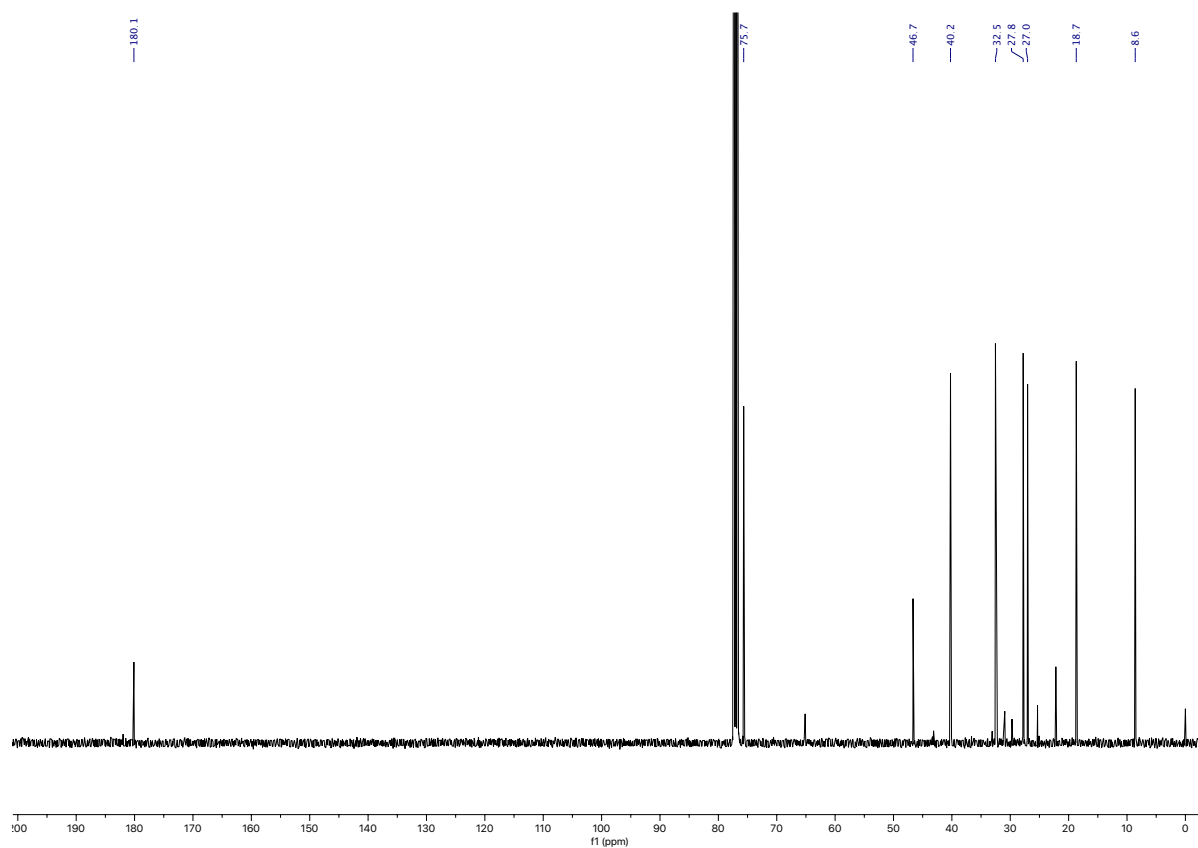
5.4 5.2 5.0 4.8 4.6 4.4 4.2 4.0 3.8 3.6 3.4 3.2 3.0 2.8 2.6 2.4 2.2 2.0 1.8 1.6 1.4 1.2 1.0
f1 (ppm)



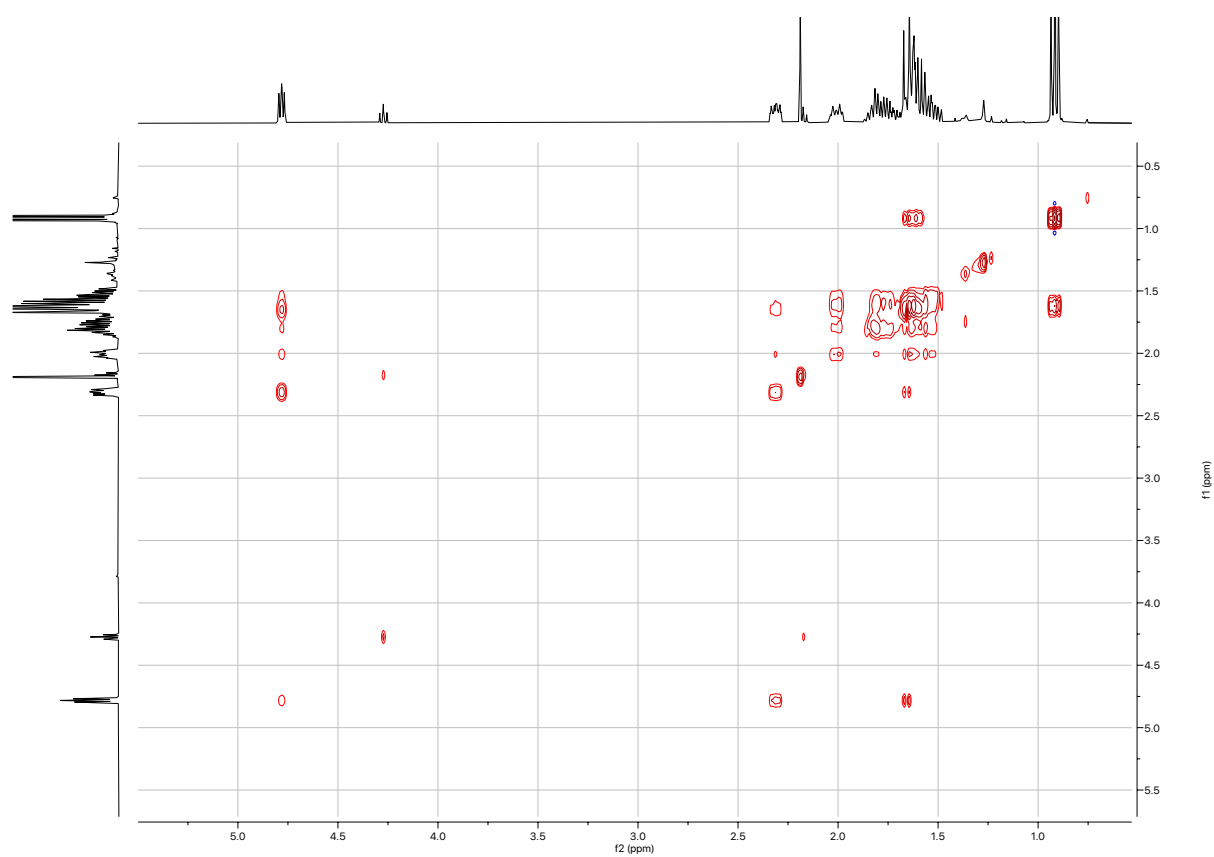
^1H NMR of **25a+25b** in CDCl_3 (labeled **25b**)



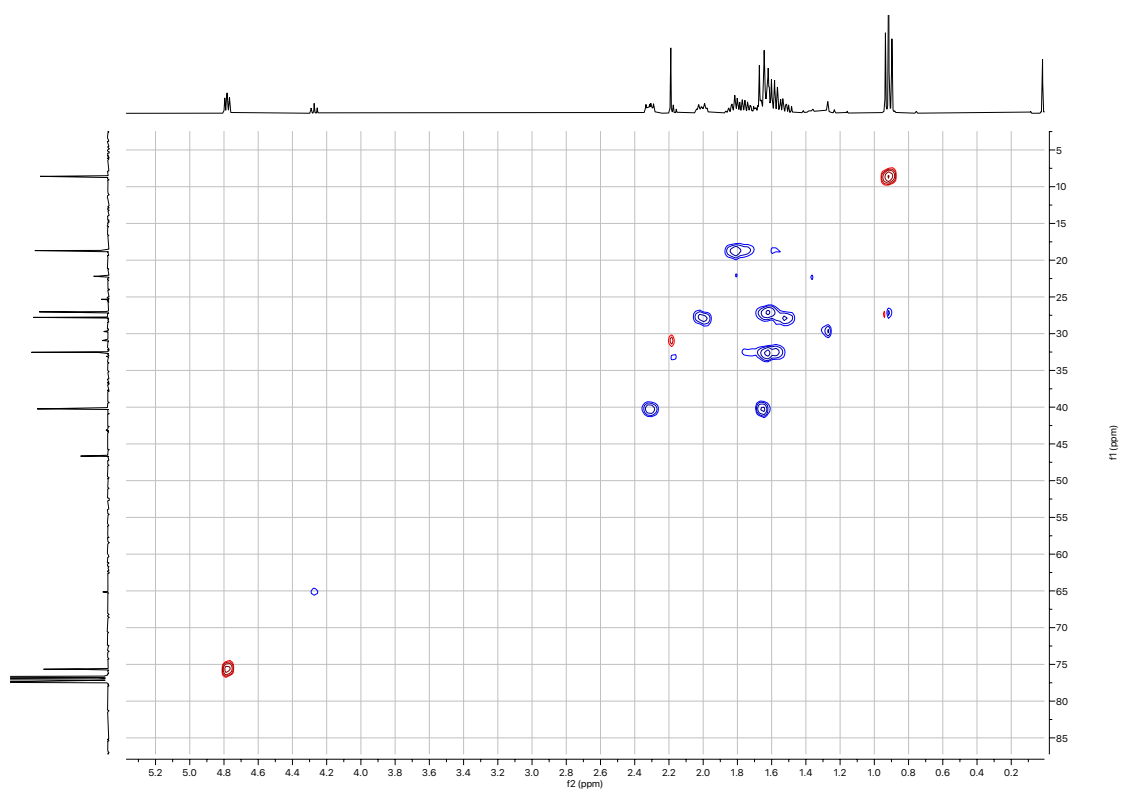
^{13}C NMR of **25a+25b** in CDCl_3 (labeled **25b**)



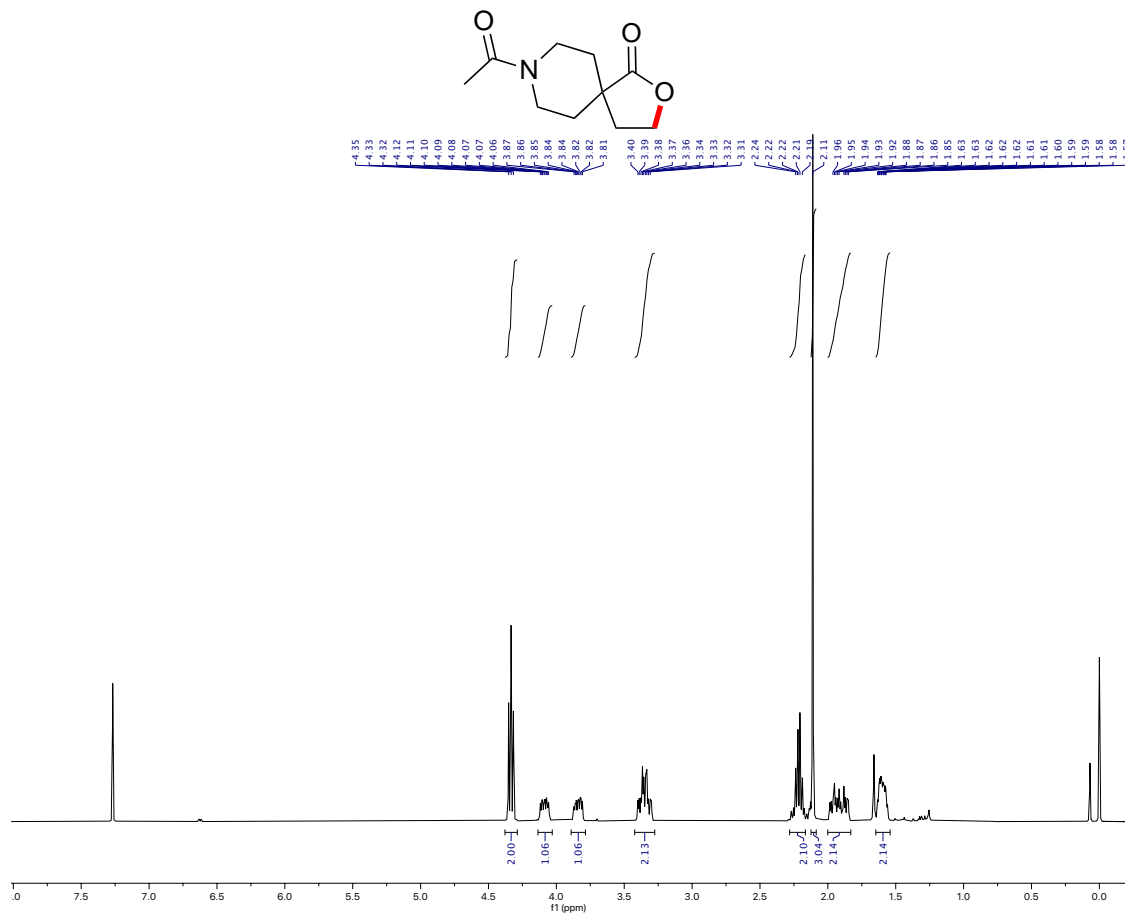
TOCSY of 25a+25b in CDCl₃



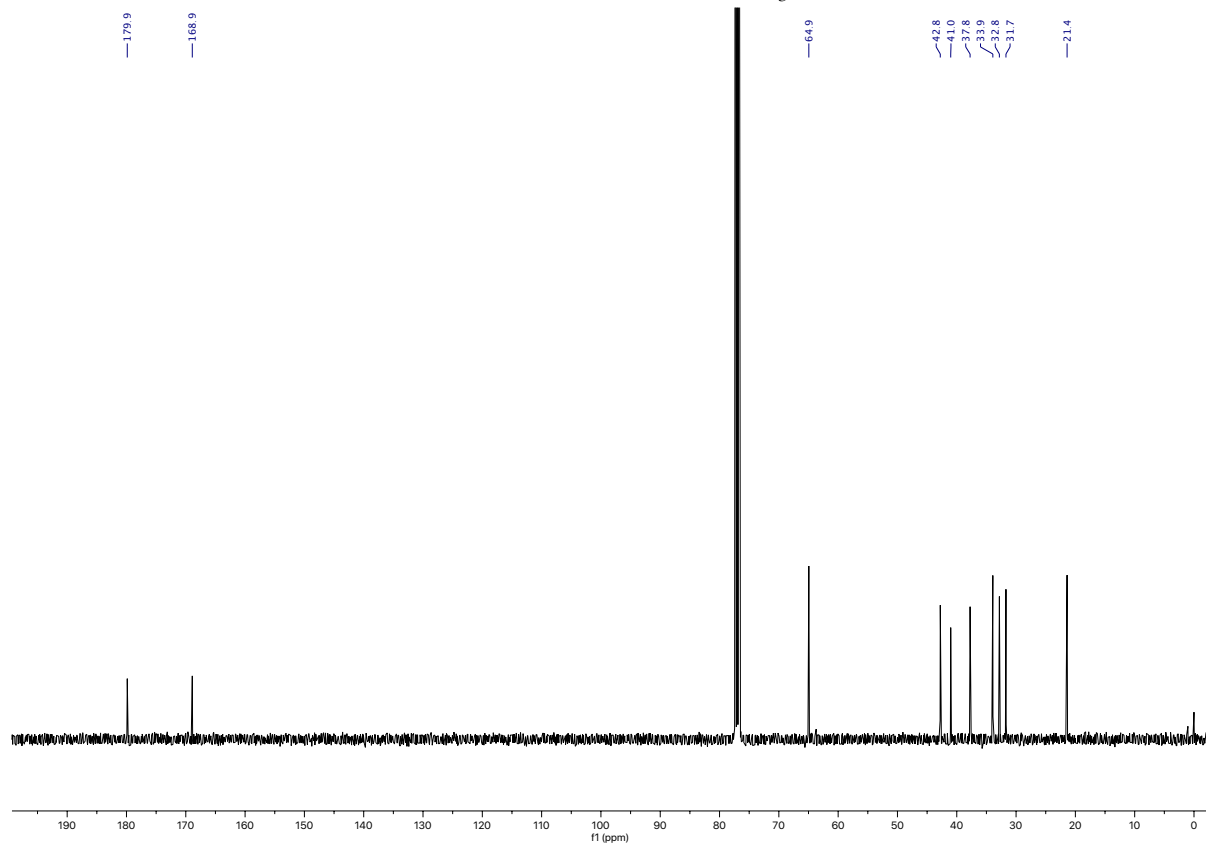
HSQC of 25a+25b in CDCl₃



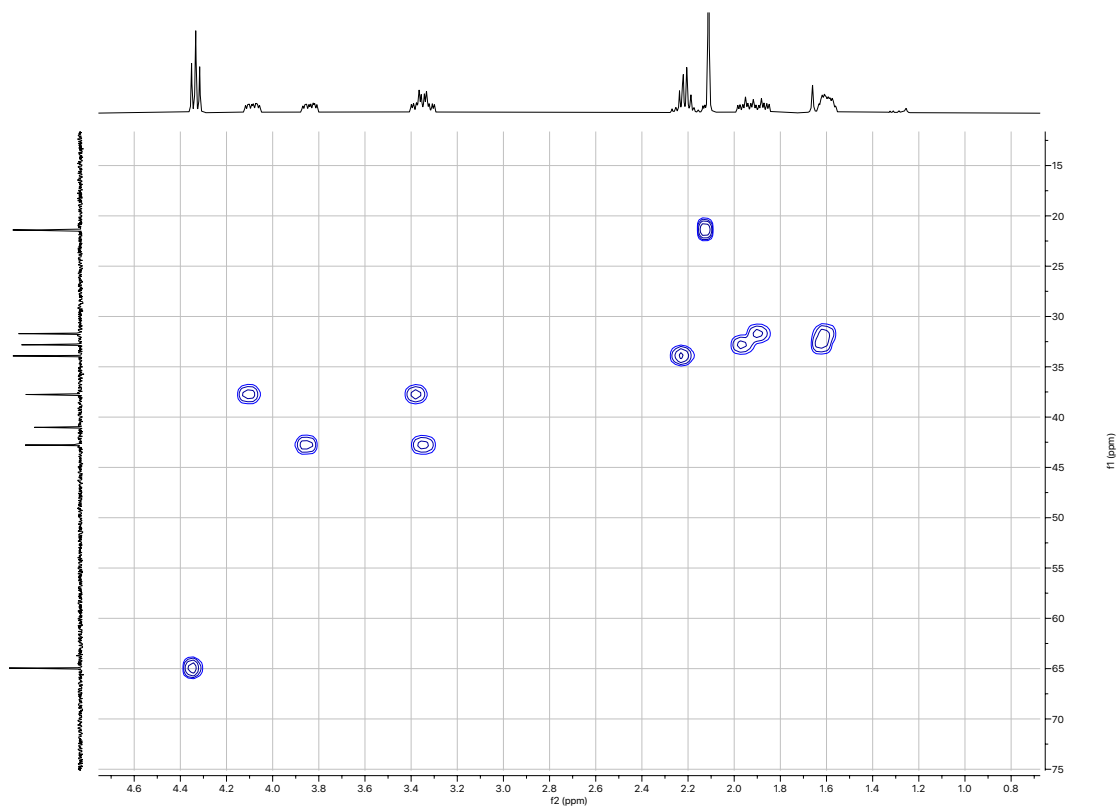
¹H NMR of 26a in CDCl₃



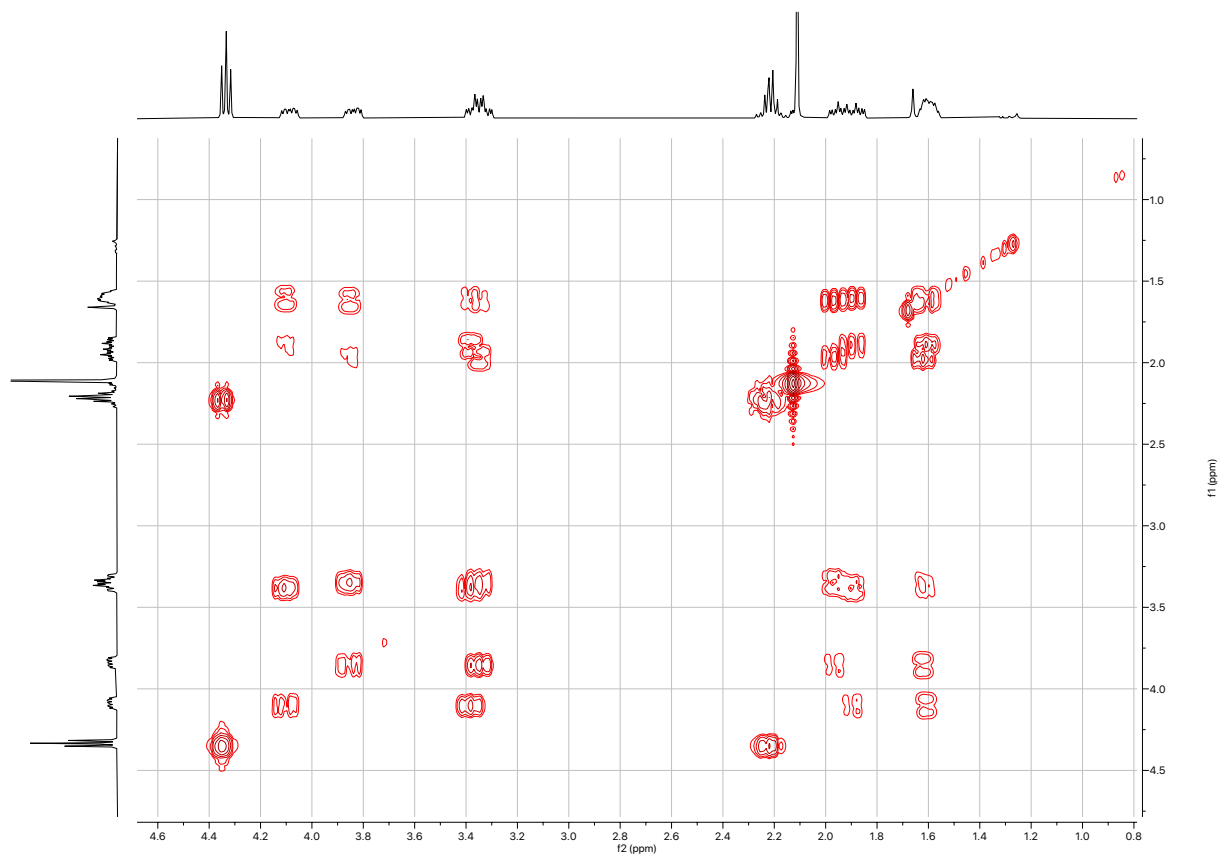
¹³C NMR of 26a in CDCl₃



HSQC of 26a in CDCl₃



COSY of 26a in CDCl₃



III.GC Traces

Selected GC traces of the crude mixtures from the oxidation of 1.

Table 1. Entry 2

(S,S)-Fe(TIPSPdp)

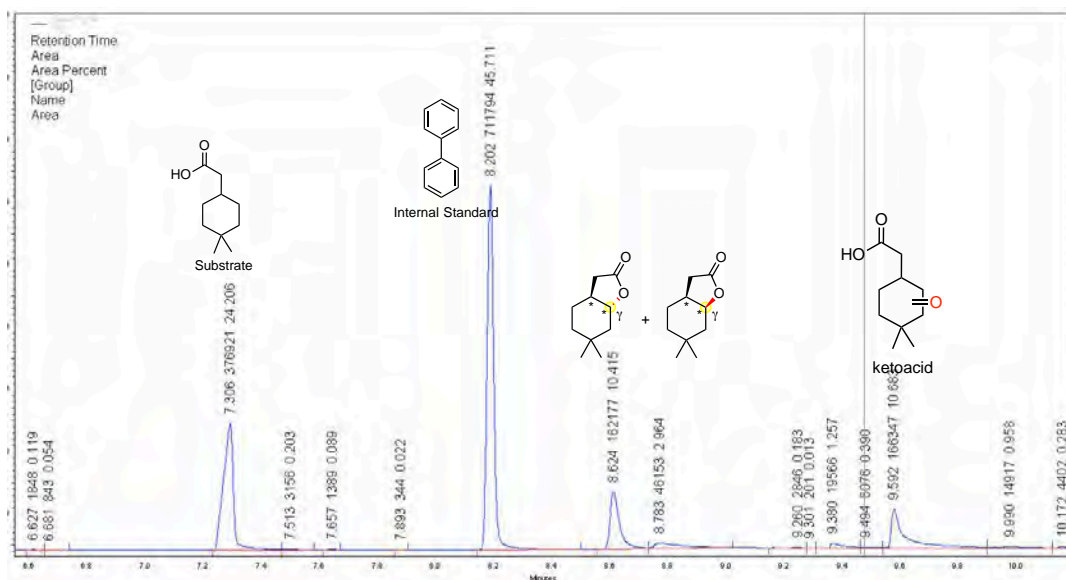


Table 1. Entry 3

(S,S)-Mn(pdp)

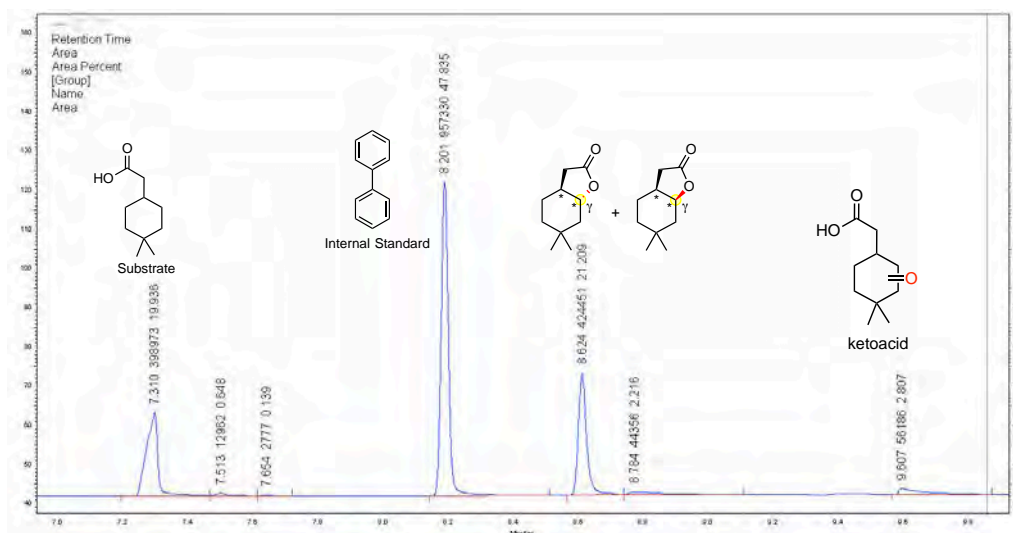
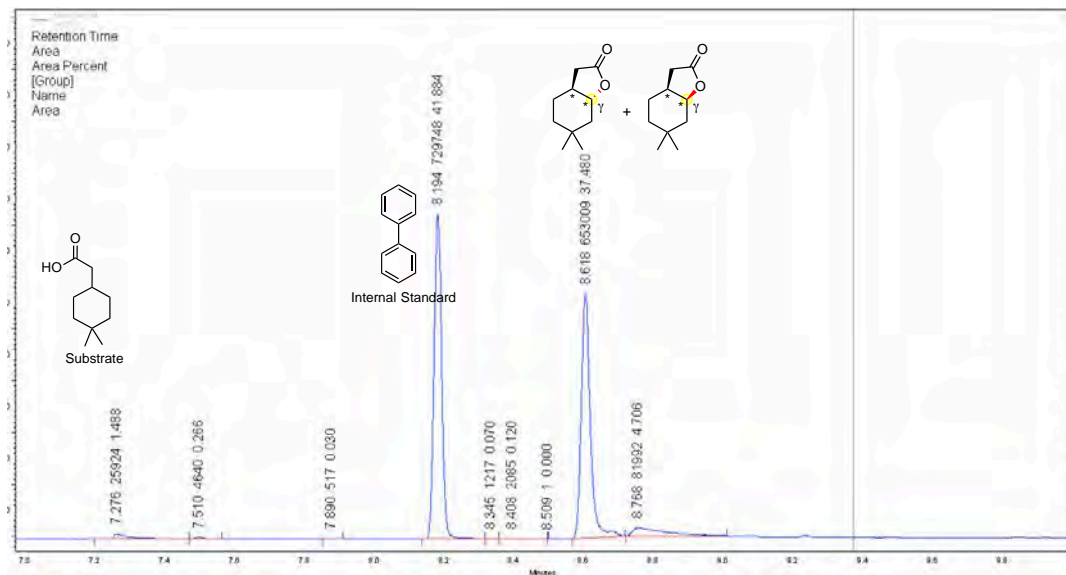


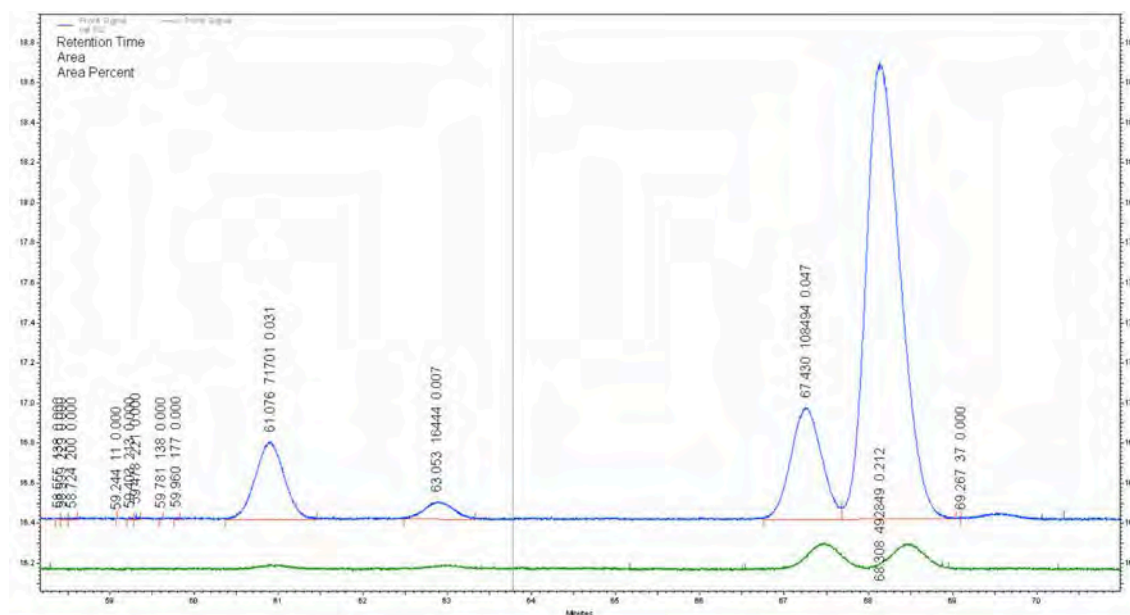
Table 1. Entry 11
Optimized Condition



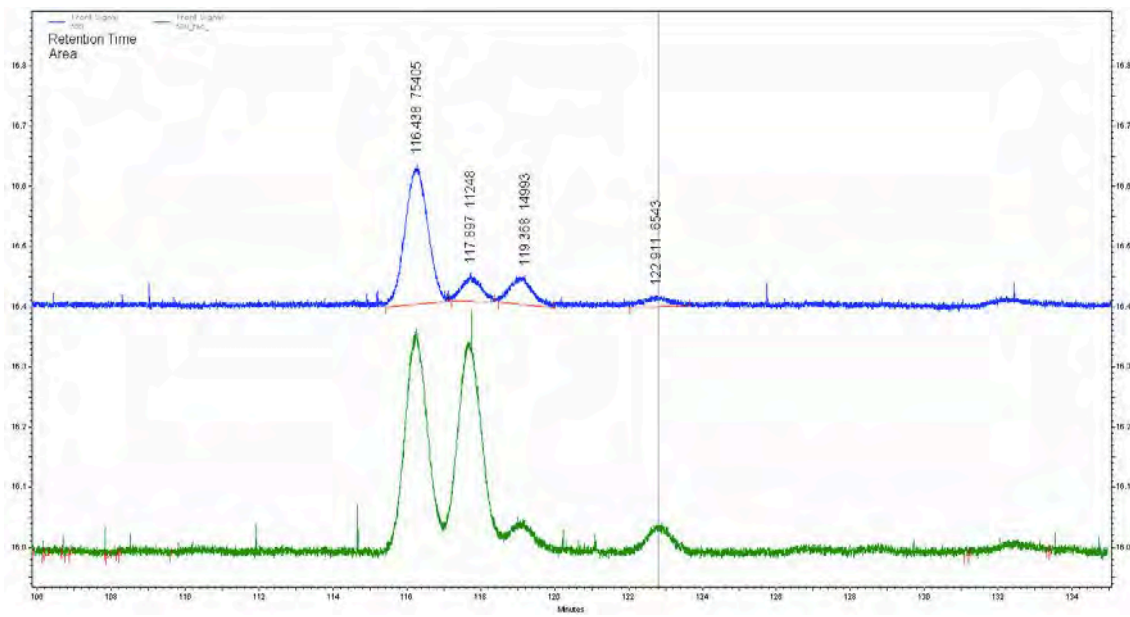
GC traces for the determination of the enantiomeric excesses

The racemic products were obtained by substrate oxidations with *rac*-Mn(TIPSMcp) complex. The green trace is referred to the racemic products while the blue one is referred to the chiral products.

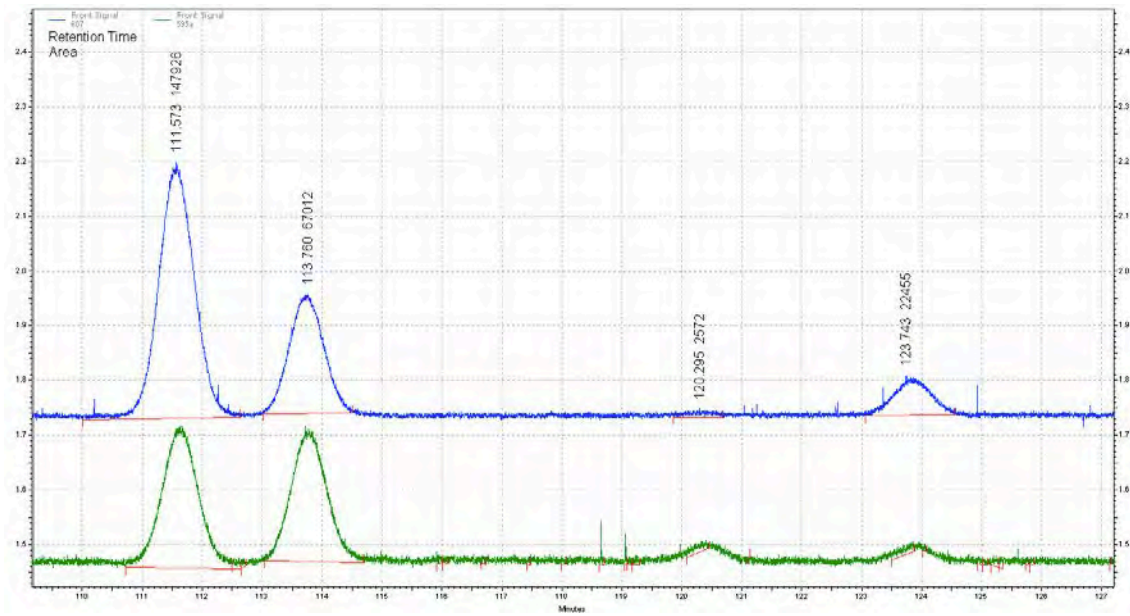
Oxidation of 1



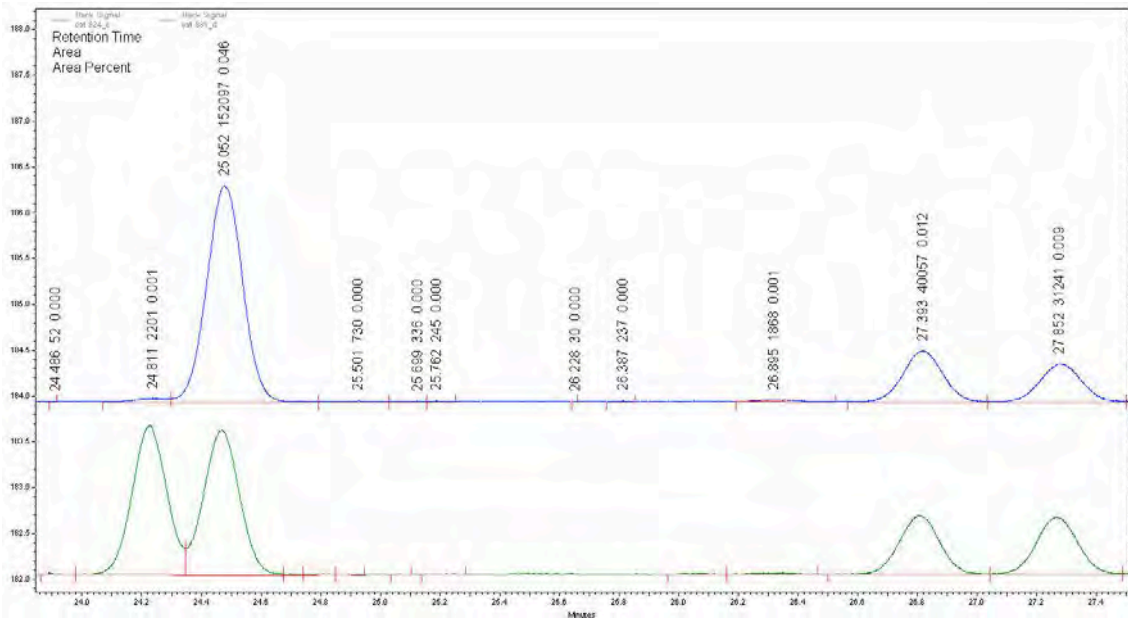
Oxidation of 2



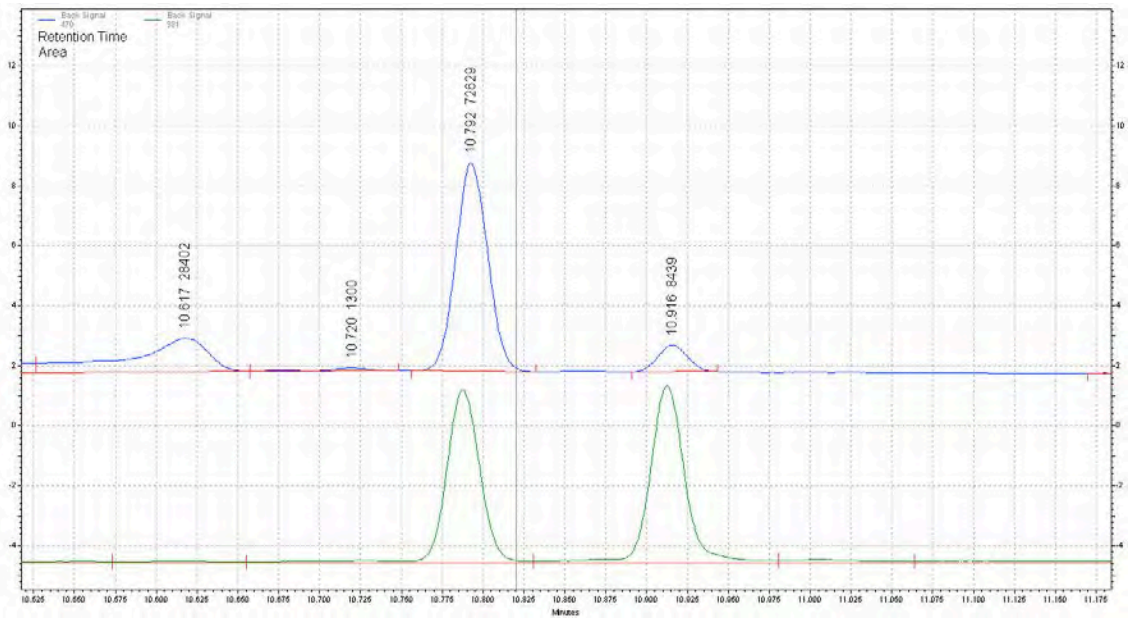
Oxidation of 3



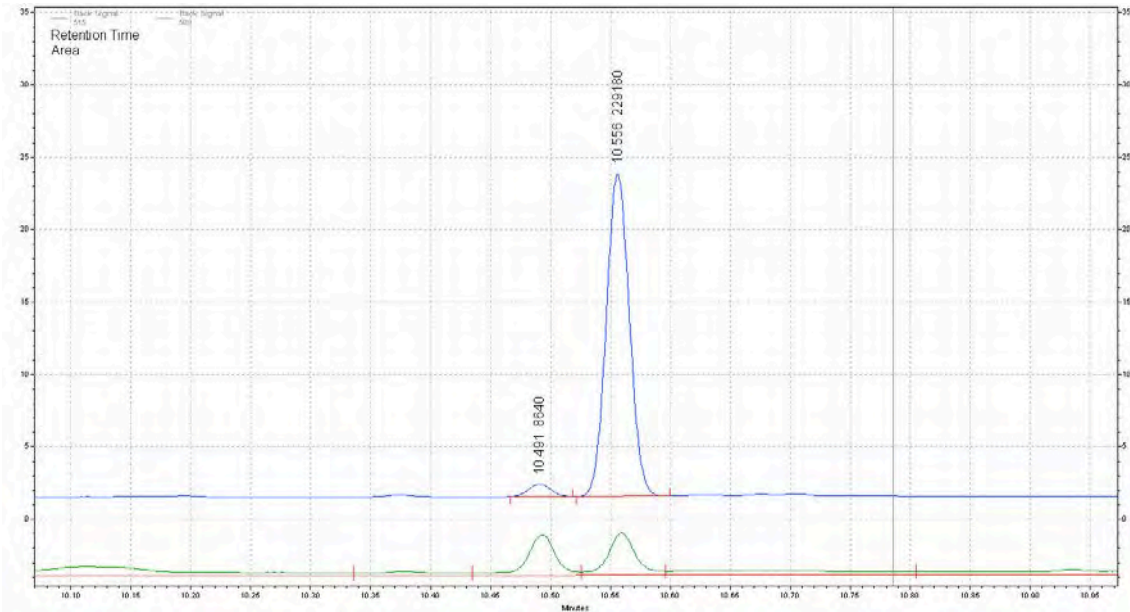
Oxidation of 4



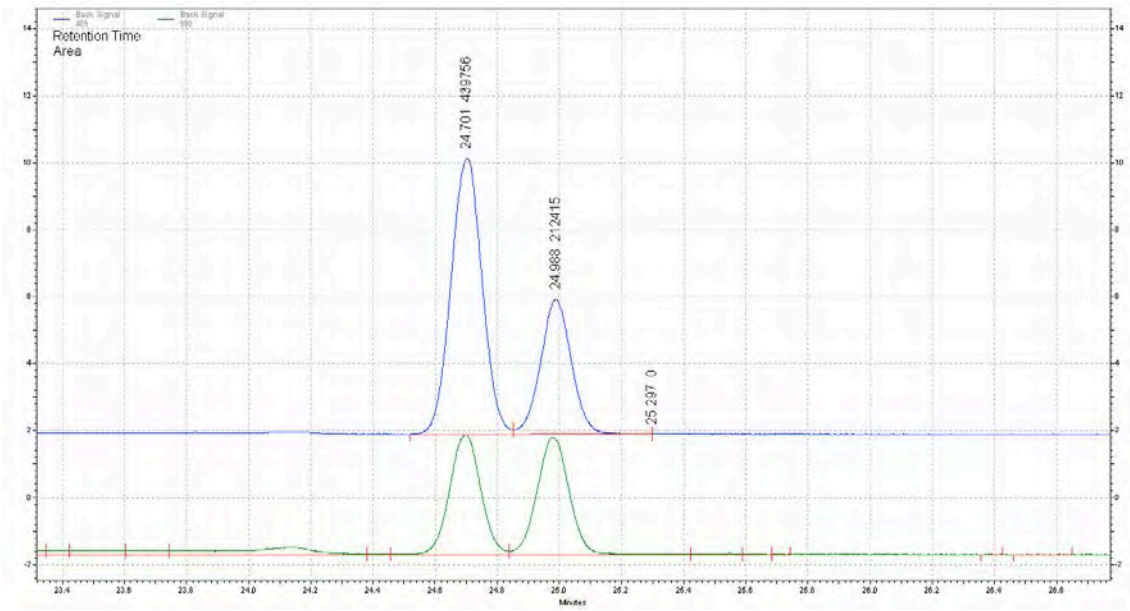
Oxidation of 6



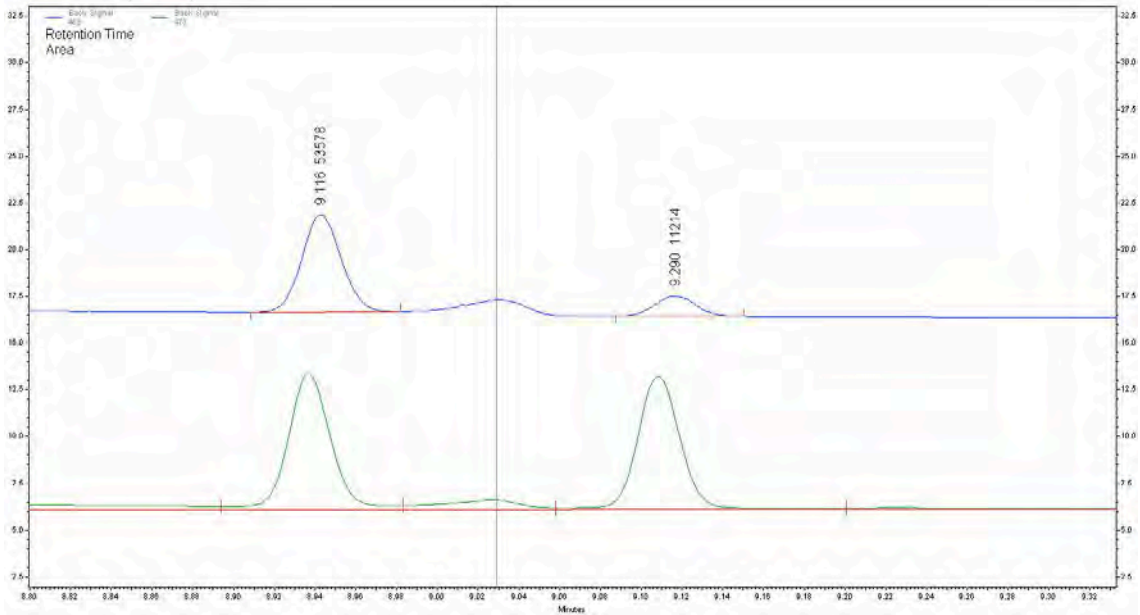
Oxidation of 7



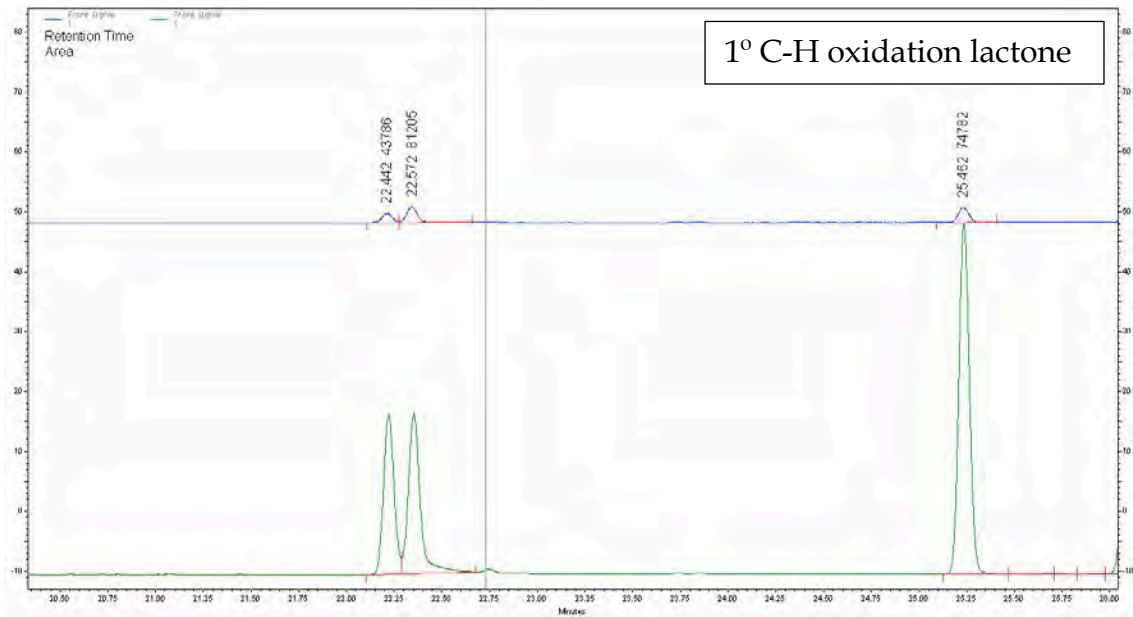
Oxidation of 9



Oxidation of 10



Oxidation of 24



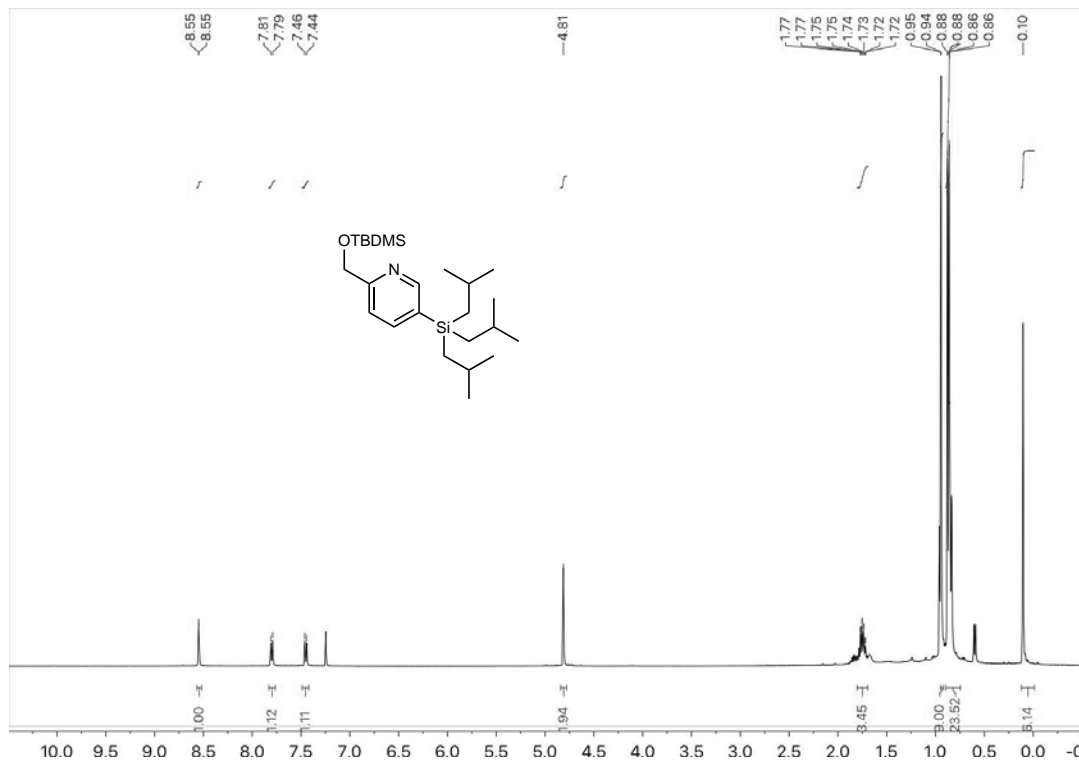
ANNEX CHAPTER IV

NMR SPECTRA, GC TRACES and X-Ray ANALYSIS

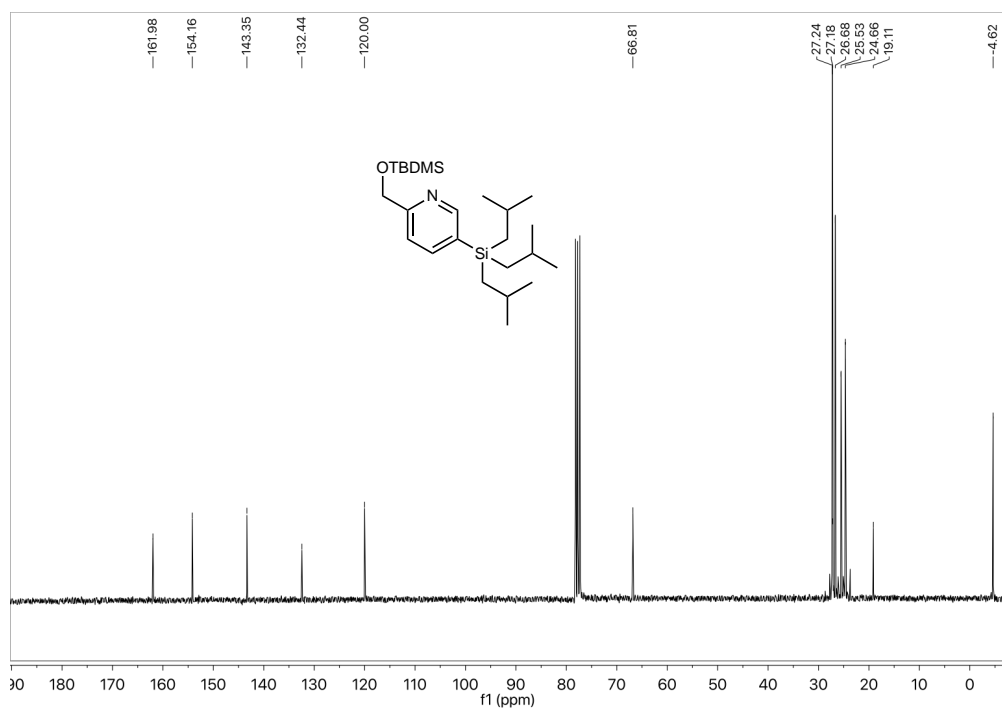
IV. NMR Spectra

IV. NMR characterization of the ligand precursors and ligands

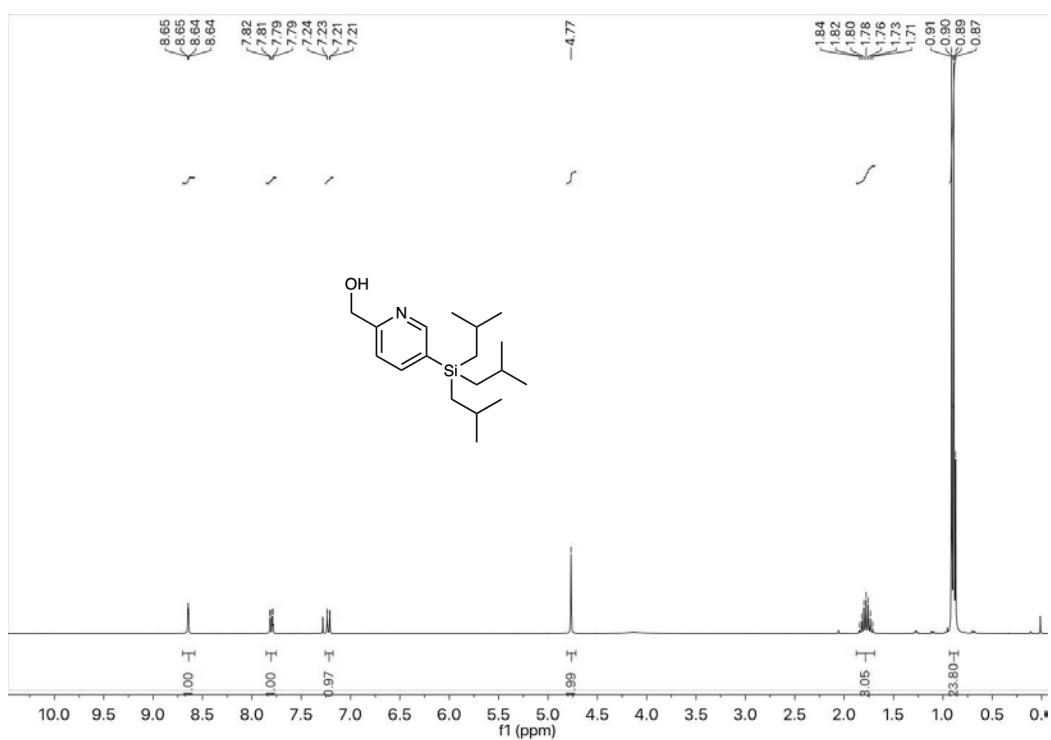
^1H NMR of $^{\text{TIBS}}\text{PyOTBDMS}$ in CDCl_3



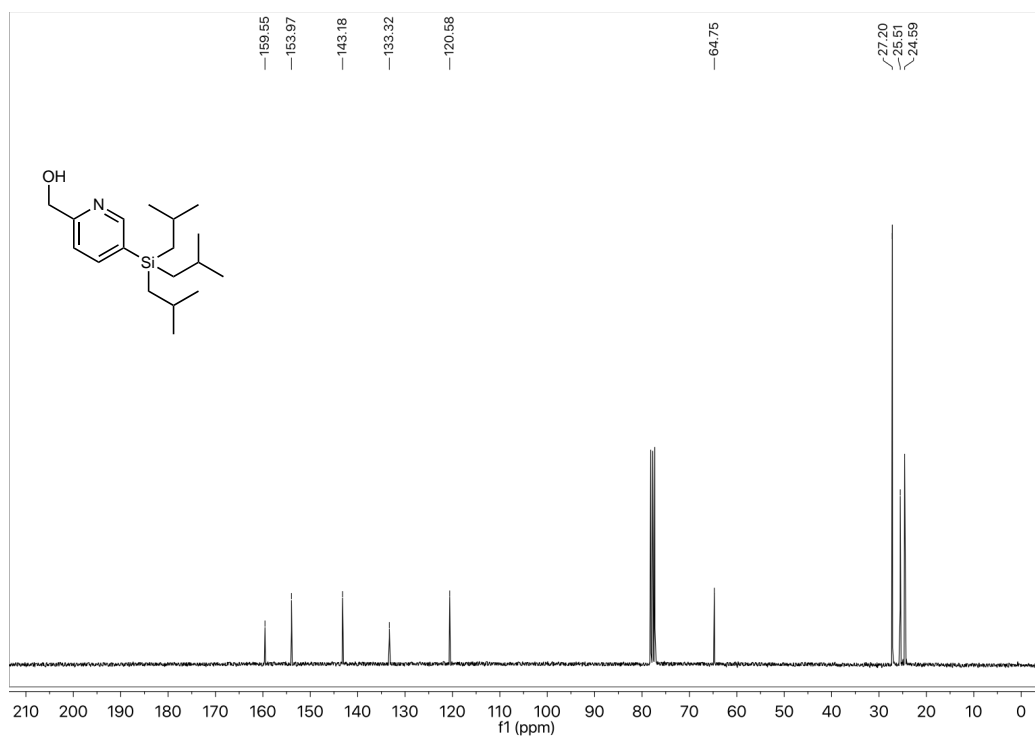
^{13}C NMR of $^{\text{TIBS}}\text{PyOTBDMS}$ in CDCl_3



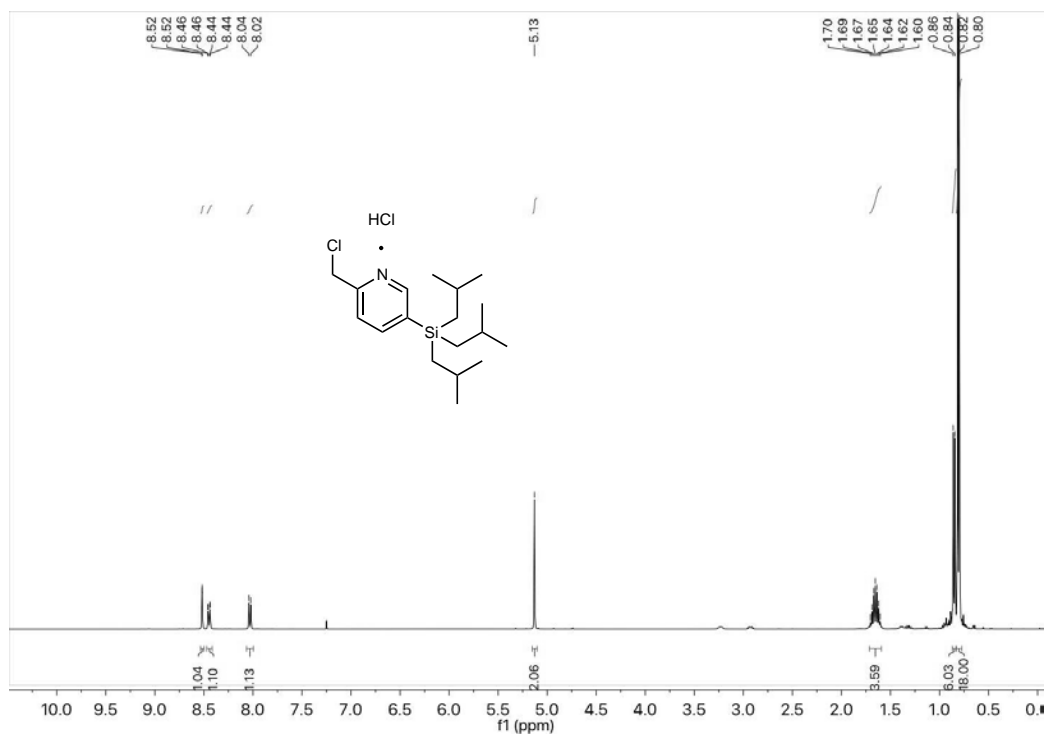
¹H NMR of TIBSPyOH in CDCl₃



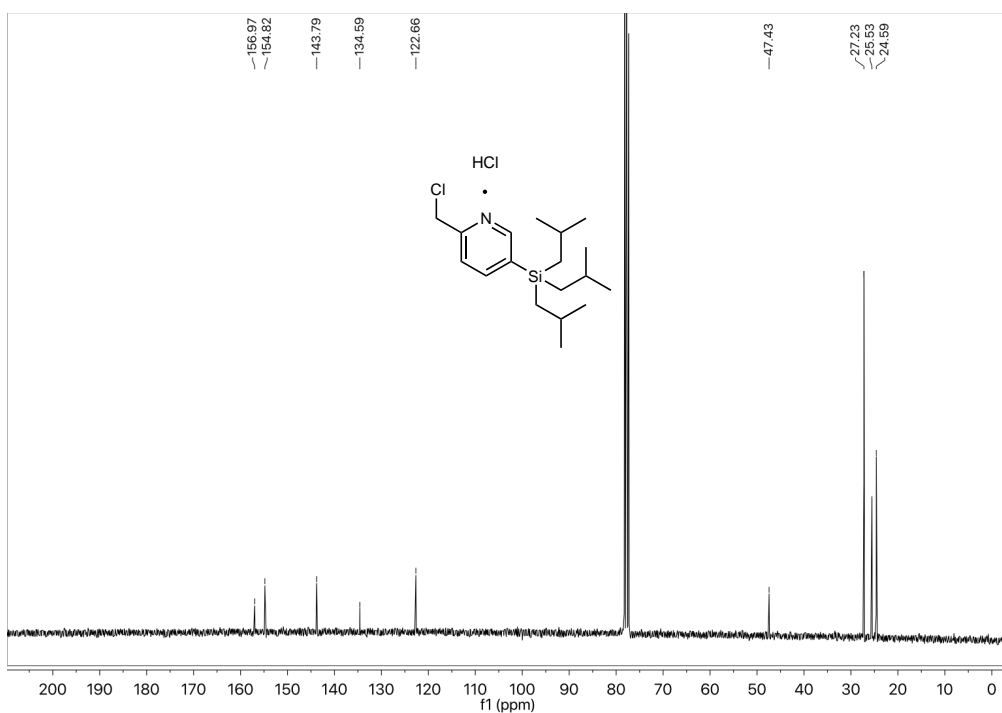
¹³C NMR of TIBSPyOH in CDCl₃



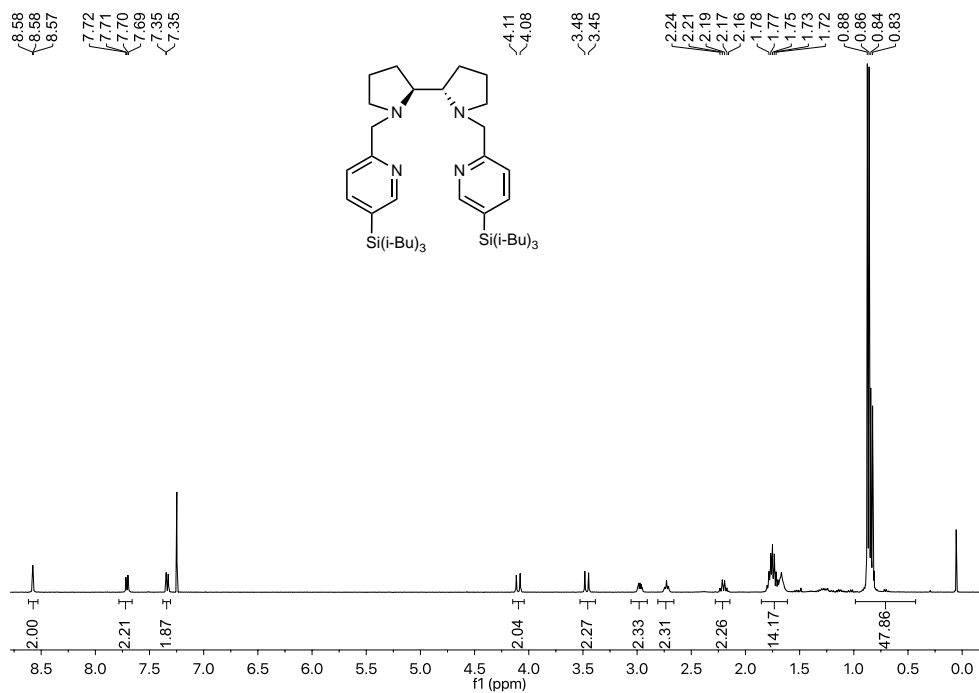
^1H NMR of TIBSPyCl·HCl in CDCl_3



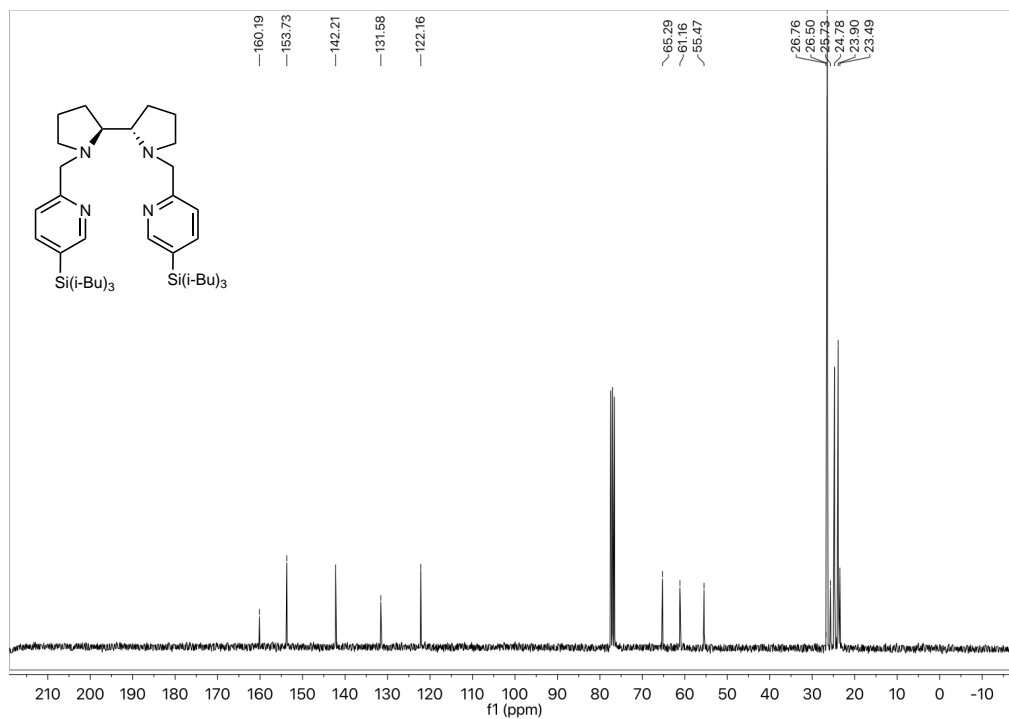
^{13}C NMR of TIBSPyCl·HCl in CDCl_3



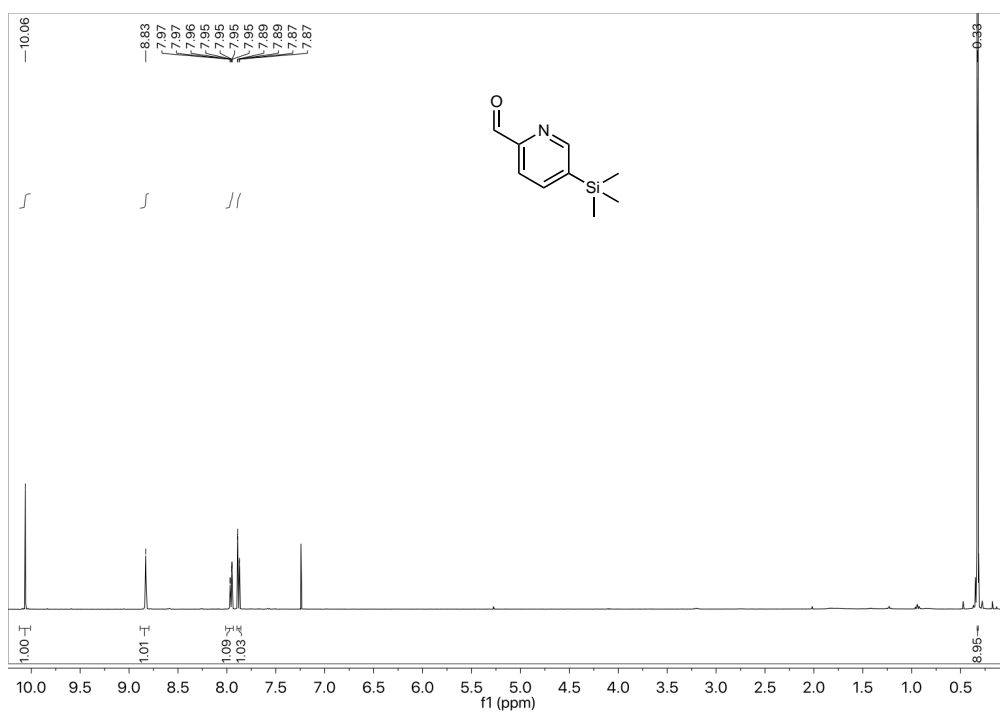
^1H NMR of (*S,S*)-^tBuSdp in CDCl₃



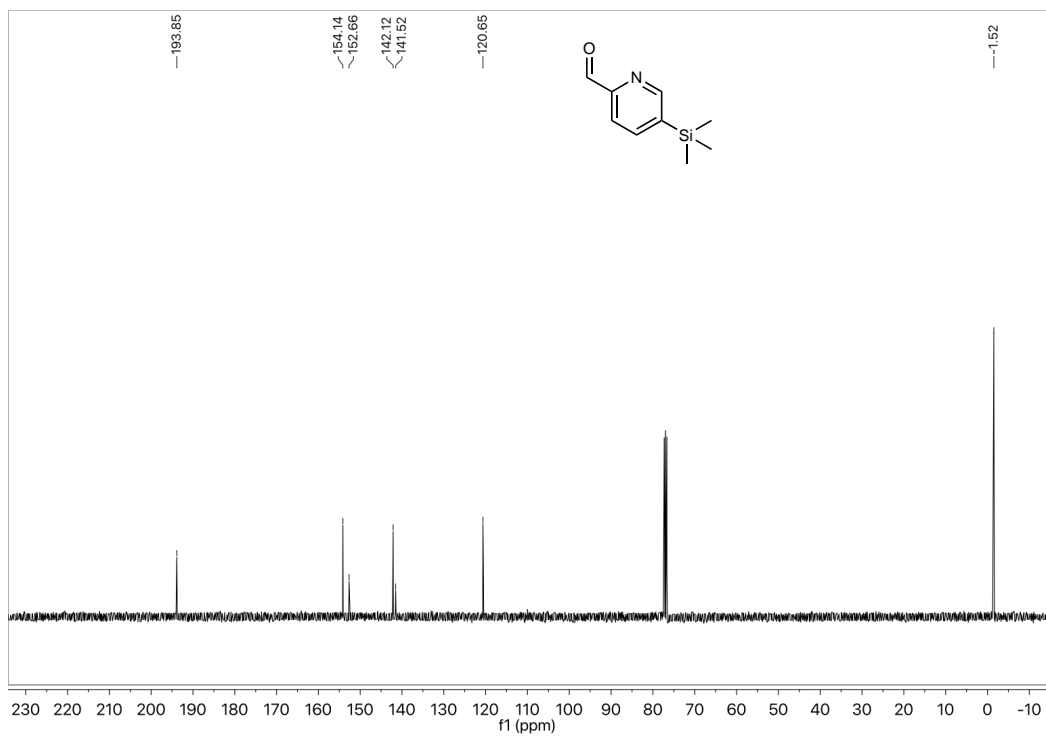
^{13}C NMR of (*S,S*)-(^tBuSdp) in CDCl₃



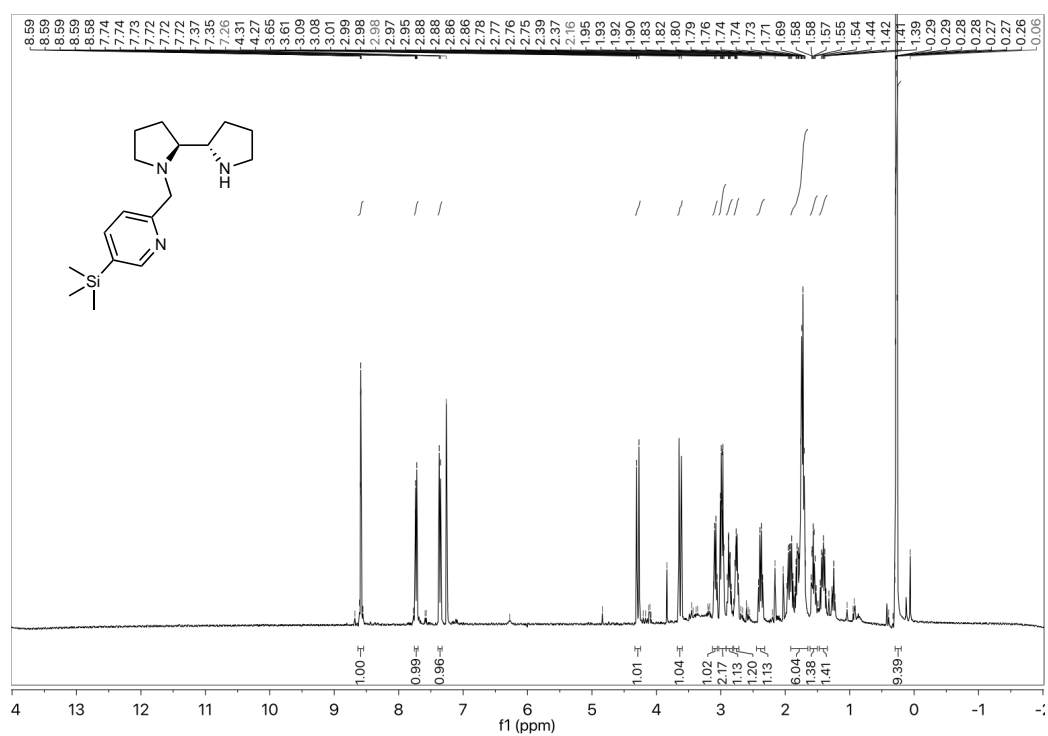
^1H NMR of TMS-PyCHO in CDCl_3



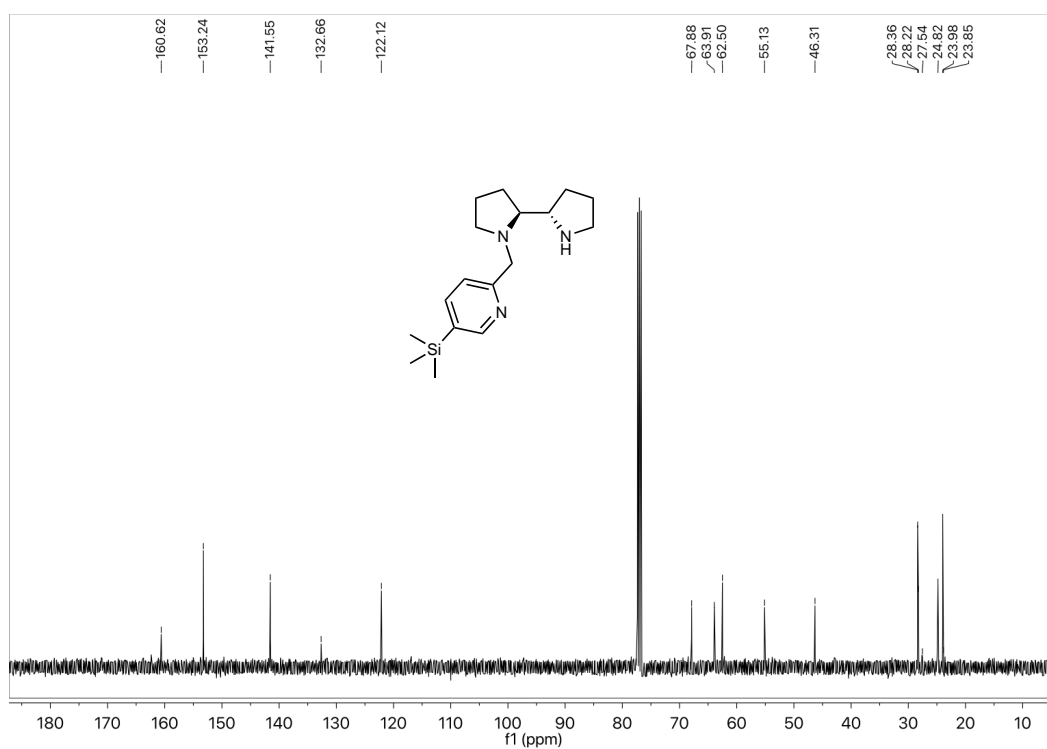
^{13}C NMR of TMS-PyCHO in CDCl_3



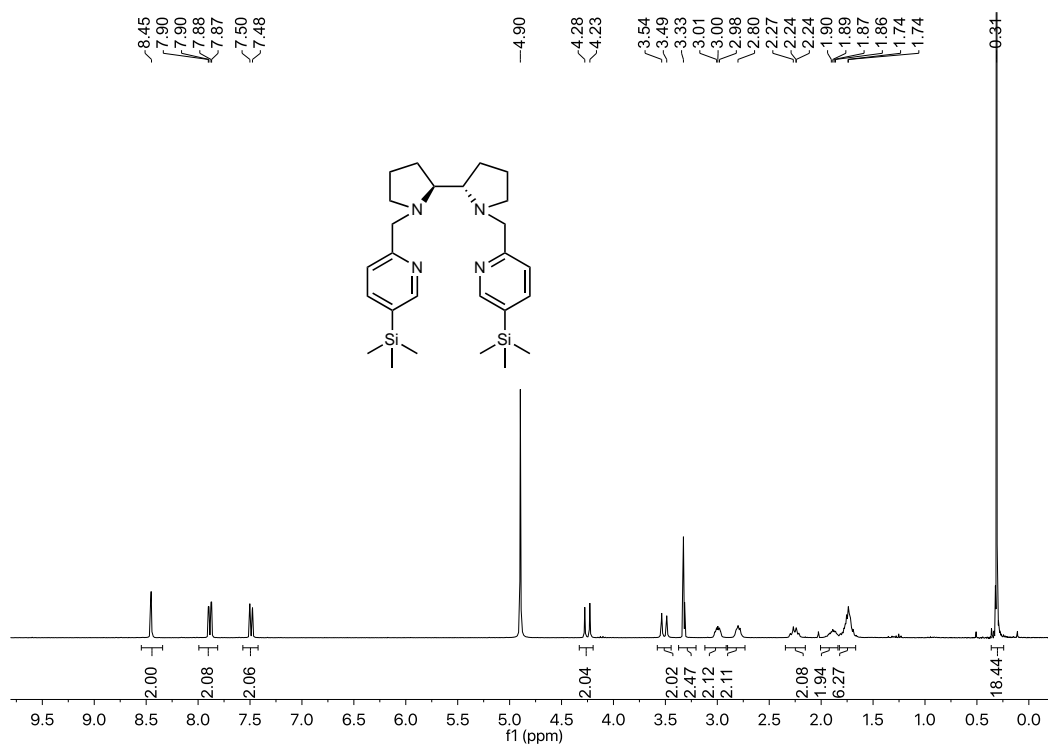
^1H NMR of (*S,S*)-TMS₂ph in CDCl₃



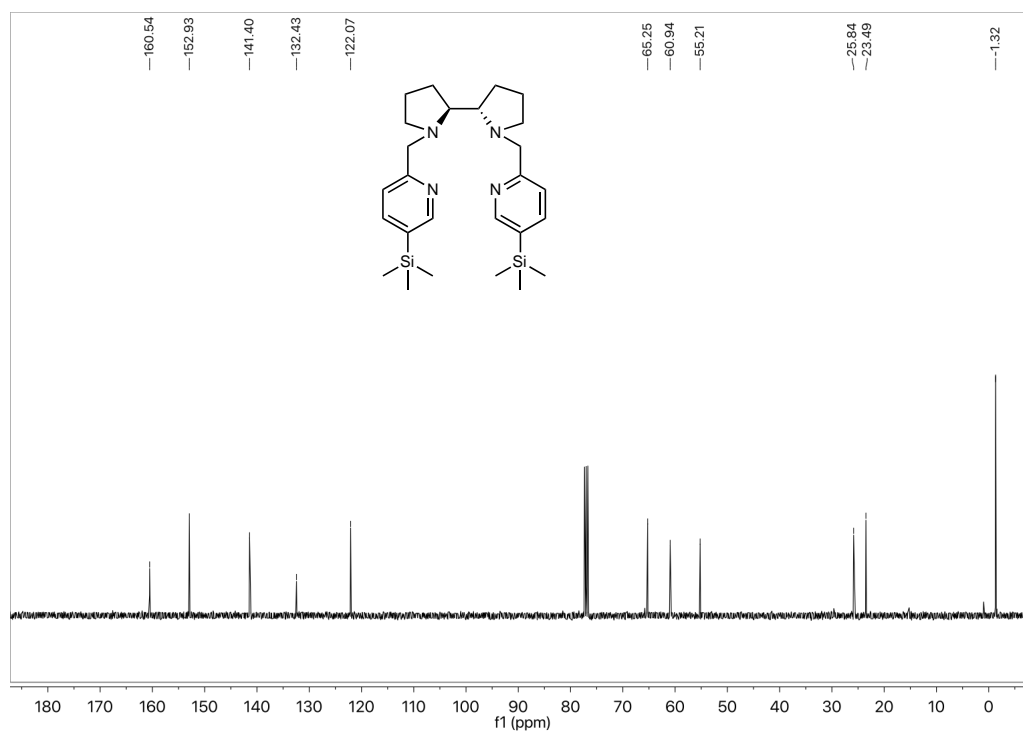
^{13}C NMR of (*S,S*)-TMS₂ph in CDCl₃



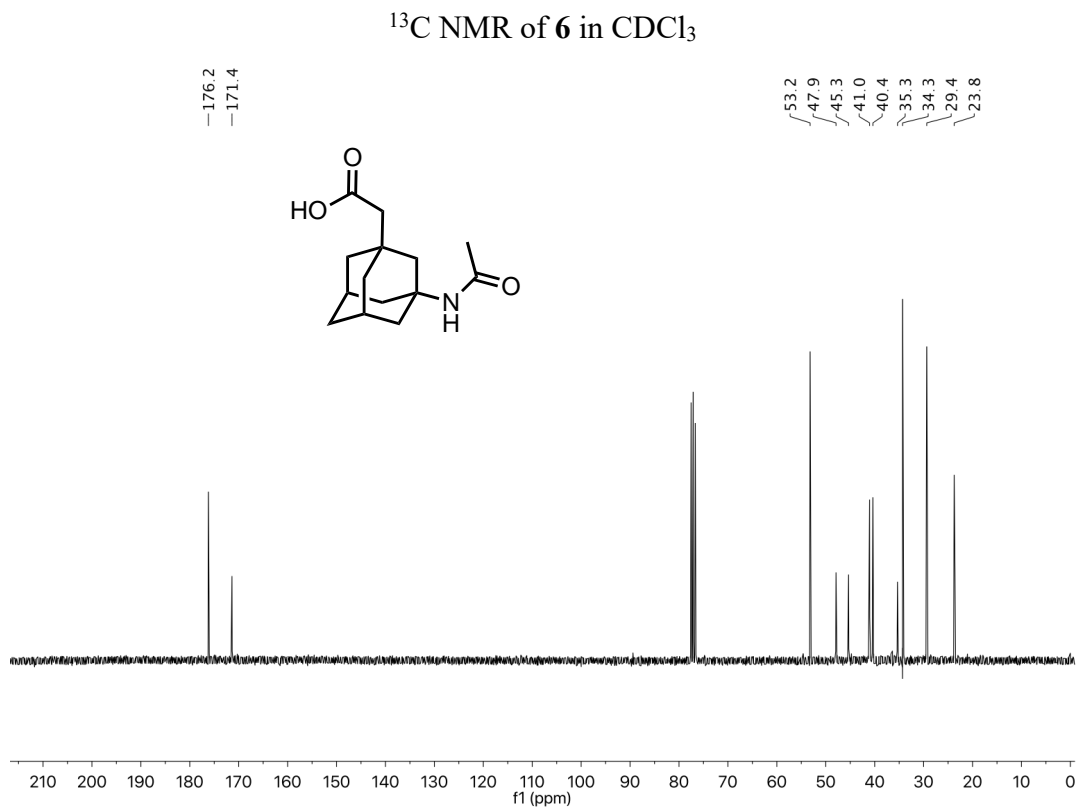
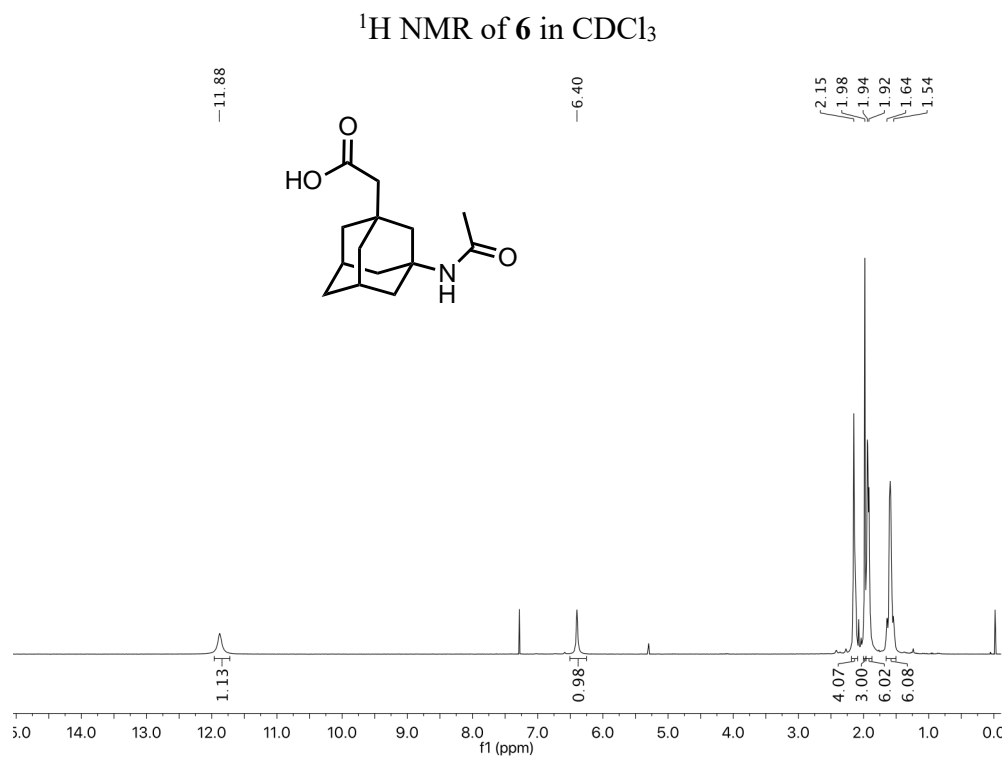
^1H NMR of (*S,S*)-TMS₂pdp in CDCl₃



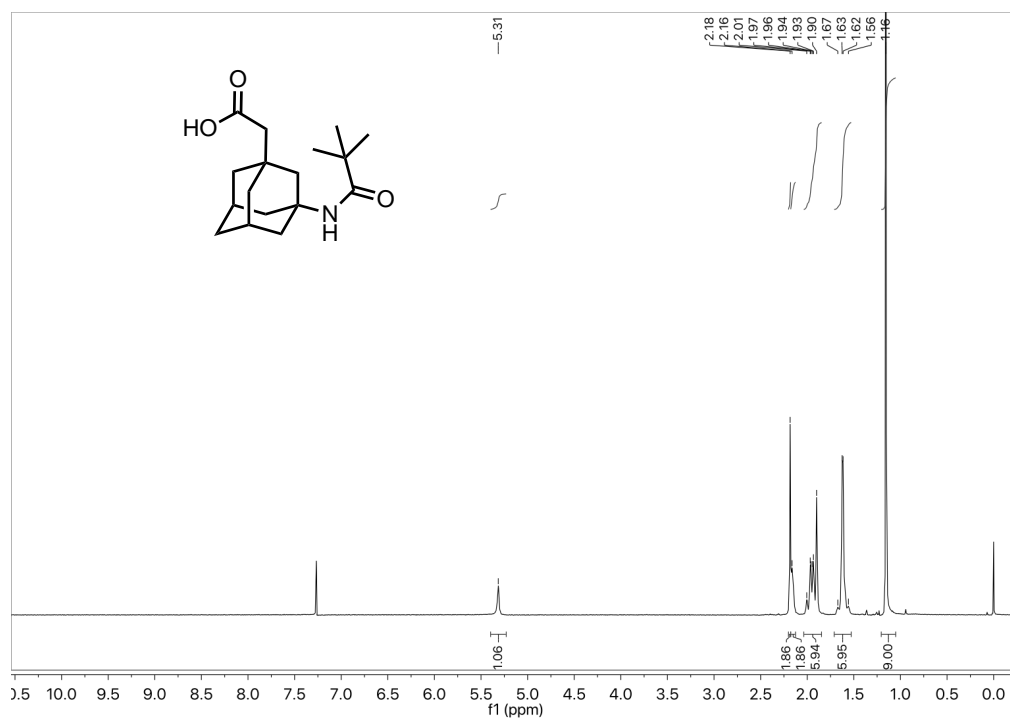
^{13}C NMR of (*S,S*)-TMS₂pdp in CDCl₃



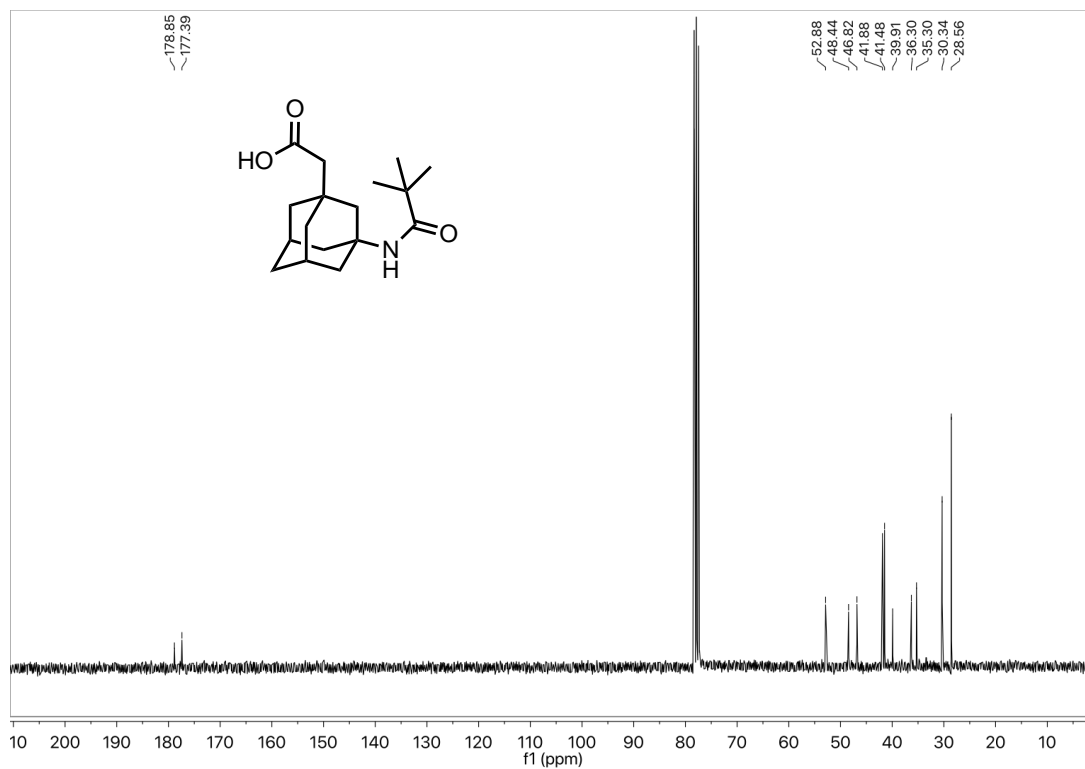
IV. NMR characterization of the substrates



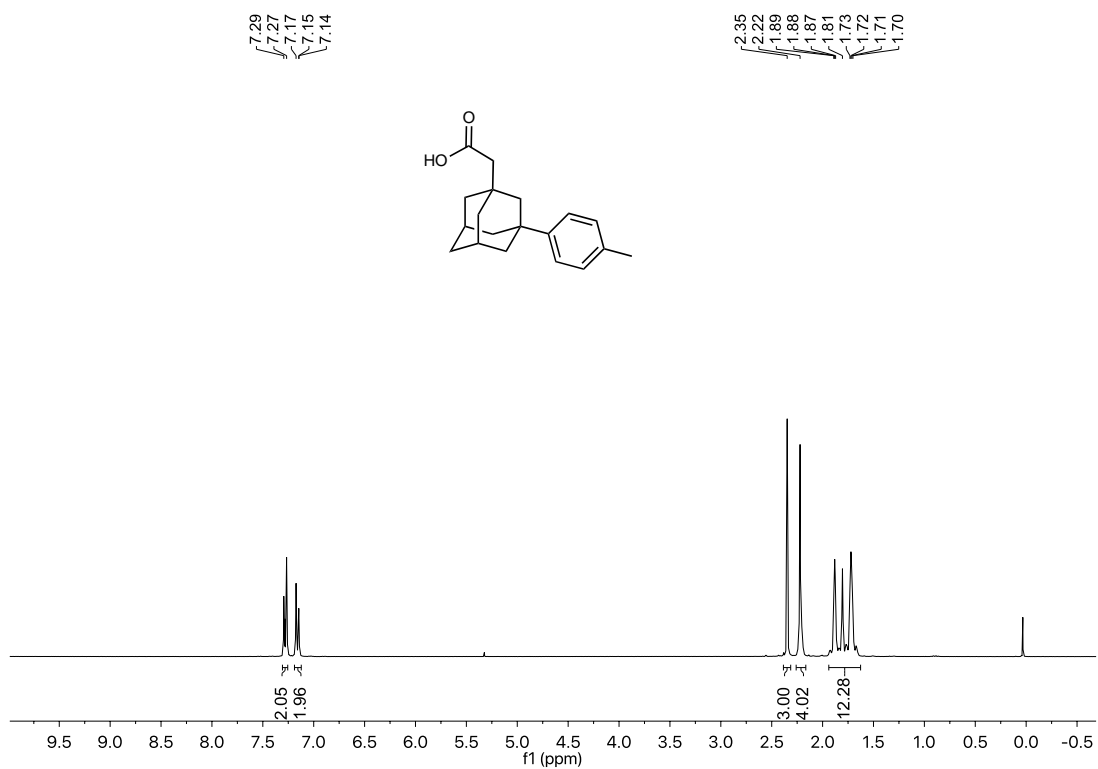
¹H NMR of 7 in CDCl₃



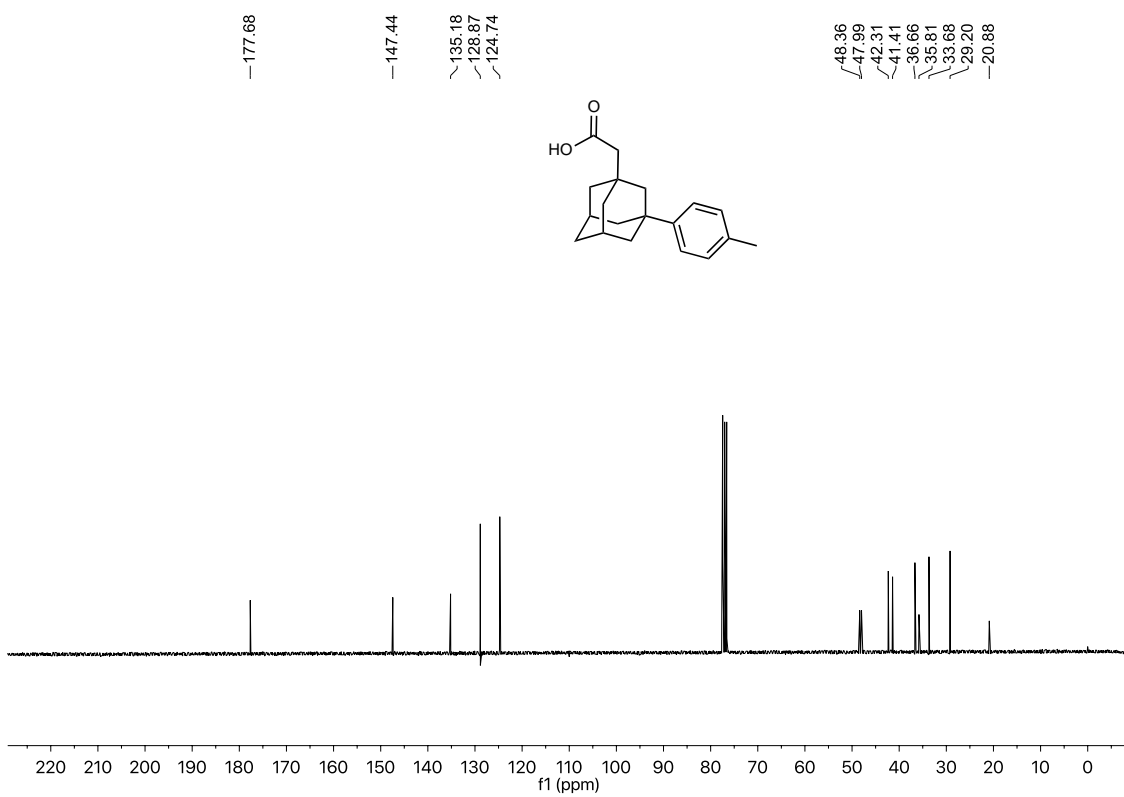
¹³C NMR of 7 in CDCl₃



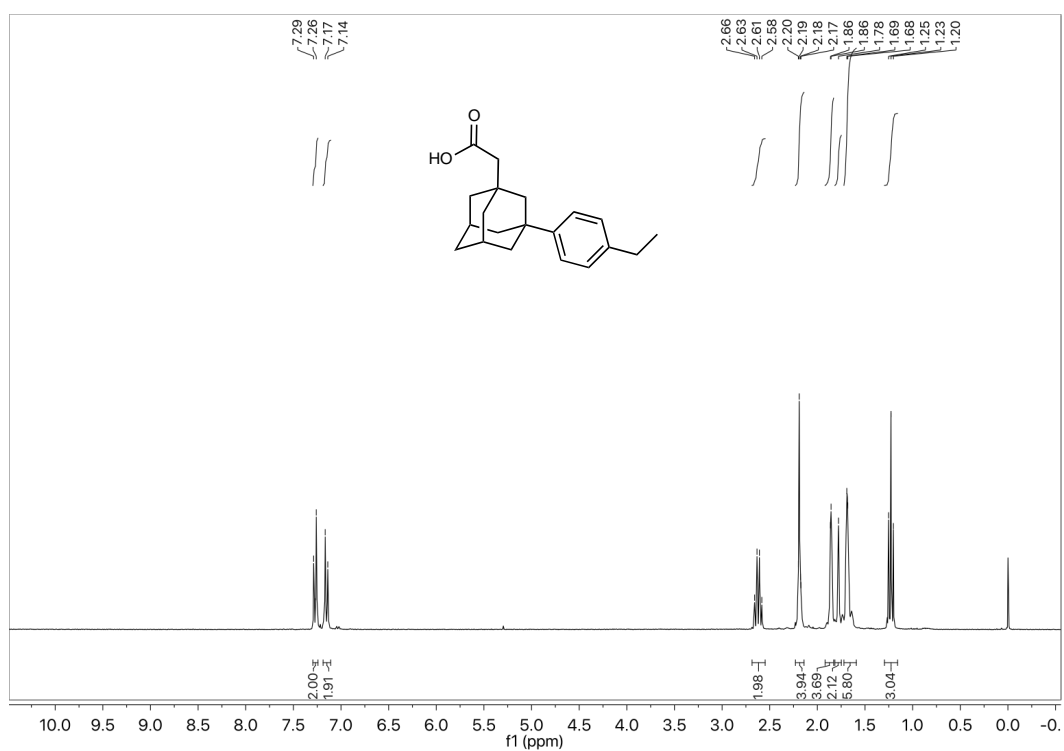
^1H NMR of **13** in CDCl_3



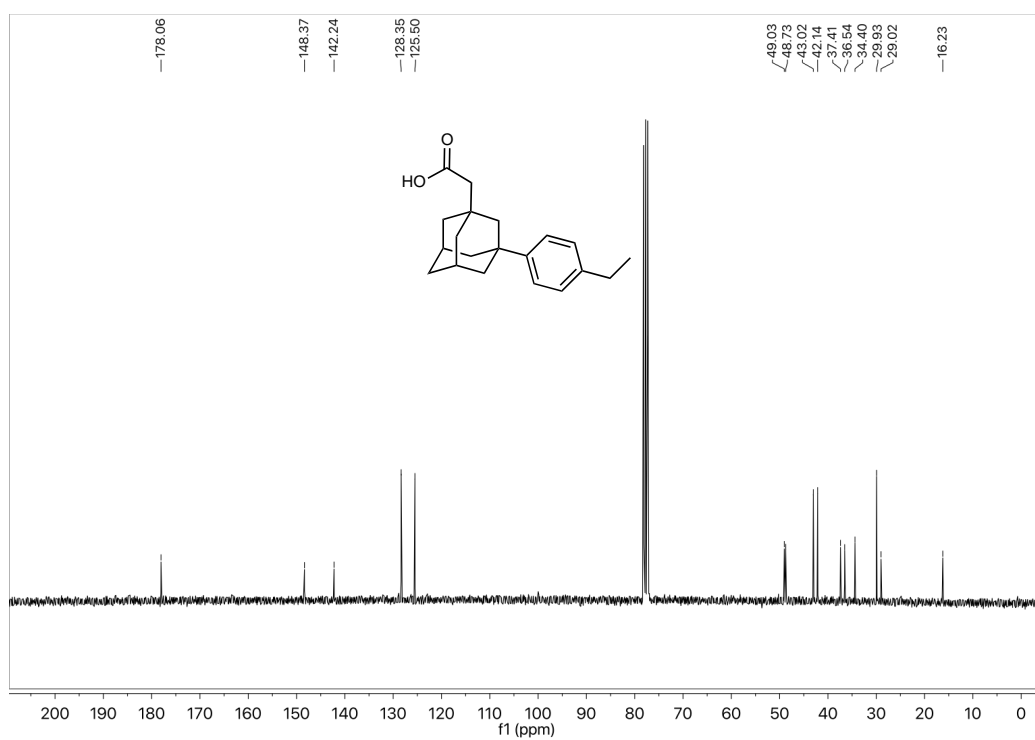
^{13}C NMR of **13** in CDCl_3



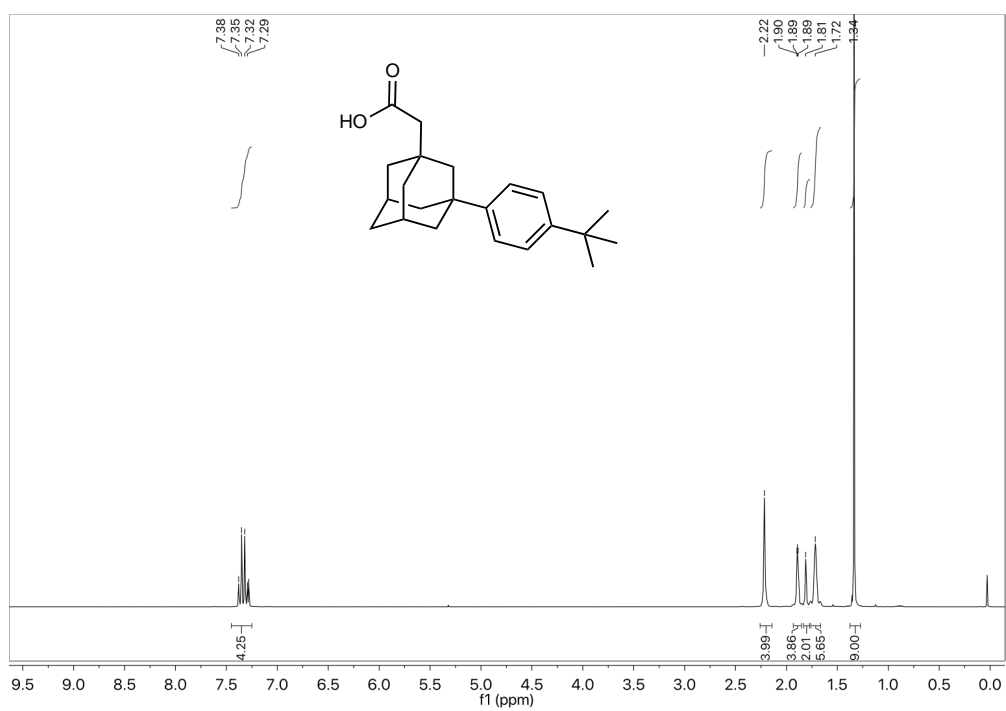
¹H NMR of **14** in CDCl₃



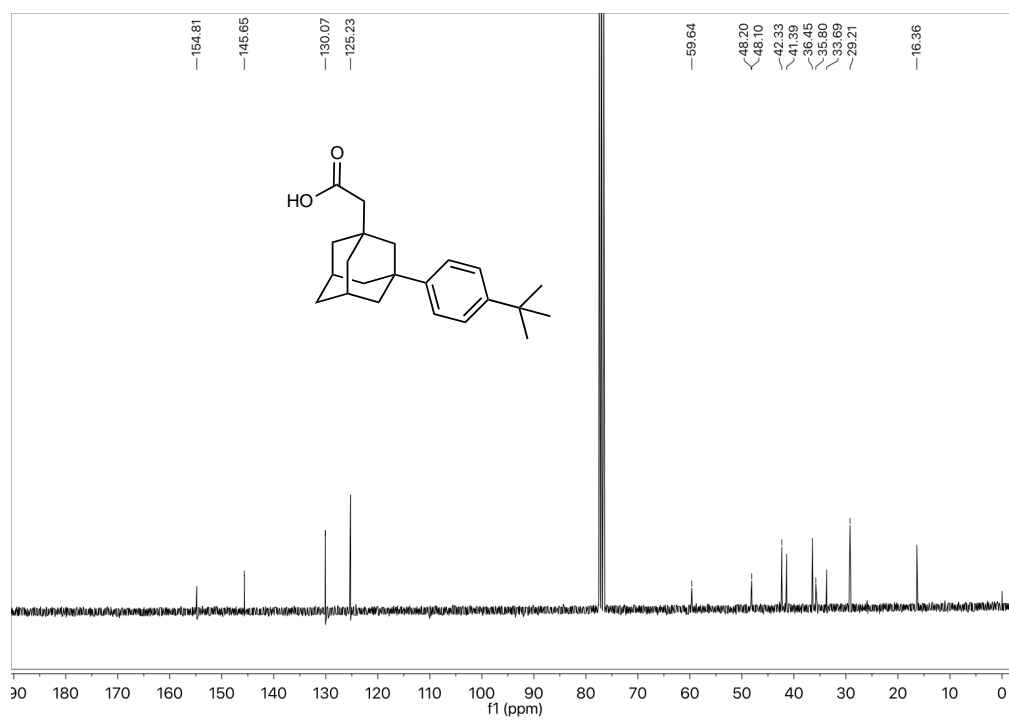
¹³C NMR of **14** in CDCl₃



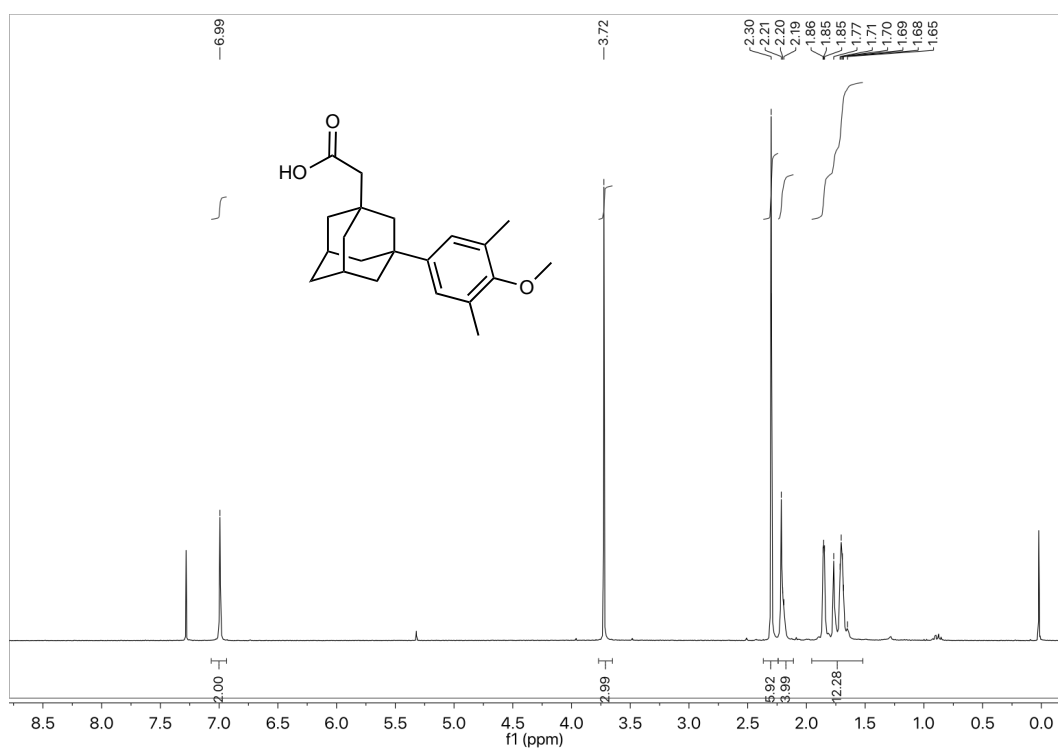
^1H NMR of **15** in CDCl_3



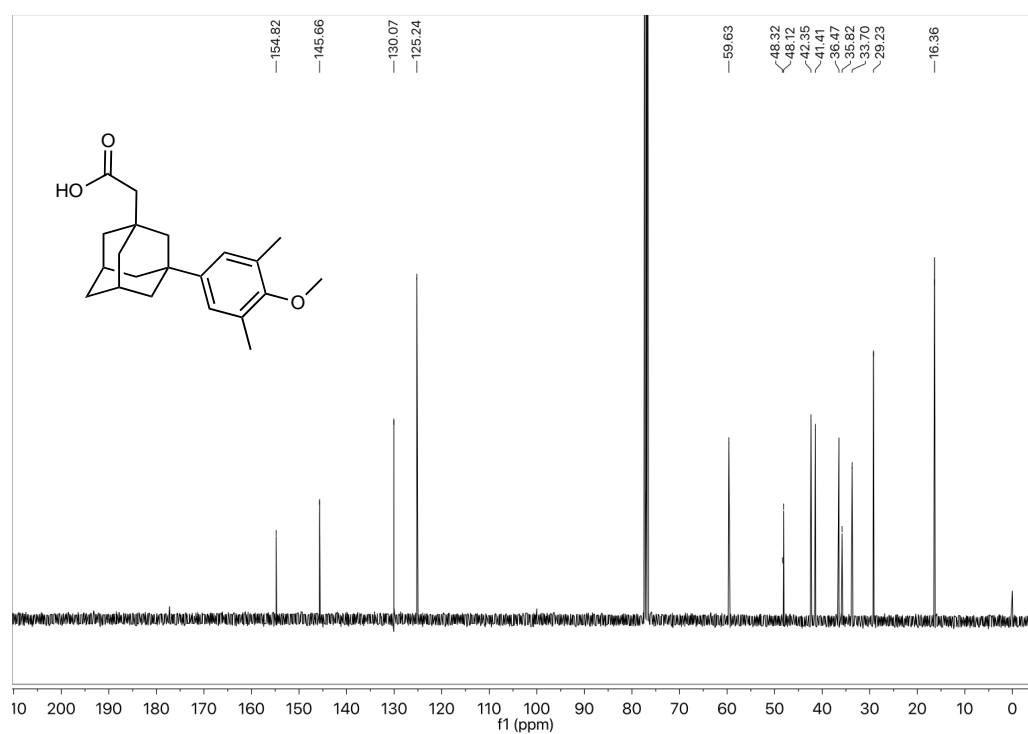
^{13}C NMR of **15** in CDCl_3



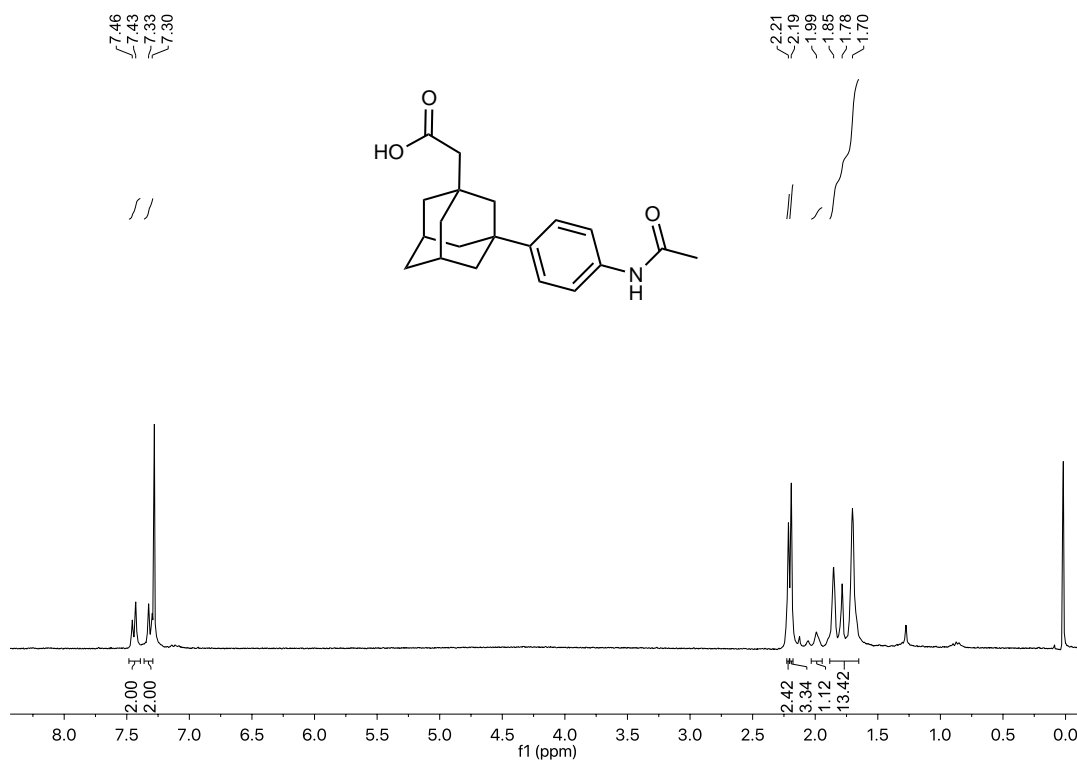
^1H NMR of **16** in CDCl_3



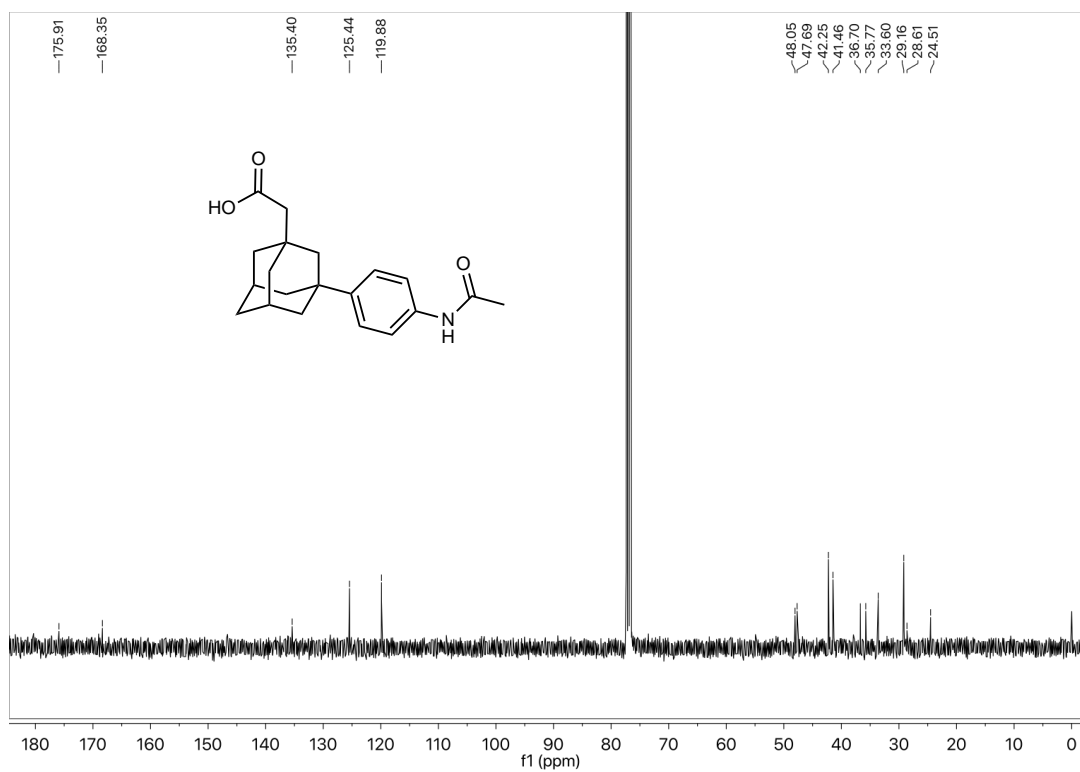
^{13}C NMR of **16** in CDCl_3



^1H NMR of **17** in CDCl_3

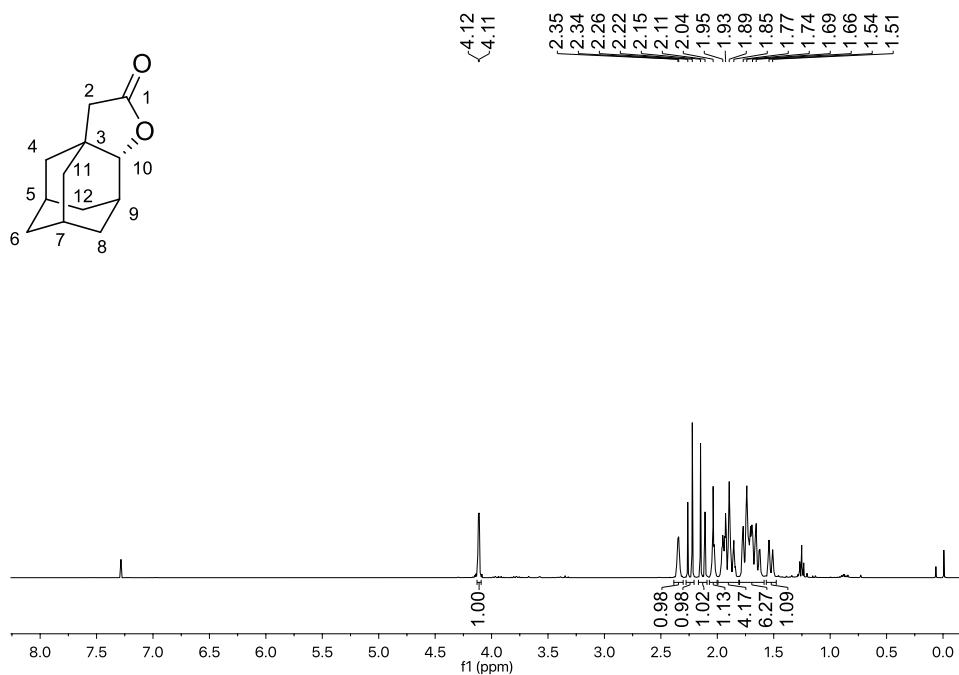


^{13}C NMR of **17** in CDCl_3



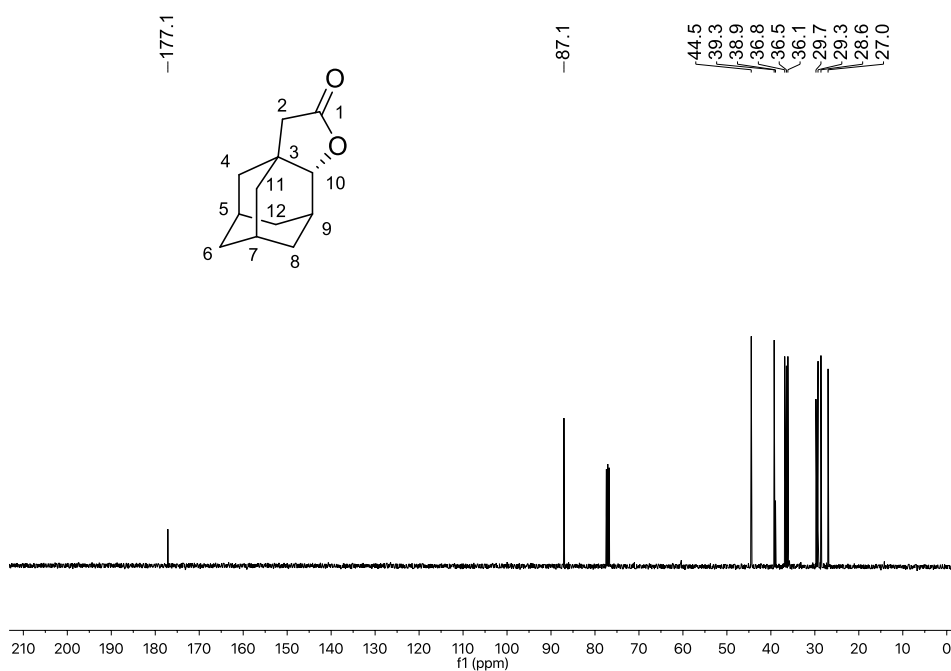
IV. NMR characterization of lactone products

^1H NMR of **1a** in CDCl_3



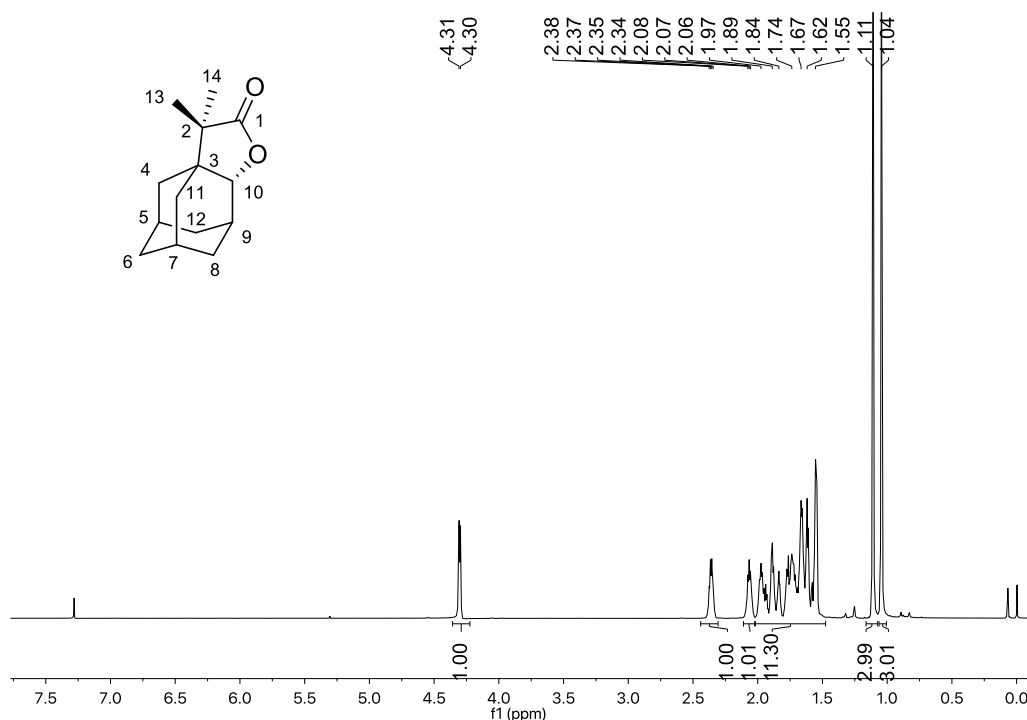
^1H NMR (400 MHz, CDCl_3) δ 4.11 (d, $J = 3.0$ Hz, 1H, C_{10} [1H]), 2.35 (d, $J = 3.2$ Hz, 1H; C_9 [1H]), 2.30 – 2.08 (df, 2H; C_2 [2H]), 2.03 (m, 1H; C_{12} [1H]), 1.99 – 1.81 (m, 4H; C_5 [1H] + C_7 [1H] + C_4 [2H]), 1.80 – 1.59 (m, 6H; C_{11} [2H] + C_6 [2H] + C_8 [2H]), 1.53 (dt, $J = 12.9, 2.8$ Hz, 1H; C_{12} [1H]).

^{13}C NMR of **1a** in CDCl_3



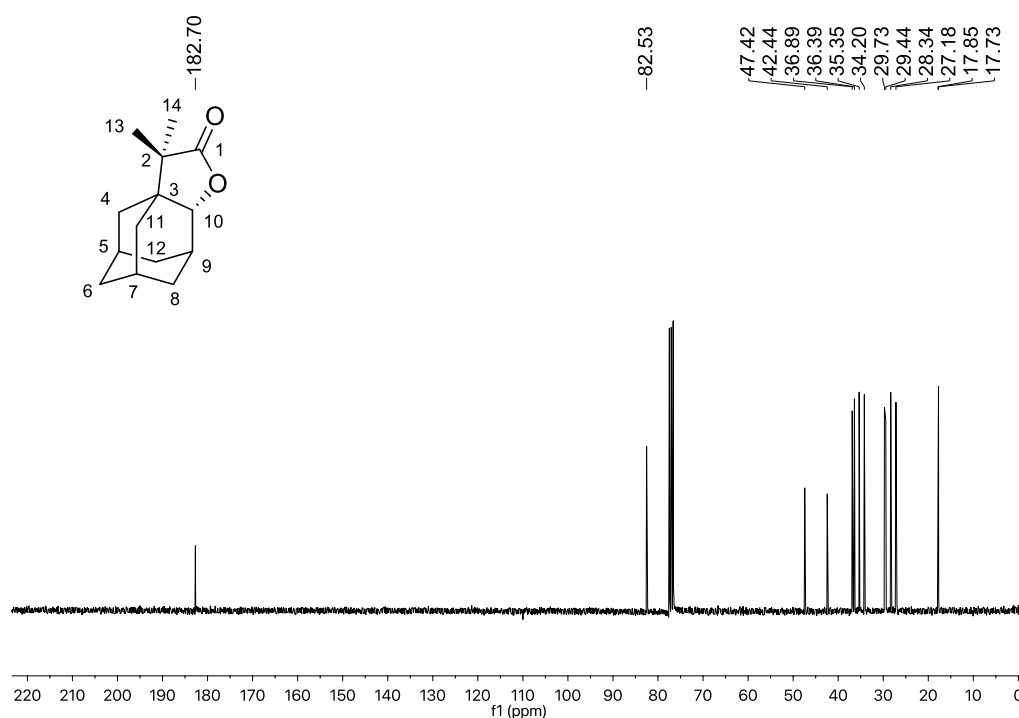
^{13}C NMR (101 MHz, CDCl_3) δ 177.1 (C_1), 87.0 (C_{10}), 44.5 (C_2), 39.2 (C_3), 38.9 (C_4 or C_{12}), 36.8 (C_4 or C_{12}), 36.5 (C_8 or C_{11}), 36.1 (C_8 or C_{11}), 29.7 (C_9), 29.3 (C_6), 28.6 (C_5 or C_7), 27.0 (C_5 or C_7).

¹H NMR of **2a** in CDCl₃



¹H NMR (300 MHz, CDCl₃) δ 4.30 (d, $J = 3.3$ Hz, 1H; C_{10} [1H]), 2.36 (h, $J = 3.2$ Hz, 1H; C_9 [1H]), 2.07 (m, 1H; C_{12} [1H]), 2.02 – 1.50 (m, 11H; C_{11} [2H] + C_6 [2H] + C_4 [2H] + C_8 [2H] + C_{12} [1H] + C_5 [1H] + C_7 [1H]), 1.11 (s, 3H; C_{14} [3H]), 1.04 (s, 3H; C_{13} [3H]).

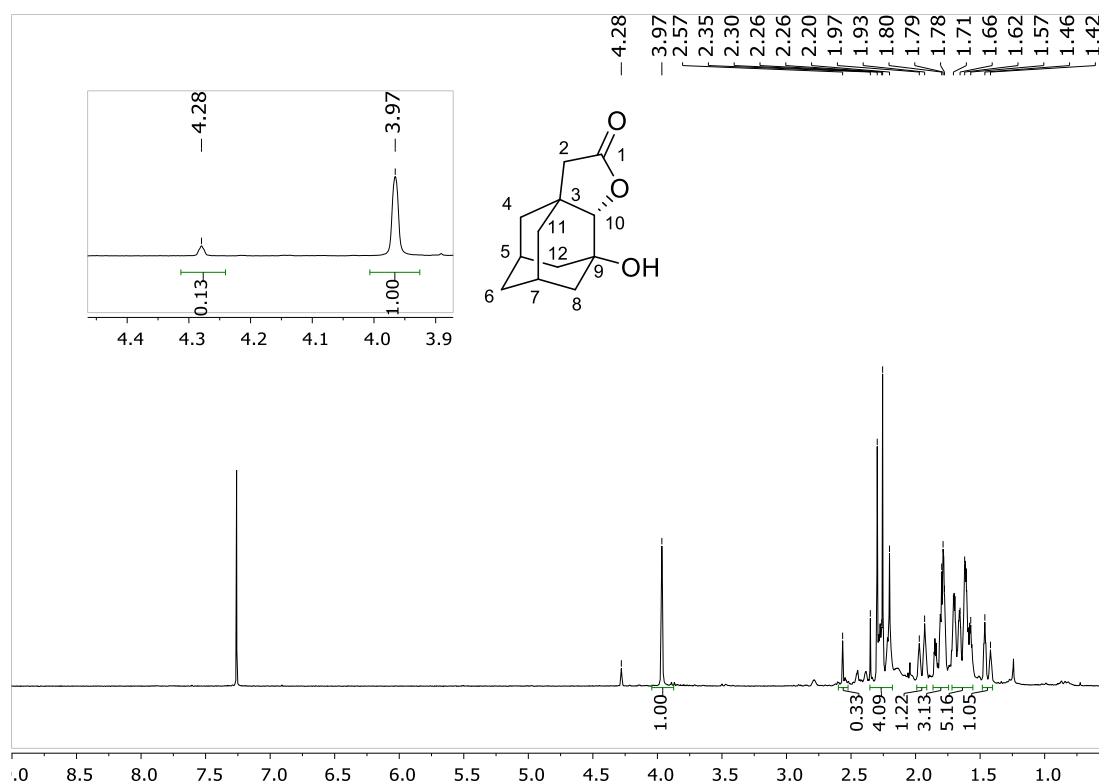
¹³C NMR of **2a** in CDCl₃



¹³C NMR (75 MHz, CDCl₃) δ 182.7 (C_1), 82.5 (C_{10}), 47.42 (C_2), 42.4 (C_3), 36.9 (C_4 or C_{12}), 36.4 (C_4 or C_{12}), 35.3 (C_8 or C_{11}), 34.2 (C_8 or C_{11}), 29.7 (C_9), 29.4 (C_6), 28.3 (C_5 or C_7), 27.2 (C_5 or C_7), 17.8 (C_{14}), 17.7 (C_{13}).

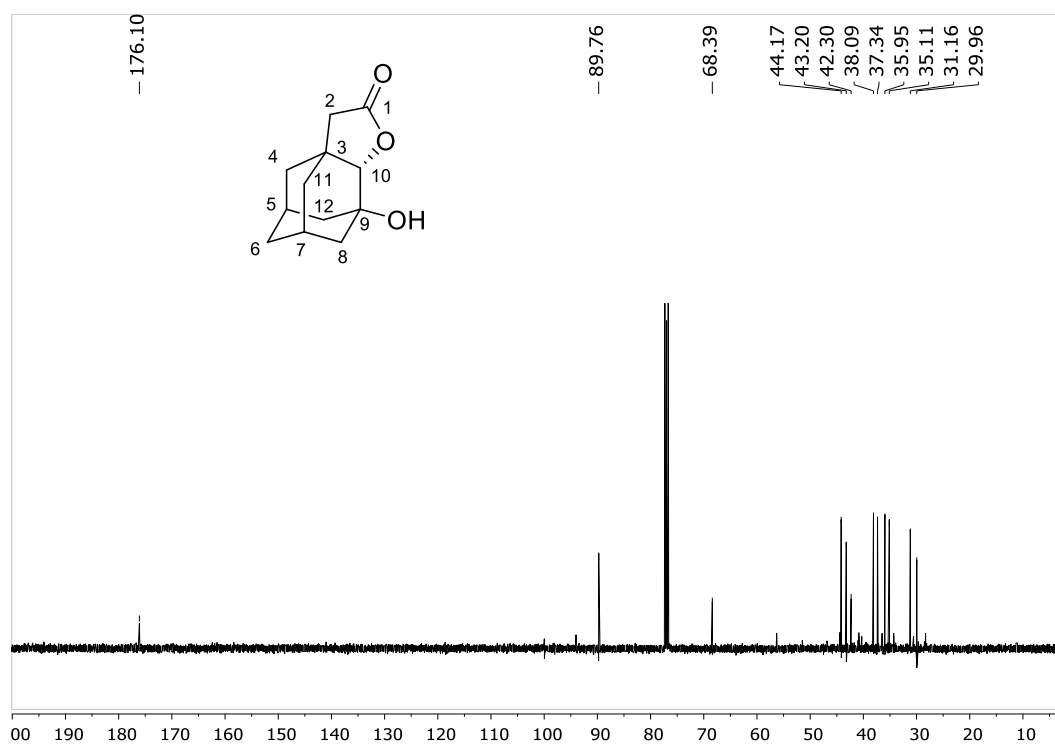
IV. NMR characterization of lactone products (Section A, X=HBA)

^1H NMR of **4a** in CDCl_3

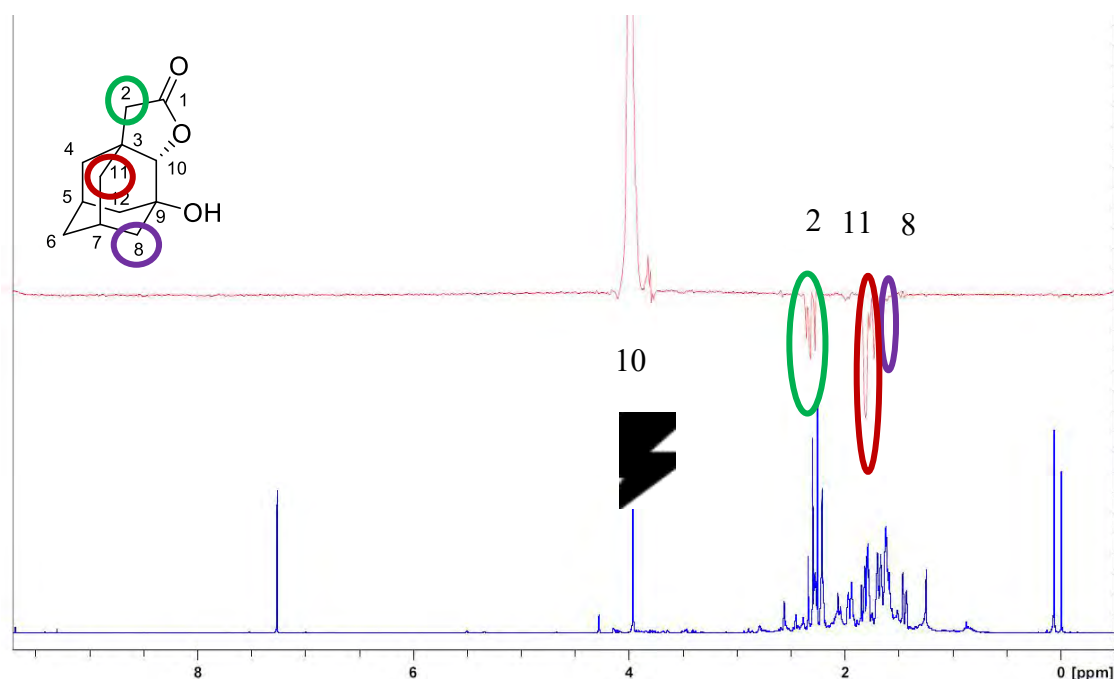


^1H NMR (400 MHz, CDCl_3) δ 3.96 (s, 1H; C_{10} [1H]), 2.39 – 2.17 (m; C_2 [2H] + C_5 [1H] + C_7 [1H]), 2.00-1.91 (m, 1H; C_4 [1H]), 1.89-1.72 (m, 3H; C_{12} [2H] + C_{11} [1H]), 1.72-1.56 (m, 5H; C_6 [2H] + C_4 [1H] + C_8 [1H] + C_{11} [1H]), 1.50-1.40 (m, 1H; C_8 [1H]). In the inset an expansion with the lactone signals is displayed. Isolated product contains a small amount of **4b** (13%), which accounts for the minor peaks in the spectra (i.e. at 4.28 and 2.57ppm).

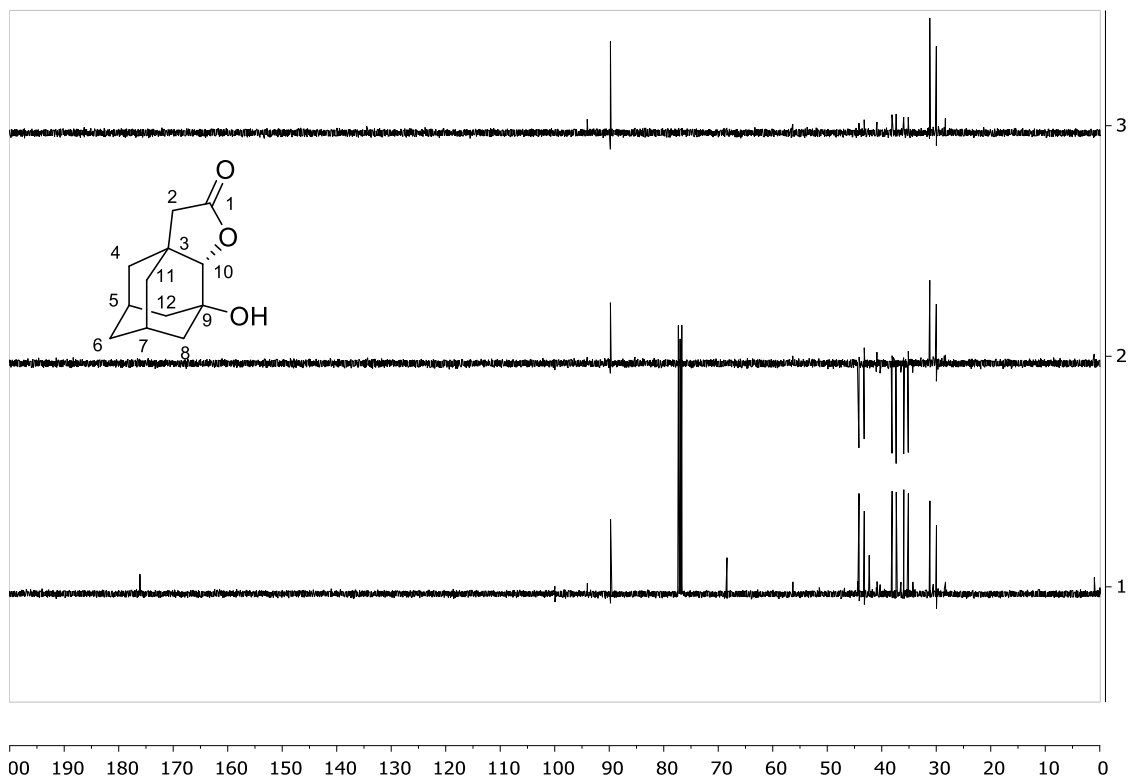
¹³C NMR of **4a** in CDCl₃



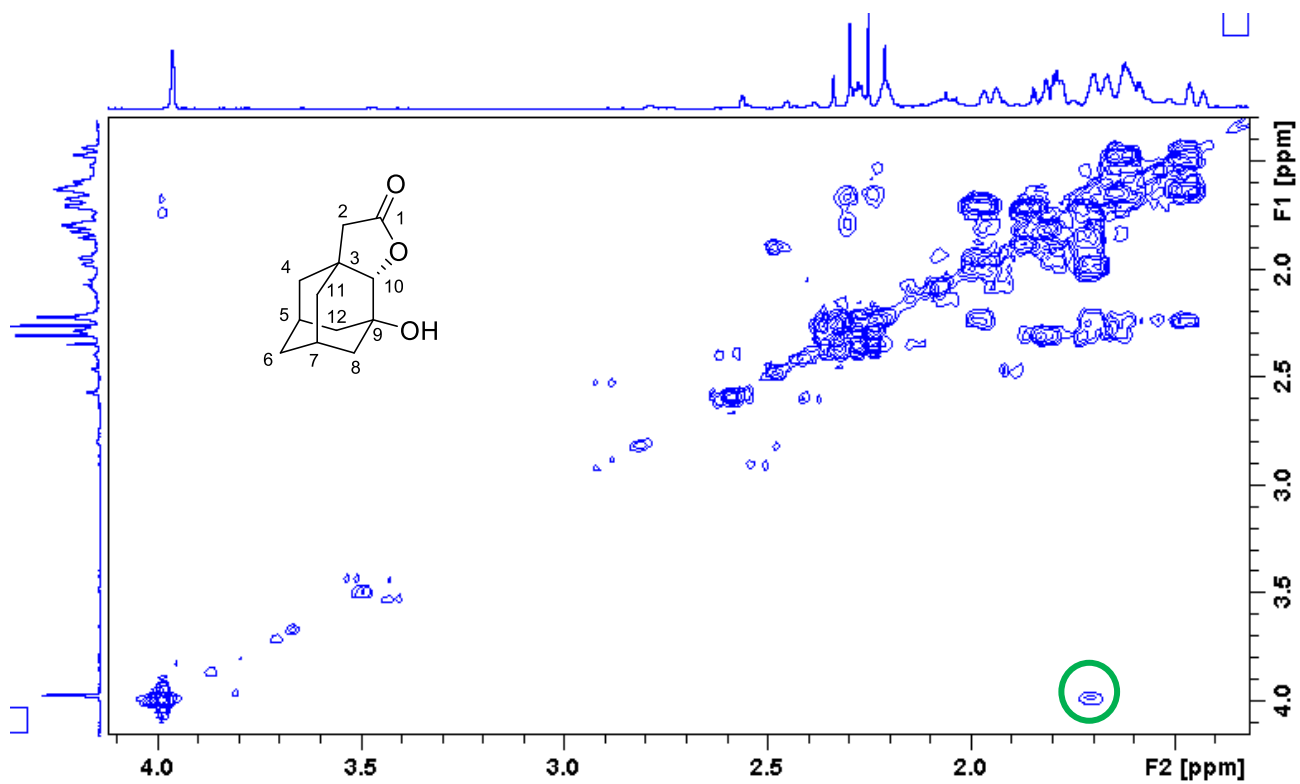
¹³C NMR (101 MHz, CDCl₃) δ 176.1 (*C*₁), 89.8 (*C*₁₀), 68.4 (*C*₉), 44.4 (*C*₂), 43.2 (*C*₁₂), 42.3 (*C*₃), 38.1 (*C*₄), 37.3 (*C*₁₁), 35.9 (*C*₈), 35.1 (*C*₆), 31.2 (*C*₅ or *C*₇), 30.0 (*C*₅ or *C*₇).



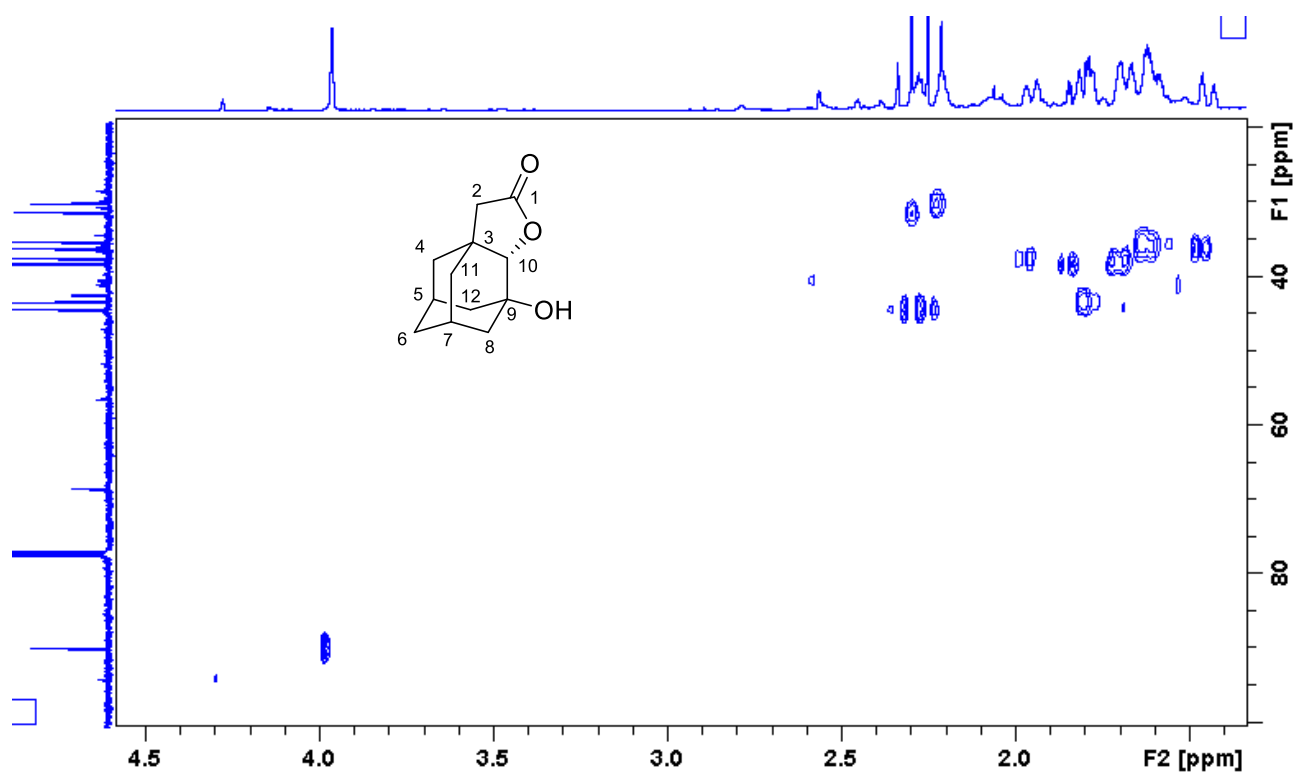
Stacking of the ¹H NMR spectrum of **4a** (bottom) with its selective NOESY obtained after irradiating at 3.96 δ (lactone signal, C₁₀-H). The signals that show a NOESY correlation with C₁₀-H are visible in a negative phase.



Stacking of the ^{13}C NMR spectrum of **4a** (bottom) stacked with its DEPT90 (top) and its DEPT 135 (middle) spectra.

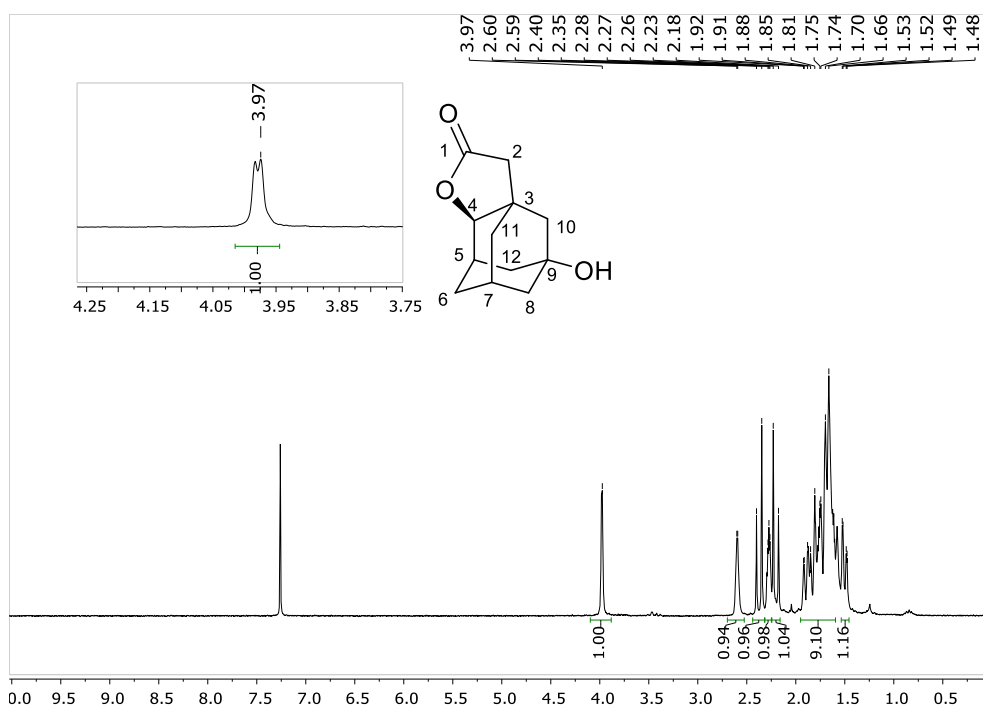


COSY of **4a**. Note the coupling of $\text{C}_{10}\text{-H}$ with a methylene $\text{C}_8\text{-H}$ (highlighted in green).



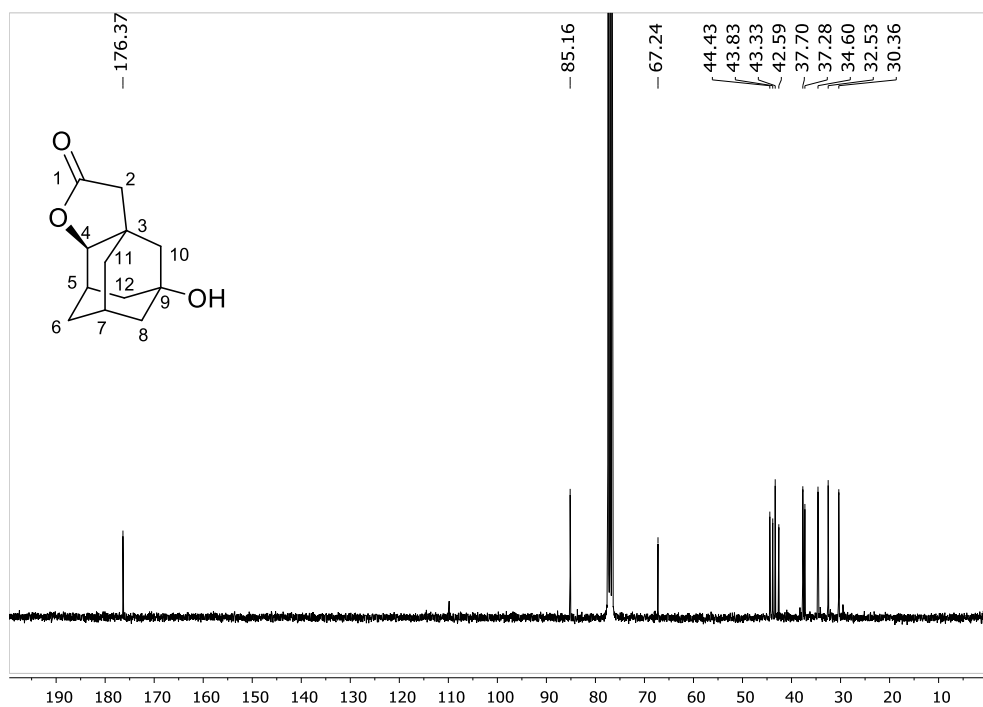
HSQC of 4a

¹H NMR of **4b** in CDCl₃

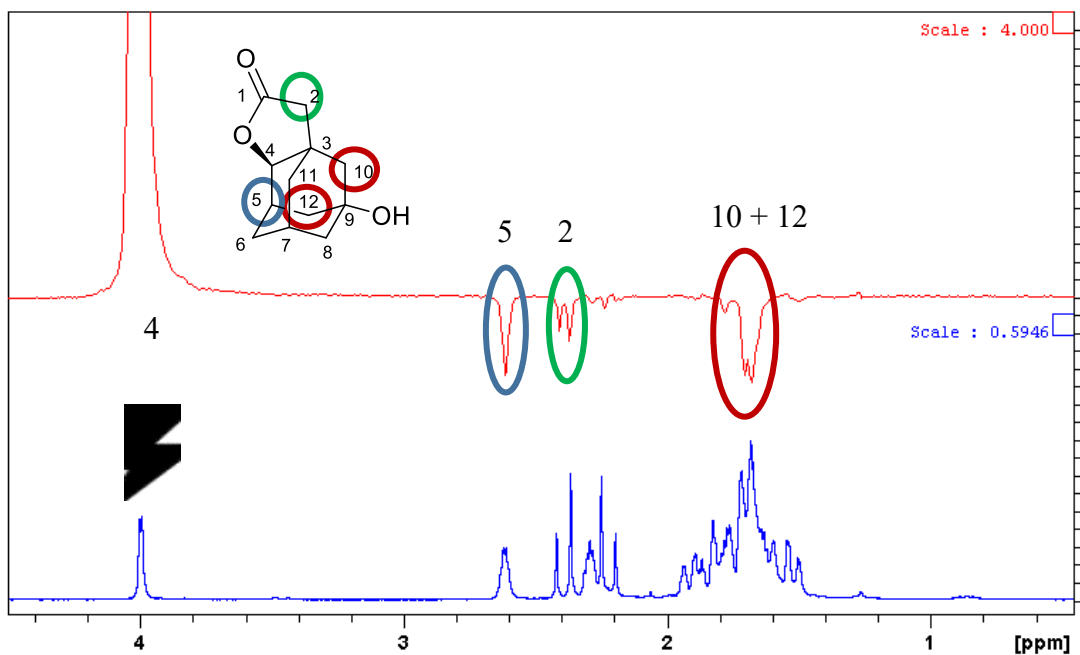


¹H NMR (300 MHz, CDCl₃) δ 3.98 (s, 1H; C₄ [1H]), 2.70 – 2.53 (m, 1H; C₅ [1H]), 2.37 (d, *J* = 16.1 Hz, 1H; C₂ [1H]), 2.32 – 2.25 (m, 1H; C₇ [1H]), 2.20 (d, *J* = 16.1 Hz, 1H; C₂ [1H]), 1.95 – 1.59 (m, 9H; C₄ [2H] + C₁₀ [2H] + C₈ [2H] + C₆ [1H] + C₁₂ [2H]), 1.50 (dd, *J* = 12.3, 2.4 Hz, 1H; C₆ [1H]).

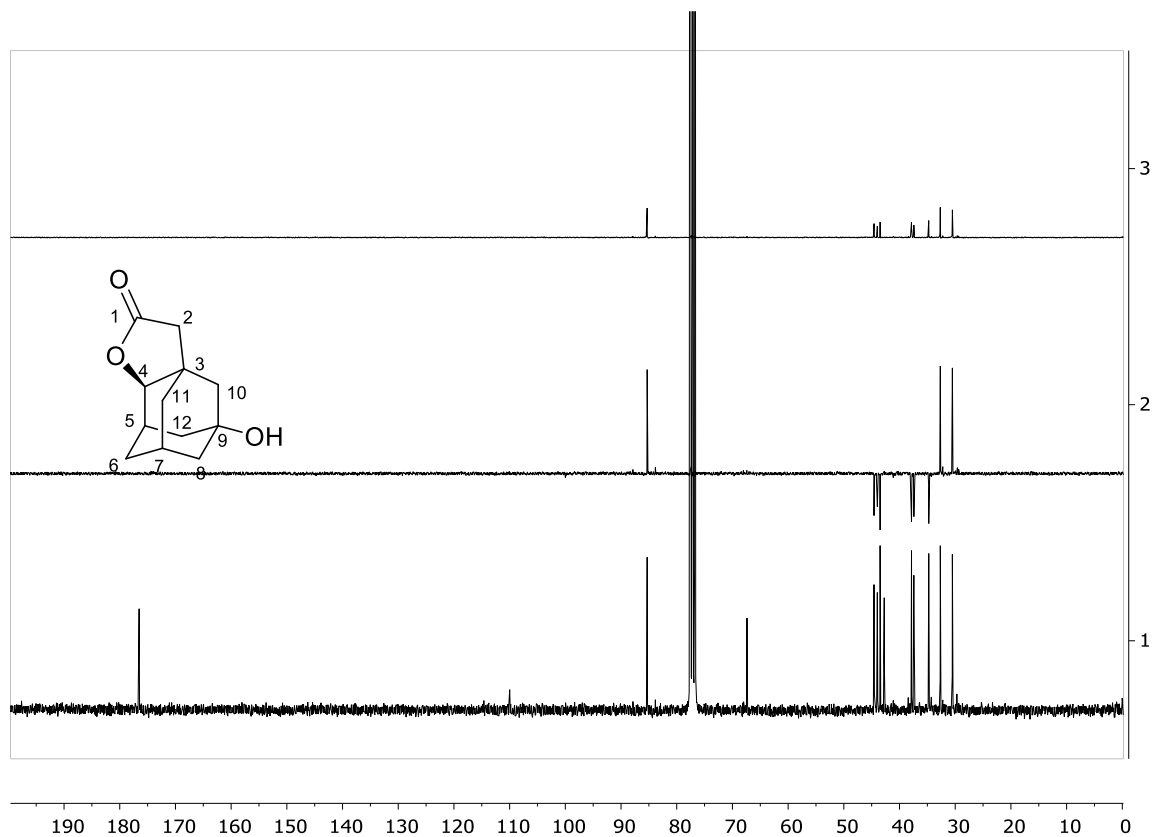
¹³C NMR of **4b** in CDCl₃



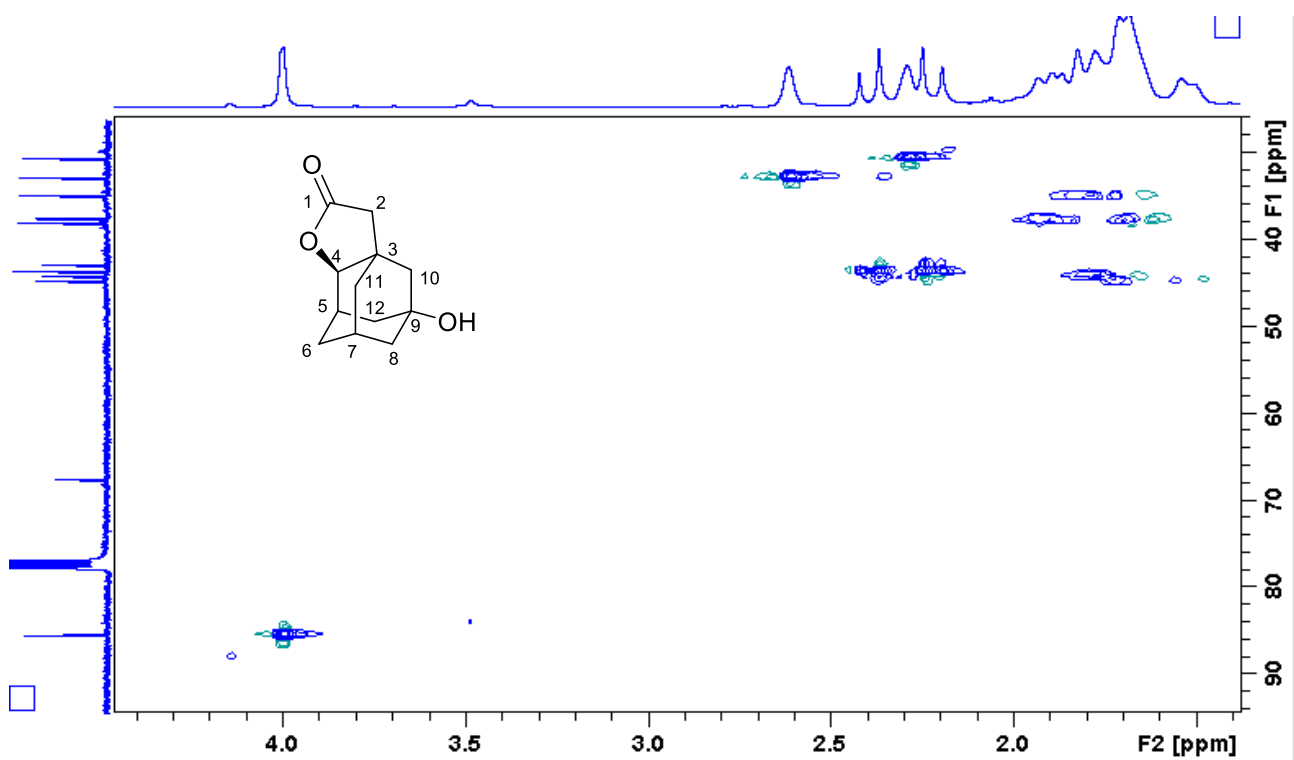
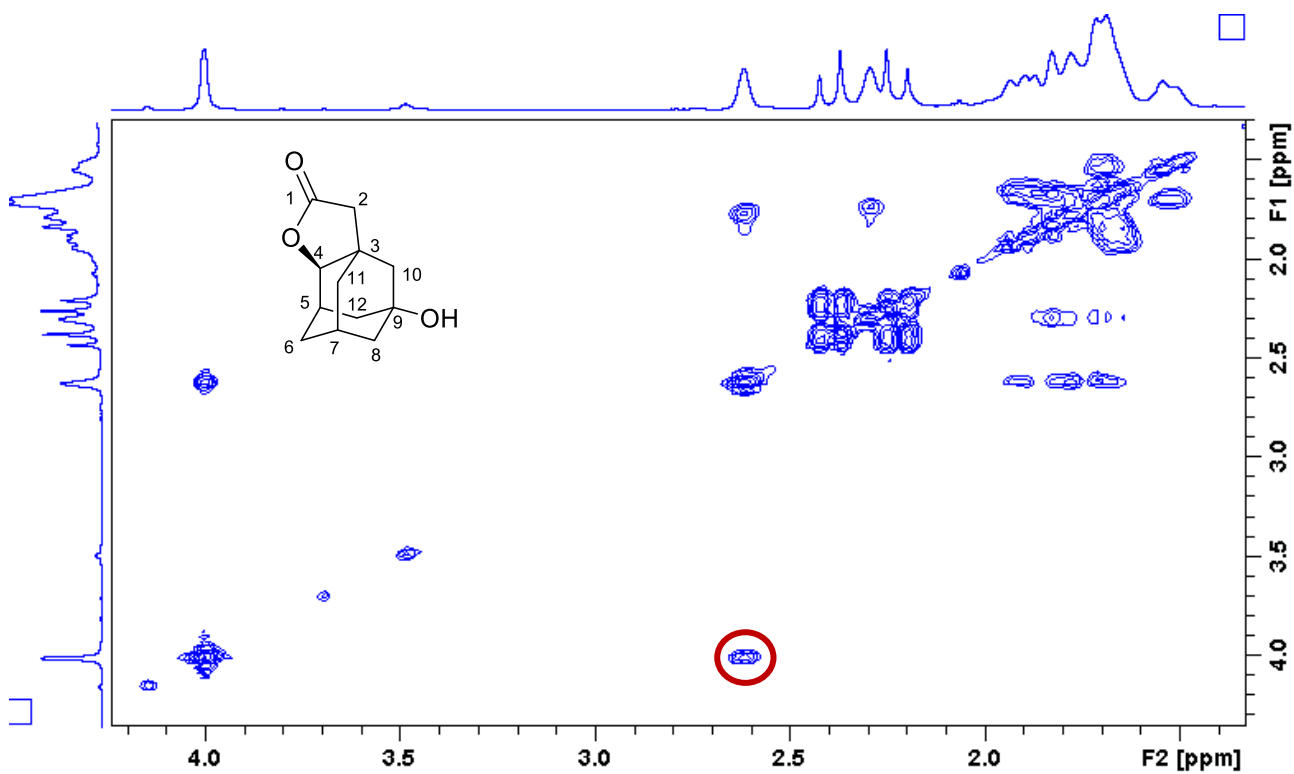
¹³C NMR (75 MHz, CDCl₃) δ 176.4 (C₁), 85.2 (C₄), 67.2 (C₉), 44.4 (C₆), 43.8, 43.3 (C₂), 42.6 (C₃), 37.7, 37.3, 34.6, 32.5 (C₇), 30.4 (C₅).



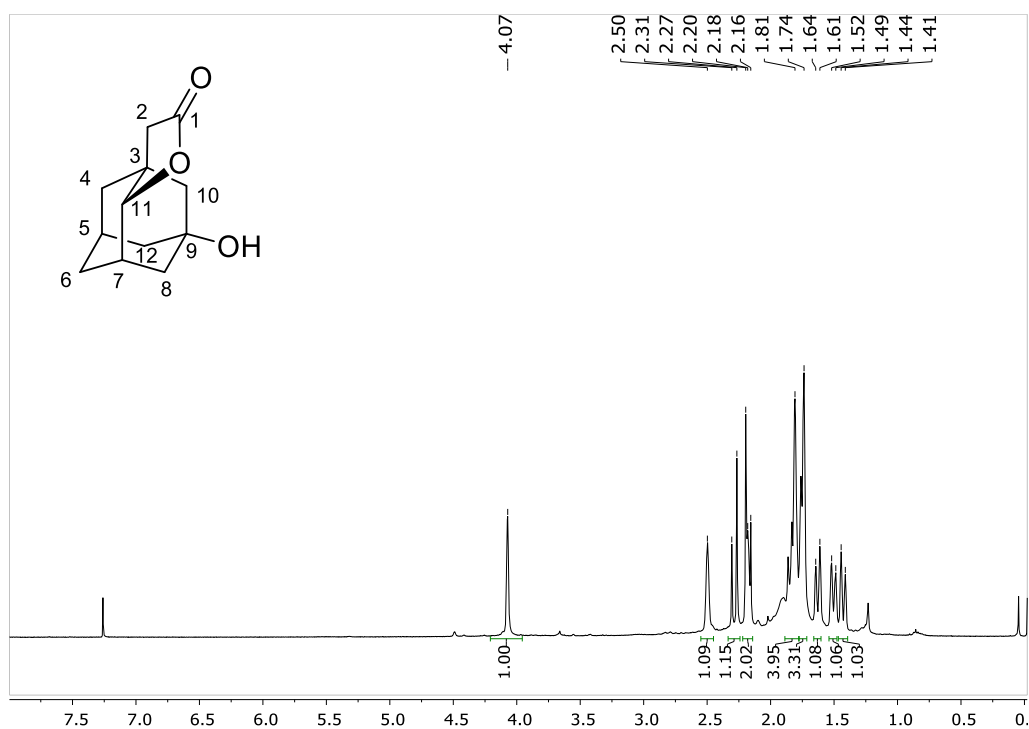
Stacking of the ^1H NMR spectrum of **4b** (bottom) with its selective NOESY obtained after irradiating at $3.98\ \delta$ (lactone signal, $\text{C}_4\text{-H}$). The signals that show a NOESY correlation with $\text{C}_4\text{-H}$ are visible in a negative phase.



Stacking of the ^{13}C NMR spectrum of **4b** (bottom) stacked with its DEPT90 (top) and its DEPT 135 (middle) spectra.

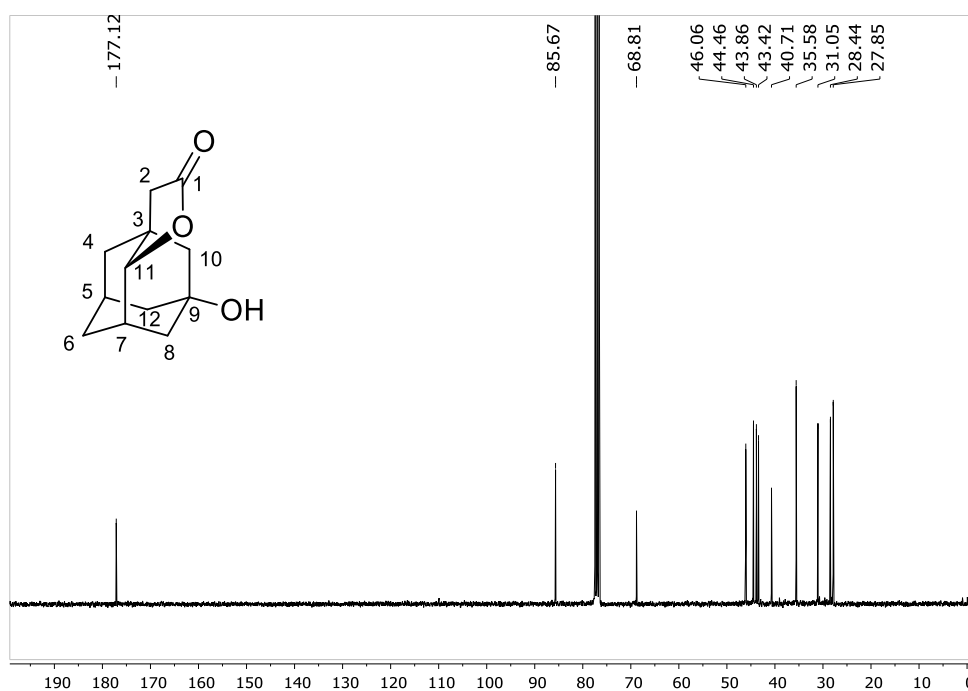


¹H NMR of **4c** in CDCl₃

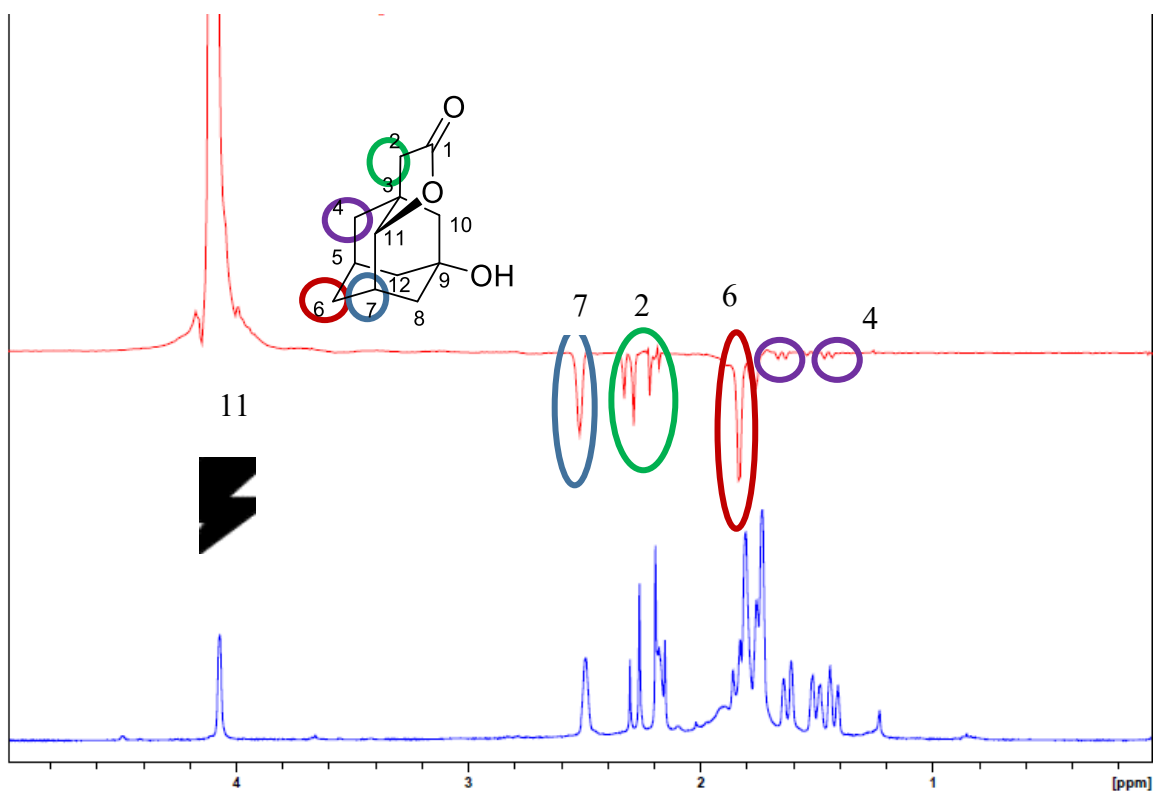


¹H NMR (400 MHz, CDCl₃) δ 4.07 (s, 1H; C₄[1H]), 2.50 (s, 1H; C₅[1H]), 2.29 (d, *J* = 16.0 Hz, 1H; C₂[1H]), 2.22 – 2.14 (m, 2H; C₂[1H] + C₇[1H]), 1.81 (m, 4H; C₆[2H] + C₁₀[1H] + C₈[1H]), 1.74 (m, 3H; C₁₂[2H] + C₈[1H]), 1.63 (d, *J* = 13.1 Hz, 1H; C₈[1H]), 1.50 (d, *J* = 13.2 Hz, 1H; C₄[1H]), 1.43 (d, *J* = 13.1 Hz, 1H; C₈[1H]).

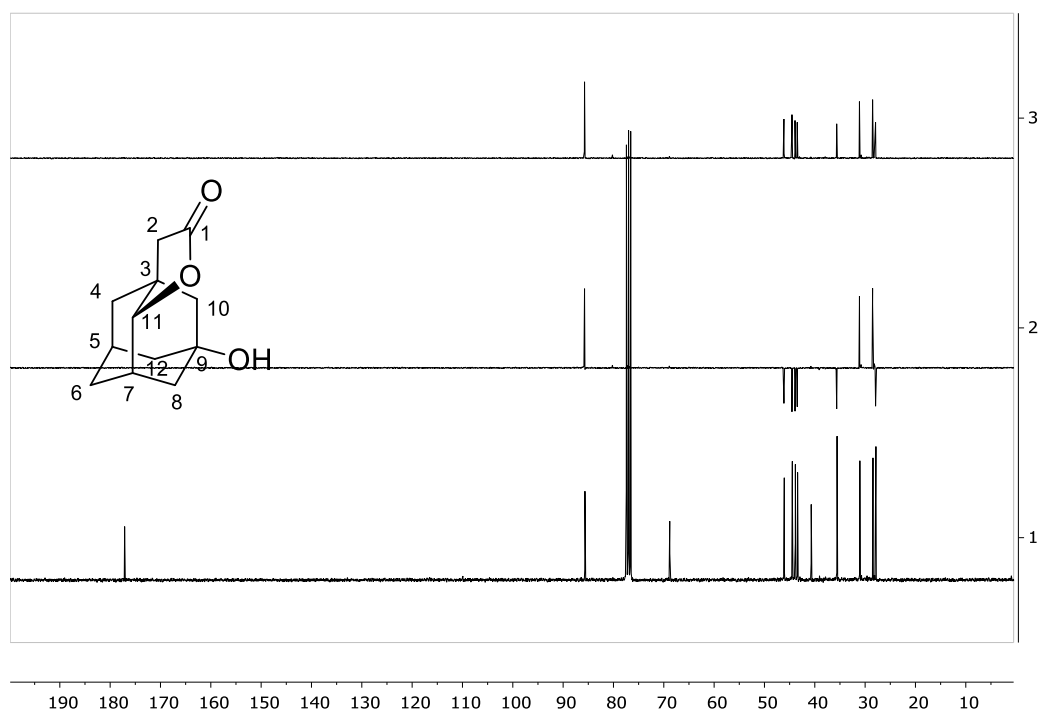
¹³C NMR of **4c** in CDCl₃



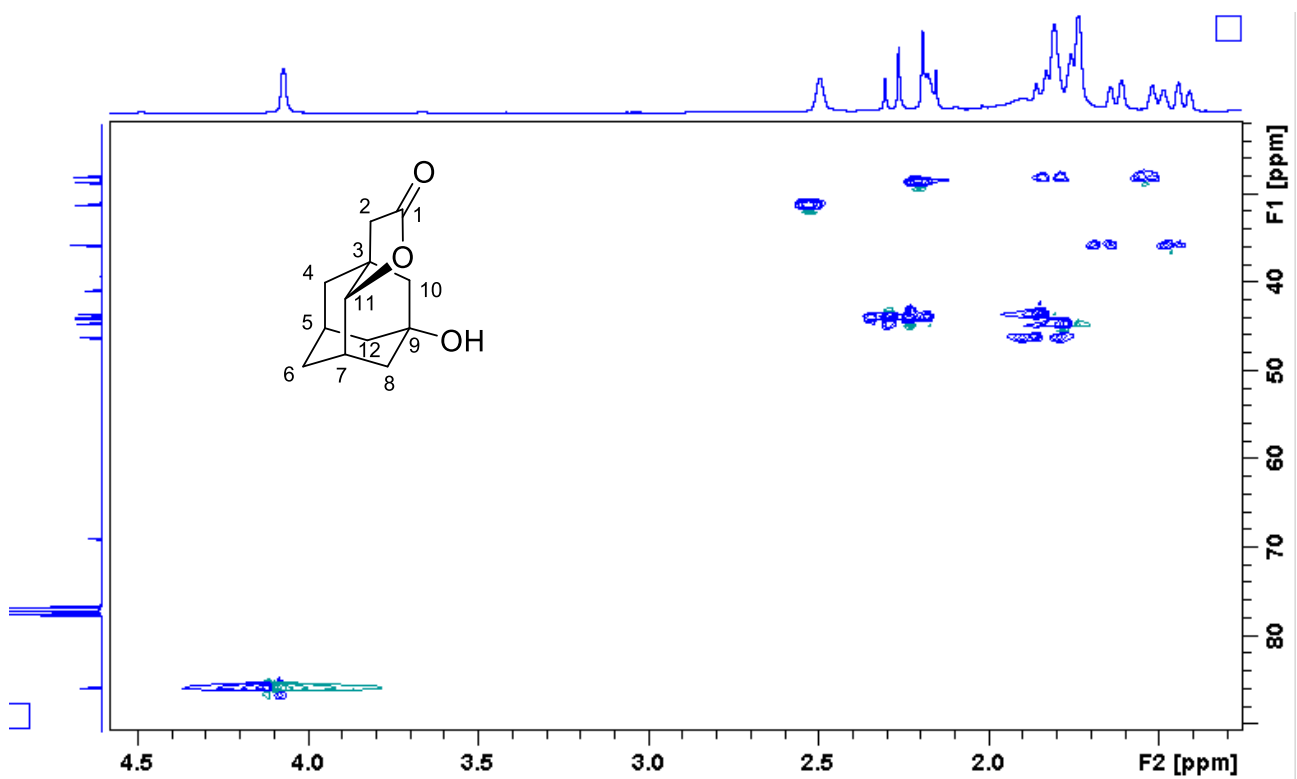
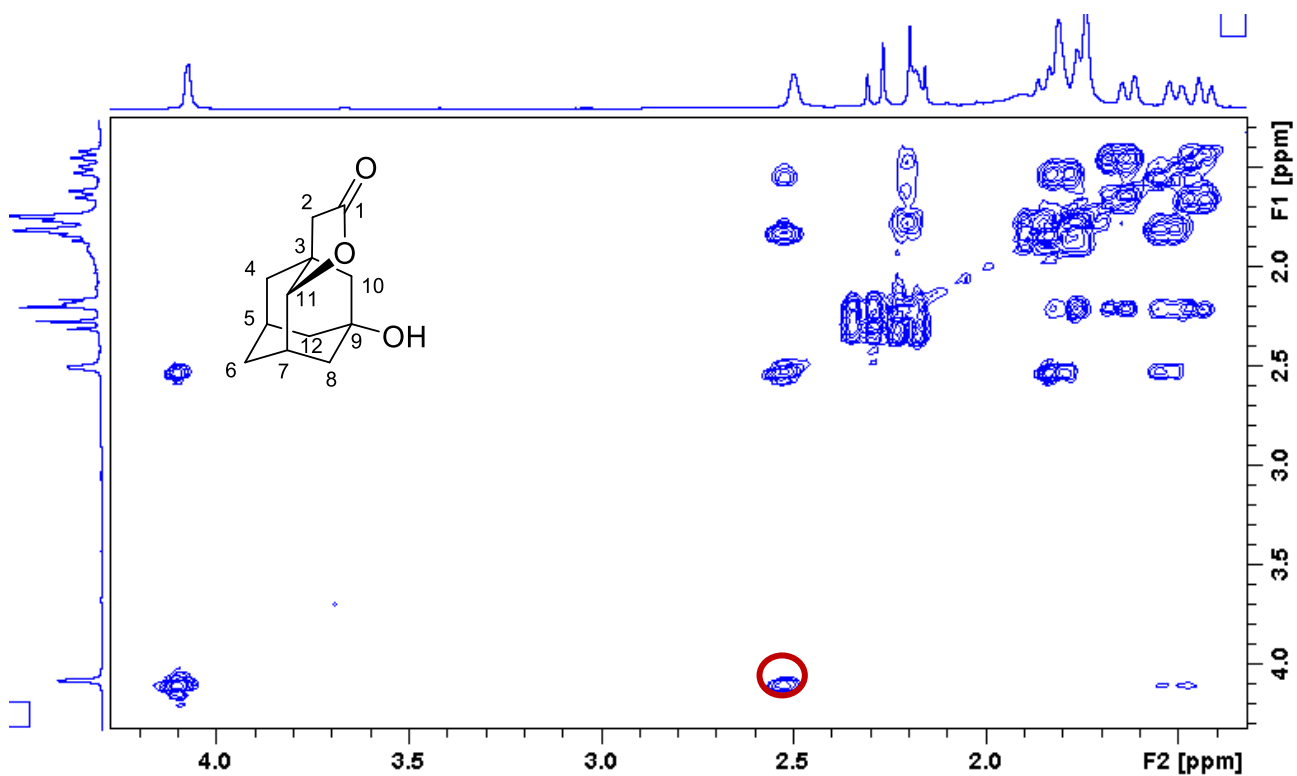
¹³C NMR (75 MHz, CDCl₃) δ 177.1 (C₁), 85.7 (C₁₁), 68.8 (C₉), 46.1 (C₁₀), 44.5 (C₁₂), 43.9 (C₂), 43.4 (C₆), 40.7 (C₃), 35.58 (C₄), 31.0 (C₇), 28.4 (C₅), 27.8 (C₈).



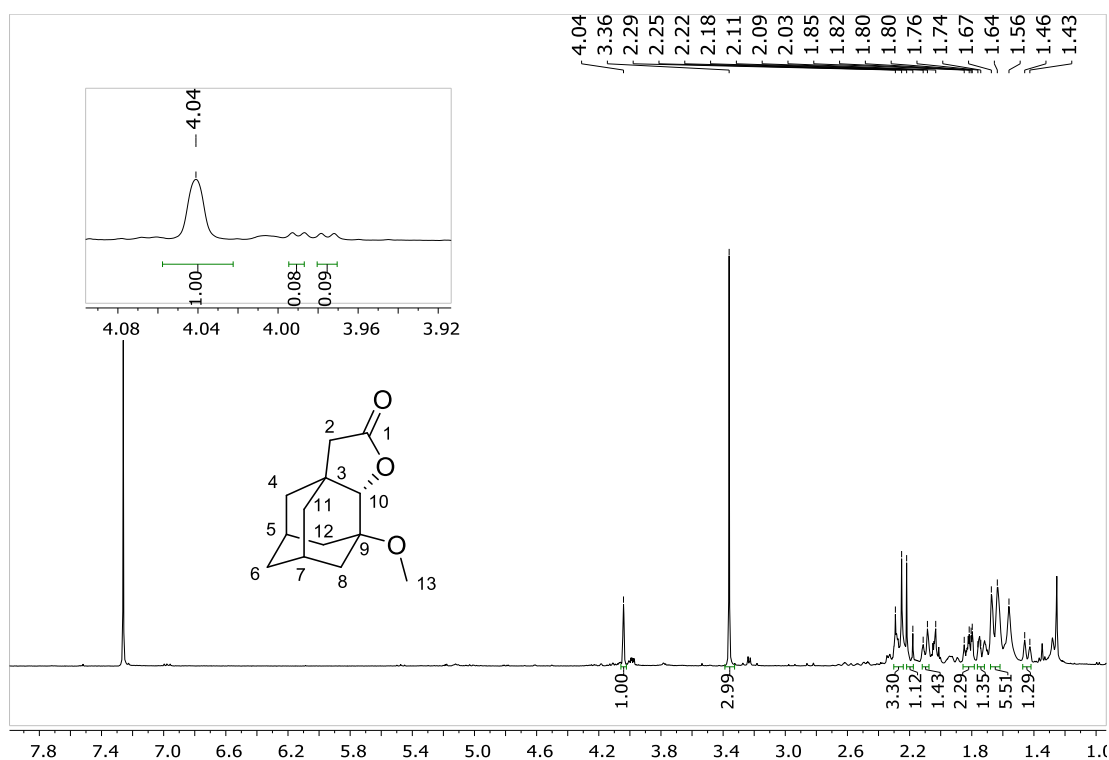
Stacking of the ^1H NMR spectrum of **4c** (bottom) with its selective NOESY obtained after irradiating at $4.07\ \delta$ (lactone signal, $\text{C}_{11}\text{-H}$). The signals that show a NOESY correlation with $\text{C}_{11}\text{-H}$ are visible in a negative phase.



Stacking of the ^{13}C NMR spectrum of **4c** (bottom) stacked with its DEPT90 (top) and its DEPT 135 (middle) spectra.

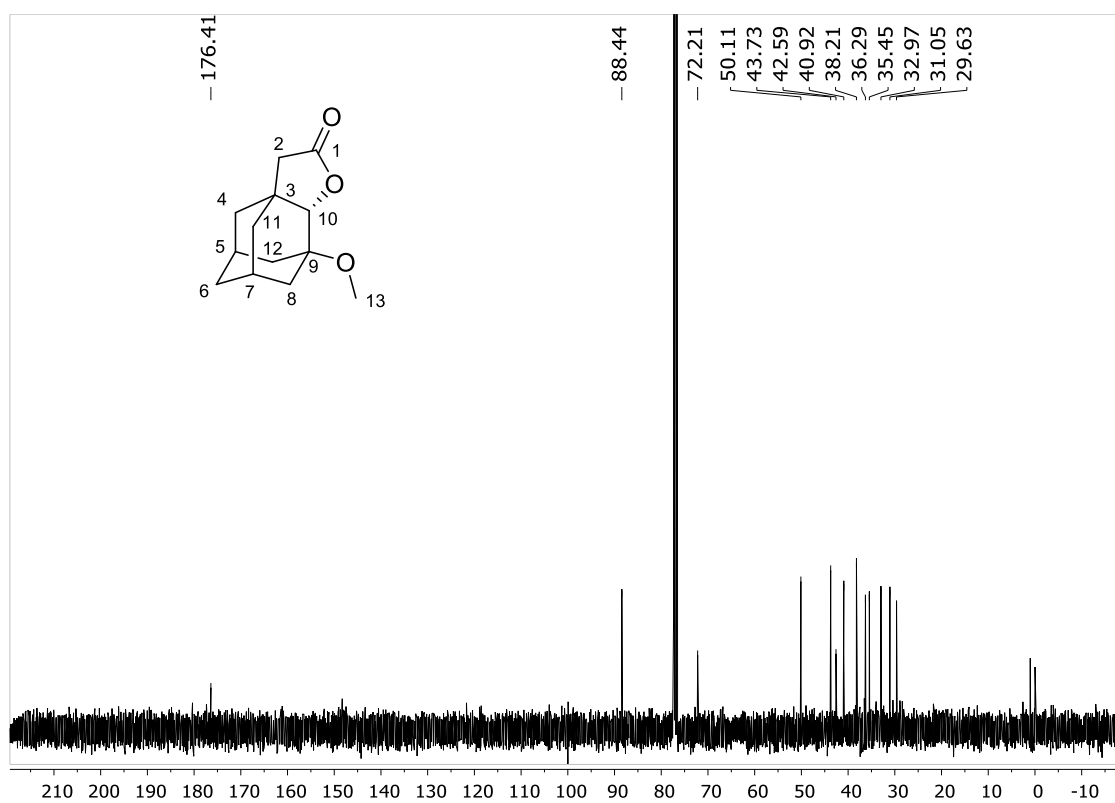


¹H NMR of **5a** in CDCl₃



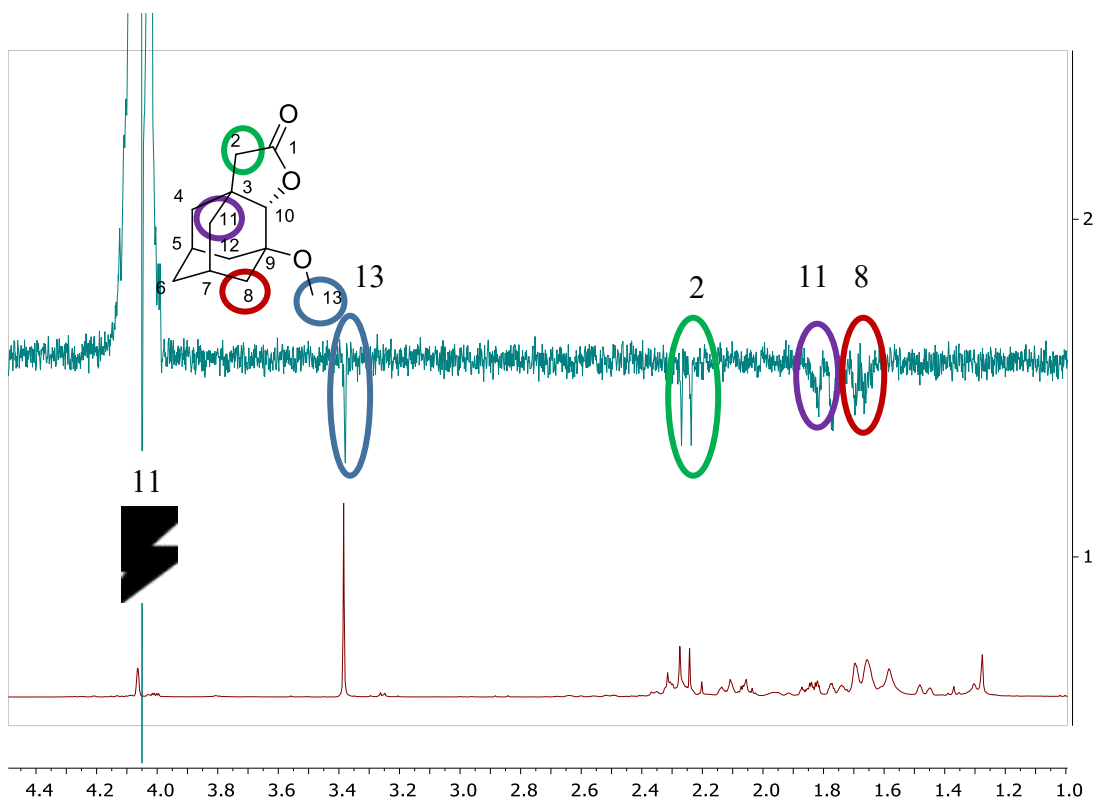
¹H NMR (400 MHz, CDCl₃) δ 4.04 (s, 1H; C₁₀ [1H]), 3.36 (s, 3H; C₁₃ [3H]), 2.27 (d, *J* = 16.0 Hz, 3H; C₂ [1H] + C₅ [1H] + C₇ [1H]), 2.20 (d, *J* = 16.0 Hz, 1H; C₂ [1H]), 2.10 (d, *J* = 11.0 Hz, 1H; C₁₂ [1H]), 1.86 – 1.78 (m, 2H; C₄ [1H] + C₁₁ [1H]), 1.75 (m, *J* = 7.4 Hz, 1H; C₈ [1H]), 1.65 (m, *J* = 15.4 Hz, 5H; C₆ [2H] + C₁₂ [1H] + C₈ [1H] + C₁₁ [1H]), 1.44 (d, *J* = 13.3 Hz, 1H; C₄ [1H]). In the inset an expansion of the lactone signals is displayed. **5a** contains small amounts (<10% each) of lactones **5b** and **5c**, that account for small peaks in the spectra.

¹³C NMR of **5a** in CDCl₃

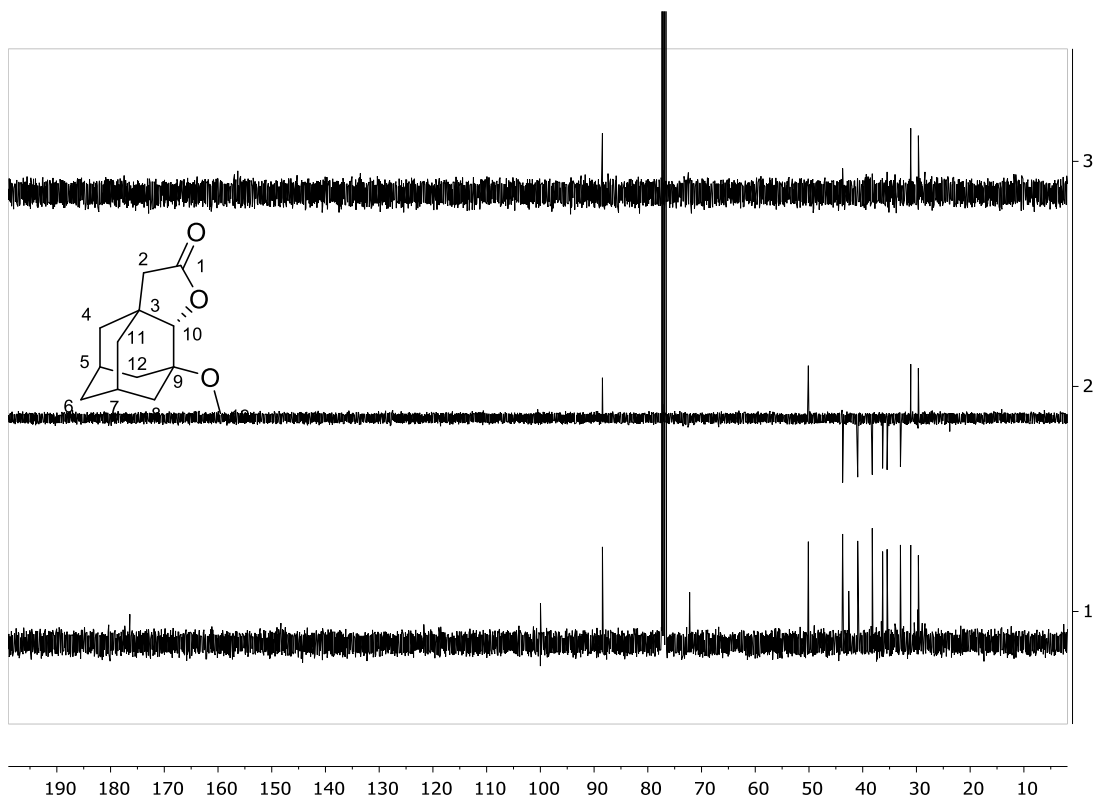


¹³C NMR (101 MHz, CDCl₃) δ 176.4 (C₁), 88.4 (C₁₀), 72.2 (C₉), 50.1 (C₁₃), 43.7 (C₂), 42.6 (C₃), 40.9 (C₈), 38.21 (C₄ or C₁₁), 36.3 (C₄ or C₁₁), 35.4 (C₆), 33.0 (C₁₂), 31.0 (C₅ or C₇), 29.6 (C₅ or C₇).

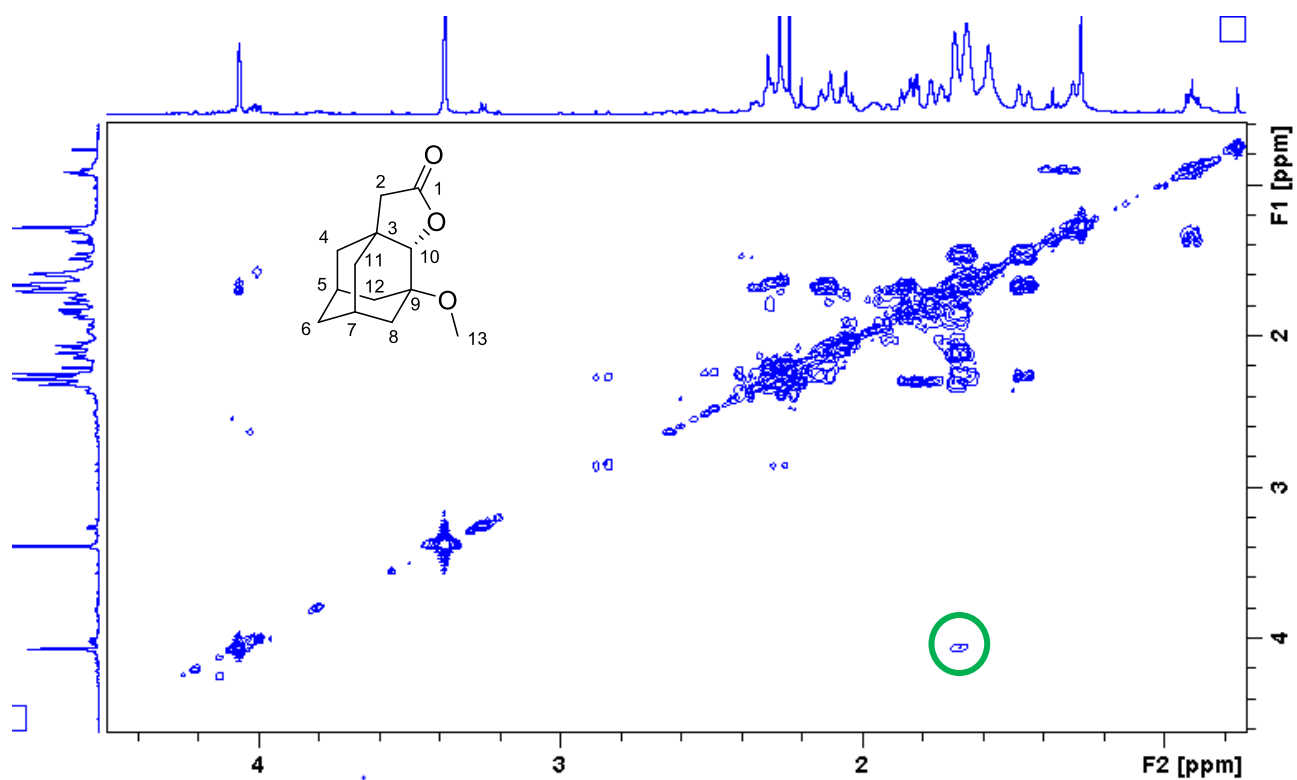
Additional small peaks are due to isomers **5b** and **5c**.



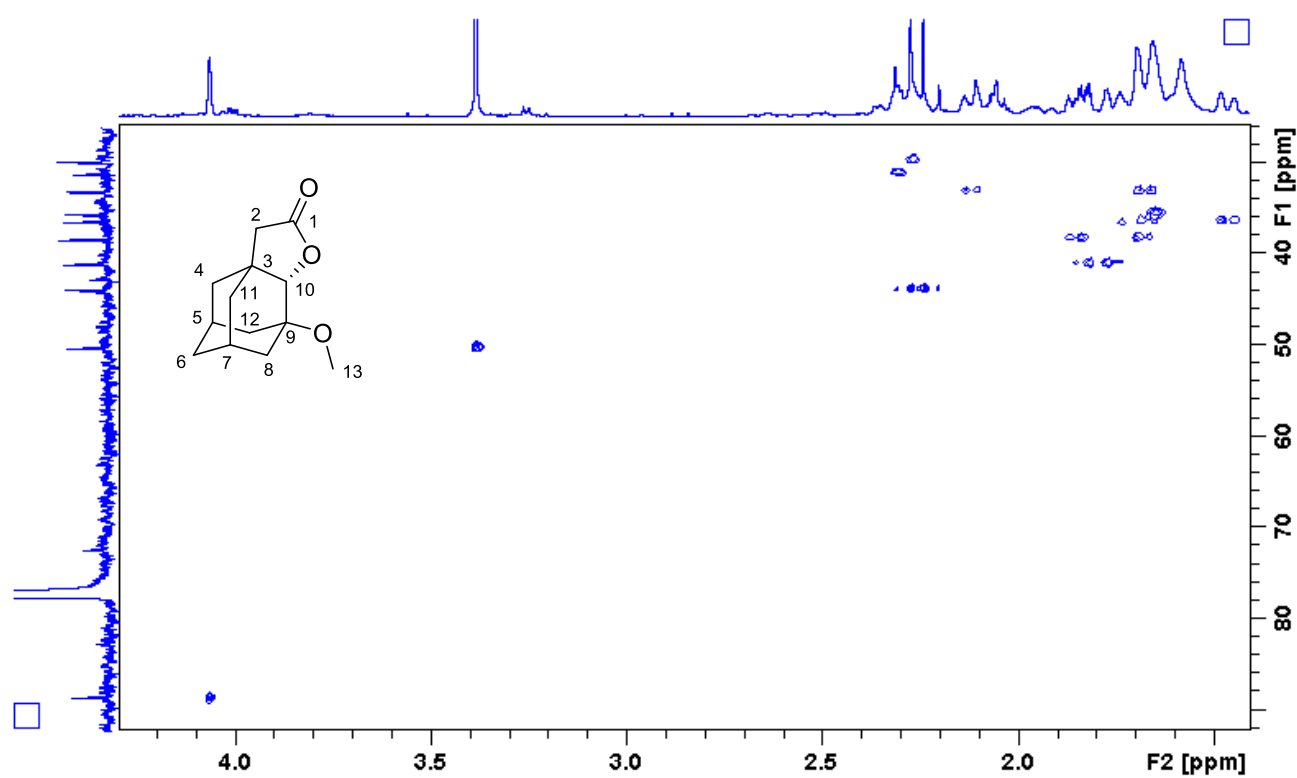
Stacking of the ¹H NMR spectrum of **5a** (bottom) with its selective NOESY obtained after irradiating at 4.04 δ (lactone signal, C₁₀-H). The signals that show a NOESY correlation with C₁₀-H are visible in a negative phase.



Stacking of the ¹³C NMR spectrum of **5a** (bottom) stacked with its DEPT90 (top) and its DEPT 135 (middle) spectra.

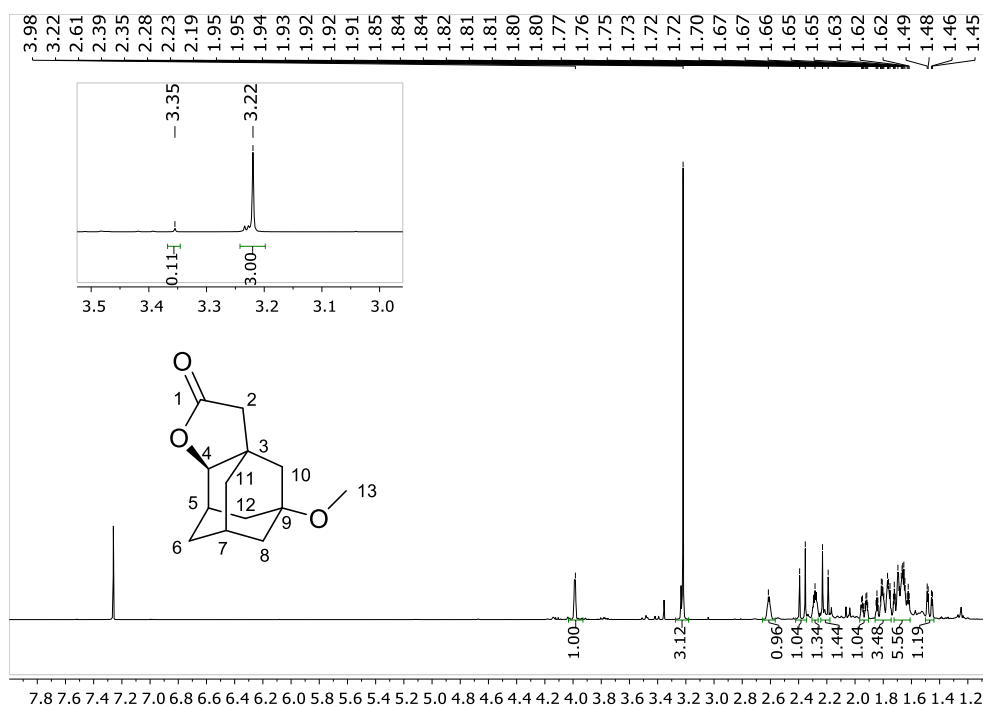


COSY of **5a**. Note the coupling of C₁₀-H with secondary C₈-H bond (highlighted in green).



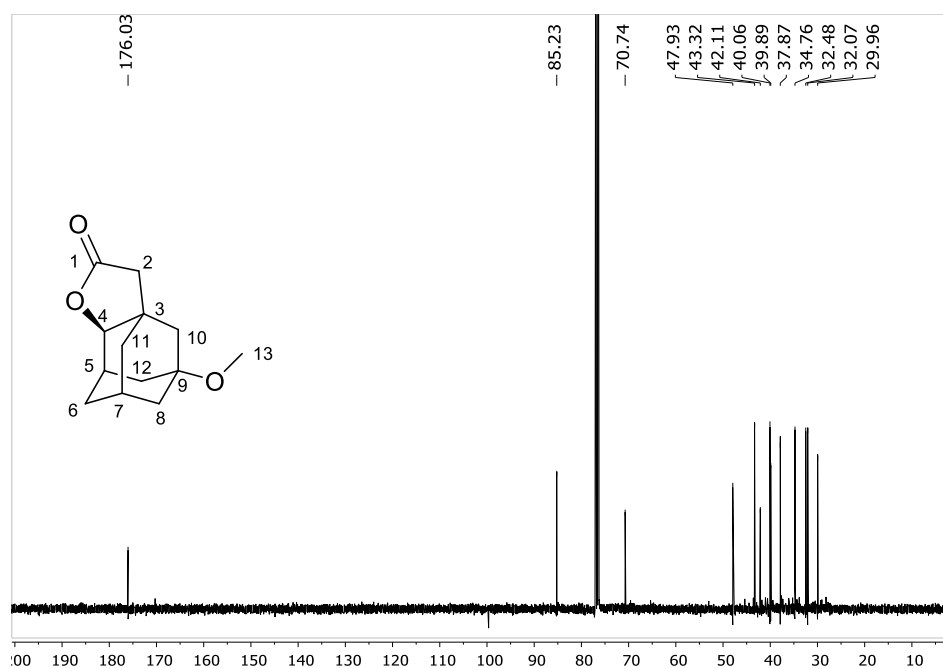
HSQC of **5a**

^1H NMR of **5b** in CDCl_3

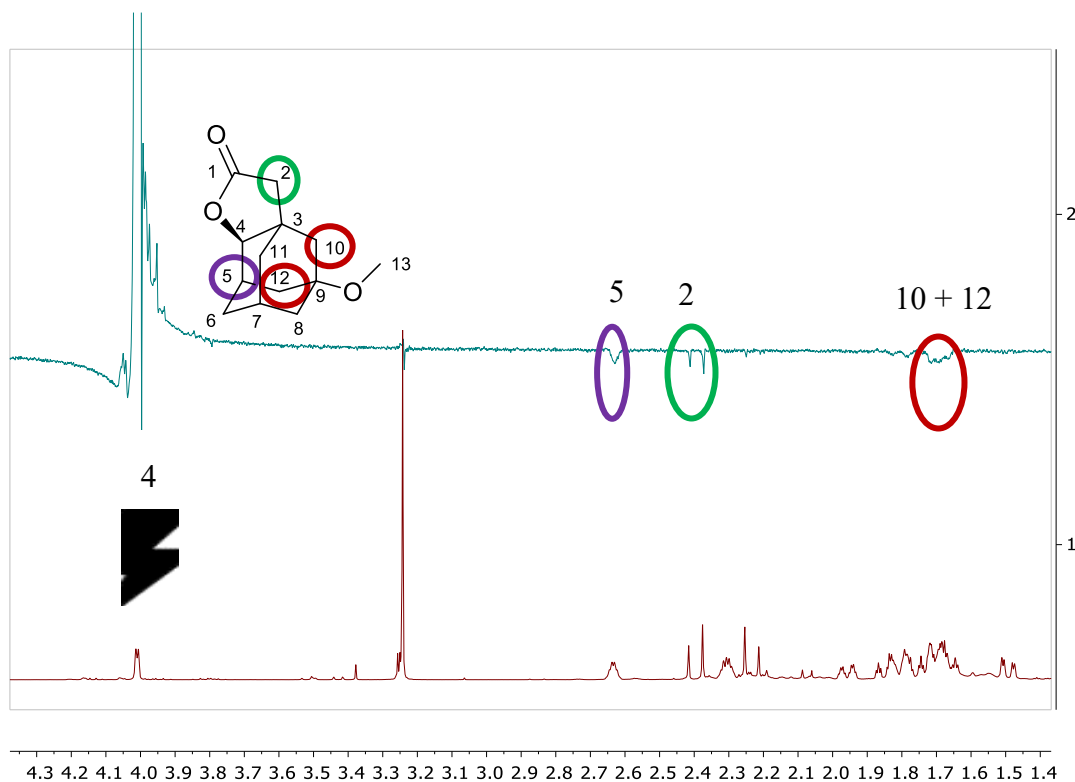


^1H NMR (400 MHz, CDCl_3) δ 3.98 (s, 1H; $C_4[1H]$), 3.22 (s, 3H; $C_{13}[1H]$), 2.61 (s, 1H; $C_5[1H]$), 2.37 (d, $J = 16.1$ Hz, 1H; $C_2[1H]$), 2.28 (s, 1H; $C_7[1H]$), 2.21 (d, $J = 16.1$ Hz, 1H; $C_2[1H]$), 1.94 (dq, $J = 12.2, 2.5$ Hz, 1H; $C_{12}[1H]$), 1.86 – 1.76 (m, 3H; $C_6[1H] + C_8[1H] + C_{11}[1H]$), 1.76 – 1.61 (m, 5H; $C_{10}[2H] + C_8[1H] + C_{11}[1H] + C_{12}[1H]$), 1.47 (dd, $J = 12.1, 2.7$ Hz, 1H; $C_8[1H]$). The sample contains traces (5%) of **5c** (which account for the small additional signals) In the inset an expansion of the OCH_3 signals is displayed.

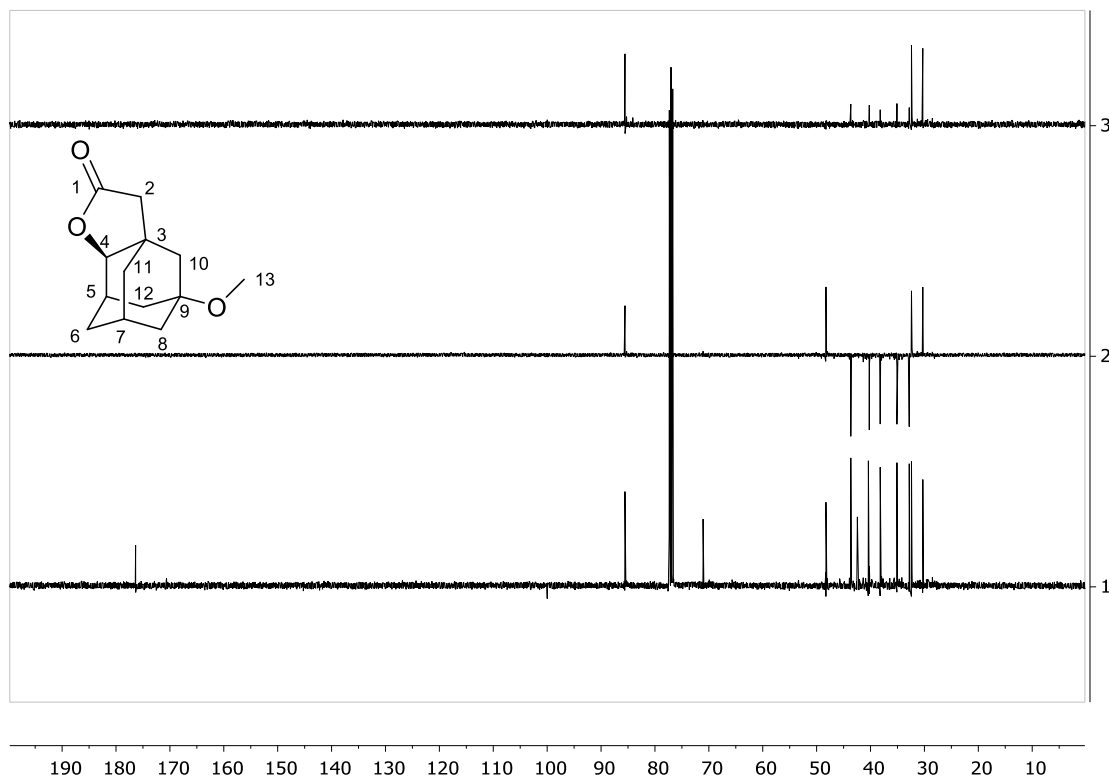
¹³C NMR of **5b** in CDCl₃



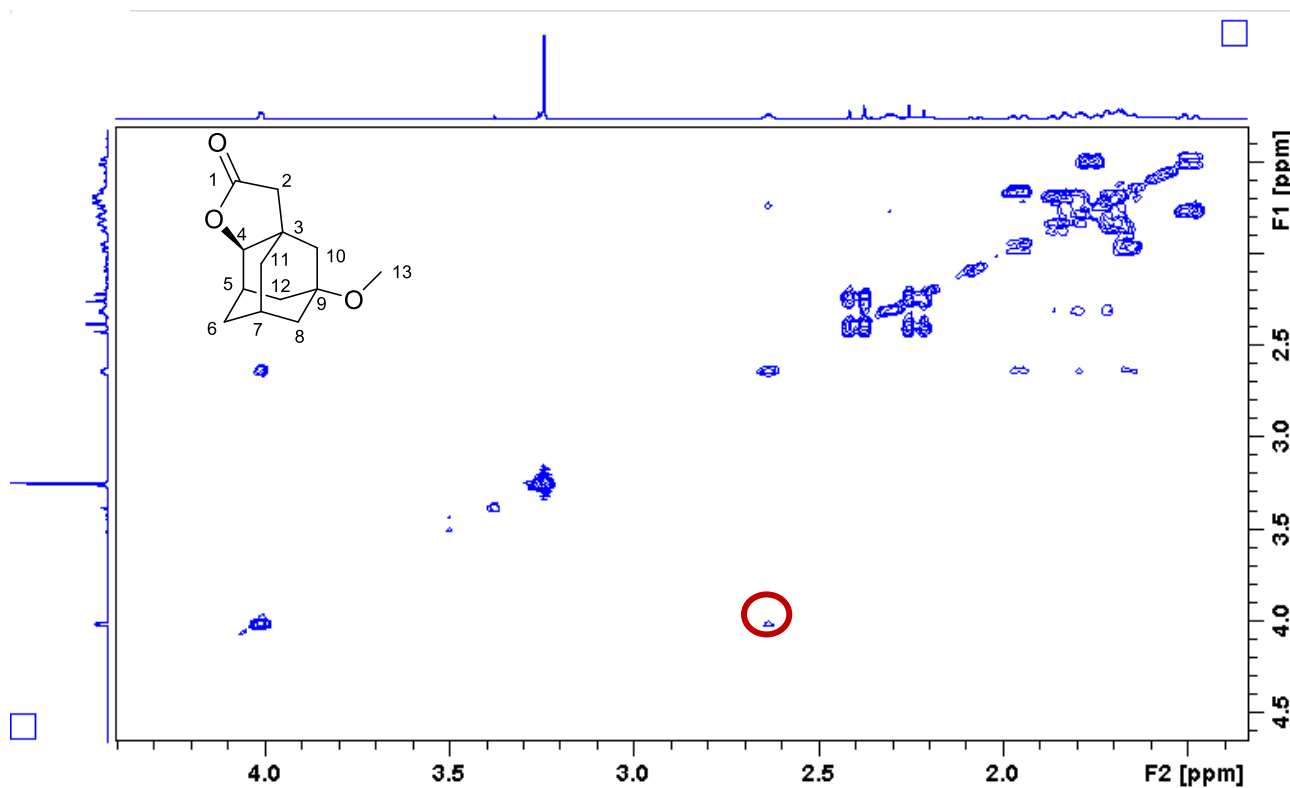
¹³C NMR (101 MHz, CDCl₃) δ 176.0 (C₁), 85.2 (C₄), 70.7 (C₉), 47.9 (C₁₃), 43.3 (C₂), 42.1 (C₃), 40.1 (C₈ or C₁₀), 39.9 (C₈ or C₁₀), 37.9 (C₁₁), 34.8 (C₆), 32.5 (C₁₂), 32.07 (C₅), 30.0 (C₇).



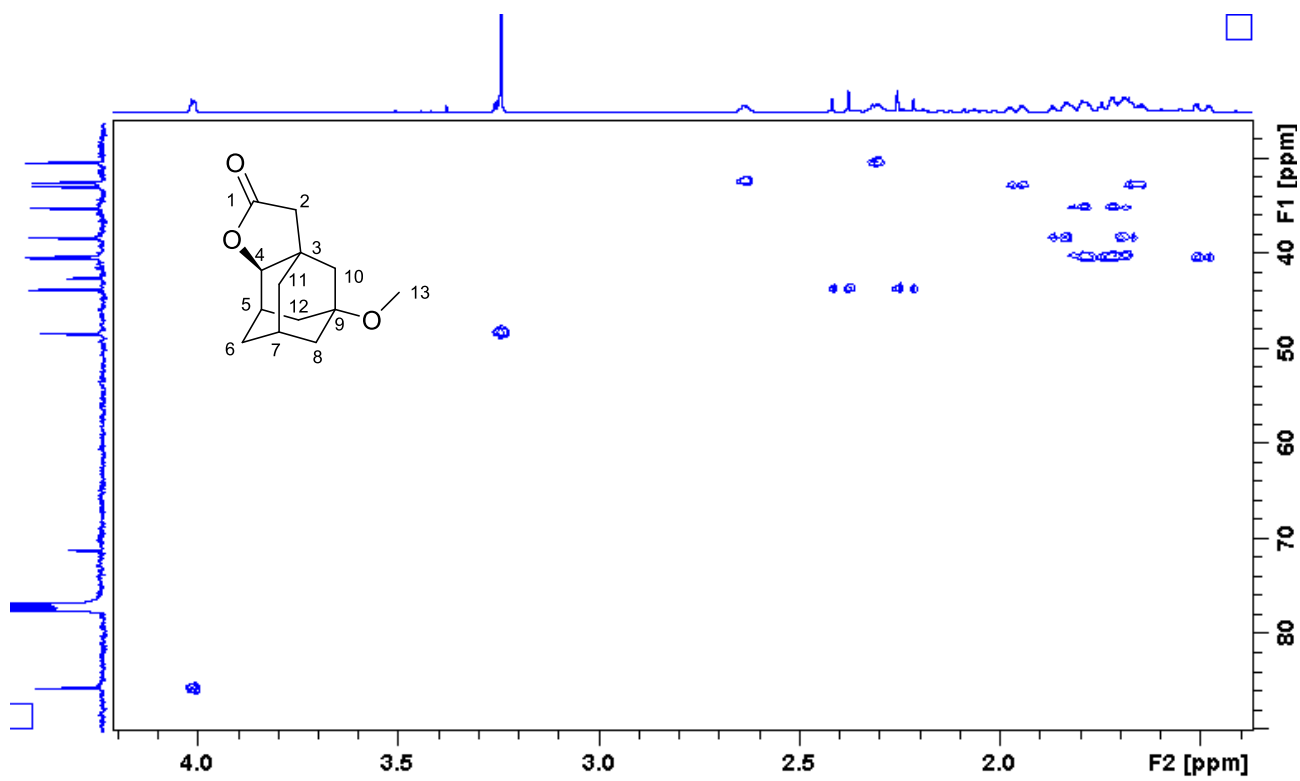
Stacking of the ¹H NMR spectrum of **5b** (bottom) with its selective NOESY obtained after irradiating at 3.98 δ (lactone signal, C₄-H). The signals that show a NOESY correlation with C₄-H are visible in a negative phase



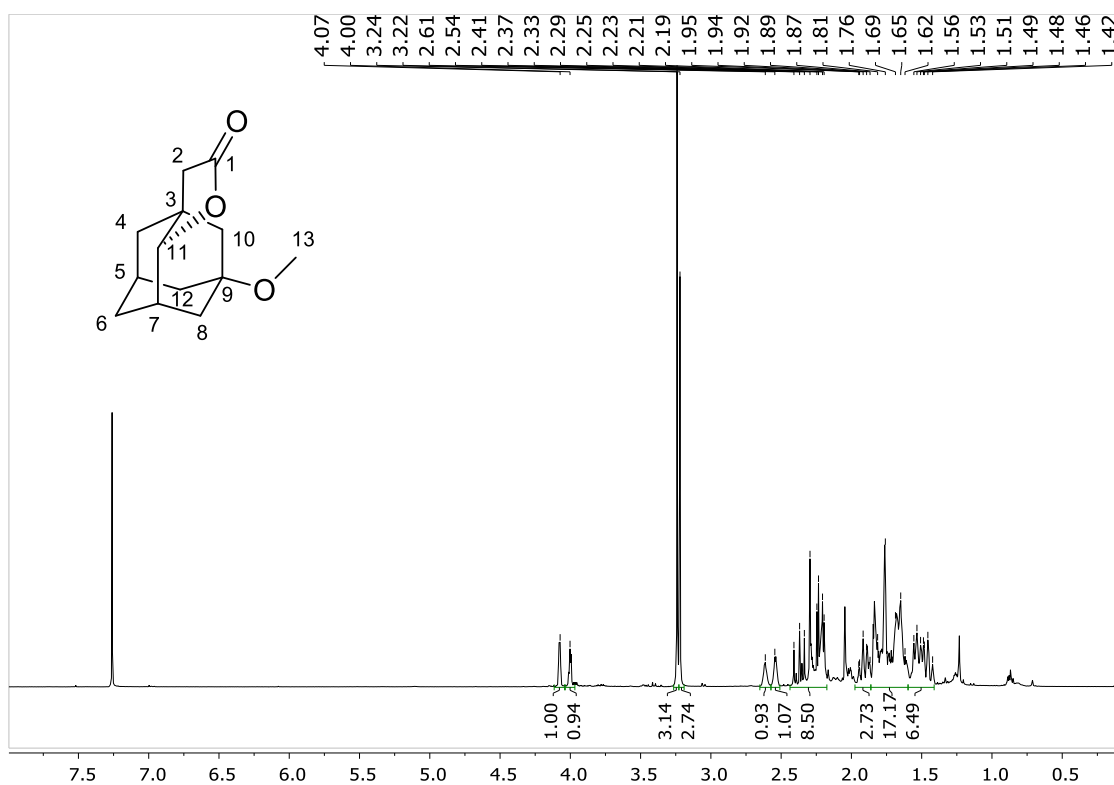
Stacking of the ^{13}C NMR spectrum of **5b** (bottom) stacked with its DEPT90 (top) and its DEPT 135 (middle) spectra.



COSY of **5b**. Note the coupling of $\text{C}_4\text{-H}$ with tertiary $\text{C}_5\text{-H}$ bond (highlighted in red).

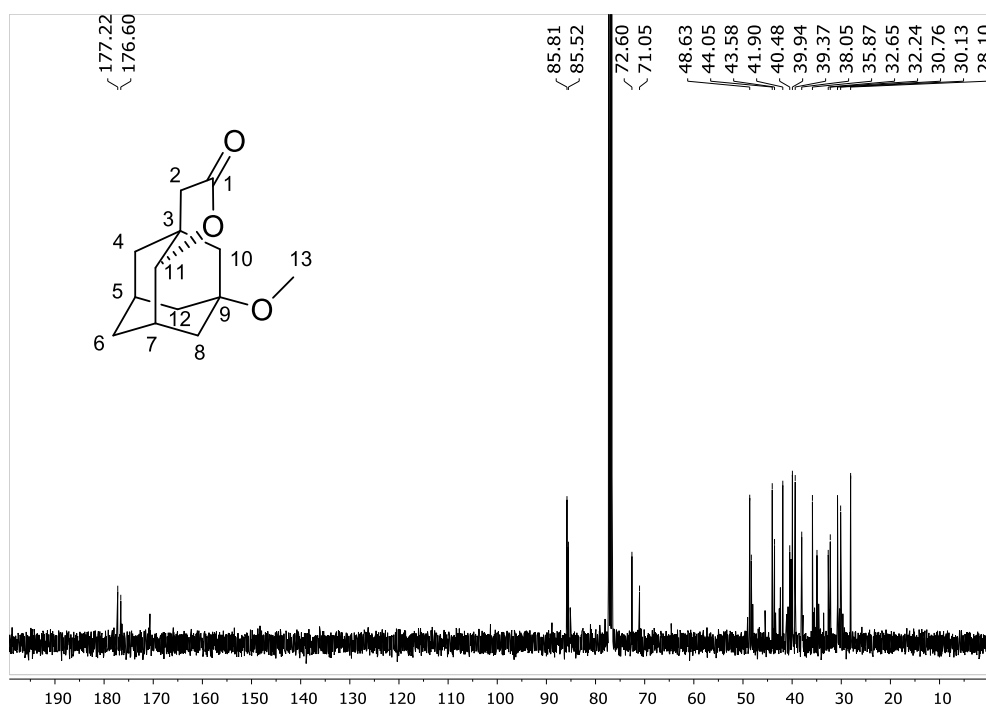


¹H NMR of **5c** (in roughly 1:1 mixture with **5b**) in CDCl₃

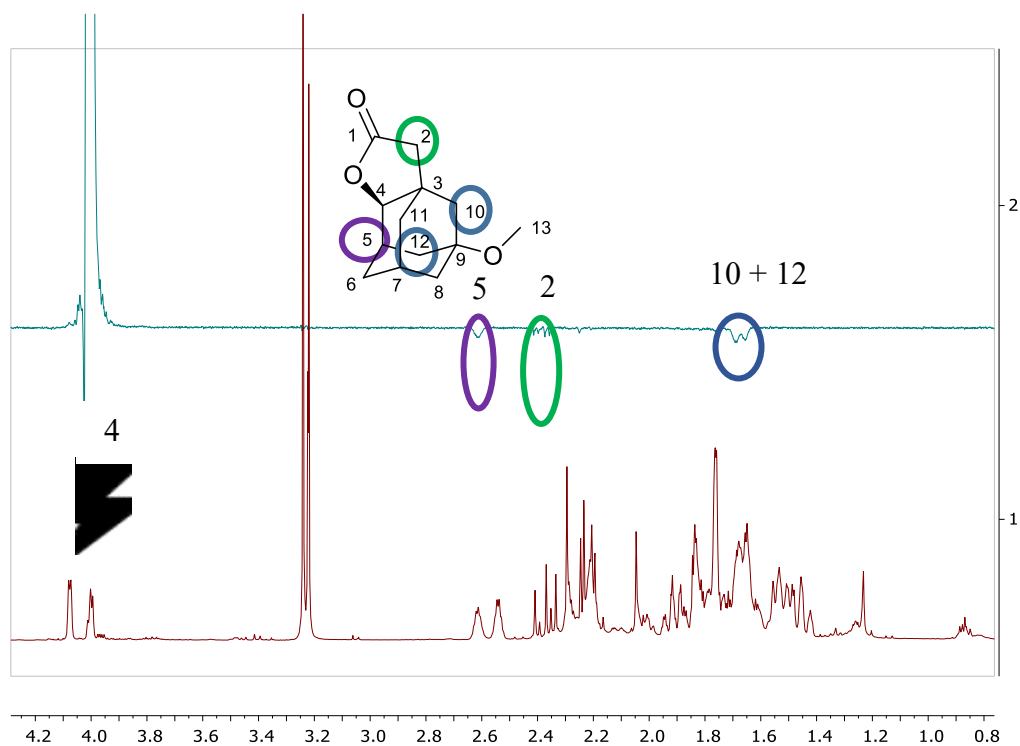


¹H NMR (400 MHz, CDCl₃) δ 4.07 (s, 1H; C₁₁ [1H] of **5c**), 3.98 (s, 1H; C₄ [1H] of **5b**), 3.24 (s, 3H; C₁₃ [3H] of **5c**), 3.22 (s, 3H; C₁₃ [3H] of **5b**), 2.61 (s, 1H; C₅ [1H] of **5b**), 2.54 (s, 1H; C₇ [1H] of **5c**), 2.44 – 2.17 (m, 8H), 1.97 – 1.86 (m, 3H), 1.86 – 1.60 (m, 17H), 1.60 – 1.41 (m, 6H).

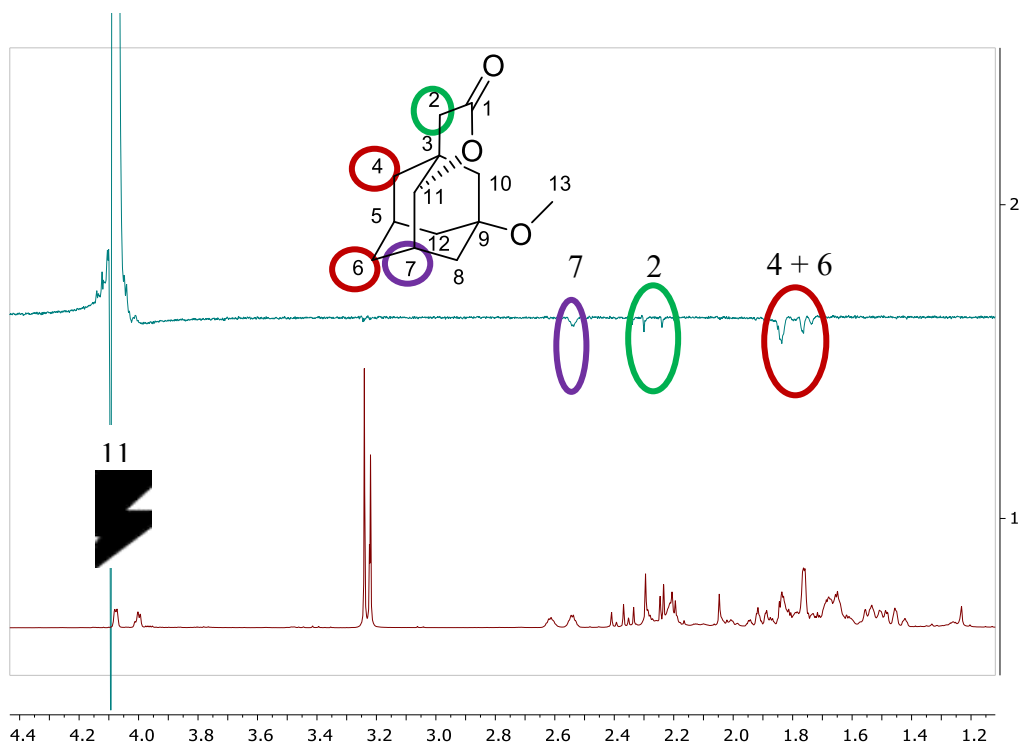
^{13}C NMR of **5c** (in roughly 1:1 mixture with **5b**) in CDCl_3



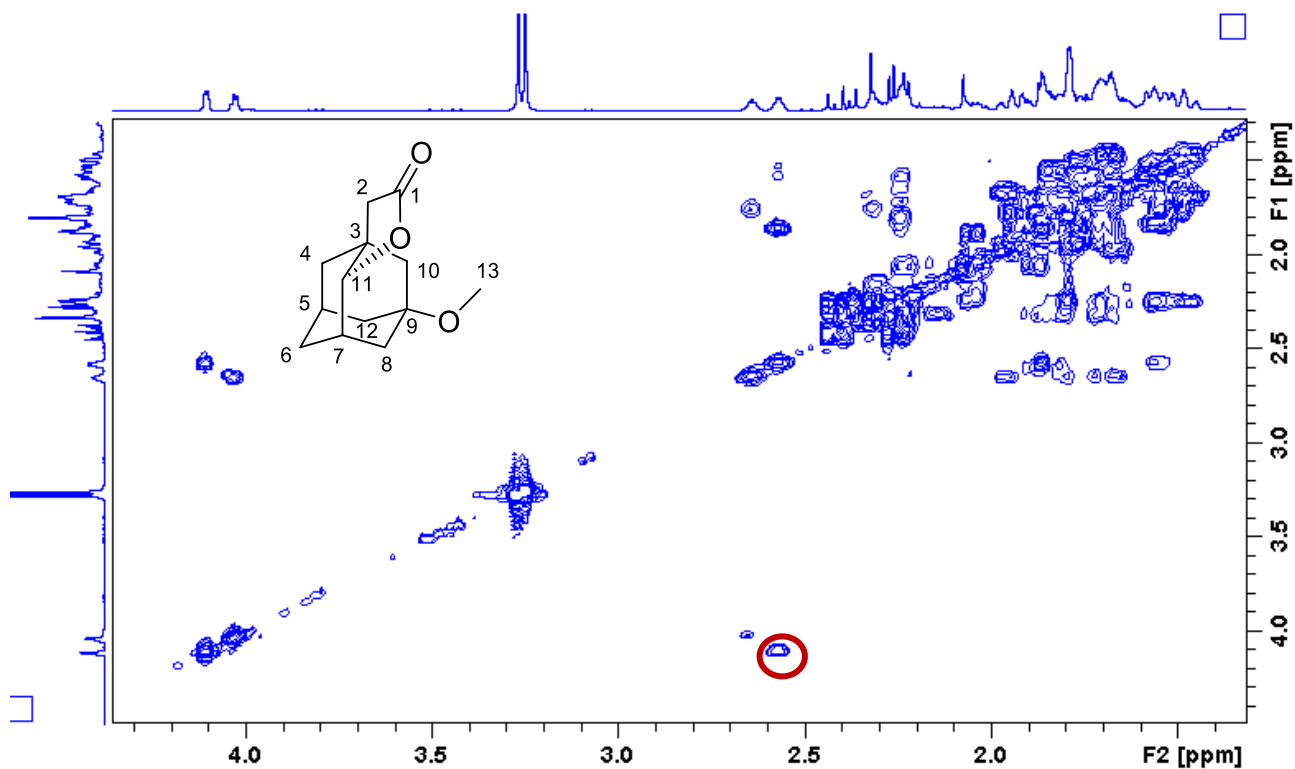
^{13}C NMR (101 MHz, CDCl_3) δ 177.2 (C_1 of **5c**), 176.6 (C_1 of **5b**), 85.8 (C_{11} of **5c**), 85.5 (C_4 of **5b**), 72.6 (C_{13} of **5b**), 71.0 (C_{13} of **5c**), 48.6, 48.3, 44.0, 43.6, 41.9, 40.5, 39.9, 39.4, 38.0, 35.9, 34.9, 32.6, 32.2, 30.8, 30.1, 28.1.



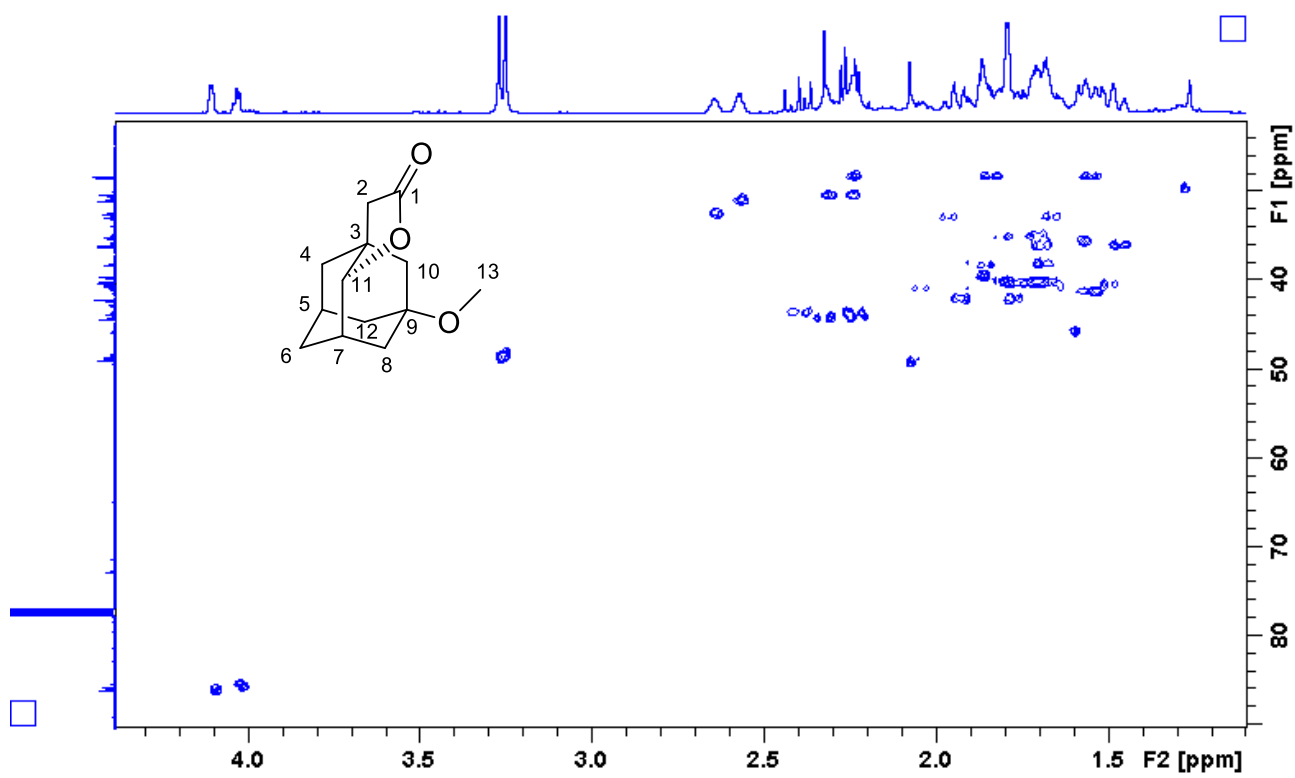
Stacking of the ^1H NMR spectrum of **5b** (bottom) with its selective NOESY obtained after irradiating at 3.98 δ (lactone signal, C_4 -H). The signals that show a NOESY correlation with C_4 -H are visible in a negative phase.



Stacking of the ^1H NMR spectrum of **5c** (bottom) with its selective NOESY obtained after irradiating at 4.07 δ (lactone signal, $\text{C}_{11}\text{-H}$). The signals that show a NOESY correlation with $\text{C}_{11}\text{-H}$ are visible in a negative phase.

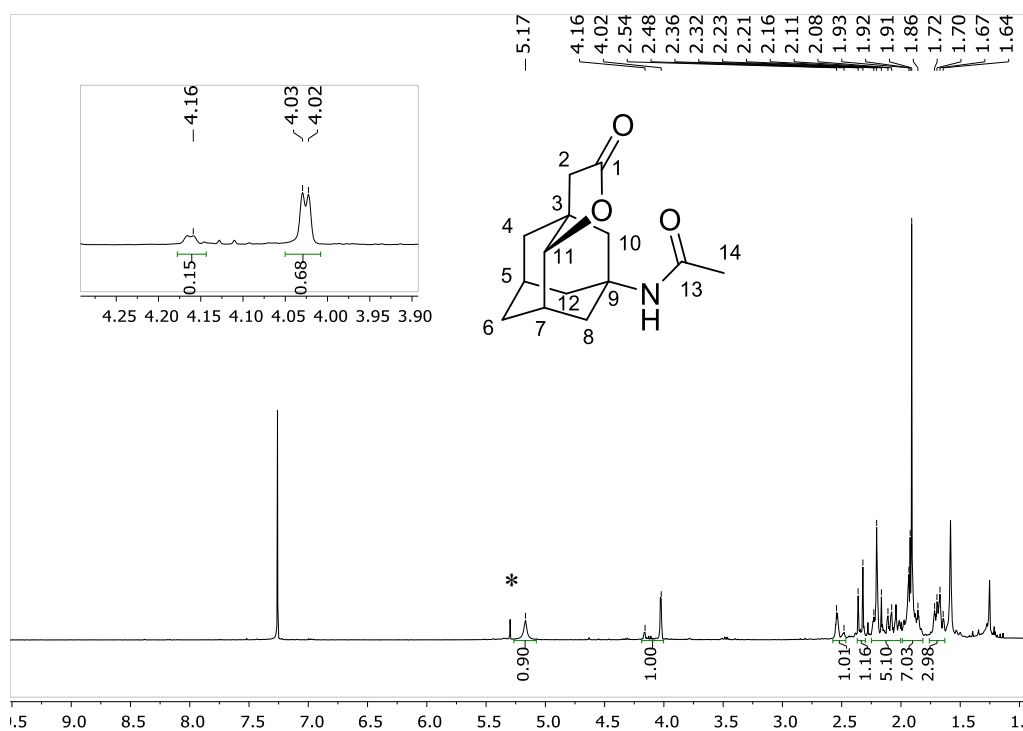


COSY of **5c** (in mixture with **5b**). Note the coupling of $\text{C}_{11}\text{-H}$ with tertiary $\text{C}_7\text{-H}$ bond (highlighted in red).



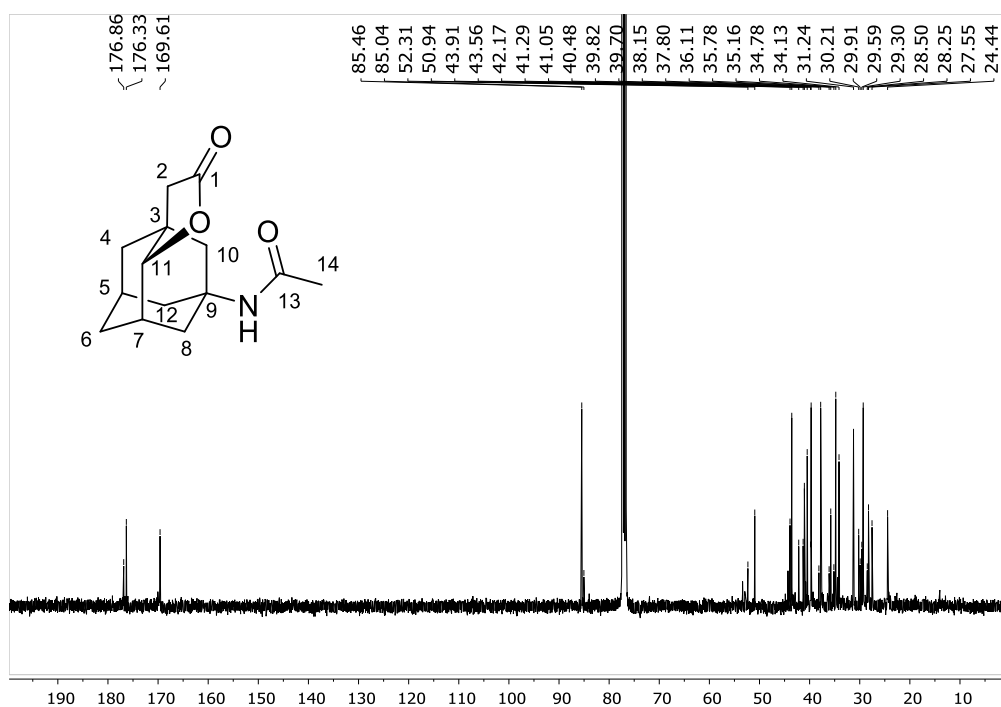
HSQC of **5c** (in mixture with **5b**).

^1H NMR of **6** oxidation in CDCl_3

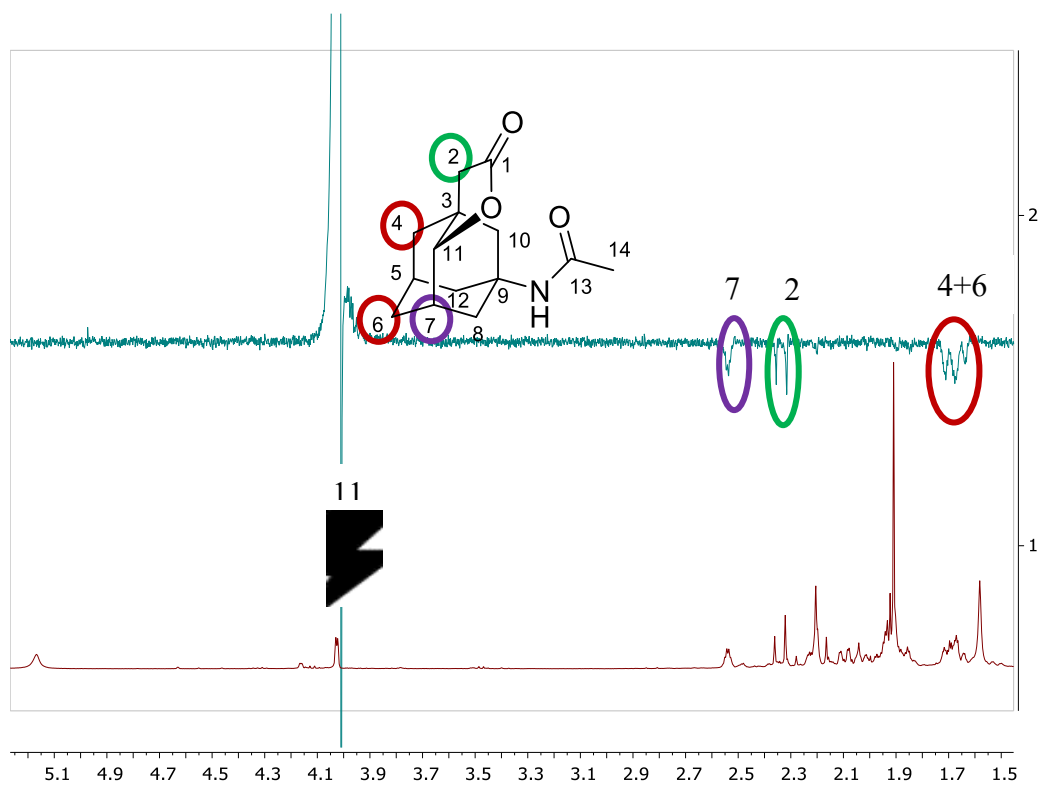


^1H NMR (400 MHz, CDCl_3) δ 5.17 (s, 1H, NH), 4.03 (d, $J = 2.8$ Hz, 1H, C_{11} [1H] *endo*), 2.51 (d, $J = 25.1$ Hz, 1H, C_7 [1H]), 2.34 (d, $J = 16.1$ Hz, 1H; C_2 [1H]), 2.25 – 2.00 (m, 5H; C_2 [1H] + C_5 [1H] + C_8 [1H] + C_{10} [2H]), 1.92 (d, $J = 5.3$ Hz, 7H, C_{14} [3H] + C_4 [1H] + C_6 [1H] + C_{12} [2H]), 1.76 – 1.63 (m, 3H; C_4 [1H] + C_6 [1H] + C_8 [1H]). In the inset an expansion with the proximal and distal lactones is displayed. Small peaks in the spectrum (i.e. at 2.55) are the signals of the distal isomers. The peak marked with an asterisk is CH_2Cl_2 .

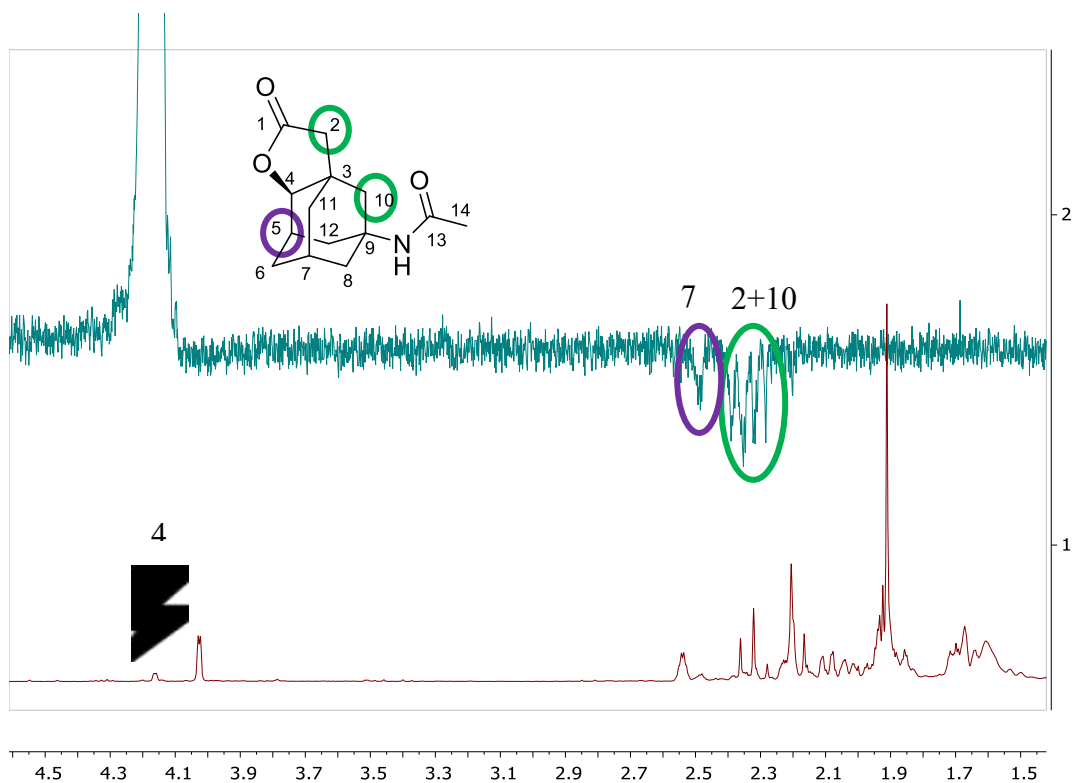
^{13}C NMR of **6** oxidation in CDCl_3



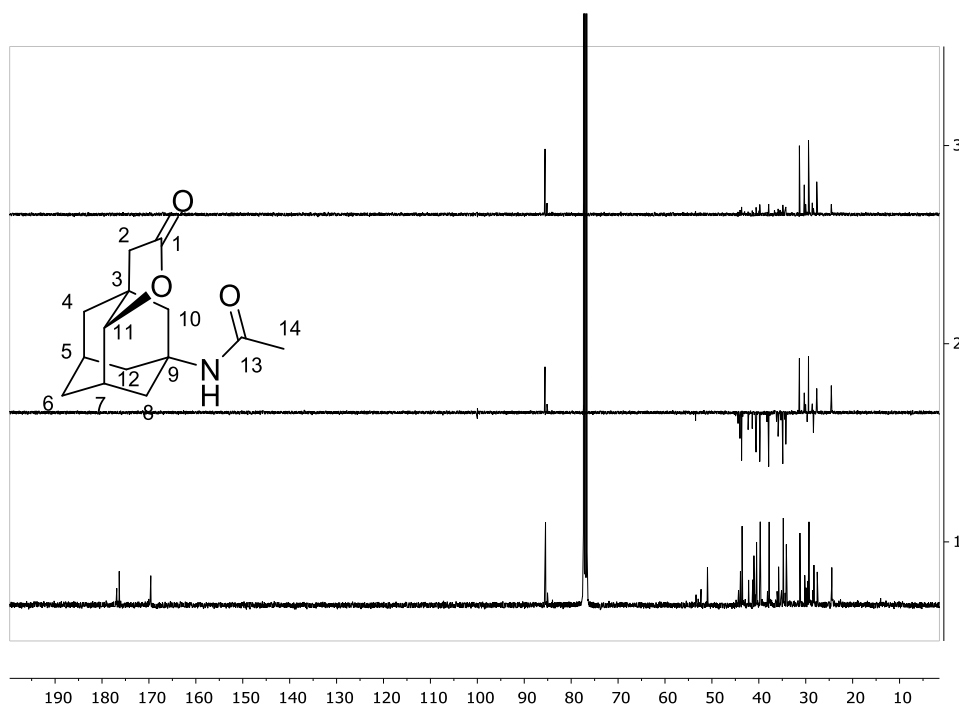
^{13}C NMR (101 MHz, CDCl_3) δ 176.9 (C_1 *exo*), 176.3 (C_1 *endo*), 169.6 (C_{13}), 85.5 (C_{11} *endo*), 85.0 (C_4 *exo*), 52.3, 50.9, 43.9, 43.6, 42.2, 41.3, 41.0, 40.5, 39.8, 39.7, 38.1, 37.8, 36.1, 35.8, 35.2, 34.8, 34.1, 31.2, 30.2, 29.9, 29.6, 29.3, 28.5, 28.2, 27.5, 24.4.



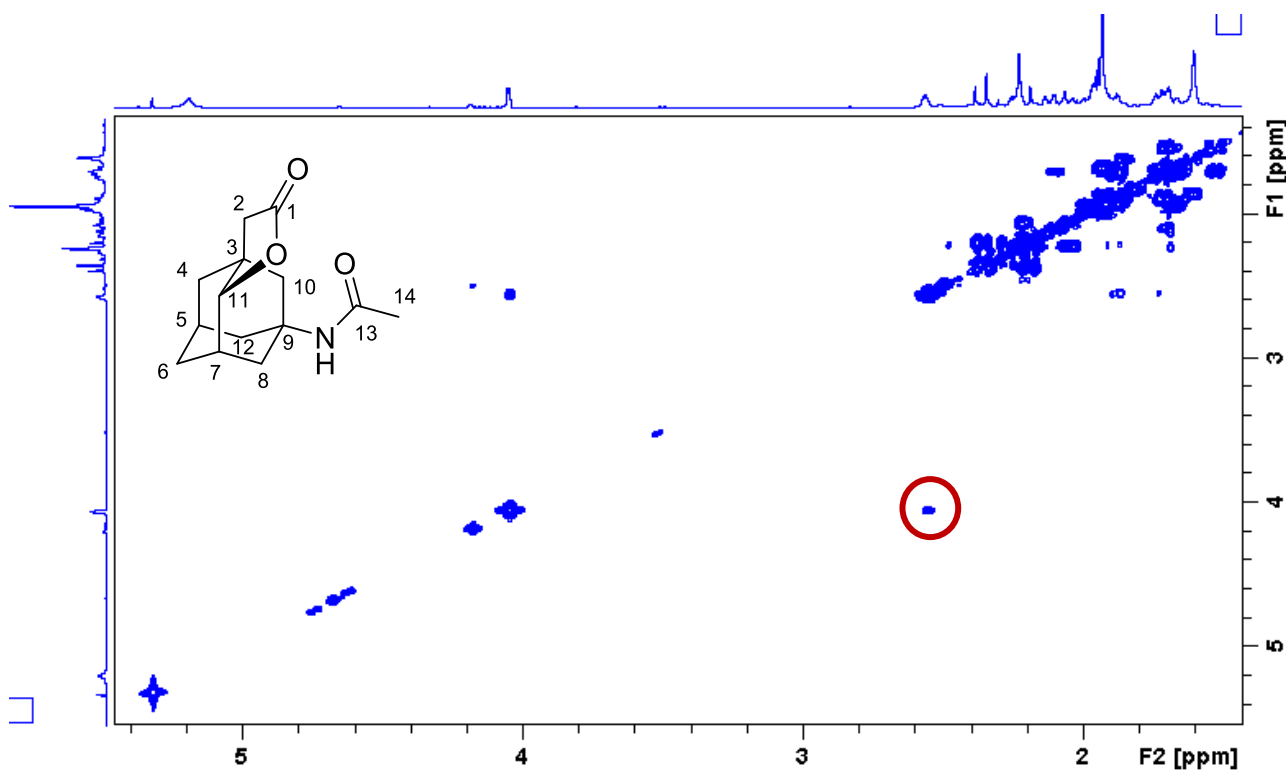
Stacking of the ^1H NMR spectrum of **6c** (bottom) with its selective NOESY obtained after irradiating at 4.02 δ (lactone signal, C_{11} -H). The signals that show a NOESY correlation with C_{11} -H are visible in a negative phase.



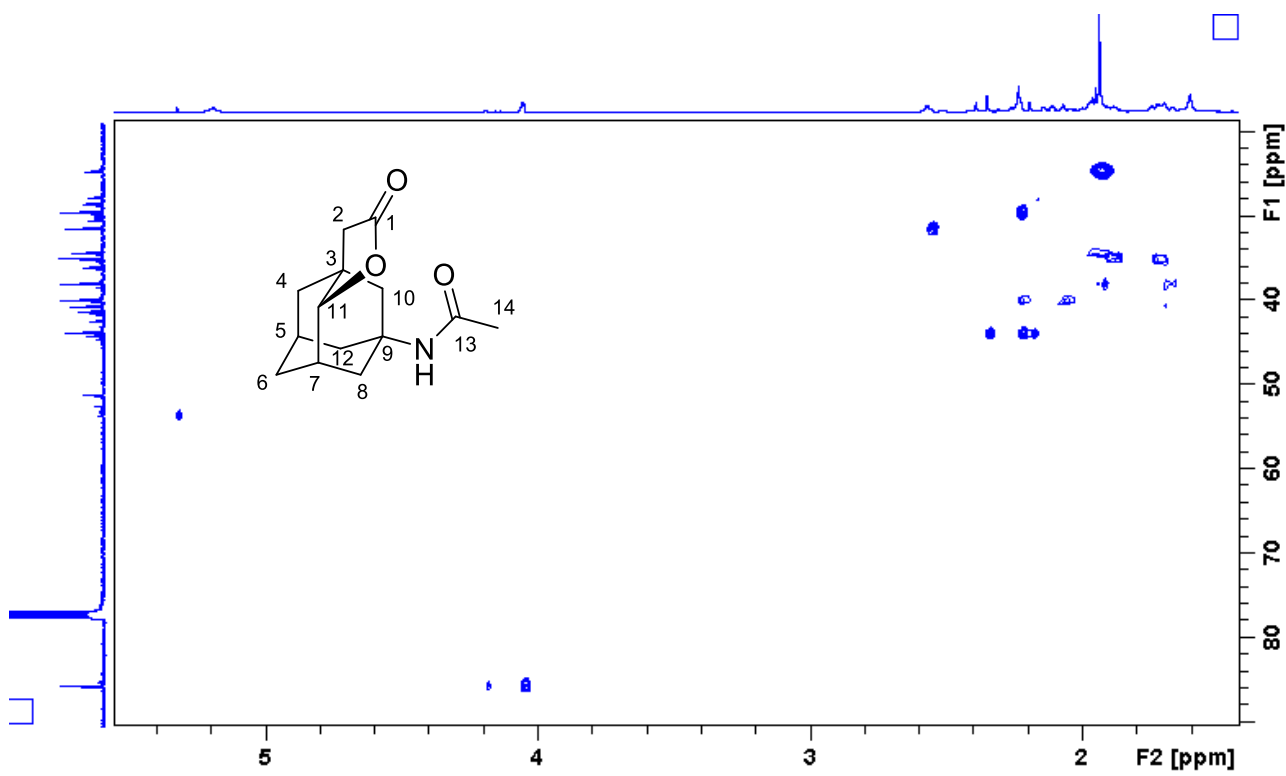
Stacking of the ^1H NMR spectrum of **6b** (bottom) with its selective NOESY obtained after irradiating at 4.16 δ (lactone signal, $\text{C}_4\text{-H}$). The signals that show a NOESY correlation with $\text{C}_4\text{-H}$ are visible in a negative phase. Due to the low amount of the *exo* isomer **6b**, not all the NOESY signals are detectable.



Stacking of the ^{13}C NMR spectrum of **6 oxidation** (bottom) stacked with its DEPT90 (top) and its DEPT 135 (middle) spectra.

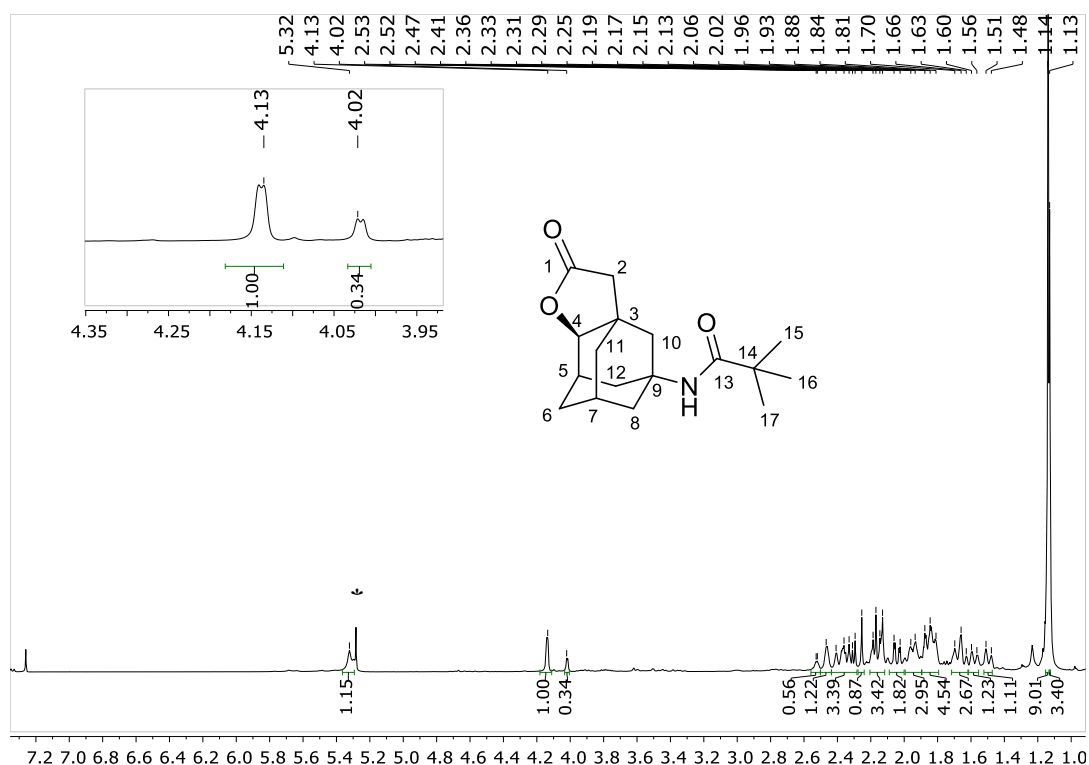


COSY of **6** oxidation. Note the coupling of lactone signal C₁₁-H with tertiary C₇-H bond (highlighted in red).



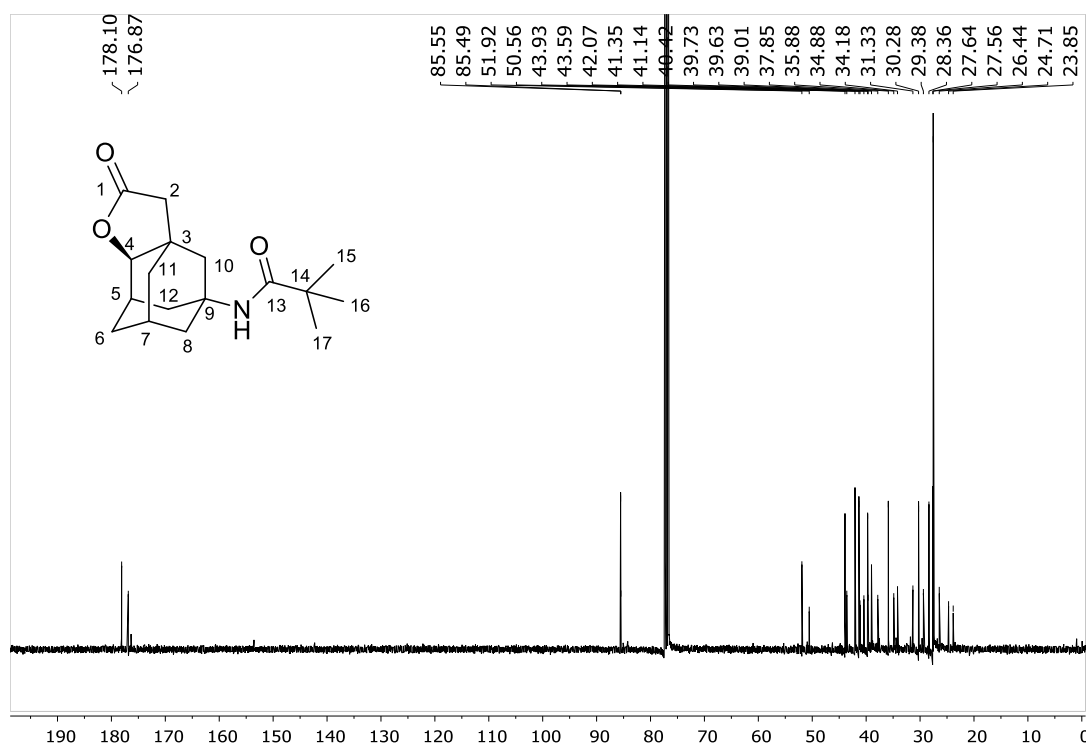
HSQC of **6** oxidation

¹H NMR of **7** oxidation in CDCl₃

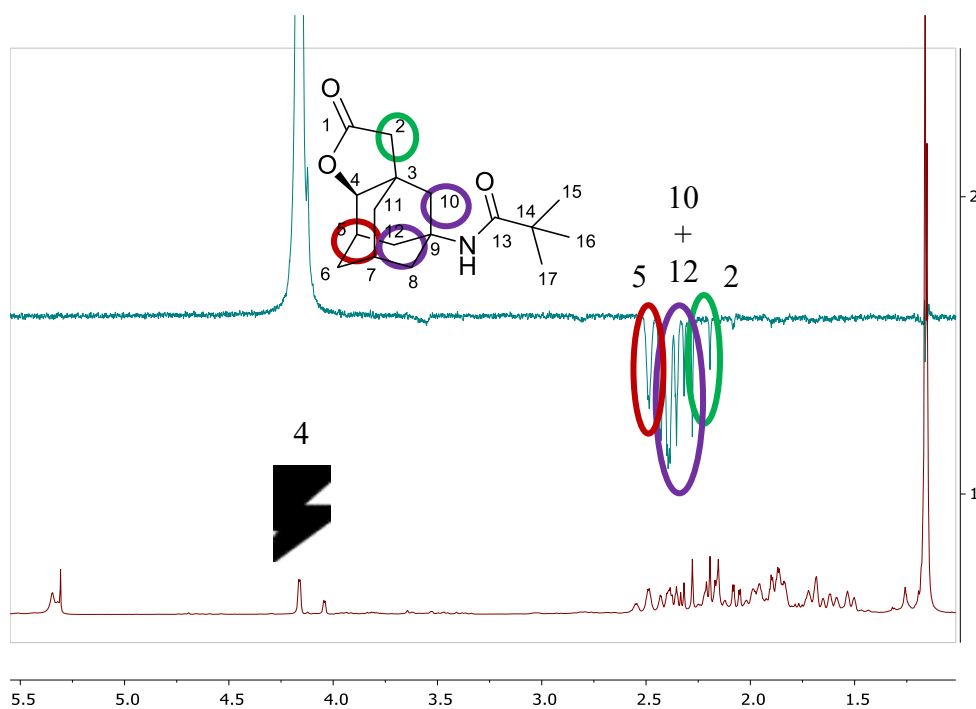


¹H NMR (400 MHz, CDCl₃) δ 5.32 (s, 1H, *NH*), 4.13 (s, 1H, *C4[H] exo*), 4.02 (s, 0.34H, *C11[H] endo*), 2.56 – 2.50 (m, 0.5H, *C7 [1H] endo*), 2.47 (s, 1H; *C5 [1H] exo*), 2.44 – 2.28 (m, 3H), 2.25 (s, 1H), 2.16 (m, 3H), 2.04 (m, 2H), 1.95 (m, 3H), 1.90 – 1.79 (m, 5H), 1.66 (m, 3H), 1.58 (m, 1H), 1.49 (m, 1H), 1.14 (s, 9H, *tBu exo*), 1.13 (s, 3H, *tBu endo*). In the expansion the lactone signals are displayed. It is a roughly 3:1 **7b**:**7c** mixture. The peak marked with an asterisk is CH₂Cl₂.

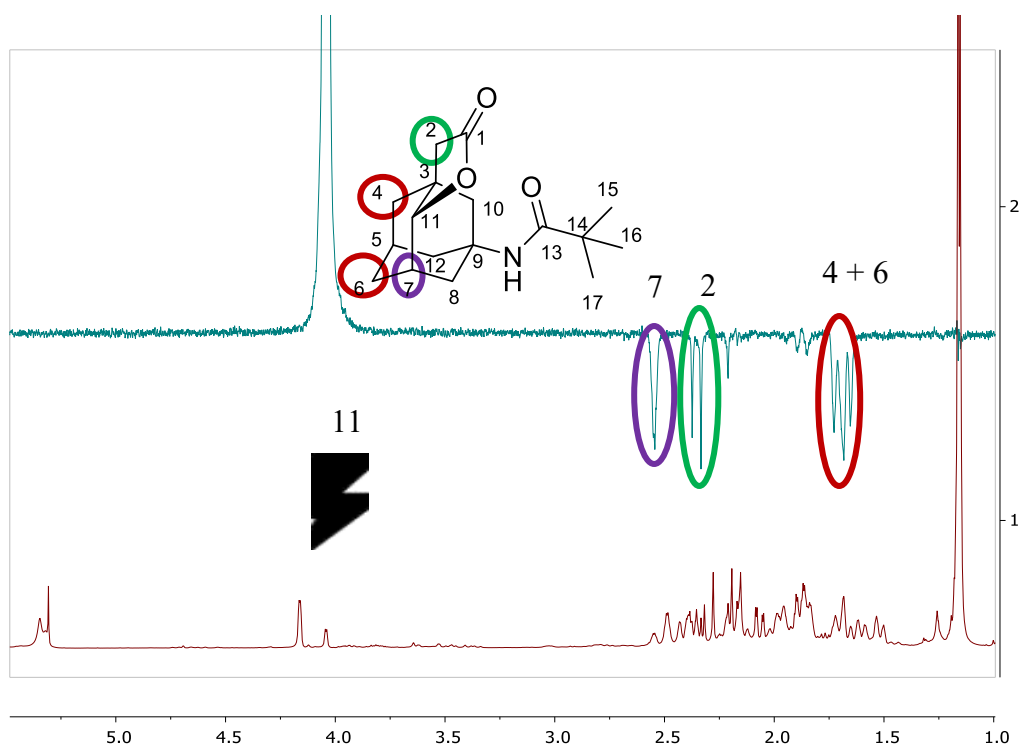
¹³C NMR of **7** oxidation (roughly 3:1 **7b**:**7c** mixture) in CDCl₃



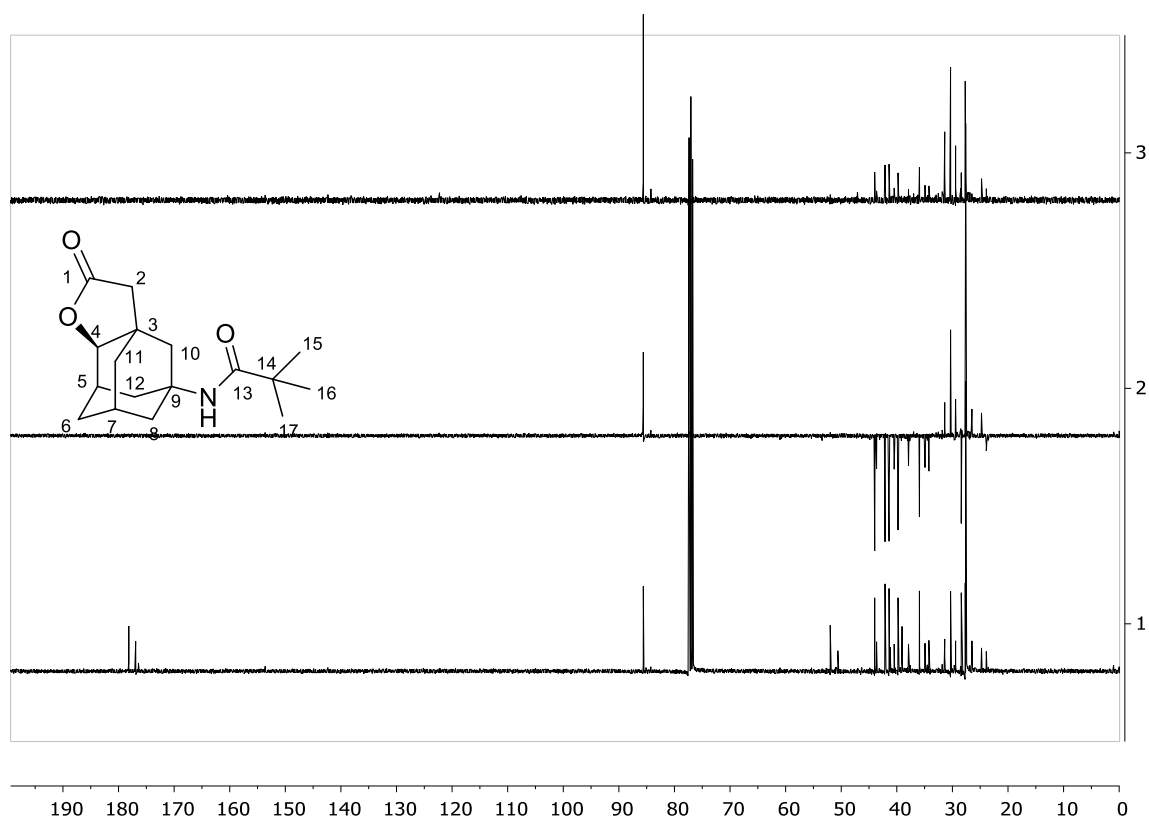
¹³C NMR (101 MHz, CDCl₃) δ 178.1, 176.9, 85.5 (*C*₄ *exo*), 85.5 (*C*₄ *endo*), 51.9, 50.6, 43.9, 43.6, 42.1, 41.3, 41.1, 40.4, 39.7, 39.6, 39.0, 37.8, 35.9, 34.9, 34.2, 31.3, 30.3, 29.4, 28.4, 27.6, 27.6, 26.4, 24.7 (*C*₁₅ + *C*₁₆ + *C*₁₇ *endo*), 23.8 (*C*₁₅ + *C*₁₆ + *C*₁₇ *exo*).



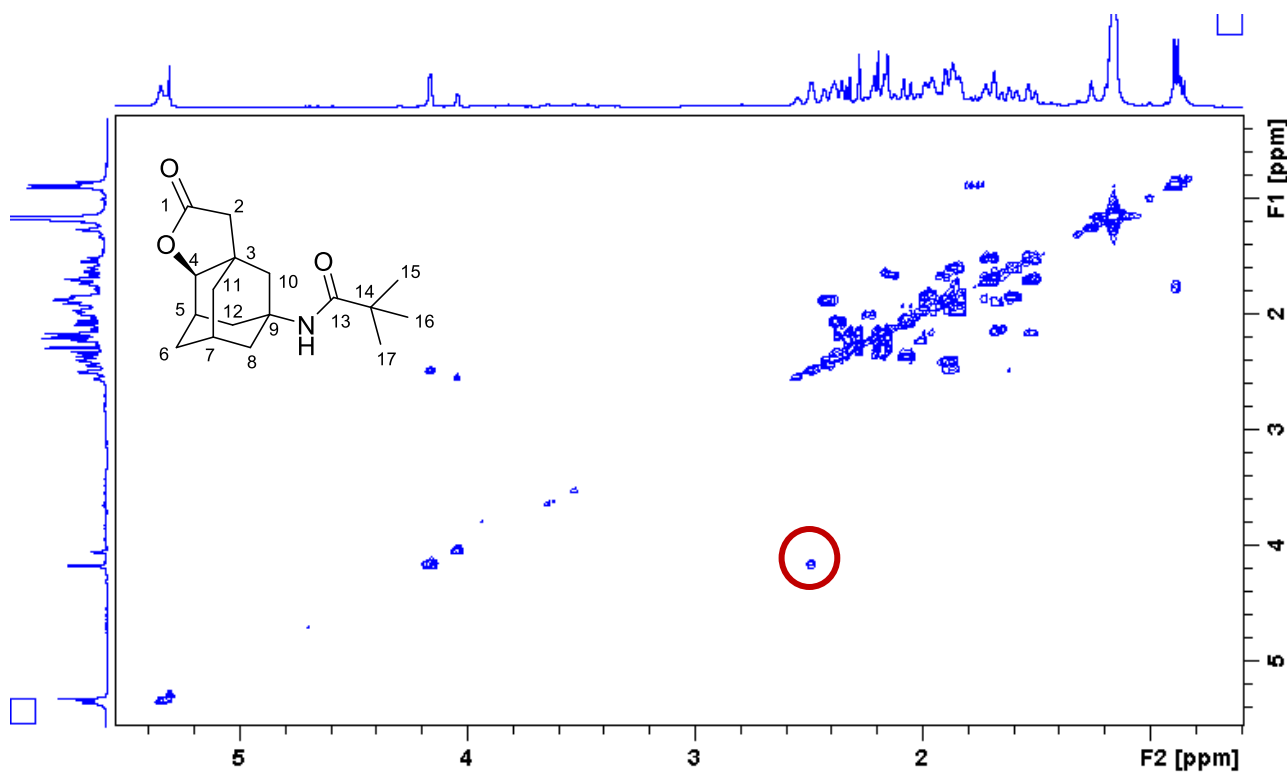
Stacking of the ¹H NMR spectrum of **7b** (bottom) with its selective NOESY obtained after irradiating at 4.13 δ (lactone signal, *C*₄-H). The signals that show a NOESY correlation with *C*₄-H are visible in a negative phase.



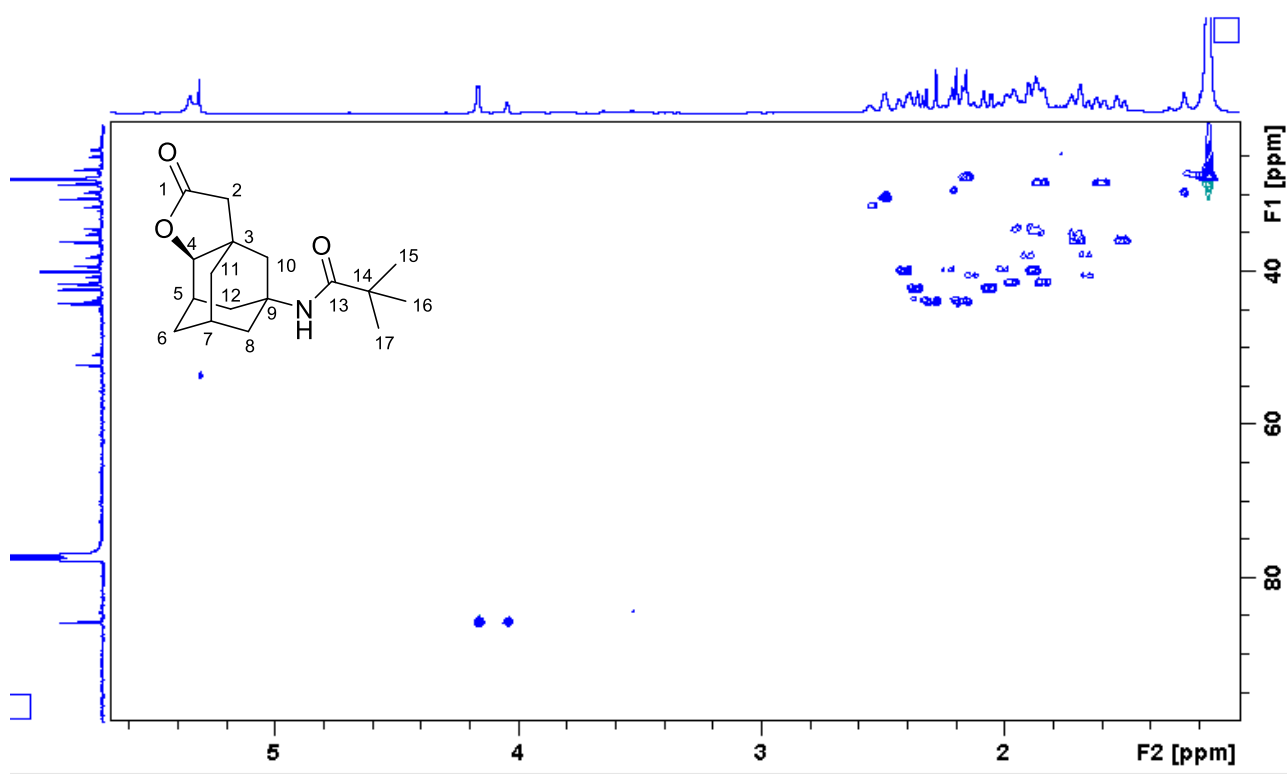
Stacking of the ^1H NMR spectrum of **7c** (bottom) with its selective NOESY obtained after irradiating at 4.02 δ (lactone signal, C₁₁-H). The signals that show a NOESY correlation with C₁₁-H are visible in a negative phase.



Stacking of the ^{13}C NMR spectrum of **7 oxidation** (bottom) stacked with its DEPT90 (top) and its DEPT 135 (middle) spectra.



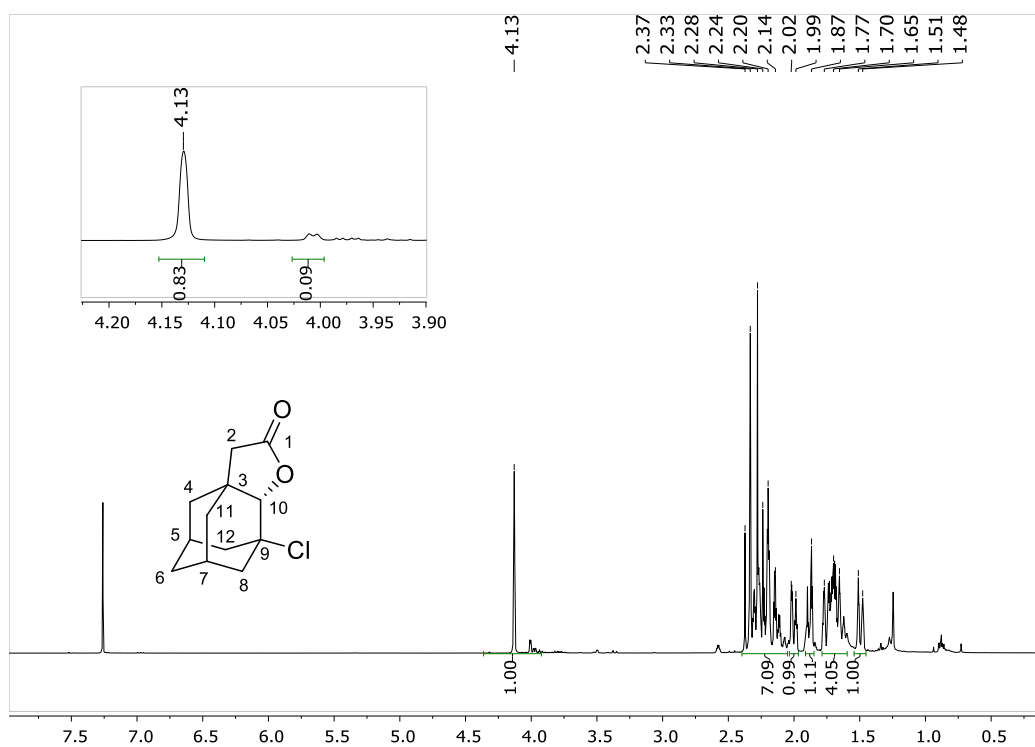
COSY of 7 oxidation. Note the coupling of the main lactone product **6b** signal C₄-H with tertiary C₅-H bond (highlighted in red).



HSQC of 7 oxidation

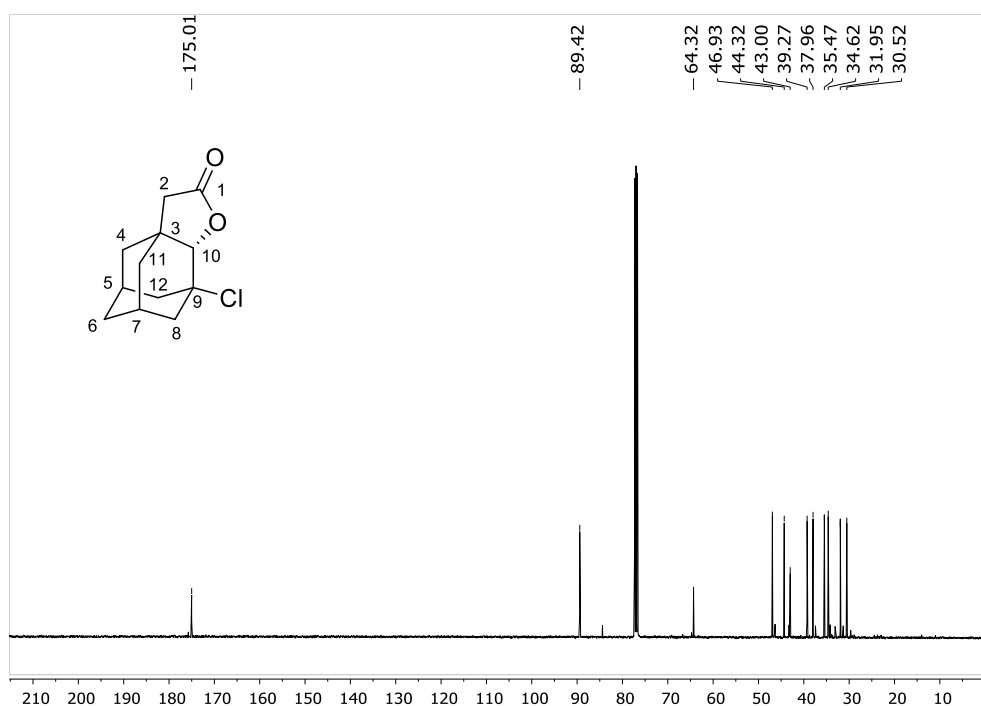
Products of acetate-adamantane acetic acid **8** oxidation (**8a**, **8b** and **8c**) have been identified by comparison of their GC retention times with samples of **8a**, **8b** and **8c** obtained by acetylation of **4a**, **4b** and **4c** (in turn obtained by separation of the products derived by **4** oxidation).

^1H NMR of **9a** in CDCl_3

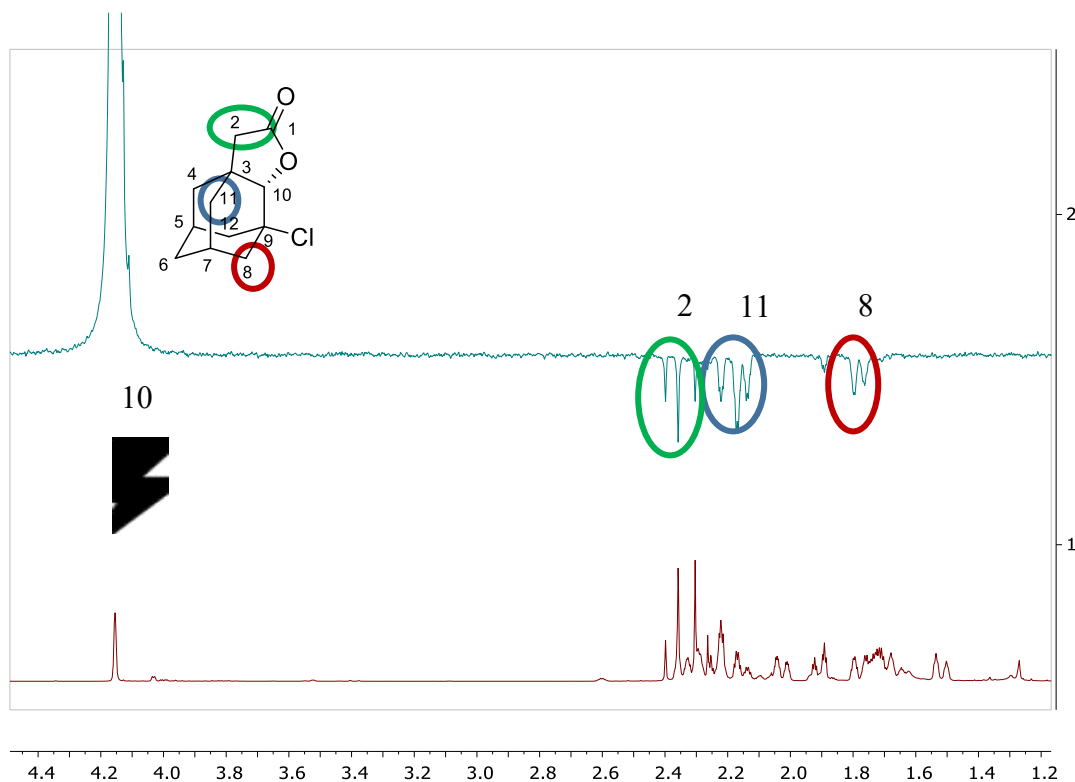


^1H NMR (400 MHz, CDCl_3) δ 4.13 (s, 1H, C_{10} [1H]), 2.40 – 2.05 (m, 7H; C_2 [2H] + C_5 [1H] + C_7 [1H] + C_4 [2H] + C_{12} [1H]), 2.00 (d, $J = 14.2$ Hz, 1H; C_{12} [1H]), 1.87 (s, 1H, C_8 [1H]), 1.79 – 1.60 (m, 4H; C_{11} [1H] + C_8 [1H] + C_6 [2H]), 1.49 (d, $J = 13.2$ Hz, 1H; C_{11} [1H]). In the expansion an enlargement of the lactone signal (with 10% of **9b**) is displayed.

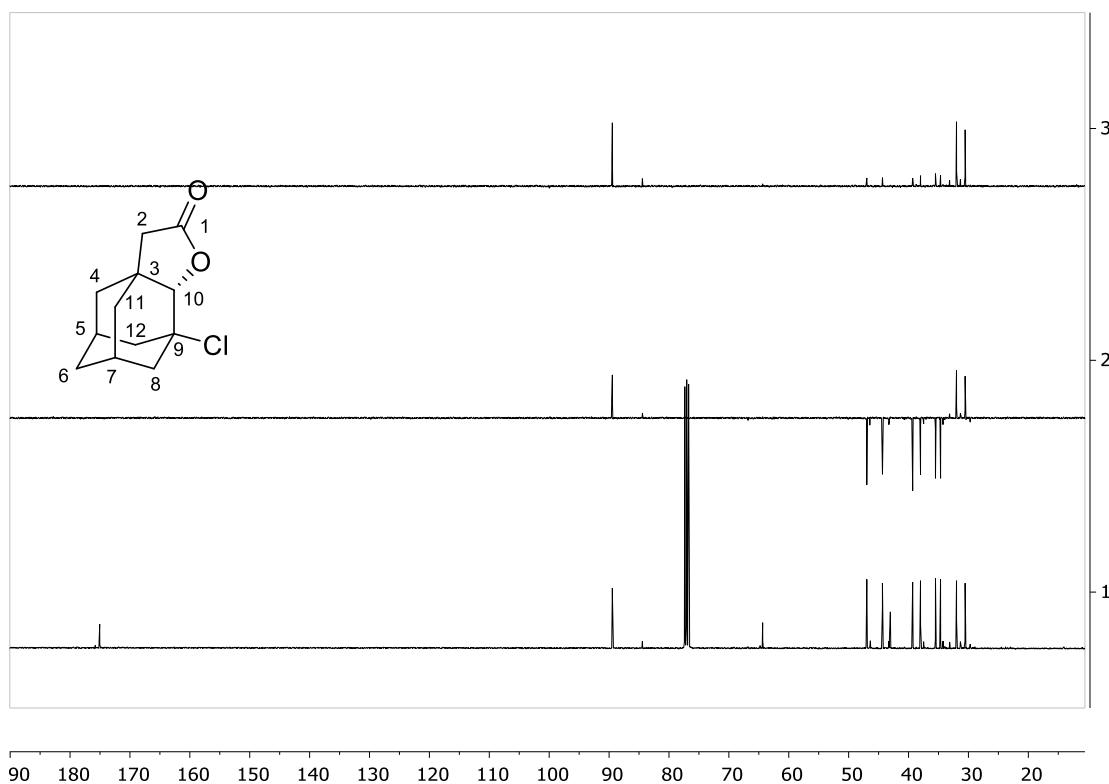
^{13}C NMR of **9a**



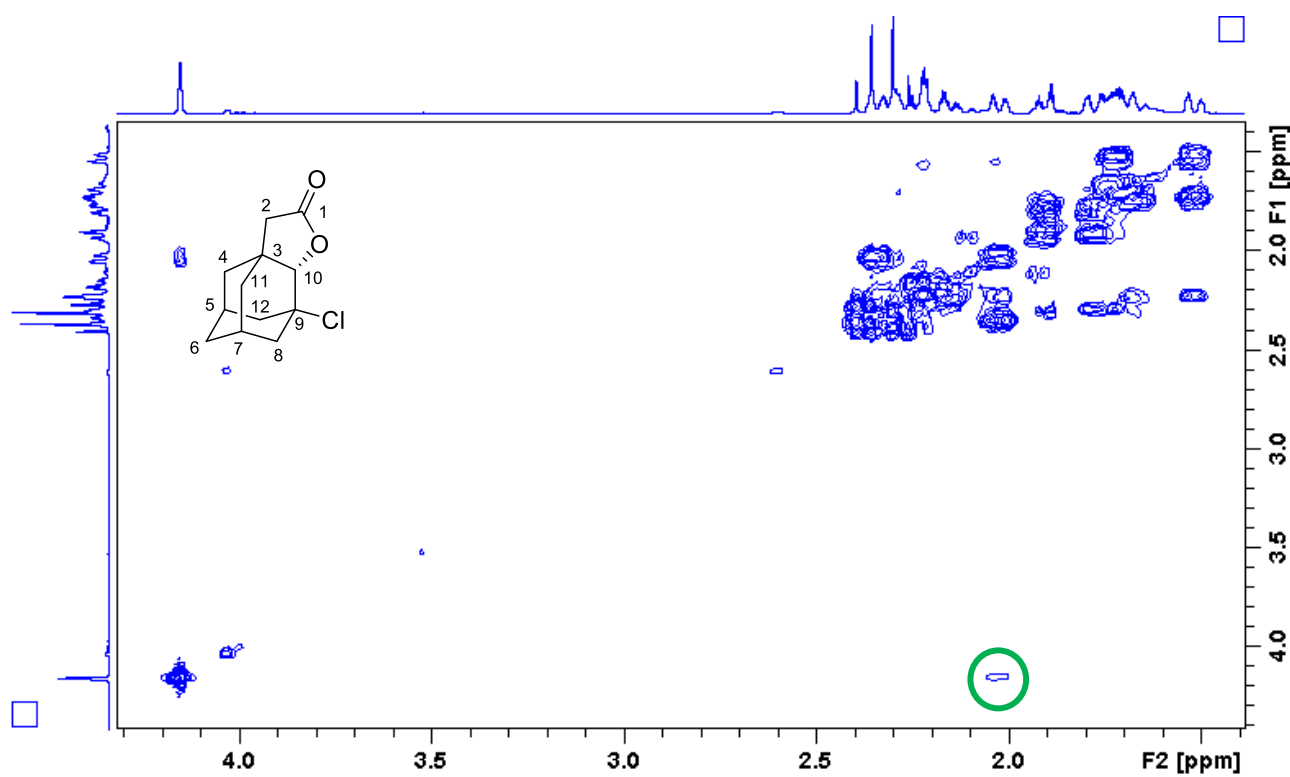
^{13}C NMR (101 MHz, CDCl_3) δ 175.0 (C1), 89.4 (C10), 64.3 (C9), 46.9 (C4), 44.3 (C2), 43.0 (C3), 39.3 (C8 or C12), 38.0 (C8 or C12), 35.5 (C11), 34.6 (C6), 31.9 (C5 or C7), 30.5 (C5 or C7). The small signals (i.e. close to C10, 85 ppm) are of isomer **9b**.



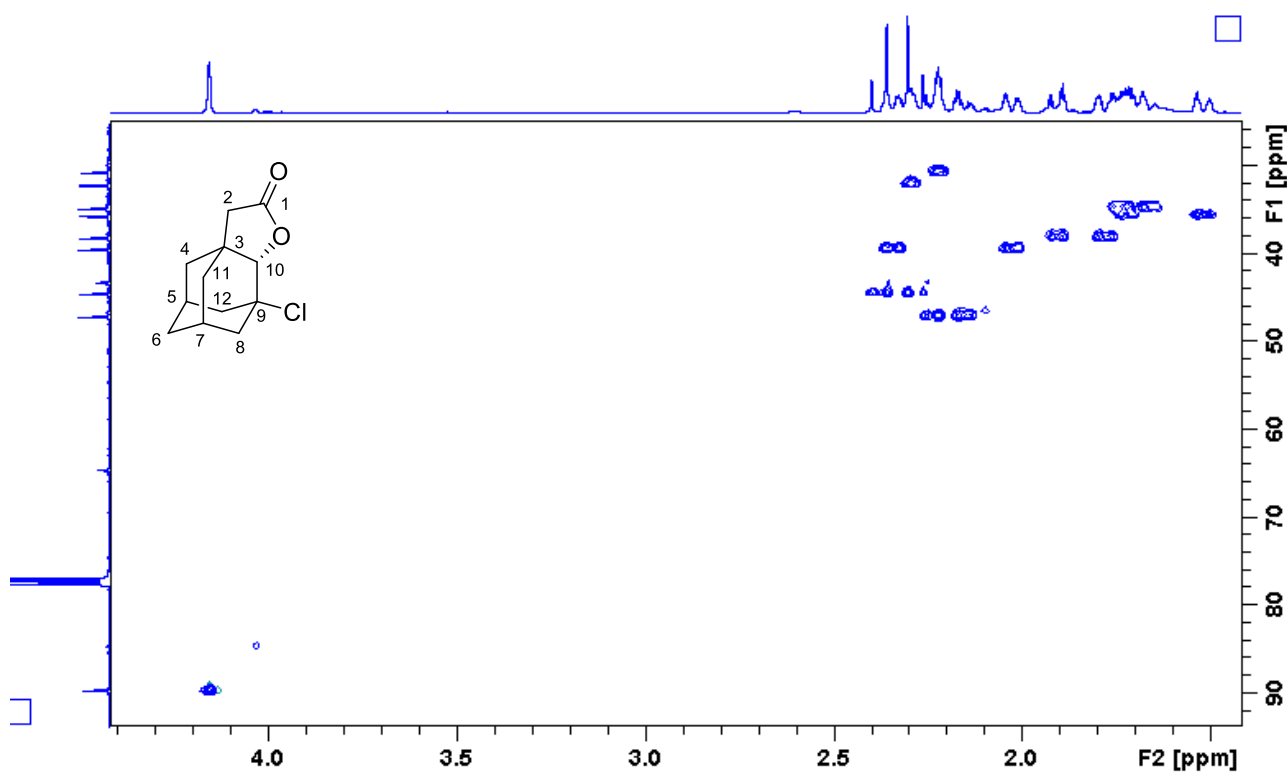
Stacking of the ^1H NMR spectrum of **9a** (bottom) with its selective NOESY obtained after irradiating at 4.13 δ (lactone signal, $\text{C}_{10}\text{-H}$). The signals that show a NOESY correlation with $\text{C}_{10}\text{-H}$ are visible in a negative phase.



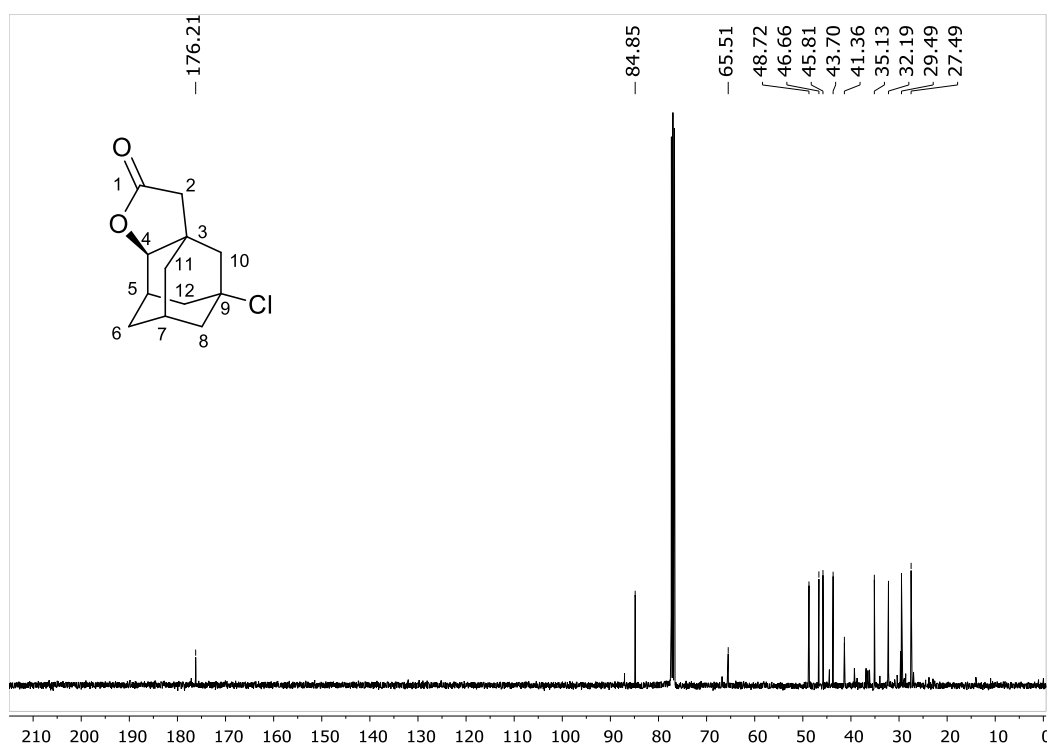
Stacking of the ^{13}C NMR spectrum of **9a** (bottom) stacked with its DEPT90 (top) and its DEPT 135 (middle) spectra.



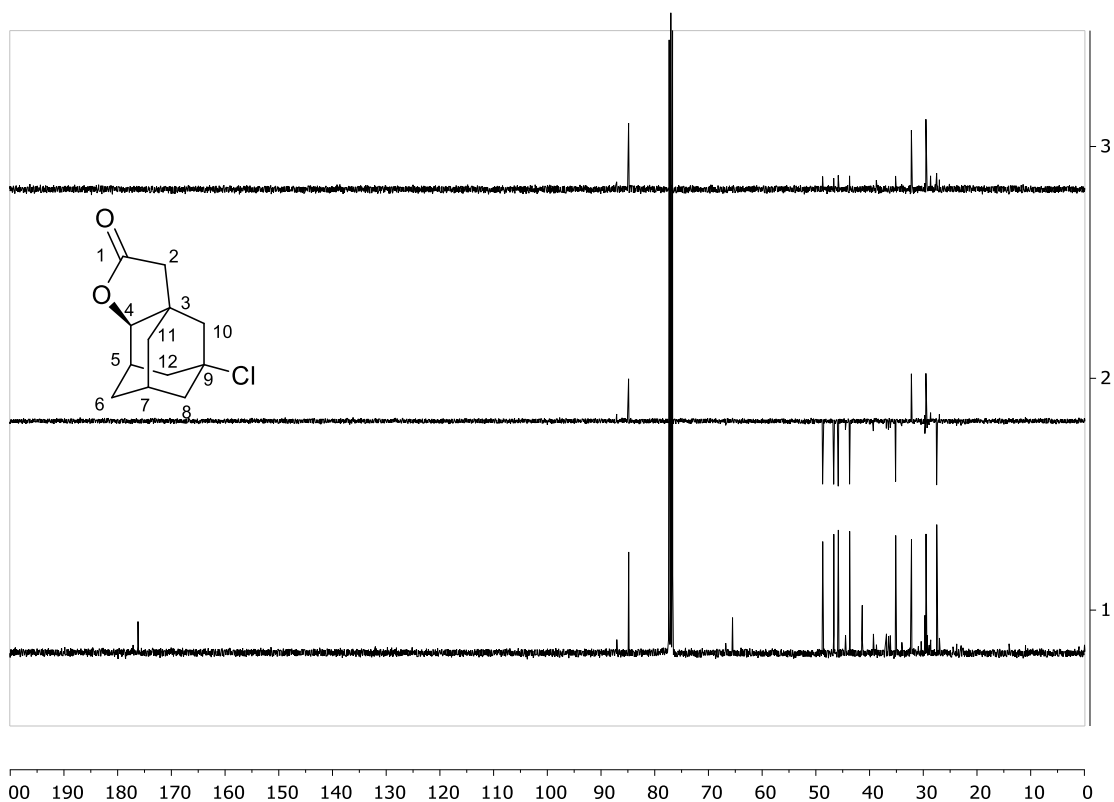
COSY of **9a**. Note the coupling of lactone signal $\text{C}_{10}\text{-H}$ with secondary $\text{C}_8\text{-H}$ (highlighted in green).



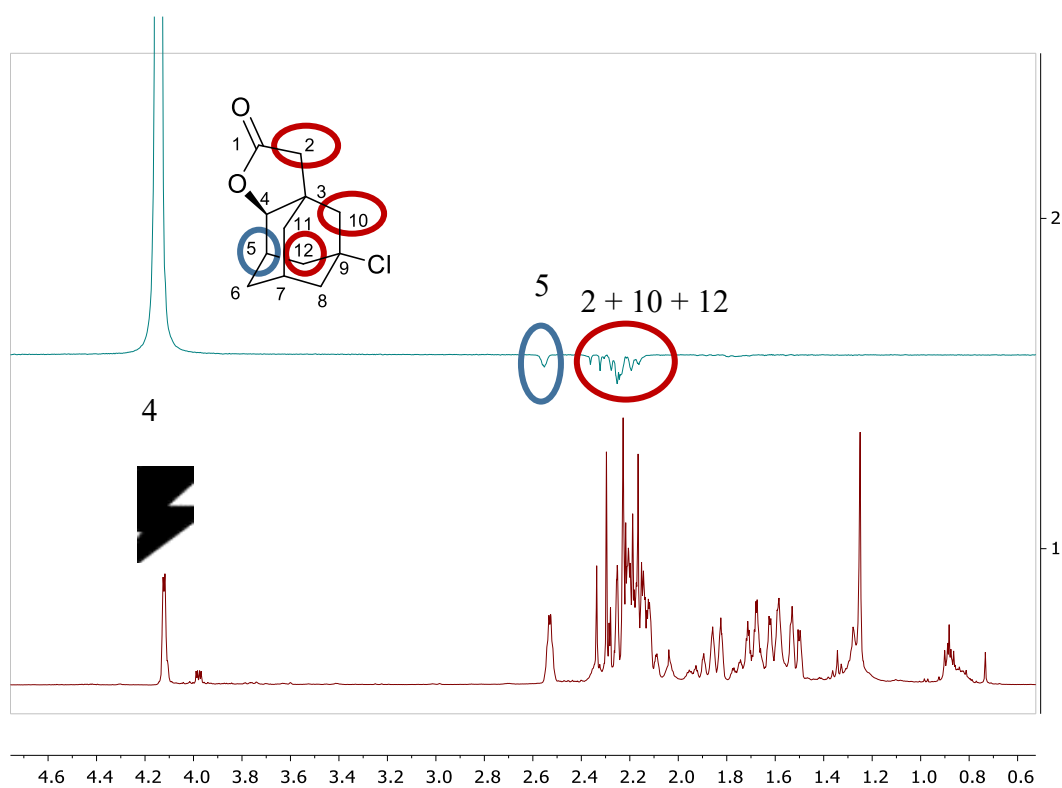
¹³C NMR of **9b** in CDCl₃



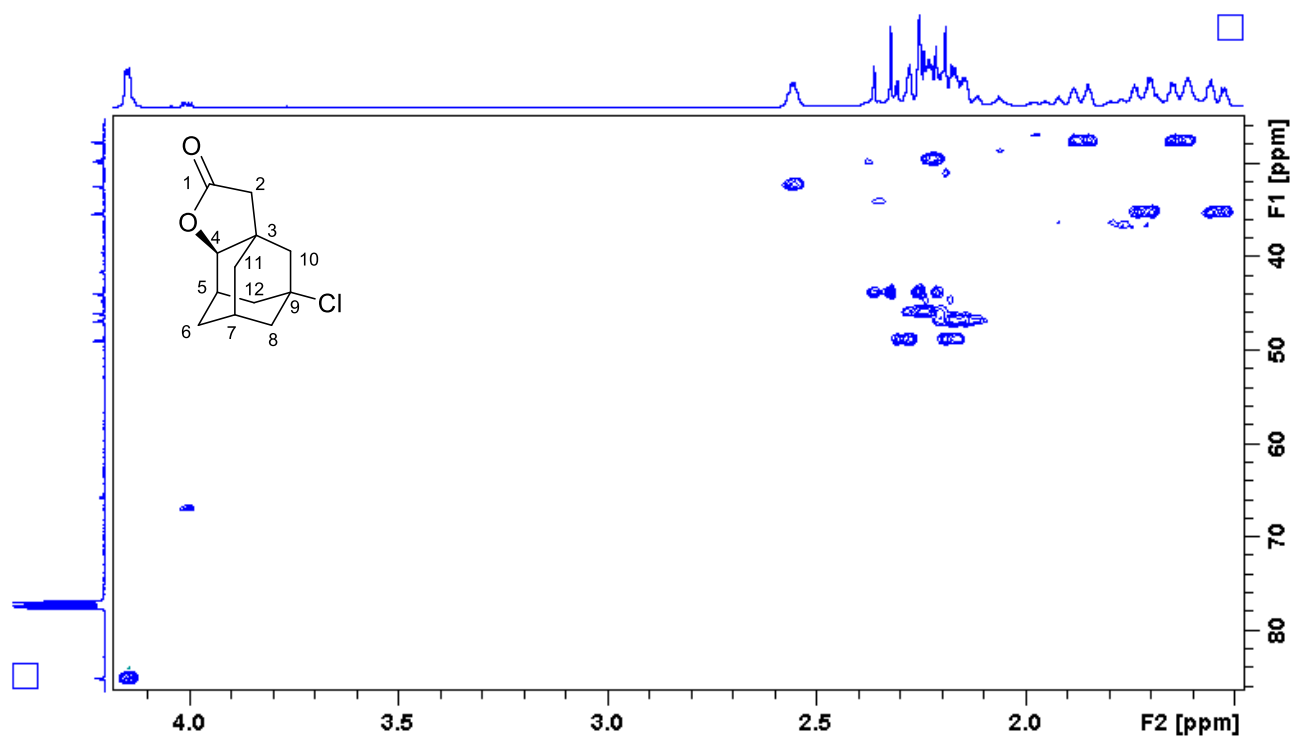
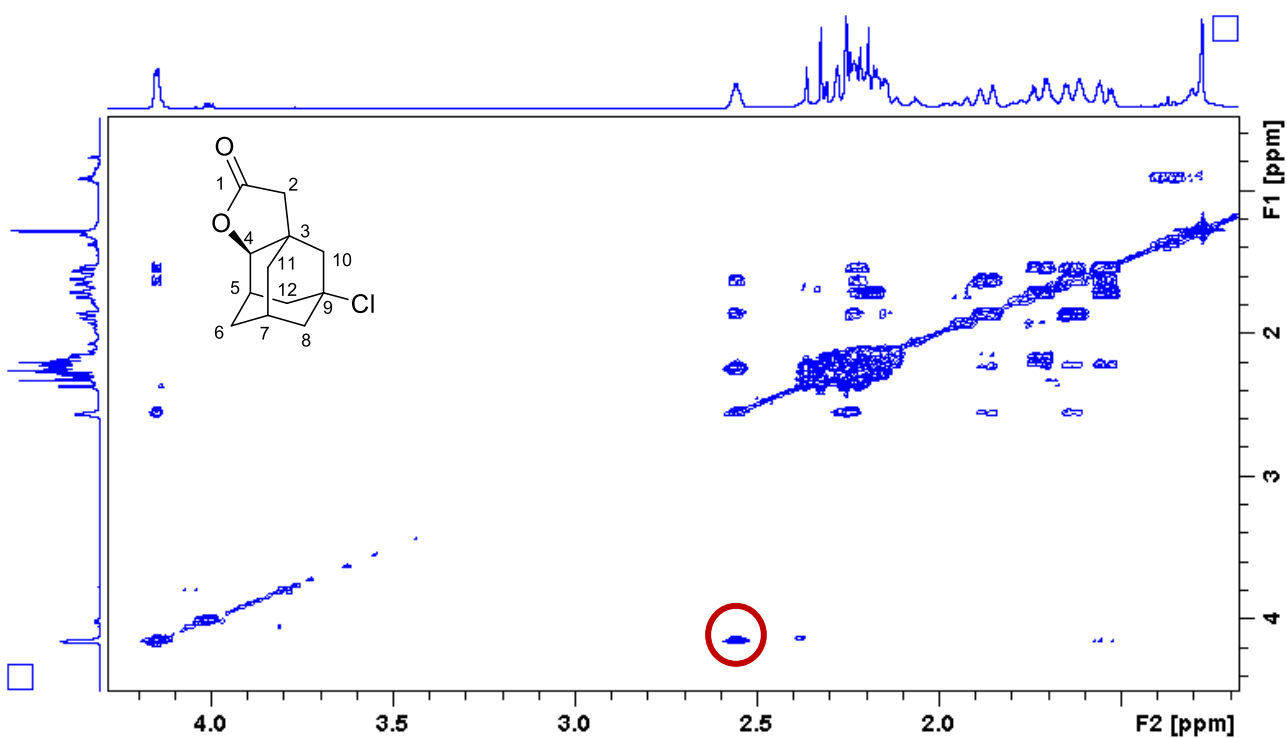
¹³C NMR (101 MHz, CDCl₃) δ : 176.2 (*C*₁), 84.8 (*C*₄), 65.5 (*C*₉), 48.7 (*C*₁₂), 46.7 (*C*₁₀), 45.8 (*C*₈), 43.7 (*C*₂), 41.4 (*C*₃), 35.1 (*C*₁₁), 32.2 (*C*₅), 29.5 (*C*₇), 27.5 (*C*₆). A small amount of **9c** (12%) accounts for the small peaks visible in the spectrum



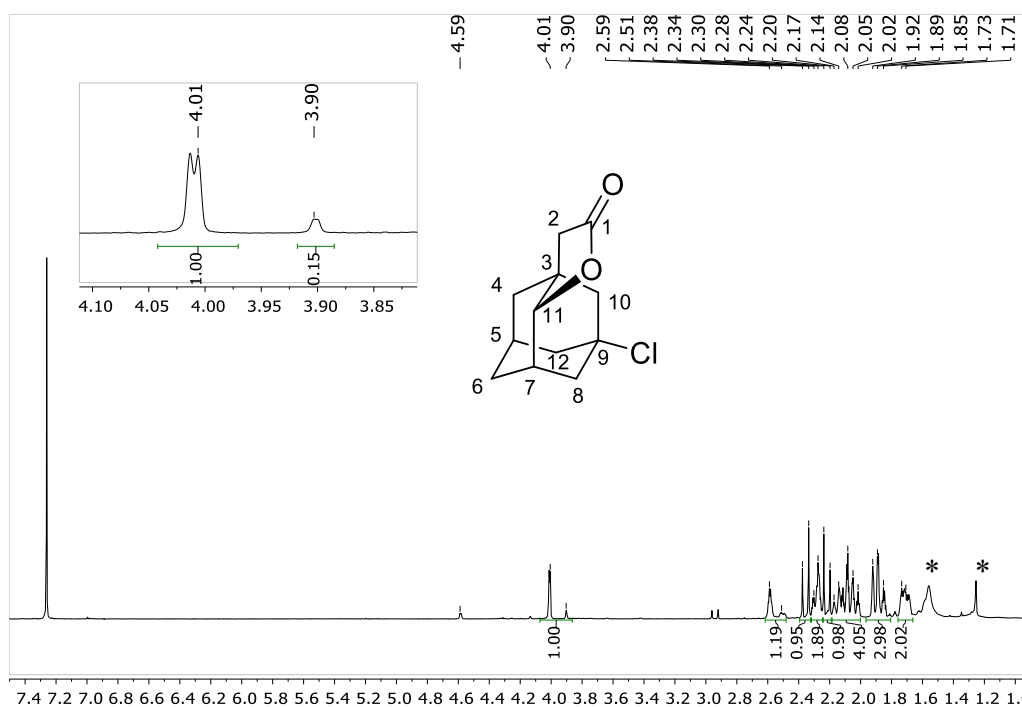
Stacking of the ^{13}C NMR spectrum of **9b** (bottom) stacked with its DEPT90 (top) and its DEPT 135 (middle) spectra.



Stacking of the ^1H NMR spectrum of **9b** (bottom) with its selective NOESY obtained after irradiating at $4.12\ \delta$ (lactone signal, $\text{C}_4\text{-H}$). The signals that show a NOESY correlation with $\text{C}_4\text{-H}$ are visible in a negative phase.

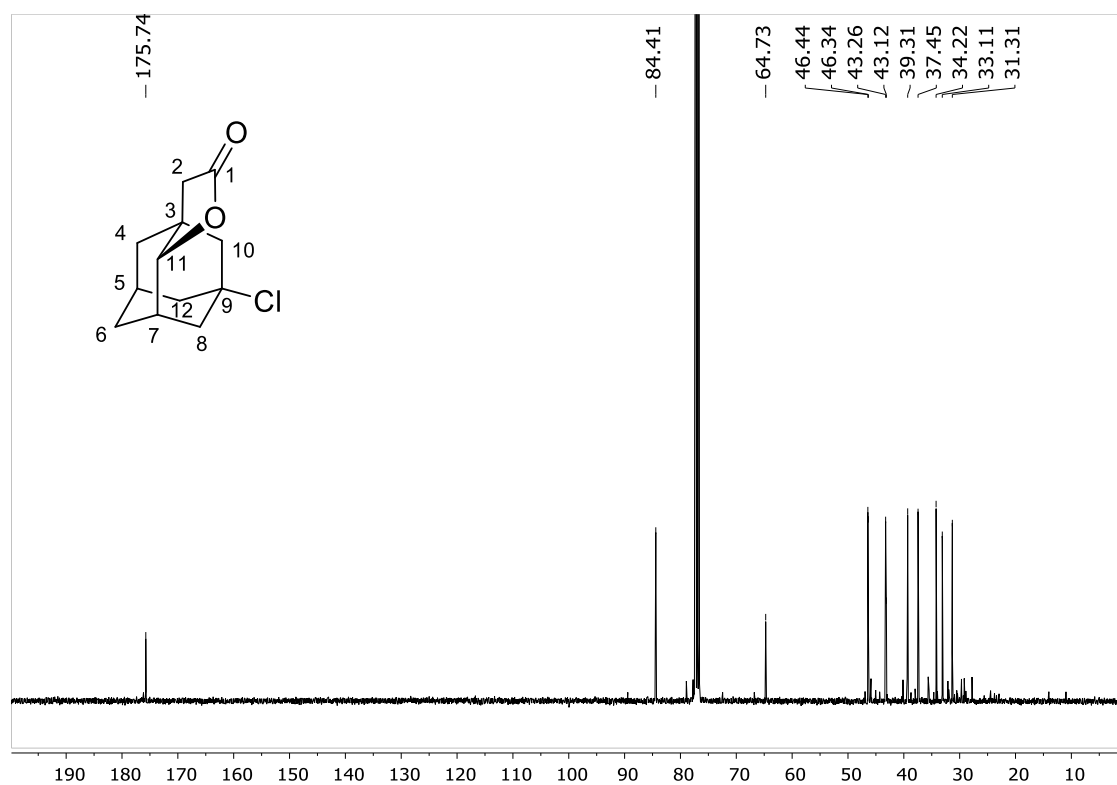


^1H NMR of **9c** in CDCl_3

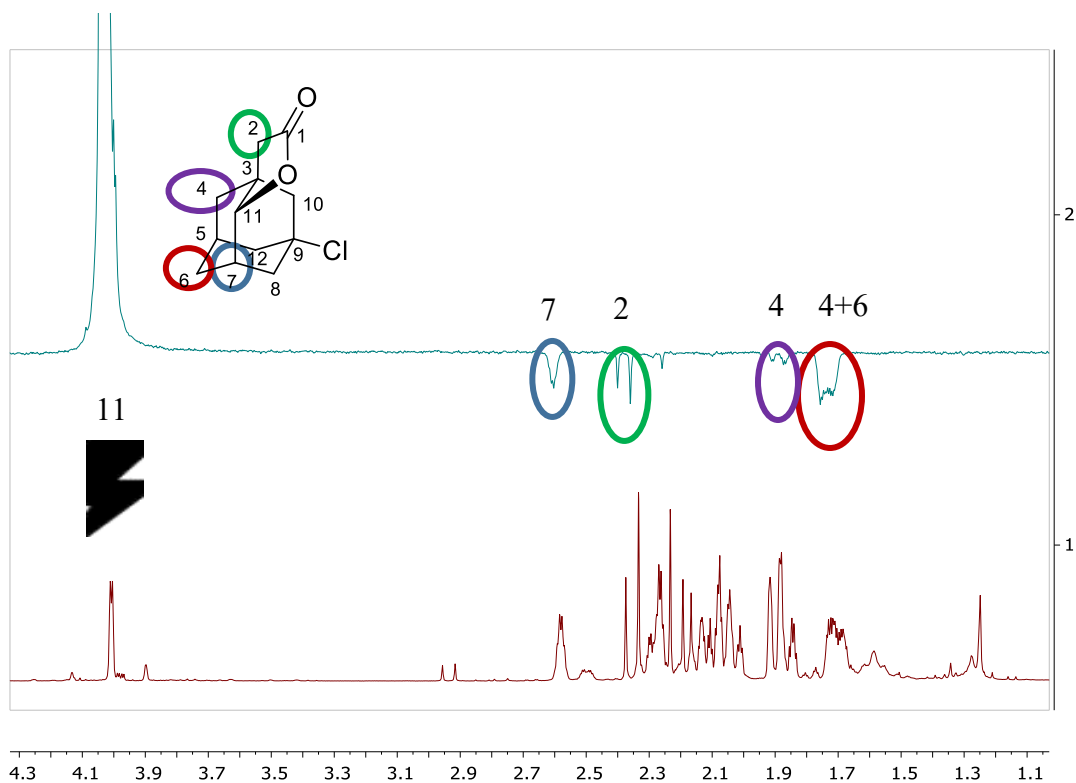


^1H NMR (400 MHz, CDCl_3) δ 4.00 (s, 1H; $\text{C}_{11}[1\text{H}]$), 2.58 (s, 1H; $\text{C}_7[1\text{H}]$), 2.36 (d, $J = 16.2$ Hz, 1H; $\text{C}_2[1\text{H}]$), 2.26 (m, 2H; $\text{C}_5[1\text{H}] + \text{C}_8[1\text{H}]$), 2.21 (d, $J = 16.1$ Hz, 1H; $\text{C}_2[1\text{H}]$), 2.17 – 2.01 (m, 5H; $\text{C}_{12}[2\text{H}] + \text{C}_{10}[1\text{H}] + \text{C}_8[1\text{H}]$), 1.86 (m, $J = 15.1$ Hz, 3H; $\text{C}_6[1\text{H}] + \text{C}_4[1\text{H}] + \text{C}_{10}[1\text{H}]$), 1.72 (m, 2H; $\text{C}_6[1\text{H}] + \text{C}_4[1\text{H}]$). The peak marked with asterisks are water and acetone. A small amount of **9b** (15%) accounts the small peaks visible in the spectrum.

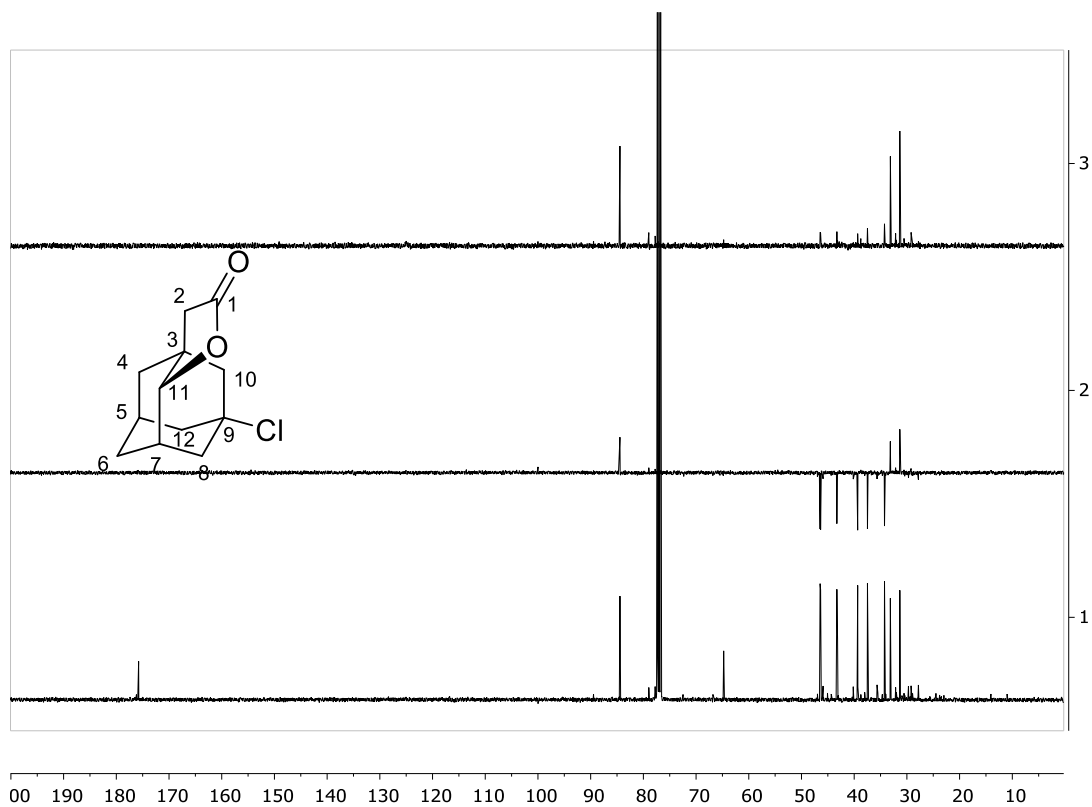
^{13}C NMR of **9c** in CDCl_3



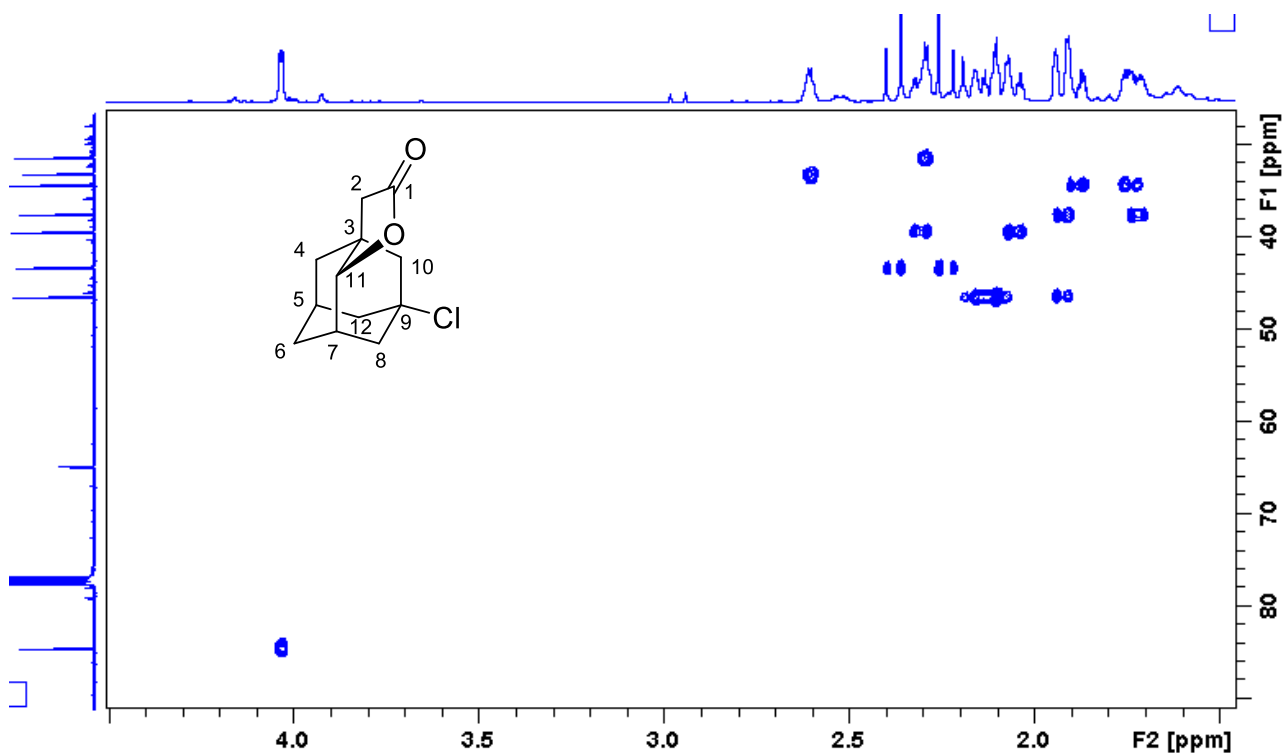
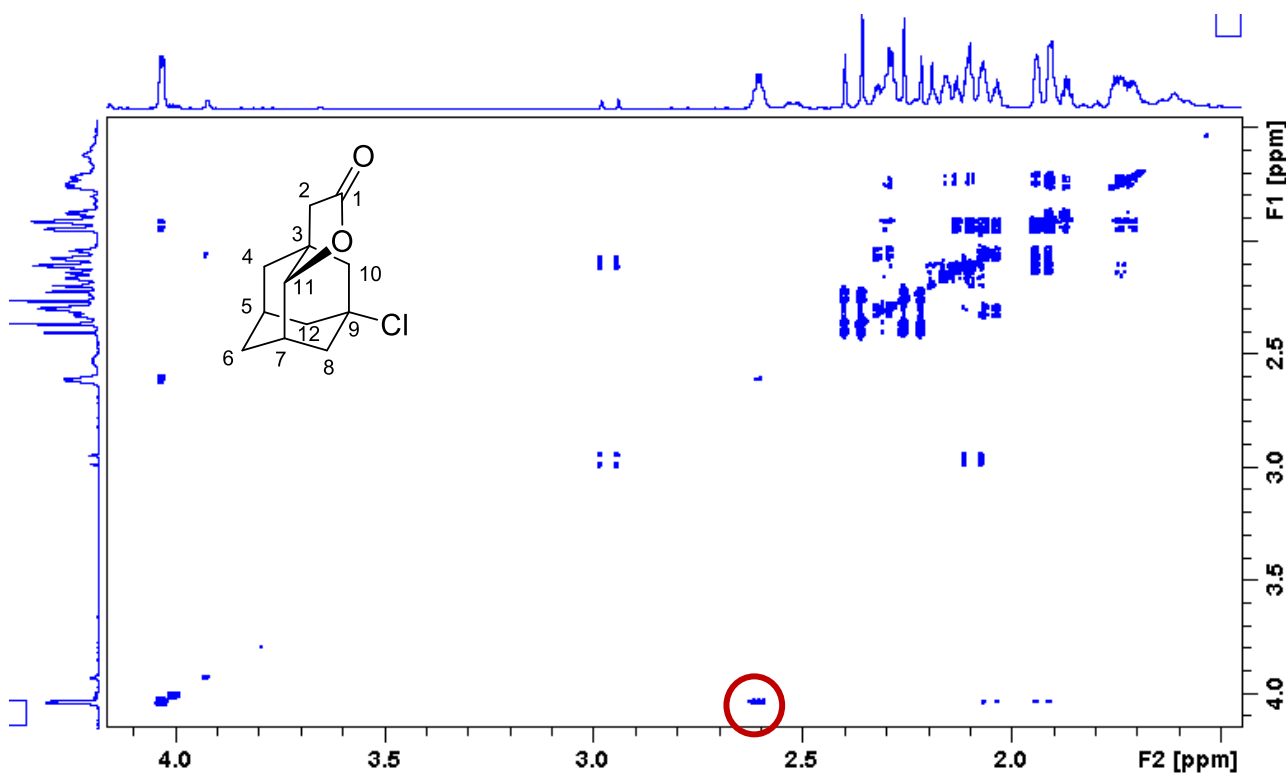
^{13}C NMR (101 MHz, CDCl_3) δ 175.7 (C1), 84.4 (C11), 64.7 (C9), 46.4 (C10 or C12), 46.3 (C10 or C12), 43.3 (C2), 43.1 (C3), 39.3 (C8), 37.4 (C4), 34.2 (C6), 33.1 (C7), 31.3 (C5). A small amount of **9b** (15%) accounts the small peaks visible in the spectrum.



Stacking of the ^1H NMR spectrum of **9c** (bottom) with its selective NOESY obtained after irradiating at 4.00 δ (lactone signal, $\text{C}_{11}\text{-H}$). The signals that show a NOESY correlation with $\text{C}_{11}\text{-H}$ are visible in a negative phase.

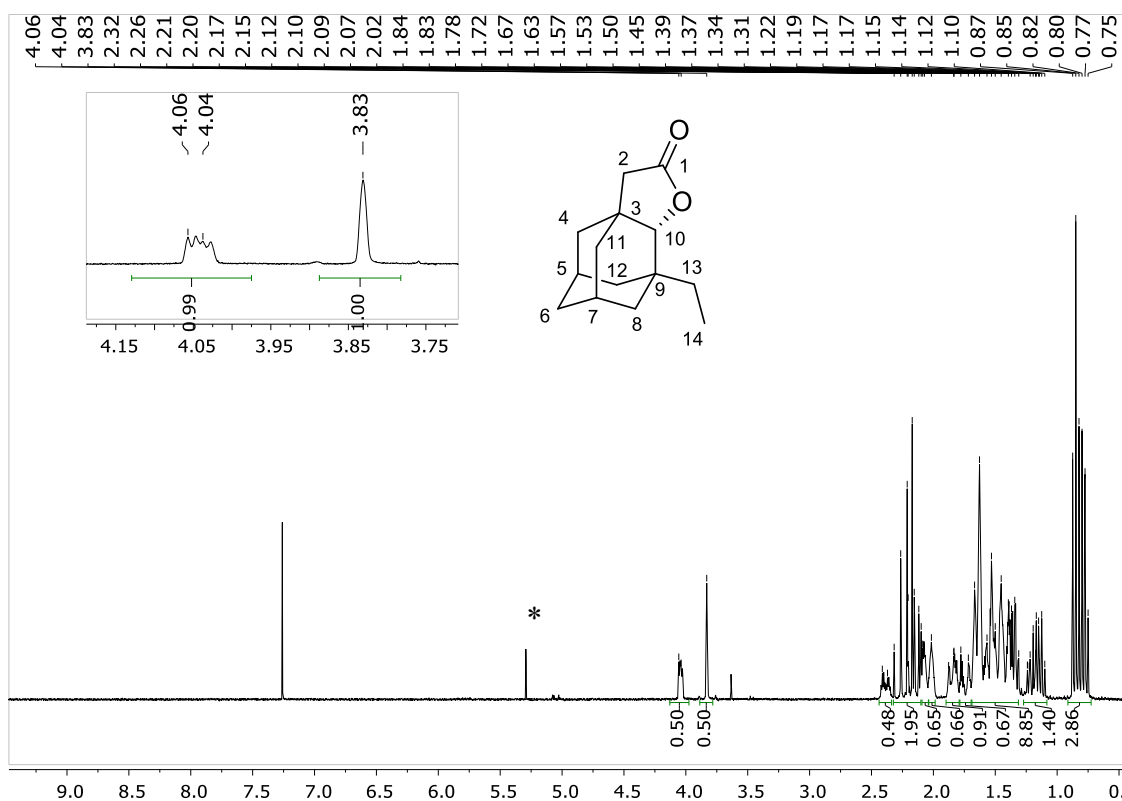


Stacking of the ^{13}C NMR spectrum of **9c** (bottom) stacked with its DEPT90 (top) and its DEPT 135 (middle) spectra.



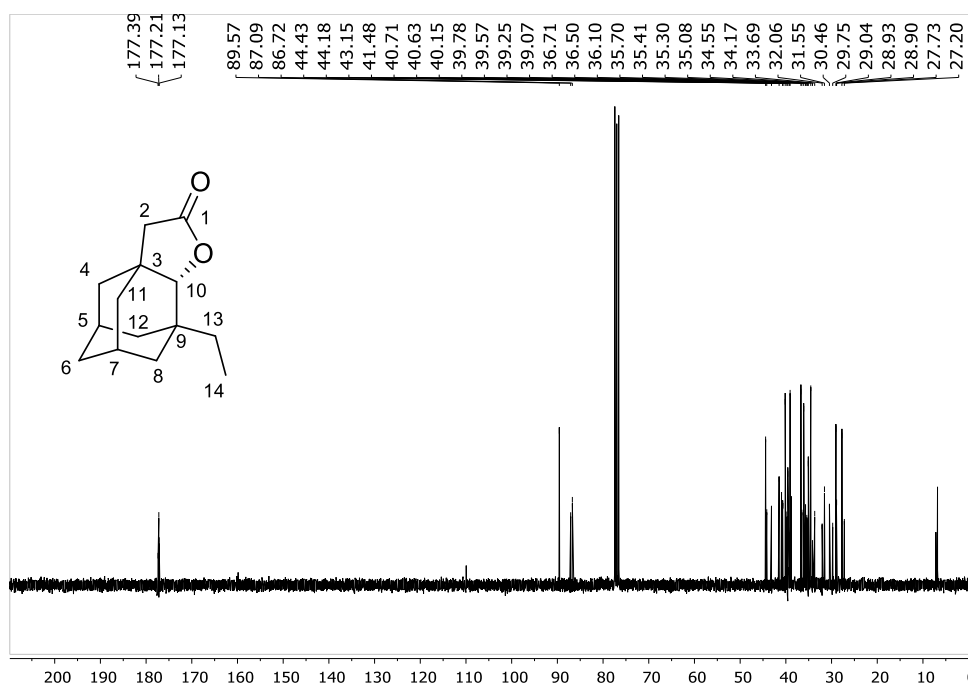
IV. NMR Characterization of lactones (Section B, X=non-HBA)

$^1\text{H-NMR}$ of **10** oxidation in CDCl_3

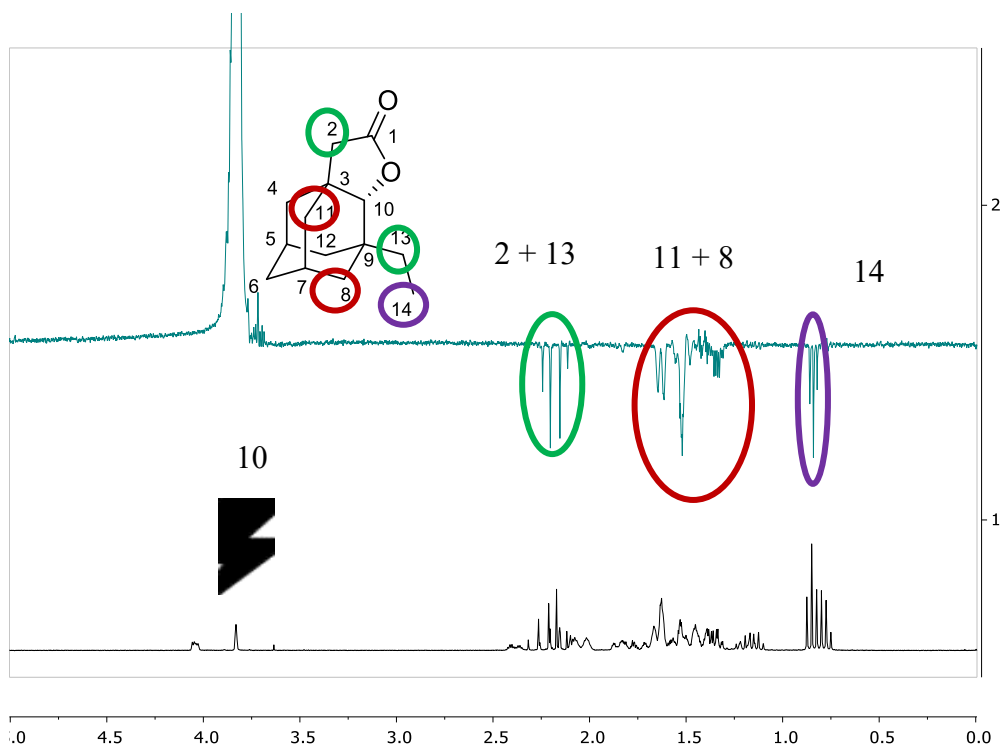


$^1\text{H NMR}$ (300 MHz, CDCl_3) δ 4.06-4.04 (m, 1H, $\text{C}_4\text{-H}$ and $\text{C}_{11}\text{-H}$ of distal **10b** and **10c**), 3.83 (s, 1H, $\text{C}_{10}\text{-H}$ of **10a**), 2.32 – 2.10 (m, 2H), 2.08 (d, $J = 4.2$ Hz, 1H), 2.02 (s, 1H), 1.90 – 1.79 (m, 1H), 1.75 (d, $J = 18.2$ Hz, 1H), 1.69 – 1.31 (m, 9H), 1.27 – 1.08 (m, 1H), 0.91 – 0.73 (m, 3H). In the inset an enlargement of the lactone signals is displayed. All three lactones are present in the spectrum, roughly in a 2:1:1 ratio (**10a**:**10b**:**10c**). The peak marked with an asterisk is CH_2Cl_2 .

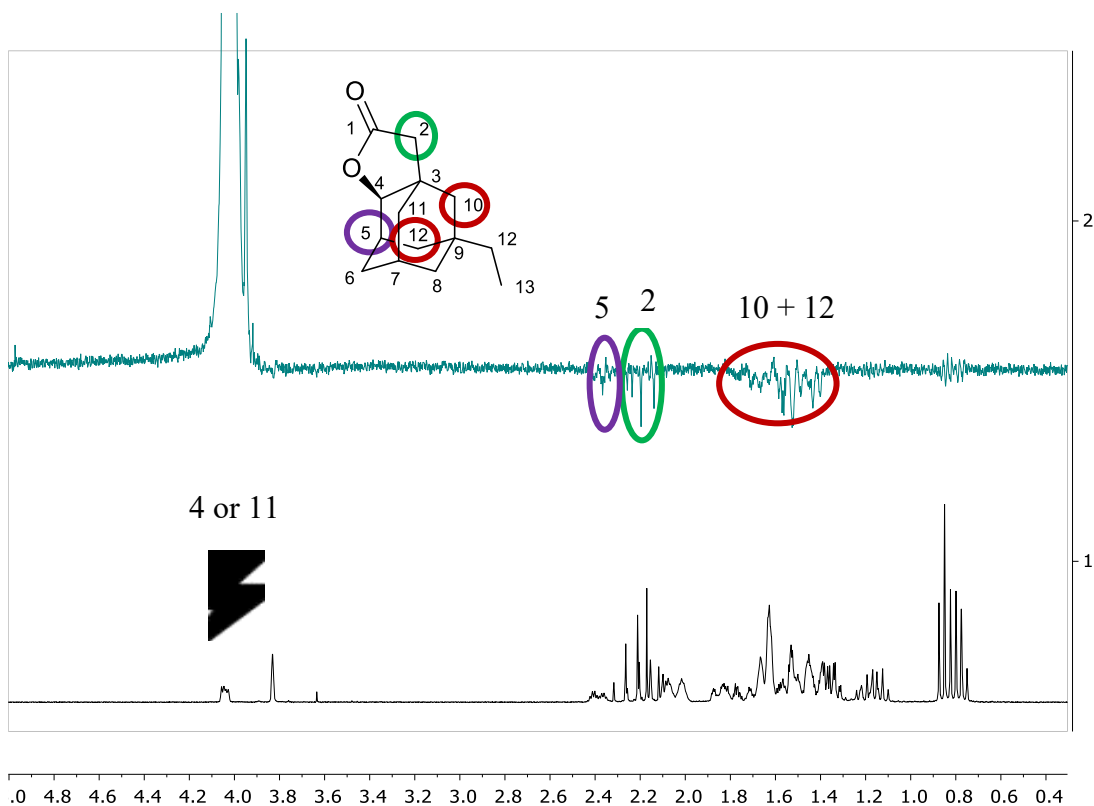
¹³C-NMR of **10** oxidation in CDCl₃



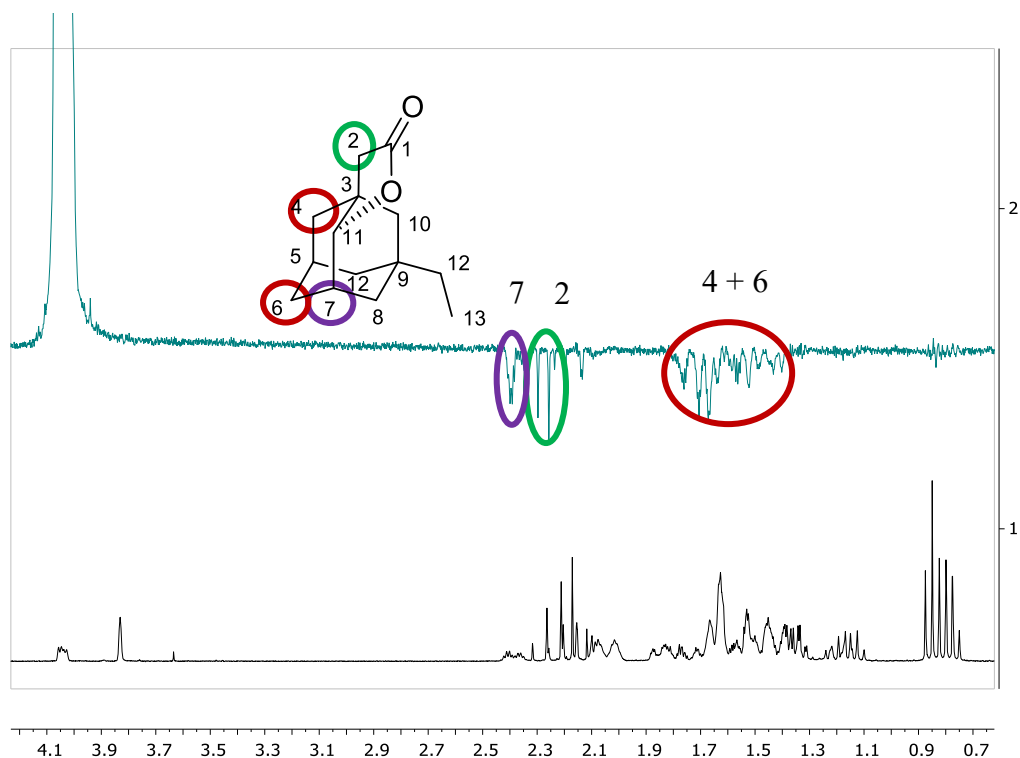
¹³C NMR (75 MHz, CDCl₃) δ 177.4, 177.2, 177.1, 89.6, 87.1, 86.7, 44.4, 44.2, 43.1, 41.5, 40.7, 40.6, 40.1, 39.8, 39.6, 39.2, 39.1, 36.7, 36.5, 36.1, 35.7, 35.4, 35.3, 35.1, 34.5, 34.2, 33.7, 32.1, 31.5, 30.5, 29.7, 29.0, 28.9, 28.9, 27.7, 27.2, 7.1, 6.8, 6.8. All three lactones are present in the spectrum, roughly in a 2:1:1 ratio (**10a**:**10b**:**10c**). The largest peaks correspond to the proximal lactone **10a**, while the smaller peaks to distal lactones **10b** and **10c**.



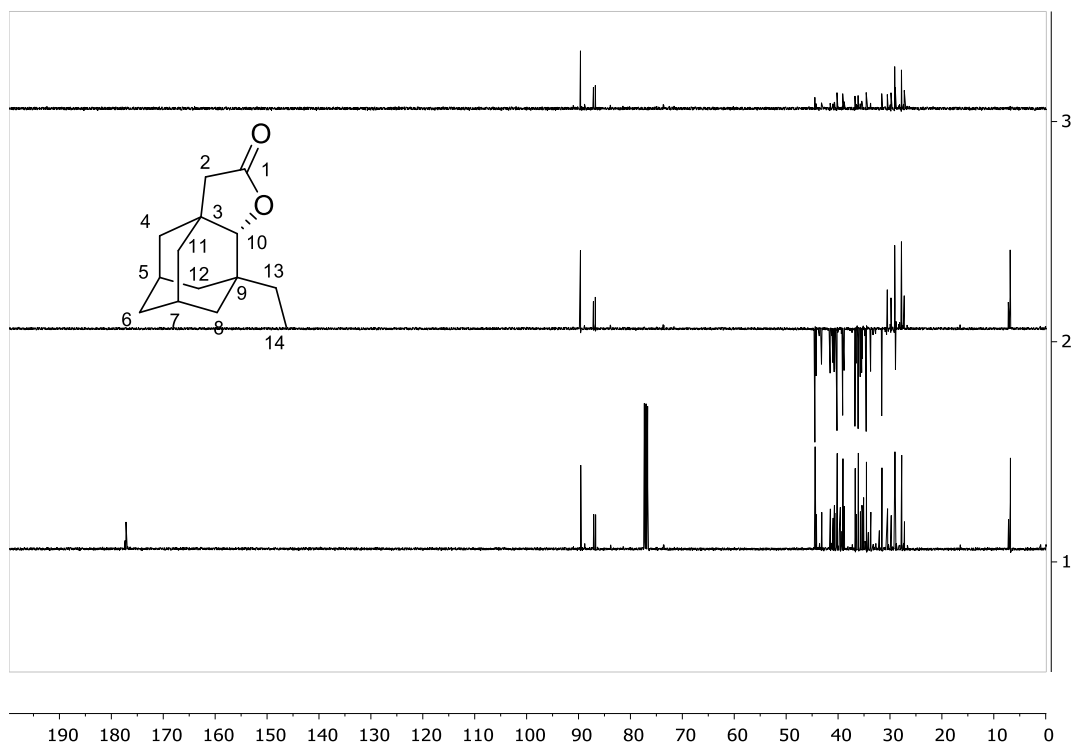
Stacking of the ^1H NMR spectrum of **10a** (bottom) with its selective NOESY obtained after irradiating at 3.82 δ (lactone signal, C₁₀-H). The signals that show a NOESY correlation with C₁₀-H are visible in a negative phase.



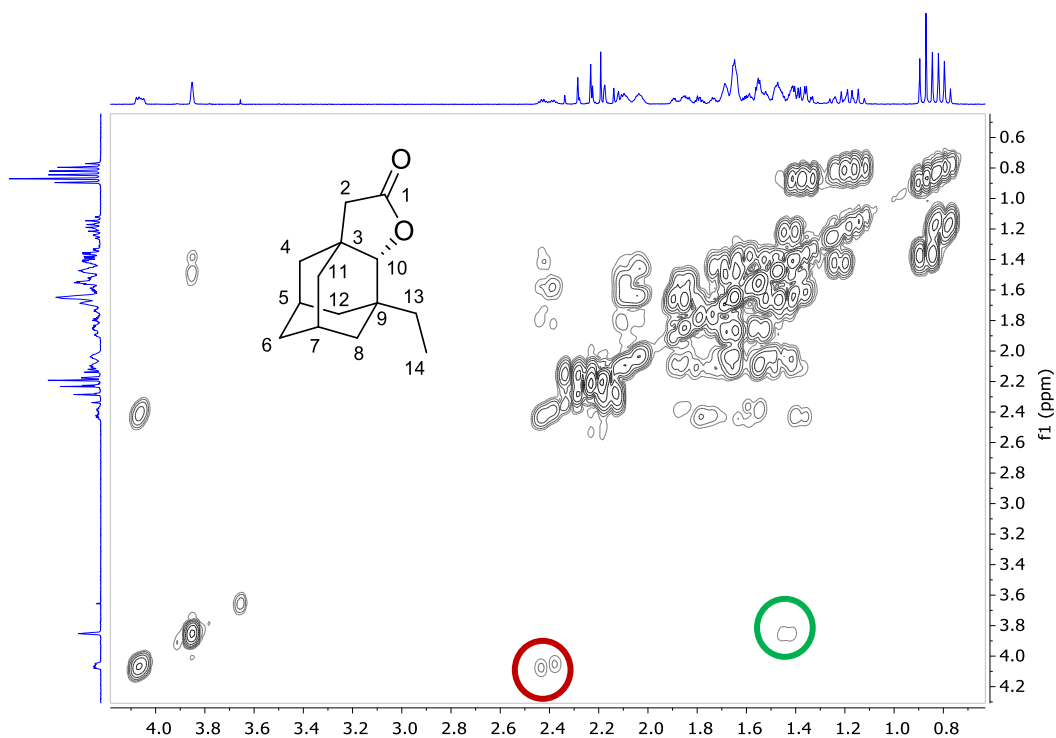
Stacking of the ^1H NMR spectrum of **10** oxidation (bottom) with its selective NOESY obtained after irradiating at 4.05 δ (lactone signal of **10b**, C₄-H). The signals that show a NOESY correlation with C₄-H are visible in a negative phase.



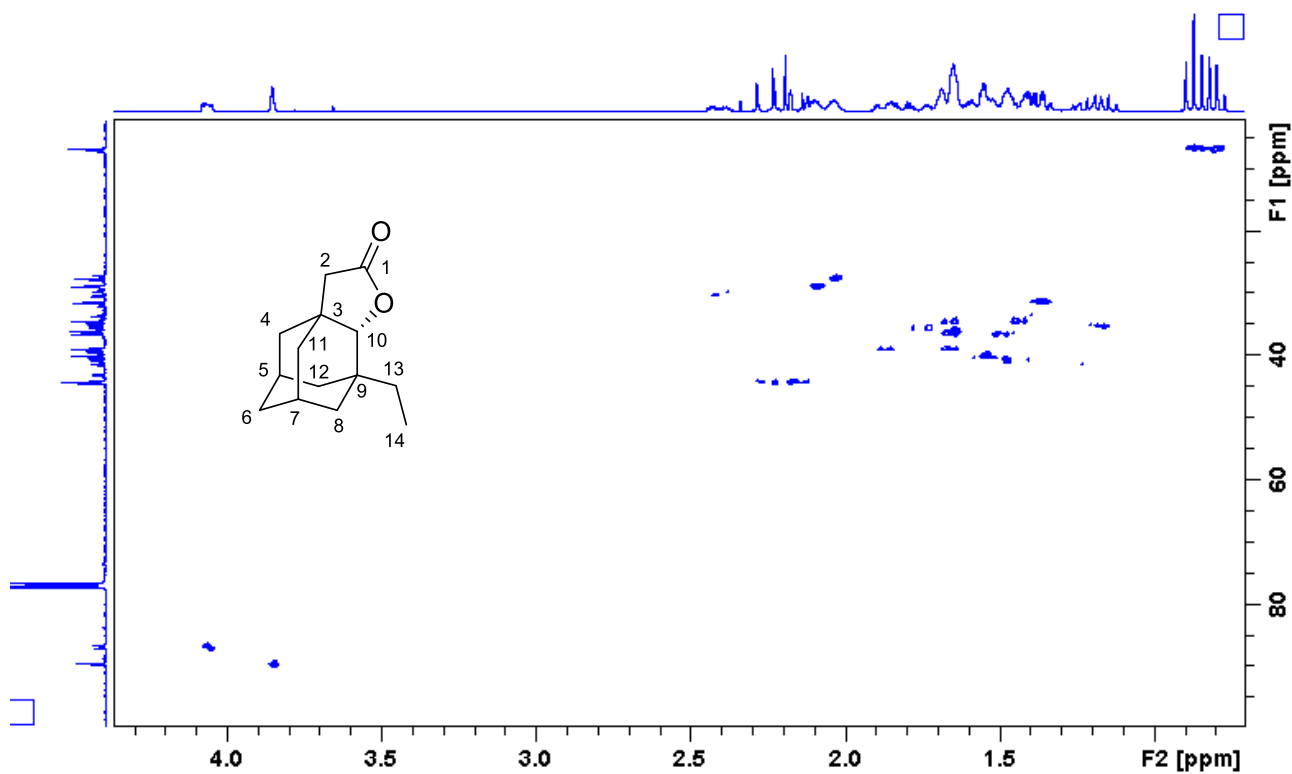
Stacking of the ^1H NMR spectrum of **10** oxidation (bottom) with its selective NOESY obtained after irradiating at 4.02 δ (lactone signal of **10c**, $\text{C}_{11}\text{-H}$). The signals that show a NOESY correlation with $\text{C}_{11}\text{-H}$ are visible in a negative phase.



Stacking of the ^{13}C NMR spectrum of **10** oxidation (bottom) stacked with its DEPT90 (top) and its DEPT 135 (middle) spectra.

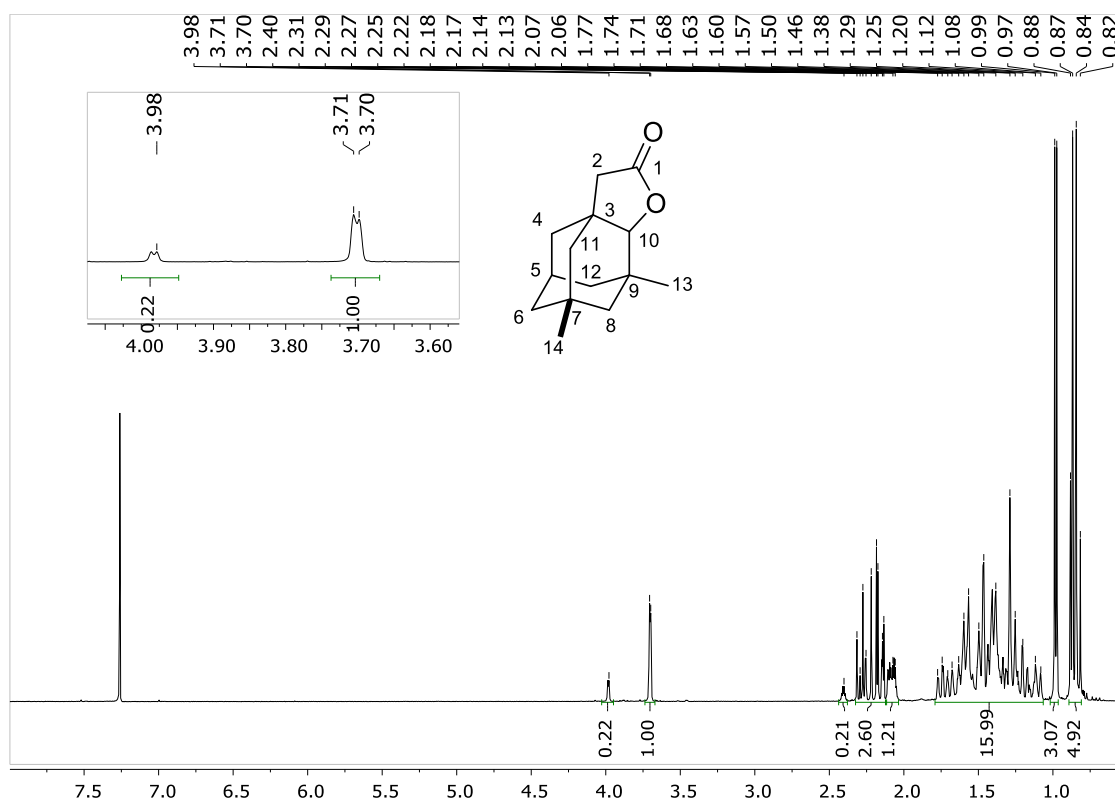


COSY of **10** oxidation. Note the coupling of lactones exo and endo signals C₄-H (left) and C₁₁-H (right, main product) with tertiary C₅-H and C₇-H bond, respectively (highlighted in red). Note also the coupling of the main proximal lactone C₁₀-H (right, main product) with secondary C₈-H bond, respectively (highlighted in green).



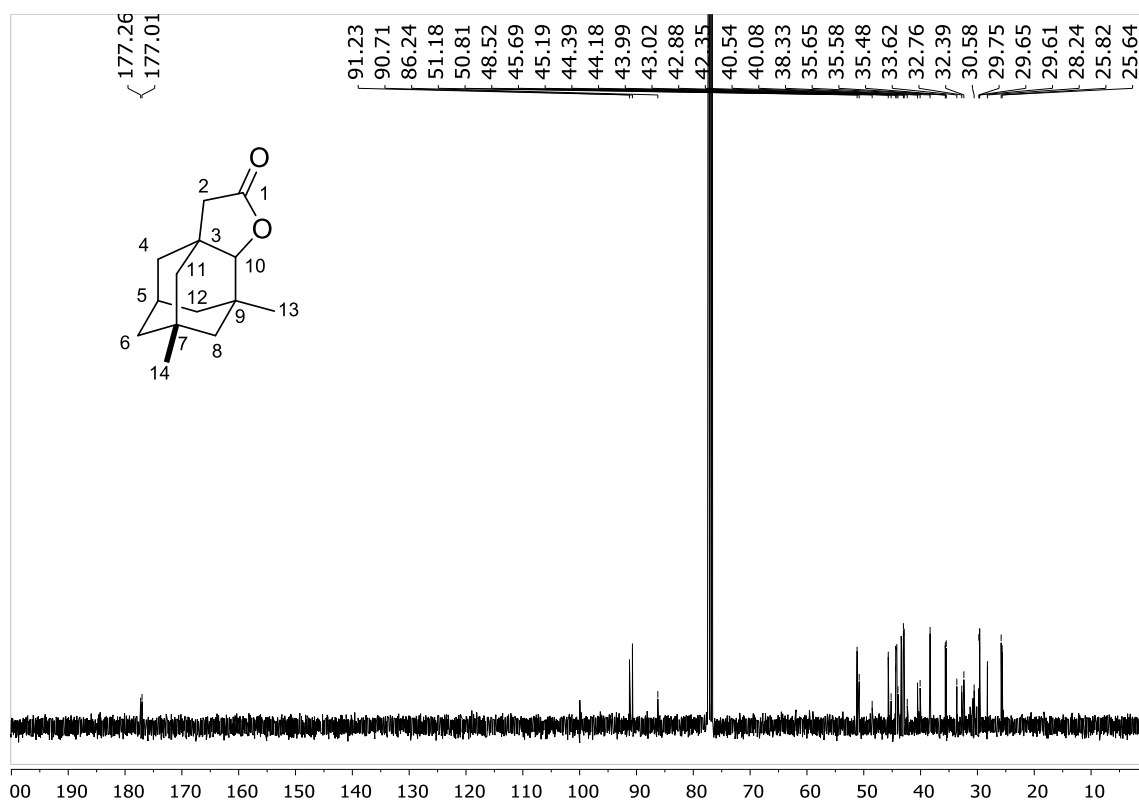
HSQC of **10** oxidation

¹H NMR of **11** oxidation in CDCl₃

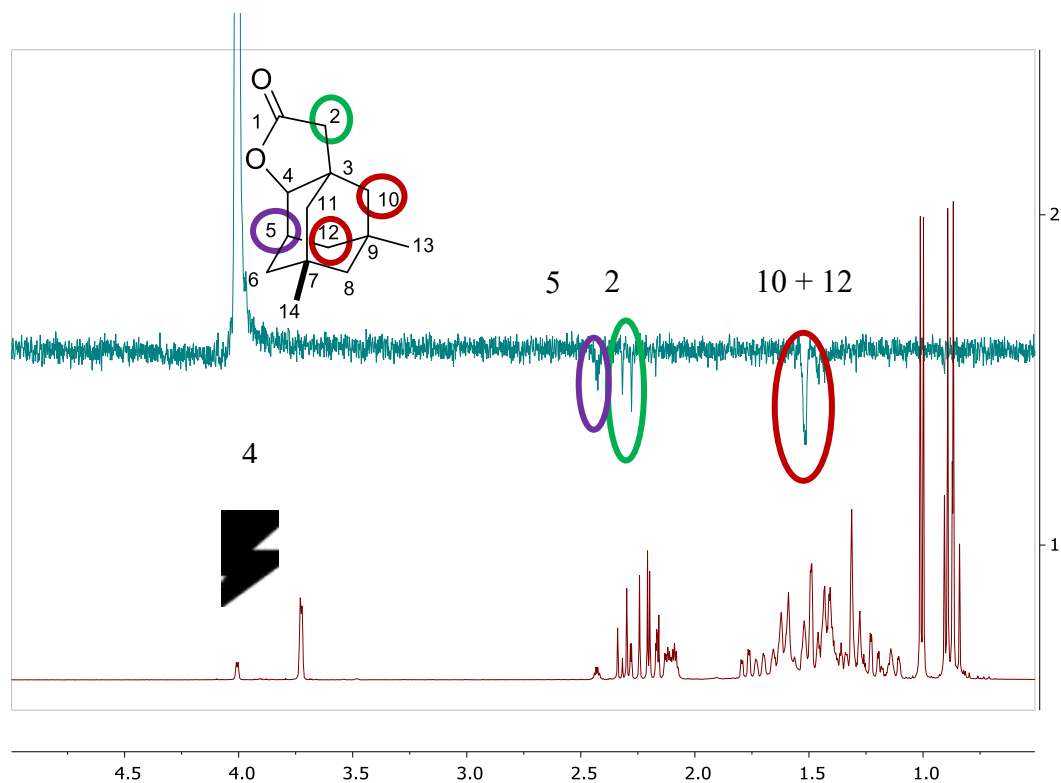


¹H NMR (400 MHz, CDCl₃) δ 3.98 (s, 0.2H, C₄[1H] **11a**), 3.70 (d, *J* = 3.0 Hz, 1H; C₁₀ [1H], **11b** + **11c**), 2.32 – 2.12 (m, 3H, C₂[2H] + C₅[1H] **11a**), 2.07 (d, *J* = 6.2 Hz, 1H), 1.79 – 1.06 (m, 16H), 0.98 (d, *J* = 5.5 Hz, 3H, C₁₃[3H] or C₁₄[3H]), 0.89 – 0.81 (m, 5H, C₁₃[3H] or C₁₄[3H]). The three lactones **11a**, **11b** (right in the inset) and **11c** (left in the inset) cannot be separated and are present in the sample.

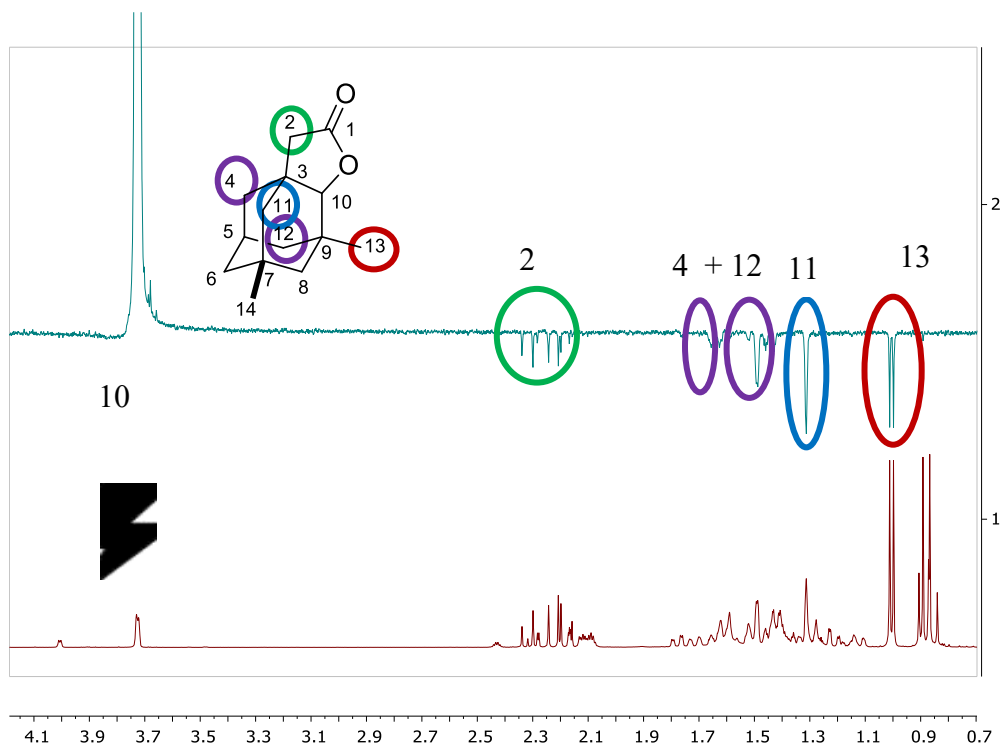
¹³C NMR of **11** oxidation in CDCl₃



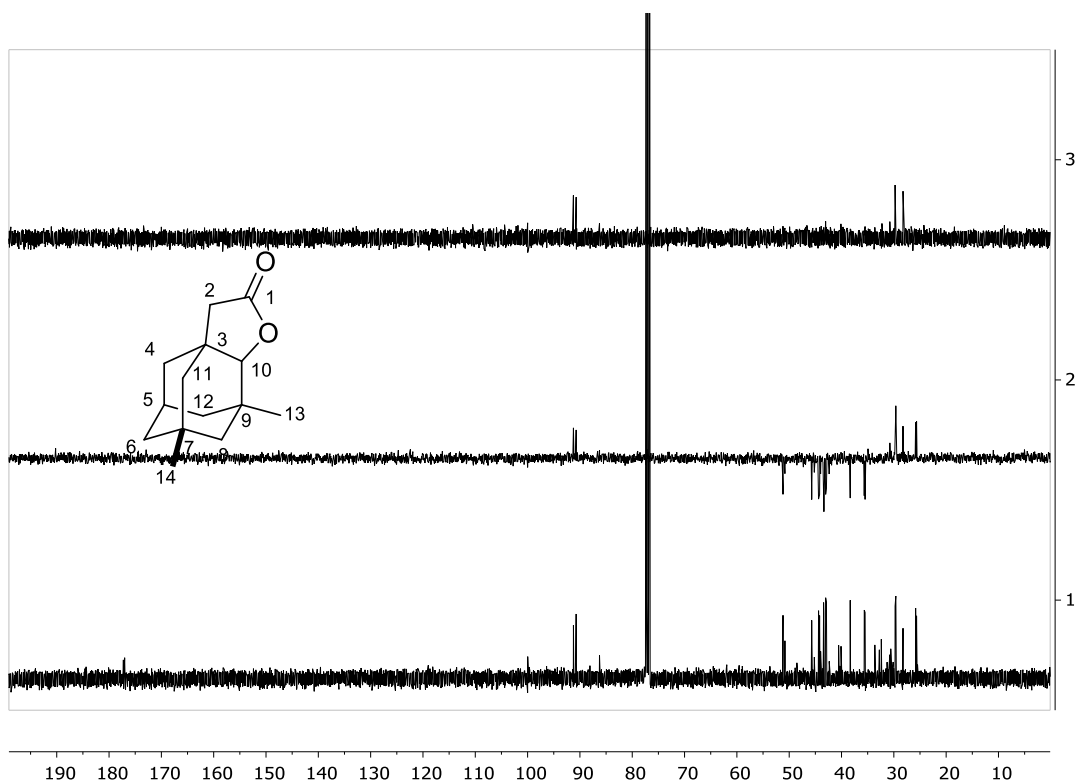
¹³C NMR (101 MHz, CDCl₃) δ 177.0 (*C*₁), 91.2 (*C*₁₀; *distal*), 90.7 (*C*₁₀; *distal*), 86.2 (*C*₄; *proximal*), 51.2, 50.8, 48.5, 45.7, 45.2, 44.4, 44.2, 44.0, 43.0, 42.9, 42.3, 40.5, 40.1, 38.3, 35.6, 35.6, 35.5, 33.6, 32.8, 32.4, 30.6, 29.7, 29.6, 29.6, 28.2, 25.8, 25.6. All the three lactones **11a**, **11b** and **11c** are present in the sample.



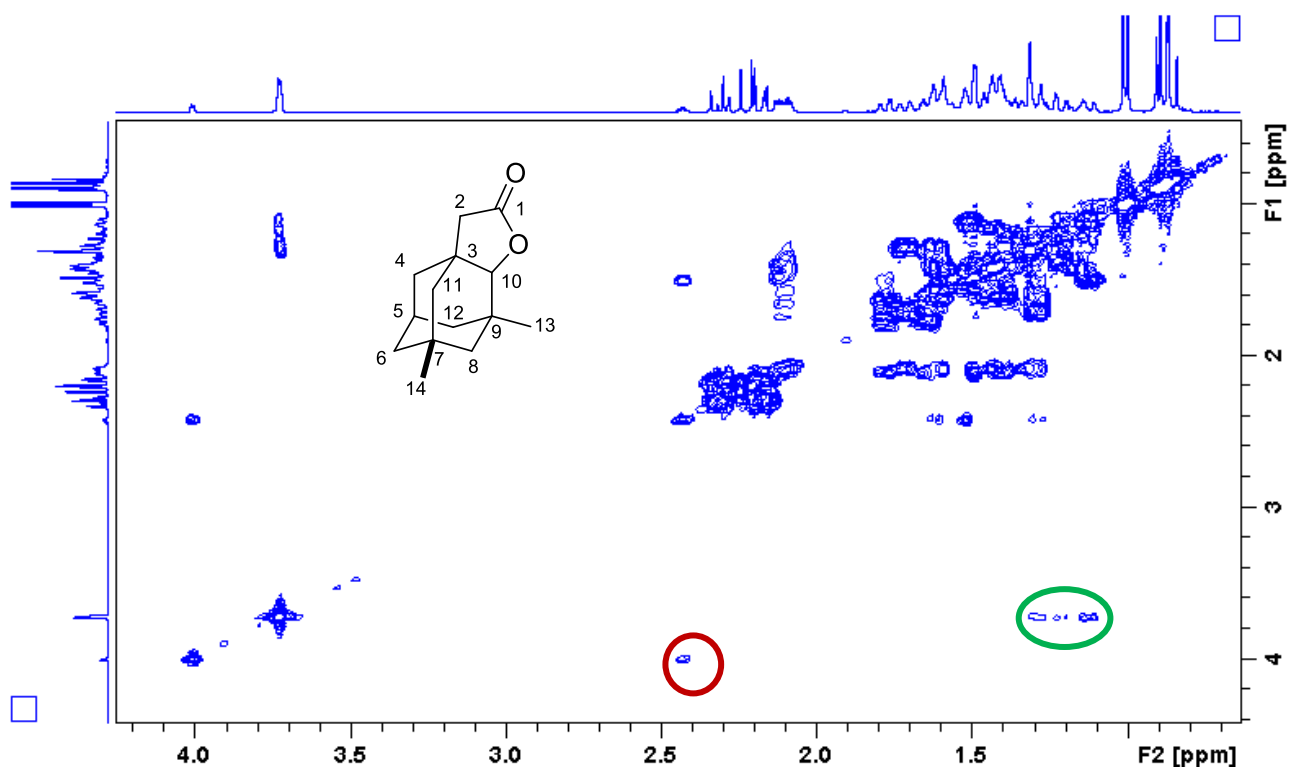
Stacking of the ^1H NMR spectrum of **11a** (bottom) with its selective NOESY obtained after irradiating at 3.98 δ (lactone signal, C₄-H). The signals that show a NOESY correlation with C₄-H are visible in a negative phase.



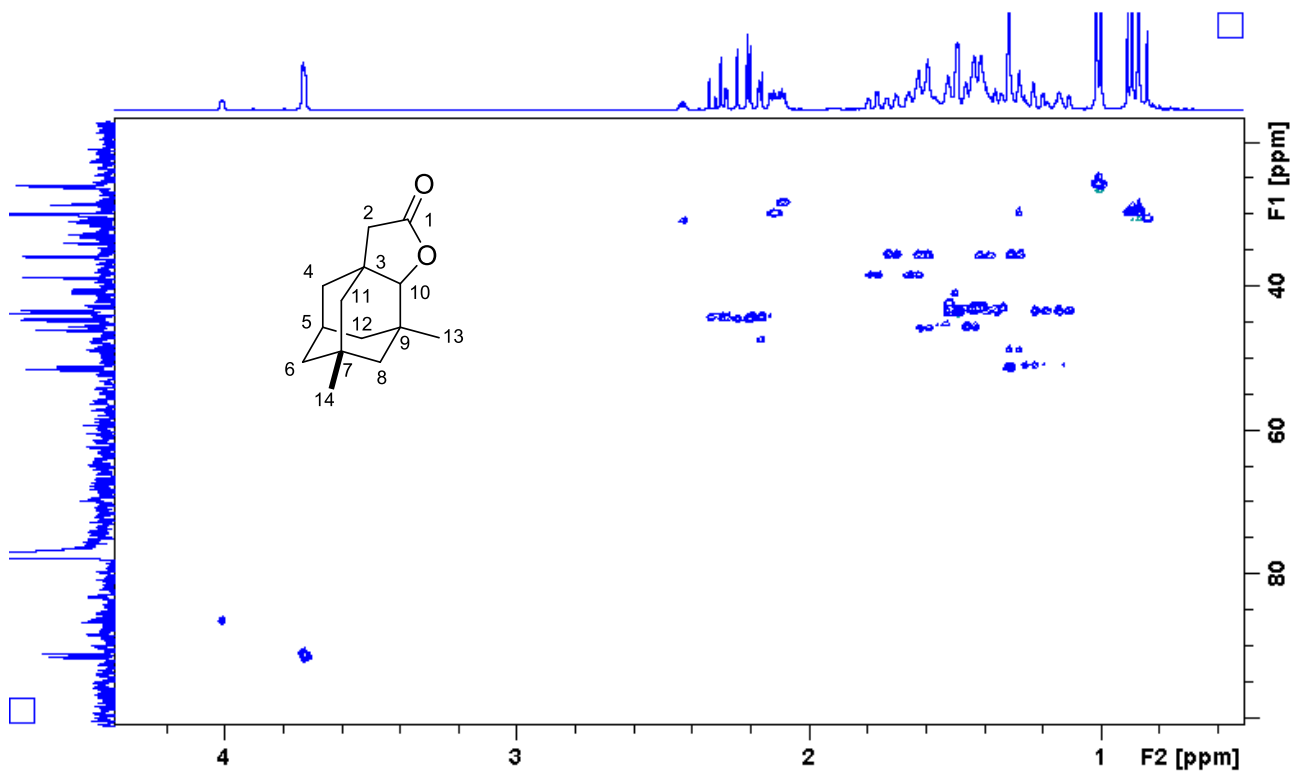
Stacking of the ^1H NMR spectrum of **11b** and **11c** (bottom) with its selective NOESY obtained after irradiating at 3.70 δ (lactone signal, C₁₀-H). The signals that show a NOESY correlation with C₁₀-H are visible in a negative phase.



Stacking of the ^{13}C NMR spectrum of **11** oxidation (bottom) stacked with its DEPT90 (top) and its DEPT 135 (middle) spectra.

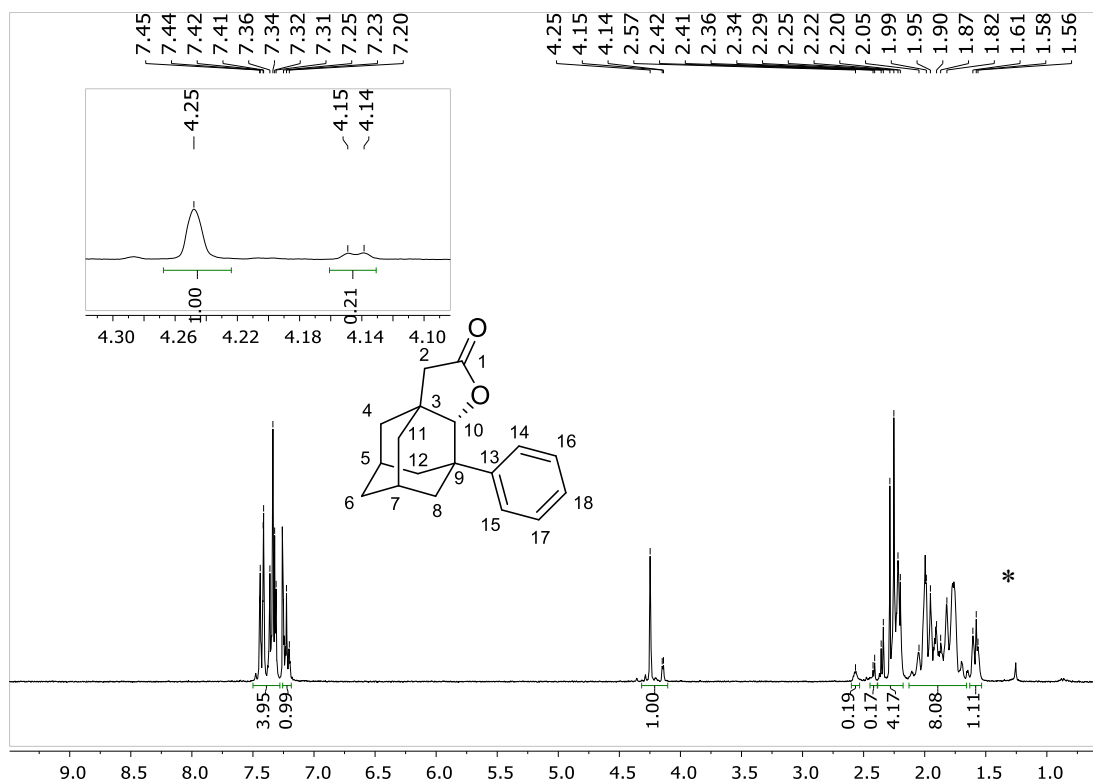


COSY of **11** oxidation. Note the coupling of distal lactone signal $\text{C}_4\text{-H}$ with tertiary $\text{C}_5\text{-H}$ bond (highlighted in red). Note also the coupling of the proximal lactones signal $\text{C}_{10}\text{-H}$ with secondary C-H bonds (highlighted in green).



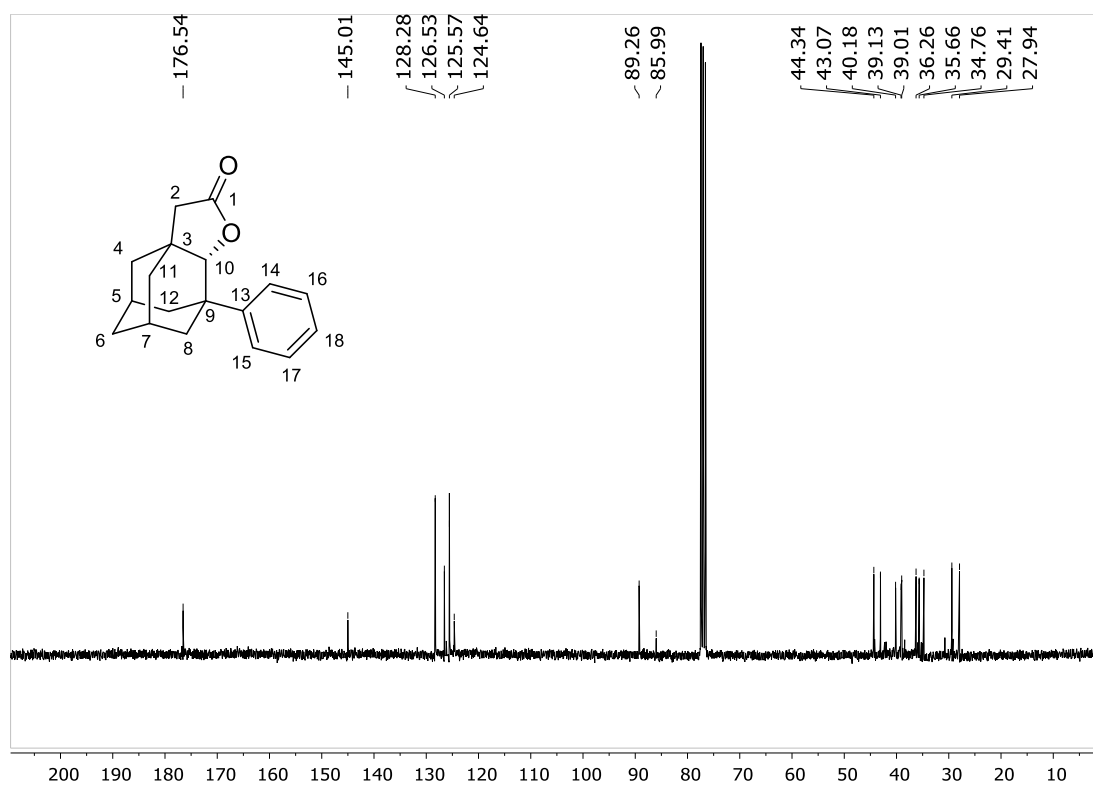
HSQC of **11** oxidation

^1H NMR of **12a** in CDCl_3

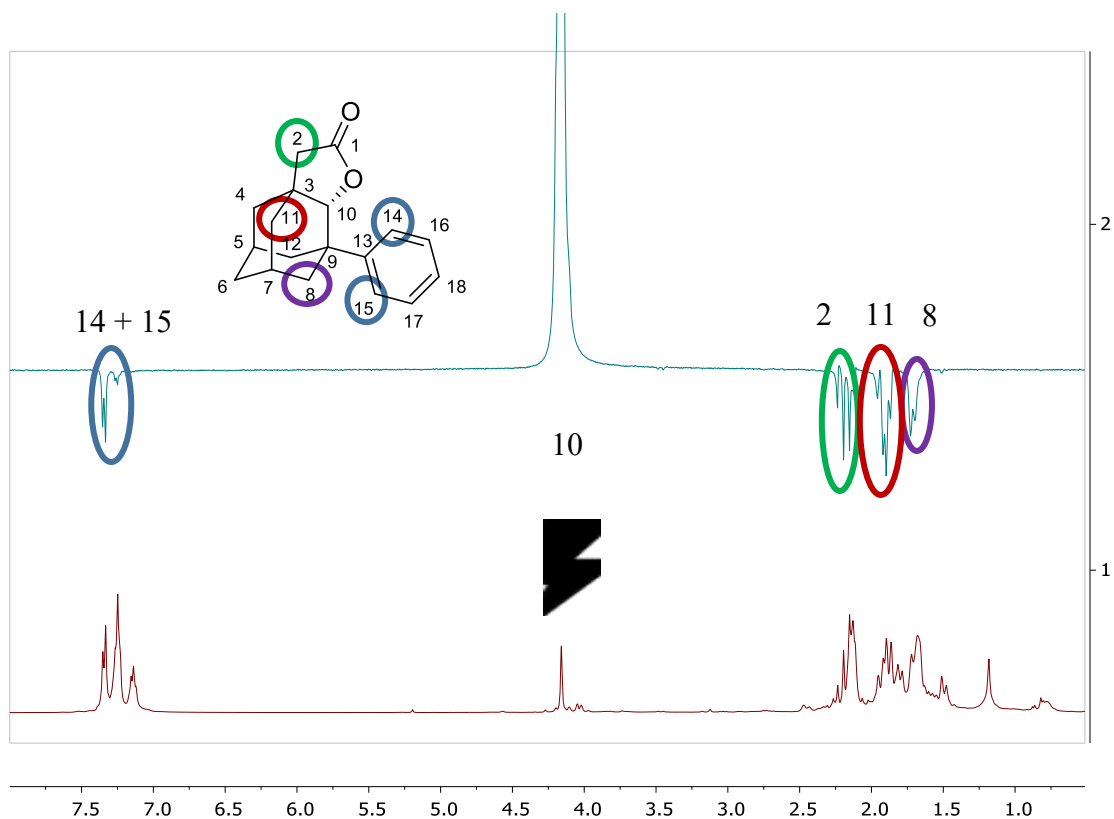


^1H NMR (400 MHz, CDCl_3 ; **12a** signals assigned. Small peaks are the signals of **12b** and **12c**) δ 7.33 (s, 2H; C_{14} [1H] + C_{15} [1H]), 7.25 (s, 3H; C_{16} [1H] + C_{17} [1H] + CHCl_3), 7.14 (s, 1H; C_{18} [1H]), 4.16 (s, 1H; C_{10} [1H]), 2.15 (s, 5H; C_2 [2H] + C_5 [1H] + C_7 [1H] + C_8 [1H]), 1.90 (s, 4H; C_4 [1H] + C_{12} [2H] + C_8 [1H]), 1.68 (s, 4H; C_6 [2H] + C_4 [1H] + C_{11} [1H]), 1.51 (m, 1H; C_{11} [1H]). In the inset an expansion with the proximal (4.25 δ) and distal lactones (4.16-4.13 δ) is displayed. The peak marked with an asterisk is acetone.

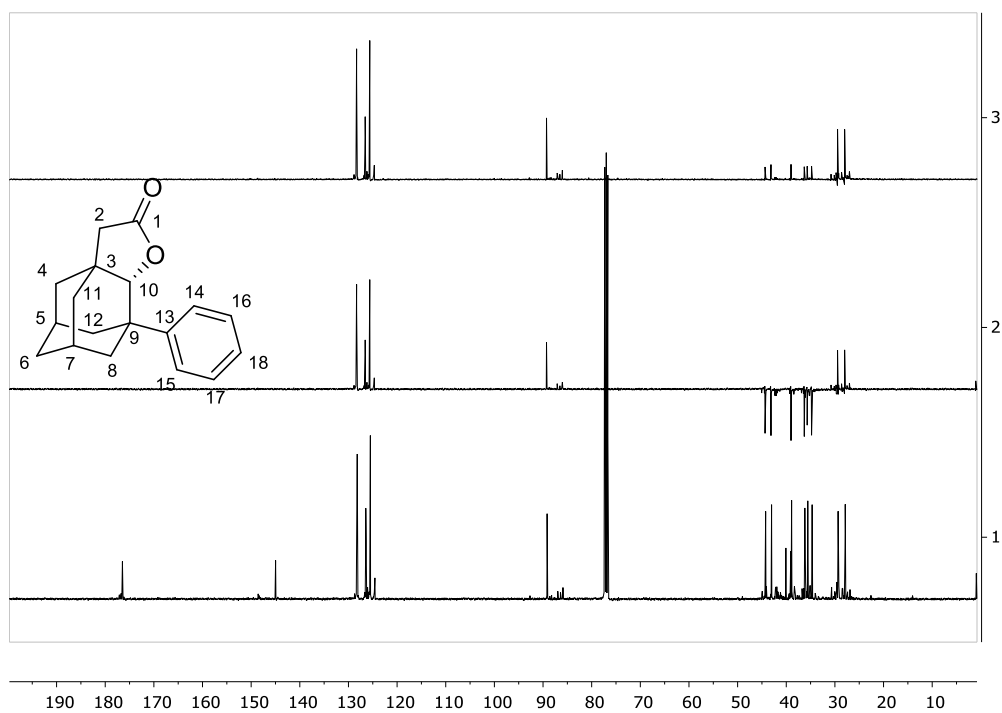
^{13}C NMR of **12a** in CDCl_3



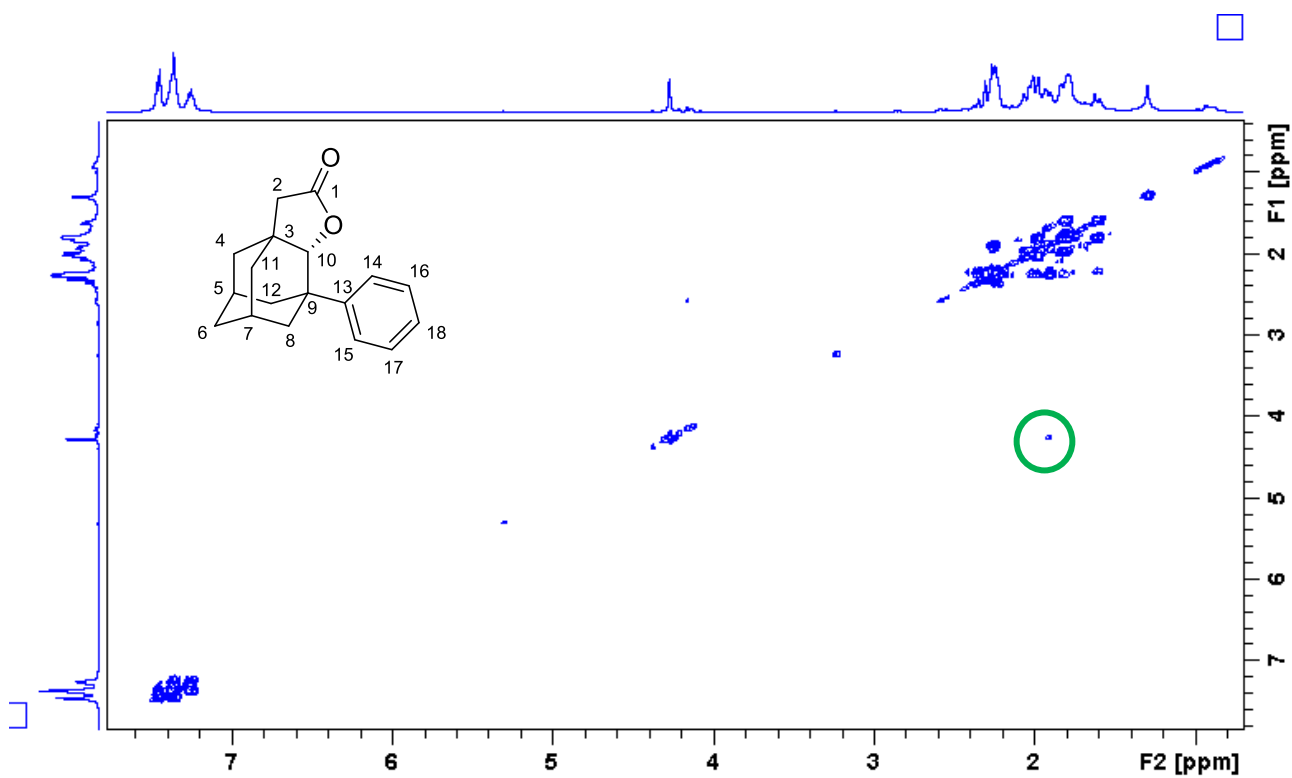
^{13}C NMR (101 MHz, CDCl_3 , **12a** signals assigned. Small peaks are the signals of **12b** and **12c**) δ 176.5 (C_1), 145.0 (C_{13}), 128.3 ($C_{14} + C_{15}$), 126.5 (C_{18}), 125.6 ($C_{14} + C_{15}$), 89.2 (C_{10}), 44.2 (C_2), 43.0 (C_{12}), 40.1 (C_3), 39.1 (C_9), 38.9 (C_4), 36.2 (C_{11}), 35.6 (C_6), 34.7 (C_8), 29.3 (C_5 or C_7), 27.9 (C_5 or C_7).



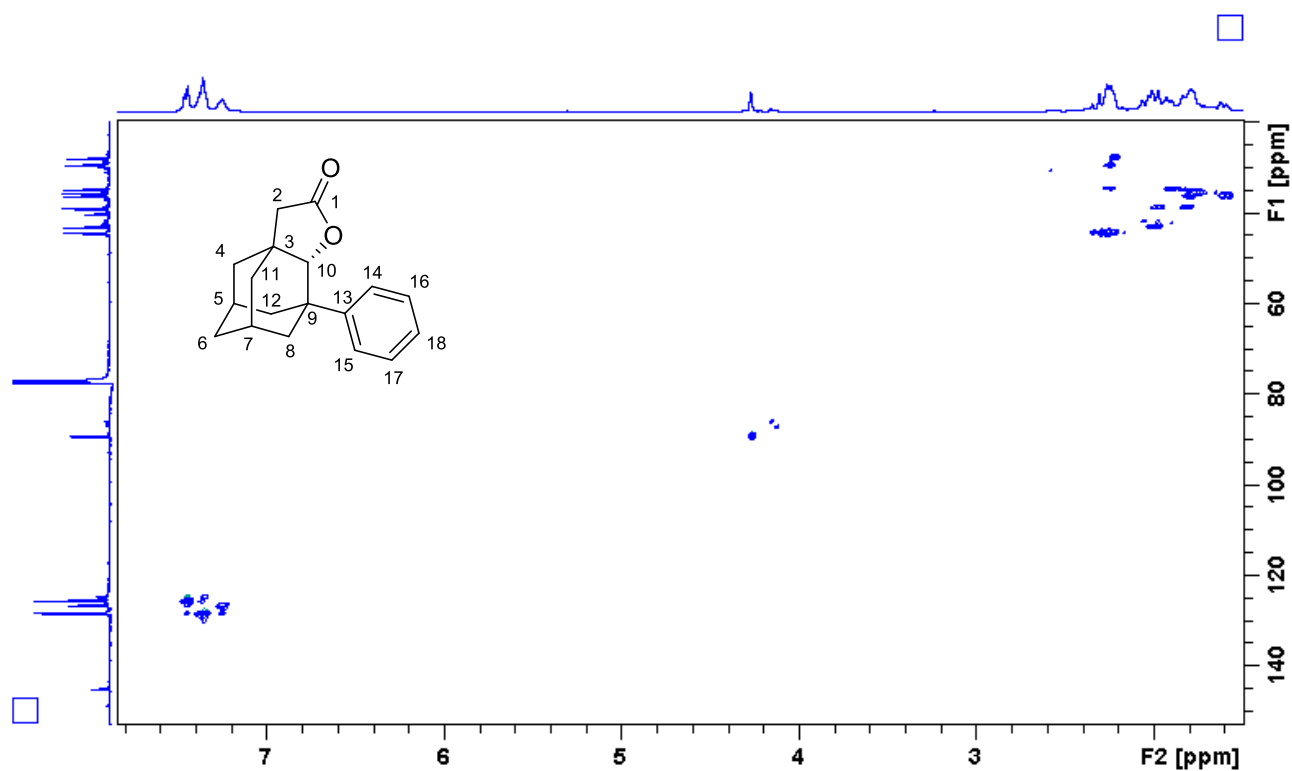
Stacking of the ^1H NMR spectrum of **12a** (bottom) with its selective NOESY obtained after irradiating at $4.25\ \delta$ (lactone signal, $\text{C}_{10}\text{-H}$). The signals that show a NOESY correlation with $\text{C}_{10}\text{-H}$ are visible in a negative phase.



Stacking of the ^{13}C NMR spectrum of **12a** (bottom) stacked with its DEPT90 (top) and its DEPT 135 (middle) spectra.

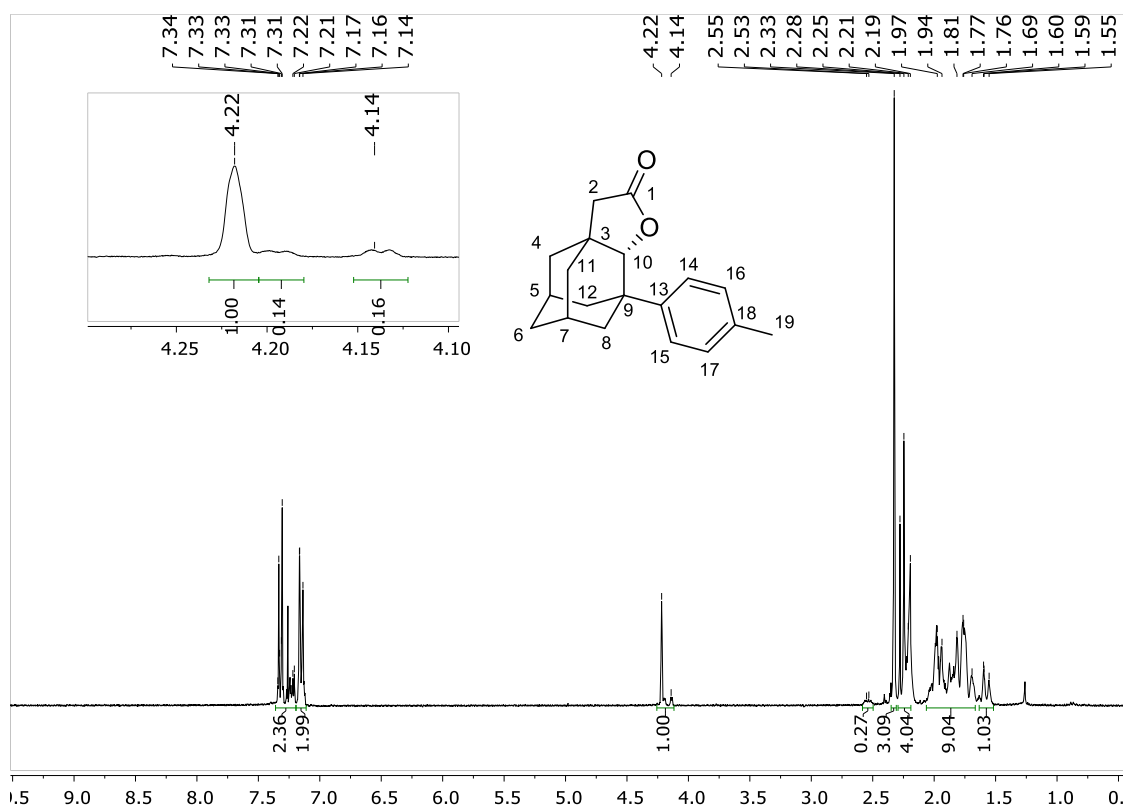


COSY of **12a**. Note the coupling the main proximal lactone C₁₀-H (right, main product) with secondary C₈-H bond, respectively (highlighted in green).



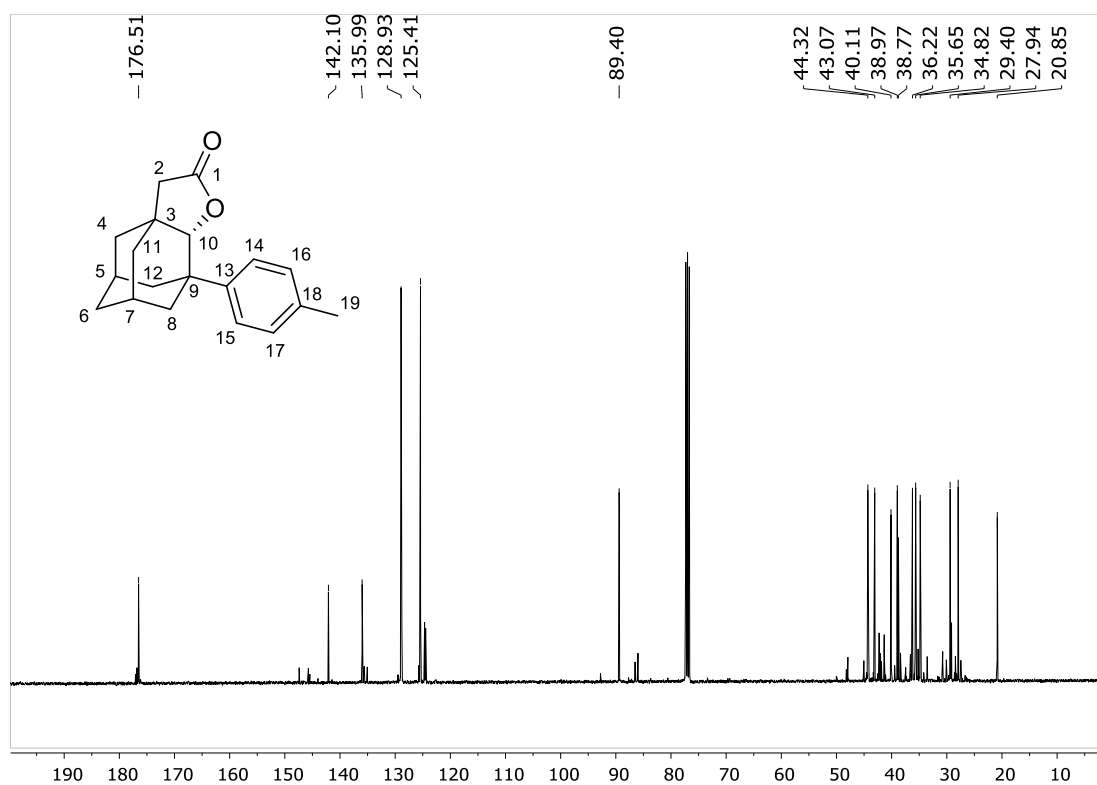
HSQC of **12a**

¹H NMR of **13a** in CDCl₃

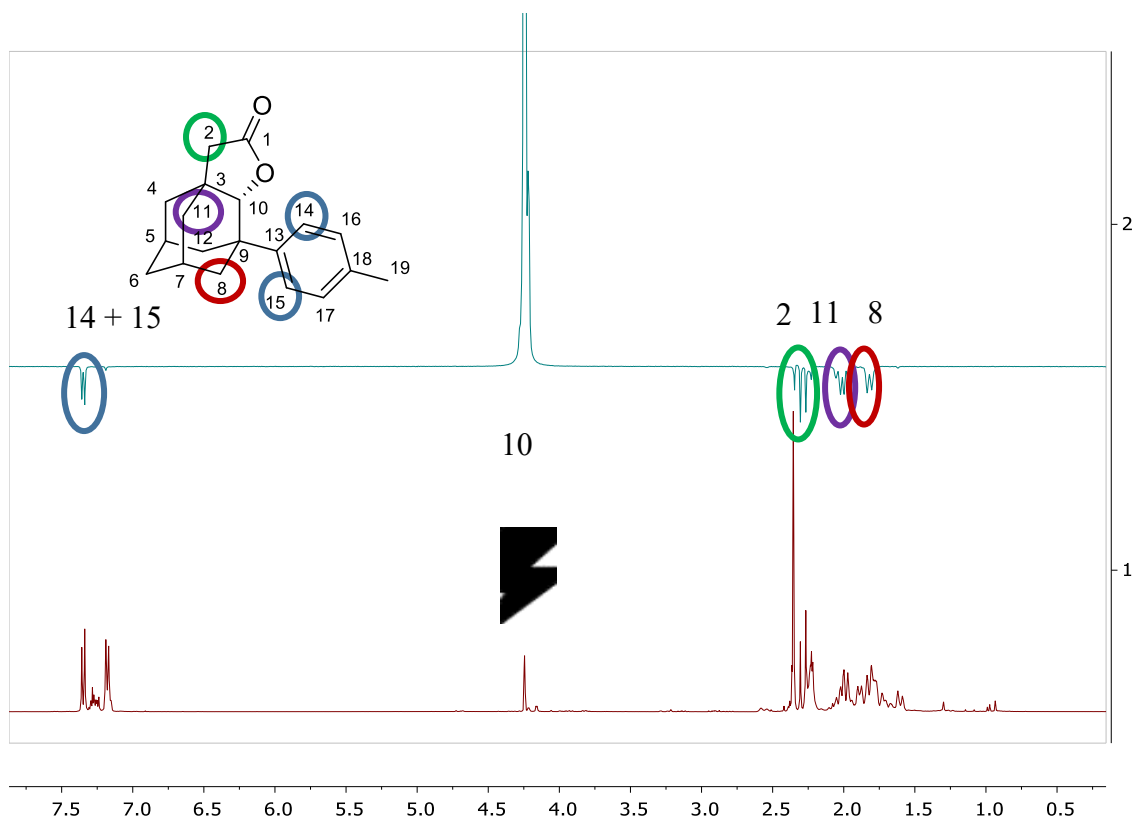


¹H NMR (400 MHz, CDCl₃) δ 7.33 (d, $J = 8.3$ Hz, 2H; C_{16} [1H] + C_{17} [1H]), 7.15 (d, $J = 8.0$ Hz, 2H; C_{14} [2H] + C_{15} [1H]), 4.22 (s, 1H; C_{10} [1H]), 2.33 (s, 1H; C_{19} [3H]), 2.20 (m, $J = 15.9$ Hz, 4H; C_2 [2H] + C_5 [1H] + C_7 [1H]), 1.97-1.59 (m, 9H; C_{11} [2H] + C_{12} [1H] + C_8 [2H] + C_6 [2H] + C_4 [1H] + C_{12} [1H]), 1.56 (m, $J = 12.7$ Hz, 1H; C_4 [1H]). In the inset an expansion with the proximal and distal lactones is shown. Small peaks in the spectrum (i.e. at 2.55) are the signals of the distal isomers **13b** and **13c**.

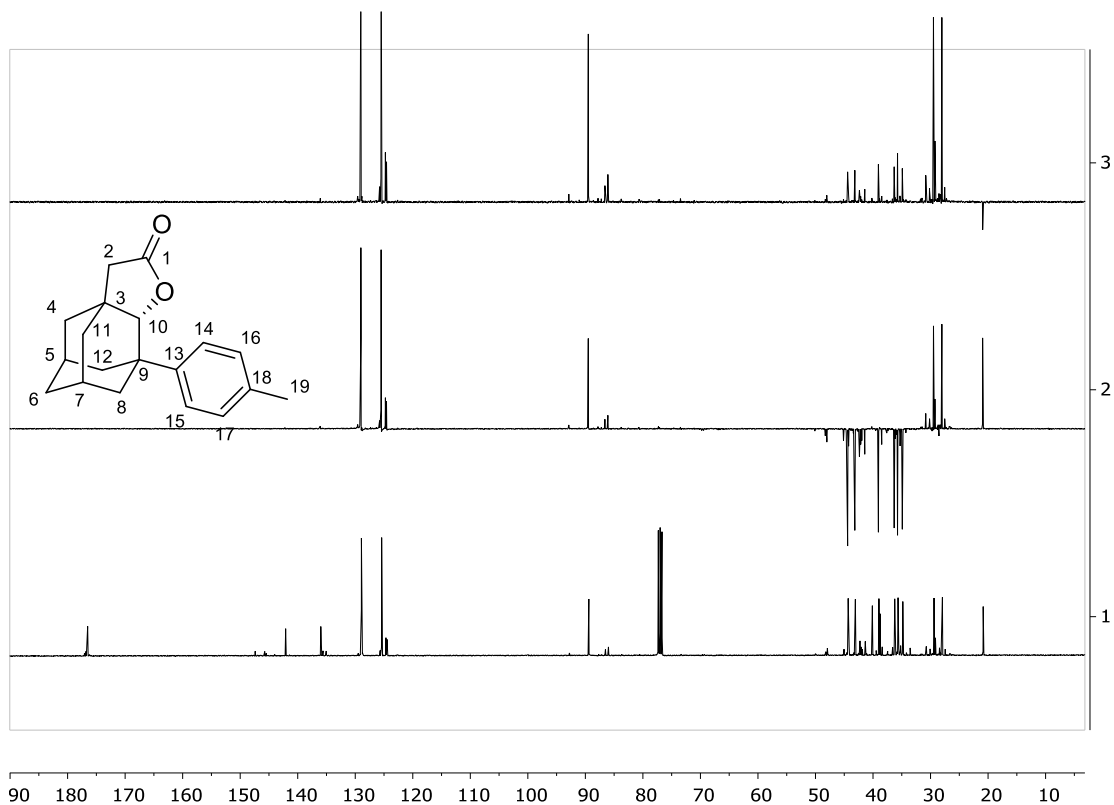
¹³C NMR of **13a** in CDCl₃



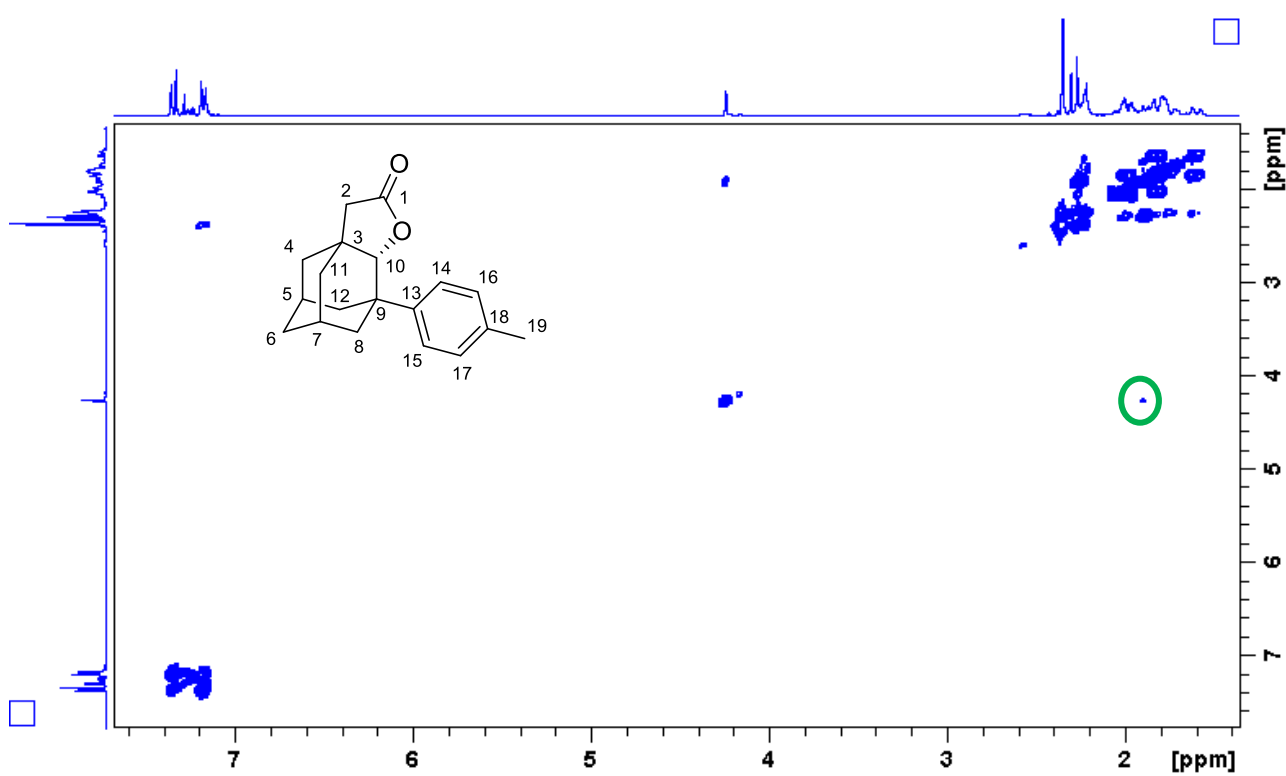
¹³C NMR (101 MHz, CDCl₃) δ 176.5 (*C*₁), 142.1 (*C*₁₃), 136.0 (*C*₁₈), 128.9 (*C*₁₆ + *C*₁₇), 125.4 (*C*₁₄ + *C*₁₅), 89.4 (*C*₁₀), 44.3 (*C*₂), 43.1 (*C*₄), 40.1 (*C*₃), 39.0 (*C*₁₂), 38.8 (*C*₉), 36.2 (*C*₁₁), 35.6 (*C*₆), 34.8 (*C*₈), 29.4 (*C*₅ or *C*₇), 27.9 (*C*₅ or *C*₇), 20.8 (*C*₁₉). Small peaks in the spectrum are the signals of the distal isomers **13b** and **13c**.



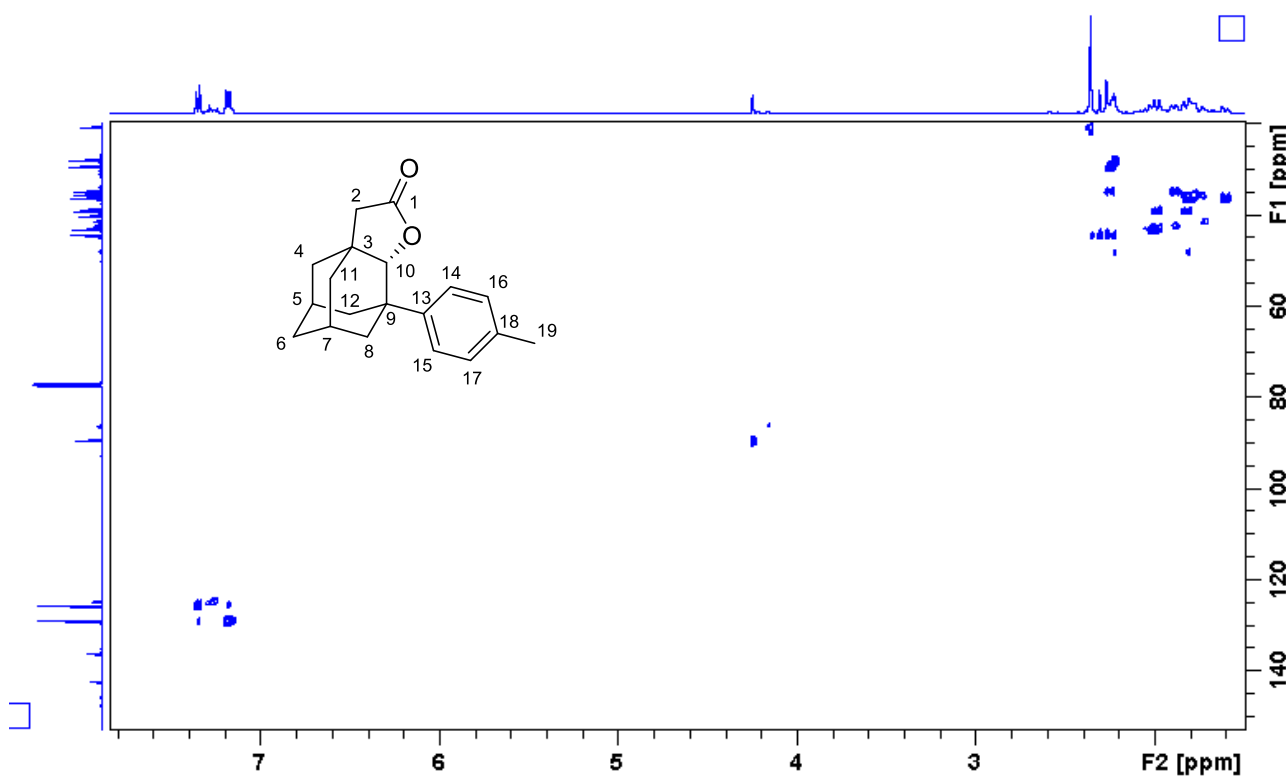
Stacking of the ^1H NMR spectrum of **13a** (bottom) with its selective NOESY obtained after irradiating at 4.22 δ (lactone signal, C₁₀-H). The signals that show a NOESY correlation with C₁₀-H are visible in a negative phase.



Stacking of the ^{13}C NMR spectrum of **13a** (bottom) stacked with its DEPT90 (top) and its DEPT 135 (middle) spectra.

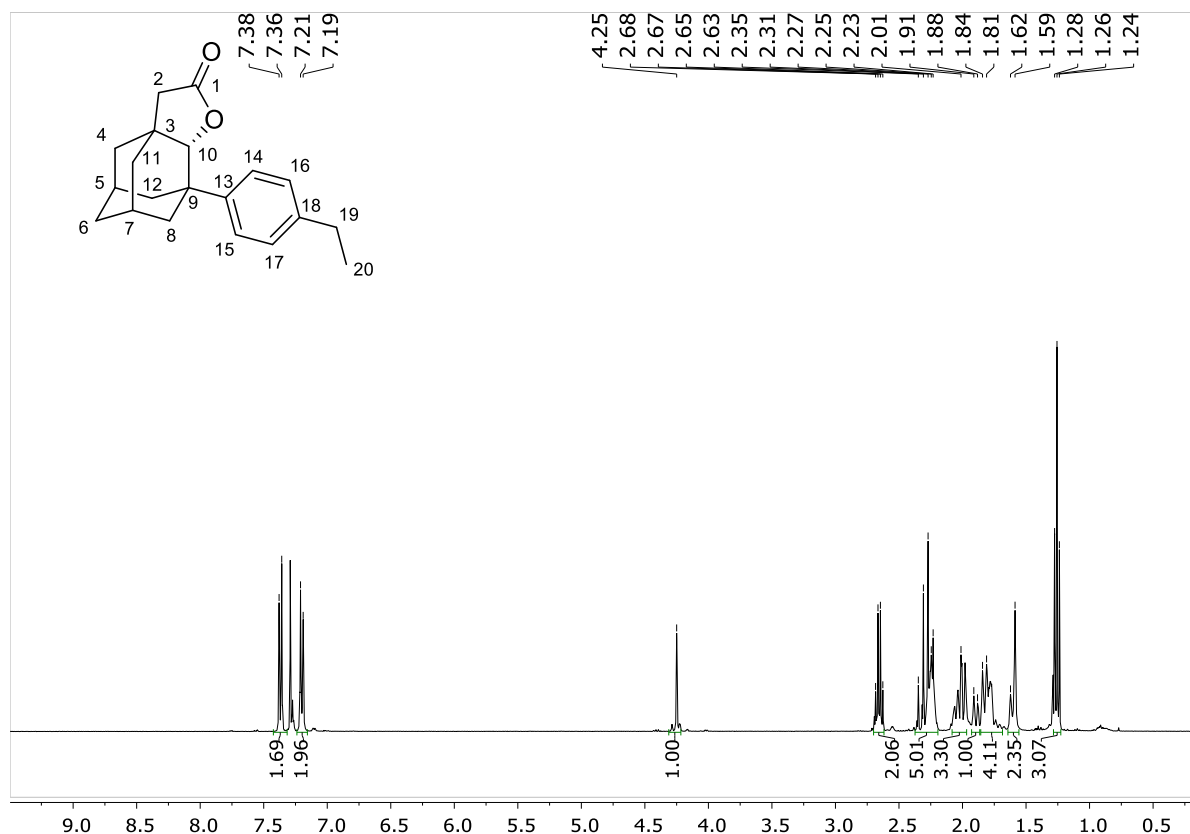


COSY of **13a**. Note the coupling the main proximal lactone C₁₀-H (right, main product) with secondary C₈-H bond, respectively (highlighted in green).



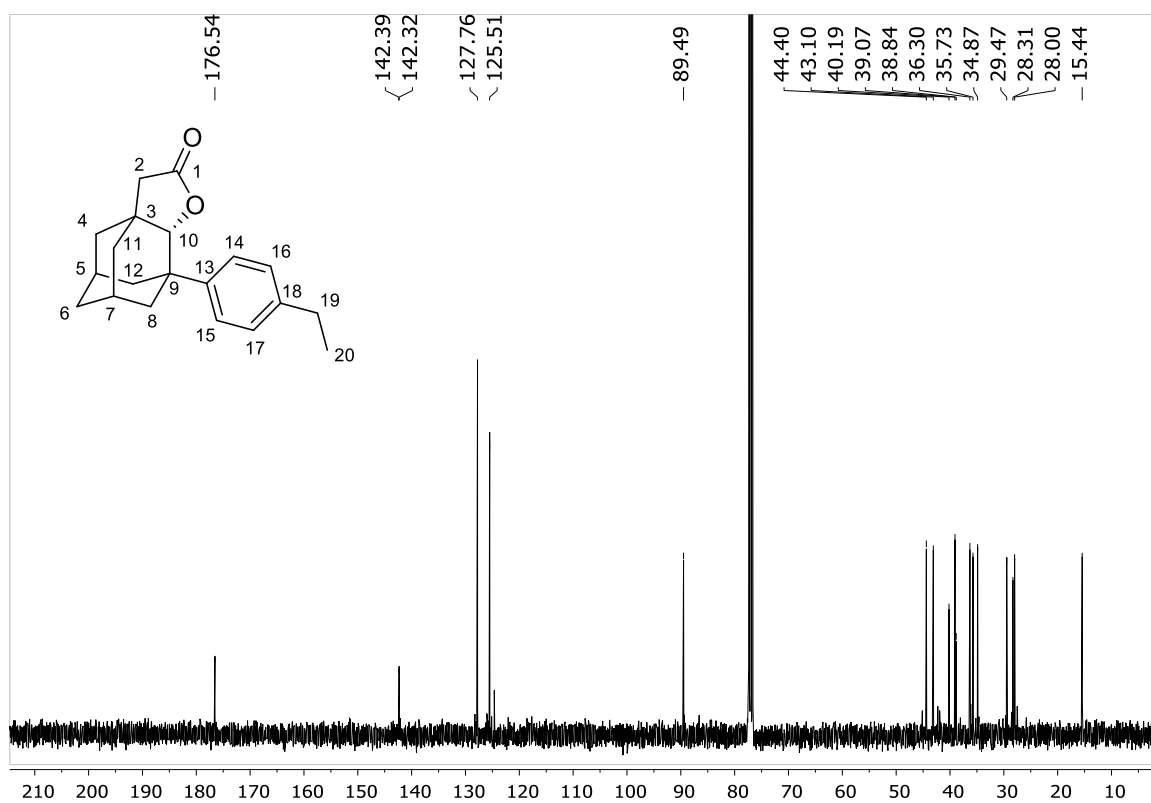
HSQC of **13a**.

¹H NMR of **14a** in CDCl₃

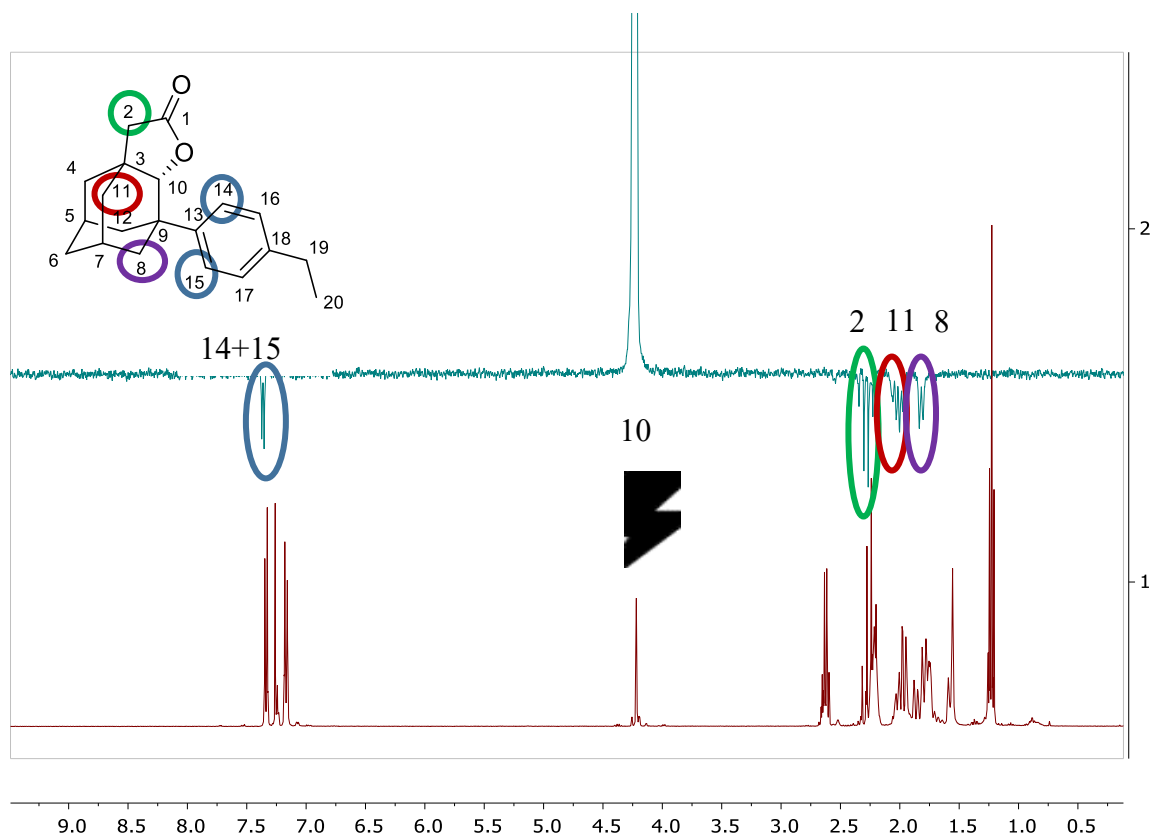


¹H NMR (400 MHz, CDCl₃) δ 7.34 (d, *J* = 8.3 Hz, 2H; C₁₄ [1H] + C₁₅ [1H]), 7.17 (d, *J* = 8.3 Hz, 2H; C₁₆ [1H] + C₁₇ [1H]), 4.22 (s, 1H; C₁₀ [1H]), 2.62 (q, *J* = 7.6 Hz, 2H; C₁₉ [2H]), 2.34 – 2.16 (m, 5H; C₂ [2H] + C₅ [1H] + C₇ [1H] + C₁₂ [1H]), 2.08-1.94 (m, 3H; C₈ [2H] + C₄ [1H]), 1.89 (d, *J* = 11.7 Hz, 1H; C₁₂ [1H]), 1.86-1.69 (m, 4H; C₆ [2H] + C₄ [1H] + C₁₁ [1H]), 1.57 (d, *J* = 14.3 Hz, 1H; C₁₁ [1H] + H₂O), 1.23 (t, *J* = 7.6 Hz, 3H; C₂₀ [3H]).

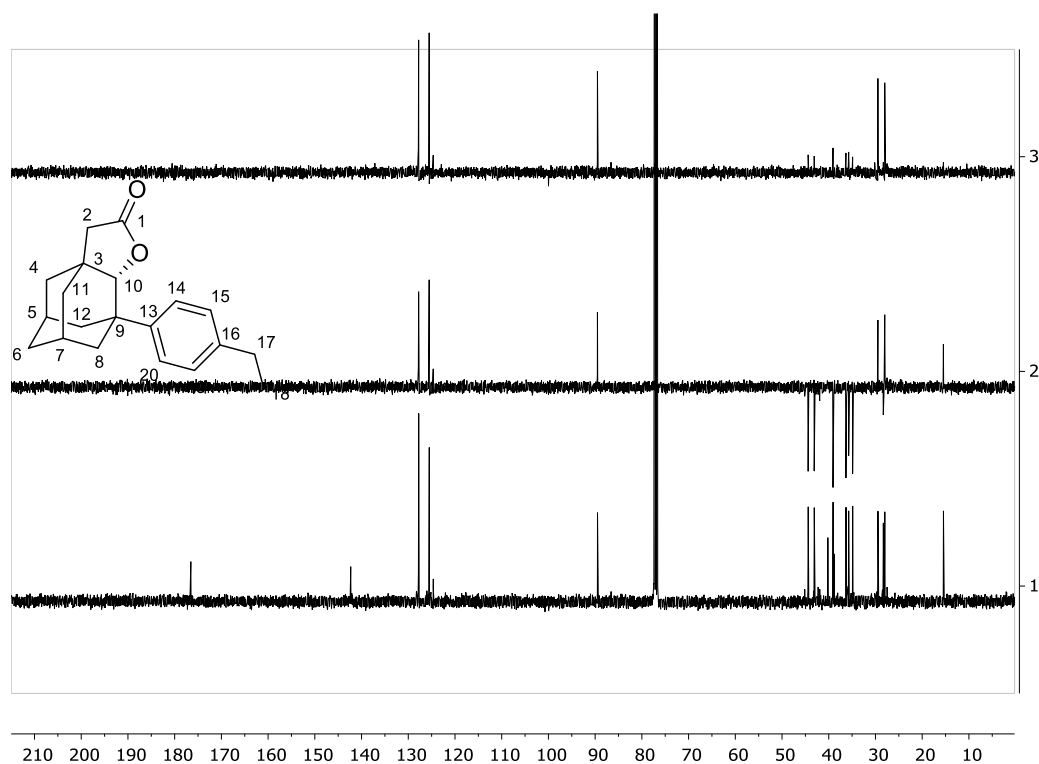
^{13}C NMR of **14a** in CDCl_3



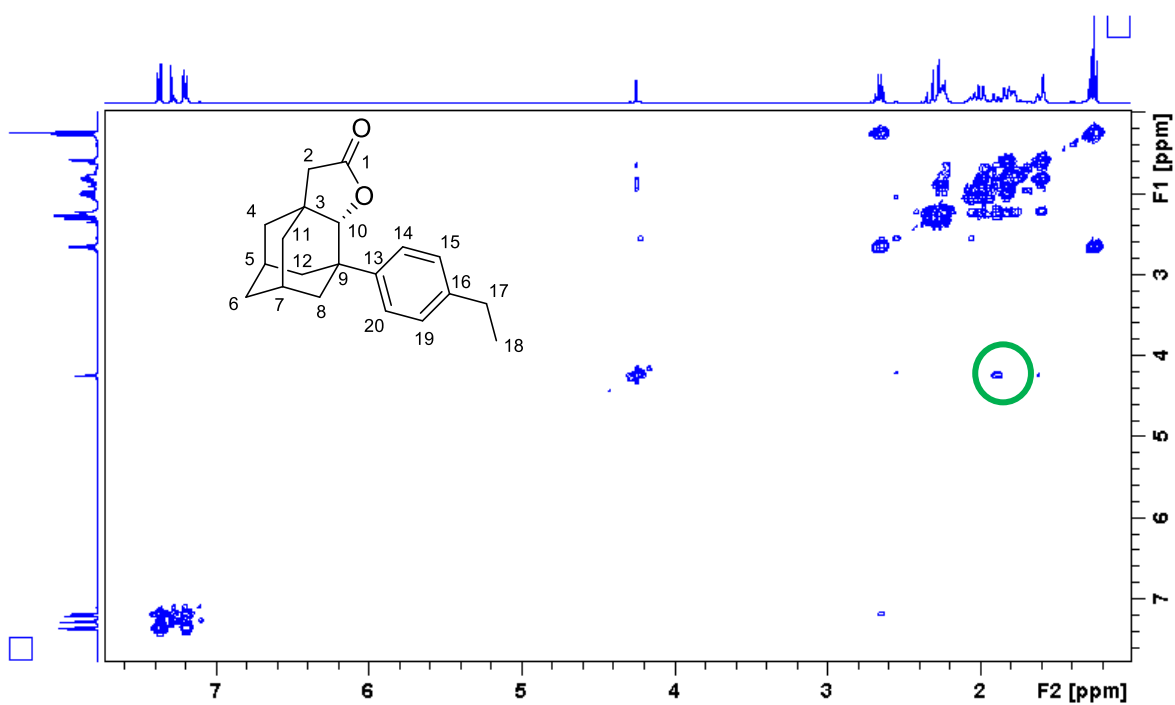
^{13}C NMR (101 MHz, CDCl_3) δ 176.5 (C_1), 142.4 (C_{13}), 142.3 (C_{18}), 127.8 ($C_{14} + C_{15}$), 125.5 ($C_{16} + C_{17}$), 89.5 (C_{10}), 44.4 (C_2), 43.1 (C_8), 40.2 (C_3), 39.1 (C_4), 38.8 (C_9), 36.3 (C_{12}), 35.7 (C_6), 34.9 (C_{12}), 29.5 (C_5), 28.3 (C_{19}), 28.0 (C_7), 15.4 (C_{20}).



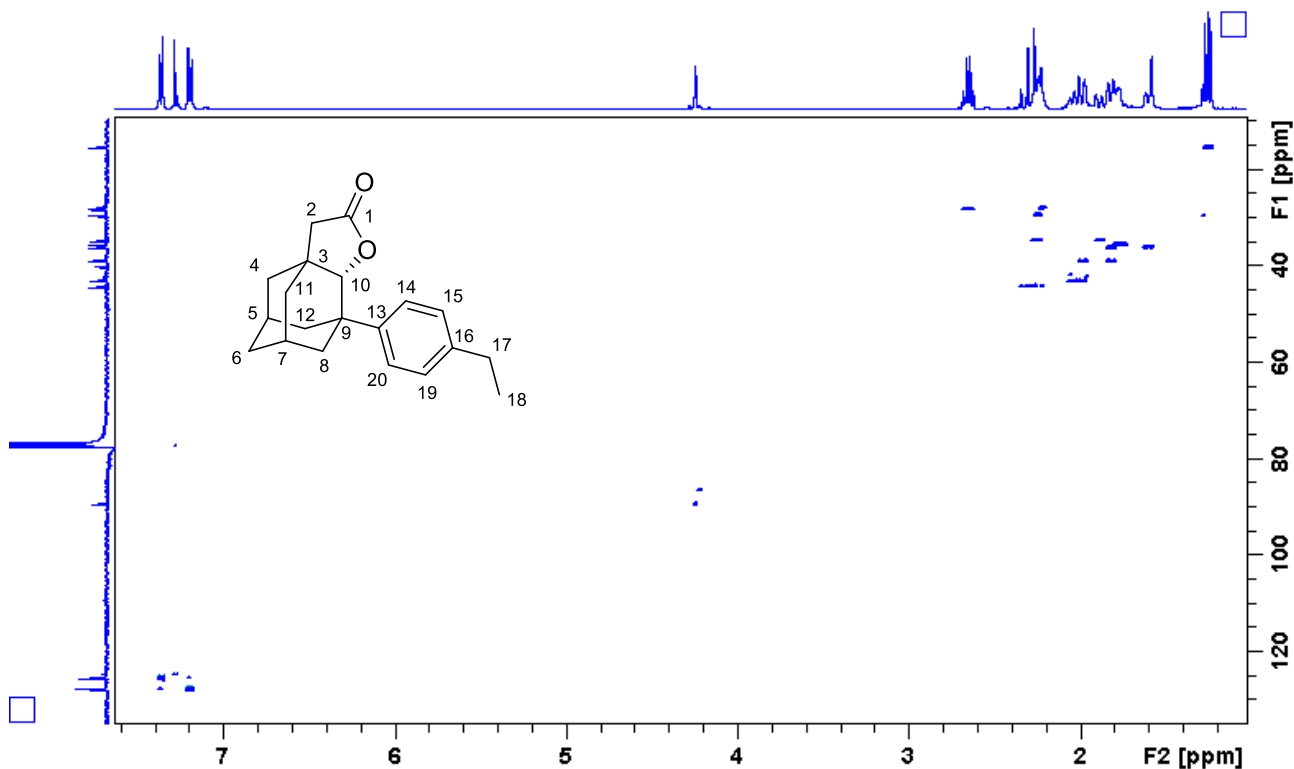
Stacking of the ^1H NMR spectrum of **14a** (bottom) with its selective NOESY obtained after irradiating at $4.25\ \delta$ (lactone signal, $\text{C}_{10}\text{-H}$). The signals that show a NOESY correlation with $\text{C}_{10}\text{-H}$ are visible in a negative phase.



Stacking of the ^{13}C NMR spectrum of **14a** (bottom) stacked with its DEPT90 (top) and its DEPT 135 (middle) spectra.

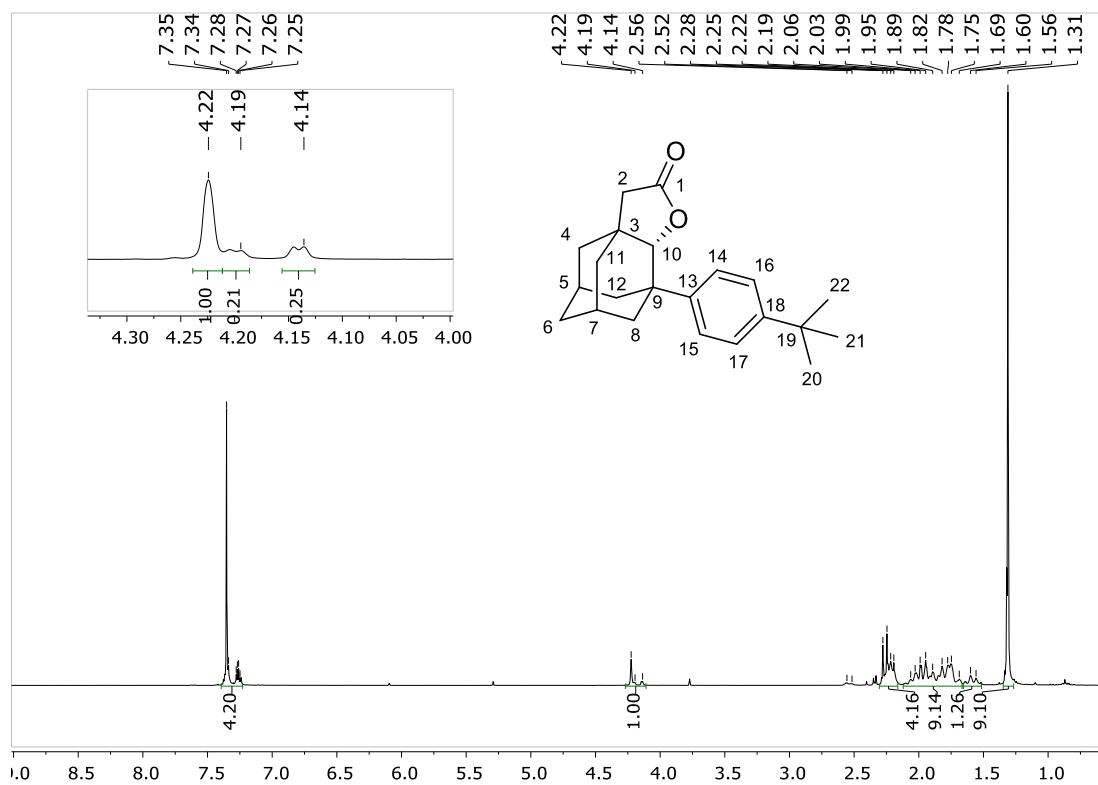


COSY of **14a**. Note the coupling the main proximal lactone C₁₀-H (right, main product) with secondary C₈-H bond, respectively (highlighted in green).



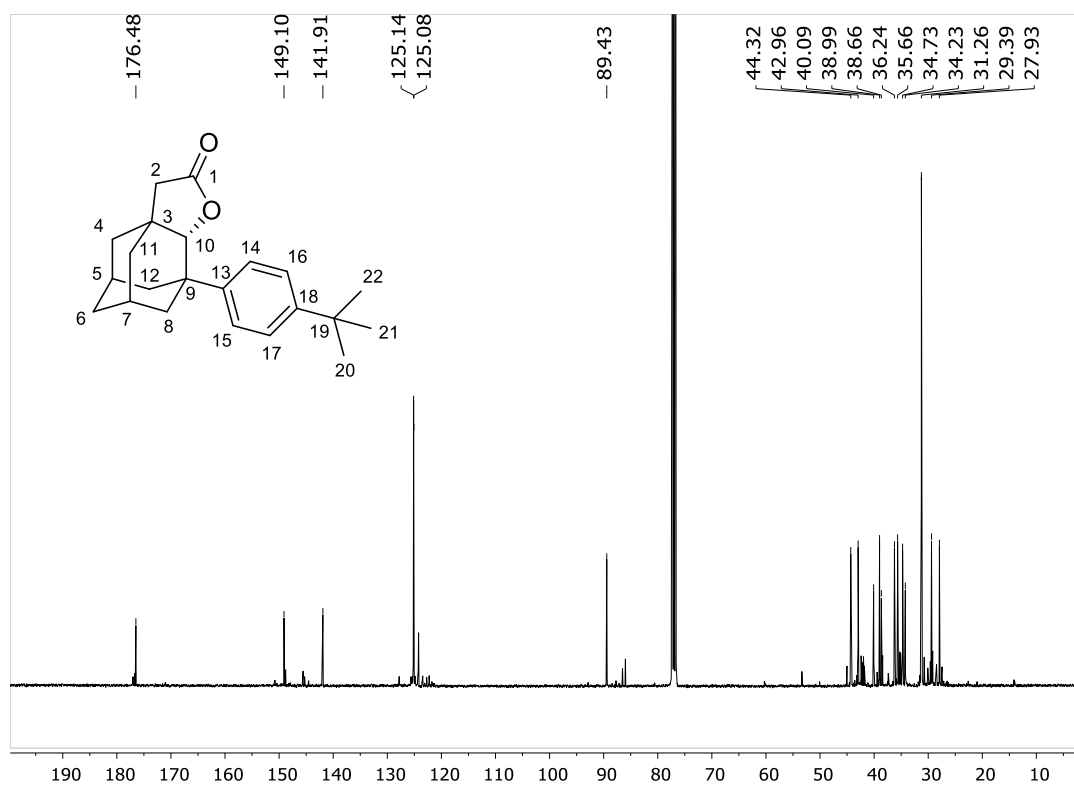
HSQC of **14a**.

¹H NMR of **15a** in CDCl₃

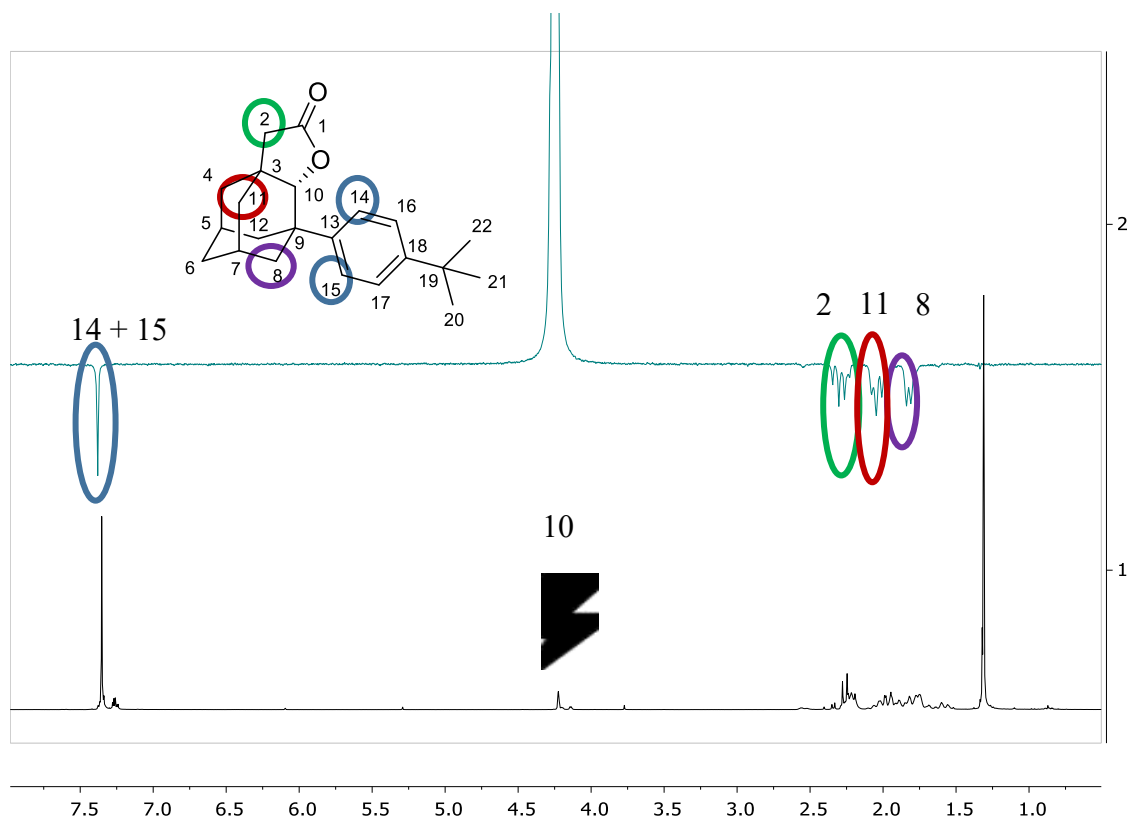


¹H NMR (400 MHz, CDCl₃) δ 7.34 (s, 4H; C₁₄ [1H] + C₁₅ [1H] + C₁₆ [1H] + C₁₇ [1H]), 4.21 (s, 1H; C₁₀ [1H]), 2.22 (m, 5H; C₂ [2H] + C₅ [1H] + C₇ [1H] + C₈ [1H]), 1.95 (m, 4H; C₁₂ [2H] + C₈ [1H] + C₄ [1H]), 1.77 (m, 4H; C₆ [2H] + C₄ [1H] + C₁₁ [1H]), 1.58 (m, 1H; C₁₁ [1H]), 1.30 (s, 9H; C₂₀ [3H] + C₂₁ [3H] + C₂₂ [3H]). In the inset an expansion with the proximal and distal lactones is displayed. Small peaks in the spectrum (i.e. at 2.55) are the signals of the distal isomers.

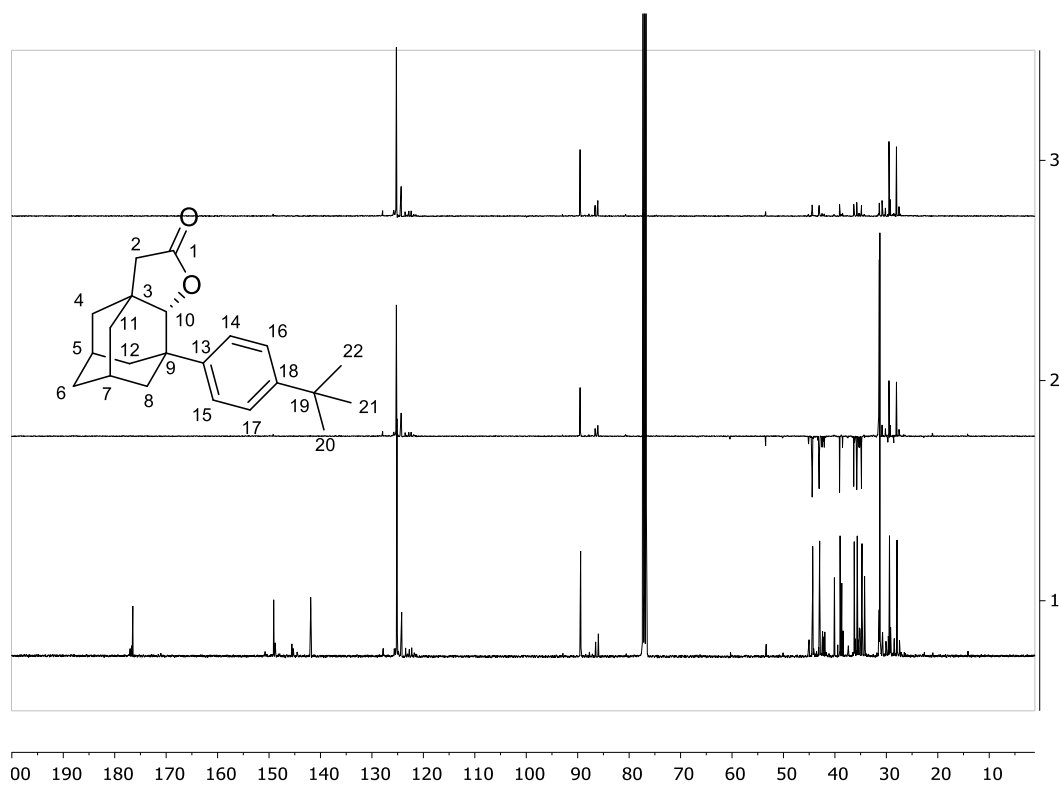
¹³C NMR of **15a** in CDCl₃



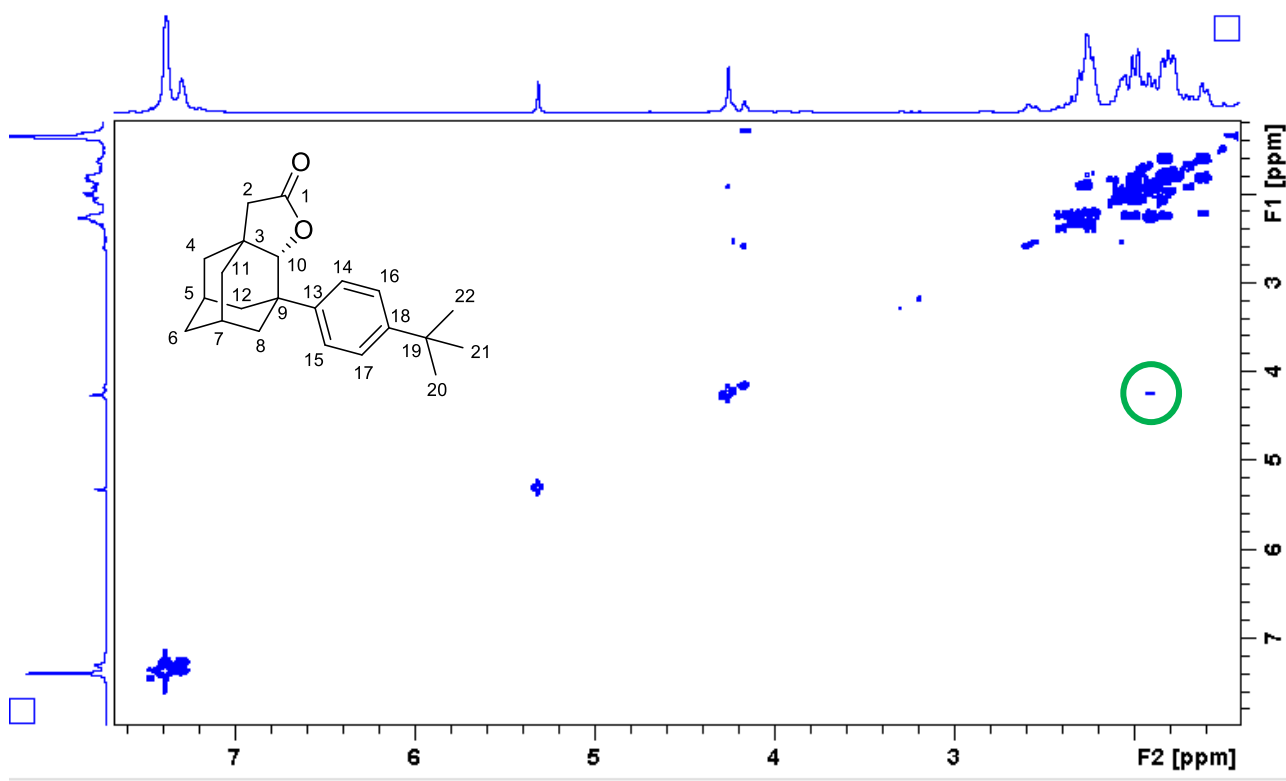
¹³C NMR (101 MHz, CDCl₃) δ 176.5 (*C*₁), 149.1(*C*₁₈), 141.9 (*C*₁₃), 125.1 (*C*₁₄ + *C*₁₅), 125.1 (*C*₁₆ + *C*₁₇), 89.4 (*C*₁₀), 44.3 (*C*₂), 43.0 (*C*₁₂), 40.1 (*C*₃), 39.0 (*C*₄), 38.7 (*C*₉), 36.2 (*C*₁₁), 35.7 (*C*₆), 34.7 (*C*₈), 34.2 (*C*₁₉), 31.3 (*C*₂₀ + *C*₂₁ + *C*₂₂), 29.4 (*C*₅ or *C*₇), 27.9 (*C*₅ or *C*₇). Small peaks in the spectrum are the signals of the distal isomers.



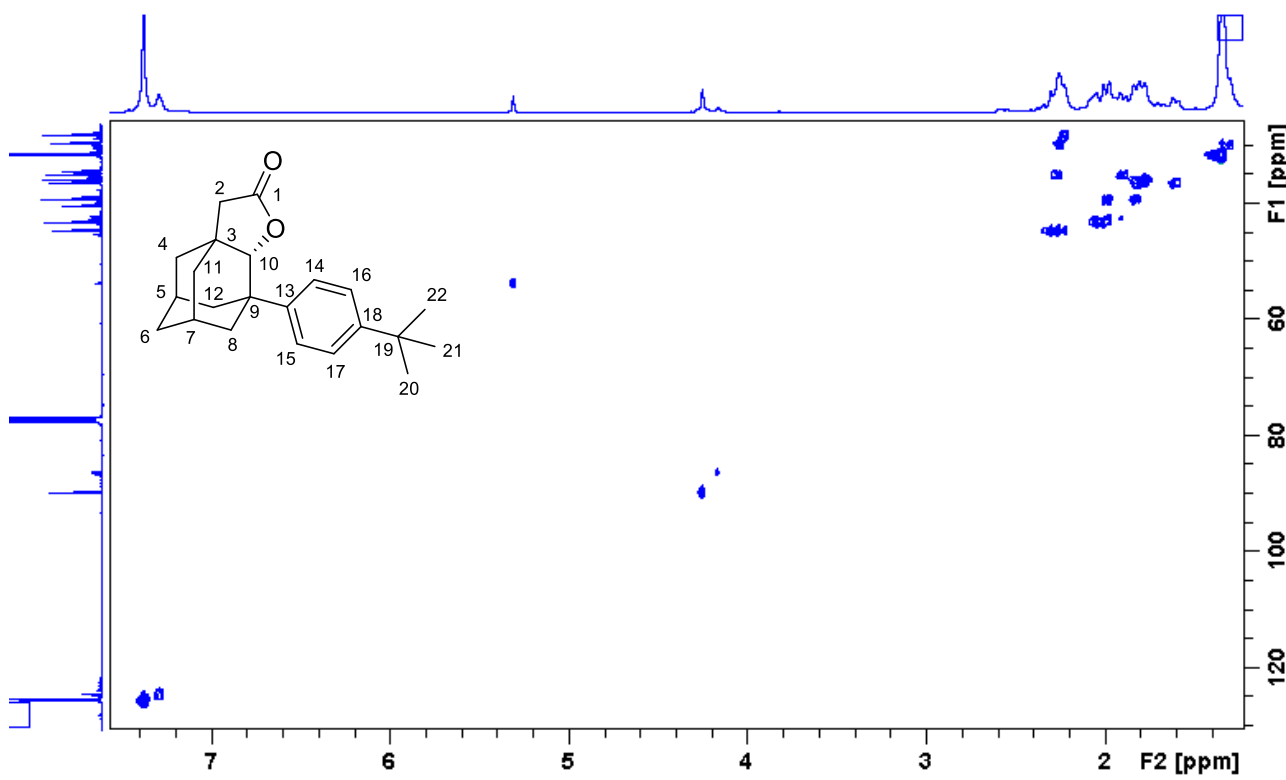
Stacking of the ¹H NMR spectrum of **15a** (bottom) with its selective NOESY obtained after irradiating at 4.21 δ (lactone signal, C₁₀-H). The signals that show a NOESY correlation with C₁₀-H are visible in a negative phase.



Stacking of the ¹³C NMR spectrum of **15a** (bottom) stacked with its DEPT90 (top) and its DEPT 135 (middle) spectra.

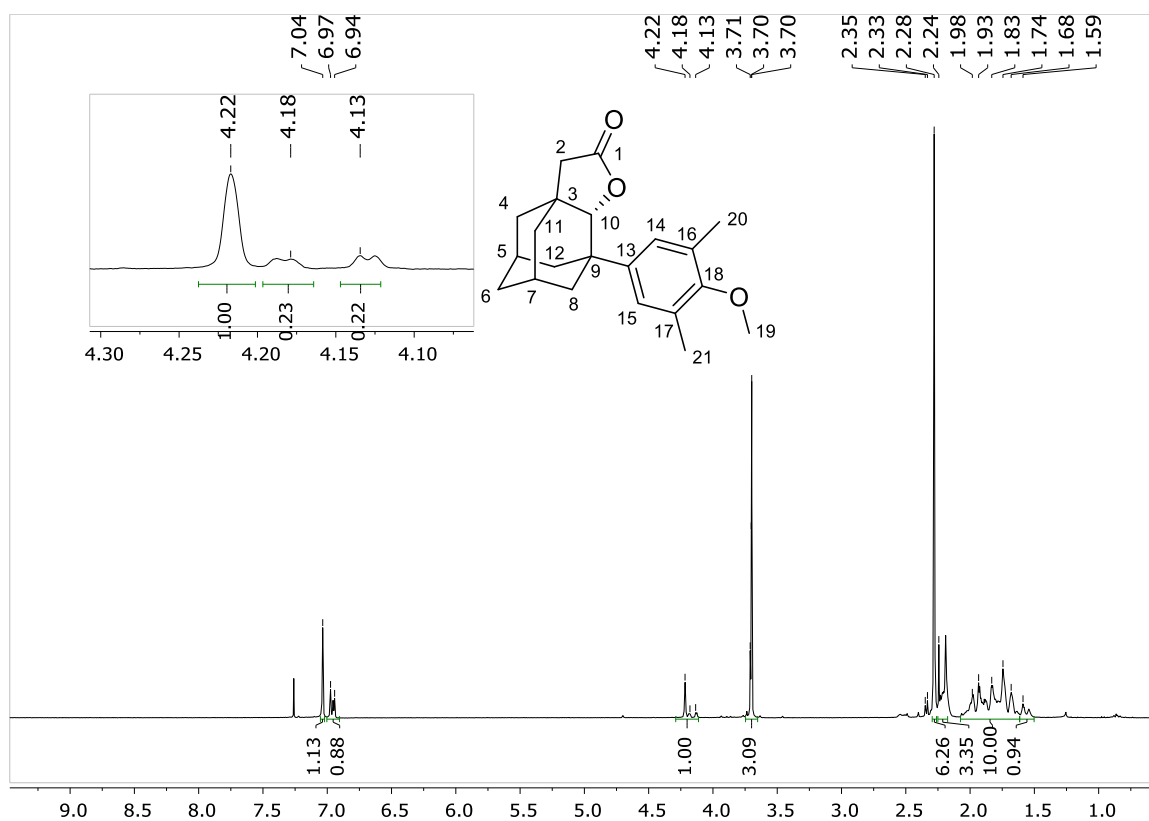


COSY of **15a**. Note the coupling the main proximal lactone C₁₀-H (right, main product) with secondary C₈-H bond, respectively (highlighted in green).



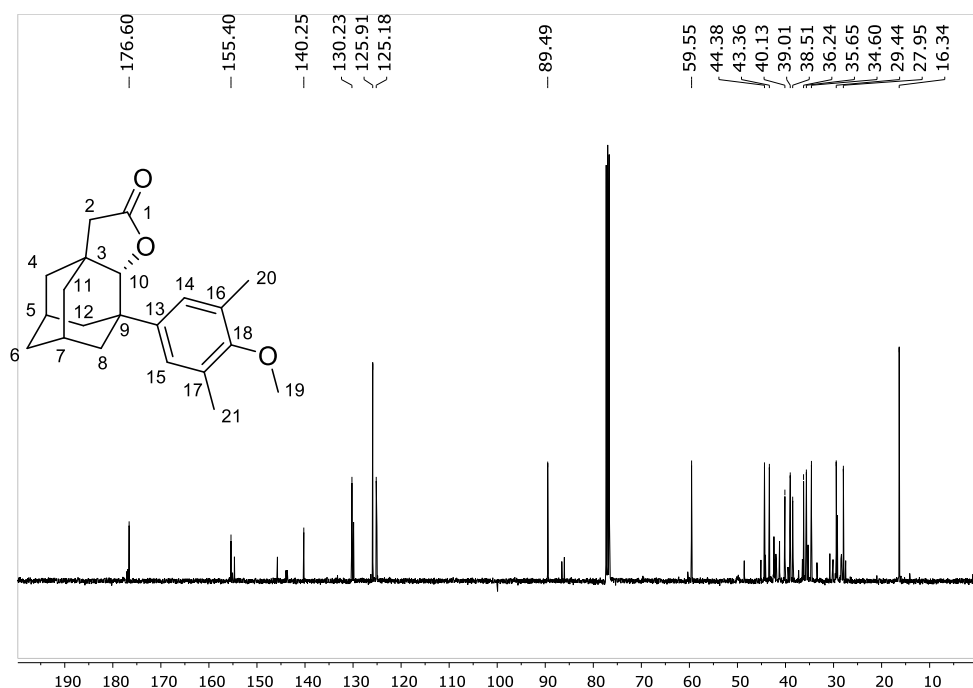
HSQC of **15a**

¹H NMR of **16a** in CDCl₃

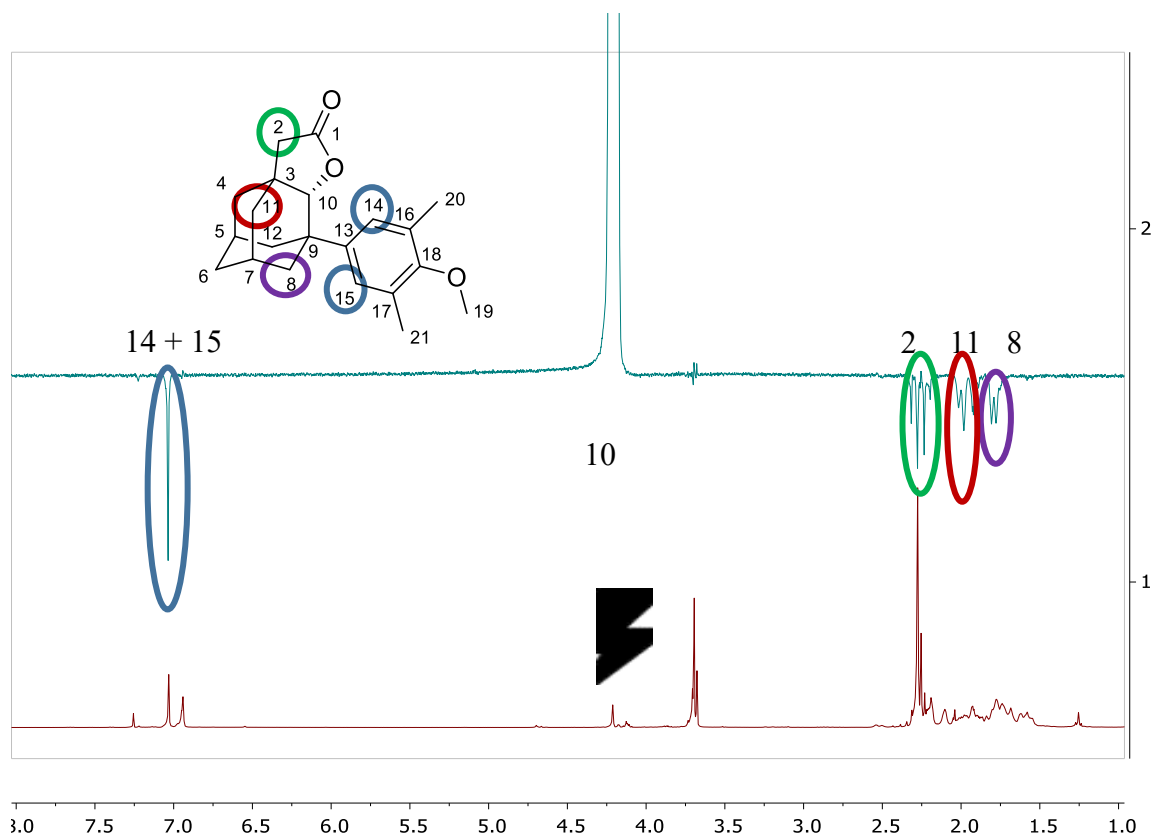


¹H NMR (300 MHz, CDCl₃) δ 7.04 (s, 1H; C₁₅[1H]), 6.95 (d, J = 9.5 Hz 1H; C₁₄[1H]), 4.18 (s, 1H; C₁₀ [1H]), 3.70 (m, 3H; C₁₉ [3H]), 2.28 (s, 6H, C₂₀ [3H] + C₂₁ [3H]), 2.24 (m, 3H; C₂ [2H] + C₈[1H]), 2.08 – 1.62 (m, 10H; C₁₂ [2H] + C₈ [1H] + C₄ [2H] + C₆ [2H] + C₅[1H] + C₇[1H] + C₁₁ [1H]), 1.81-1.69 (m, 4H; C₆ [2H] + C₄ [1H] + C₁₁ [1H]), 1.62-1.54 (m, 1H; C₁₁ [1H]). In the inset an expansion with the proximal and distal lactones is displayed. Small peaks in the spectrum (i.e. at 2.35) are the signals of the distal isomers.

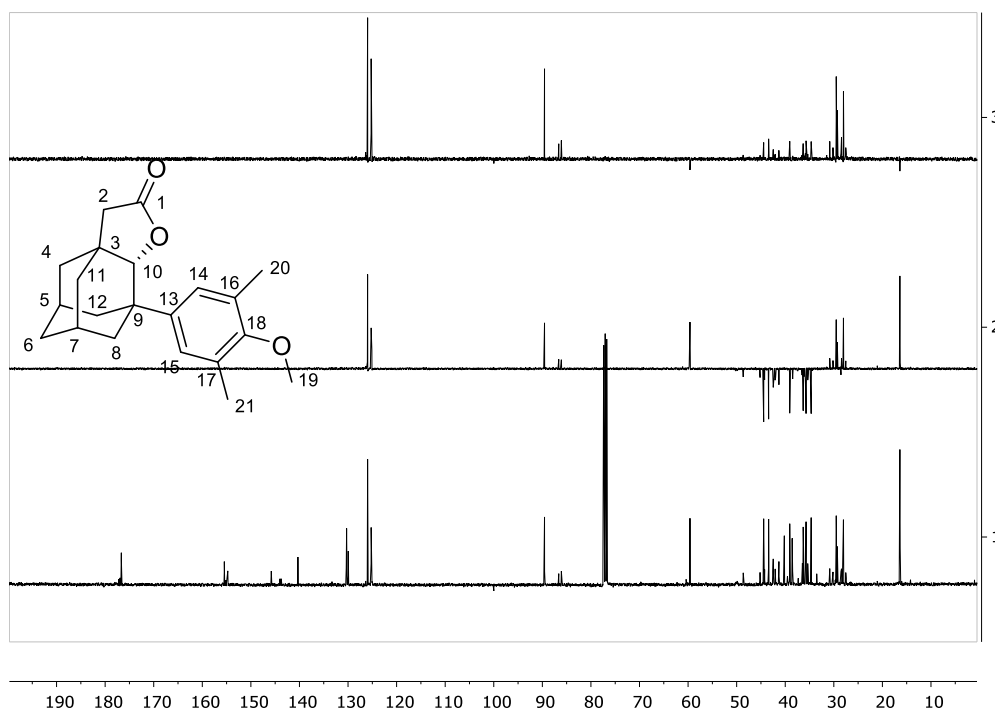
¹³C NMR of **16a** in CDCl₃



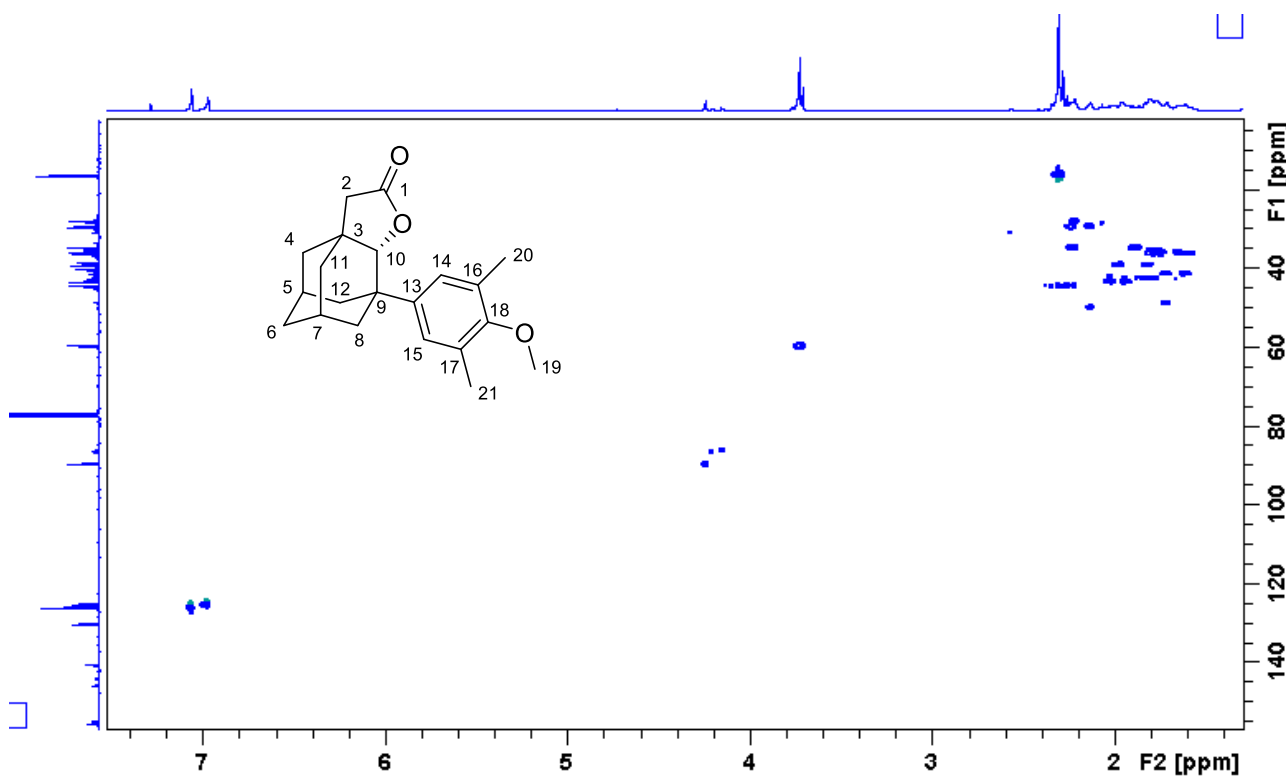
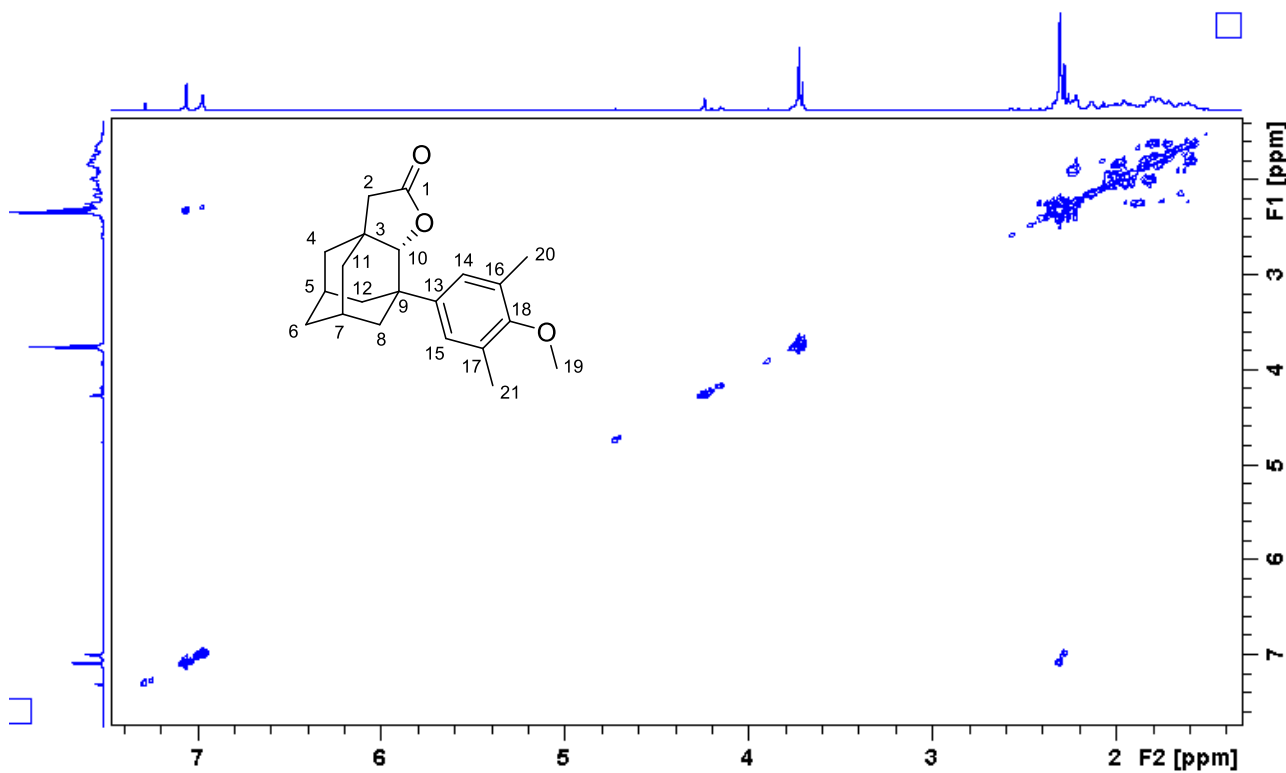
¹³C NMR (101 MHz, CDCl₃) δ 176.6 (*C*₁), 155.4 (*C*₁₈), 140.2 (*C*₁₃), 130.2 (*C*₁₆ or *C*₁₇), 125.9 (*C*₁₄ + *C*₁₅), 125.2 (*C*₁₆ or *C*₁₇), 89.5 (*C*₁₀), 59.55 (*C*₁₉), 44.4 (*C*₂), 43.4 (*C*₁₂), 40.1 (*C*₃), 39.0 (*C*₄), 38.5 (*C*₉), 36.2 (*C*₁₁), 35.6 (*C*₆), 34.6 (*C*₈), 29.4 (*C*₅ or *C*₇), 27.9 (*C*₅ or *C*₇), 16.3 (*C*₂₀ + *C*₂₁). Small peaks in the spectrum are the signals of the distal isomers.



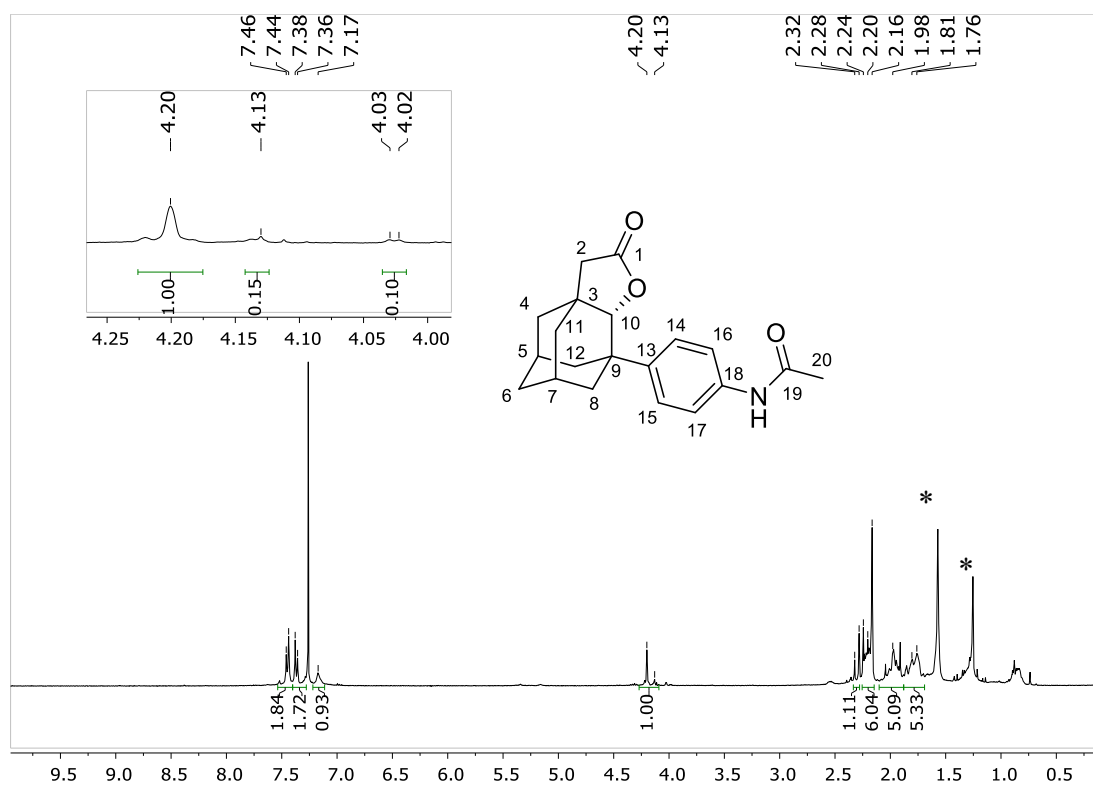
Stacking of the ^1H NMR spectrum of **16a** (bottom) with its selective NOESY obtained after irradiating at 4.21 δ (lactone signal, C₁₀-H). The signals that show a NOESY correlation with C₁₀-H are visible in a negative phase.



Stacking of the ^{13}C NMR spectrum of **16a** (bottom) stacked with its DEPT90 (top) and its DEPT 135 (middle) spectra.

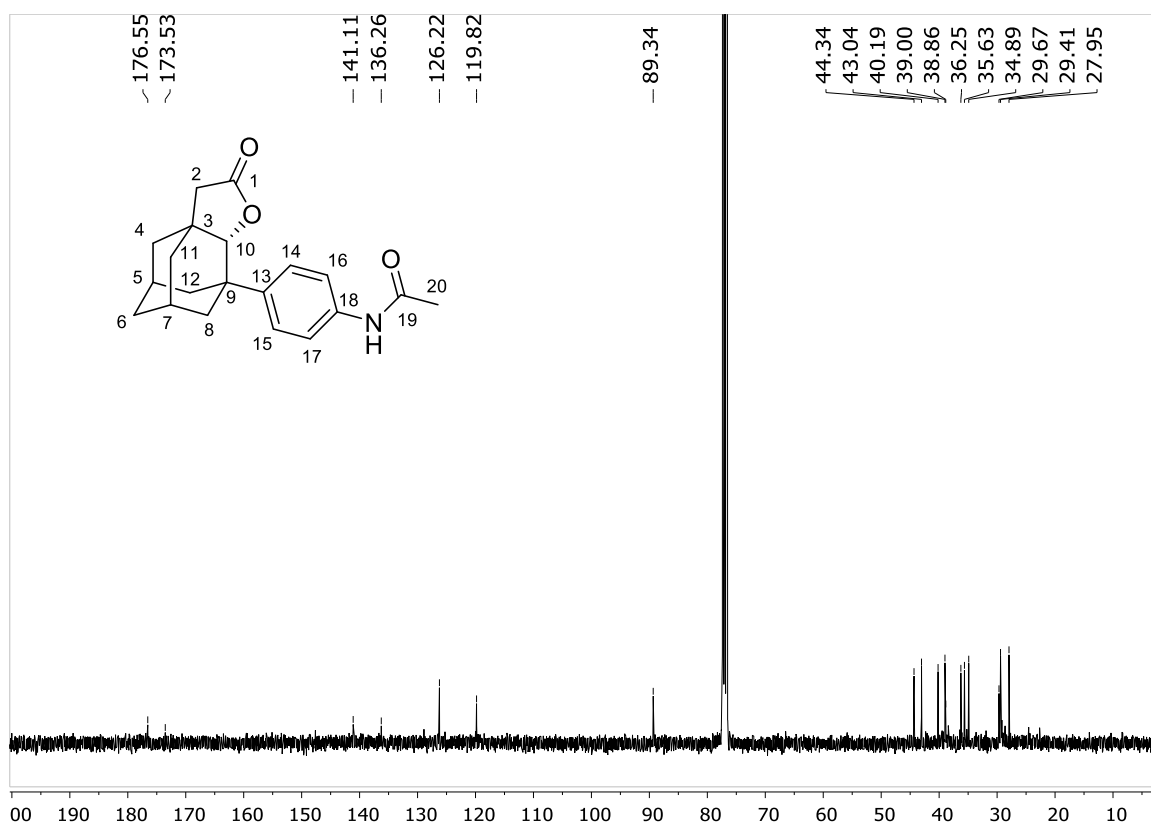


¹H NMR of **17a** in CDCl₃

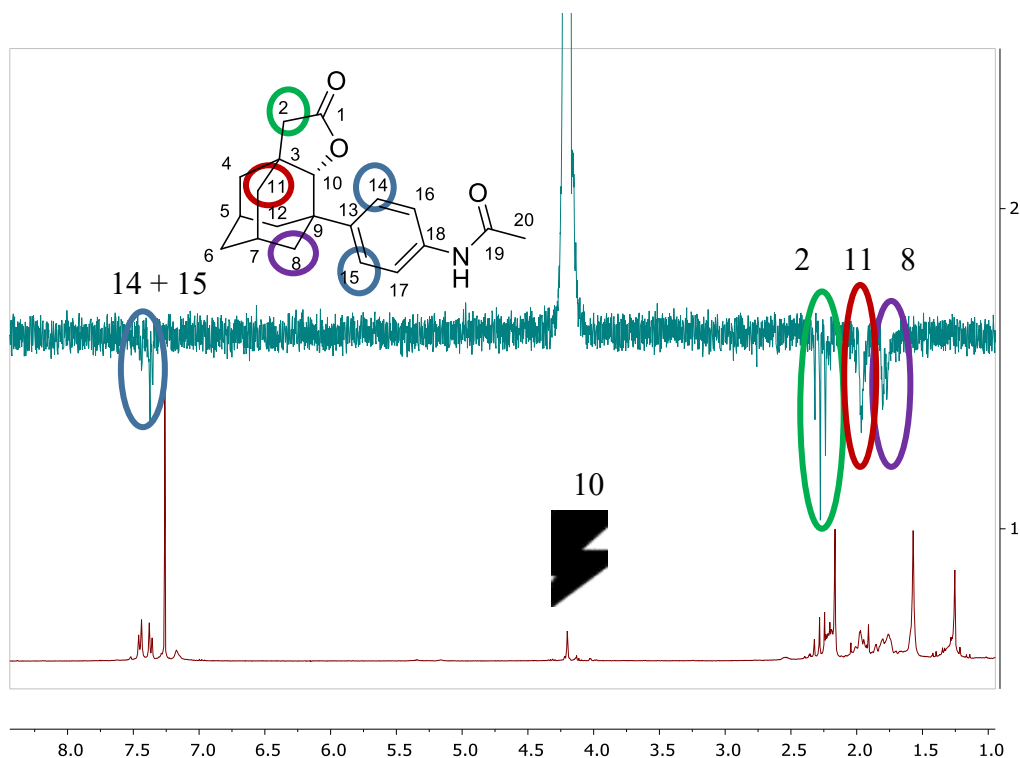


¹H NMR (400 MHz, CDCl₃) δ 7.45 (m, 2H; C₁₄ [1H] + C₁₅ [1H]), 7.36 (m, 2H; C₁₆ [1H] + C₁₇ [1H]), 4.20 (s, 1H; C₁₀ [1H]), 2.30 (d, *J* = 16.1 Hz, 1H; C₂ [1H]), 2.20 (d, *J* = 33.8 Hz, 4H), 1.97 (m, 3H), 1.80 (d, *J* = 39.5 Hz, 5H), 1.57 (d, *J* = 12.9 Hz, 1H), 1.25 (s, 3H; C₂₀ [3H]). In the inset an expansion with the proximal and distal lactones is displayed. The peaks marked with an asterisk are H₂O and acetone. Small peaks in the spectrum are the signals of the distal isomers.

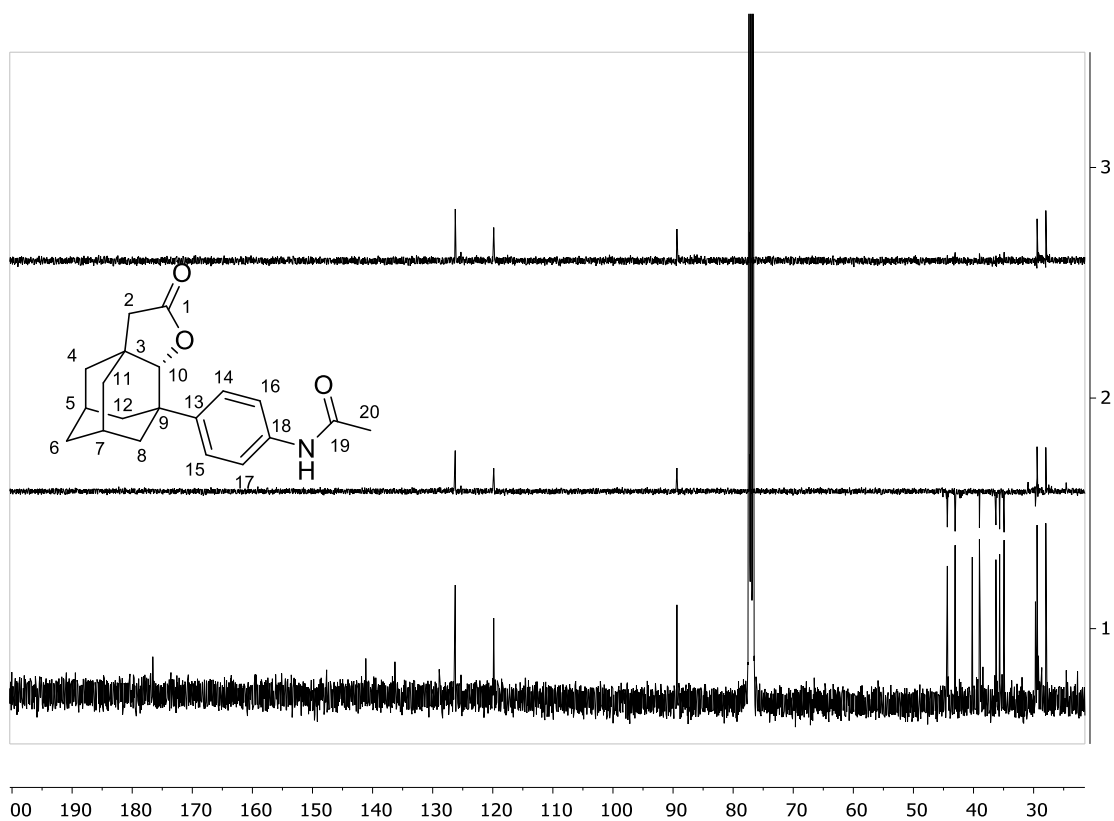
¹³C NMR of **17a** in CDCl₃



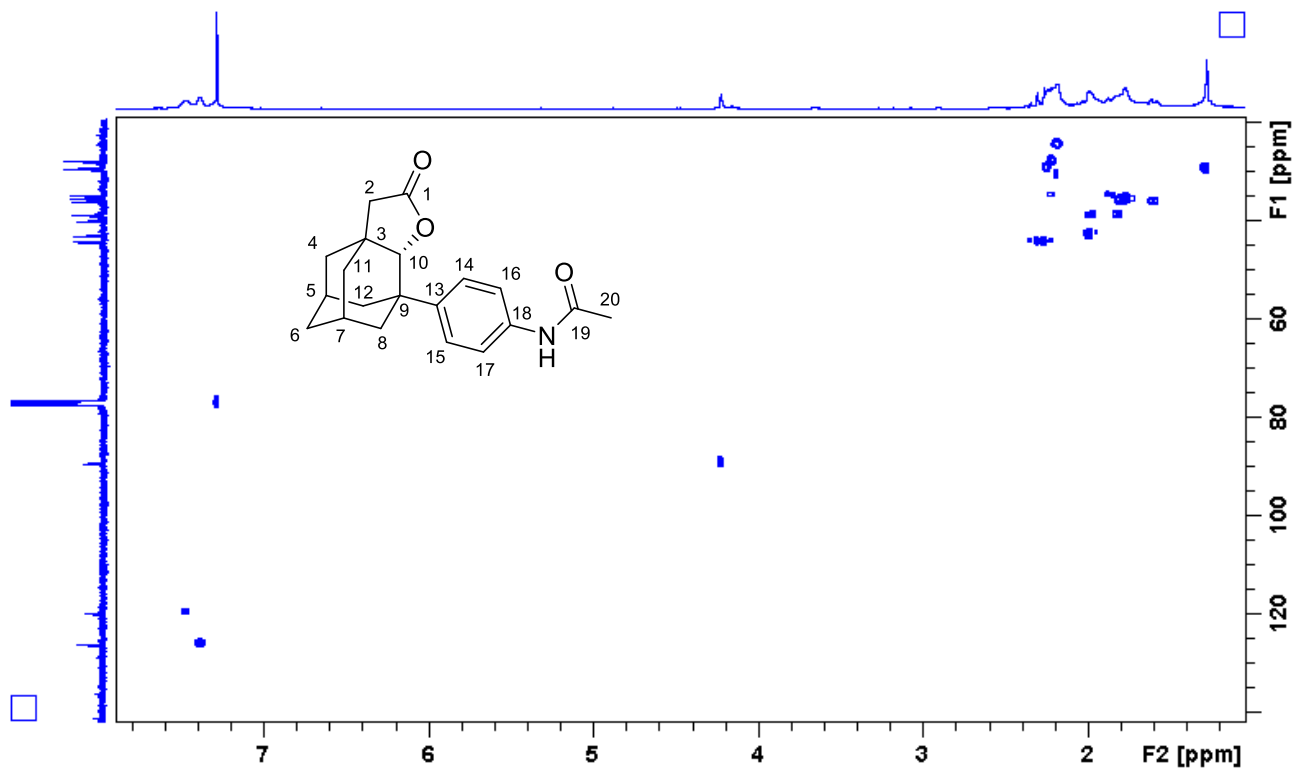
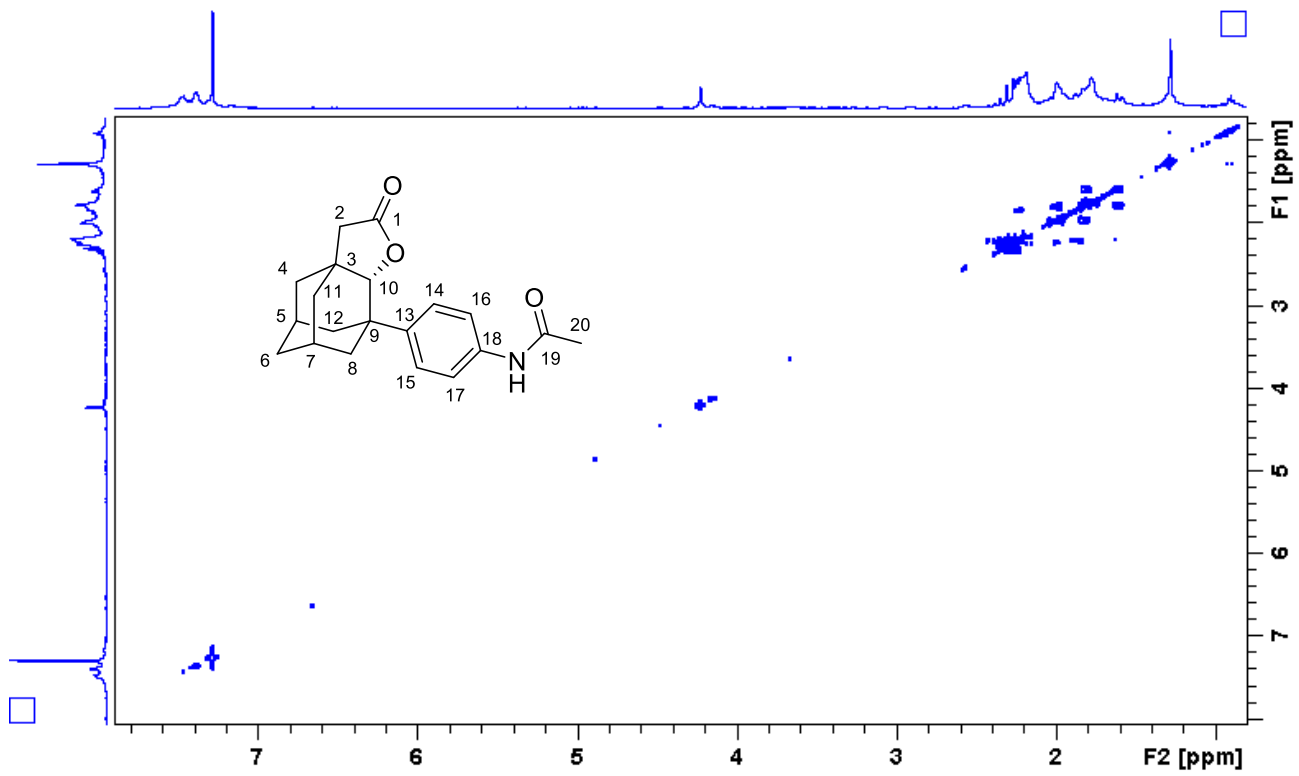
¹³C NMR (101 MHz, CDCl₃) δ 176.5 (C₁), 173.5 (C₁), 141.1 (C₁₉), 136.3 (C₁₃), 126.2 (C₁₄ + C₁₅), 119.8 (C₁₆ + C₁₇), 89.3 (C₁₀), 44.3 (C₂), 43.0, 40.2 (C₃), 39.0, 38.9 (C₉), 36.2, 35.6, 34.9, 29.7 (C₂₀), 29.4 (C₅ or C₇), 27.9 (C₅ or C₇).



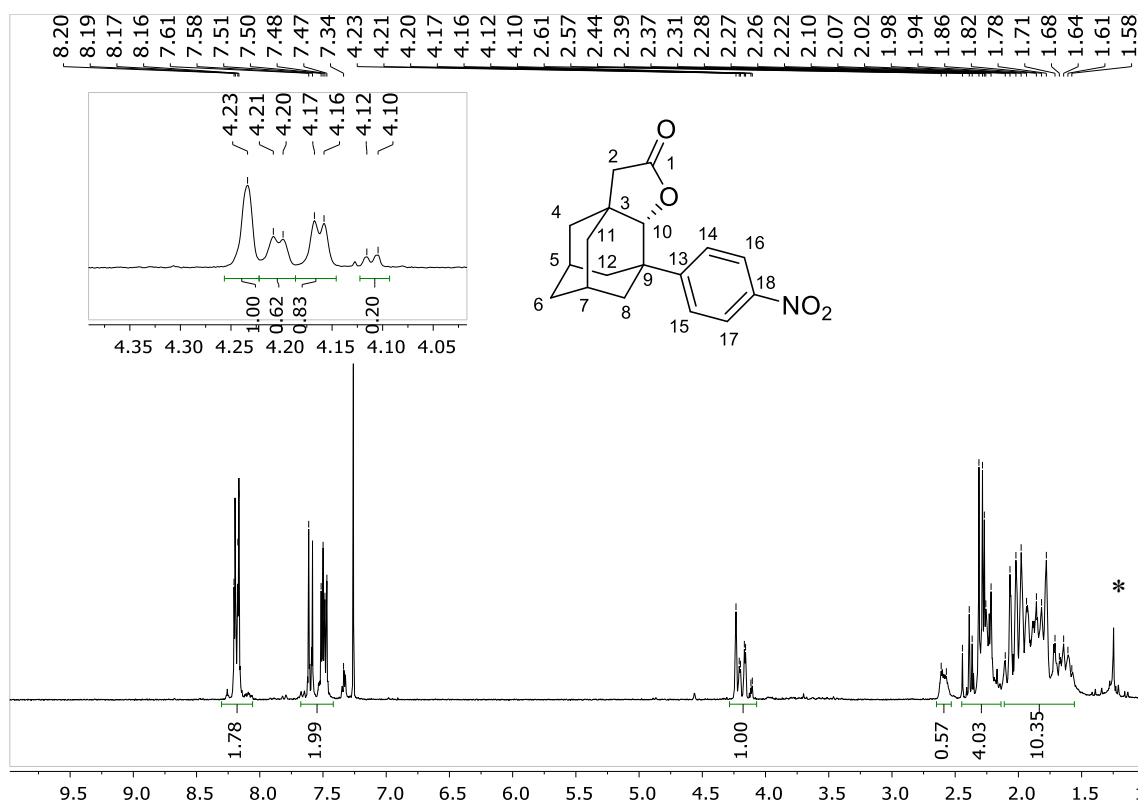
Stacking of the ¹H NMR spectrum of **17a** (bottom) with its selective NOESY obtained after irradiation at 4.20 δ (lactone signal, C₁₀-H). The signals that show a NOESY correlation with C₁₀-H are visible in a negative phase.



Stacking of the ¹³C NMR spectrum of **17a** (bottom) stacked with its DEPT90 (top) and its DEPT 135 (middle) spectra.

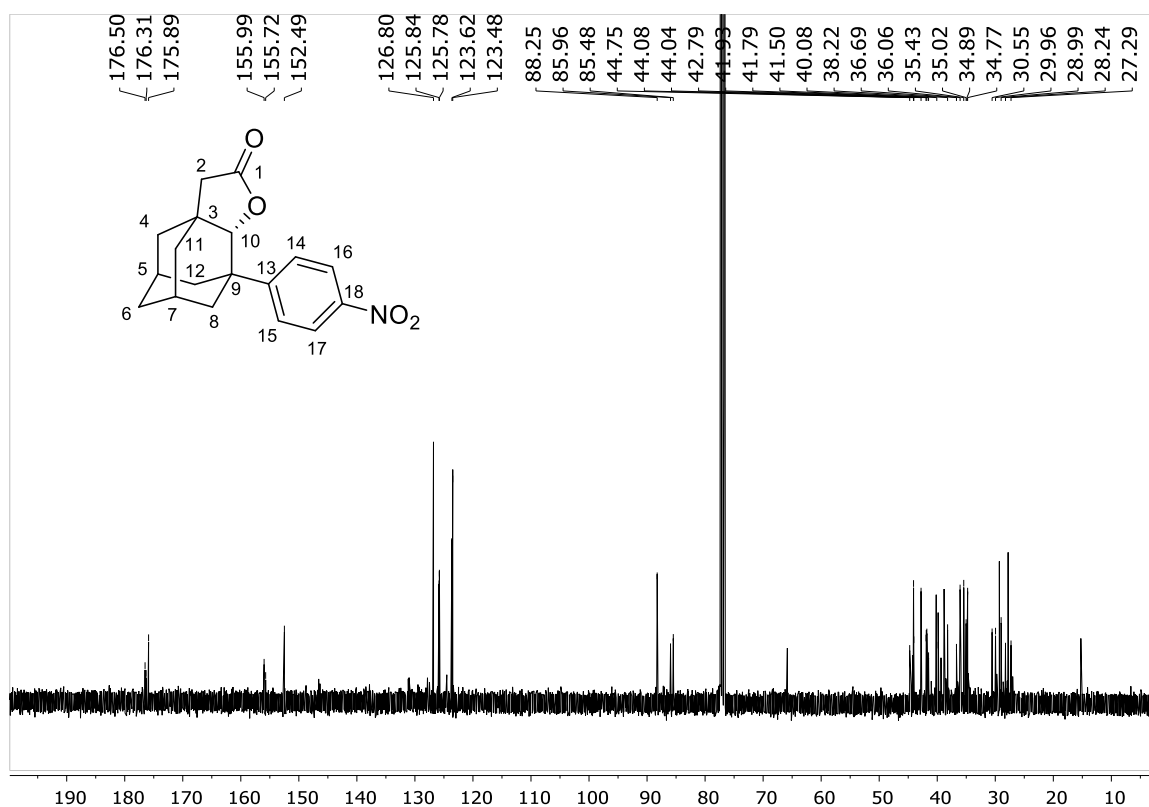


¹H NMR of **18a** in CDCl₃

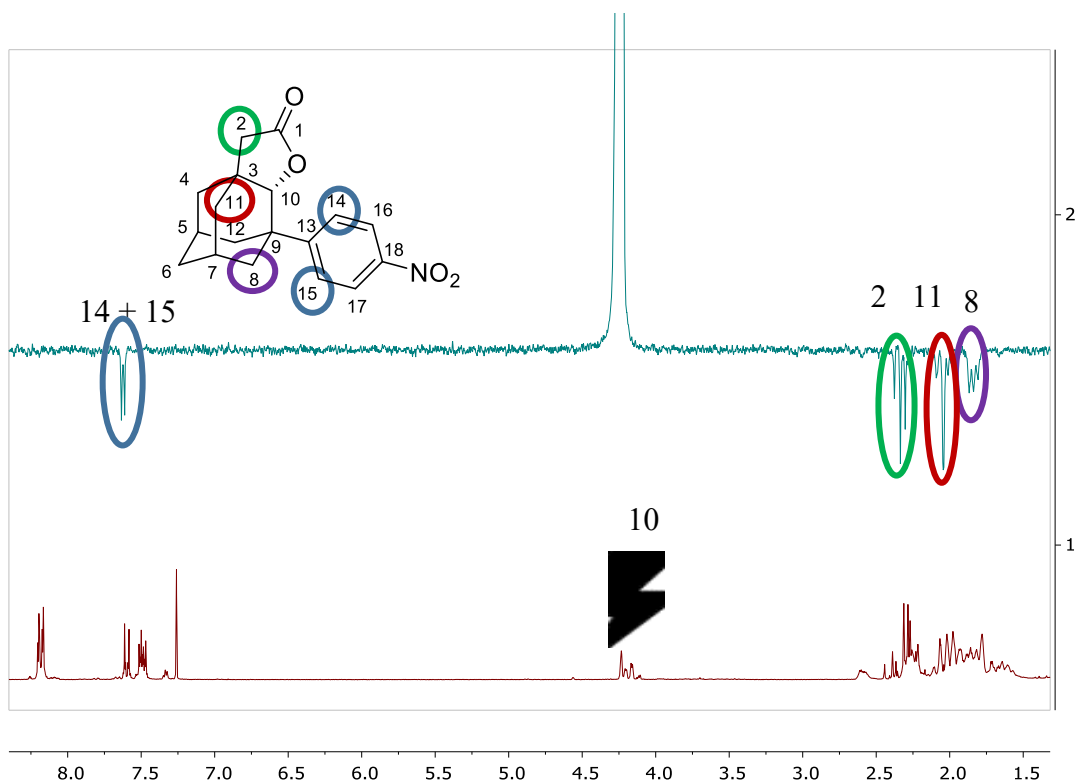


¹H NMR (400 MHz, CDCl₃) δ 8.18 (d, $J = 8.8$ Hz, 2H; C_{14} [1H] + C_{15} [1H]), 7.49 (d, $J = 8.9$ Hz, 2H; C_{16} [1H] + C_{17} [1H]), 4.23 (s, 1H; C_{10} [1H] **18a**), 4.20 (m, 1H; C_4 [1H] **18b**), 4.16 (s, 1H; C_{11} [1H] **18c**), 2.61 (d, $J = 12.7$ Hz, 0.6H, C_5 [1H] **18b** + C_7 [1H] **18c**), 2.45 – 2.14 (m, 4H, C_2 [2H] + C_5 [1H] **18a** + C_7 [1H] **18a** + C_{11} [1H] **18b**), 2.11 – 1.55 (m, 10H). The peak marked with an asterisk is H₂O. The small peak at 4.11 ppm (<10% of the lactones, along with that at 7.34 and others below the signals of **18a**, **b** and **c**) corresponds to the lactone of the *meta*-nitro isomer deriving from the oxidation of substrate **18**. Both the isomeric lactone and its parent acid are inseparable from the mixture of **18a**, **b** and **c** and from substrate **18**, respectively.

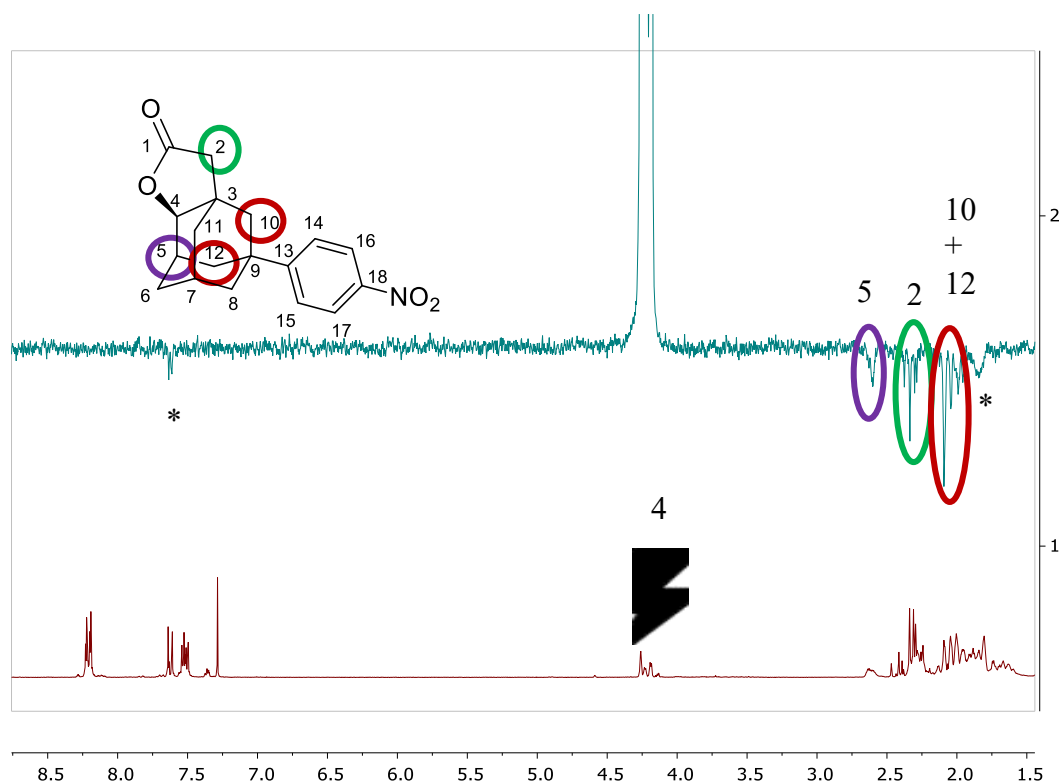
¹³C NMR of **18a** in CDCl₃



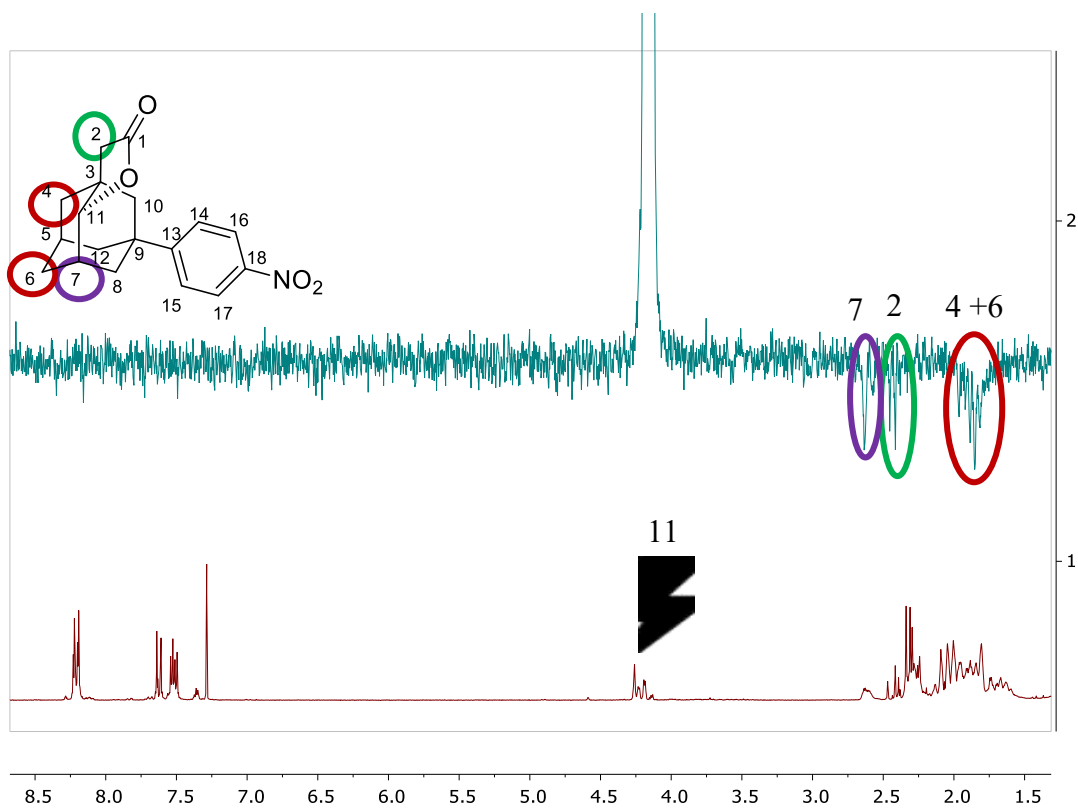
¹³C NMR (101 MHz, CDCl₃) δ 176.5, 176.3, 175.9, 156.0, 155.7, 152.5, 126.8, 125.8, 125.8, 123.6, 123.5, 88.2, 86.0, 85.5, 44.7, 44.1, 44.0, 42.8, 41.9, 41.8, 41.5, 40.1, 38.2, 36.7, 36.1, 35.4, 35.0, 34.9, 34.8, 30.5, 30.0, 29.0, 28.2, 27.3. In this sample the four species are present: the three lactones **18a**, **b** and **c** in nearly equimolar amounts and the lactone of the *meta*-nitro isomer deriving from the oxidation of substrate **18**.



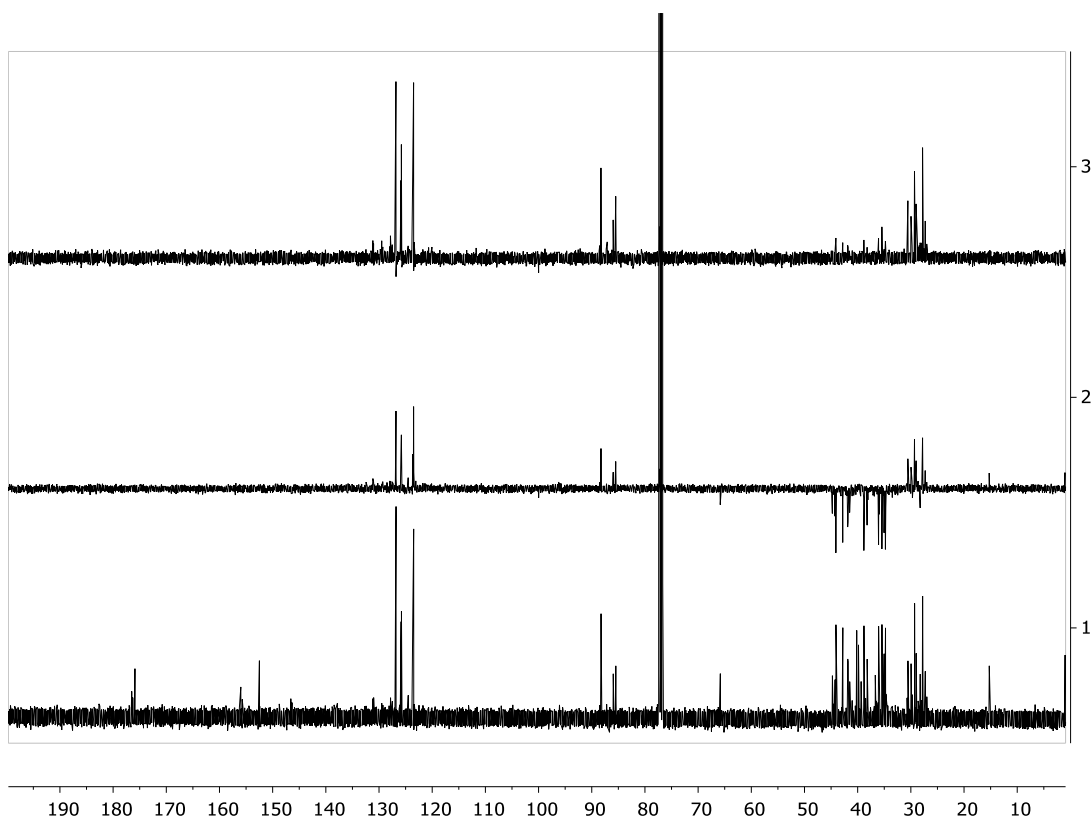
Stacking of the ¹H NMR spectrum of the oxidation of **18** (bottom) with its selective NOESY (in a negative phase) obtained after irradiation at 4.23 δ (lactone signal of **18a**, C₁₀-H).



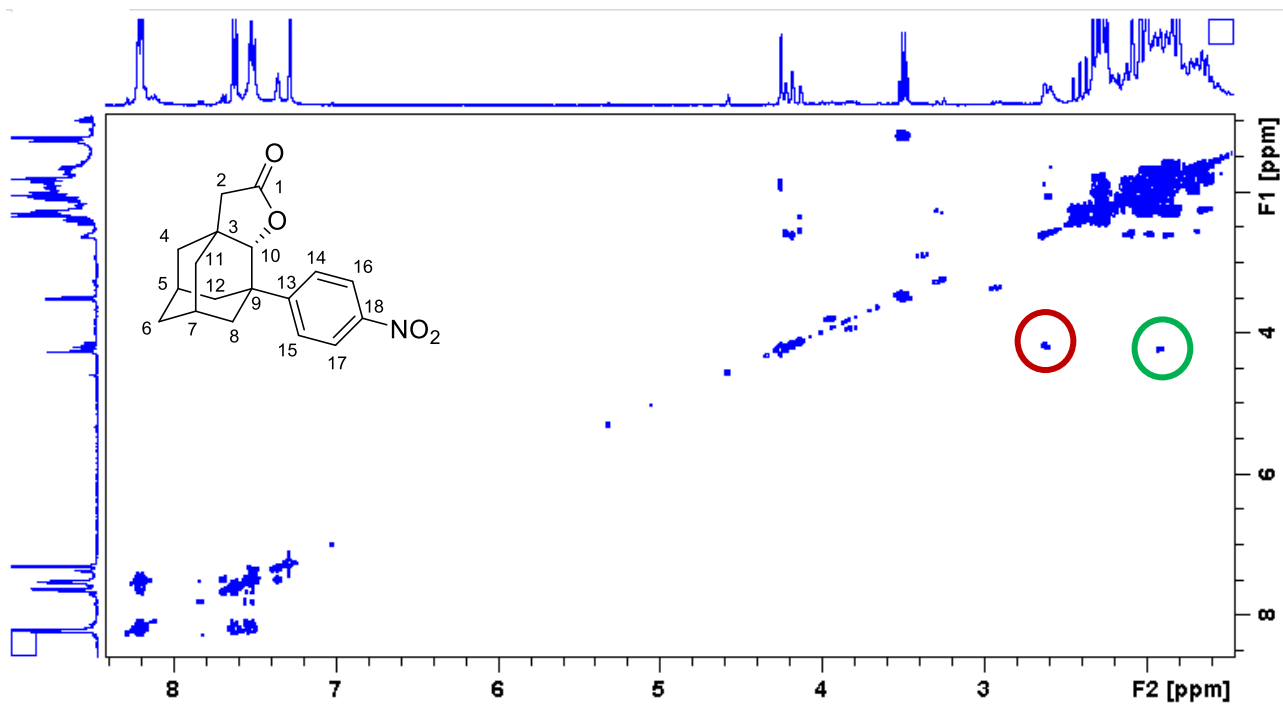
Stacking of the ¹H NMR spectrum of the oxidation of **18** (bottom) with its selective NOESY (in a negative phase) obtained after irradiation at 4.21 δ (lactone signal of **18b**, C₄-H). The peak marked with an asterisk is the residual irradiation of C₁₀-H signal of **18a**.



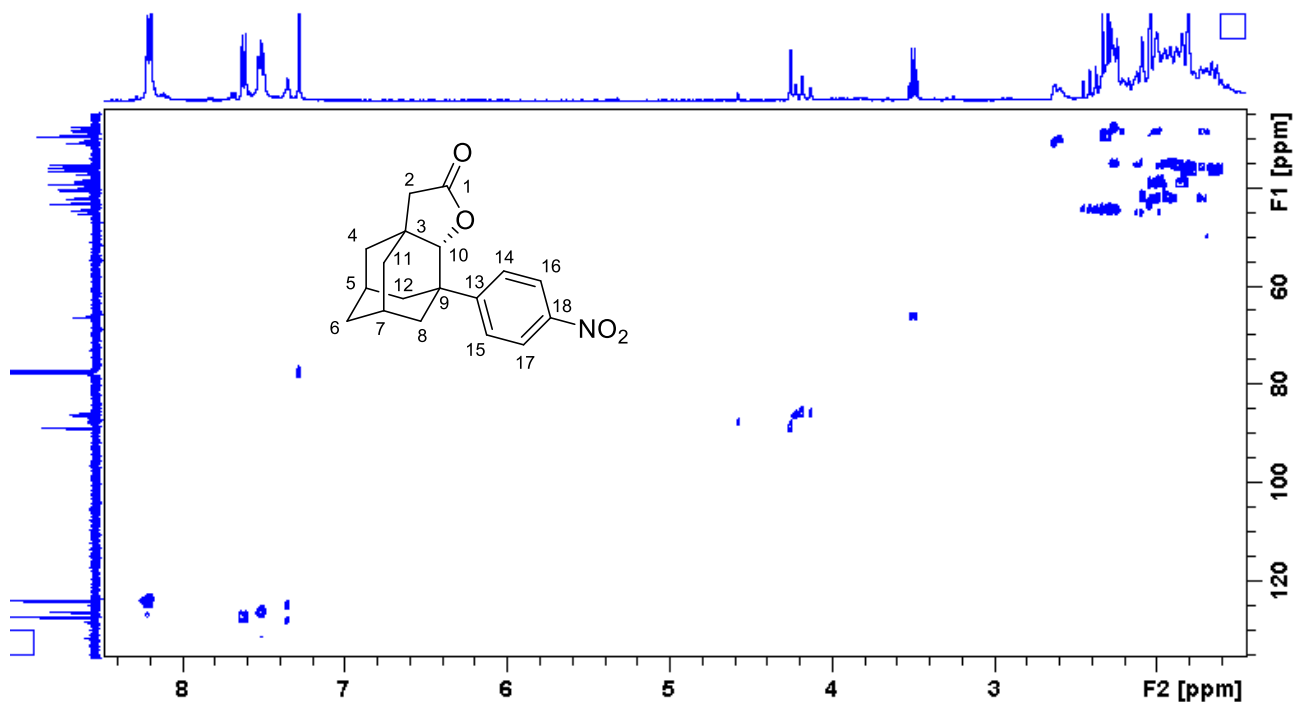
Stacking of the ^1H NMR spectrum of the oxidation of **18** (bottom) with its selective NOESY (in a negative phase) obtained after irradiation at 4.17 δ (lactone signal of **18c**, C₁₁-H).



Stacking of the ^{13}C NMR spectrum of the oxidation of **18** (bottom) stacked with its DEPT90 (top) and its DEPT 135 (middle) spectra.

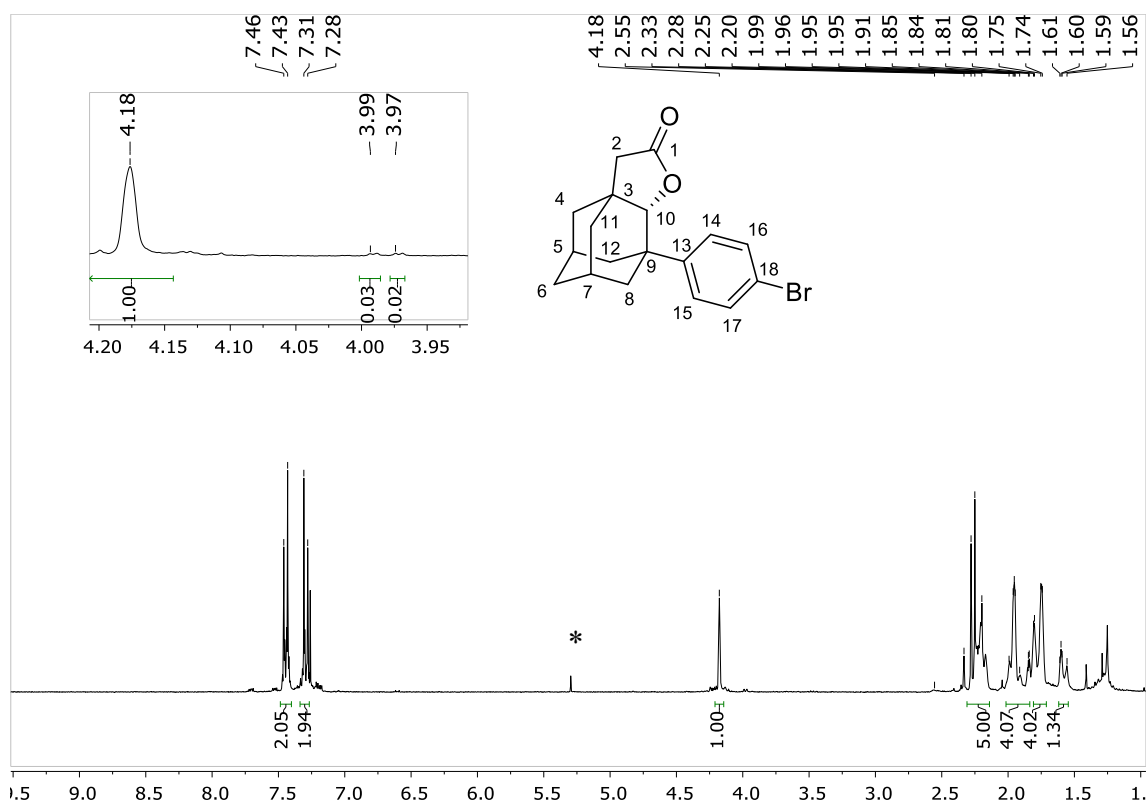


COSY of the oxidation of **18**. Note the coupling of the main proximal lactone **18a** C₁₀-H (left, main product) with secondary C₈-H bond (highlighted in green), and that of **18b** and **18c** (C₄-H and C₁₁-H signals) with tertiary C₅-H and C₇-H bond, respectively (highlighted in red).



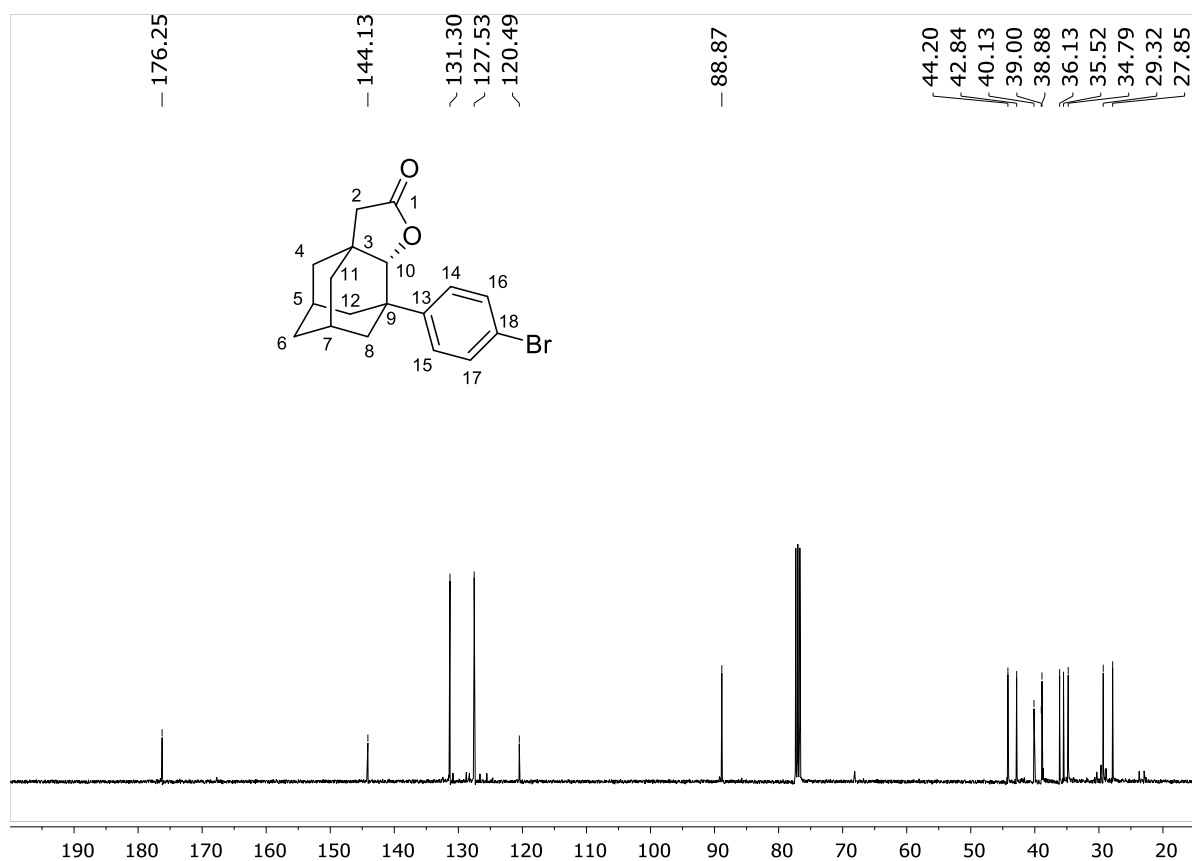
HSQC of **18a**.

¹H NMR of **19a** in CDCl₃

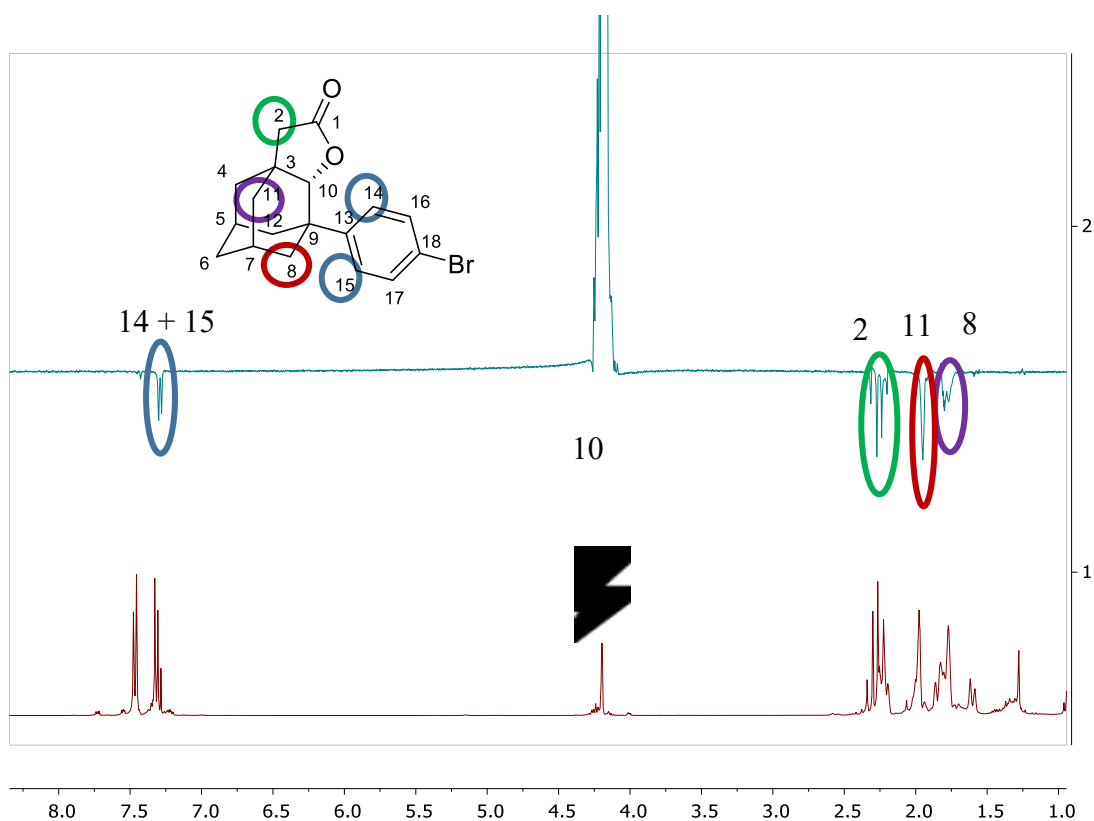


¹H NMR (400 MHz, CDCl₃) δ 7.44 (d, $J = 8.7$ Hz, 2H; $C_{14}[1H] + C_{15}[1H]$), 7.29 (d, $J = 8.7$ Hz, 2H; $C_{16}[1H] + C_{17}[1H]$), 4.17 (s, 1H; $C_{10}[1H]$), 2.32 – 2.16 (m, 5H; $C_2[2H] + C_5[1H] + C_7[1H] + C_{12}[1H]$), 1.95 (m, 3H; $C_{11}[2H] + C_4[1H]$), 1.84 – 1.72 (m, 5H; $C_6[2H] + C_4[1H] + C_8[1H] + C_{12}[1H]$), 1.58 (d, $J = 13.3$ Hz, 1H; $C_8[1H]$). Small peaks in the spectrum are the signals of the distal isomers. The peak marked with an asterisk corresponds to CH₂Cl₂.

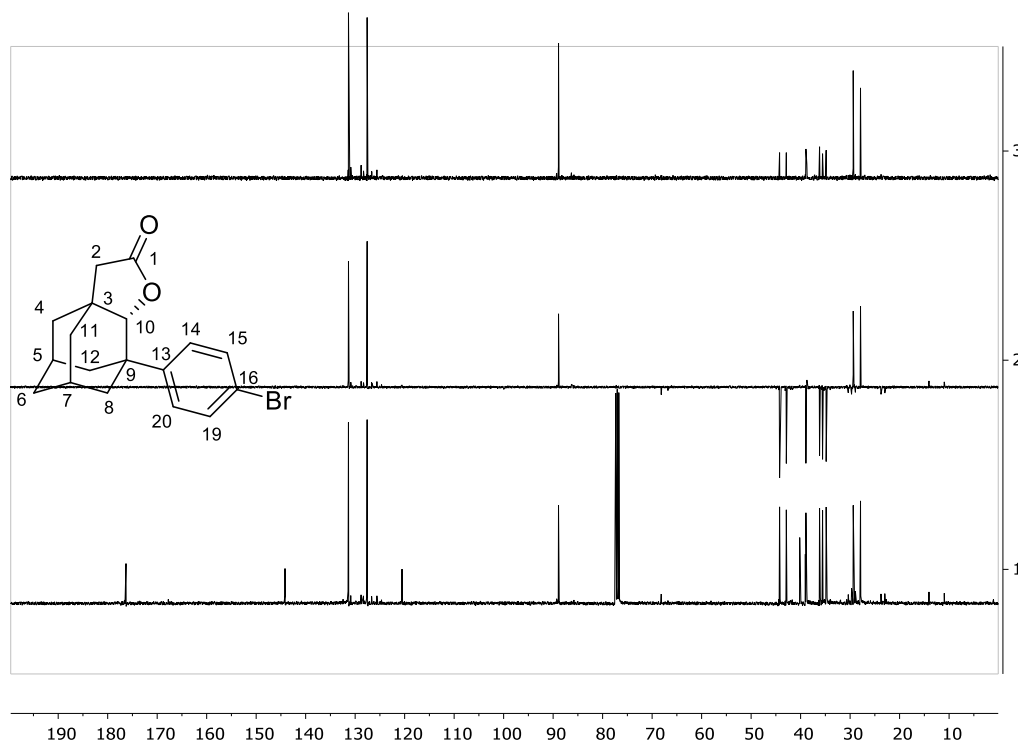
¹³C NMR of **19a** in CDCl₃



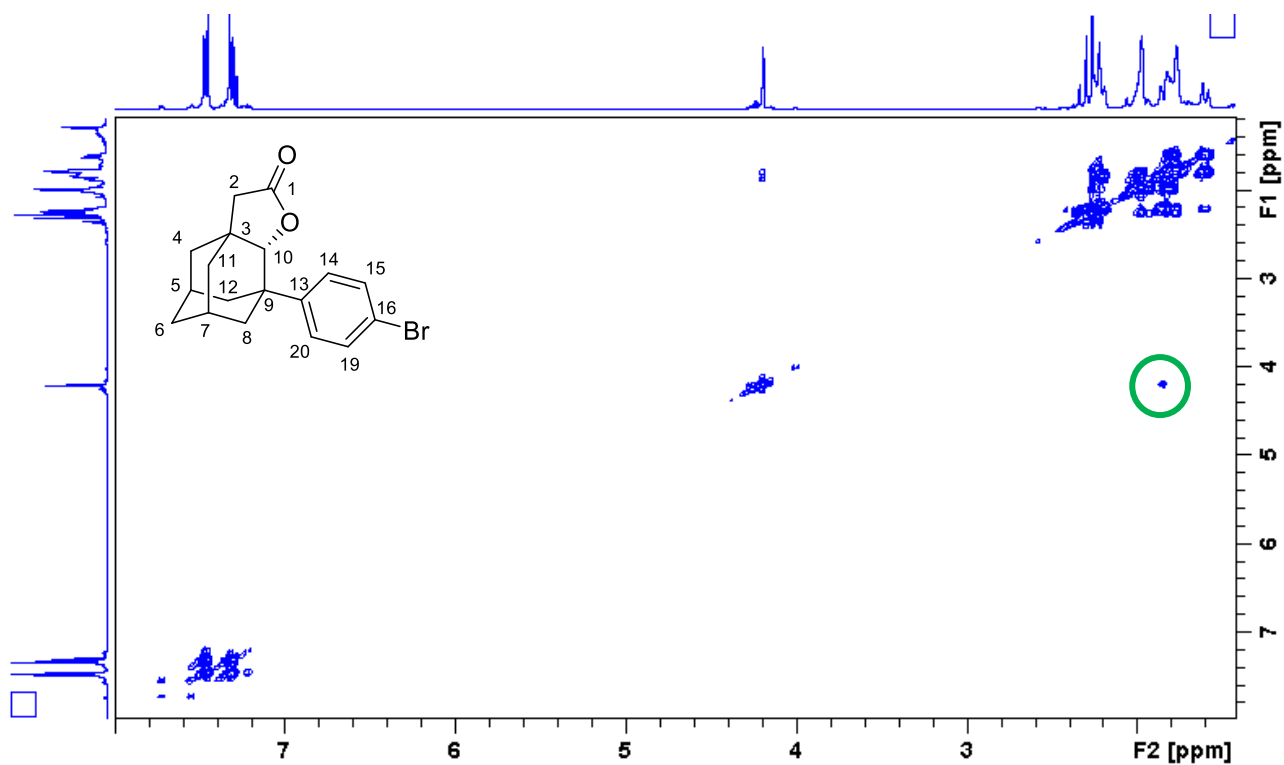
¹³C NMR (101 MHz, CDCl₃) δ 176.2 (*C*₁), 144.1 (*C*₁₃), 131.3 (*C*₁₄ + *C*₁₅), 127.5 (*C*₁₆ + *C*₁₇), 120.5 (*C*₁₈), 88.9 (*C*₁₀), 44.2 (*C*₂), 42.8 (*C*₈), 40.1 (*C*₃), 39.0 (*C*₉), 38.9 (*C*₄), 36.1 (*C*₁₁), 35.5 (*C*₆), 34.8 (*C*₁₂), 29.3 (*C*₅ or *C*₇), 27.8 (*C*₅ or *C*₇). Small peaks in the spectrum are the signals of the distal isomers.



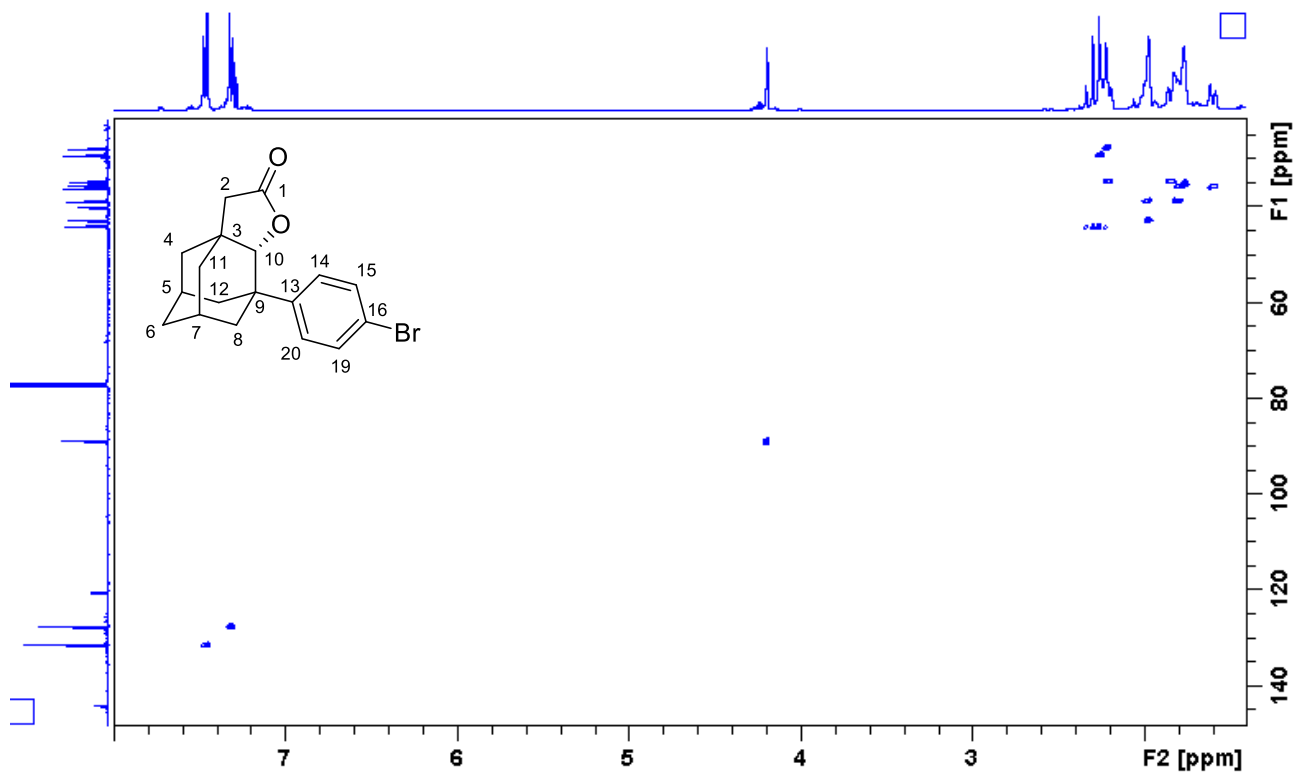
Stacking of the ^1H NMR spectrum of **19a** (bottom) with its selective NOESY obtained after irradiating at 4.17 δ (lactone signal, C₁₀-H). The signals that show a NOESY correlation with C₁₀-H are visible in a negative phase.



Stacking of the ^{13}C NMR spectrum of **19a** (bottom) stacked with its DEPT90 (top) and its DEPT 135 (middle) spectra.



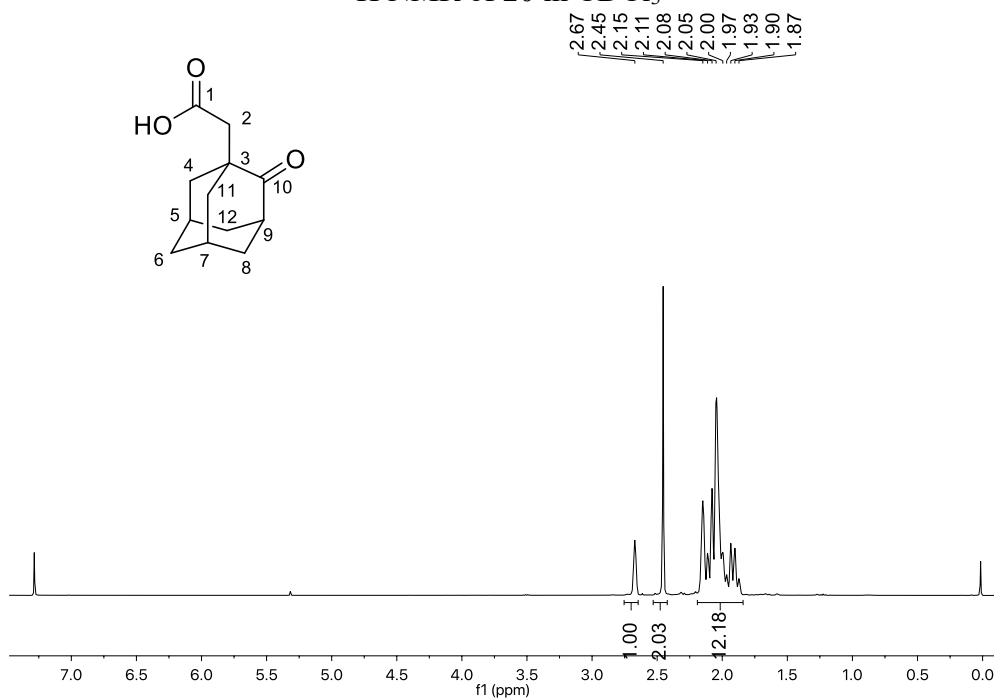
COSY of **19a**. Note the coupling the main proximal lactone C₁₀-H (right, main product) with secondary C₈-H bond, respectively (highlighted in green).



HSQC of **19a**.

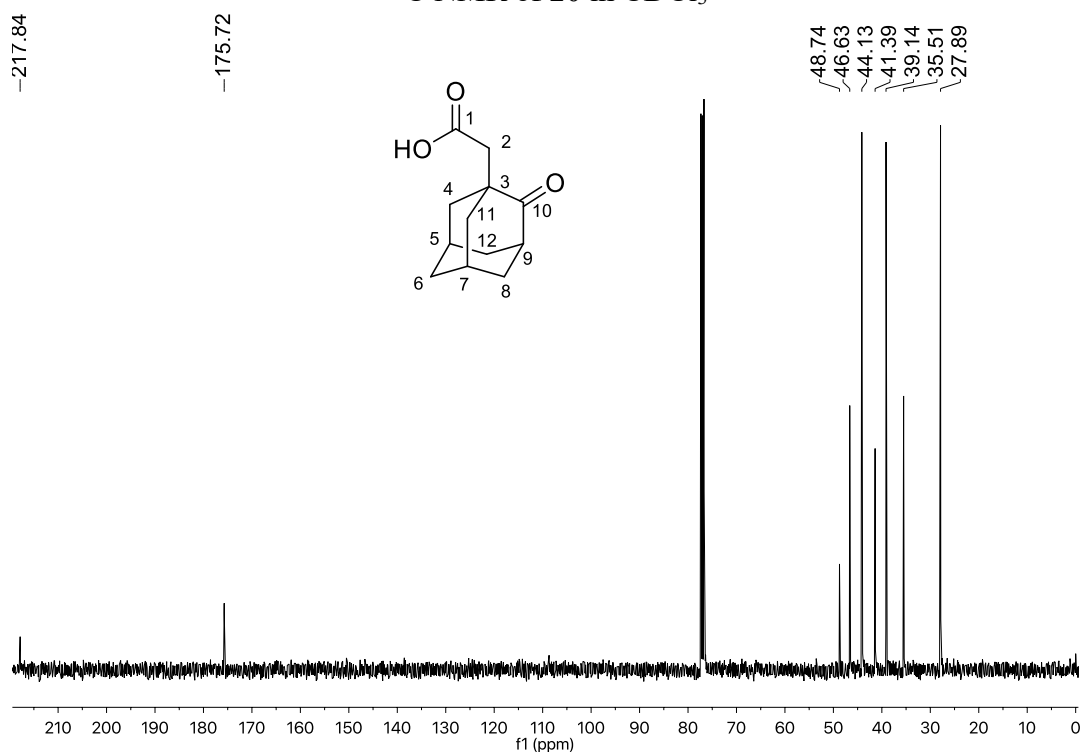
IV. NMR Characterization of the products in the synthesis of (+)-22

^1H NMR of **20** in CDCl_3



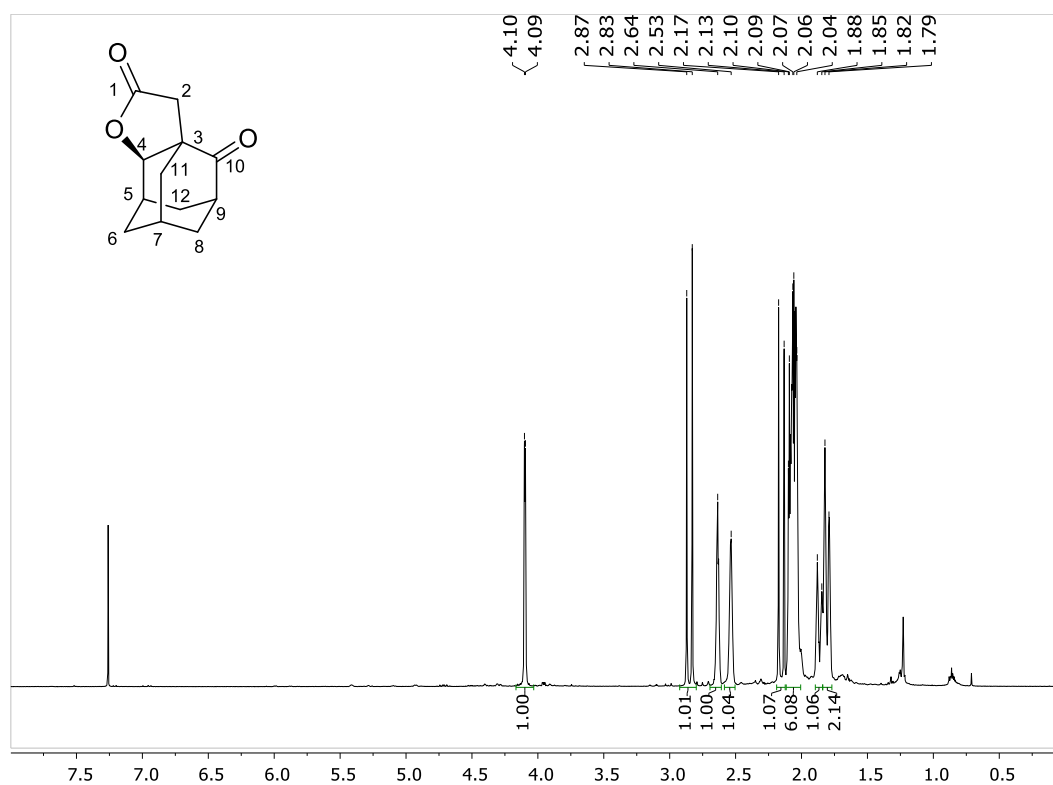
^1H NMR (400 MHz, CDCl_3) δ 2.67 (t, $J = 3.1$ Hz, 1H; C_9 [1H]), 2.45 (s, 2H; C_2 [2H]), 2.20 – 1.84 (m, 12H).

^{13}C NMR of **20** in CDCl_3



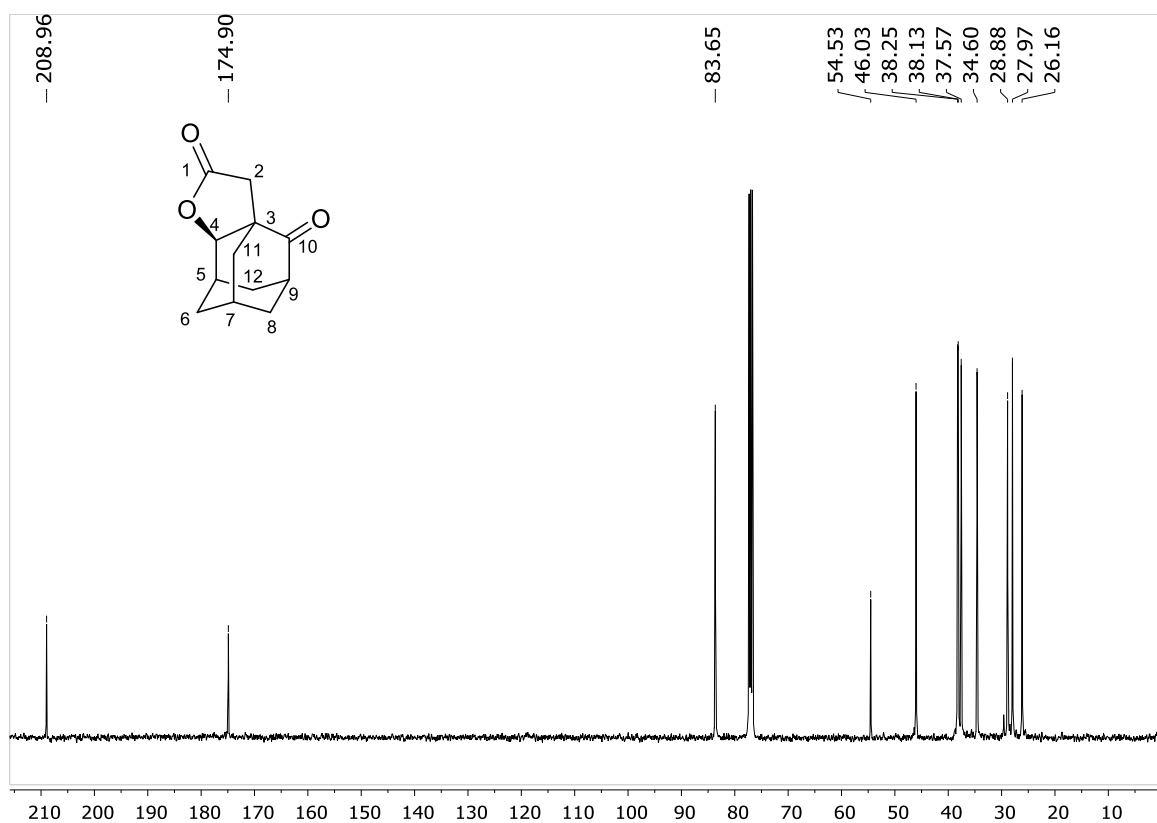
^{13}C NMR (101 MHz, CDCl_3) δ 217.8 (C_{10}), 175.72 (C_1), 48.7 (C_3), 46.6 (C_2), 44.1 ($C_4 + C_{11}$), 41.4 (C_6), 39.1 ($C_8 + C_{12}$), 35.5 (C_9), 27.9 ($C_5 + C_7$).

¹H NMR of **20b** in CDCl₃

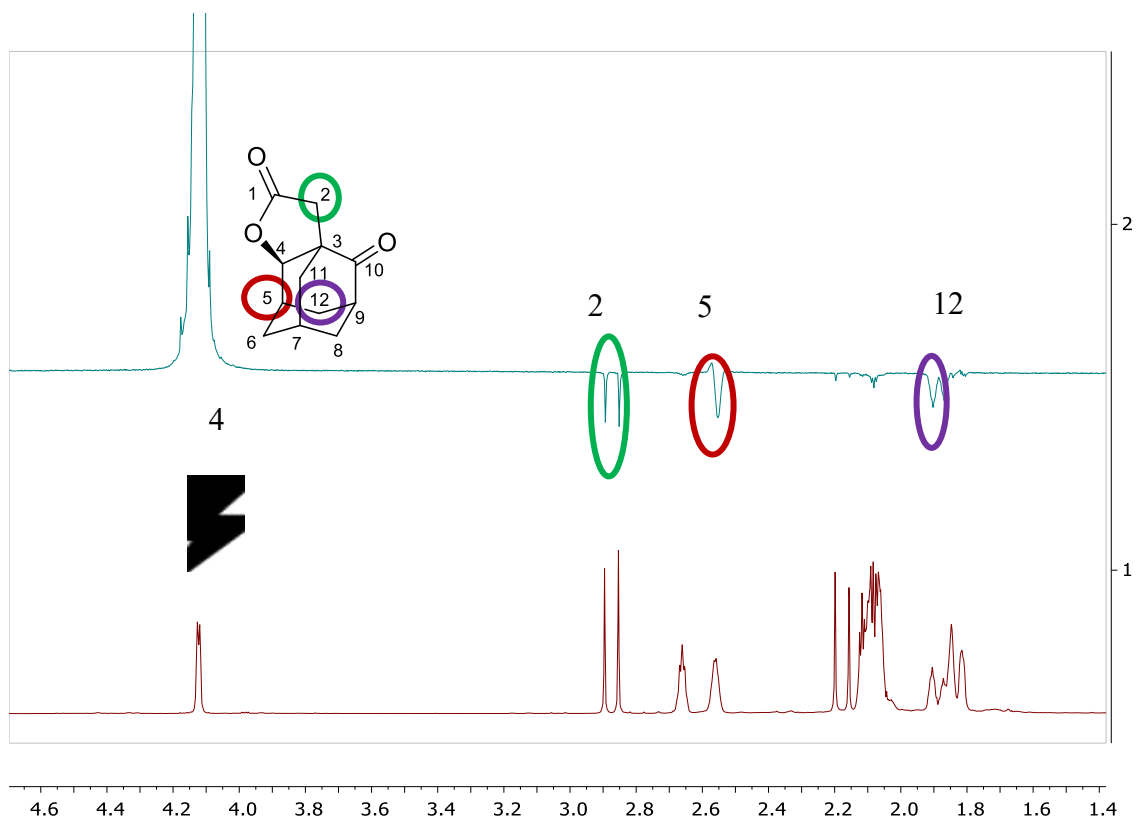


¹H NMR (400 MHz, CDCl₃) δ 4.10 (d, $J = 3.0$ Hz, 1H; C₄ [1H]), 2.85 (d, $J = 16.8$ Hz, 1H; C₂ [1H]), 2.64 (s, 1H; C₉ [1H]), 2.53 (s, 1H; C₅ [1H]), 2.15 (d, $J = 16.7$ Hz, 1H; C₂ [1H]), 2.12 – 2.01 (m, 6H; C₈ [2H] + C₁₁ [1H] + C₇ [1H] + C₆ [1H] + C₁₂ [1H]), 1.86 (d, $J = 13.6$ Hz, 1H; C₁₂ [1H]), 1.81 (d, $J = 12.2$ Hz, 2H, C₆ [1H] + C₁₁ [1H]).

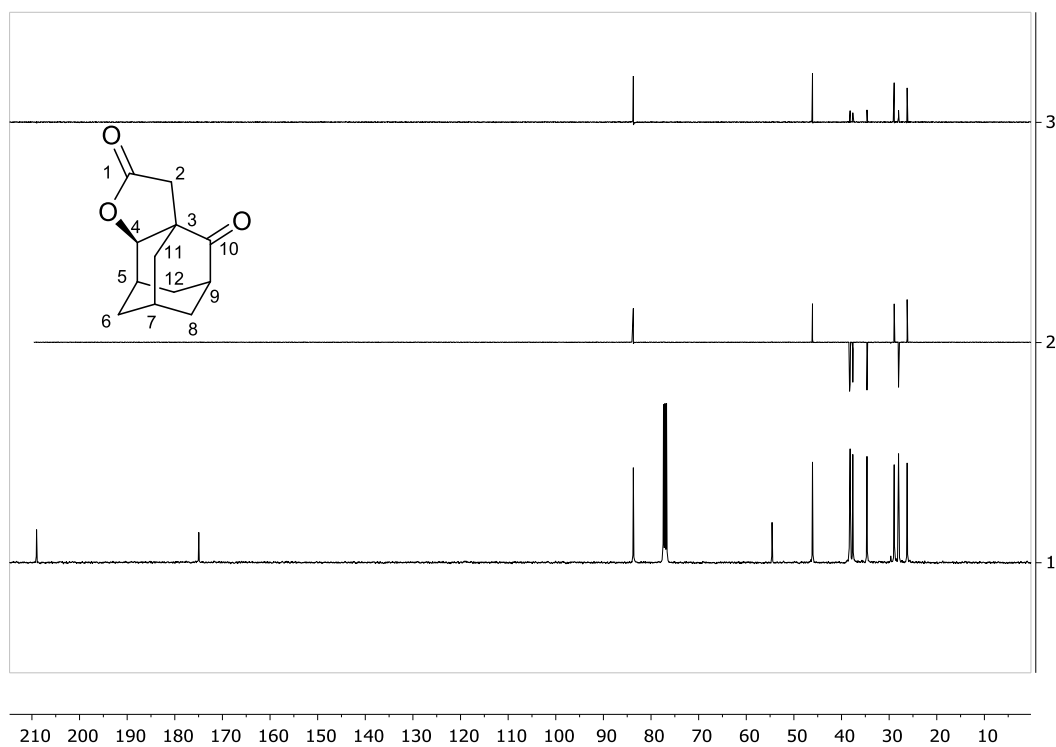
^{13}C NMR of **20b** in CDCl_3



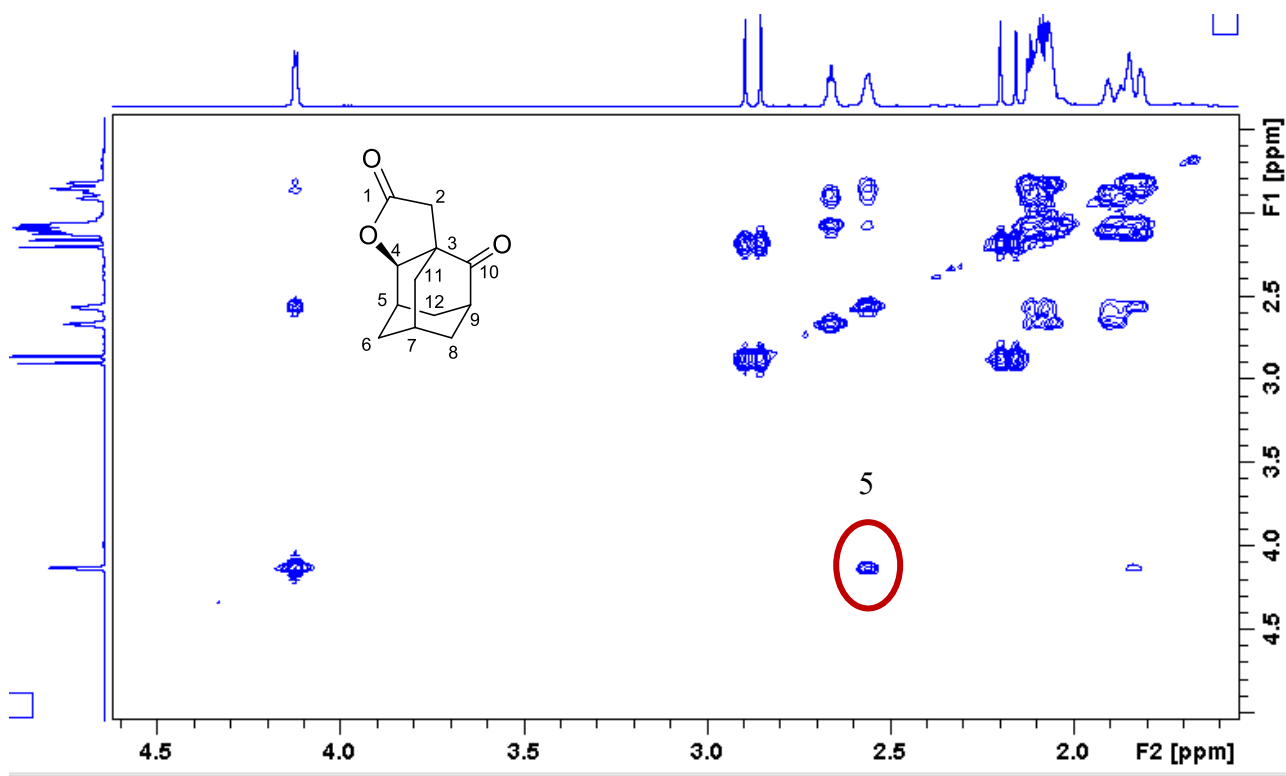
^{13}C NMR (101 MHz, CDCl_3) δ 209.0 (C_{10}), 174.9 (C_1), 83.6 (C_4), 54.5 (C_3), 46.0 (C_9), 38.2 (C_8), 38.1 (C_{11}), 37.6 (C_2), 34.6 (C_{12}), 28.9 (C_5), 28.0 (C_6), 26.2 (C_7).



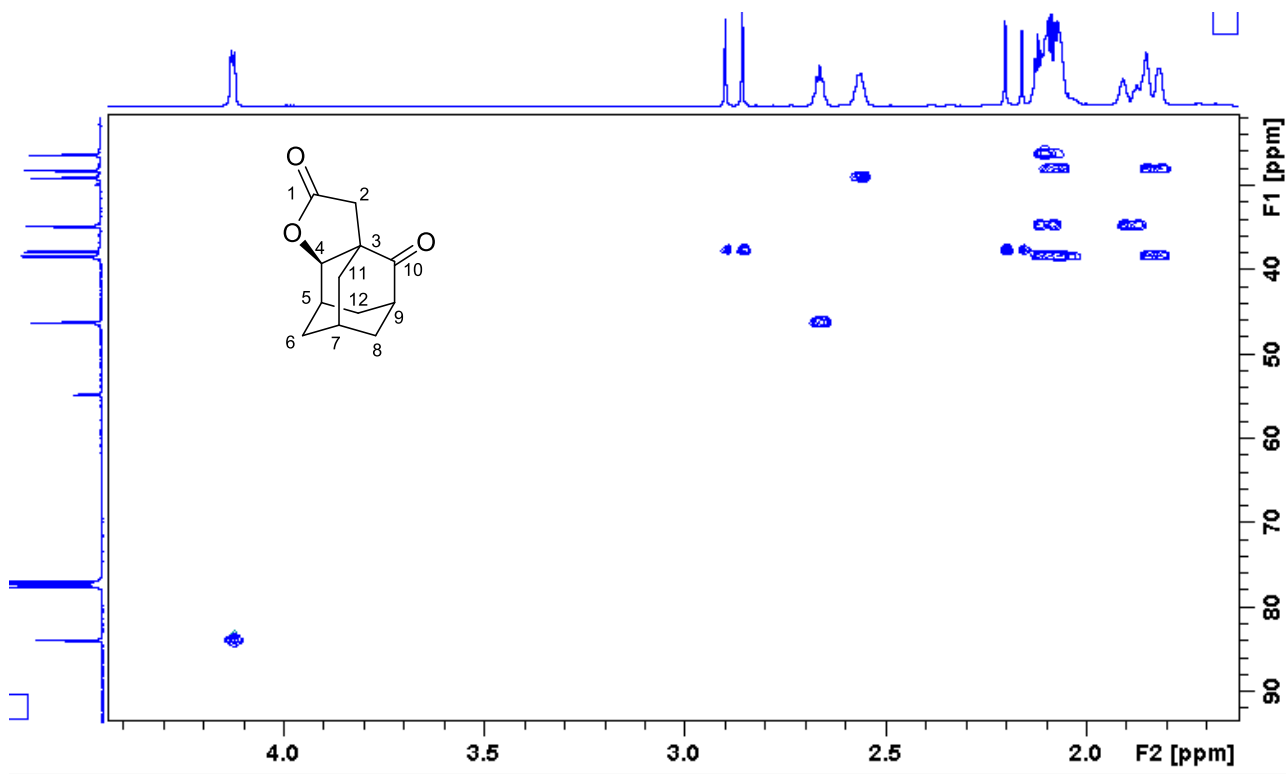
Stacking of the ^1H NMR spectrum of **20b** (bottom) with its selective NOESY obtained after irradiating at 4.10 δ (lactone signal, C₄-H). The signals that show a NOESY correlation with C₄-H are visible in a negative phase.



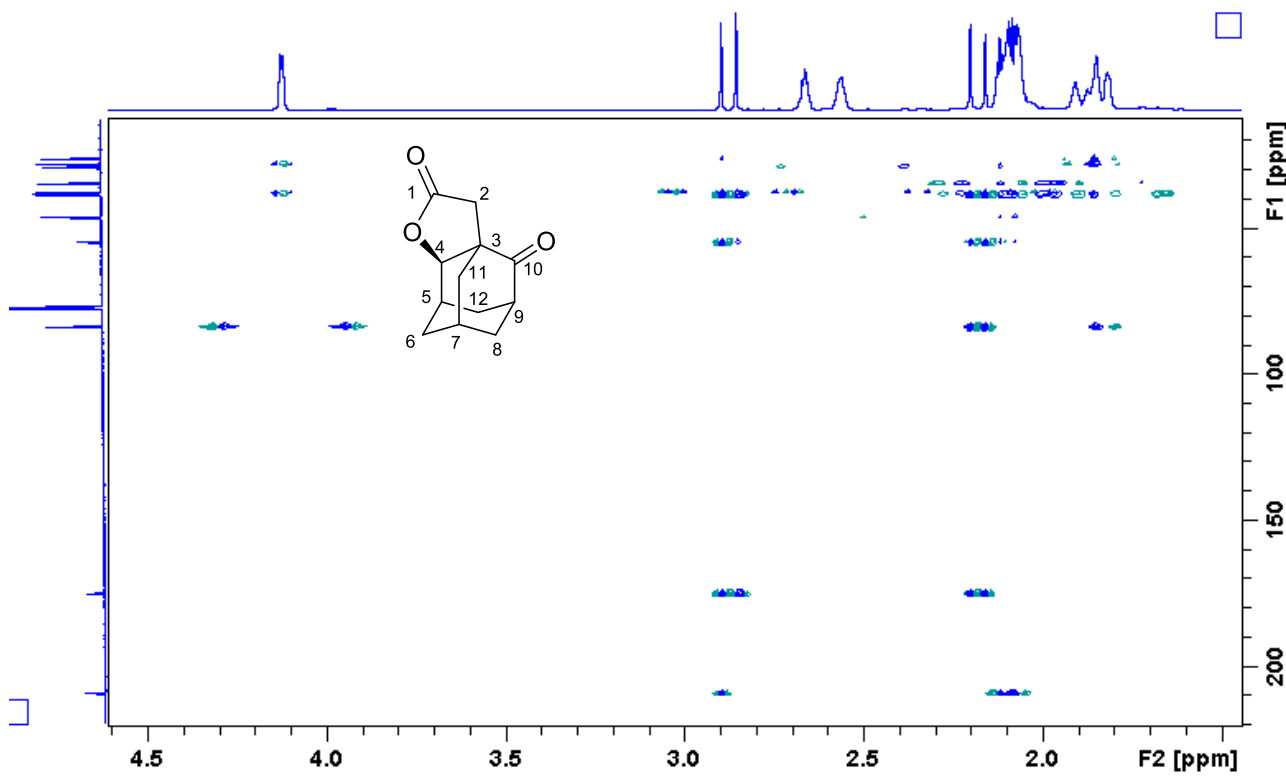
Stacking of the ^{13}C NMR spectrum of **20b** (bottom) stacked with its DEPT90 (top) and its DEPT 135 (middle) spectra.



COSY of **20b**. Correlation with tertiary C₅-H highlighted in red.



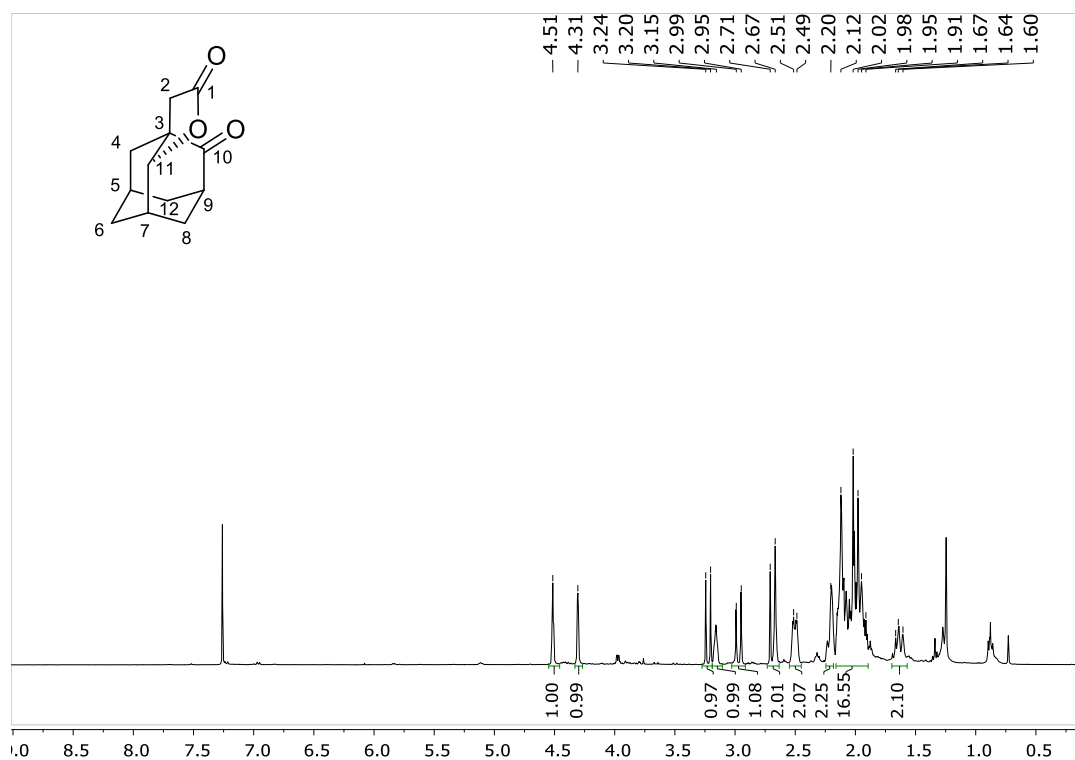
HSQC of **20b**.



HMBC of **20b**.

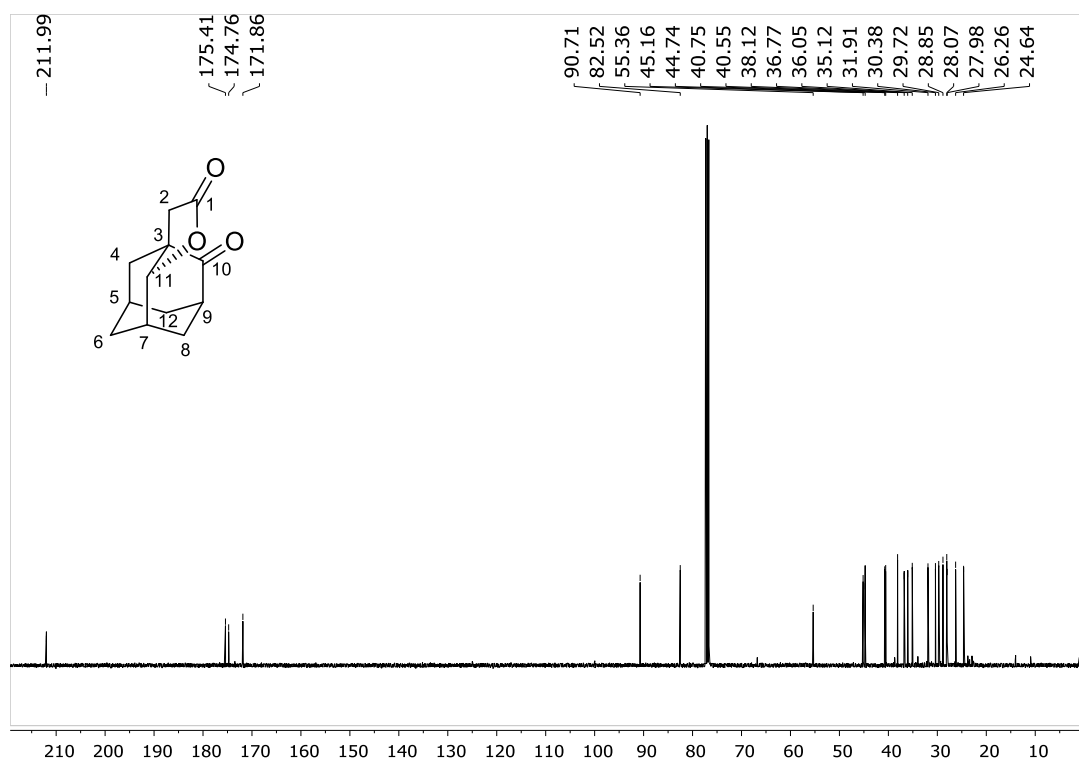
¹H NMR of **20c** in CDCl₃

(Inseparable roughly 1:1 mixture with *endo*-**21** byproduct formed in the reaction conditions)

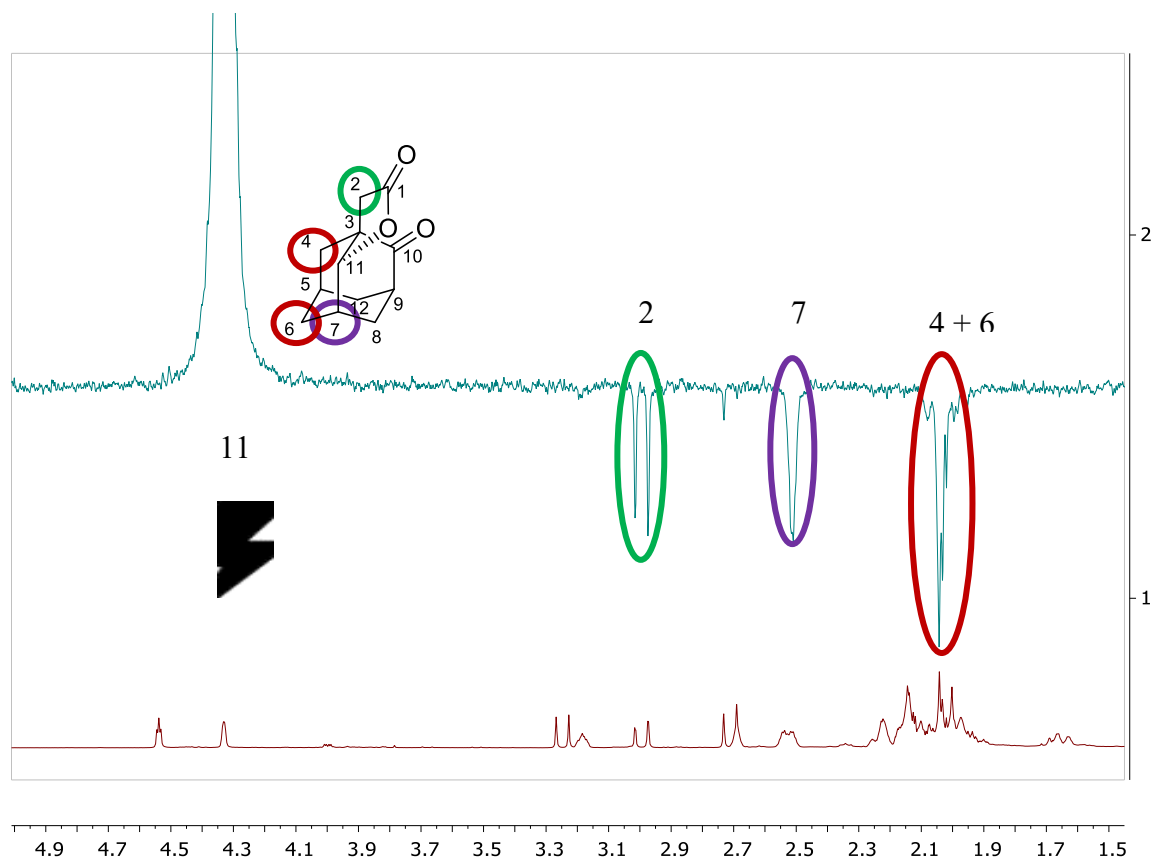


¹H NMR (400 MHz, CDCl₃) δ 4.51 (s, 1H), 4.31 (s, 1H; *C*₁₁ [1H]), 3.22 (d, *J* = 16.0 Hz, 1H), 3.15 (s, 1H), 2.97 (d, *J* = 16.5 Hz, 1H; *C*₂[1H]), 2.69 (d, *J* = 16.6 Hz, 2H *C*₇ [1H]), 2.50 (m, *J* = 10.9 Hz, 2H; *C*₇ [1H]), 2.20 (s, 2H), 2.16 – 1.89 (m, 17H), 1.70 – 1.57 (m, 2H).

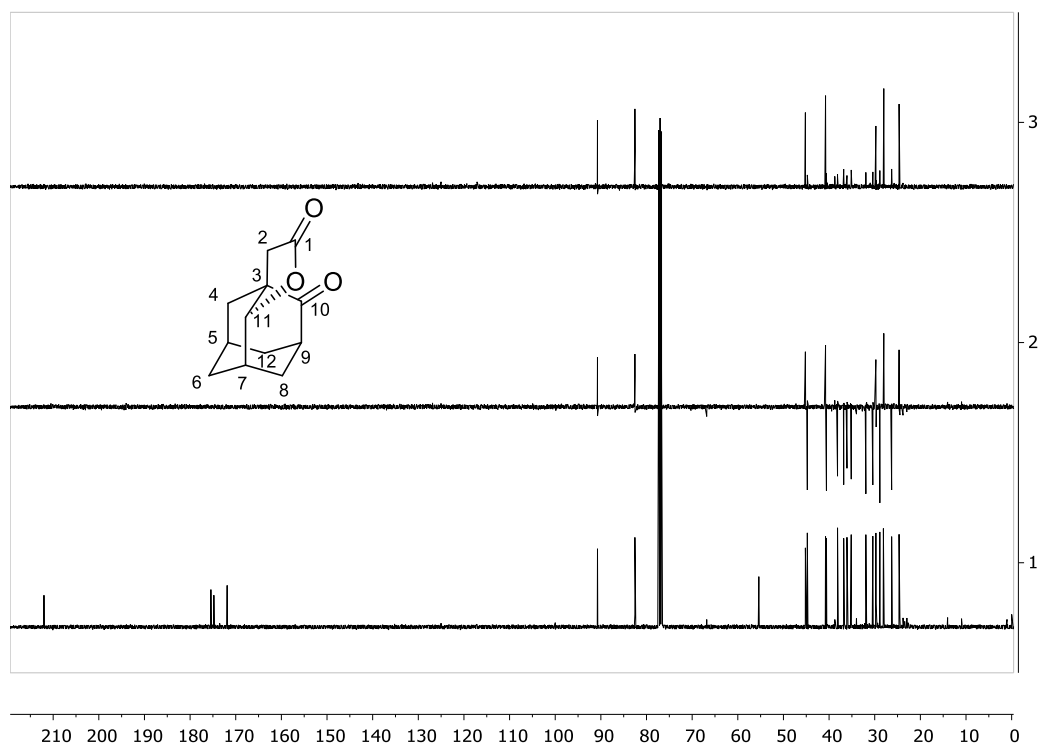
^{13}C NMR of **20c** in CDCl_3



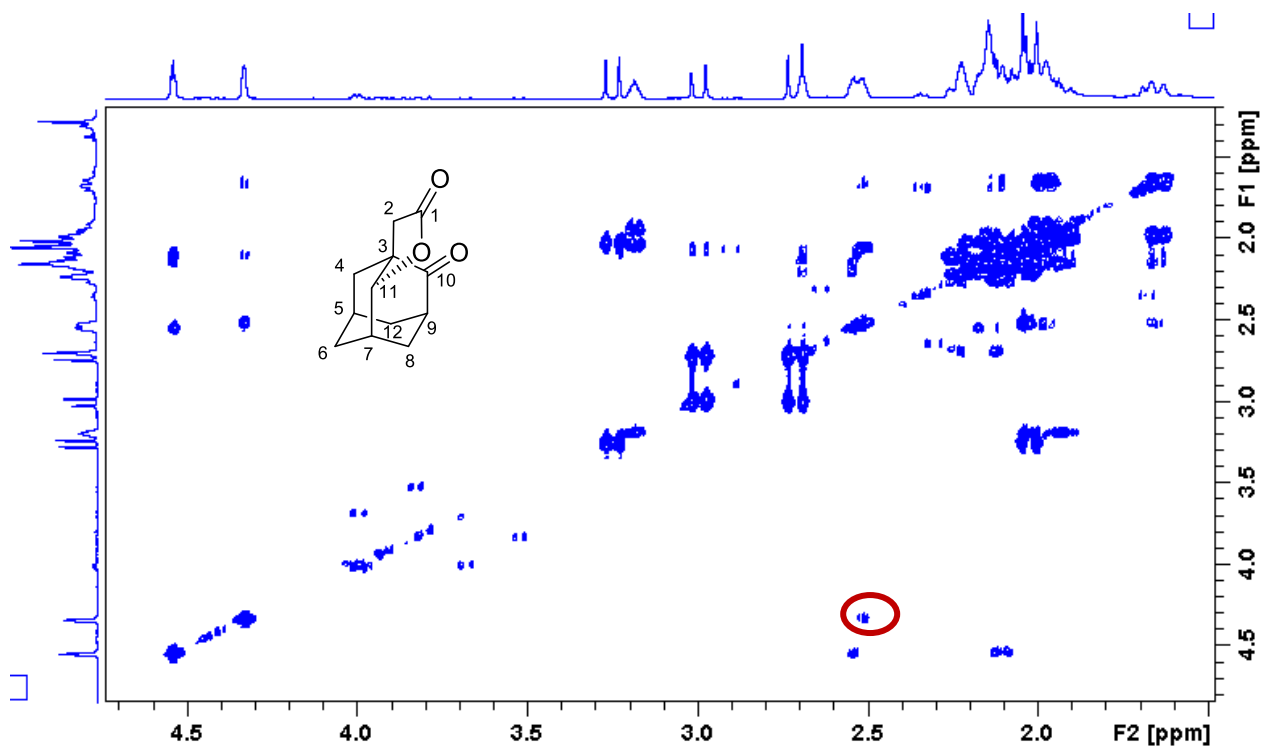
^{13}C NMR (101 MHz, CDCl_3) δ 212.0 (C_{10}), 175.4, 174.8, 171.9 (C_1), 90.7, 82.5 (C_{11}), 55.4, 45.2 (C_2), 44.7, 40.7, 40.5, 38.1, 36.8, 36.0 (C_4), 35.1, 31.9 (C_6), 30.4, 29.7, 28.8, 28.1 (C_7), 28.0, 26.3, 24.6 (C_3).



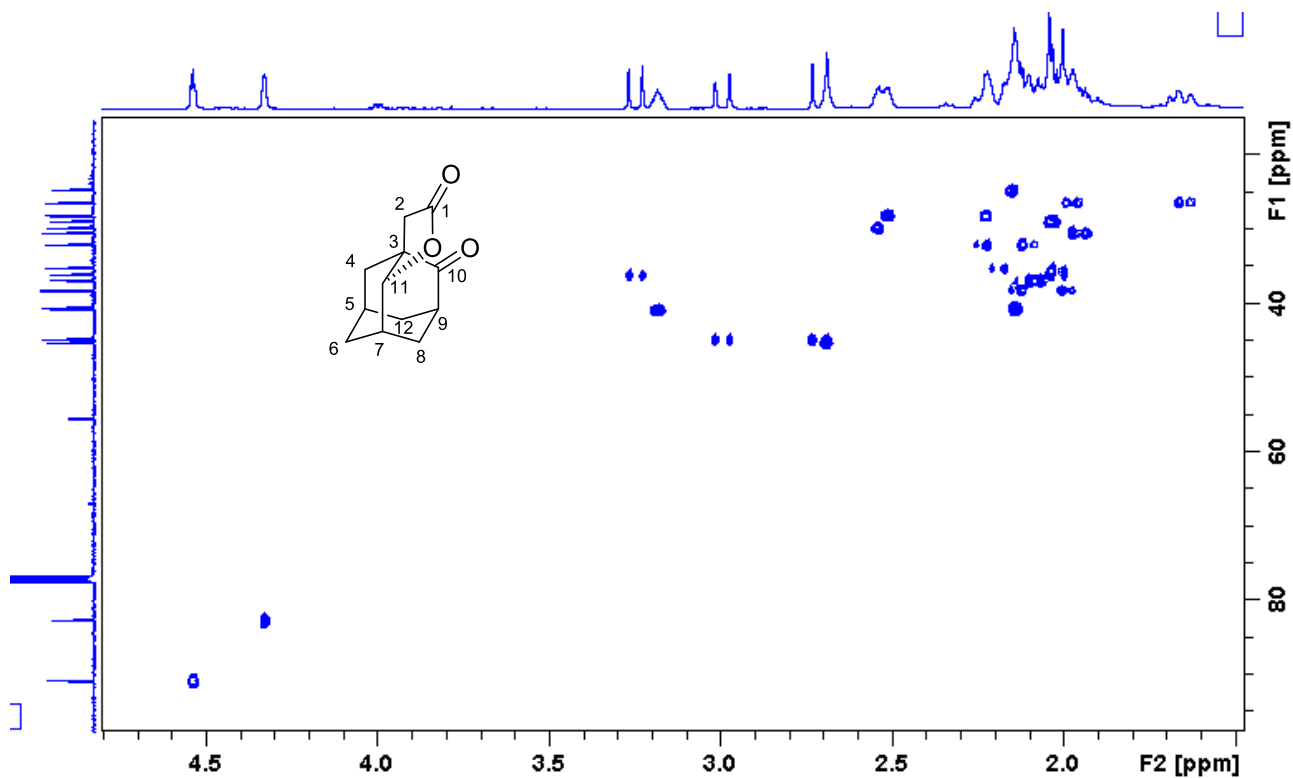
Stacking of the ^1H NMR spectrum of **20c** (bottom) with its selective NOESY obtained after irradiating at $4.31\ \delta$ (lactone signal, $\text{C}_{11}\text{-H}$). The signals that show a NOESY correlation with $\text{C}_{11}\text{-H}$ are visible in a negative phase



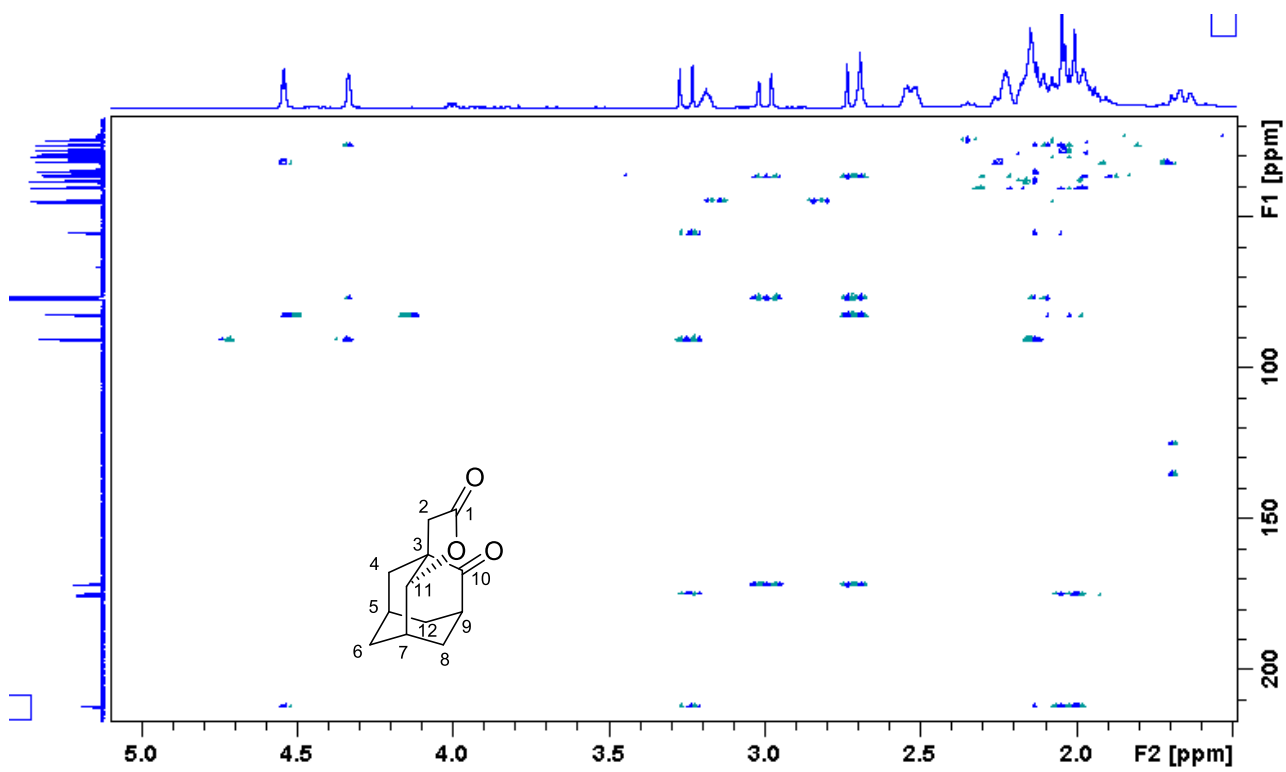
Stacking of the ^{13}C NMR spectrum of **20c** (bottom) stacked with its DEPT90 (top) and its DEPT 135 (middle) spectra.



COSY of **20c**. Note the coupling the main proximal lactone C₁₁-H (right, main product) with tertiary C₇-H bond (highlighted in red).

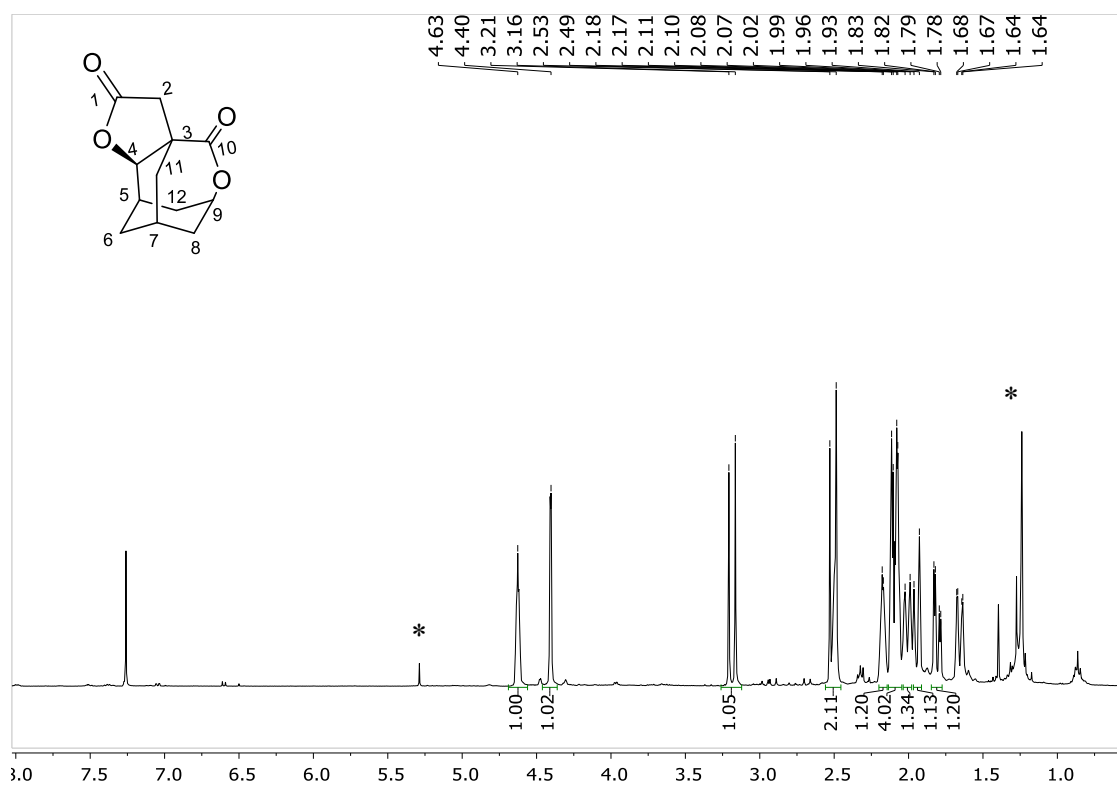


HSQC of **20c**



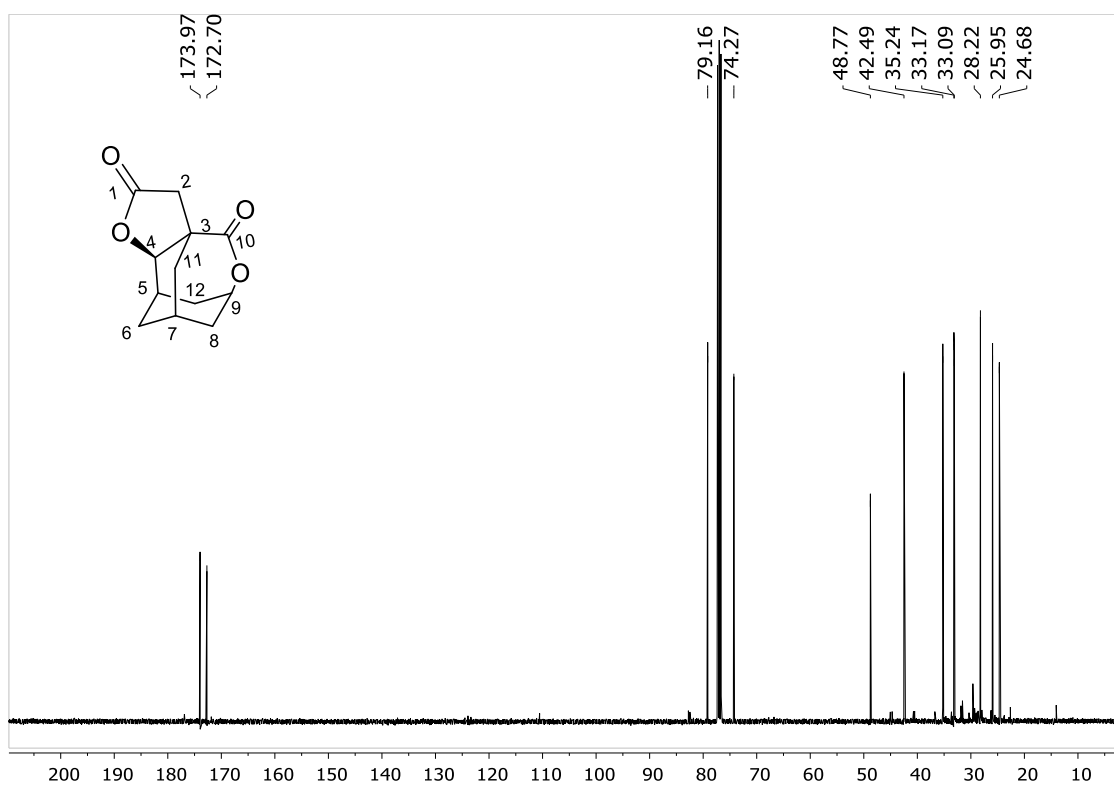
HMBC of **20c**

¹H NMR of **21-exo** in CDCl₃

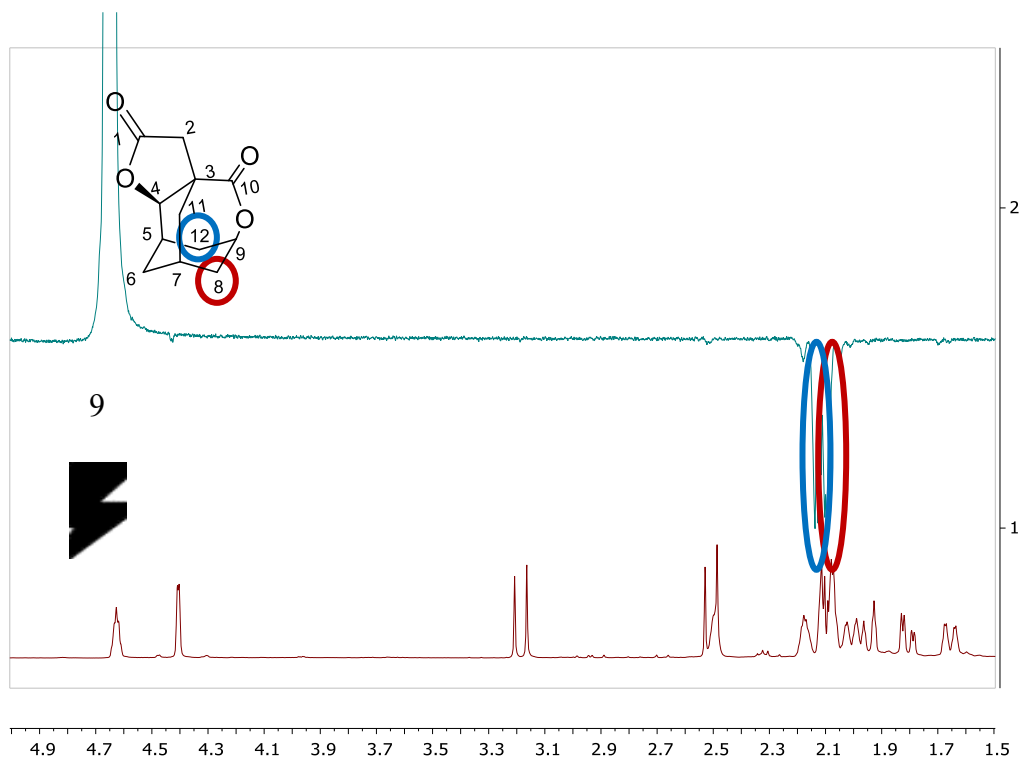


¹H NMR (400 MHz, CDCl₃) δ 4.63 (s, 1H; C₉ [1H]), 4.40 (s, 1H; C₄ [1H]), 3.19 (d, *J* = 17.4 Hz, 1H; C₂ [1H]), 2.51 (d, *J* = 17.2 Hz, 2H; C₂ [1H] + C₅ [1H]), 2.17 (m, 1H; C₂ [1H]), 2.14-2.05 (m, 4H, C₈ [2H] + C₁₂ [2H]), 2.05 – 1.96 (m, 1H; C₆ [1H]), 1.93 (m, 1H; C₁₁ [1H]), 1.81 (dd, *J* = 14.5, 3.9 Hz, 1H; C₁₁ [1H]), 1.69 – 1.62 (m, 1H; C₆ [1H]). The peak marked with an asterisk is CH₂Cl₂ (at 5.3 ppm) and acetone (at ca 1.3 ppm).

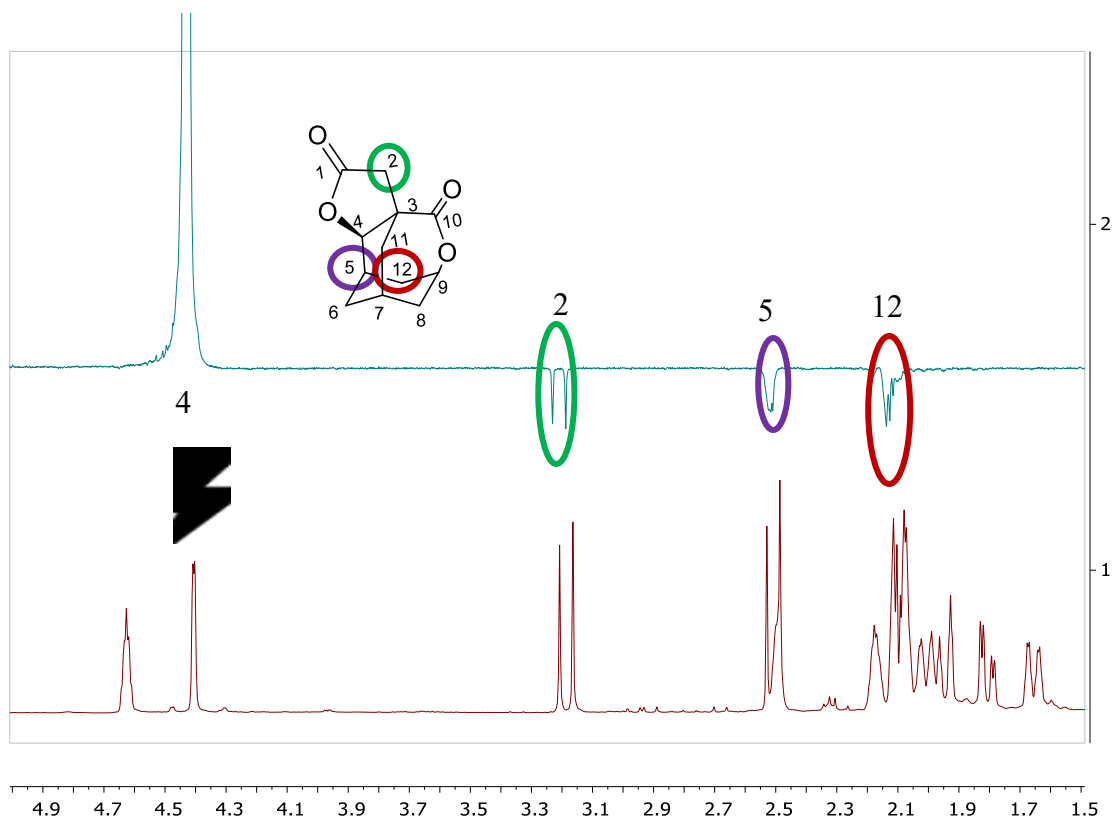
^{13}C NMR of **21** in CDCl_3



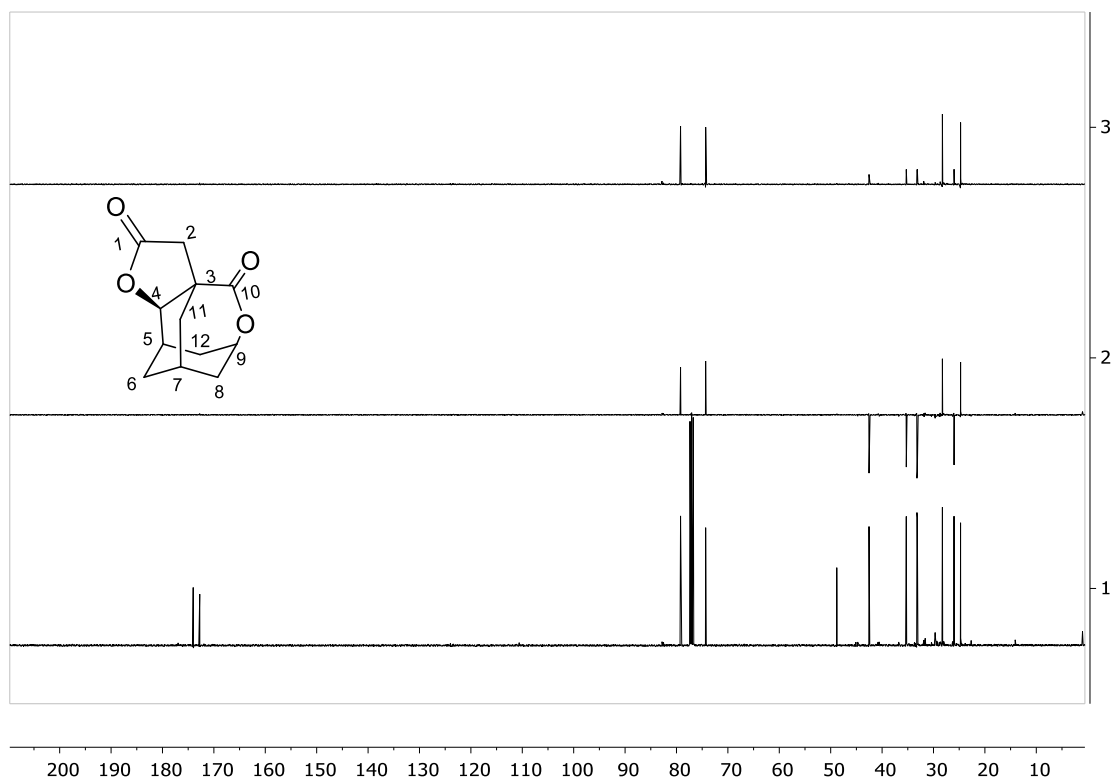
^{13}C NMR (101 MHz, CDCl_3) δ 174.0 (C_1), 172.7 (C_{10}), 79.2 (C_4), 74.3 (C_9), 48.8 (C_3), 42.5 (C_2), 35.2 (C_8), 33.2 (C_{12}), 33.1 (C_{11}), 28.2 (C_5), 25.9 (C_6), 24.7 (C_7).



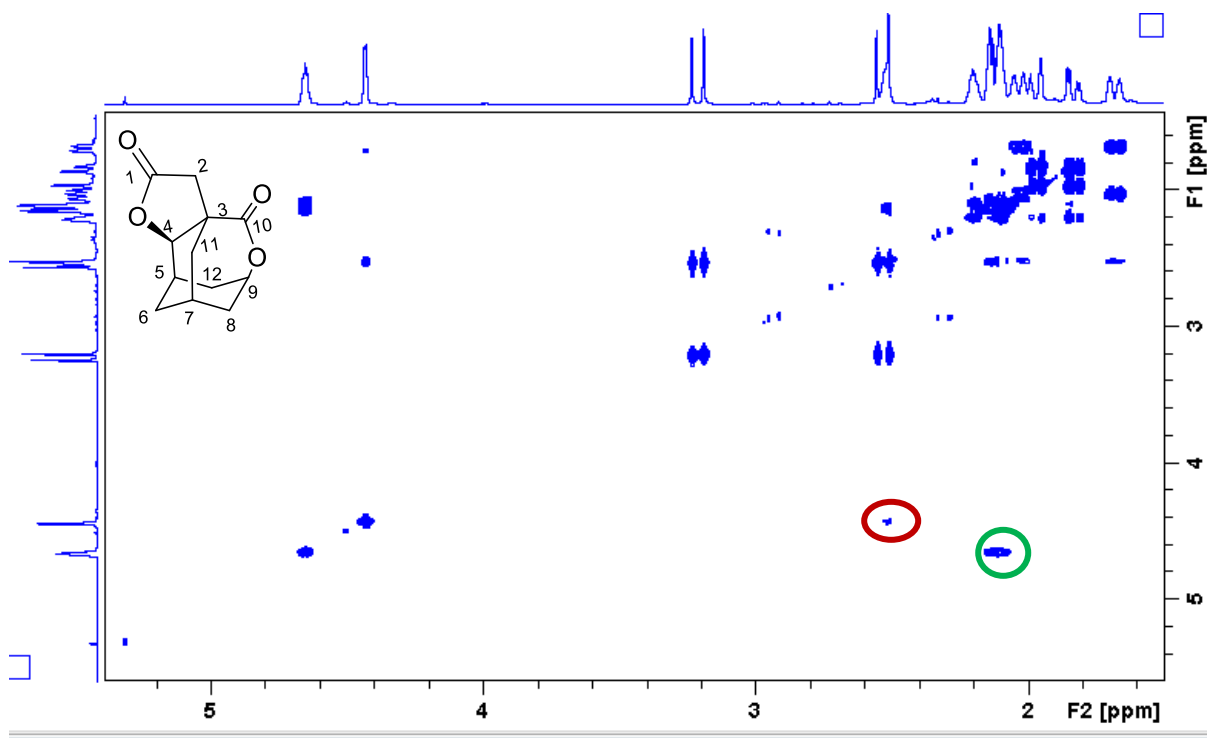
Stacking of the ^1H NMR spectrum of **21** (bottom) with its selective NOESY obtained after irradiating at 4.63 δ (lactone signal, $C_9\text{-H}$). The signals that show a NOESY correlation with $C_9\text{-H}$ are visible in a negative phase.



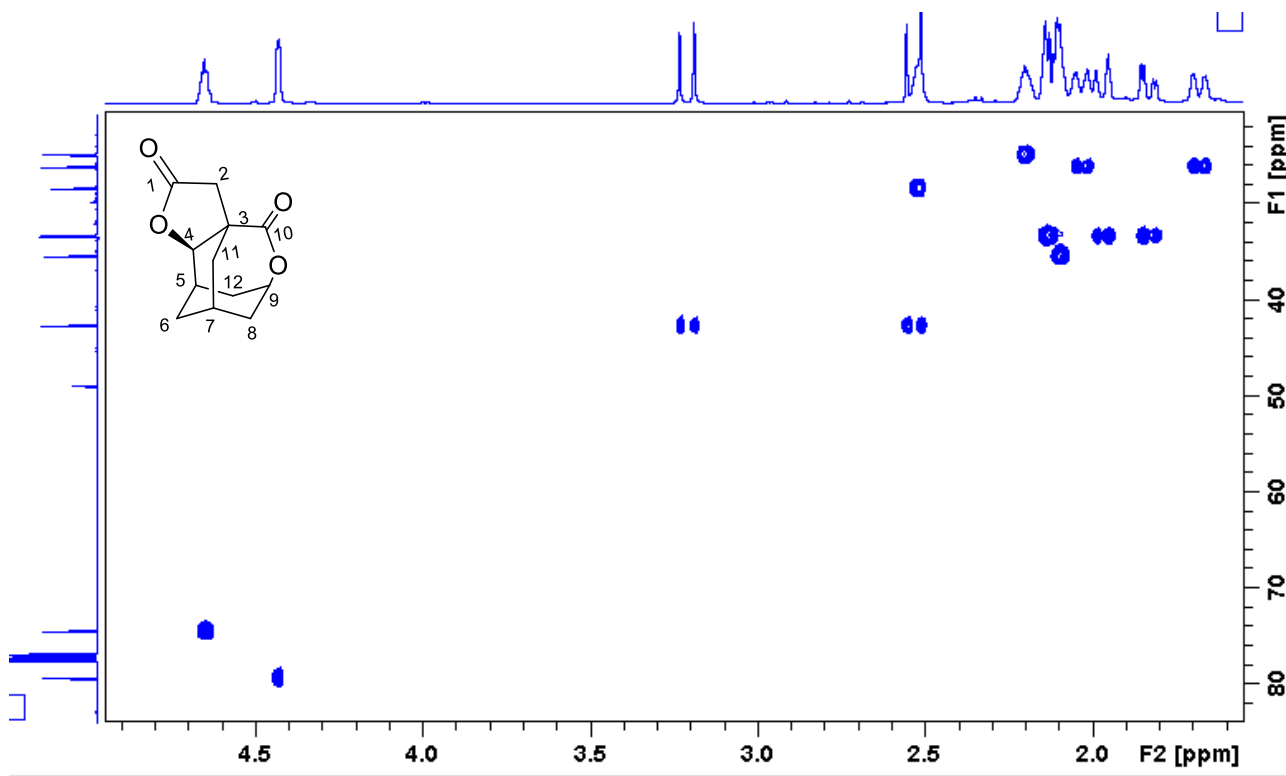
Stacking of the ¹H NMR spectrum of **21** (bottom) with its selective NOESY obtained after irradiating at 4.40 δ (lactone signal, C₄-H). The signals that show a NOESY correlation with C₄-H are visible in a negative phase.



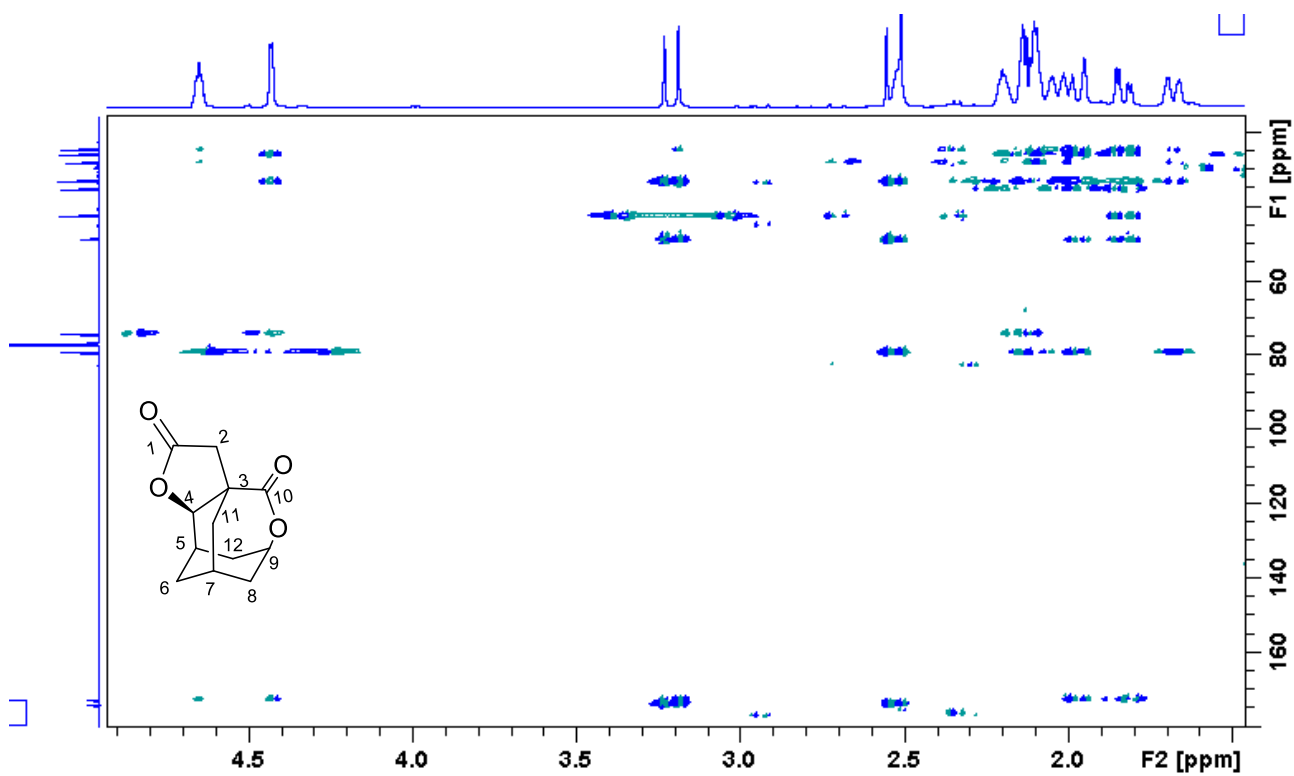
Stacking of the ^{13}C NMR spectrum of **21** (bottom) stacked with its DEPT90 (top) and its DEPT 135 (middle) spectra.



COSY of **21**. Note the coupling the main proximal lactone $\text{C}_4\text{-H}$ with tertiary $\text{C}_5\text{-H}$ bond (highlighted in red) and of lactone $\text{C}_9\text{-H}$ with secondary $\text{C}_8\text{-H}$ and $\text{C}_{12}\text{-H}$ bonds (highlighted in green).

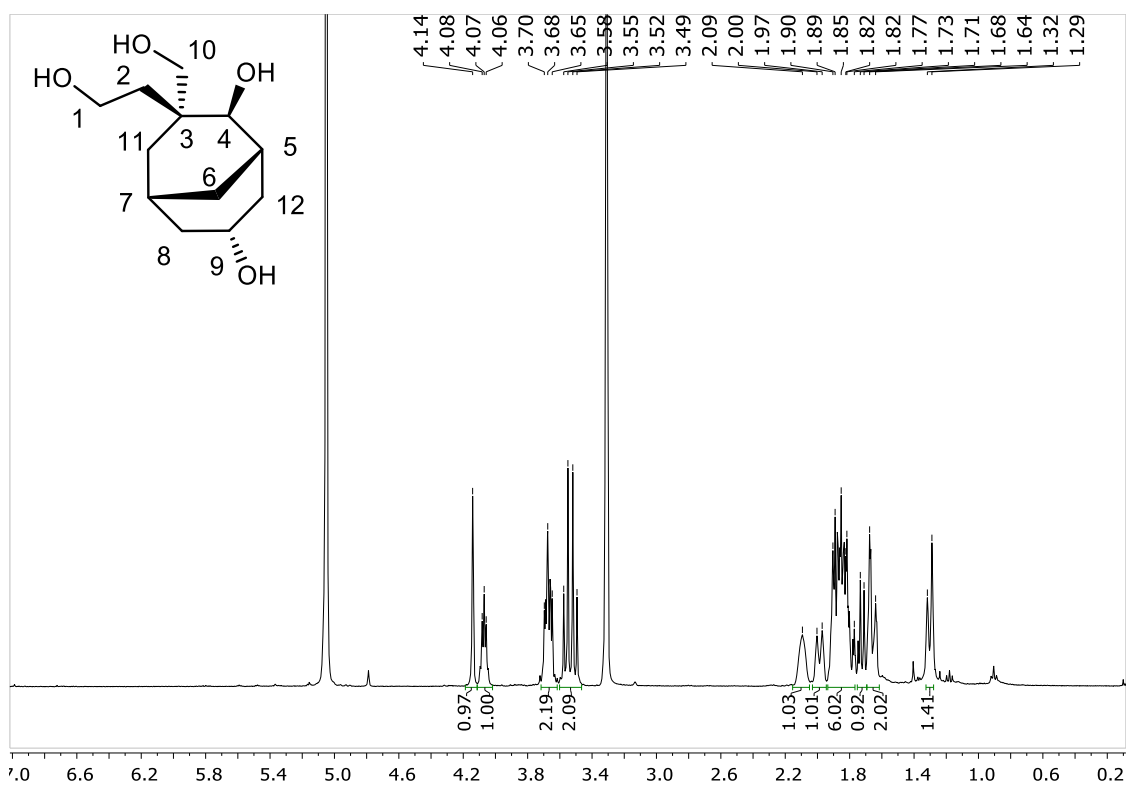


HSQC of **21**.



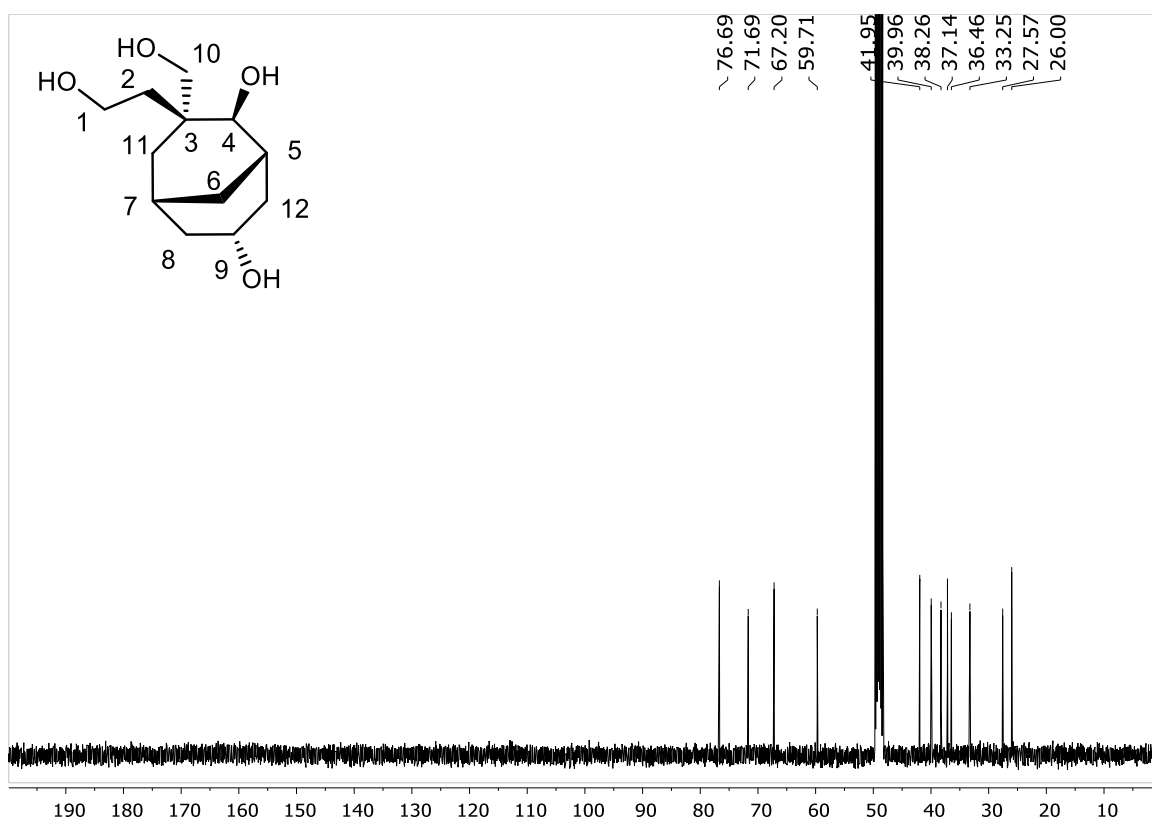
HMBC of 21.

¹H NMR of **22** in CD₃OD

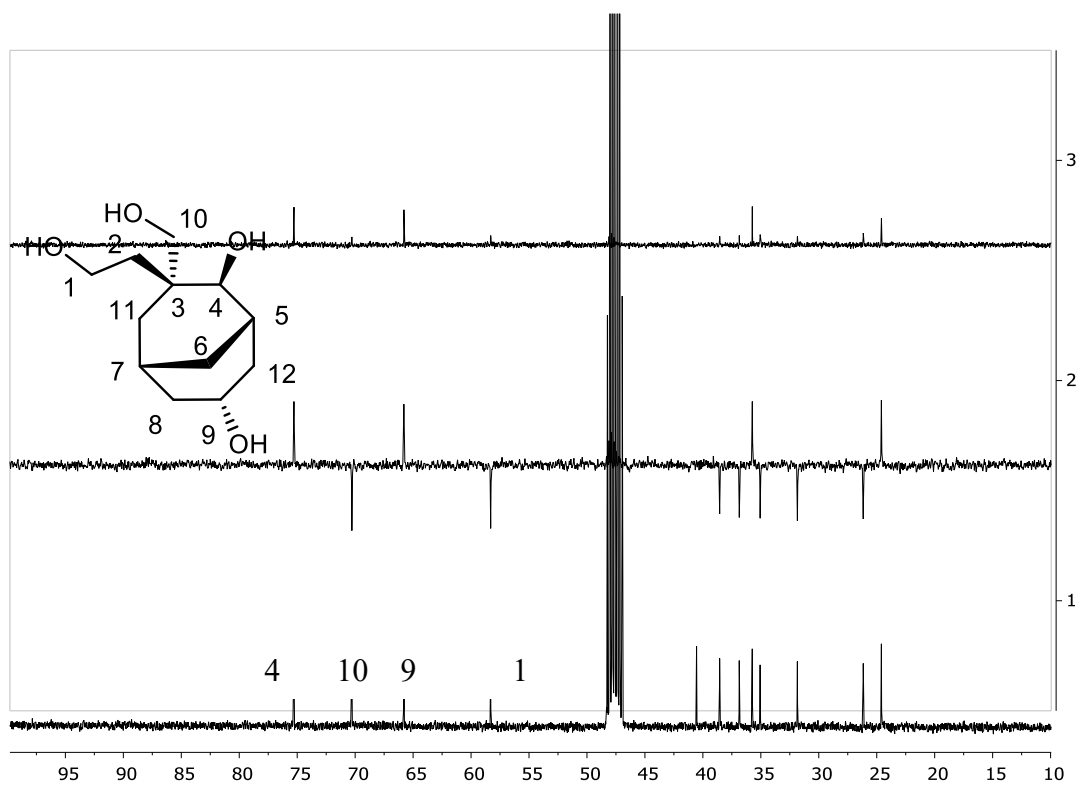


¹H NMR (400 MHz, CD₃OD) δ 4.14 (s, 1H; C₄ [1H]), 4.11 – 4.02 (m, 1H; C₉ [1H]), 3.71 – 3.73 (m, 2H; C₁ [2H]), 3.54 (q, 2H, $J = 12.2$ Hz; C₁₀ [2H]), 2.09 (m, 1H; C₇ [1H]), 1.99 (d, $J = 12.9$ Hz, 1H; C₁₂ [1H]), 1.94 – 1.77 (m, 6H; C₂ [2H] + C₅ [1H] + C₆ [2H] + C₈ [1H]), 1.72 (d, $J = 9.2$ Hz, 1H; C₁₁ [1H]), 1.66 (d, $J = 14.8$ Hz, 2H; C₈ [1H] + C₁₁ [1H]), 1.30 (d, $J = 11.3$ Hz, 1H; C₁₂ [1H]).

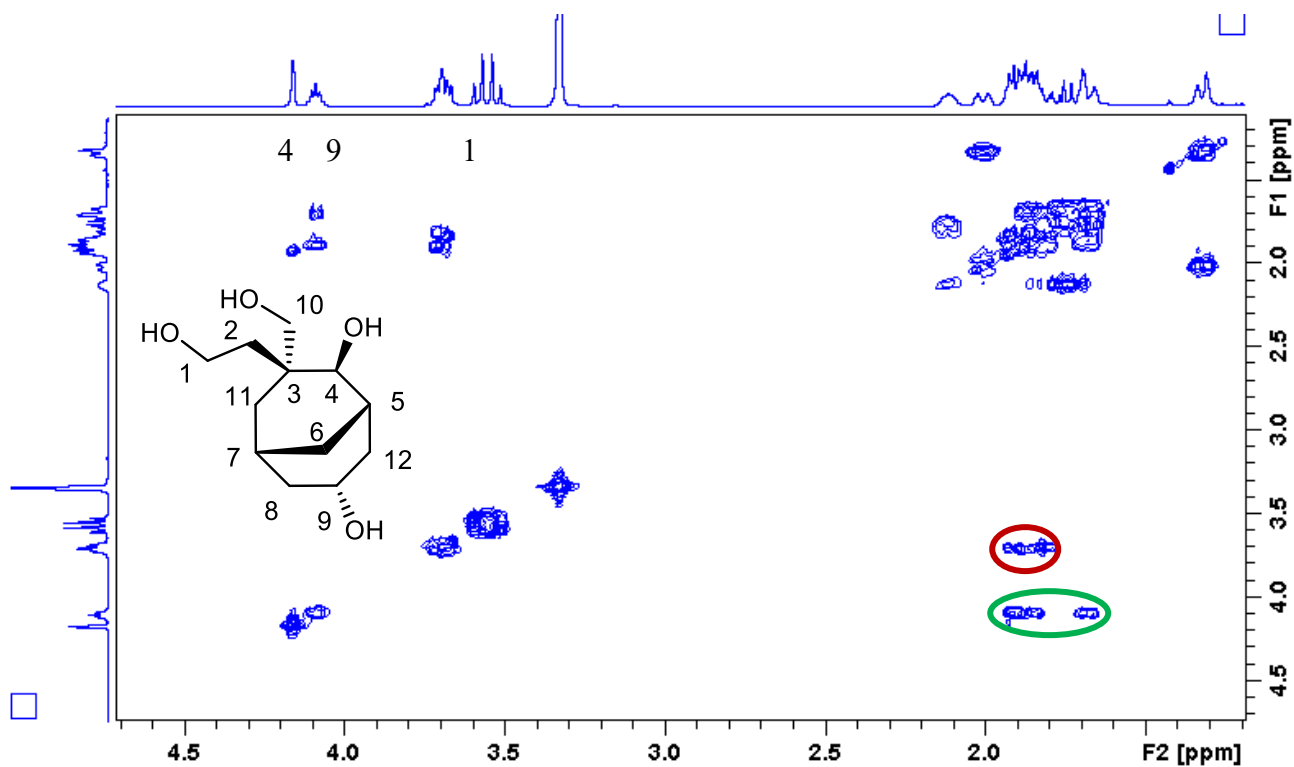
^{13}C NMR of **22** in CD_3OD



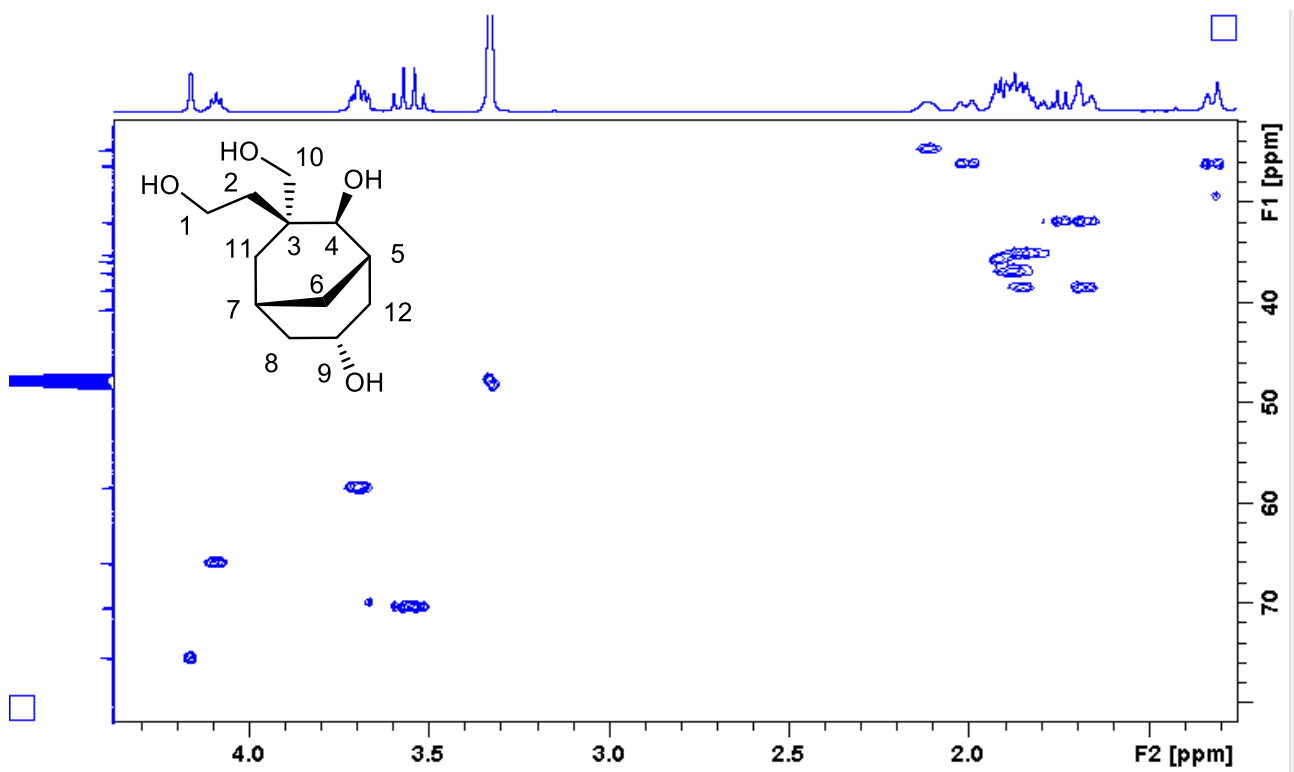
^{13}C NMR (101 MHz, CD_3OD) δ 76.7 (C_4), 71.7 (C_{10}), 67.2 (C_9), 59.7 (C_1), 41.9 (C_3), 40.0 (C_8), 38.3 (C_6), 37.1 (C_5), 36.5 (C_2), 33.2 (C_{11}), 27.6 (C_{12}), 26.0 (C_7).



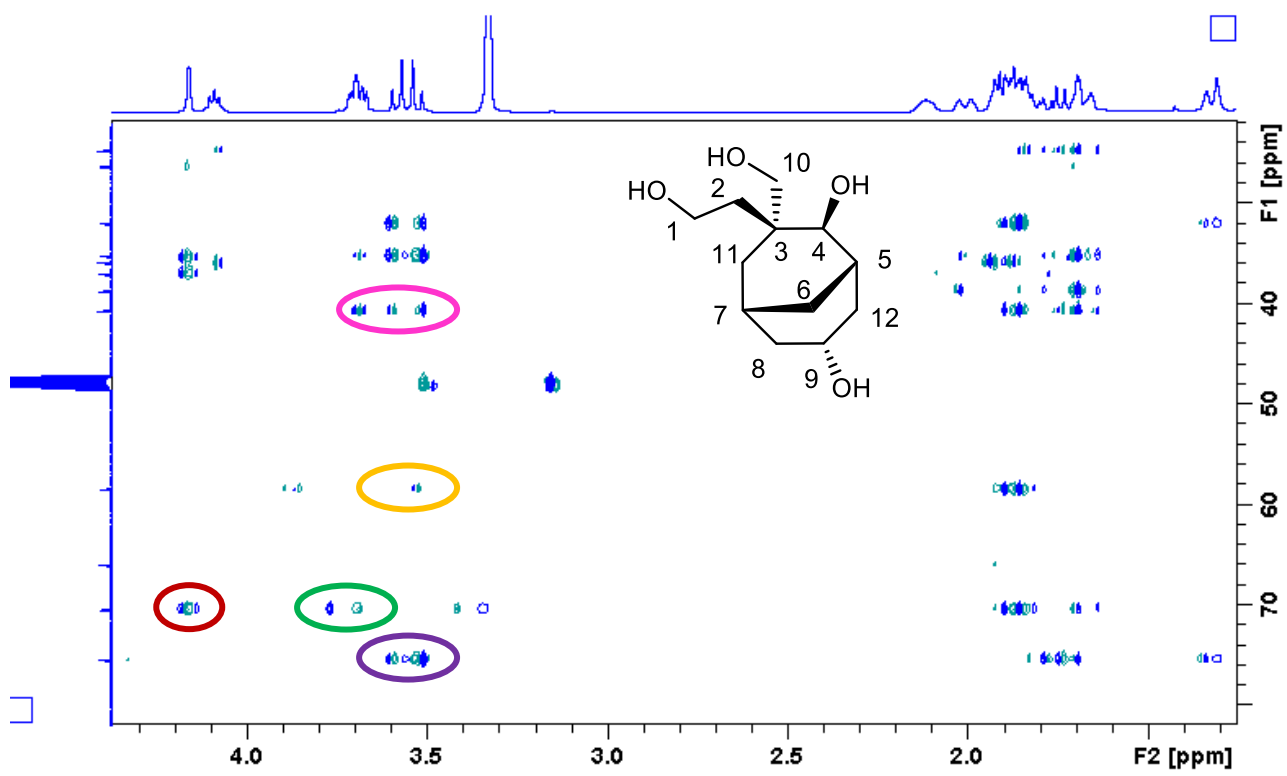
Stacking of the ^{13}C NMR spectrum of **22** (bottom) stacked with its DEPT90 (top) and its DEPT 135 (middle) spectra.



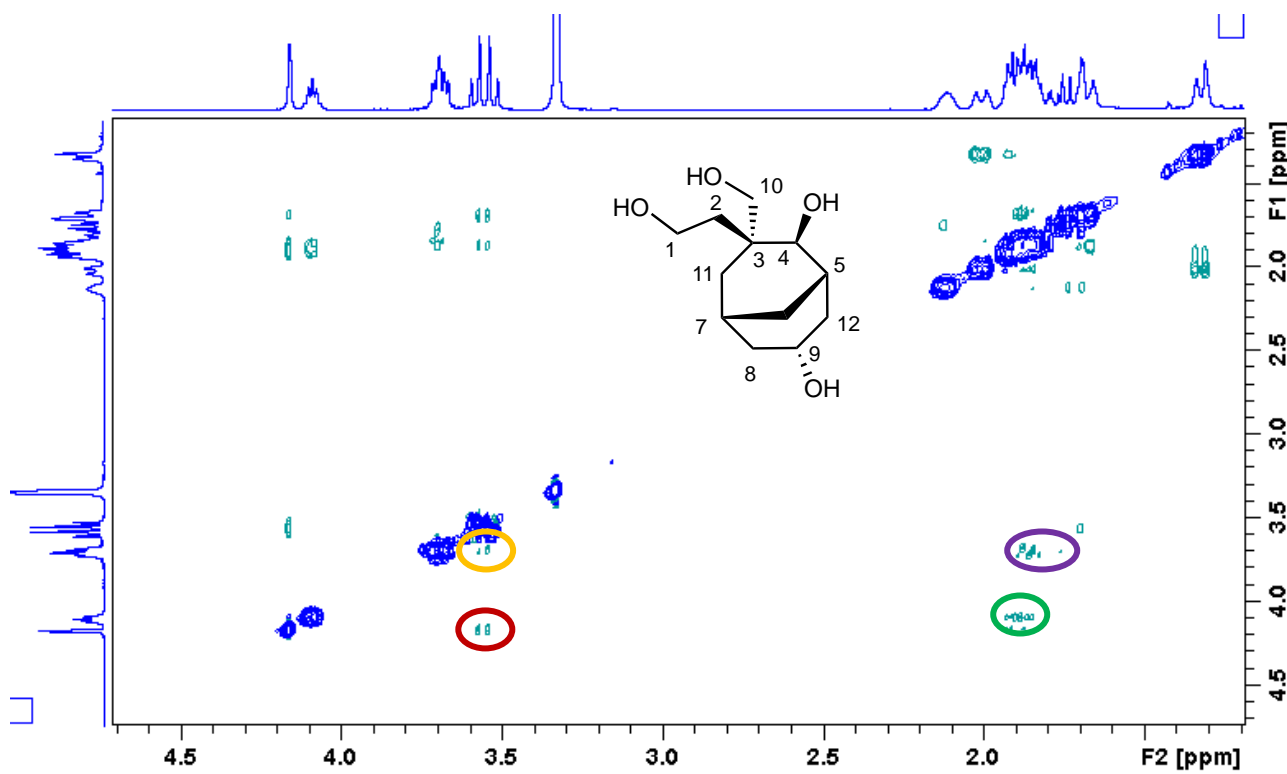
COSY of **22**. Note the correlation between C₁-H and C₂-H (highlighted in red) and the correlation between C₉-H and C₅-H (W coupling¹⁵) and C₈-H (highlighted in green).



HSQC of **22**



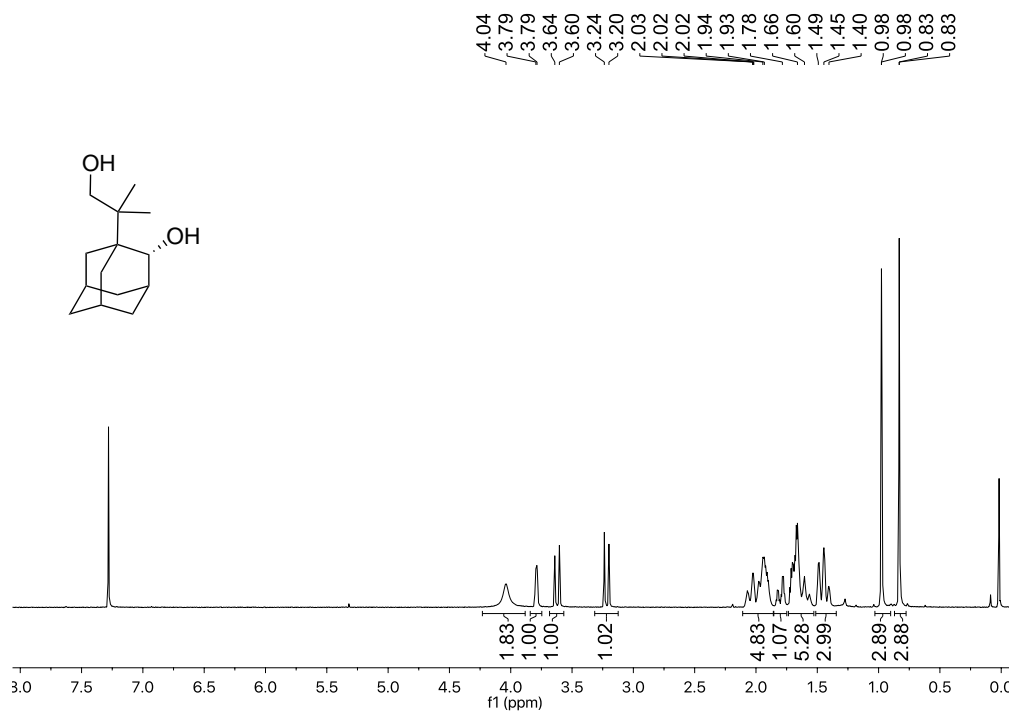
HMBC of **22**. Note the correlation between C₄-H and C₁₀ (highlighted in red), C₁-H and C₁₀ (green), C₁₀-H and C₁ (purple) and C₁₀ (orange). The correlation between C₃ and C₁-H and C₁₀-H is highlighted in pink.



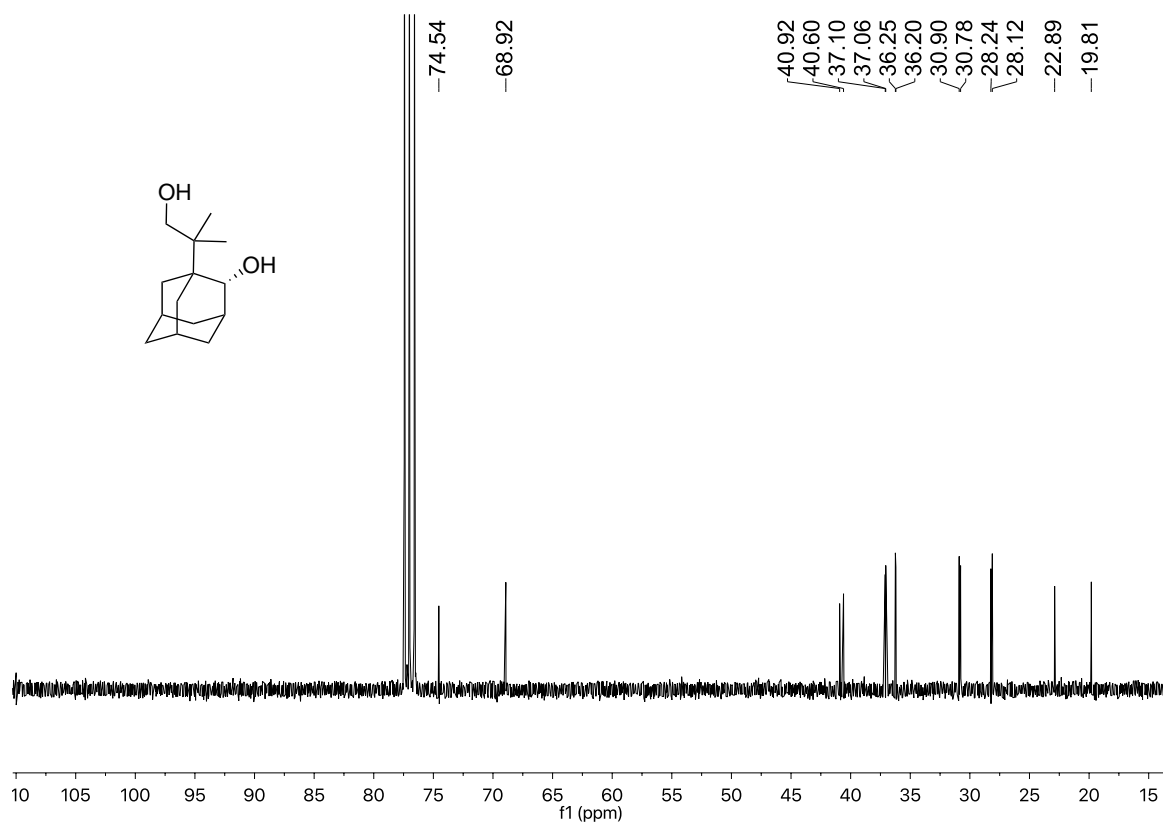
NOESY of **22**. The NOESY correlation of C₄-H with C₁₀-H is highlighted in red, while the correlation of C₉-H with C₈-H is highlighted in green. Correlation of C₁-H with C₂-H₂ is highlighted in orange and correlation of C₁₀-H with C₂-H₂ and C₁₁-H is highlighted in purple.

IV. NMR Characterization of lactone derivatization products

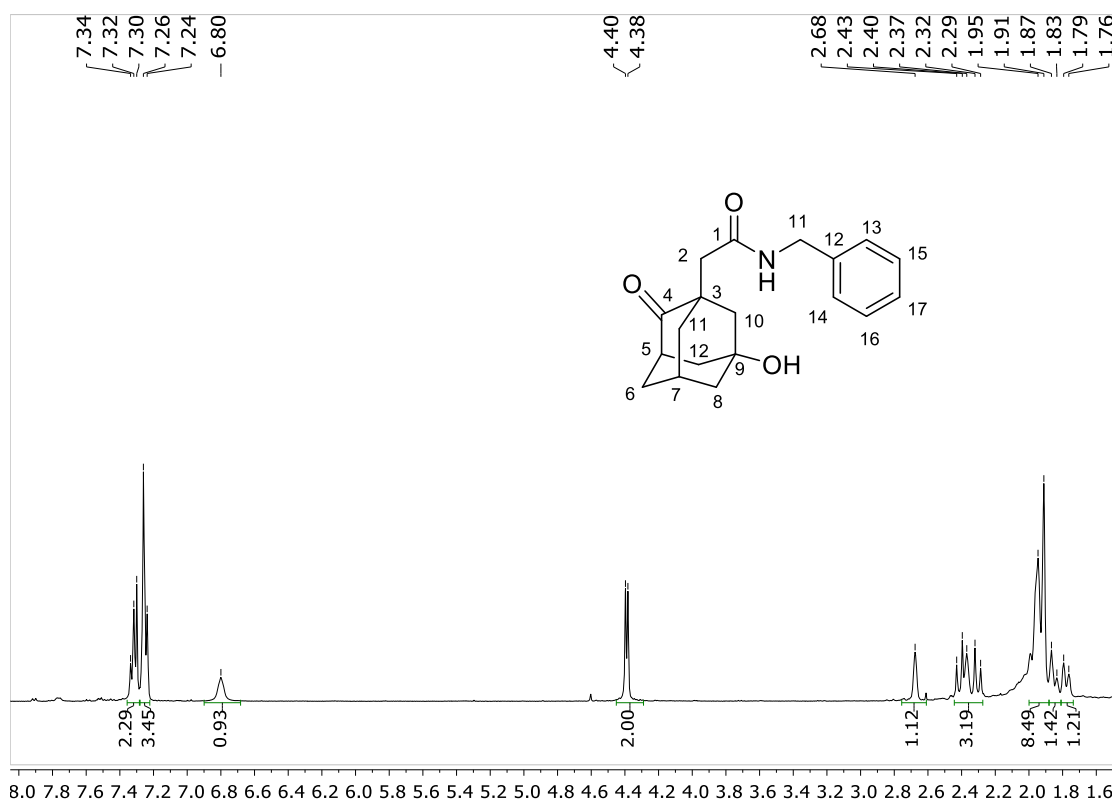
^1H NMR of **2b** in CDCl_3



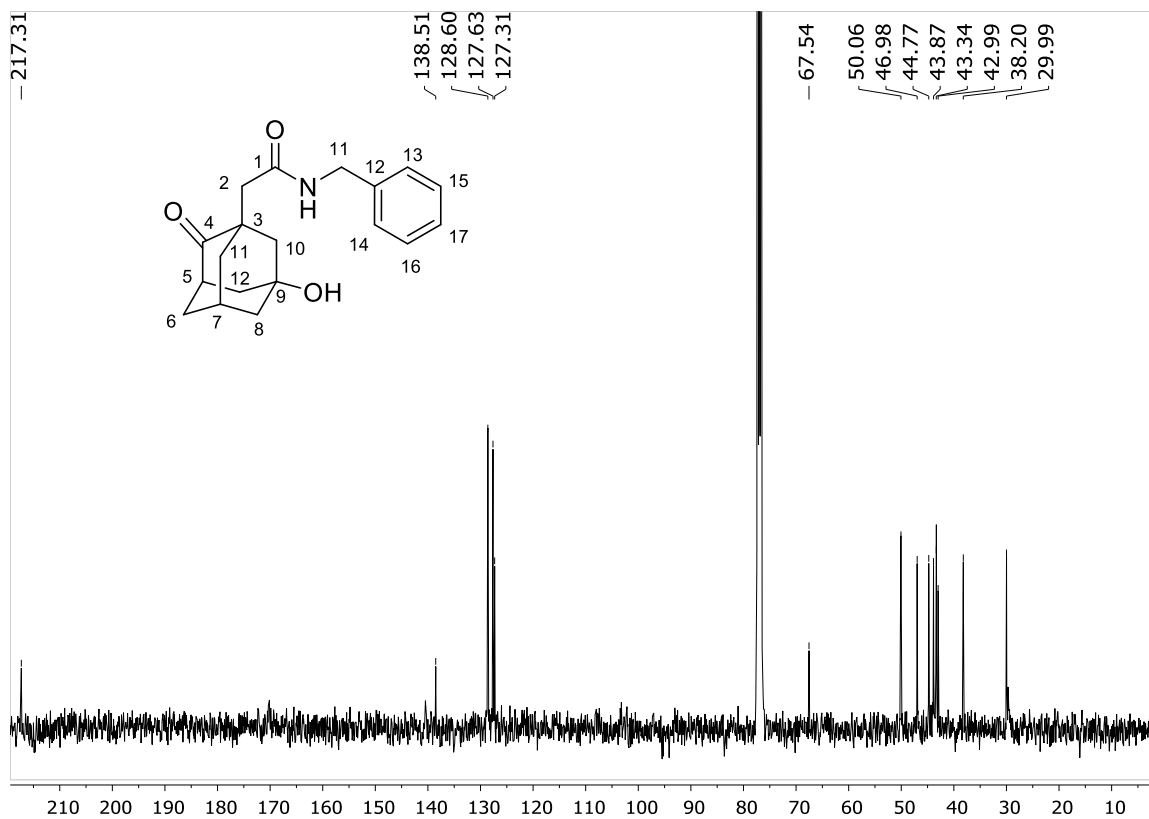
^{13}C NMR of **2b** in CDCl_3



^1H NMR of **23b** in CDCl_3



^{13}C NMR of **23b** in CDCl_3



IV.HPLC and GC chromatograms of the products

Diastereomeric ratios (d.r.) and regioisomeric ratios (r.r.) were calculated from GC analysis of the crude mixture immediately after each oxidation experiment as described in General oxidation protocol A. Unless otherwise stated, the GC analysis was performed by using HP5-column (30m).

GC method for the analysis of the products derived from oxidation of **4, 5, 8, 9, 10, 20**:

Initial: 75 °C hold time 0.5 min

Ramp 1: 190 °C (10 °C/min) hold time 0 min

Ramp 2: 300 °C (20 °C/min) hold time 0 min

GC method for the analysis of the products derived from oxidation of **6, 7** (HP-Chiral-20B column):

Initial: 75 °C hold time 0.5 min

Ramp 1: 180 °C (10 °C/min) hold time 0 min

Ramp 2: 240 °C (20 °C/min) hold time 400min

GC method for the analysis of the products derived from oxidation of **11**:

Initial: 75 °C hold time 0.5 min

Ramp 1: 160 °C (10 °C/min) hold time 60 min

Ramp 2: 240 °C (20 °C/min) hold time 15 min

GC method for the analysis of the products derived from oxidation of **12, 13, 14, 15, 16, 17, 18, 19**:

Initial: 150 °C hold time 0.5 min

Ramp 1: 190 °C (10 °C/min) hold time 0 min

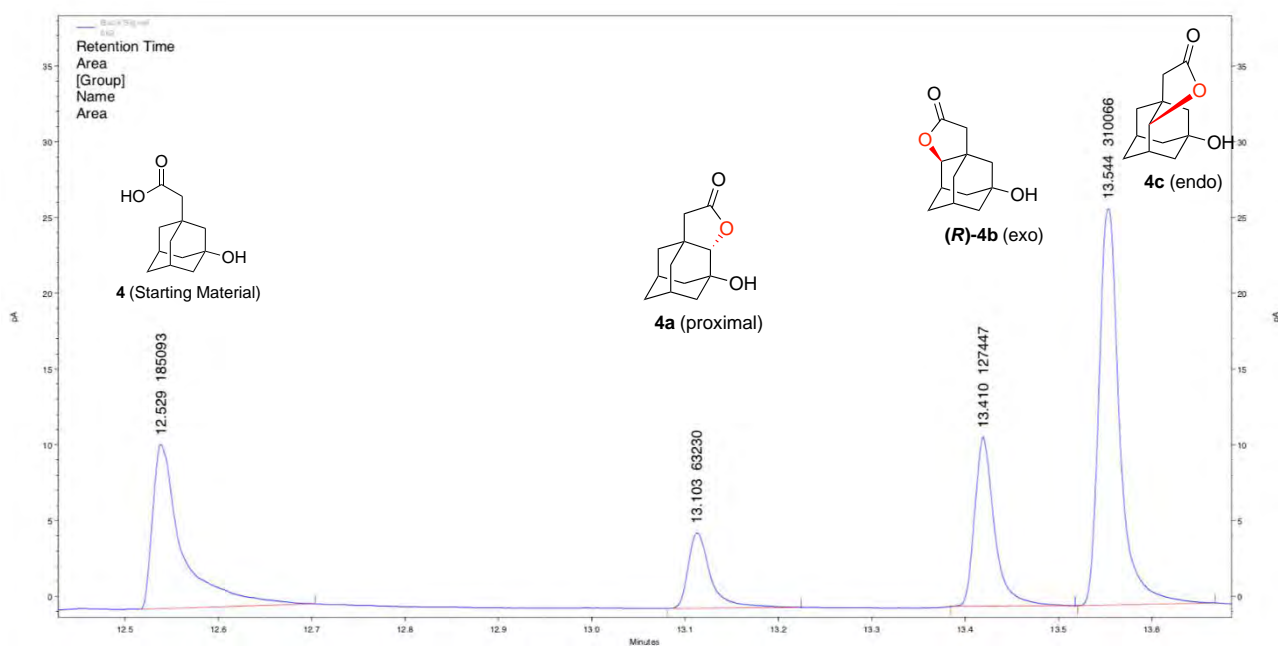
Ramp 2: 300 °C (25 °C/min) hold time 0 min

Ramp 3: 325 °C (10 °C/min) hold time 3 min

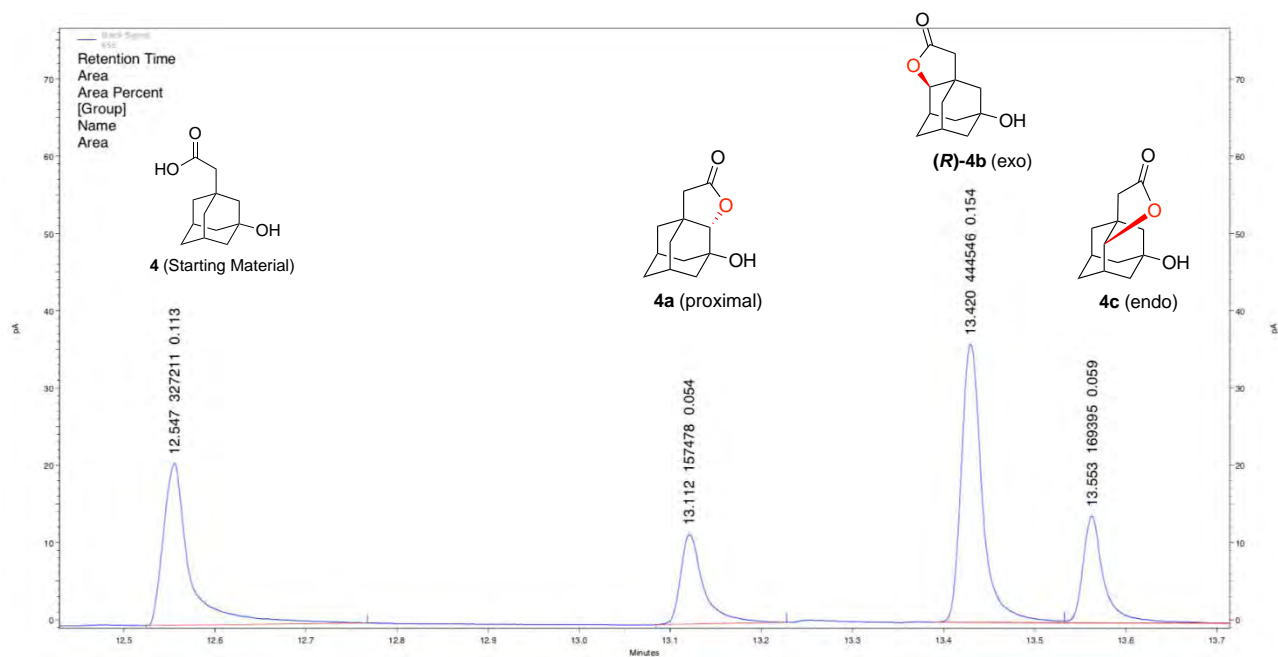
IV. GC chromatograms for the determination of the a:b:c ratios (and d.r., r.r.)

Oxidation of 4

(*S,S*)-Mn(pdp)

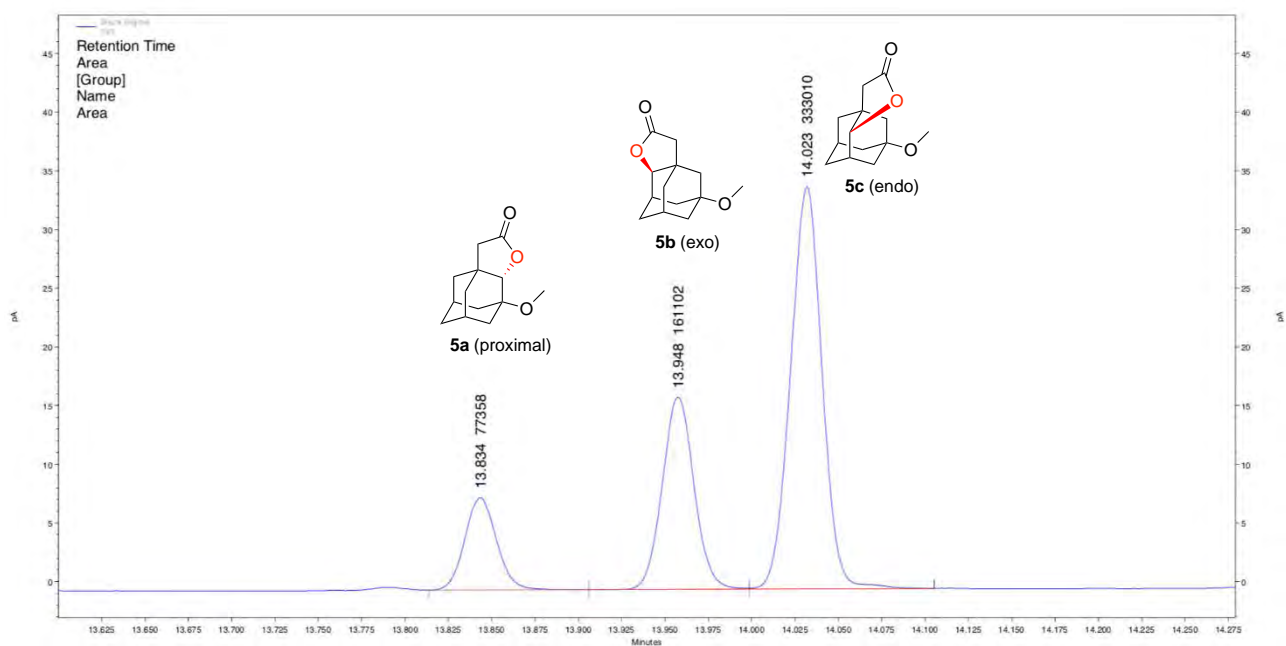


(*S,S*)-Mn(^{TiBS}pdp)

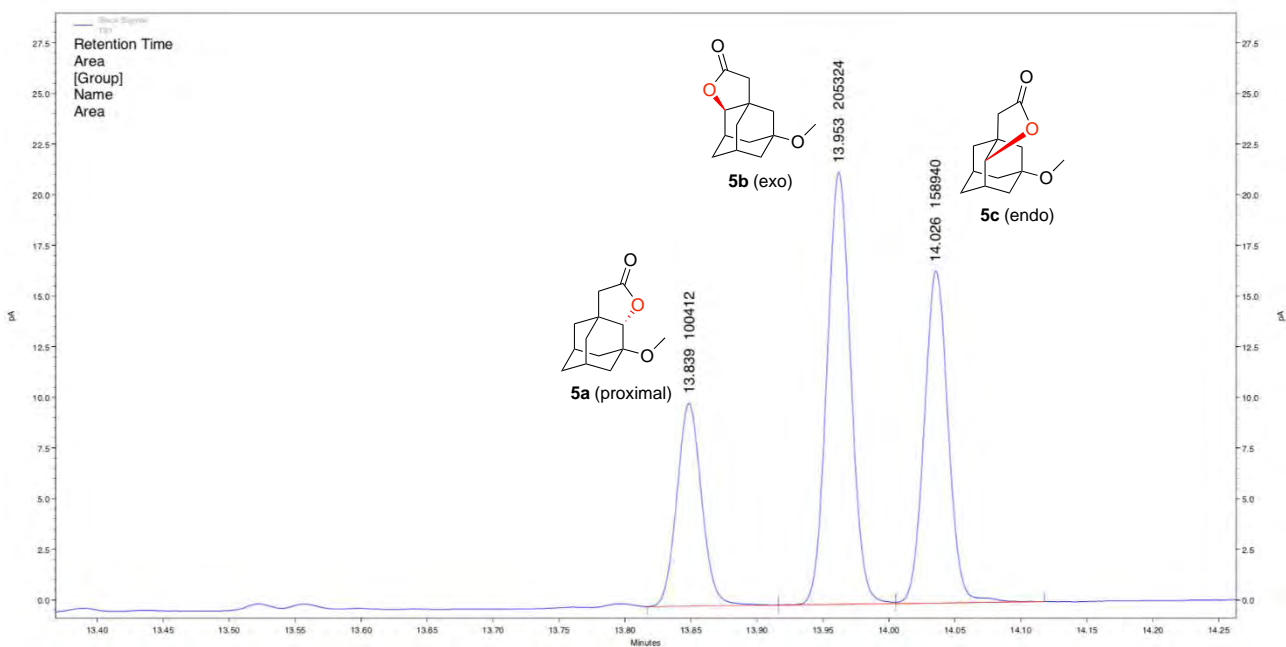


Oxidation of 5

(*S,S*)-Mn(pdp)

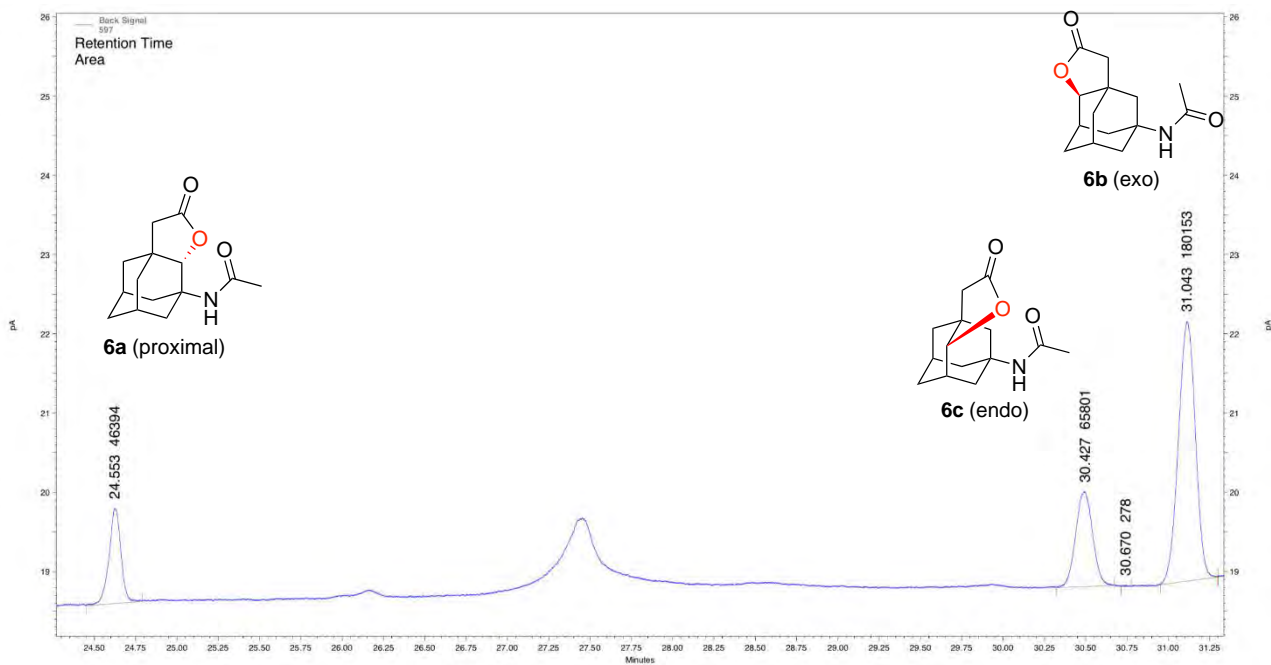


(*S,S*)-Mn(^{TiBS}pdp)

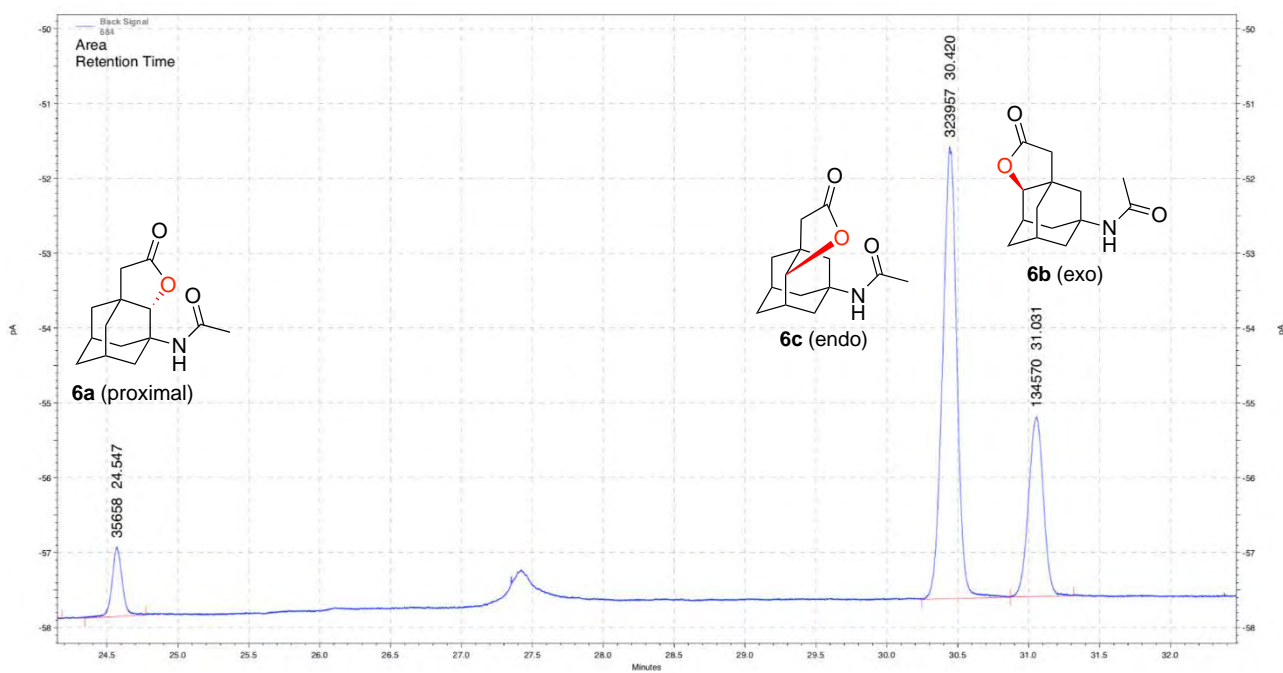


Oxidation of 6

(*S,S*)-Mn(pdp)

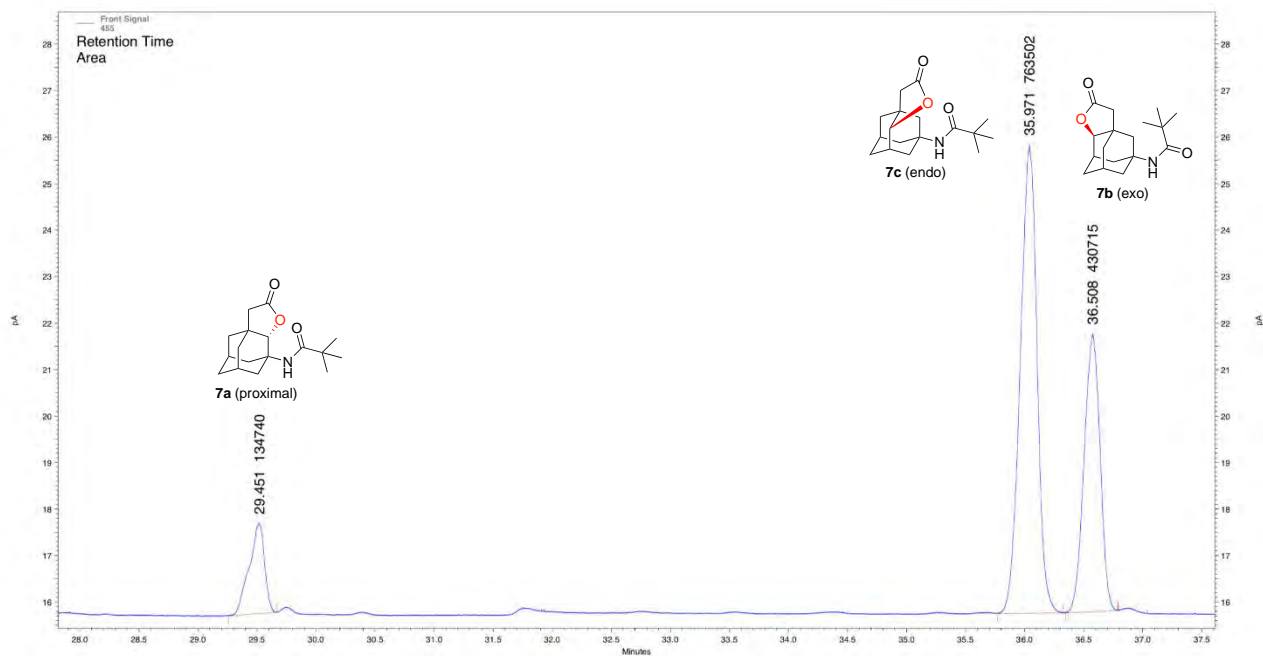


(*S,S*)-Mn(^{TIBS}pdp)

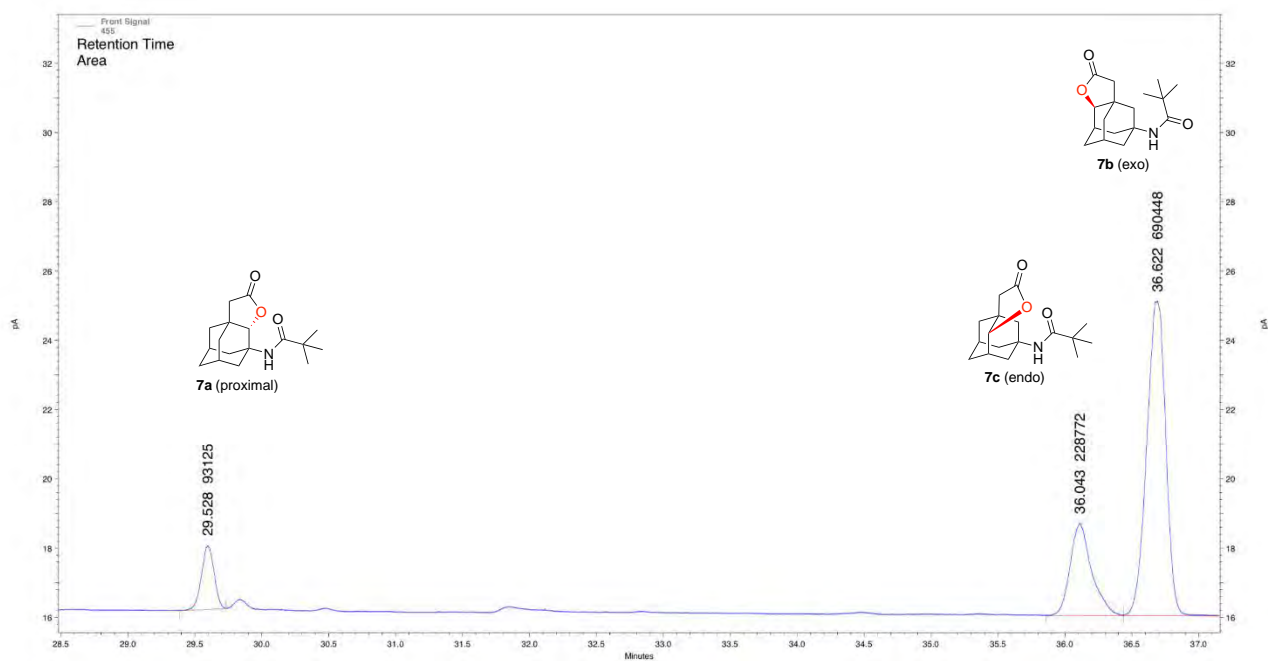


Oxidation of 7

(*S,S*)-Mn(pdp)

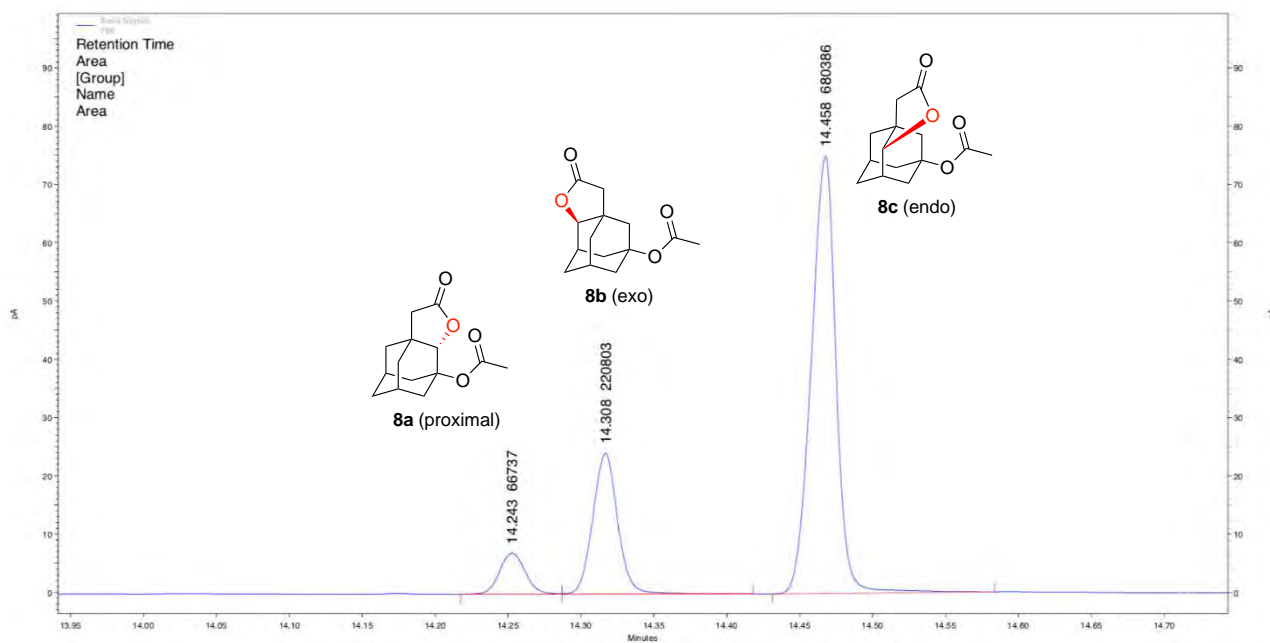


(*S,S*)-Mn(^TIBS_{pdp})

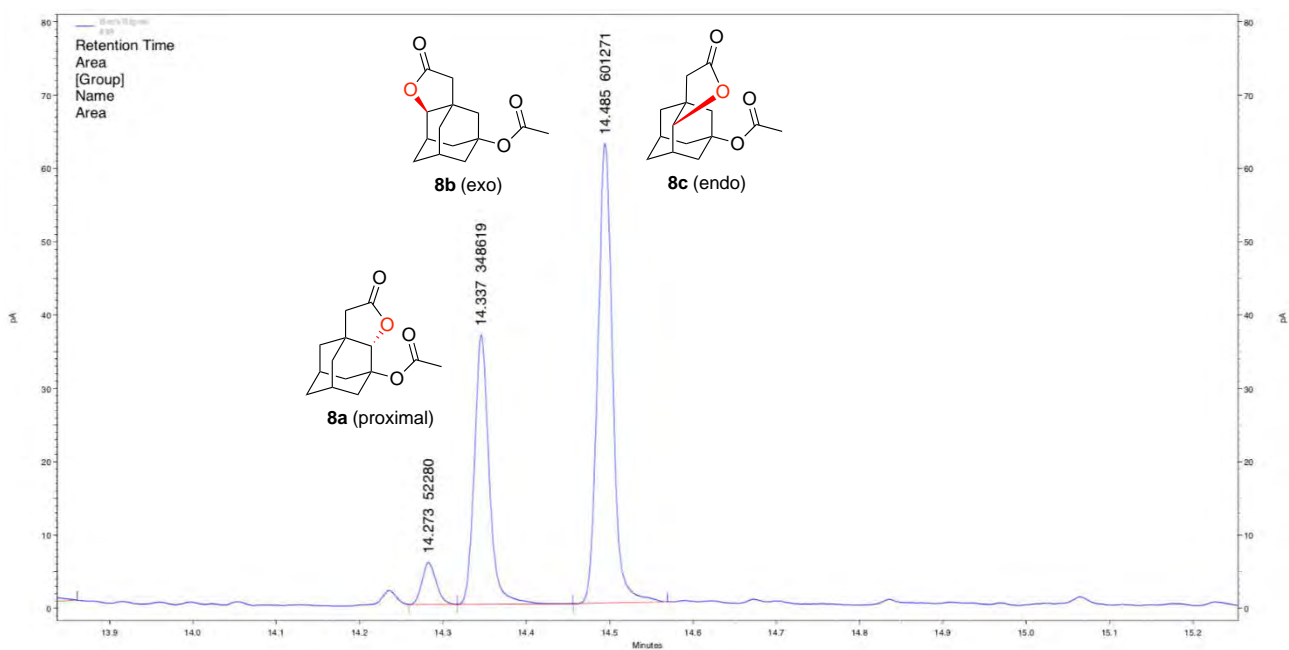


Oxidation of 8

(*S,S*)-Mn(pdp)

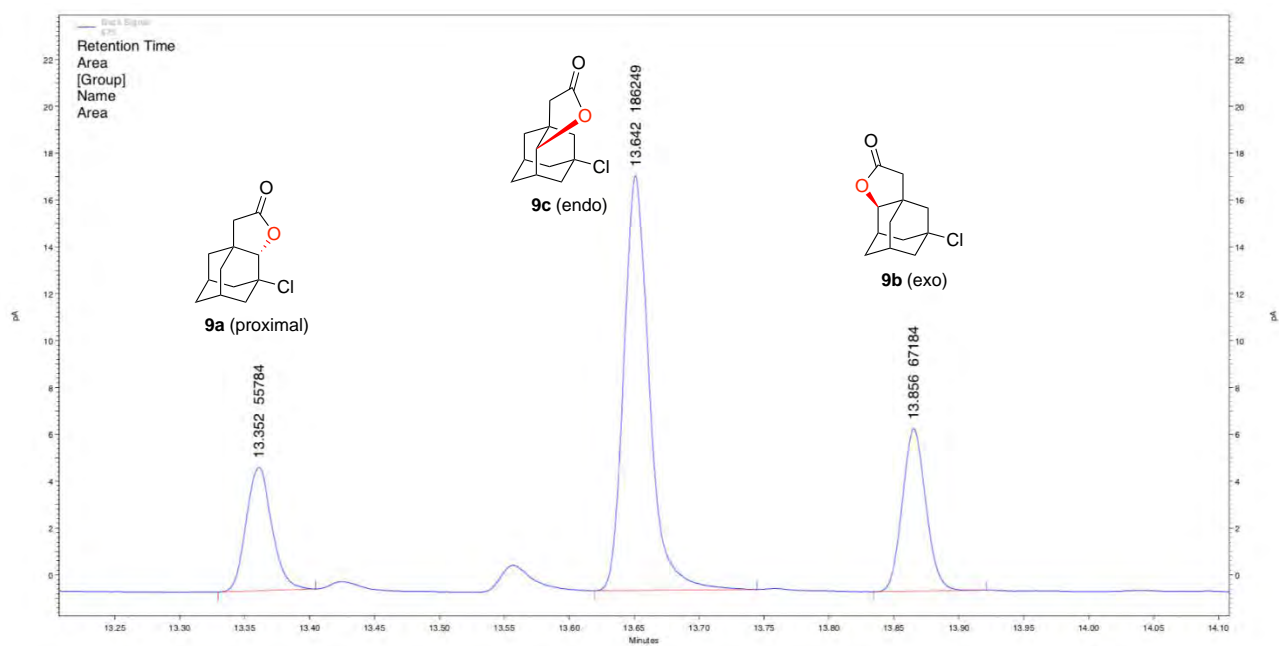


(*S,S*)-Mn(^TIBS_{pdp})

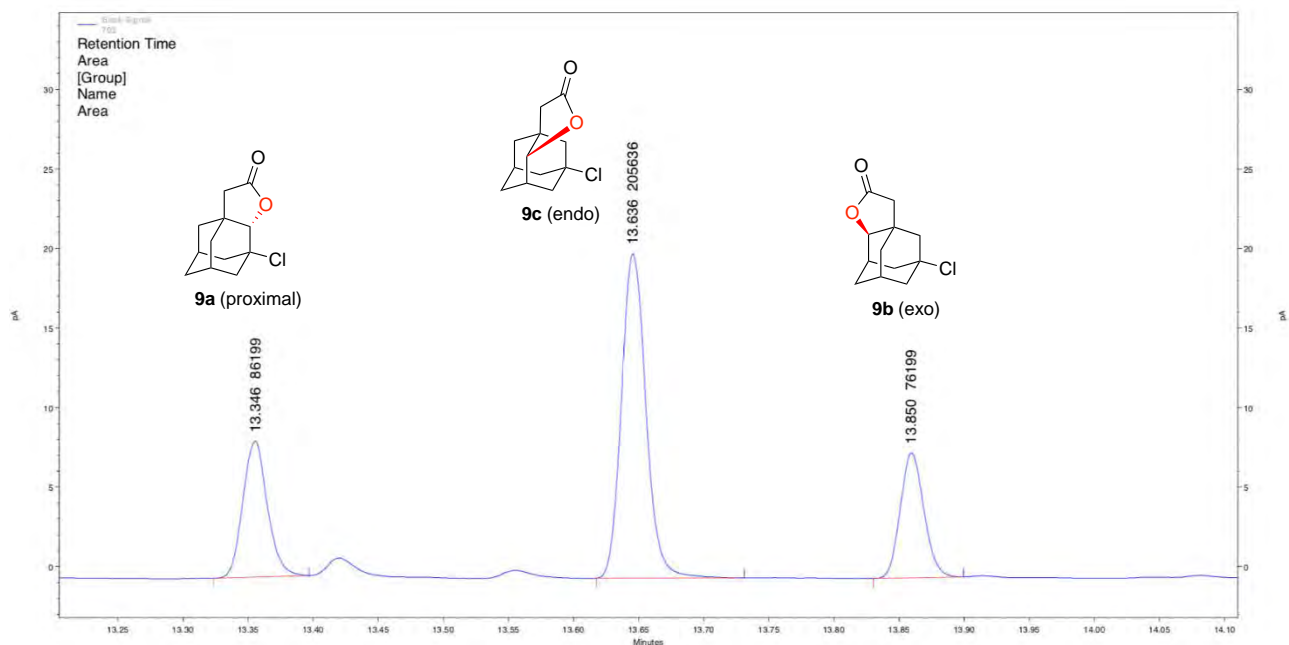


Oxidation of 9

(*S,S*)-Mn(pdp)

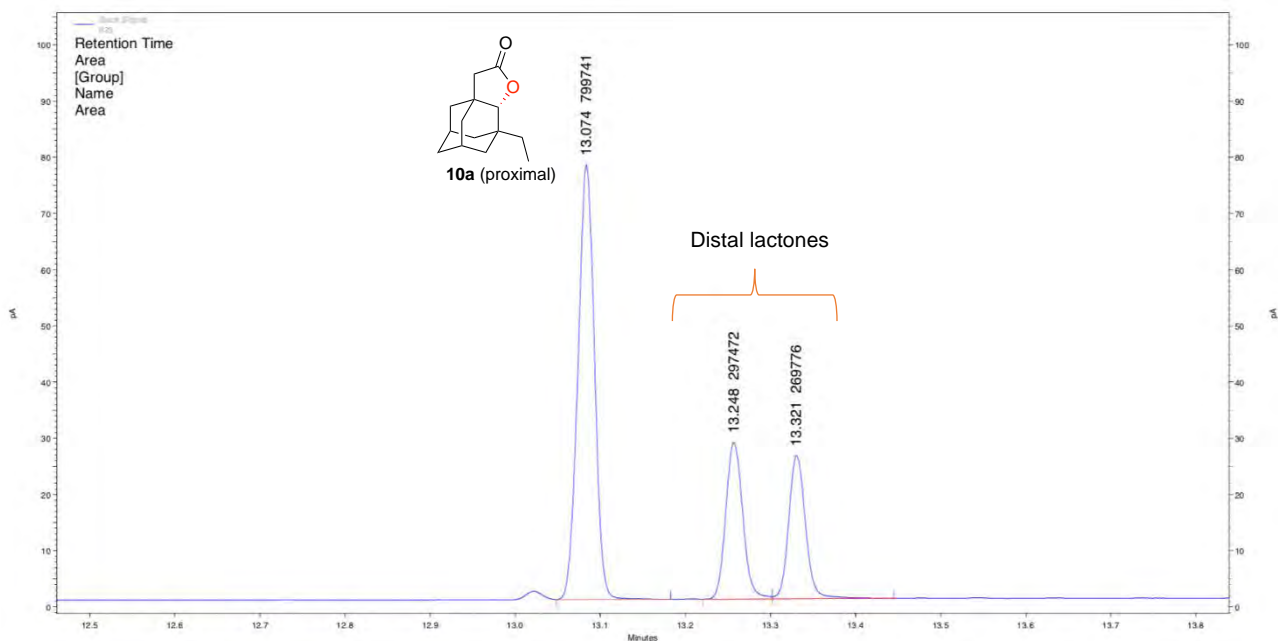


(*S,S*)-Mn(^TIBS_{pdp})

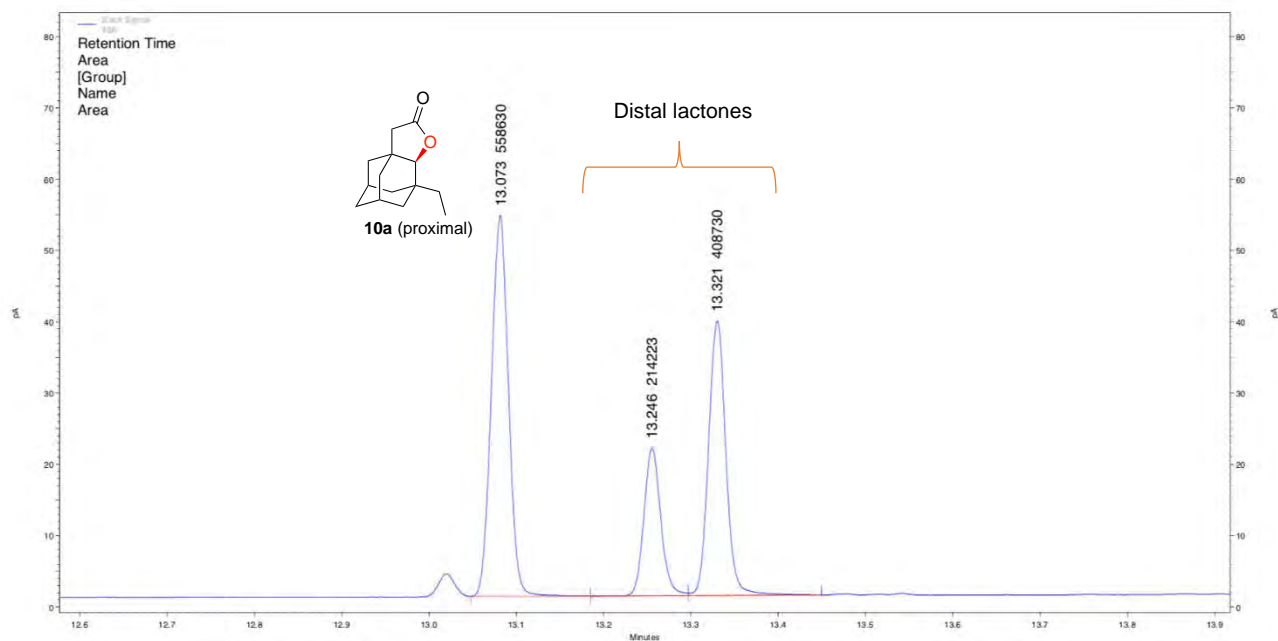


Oxidation of 10

(*S,S*)-Mn(pdp)

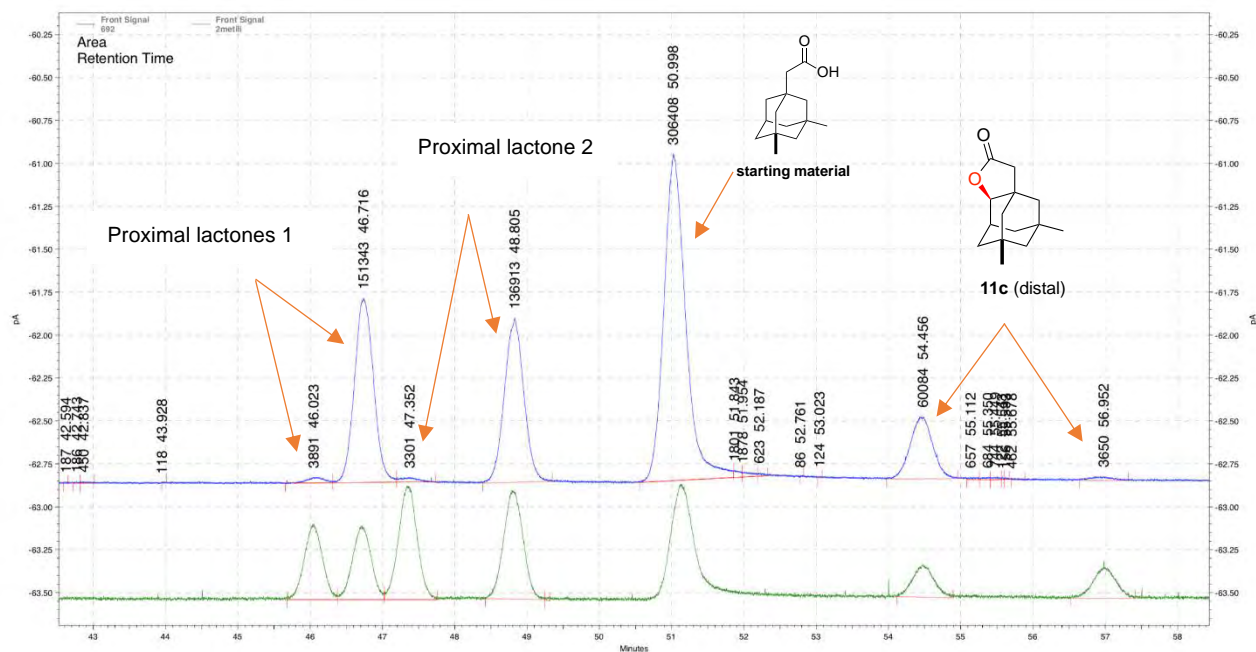


(*S,S*)-Mn(^{TIBS}pdp)

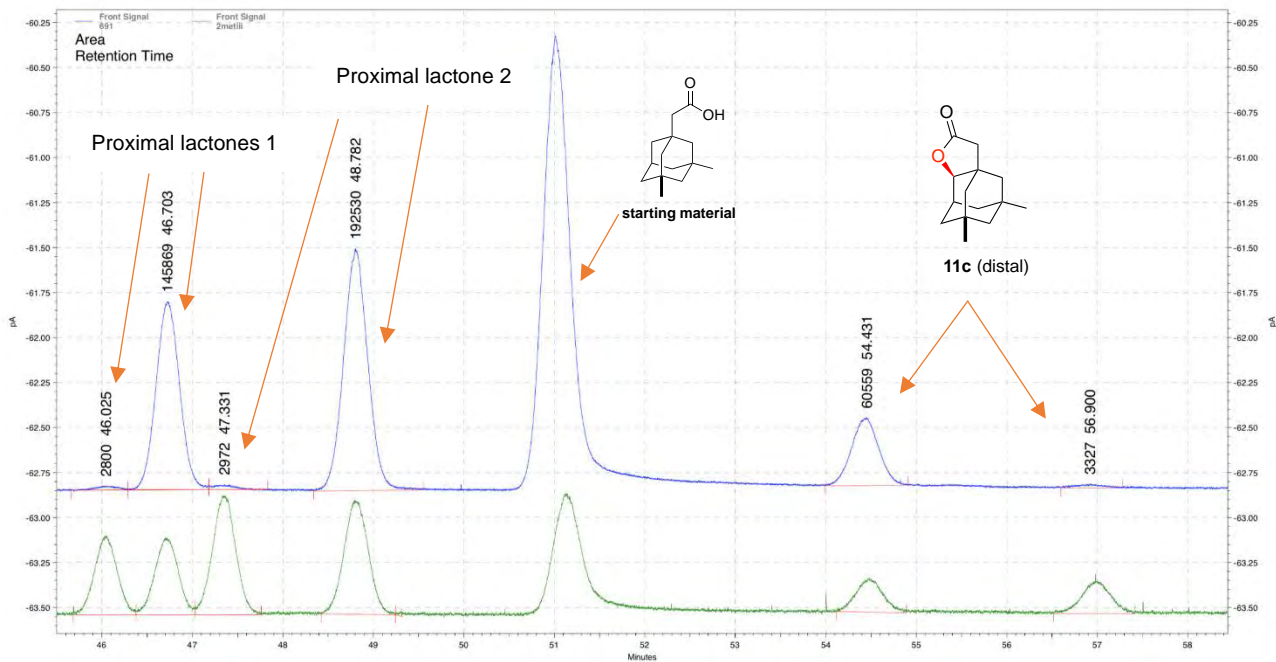


Oxidation of 11

(*S,S*)-Mn(pdp)

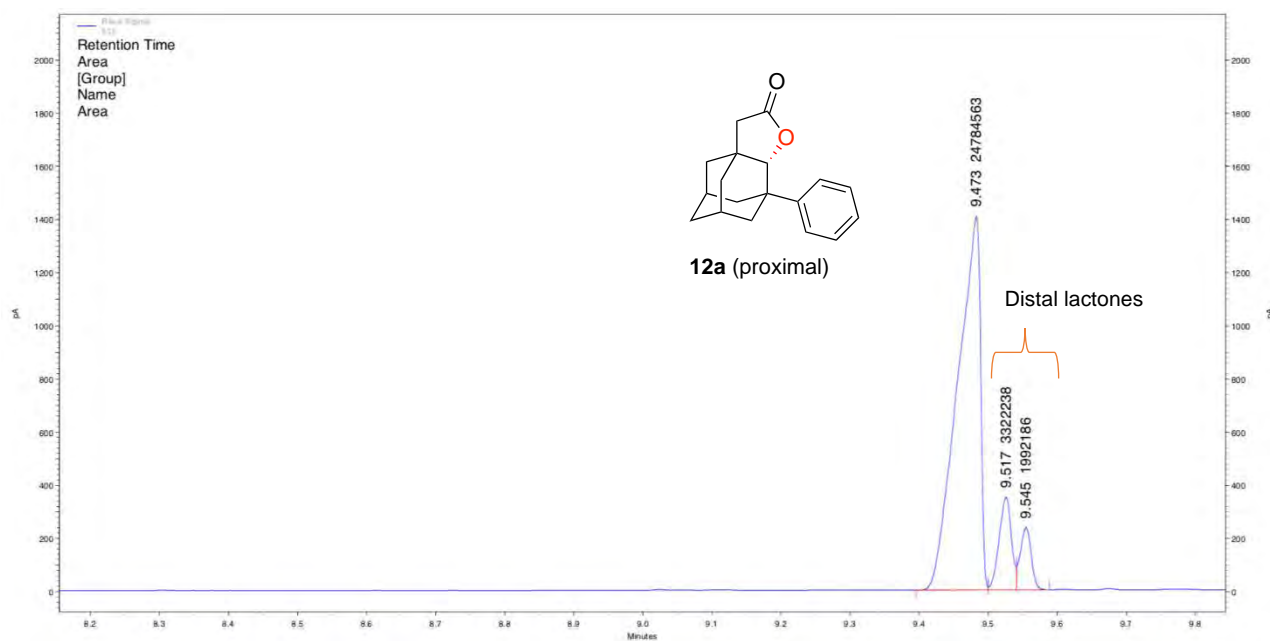


(*S,S*)-Mn(^{TiBS}pdp)

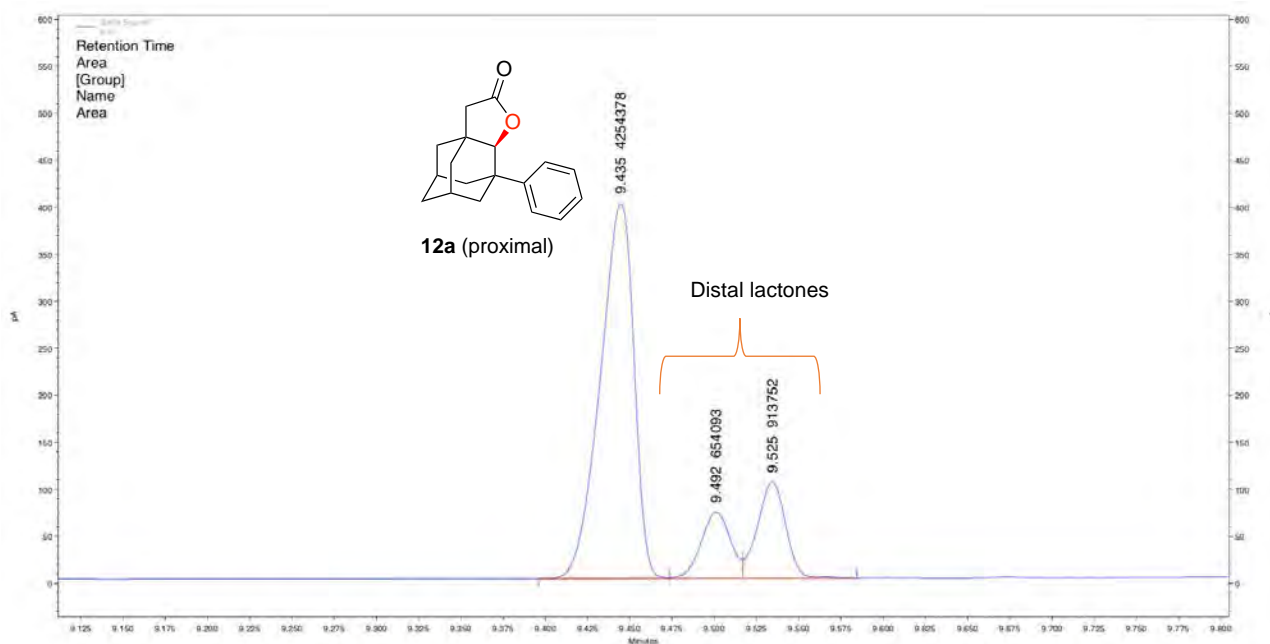


Oxidation of 12

(*S,S*)-Mn(pdp)

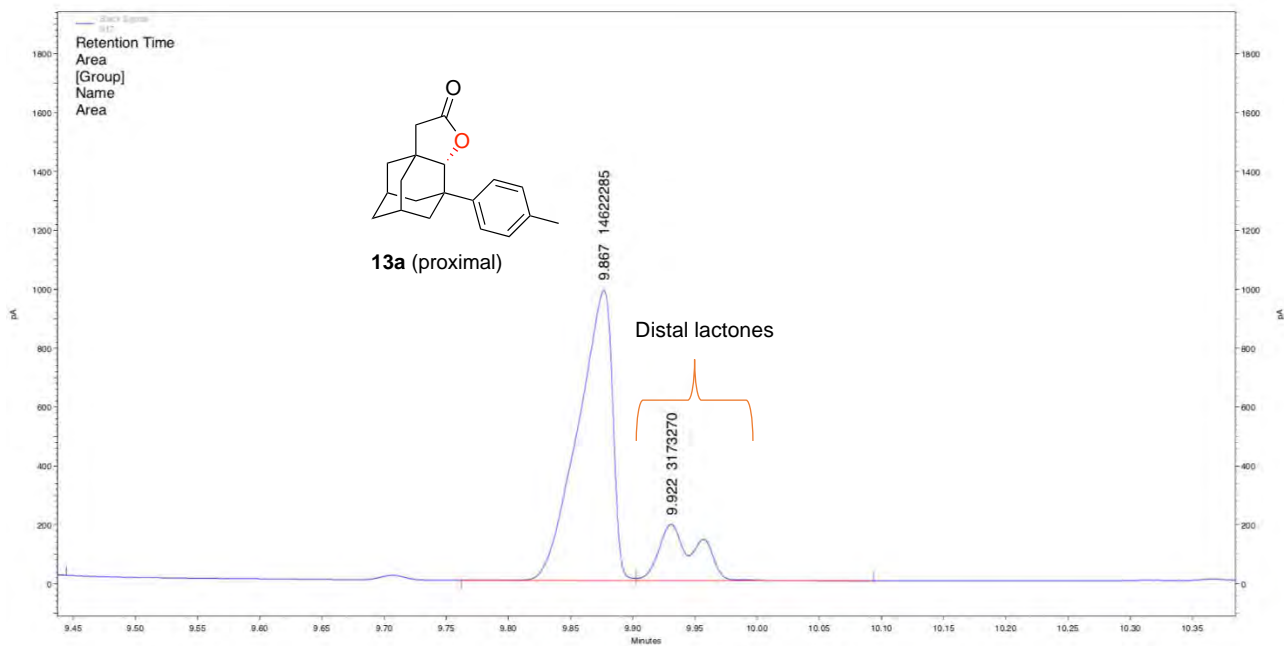


(*R,R*)-Mn(^{TiBS}pdp)

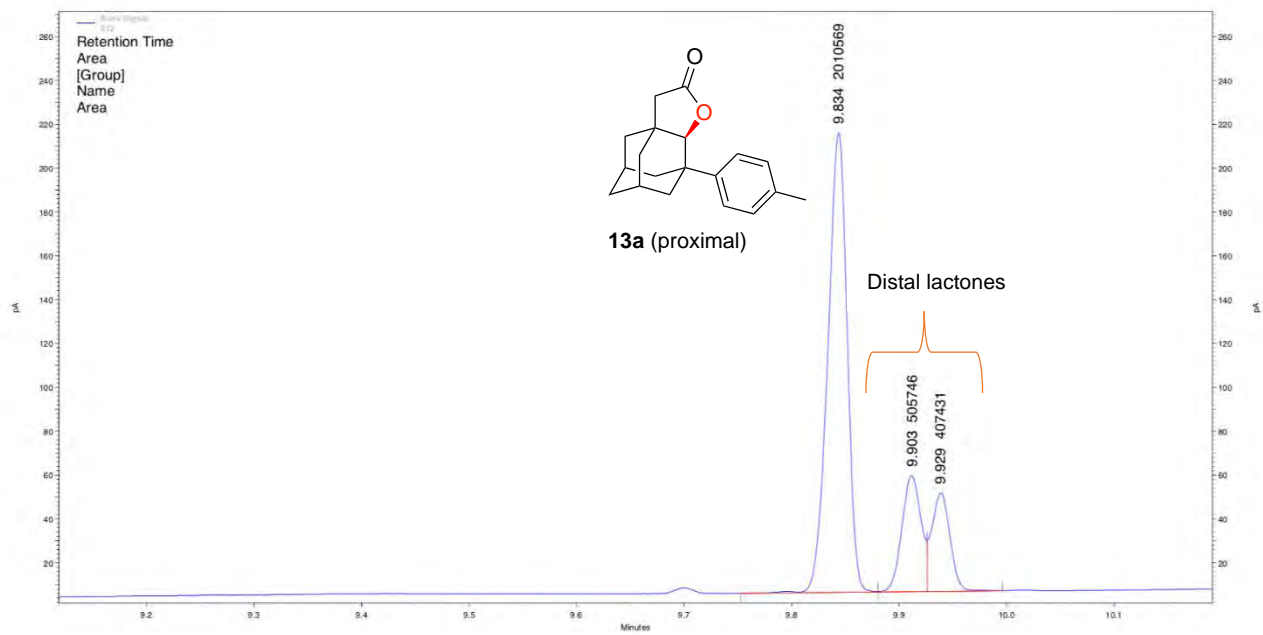


Oxidation of 13

(*S,S*)-Mn(pdp)

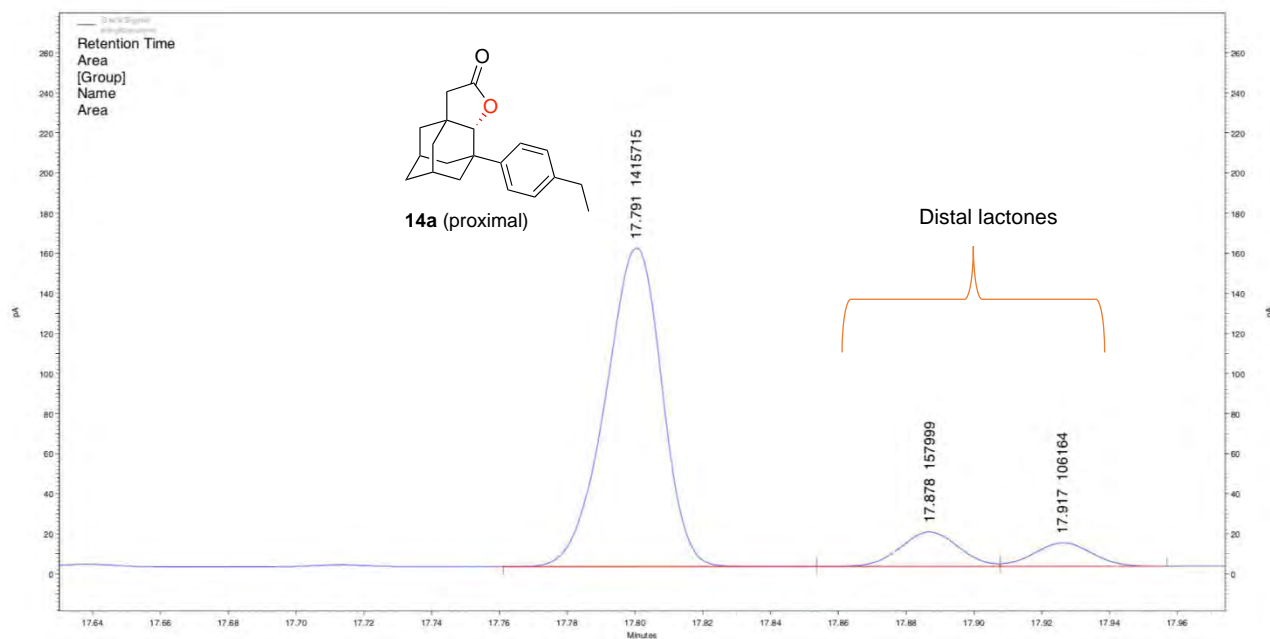


(R,R) -Mn(TIBS)pdp

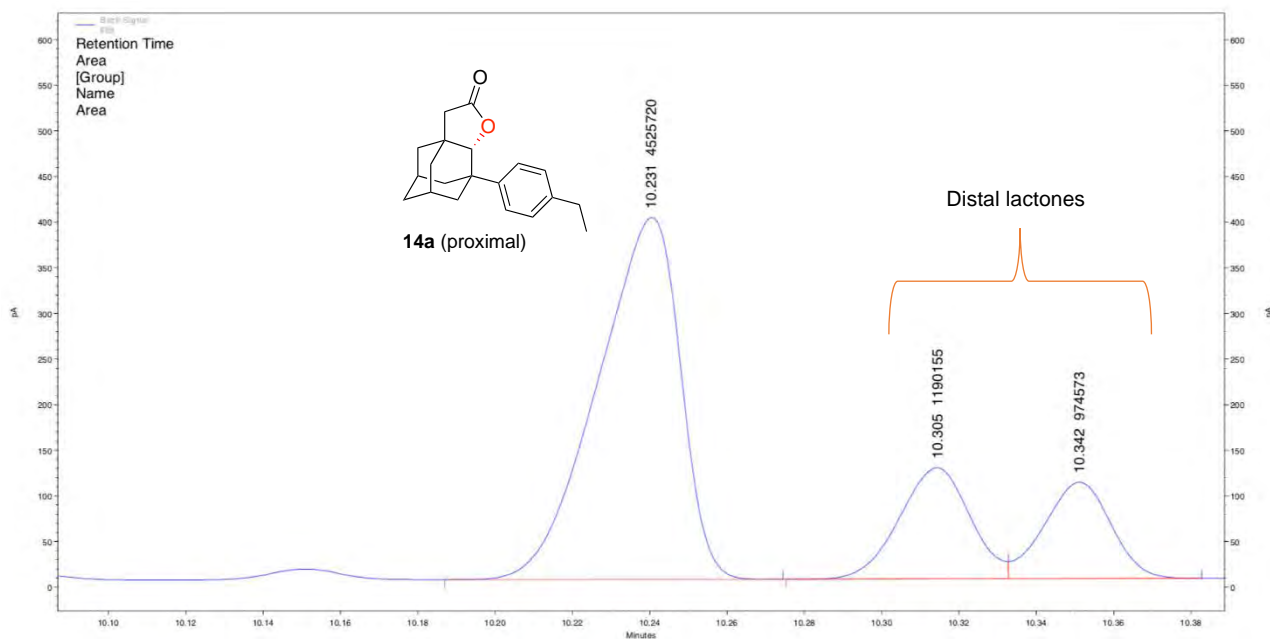


Oxidation of 14

(*S,S*)-Mn(pdp)

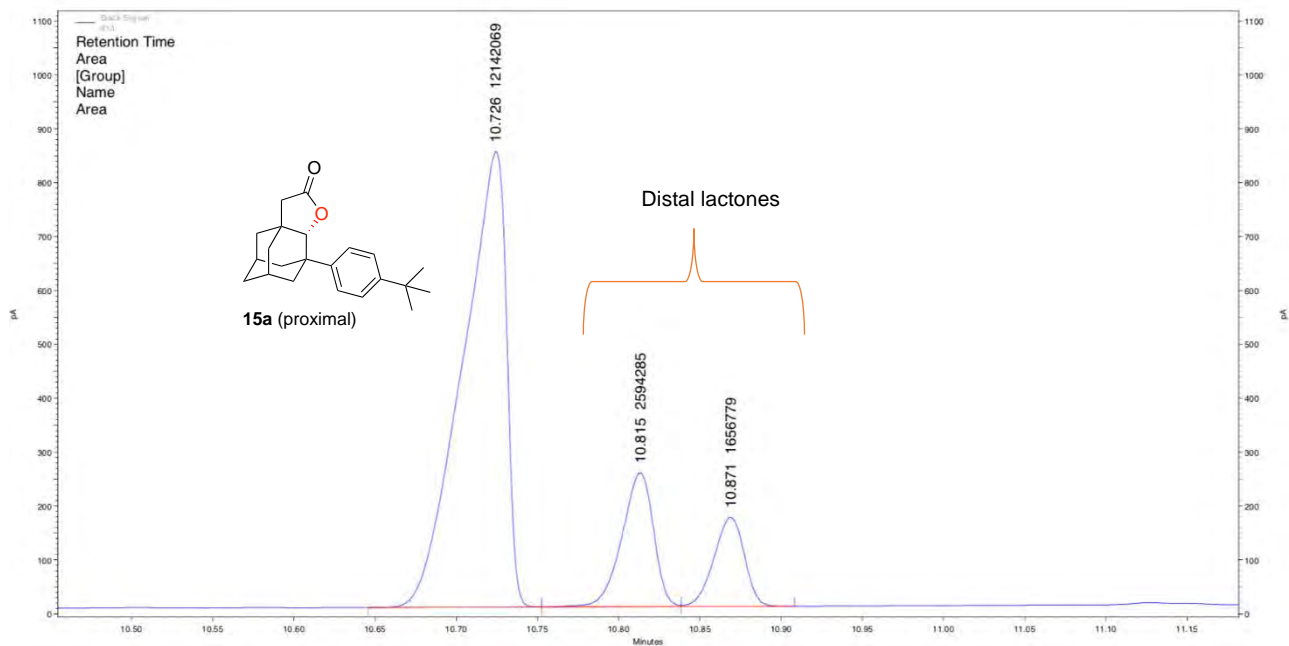


(*S,S*)-Mn(^{TiBS}pdp)

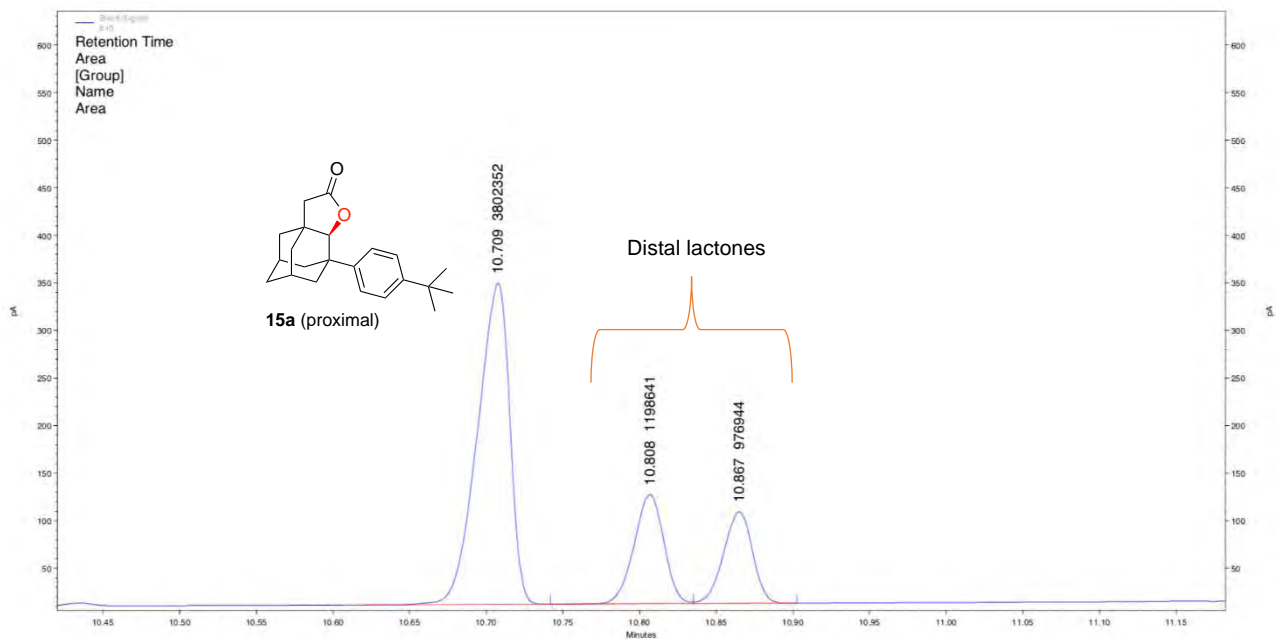


Oxidation of 15

(*S,S*)-Mn(pdp)

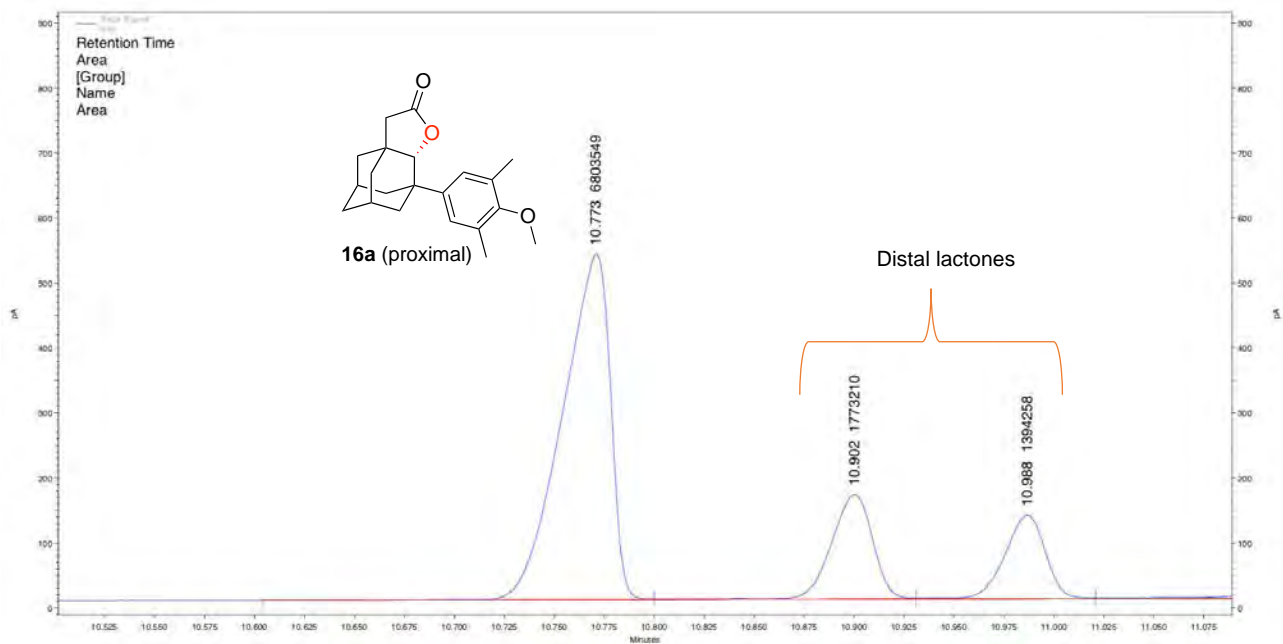


(R,R) -Mn(TIBS)pdp

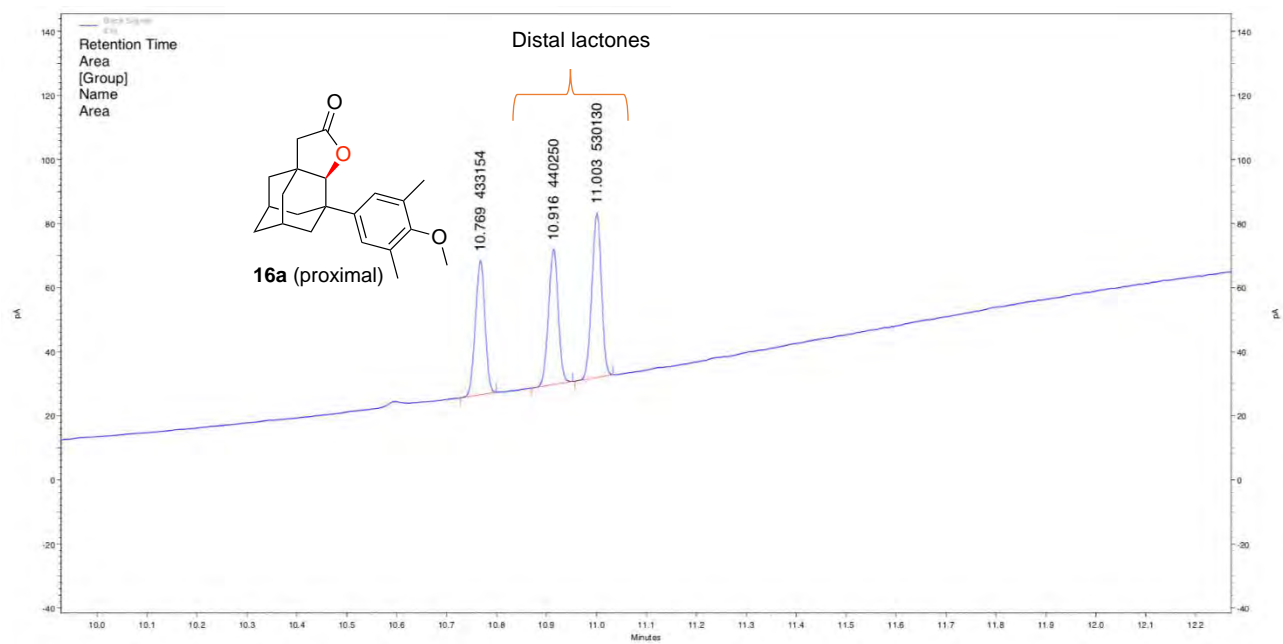


Oxidation of 16

(S,S) -Mn(pdp)

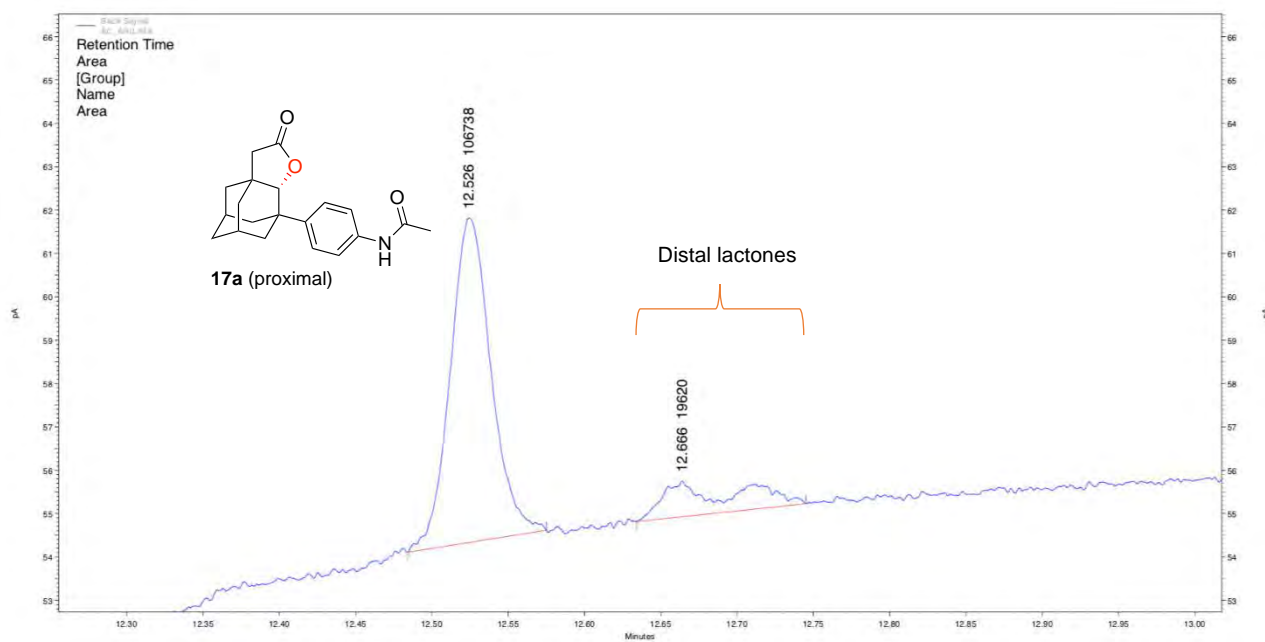


(R,R) -Mn(TIBSpdp)

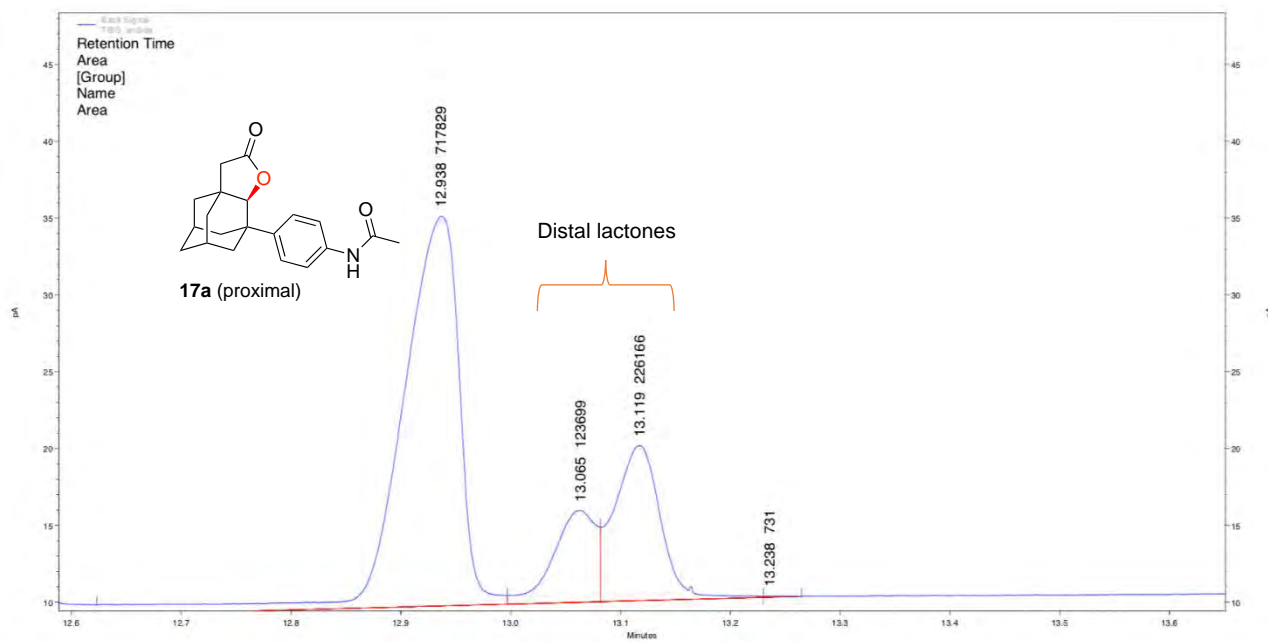


Oxidation of 17

(S,S) -Mn(pdp)

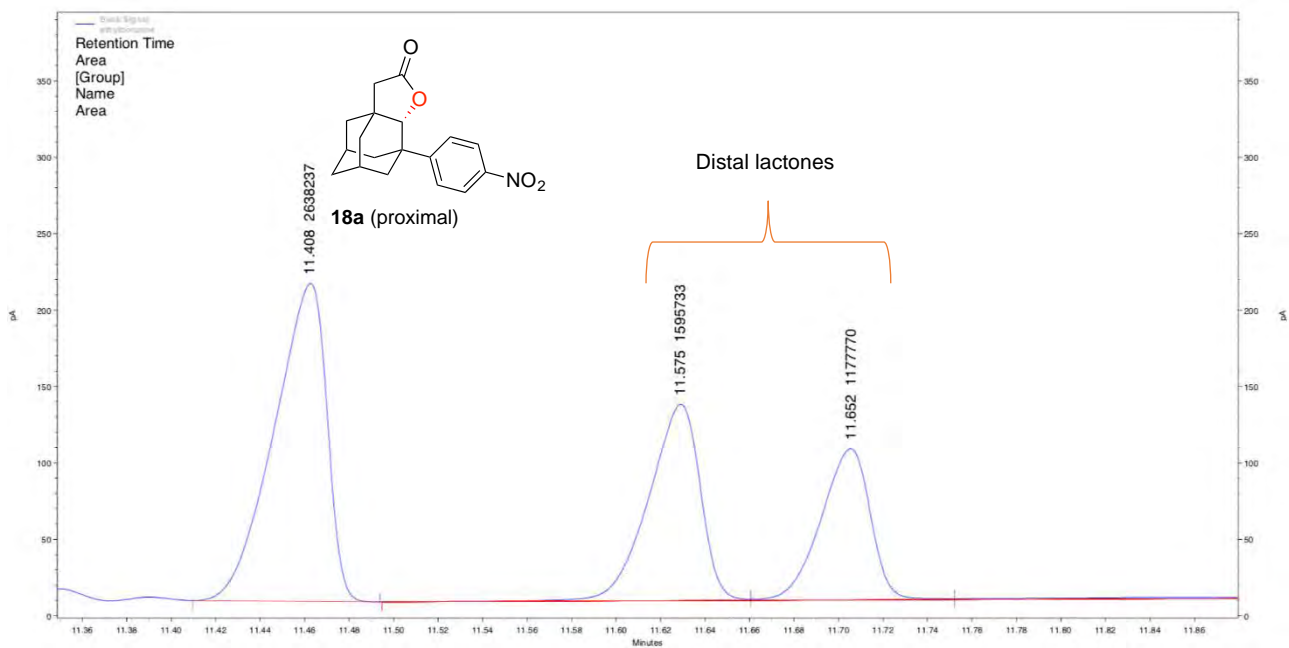


(*R,R*)-Mn(^{TIBS}pdp)

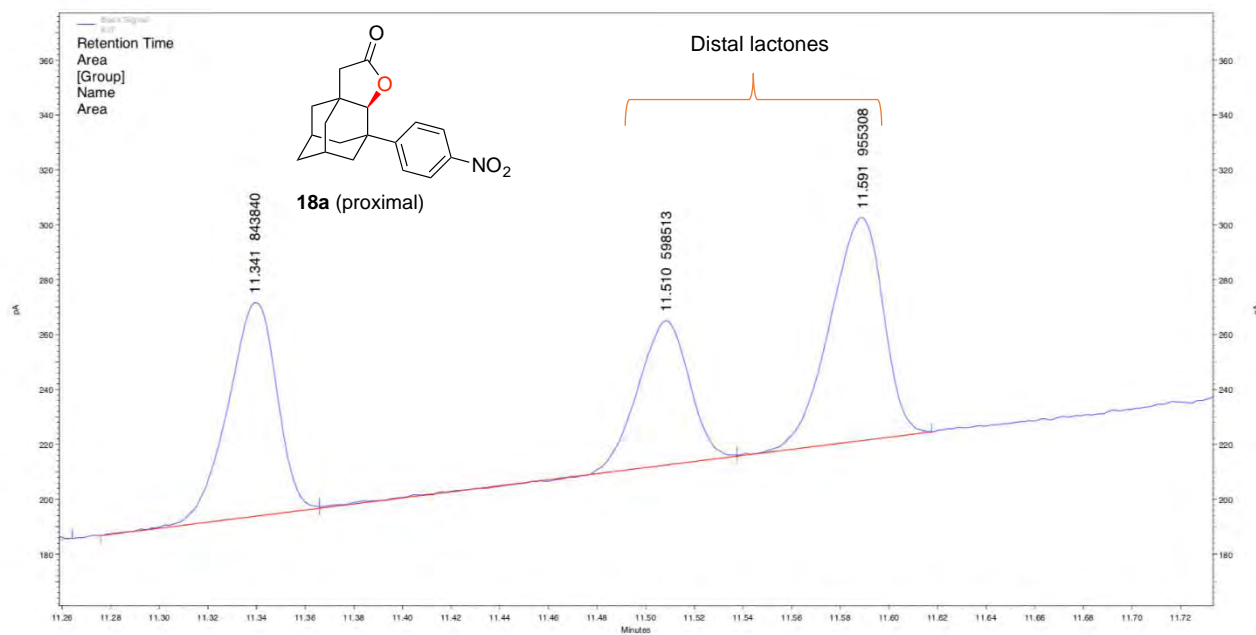


Oxidation of 18

(*S,S*)-Mn(pdp)

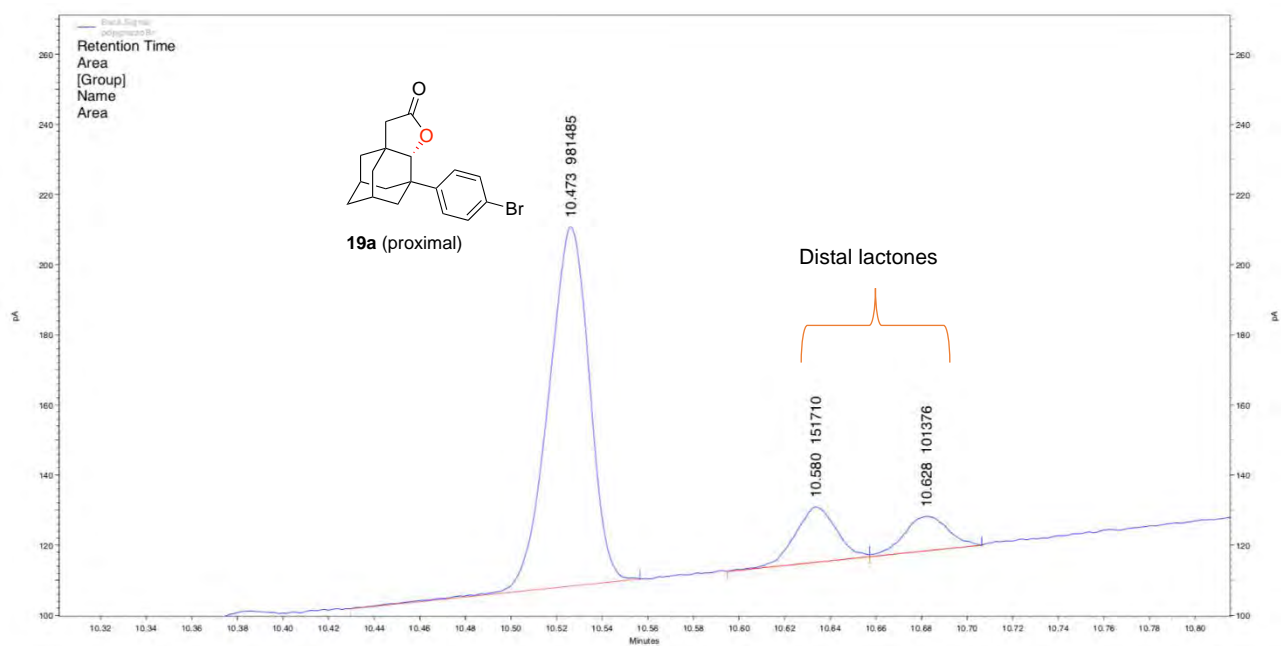


$(R,R)\text{-Mn}(\text{TIBS})\text{pdp}$

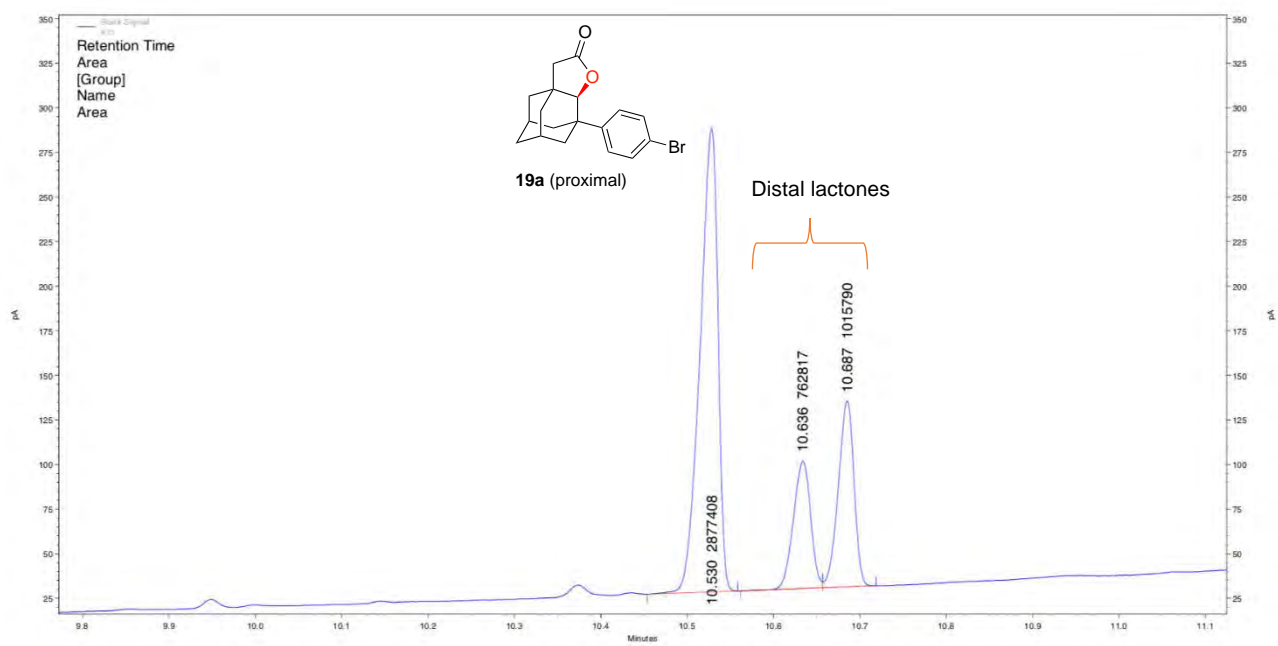


Oxidation of 19

$(S,S)\text{-Mn}(\text{pdp})$

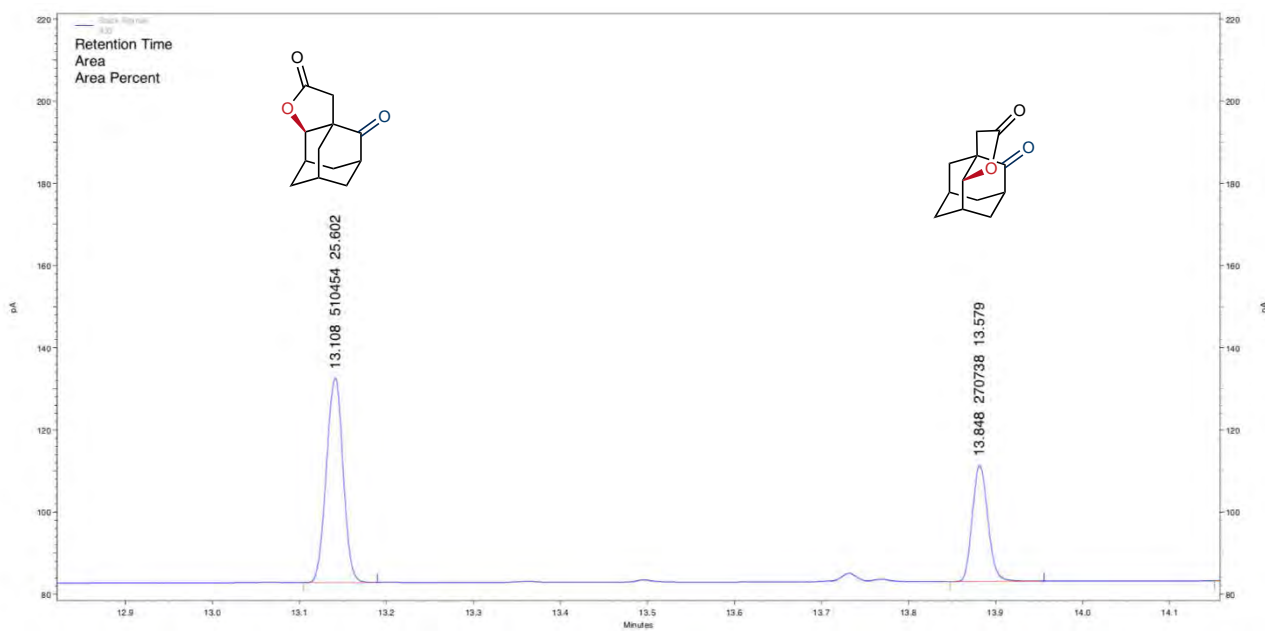


(R,R) -Mn(TIBSpdp)

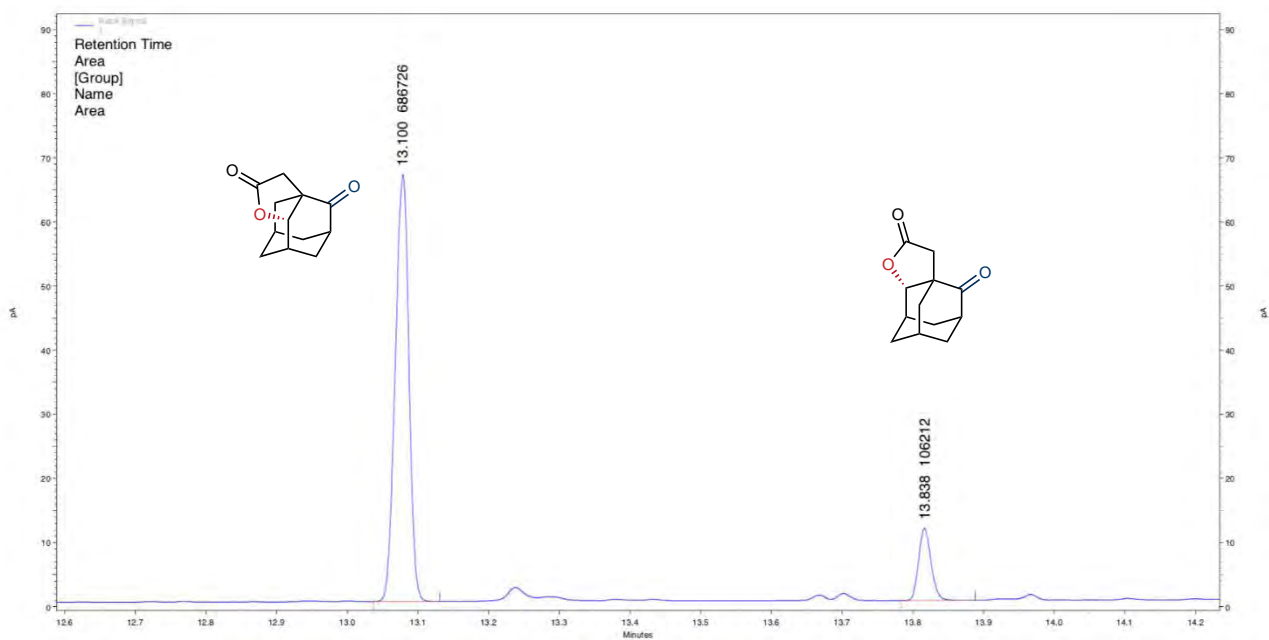


Oxidation of 20

(S,S) -Mn(pdp)



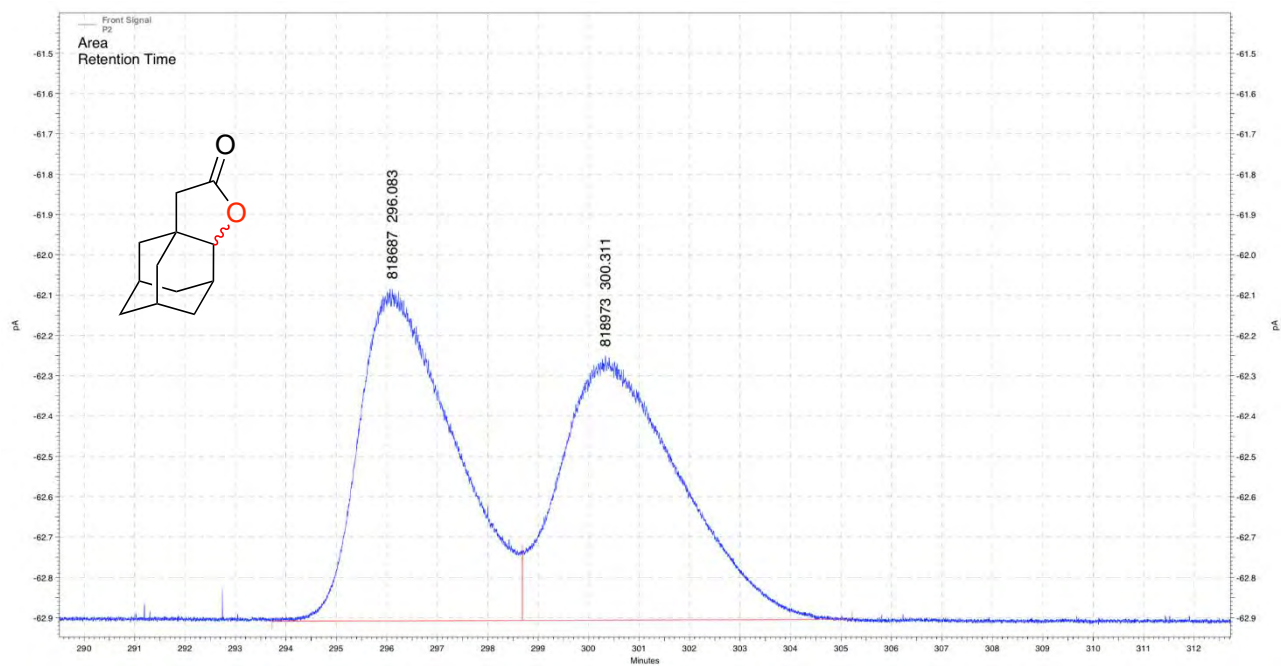
(*R,R*)-Mn(^{TIPS}pdp)



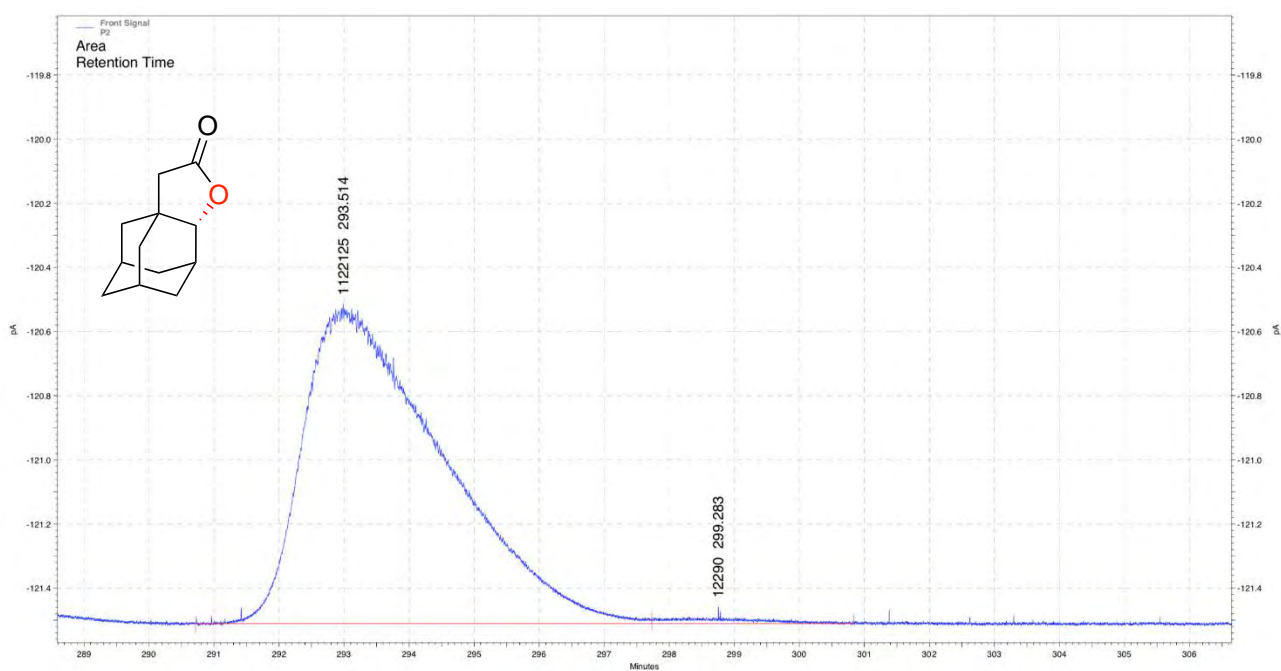
IV. GC and HPLC traces for the determination of the enantiomeric excesses

The racemic products were obtained by substrate oxidations with *rac*-Mn(^{TIPS}mcp) complex. In comparison between traces, the green trace is referred to the racemic product.

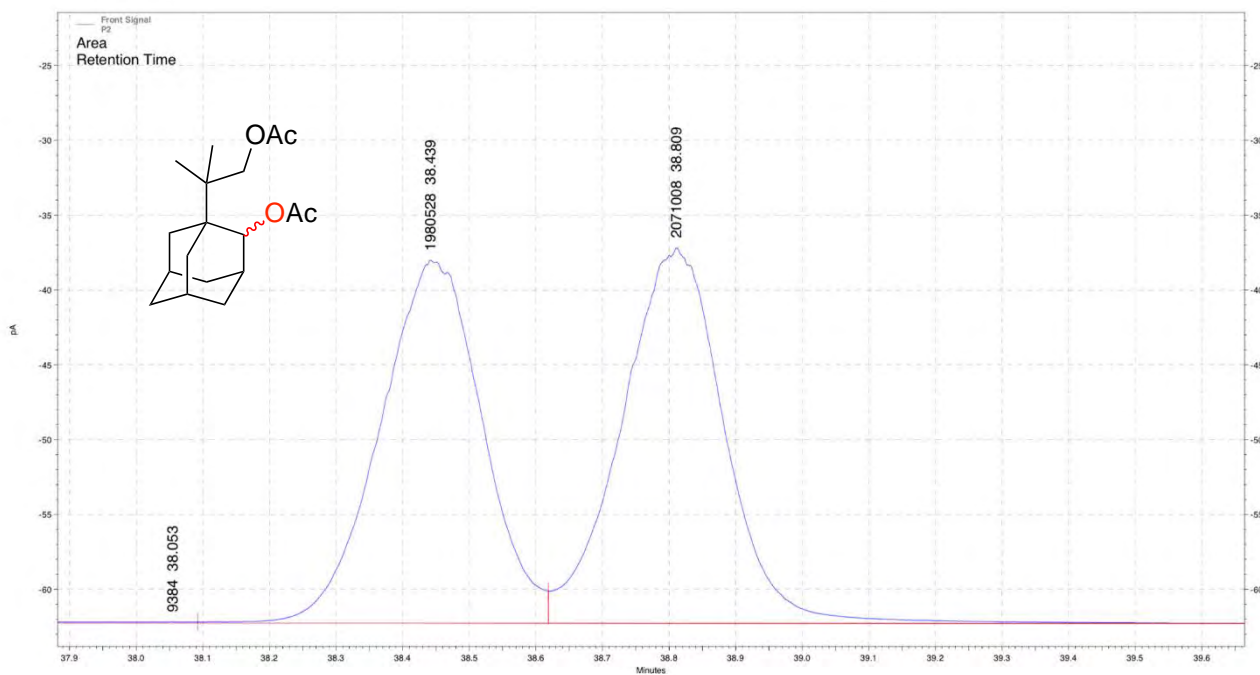
rac-1a



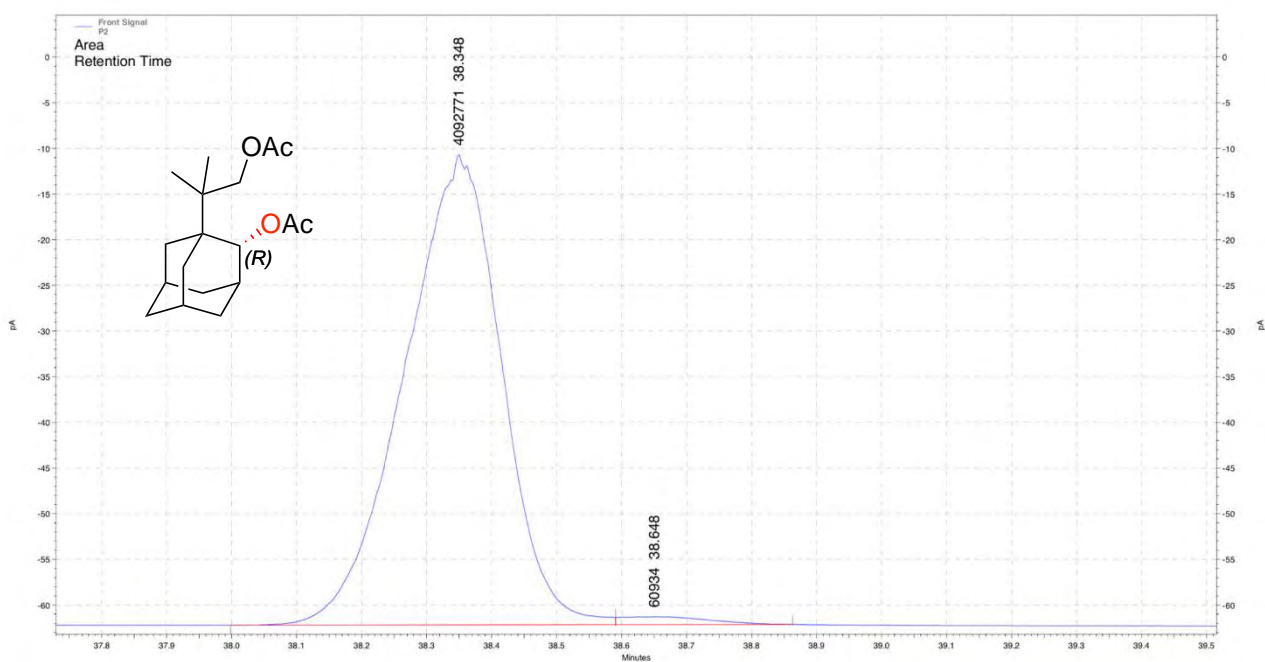
1a - (*S,S*)-Mn(^{Ti}BS₂pdp)



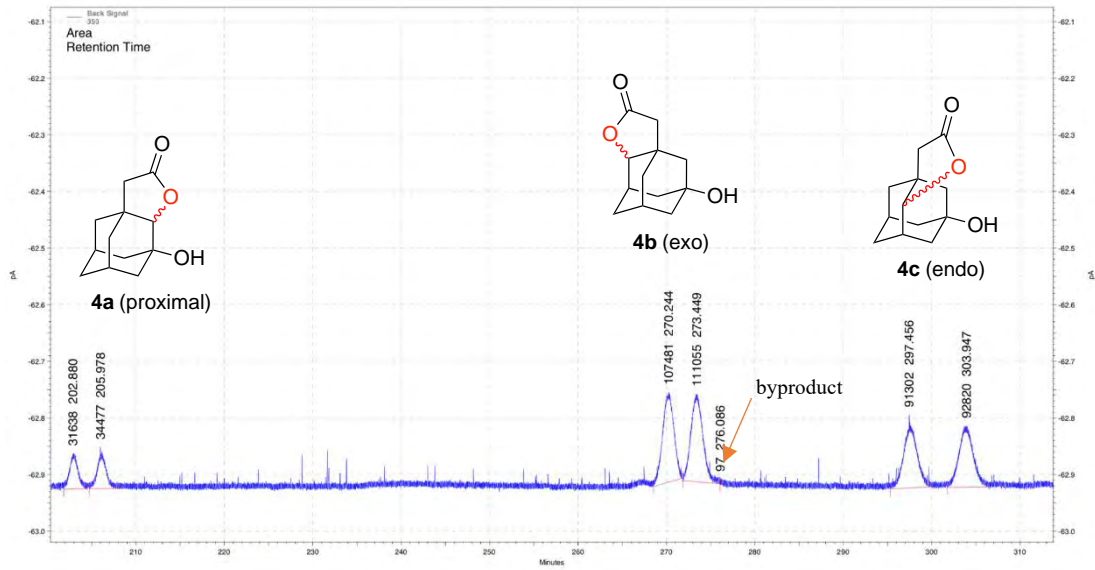
rac-2b (after derivatization)



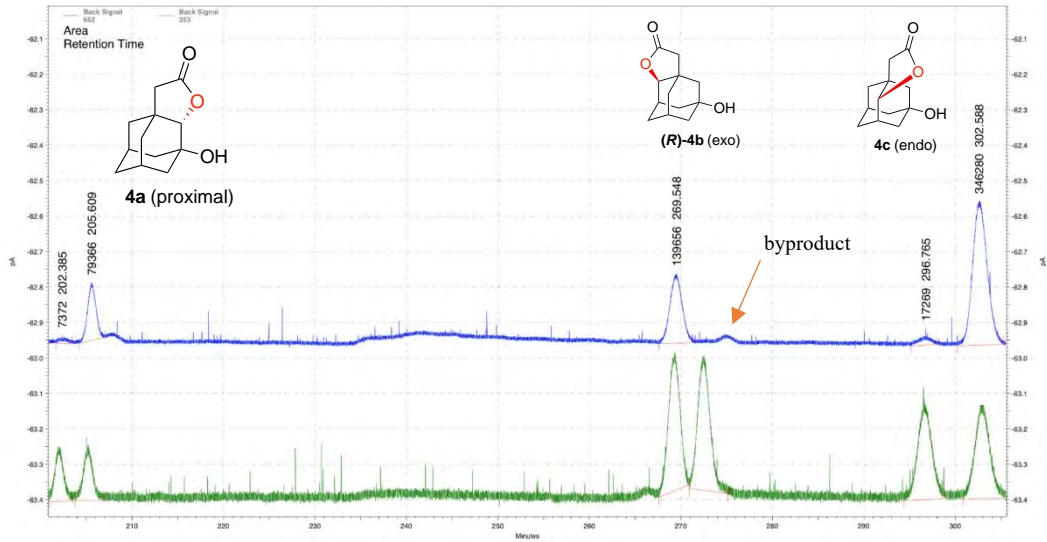
(R)-2b – obtained from oxidation of 2 catalyzed by (*S,S*)-Mn(^{Ti}BS₃pdp)



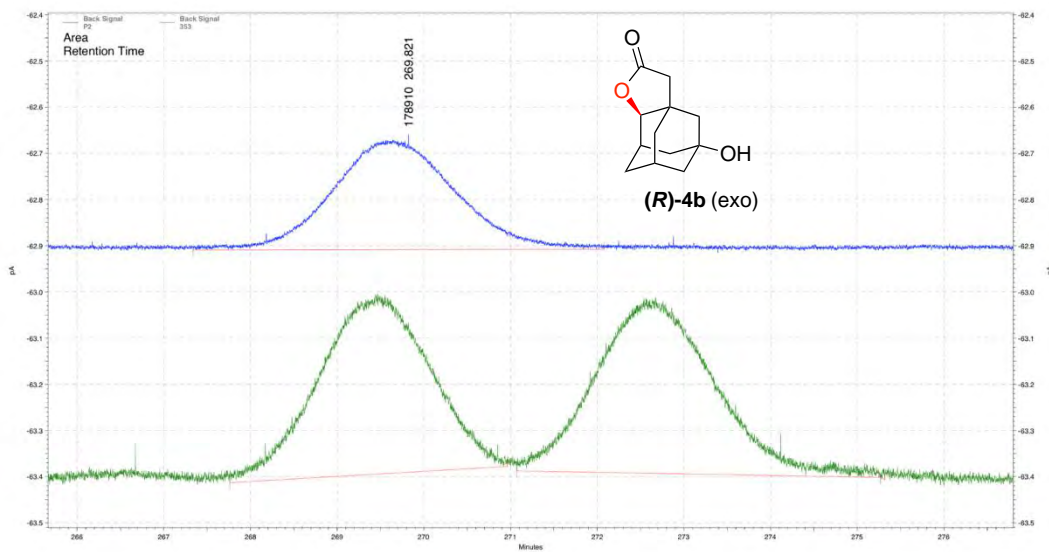
rac-4a/4b/4c



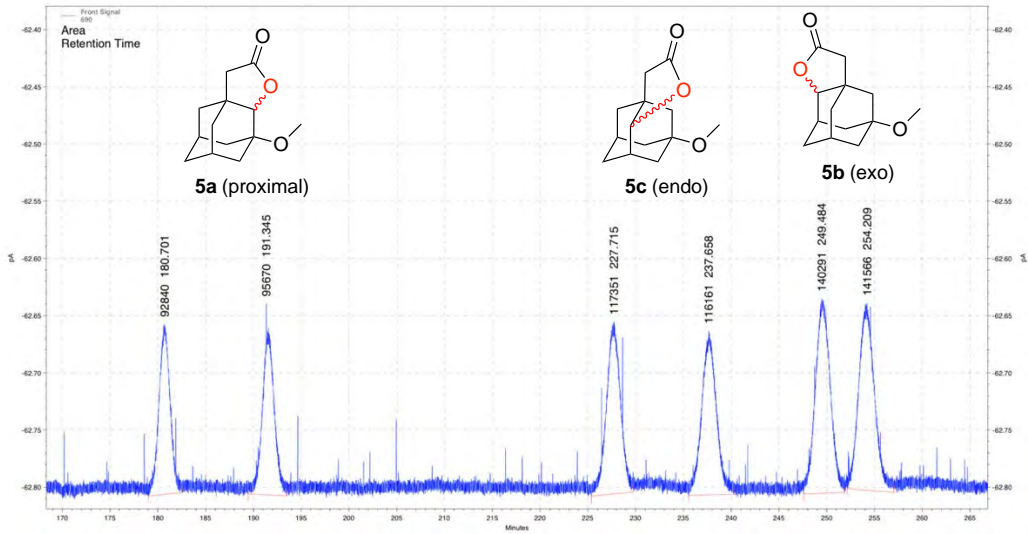
4a/4b/4c - (S,S)-Mn(pdp)



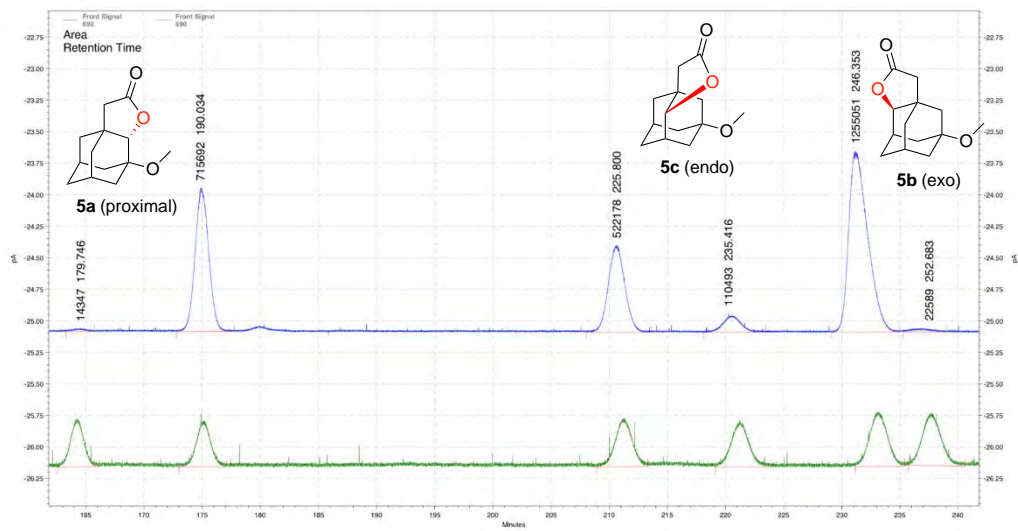
(R)-4b - (S,S)-Mn(TIBS)pdp



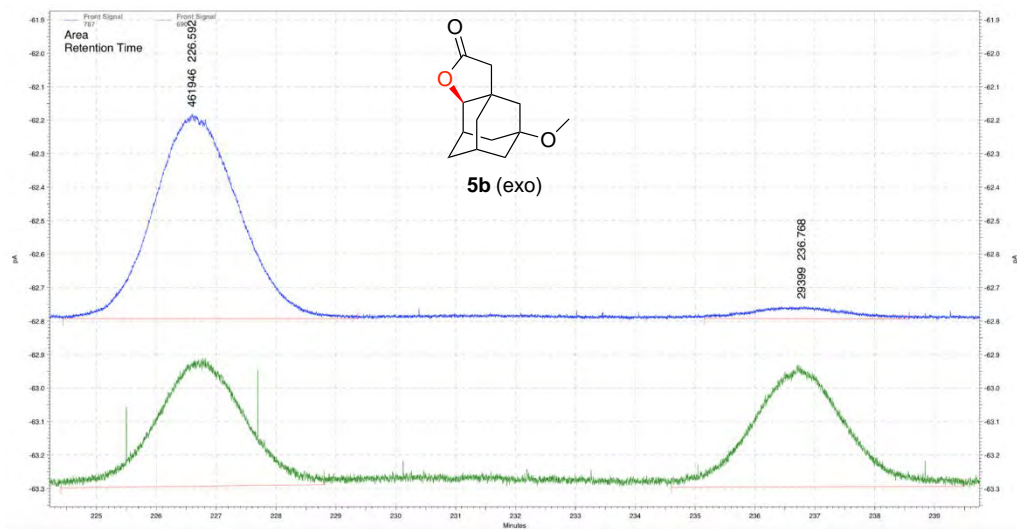
rac-5a/5b/5c



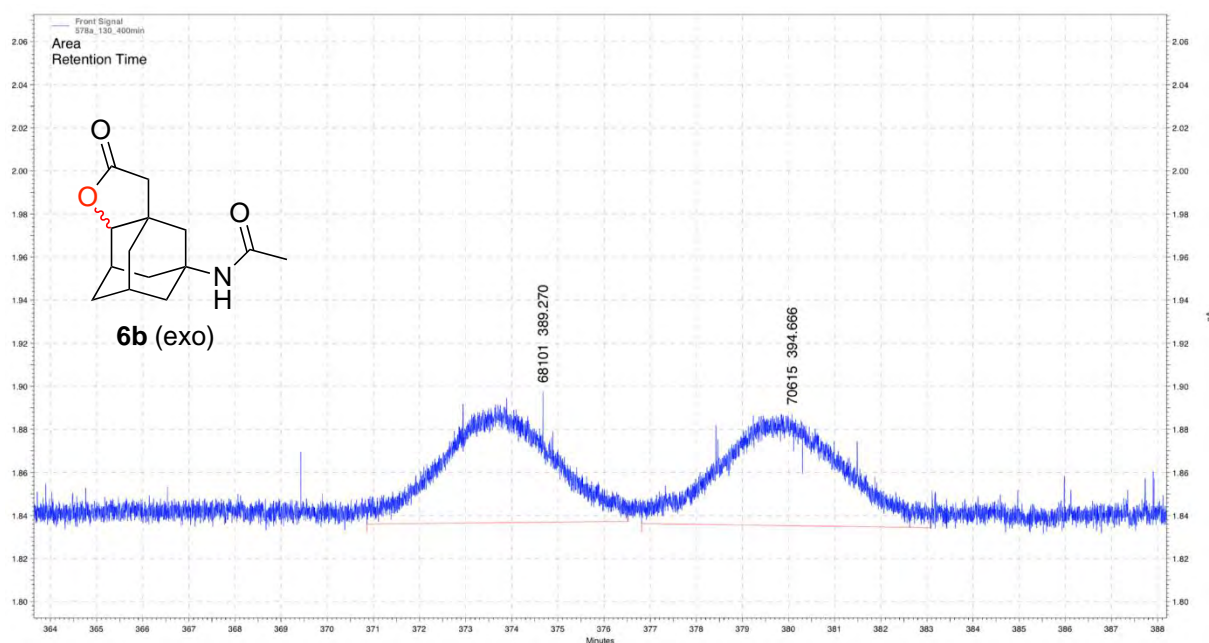
5a/5b/5c - (S,S)-Mn(TIBS₃pdp)



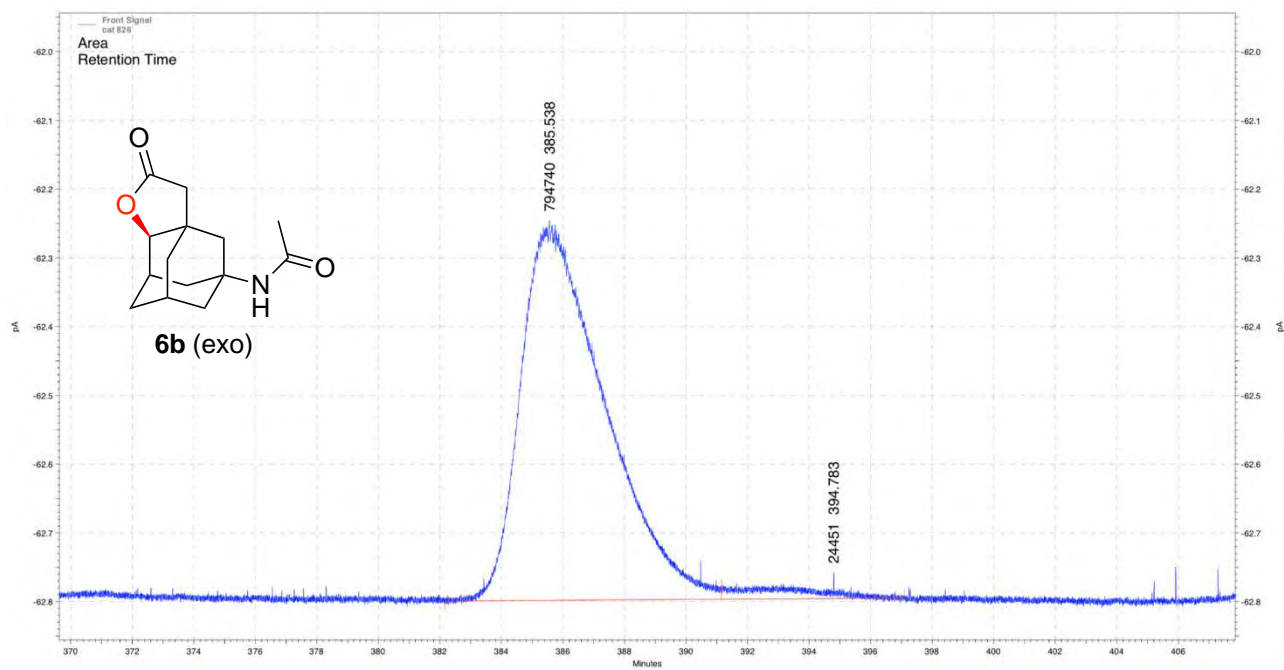
5b - (S,S)-Mn(pdp)



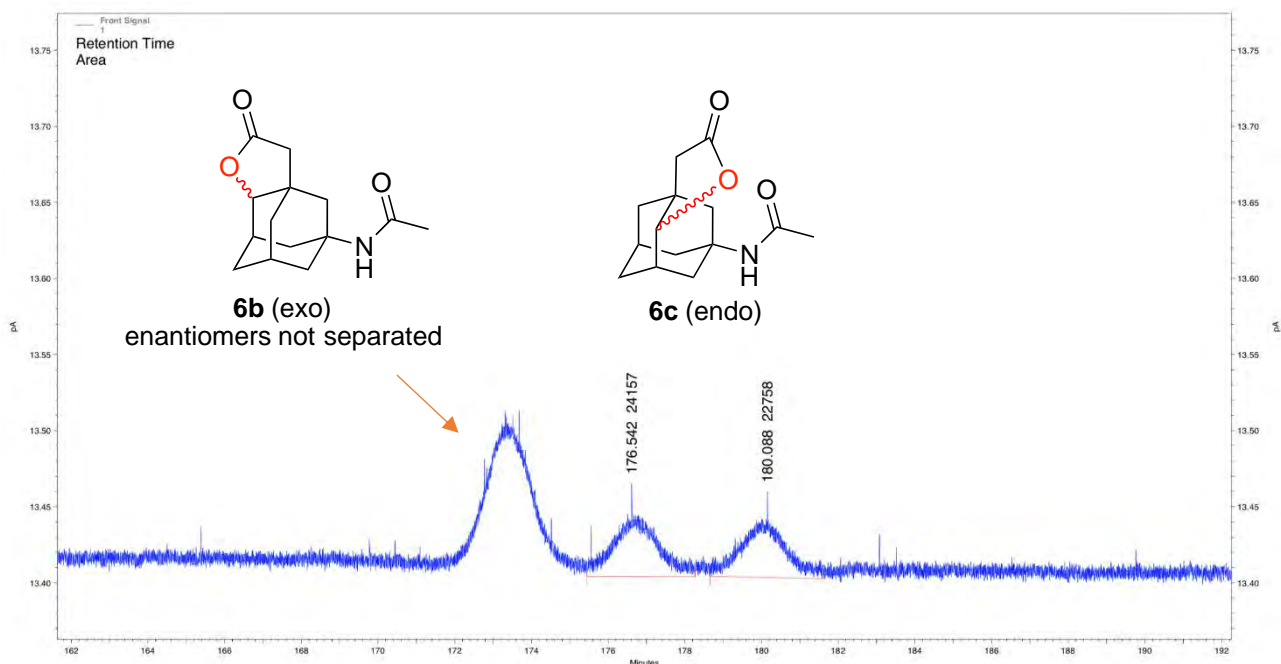
rac-6b



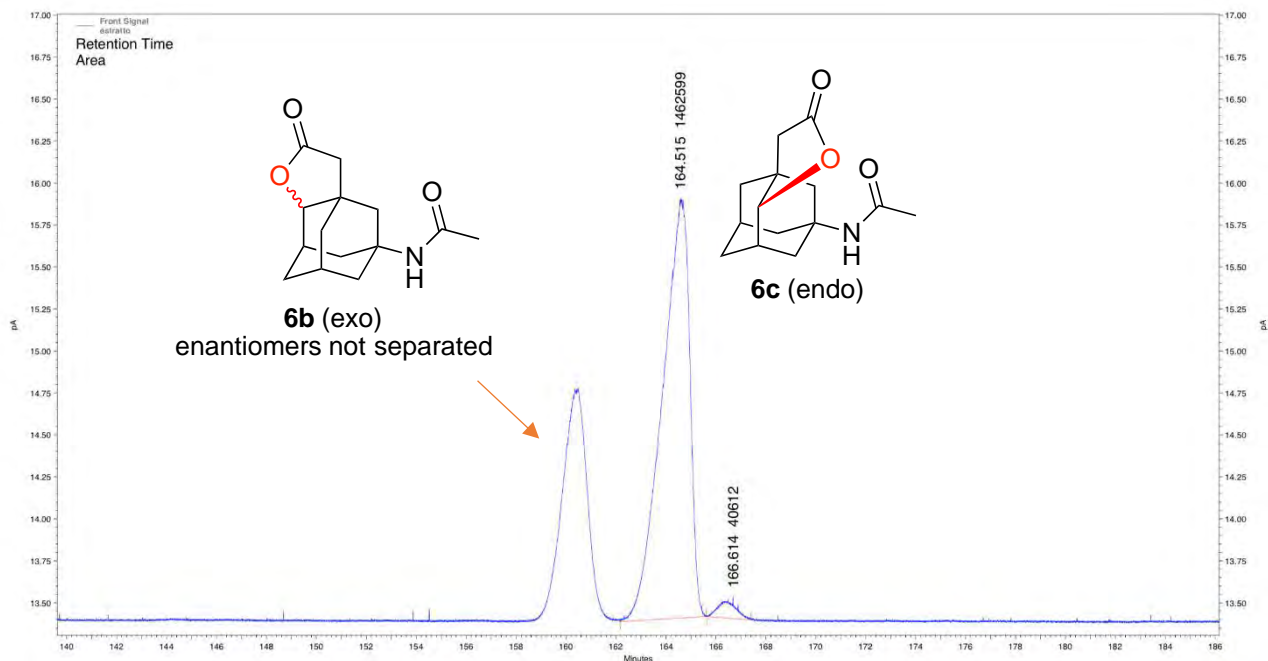
6b - (S,S)-Mn(TIBS_pd_p)



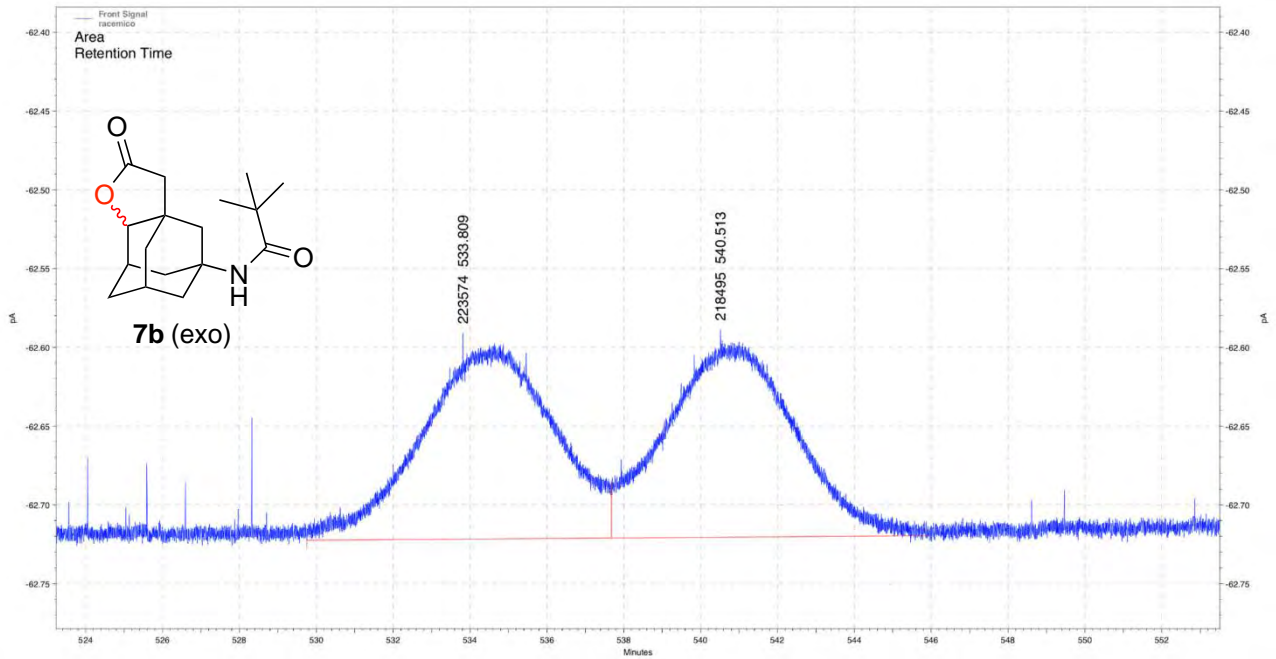
rac-6c



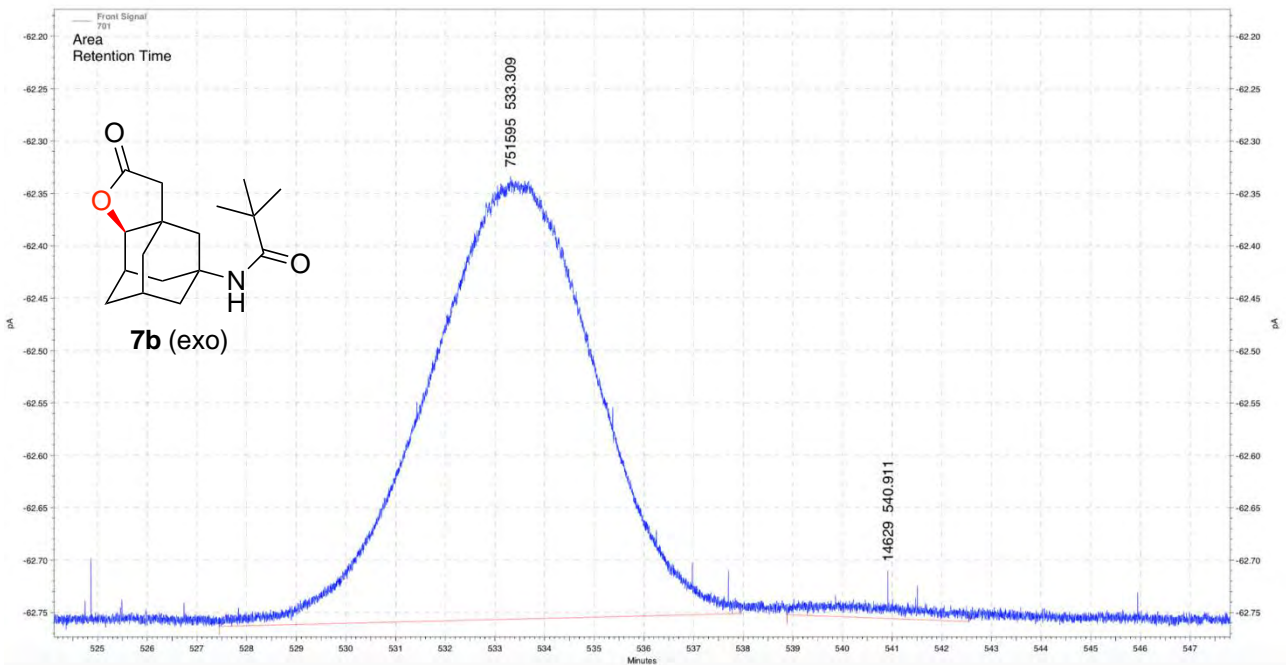
6c - (S,S)-Mn(pdp)



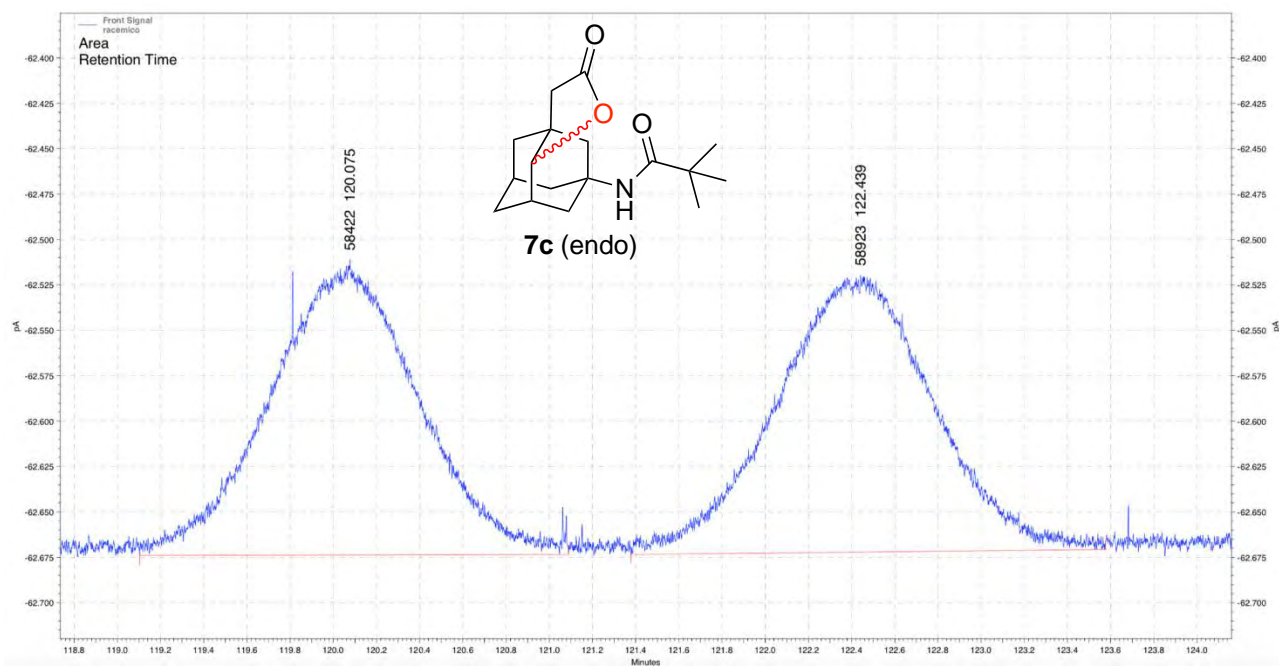
rac-7 b



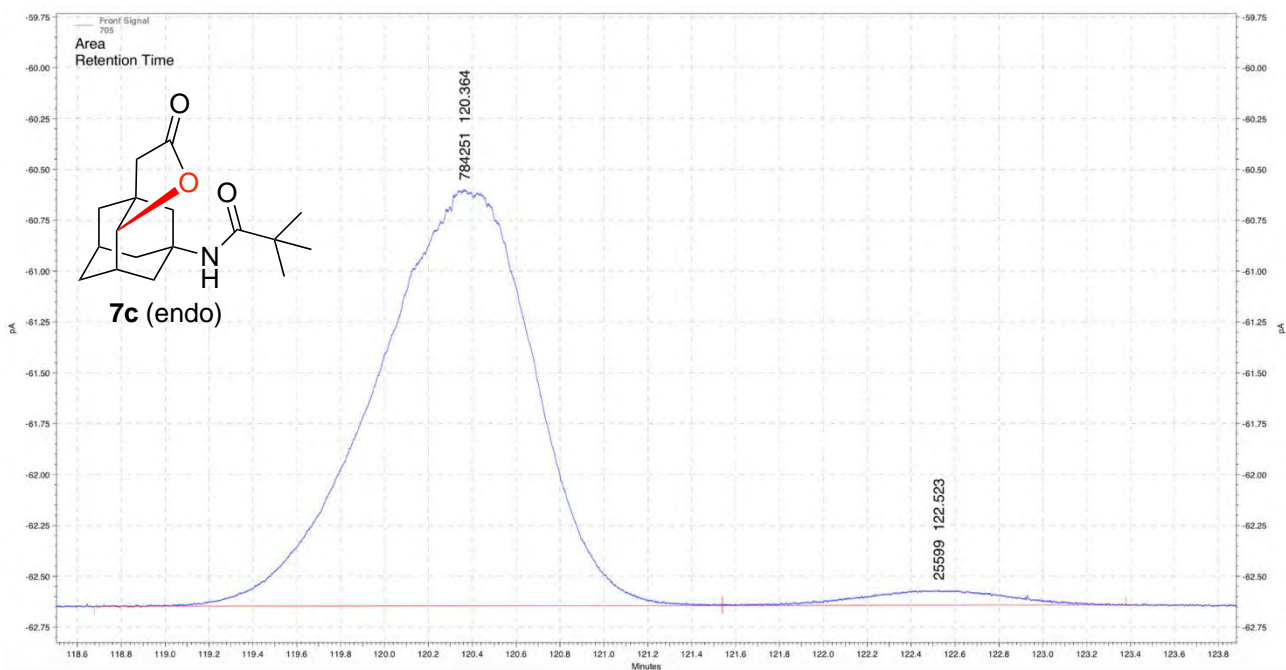
7b - (S,S)-Mn(TIBS₃pdp)



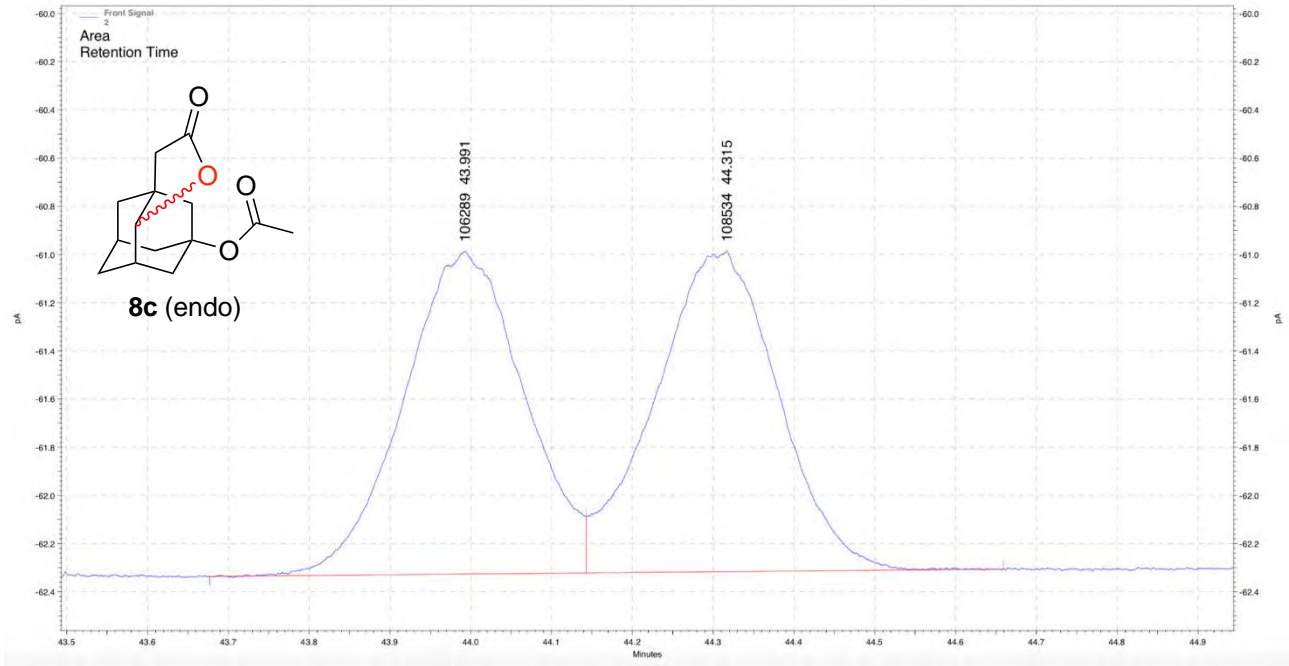
rac-7c



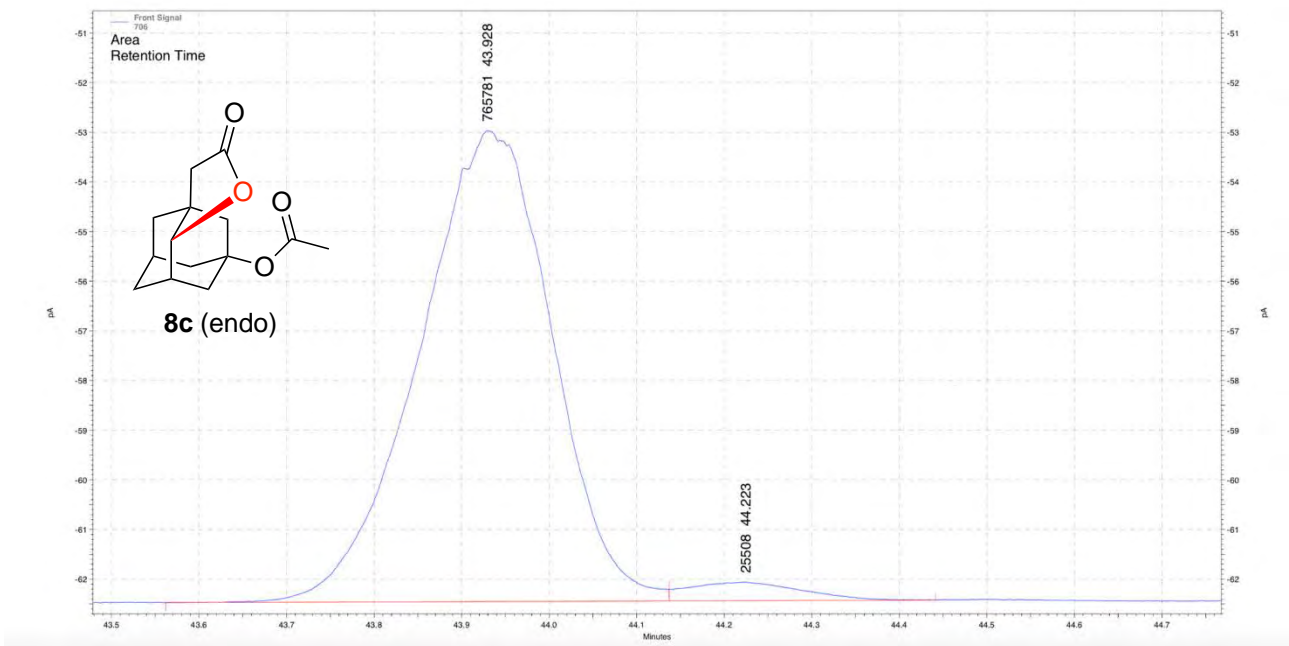
7c - (S,S)-Mn(pdp)



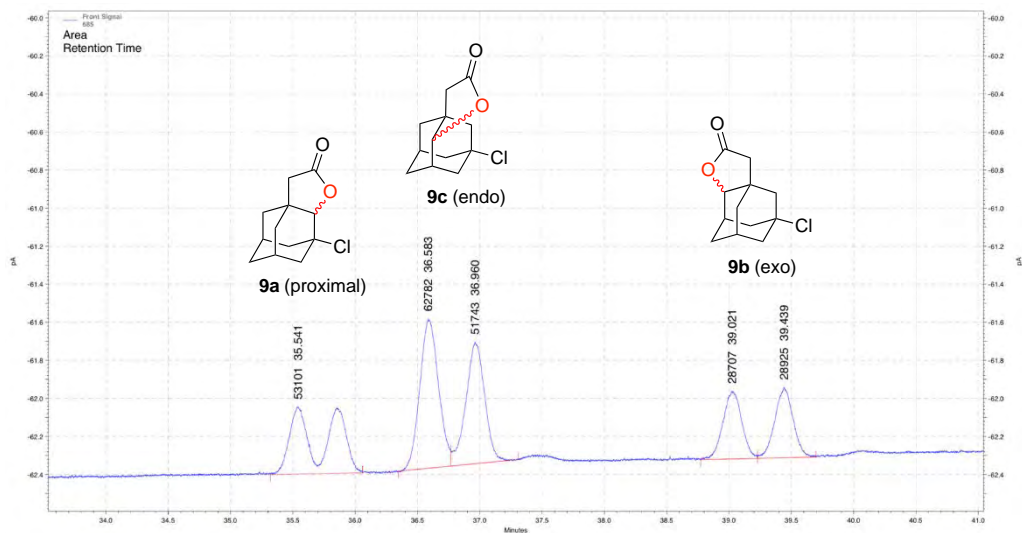
rac-8



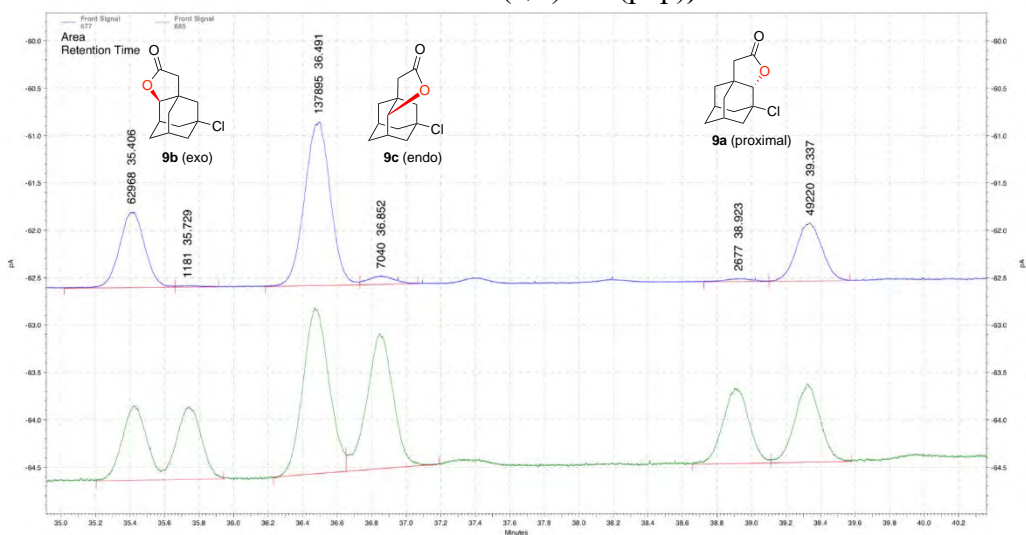
8c - (S,S)-Mn(pdp)



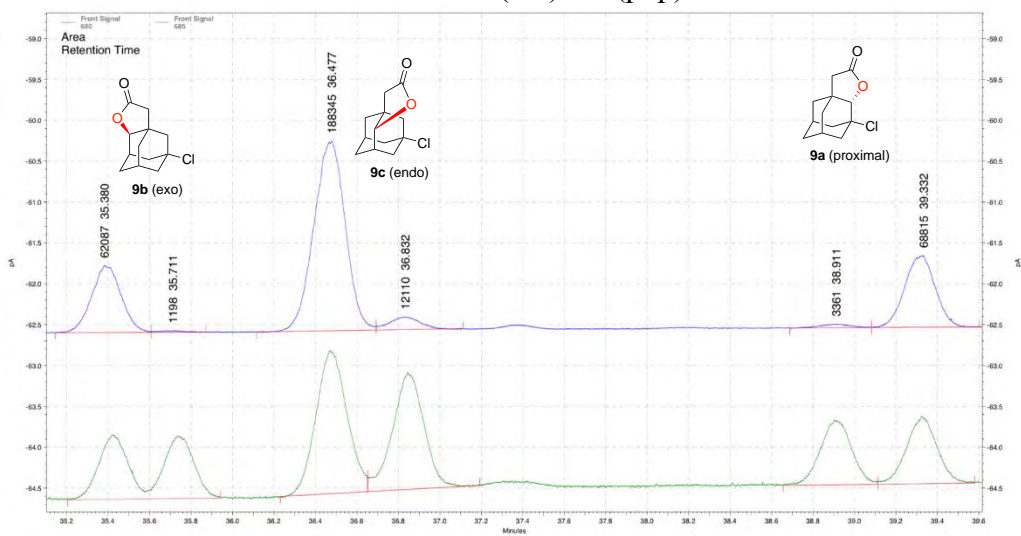
rac-9a/9b/9c



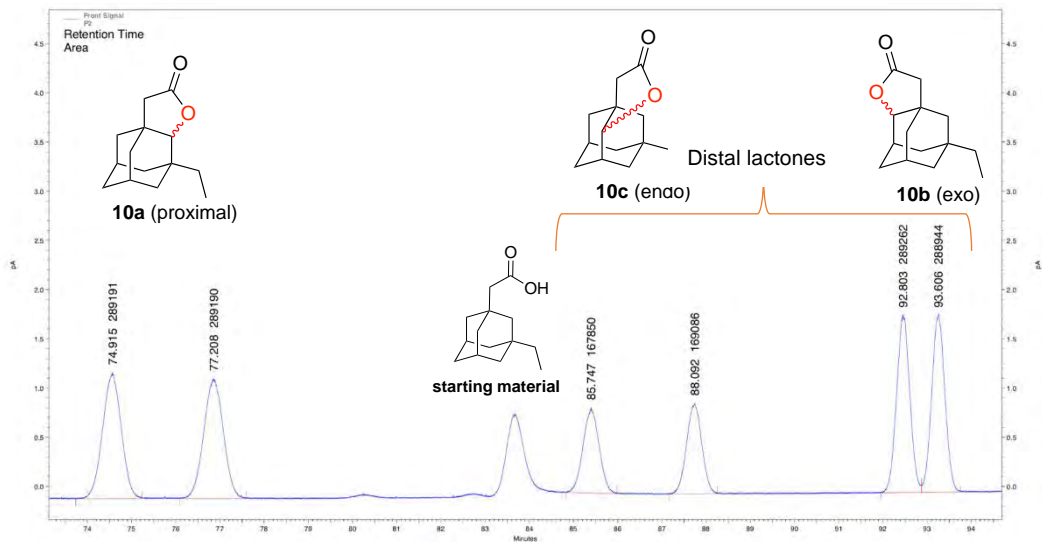
9a/9b/9c - (S,S)-Mn(pdp)



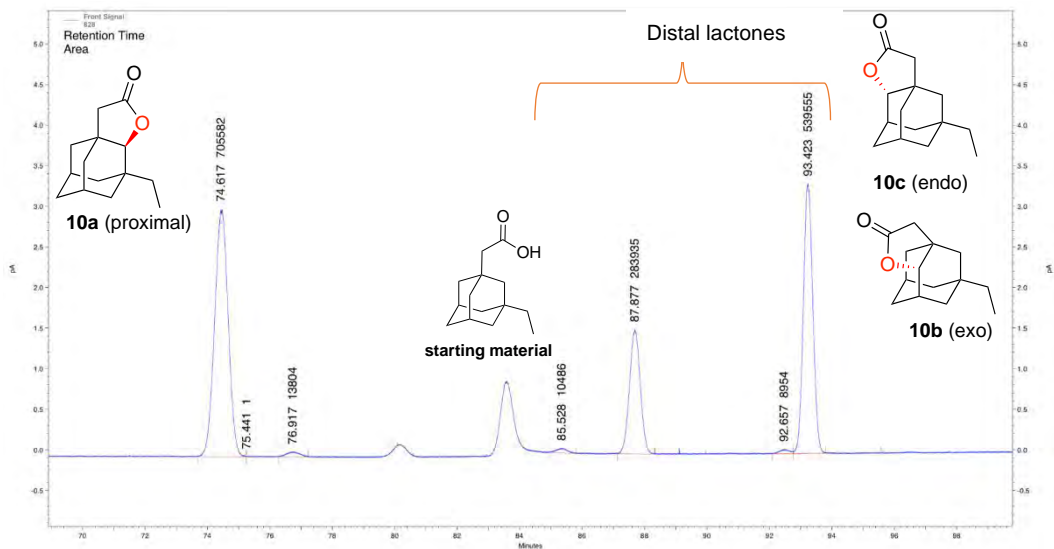
9a/9b/9c - (S,S)-Mn(pdp)



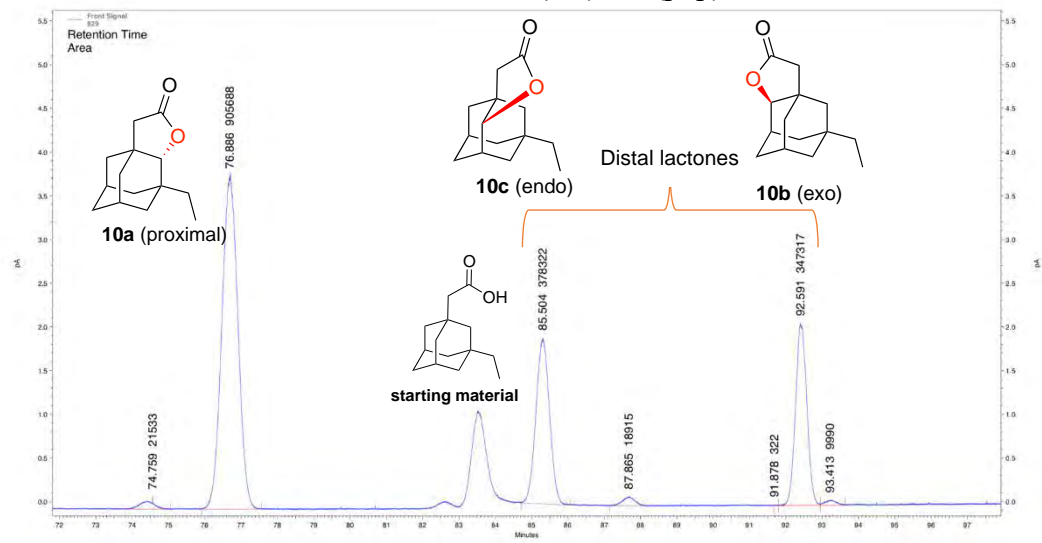
rac-10a/10b/10c



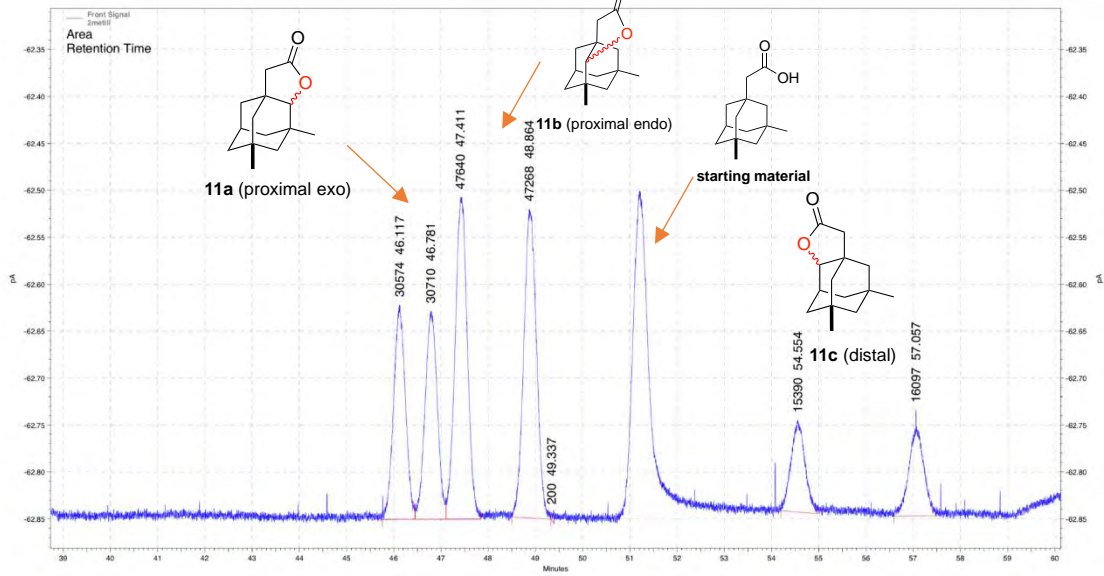
10a/10b/10c - (R,R) -Mn(TIBS)pdp



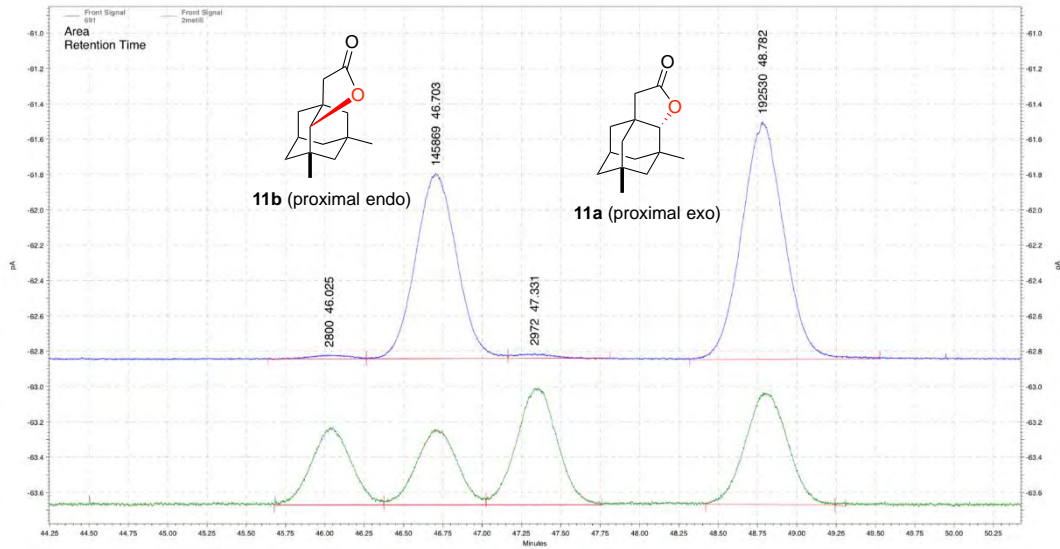
10a/10b/10c - (S,S) -Mn(pdp)



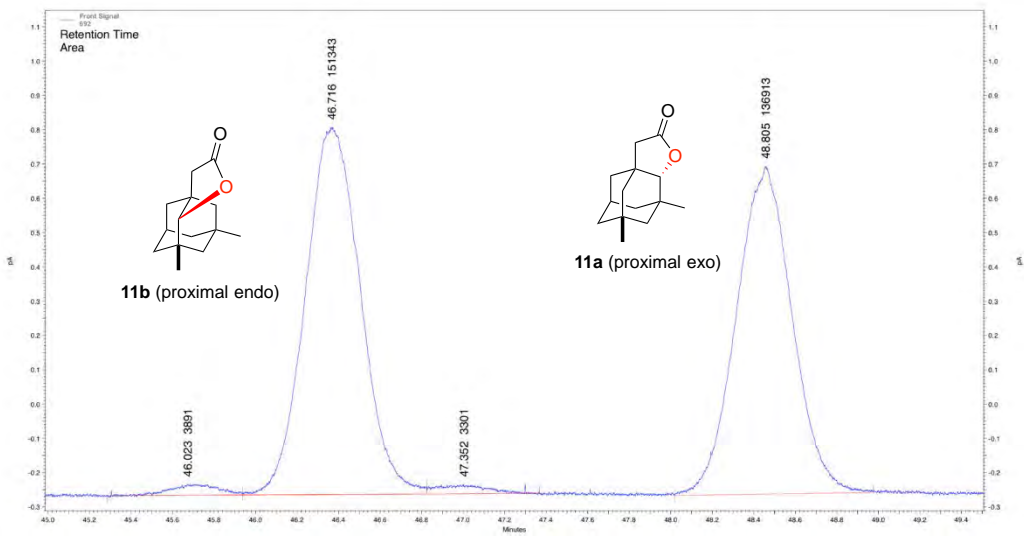
rac-11a/11b/11c



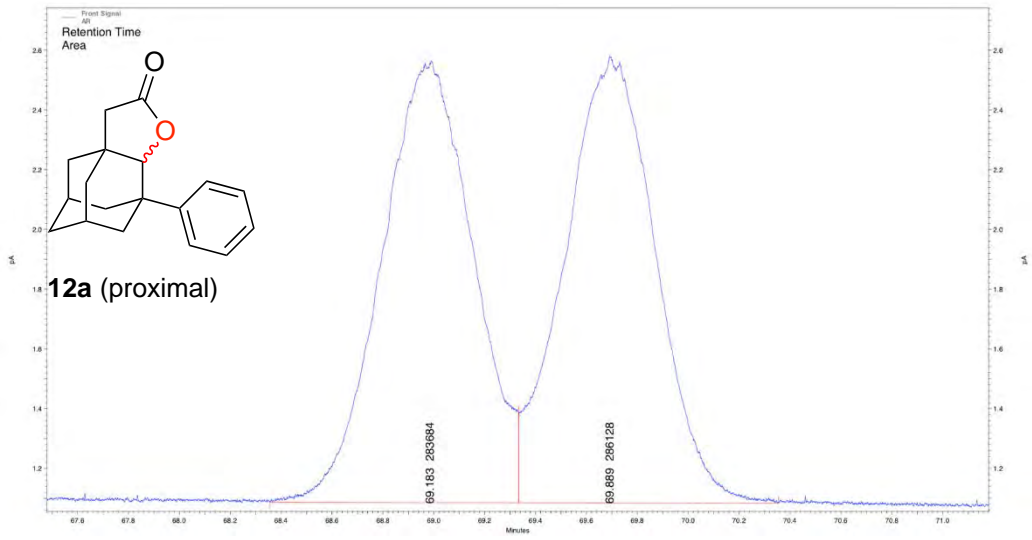
11a/11b - (S,S)-Mn(TIBS)pdp



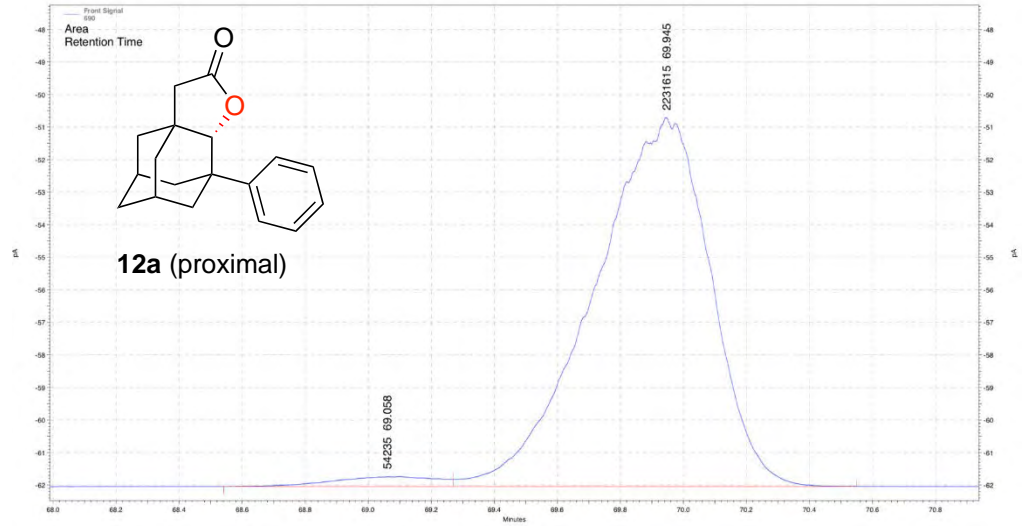
11a/11b - (S,S)-Mn(pdp)



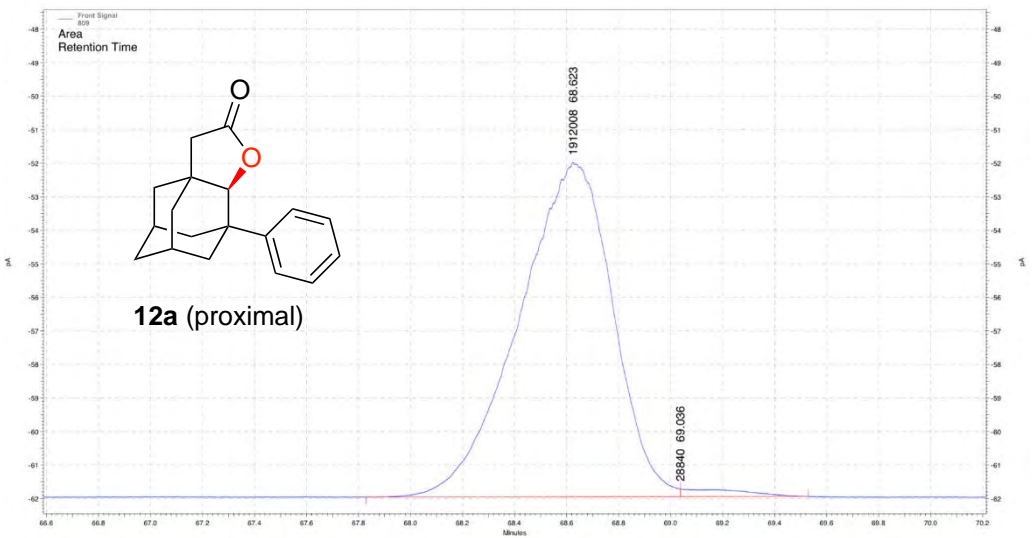
rac-12a



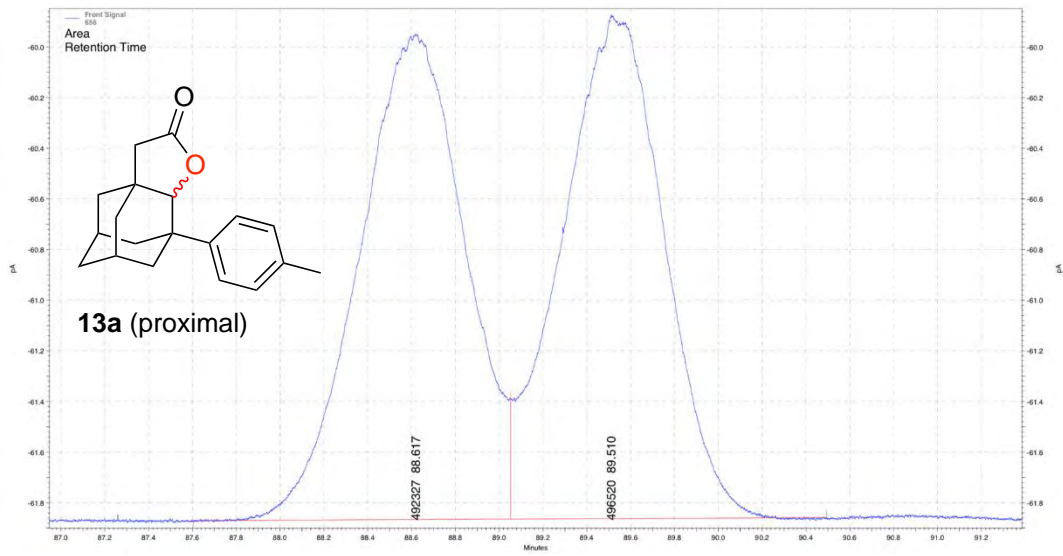
12a - (S,S)-Mn(pdp)



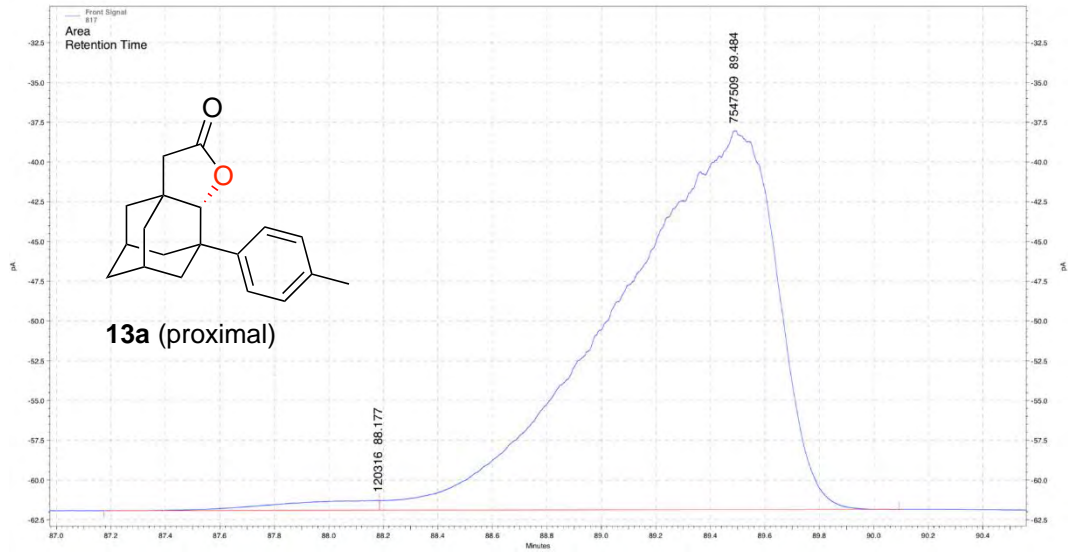
12a - (R,R)-Mn(TIBS₃pdp)



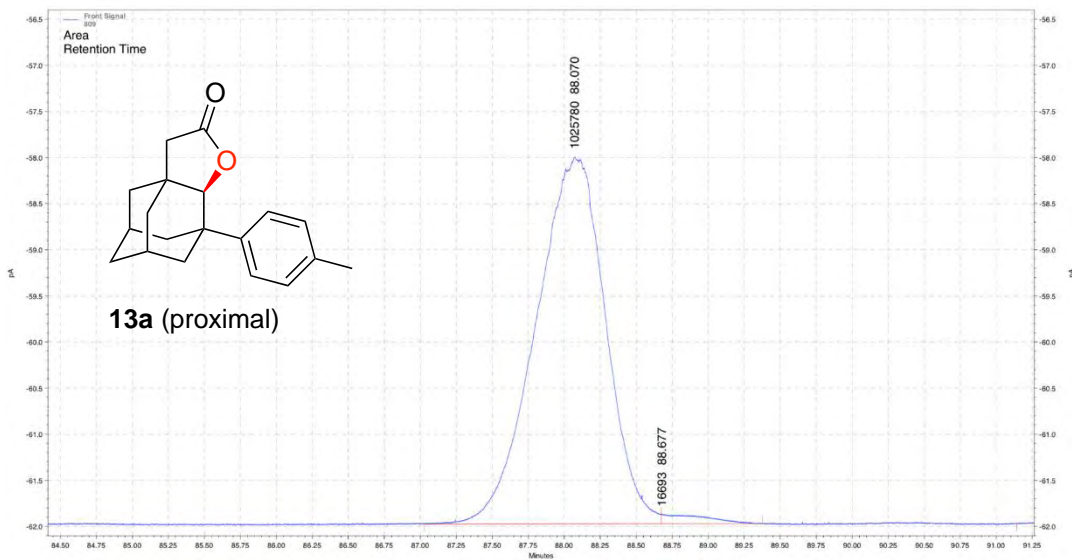
rac-13a



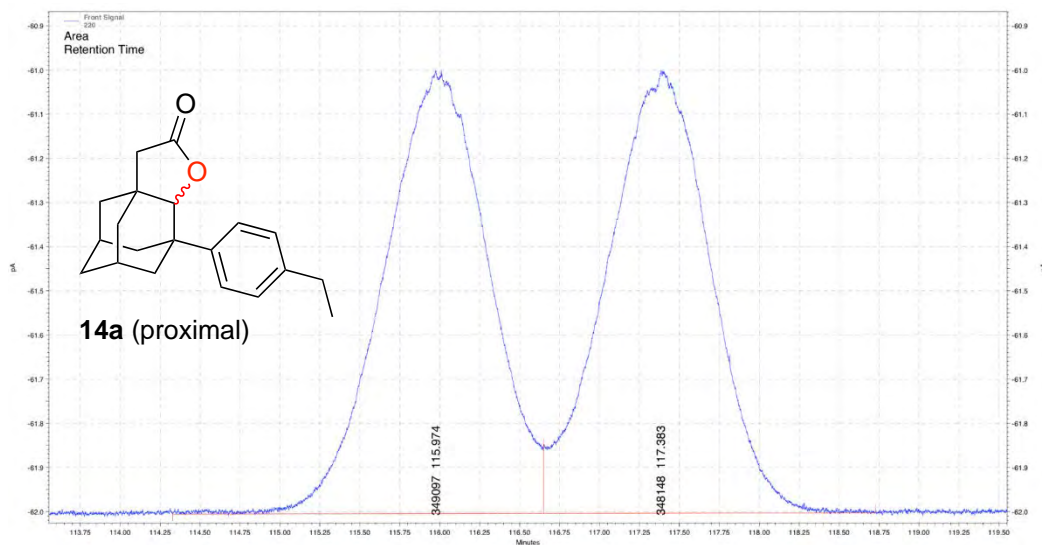
13a - (S,S)-Mn(pdp)



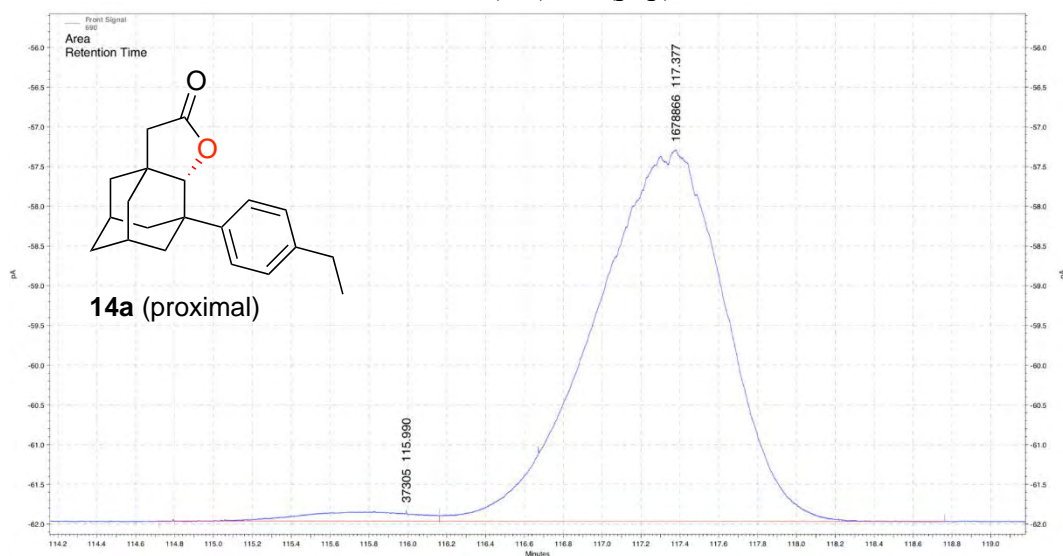
13a - (R,R)-Mn(TIBS₃pdp)



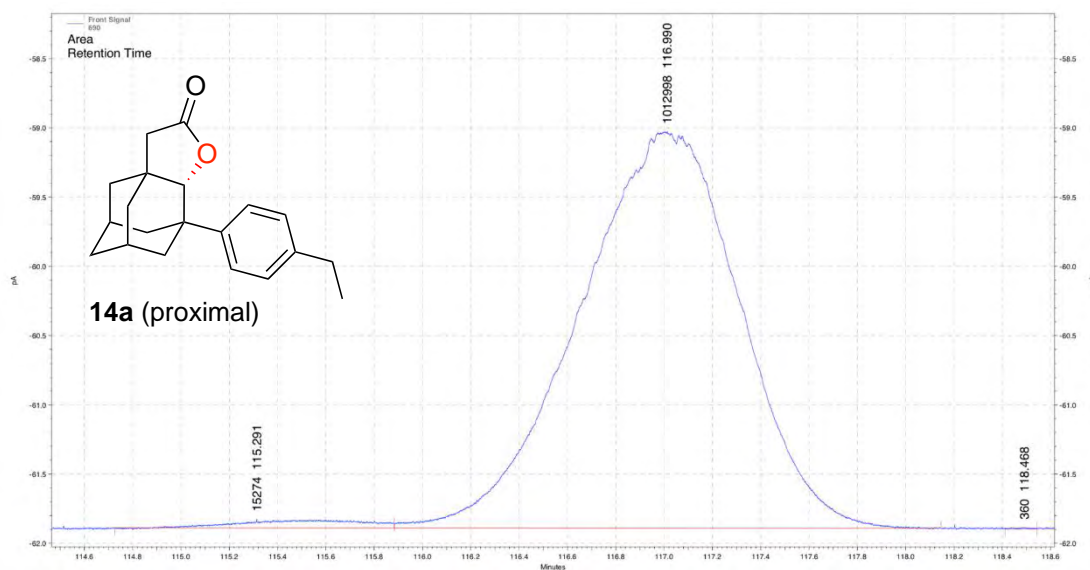
rac-14a



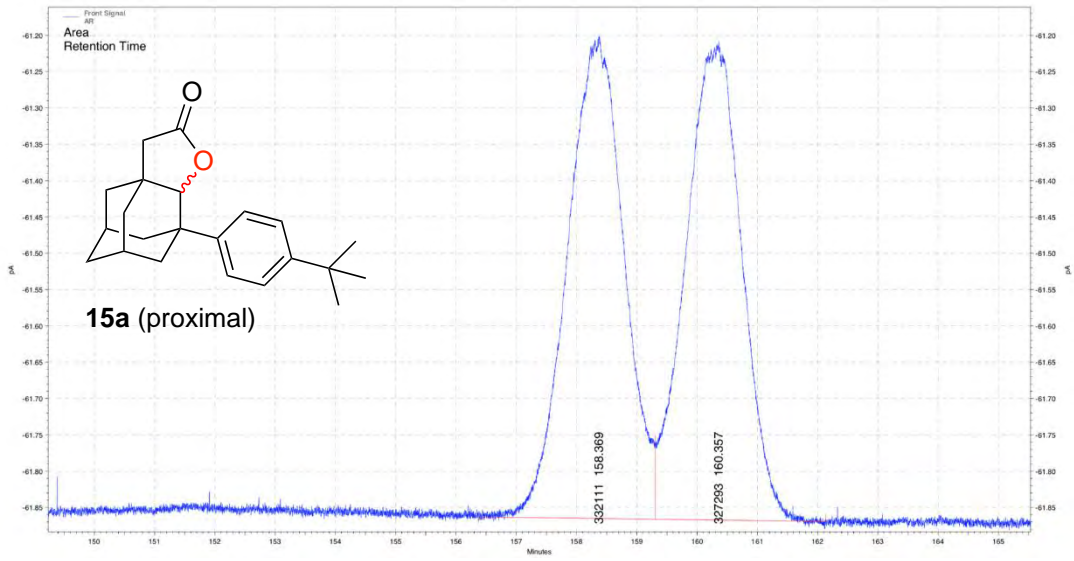
14a - (S,S)-Mn(pdp)



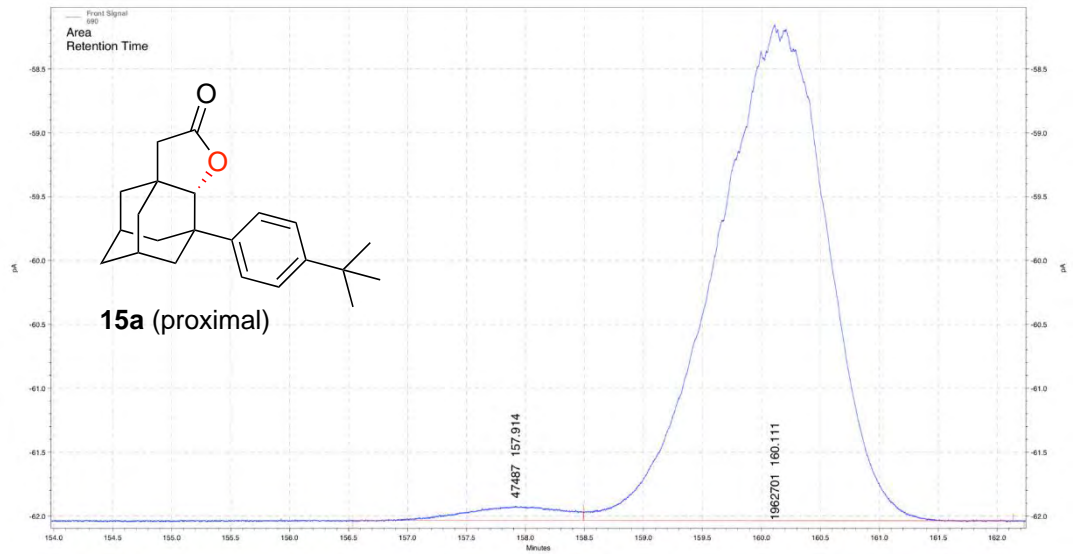
14a - (S,S)-Mn(^tIBSpdp)



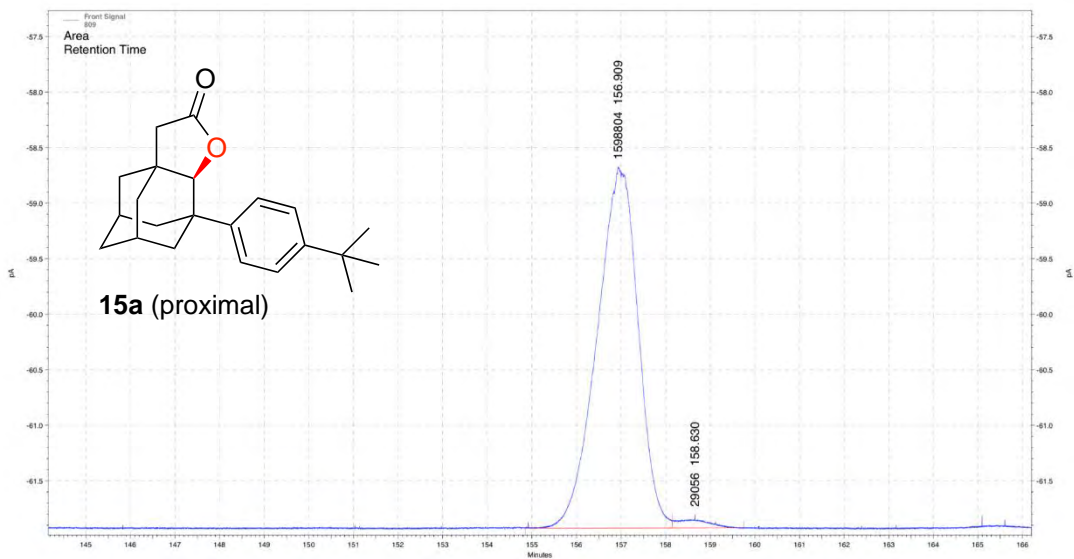
rac-15a



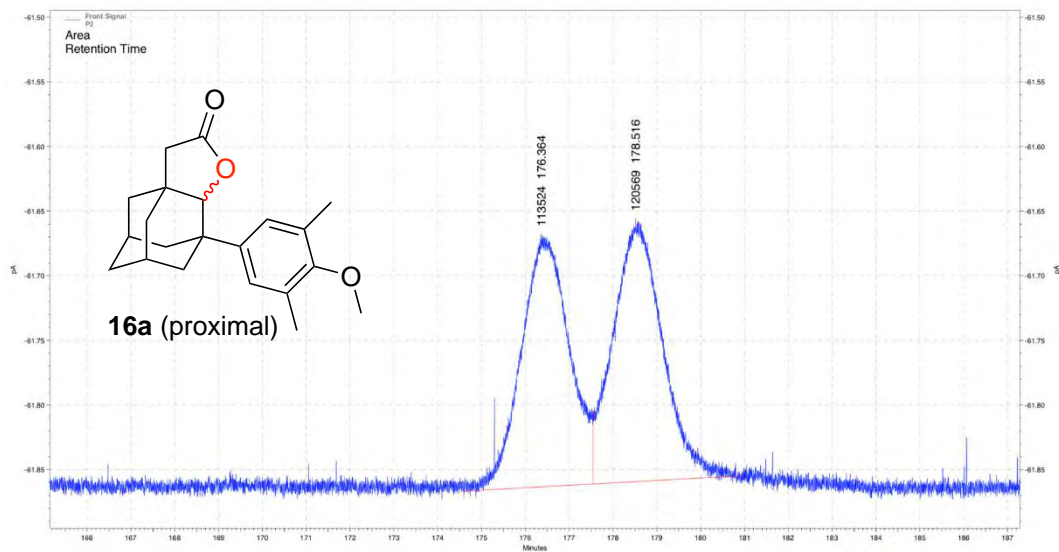
15a - (S,S)-Mn(pdp)



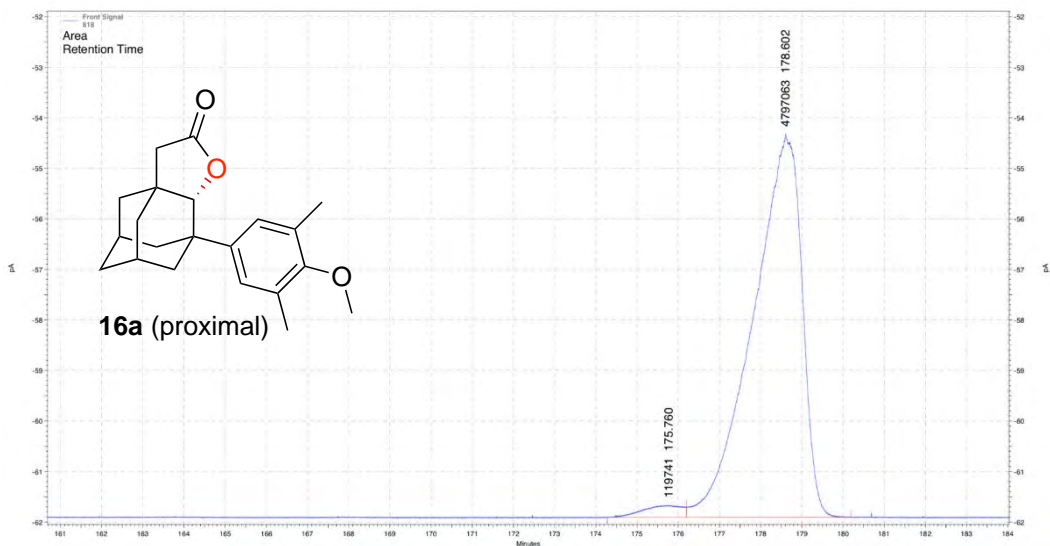
15a - (R,R)-Mn(TIBS_ppdp)



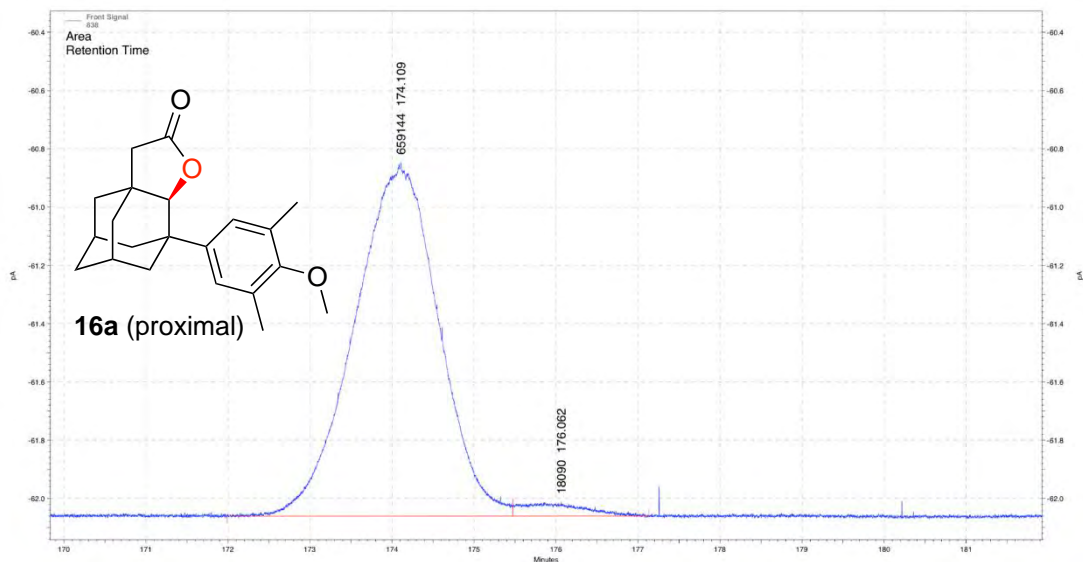
rac-16a



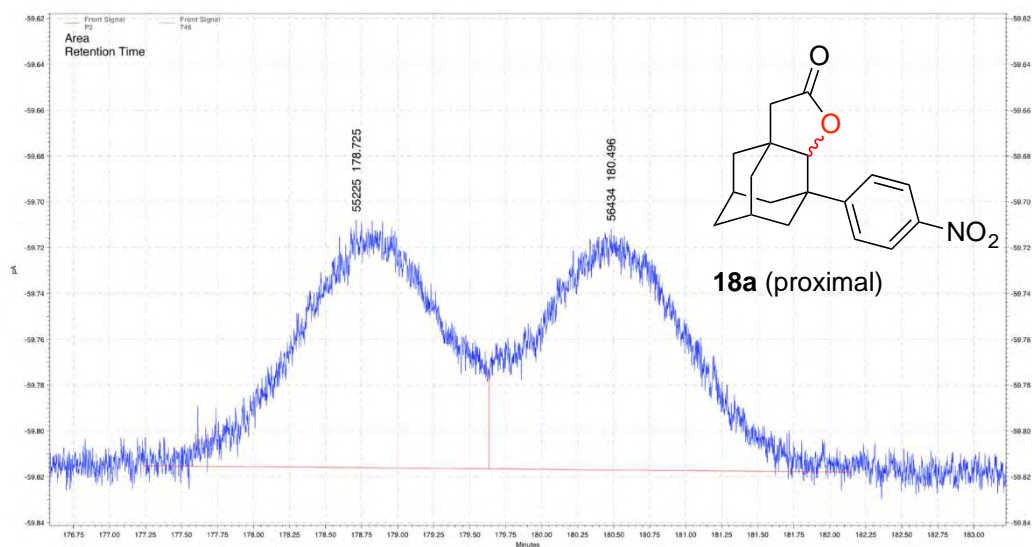
16a - (S,S)-Mn(pdp)



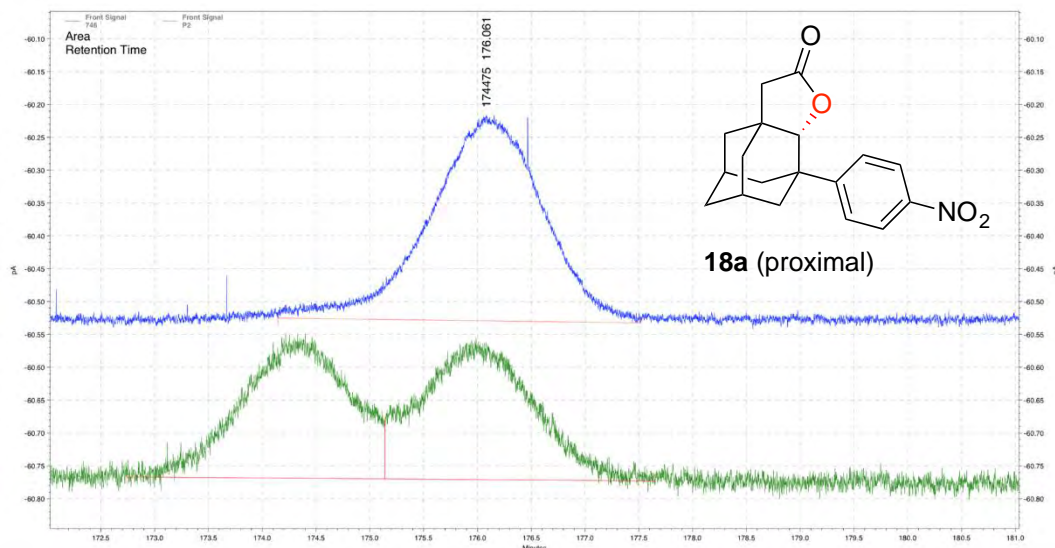
16a - (R,R)-Mn(TIBS₃pdp)



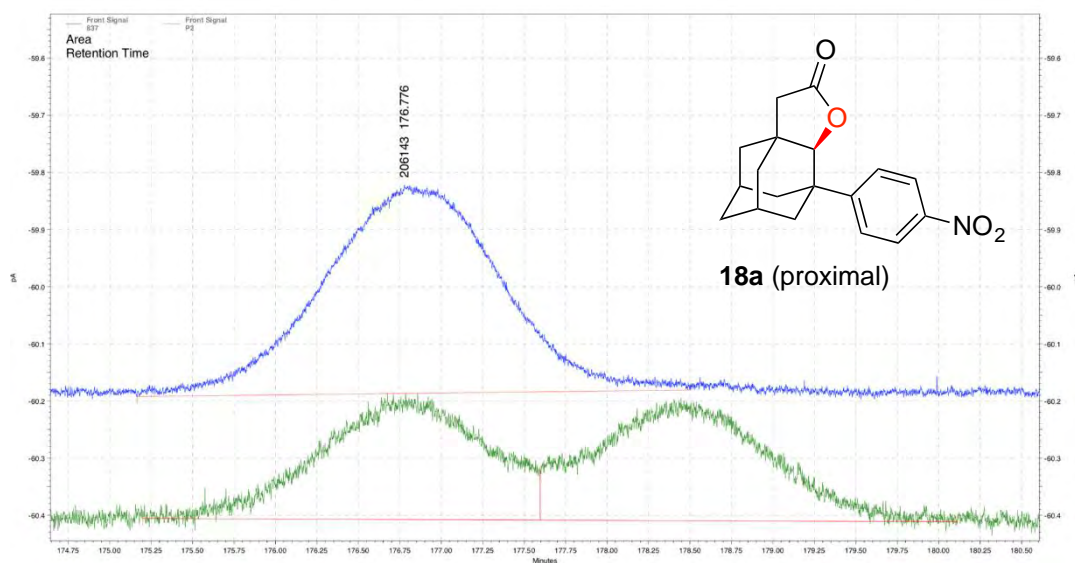
rac-18a



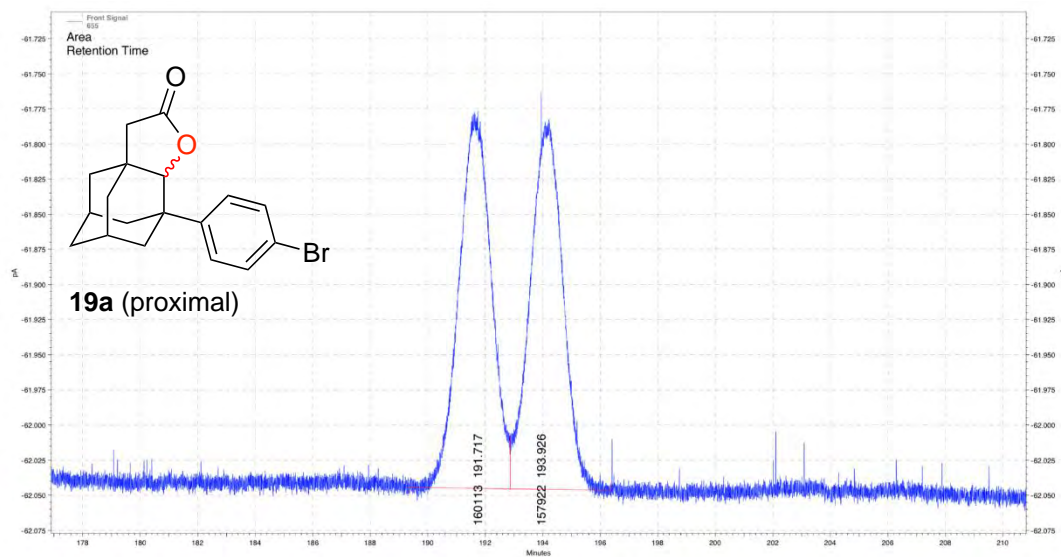
18a - (S,S)-Mn(pdp)



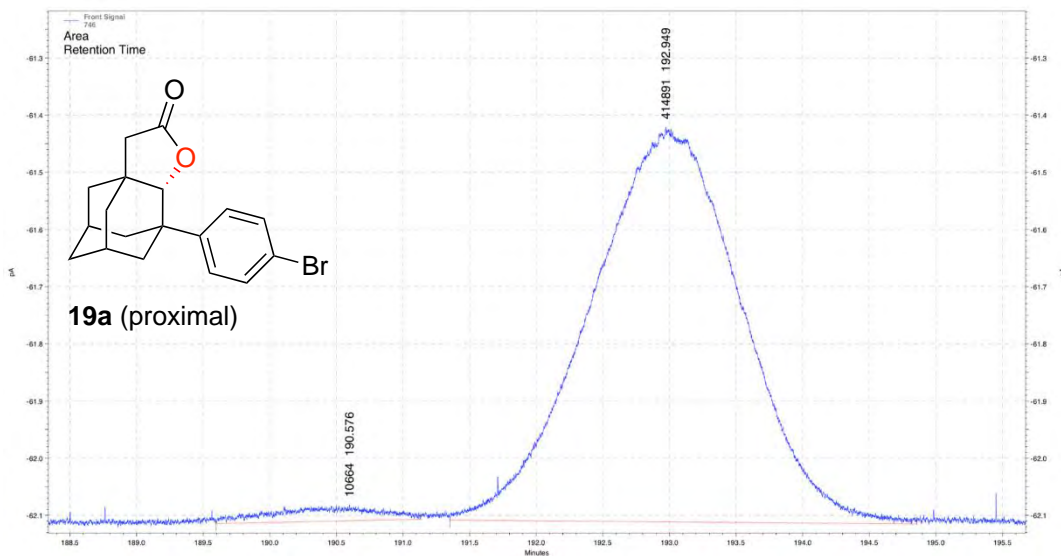
18a - (R,R)-Mn(TIBS₃pdp)



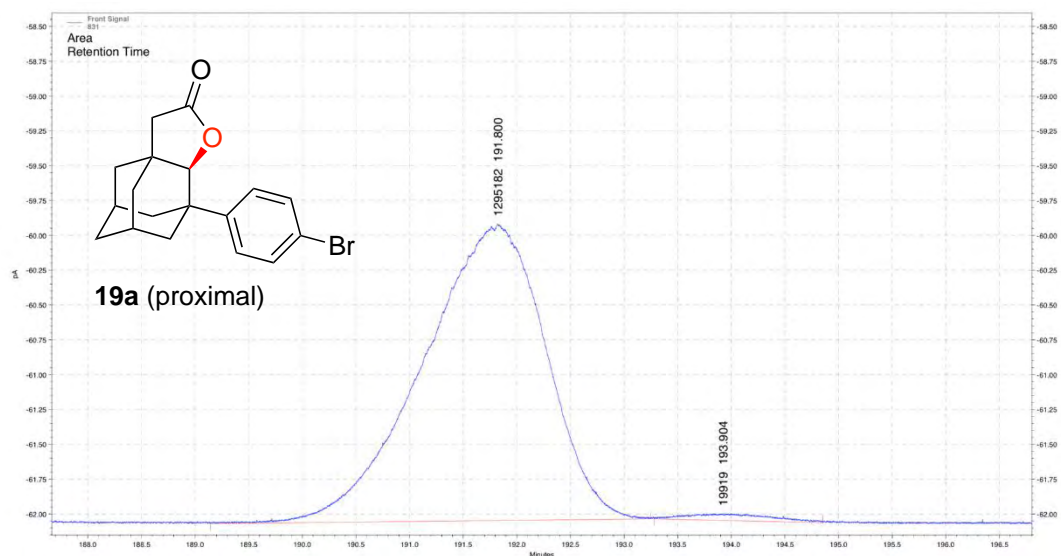
rac-19a



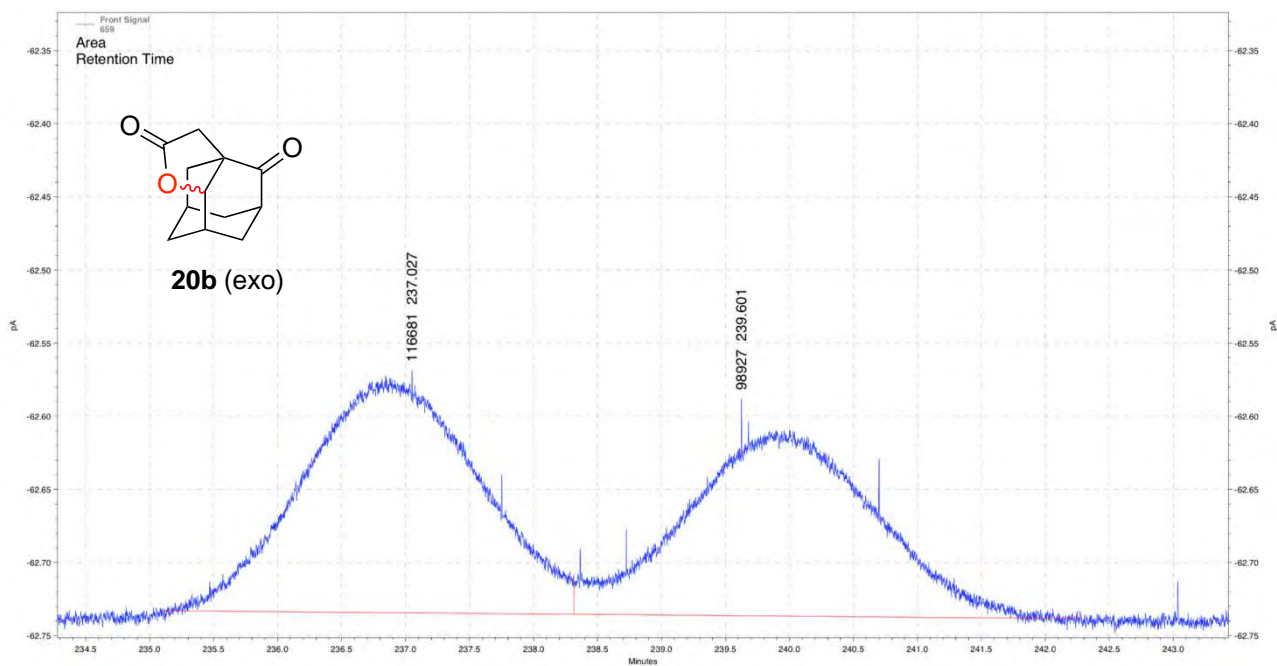
19a - (S,S)-Mn(pdp)



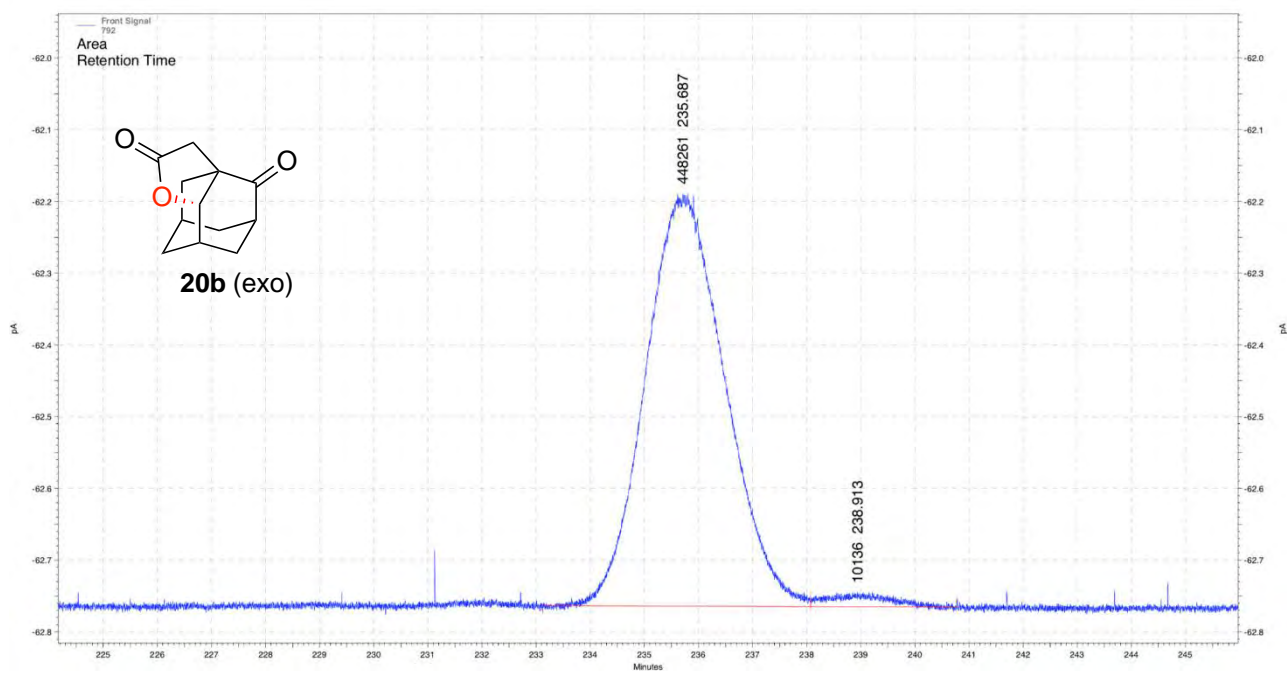
19a-(R,R)-Mn(TIBS₃pdp)



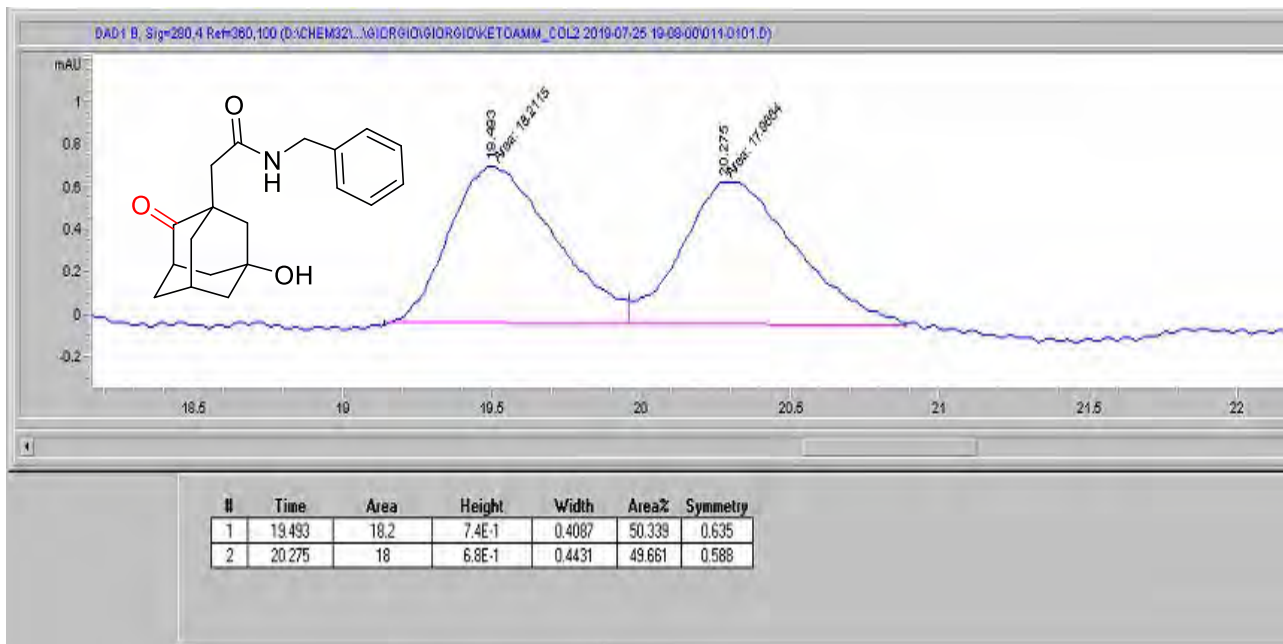
rac-20b



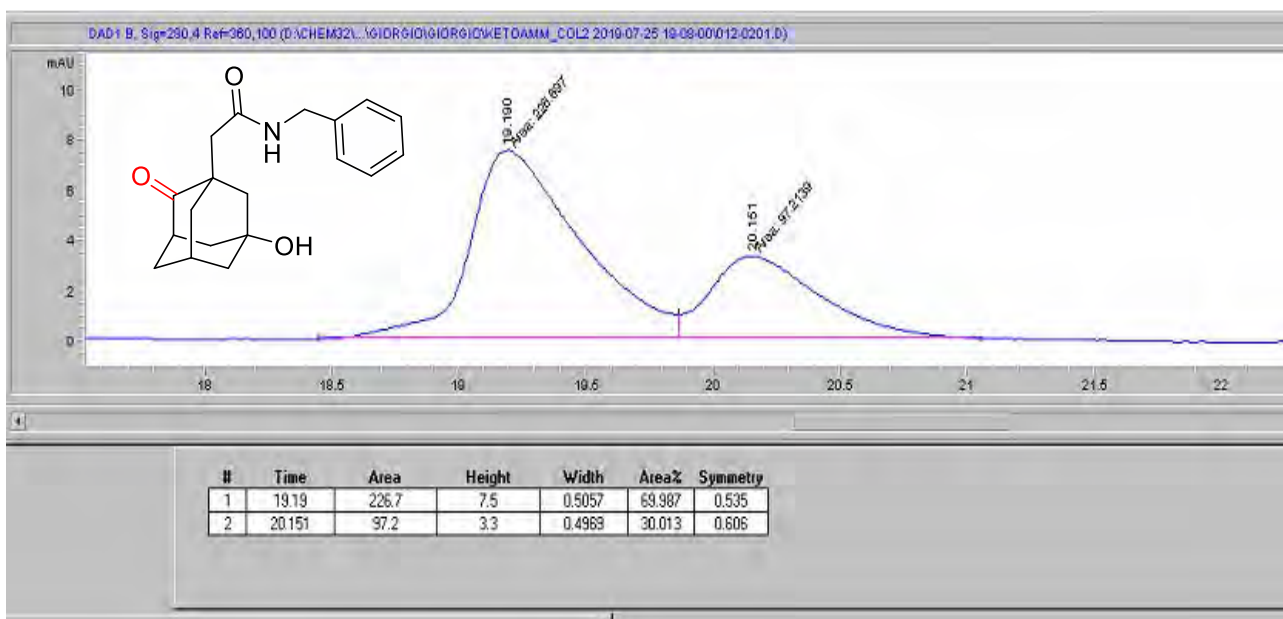
20b - (*R,R*)-Mn(^{TIBS}pdp)



rac-23b (HPLC trace)

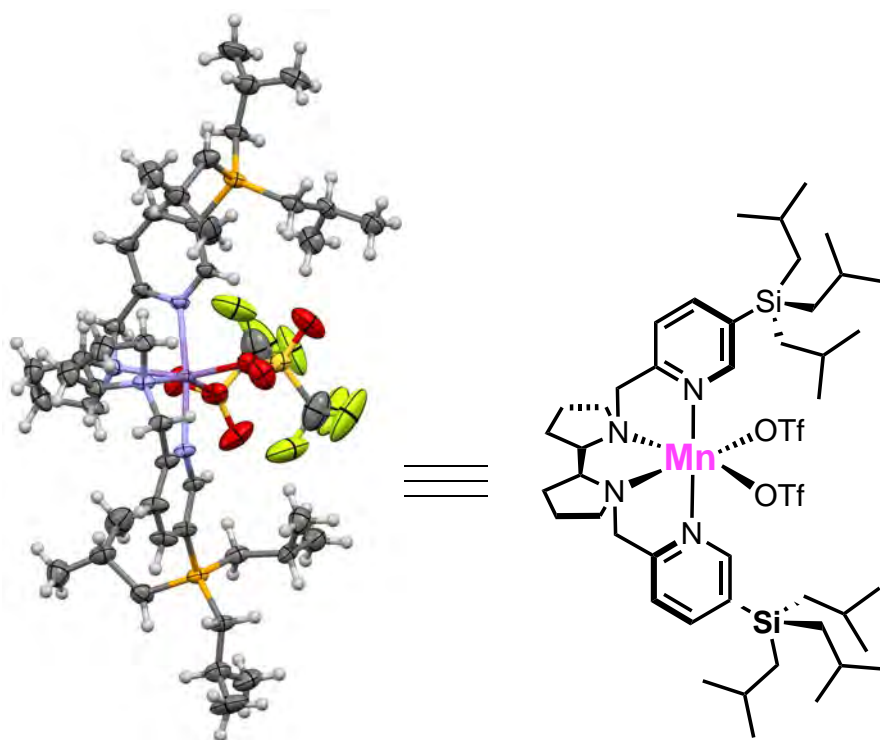


20b - (S,S)-Mn(pdp)



IV.X-ray analysis

Crystal structure of (*S,S*)-[Mn(CF₃SO₃)₂(^TIBS_{pdp})]

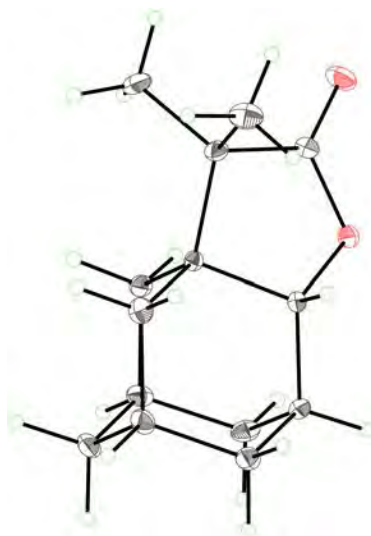


IV. Crystal data for (*S,S*)-[Mn(CF₃SO₃)₂(^TIBS_{pdp})]

Chemical formula	C ₄₆ H ₇₈ F ₆ MnN ₄ O ₆ S ₂ Si ₂
Formula weight	1072.37 g/mol
Temperature	100(2) K
Wavelength	0.71076 Å
Crystal size	0.230 x 0.300 x 0.330 mm
Crystal habit	colorless prism
Crystal system	trigonal
Space group	P 3 ₁ 2 1
Unit cell dimensions	a = 15.215(3) Å α = 90.00(3)° b = 15.215(3) Å β = 90.00(3)° c = 23.053(5) Å γ = 120.00(3)°

Volume	4622.(2) Å ³
Z	3
Density (calculated)	1.154 g/cm ³
Absorption coefficient	0.381 mm ⁻¹
F(000)	1701
Diffractionmeter	Bruker D8 QUEST ECO
Radiation source	sealed X-ray tube, Mo Kalpha
Theta range for data collection	2.35 to 27.50°
Index ranges	-19<=h<=18, -19<=k<=19, -29<=l<=29
Reflections collected	103734
Independent reflections	7073 [R(int) = 0.0366]
Coverage of independent reflections	99.7%
Absorption correction	Multi-Scan
Max. and min. transmission	0.7456 and 0.6909
Structure solution technique	direct methods
Structure solution program	SHELXT 2014/5 (Sheldrick, 2014)
Refinement method	Full-matrix least-squares on F ²
Refinement program	SHELXL-2016/6 (Sheldrick, 2016)
Function minimized	$\Sigma w(F_o^2 - F_c^2)^2$
Data / restraints / parameters	7073 / 0 / 310
Goodness-of-fit on F²	1.085
Final R indices [I>2σ(I)]	R1 = 0.0648, wR2 = 0.1845
Final R indices (all data)	R1 = 0.0681, wR2 = 0.1885
Weighting scheme	$w=1/[\sigma^2(F_o^2)+(0.1112P)^2+5.2338P]$ where $P=(F_o^2+2F_c^2)/3$
Absolute structure parameter	0.04(4)
Largest diff. peak and hole	1.179 and -0.732 eÅ ⁻³

IV. Single Crystal structure of (R)-2a:



The determination of the absolute configuration was done having in consideration the methodology proposed by Escudero et al. (Acta Crystallographica section B, Volume 70, Part 4, 2014, 660-668). Thus, a high quality, high resolution data set was acquired, with a high number of independent reflections.

Values of P2 (right), P3, Hooft parameter γ (Hooft, R. W. W., Straver, L. H. & Spek, A. L. (2008) J. Appl. Cryst. 41, 96–103) and Flack parameter using the Parsons method z (Parsons, S., Flack, H. D. & Wagner, T. (2013). Acta Cryst. B69, 249–259), were calculated with PLATON (Spek, A. L. (2003). J. Appl. Cryst. 36, 7–13).

P2(true).... 1.000
P3(true).... 1.000
P3(rac-twin) 0.7E-04
P3(false) .. 0.1E-13
Parsons z .. -0.04(14)
Hooft γ -0.12(14)

Crystal data of (+)-2a

Chemical formula	C ₁₄ H ₂₀ O ₂	
Formula weight	220.30 g/mol	
Temperature	100(2) K	
Wavelength	0.71076 Å	
Crystal size	0.030 x 0.280 x 0.430 mm	
Crystal habit	colorless plate	
Crystal system	orthorhombic	
Space group	P 21 21 21	
Unit cell dimensions	a = 6.8836(2) Å	$\alpha = 90^\circ$
	b = 9.7992(3) Å	$\beta = 90^\circ$
	c = 17.1373(5) Å	$\gamma = 90^\circ$
Volume	1155.98(6) Å ³	

Z	4
Density (calculated)	1.266 g/cm ³
Absorption coefficient	0.083 mm ⁻¹
F(000)	480
Diffractometer	Bruker D8 QUEST ECO three-circle diffractometer
Radiation source	Ceramic x-ray tube (Mo K α , λ = 0.71076 Å)
Theta range for data collection	3.81 to 41.27°
Index ranges	-12 \leq h \leq 12, -18 \leq k \leq 18, -31 \leq l \leq 31
Reflections collected	46298
Independent reflections	7693 [R(int) = 0.0316]
Coverage of independent reflections	99.2%
Absorption correction	Multi-Scan
Max. and min. transmission	0.9980 and 0.9650
Structure solution technique	direct methods
Structure solution program	SHELXT 2014/5 (Sheldrick, 2014)
Refinement method	Full-matrix least-squares on F ²
Refinement program	SHELXL-2017/1 (Sheldrick, 2017)
Function minimized	$\Sigma w(F_o^2 - F_c^2)^2$
Data / restraints / parameters	7693 / 0 / 225
Goodness-of-fit on F²	1.092
Δ/σ_{\max}	0.001
Final R indices [I$>$2σ(I)]	R1 = 0.0318, wR2 = 0.0830
Final R indices (all data)	R1 = 0.0369, wR2 = 0.0860
Weighting scheme	$w=1/[\sigma^2(F_o^2)+(0.0499P)^2+0.0493P]$ where $P=(F_o^2+2F_c^2)/3$
Absolute structure parameter	-0.16(16)
Largest diff. peak and hole	0.349 and -0.186 eÅ ⁻³
R.M.S. deviation from mean	0.043 eÅ ⁻³

IV. Single crystal structure of (+)-4b:

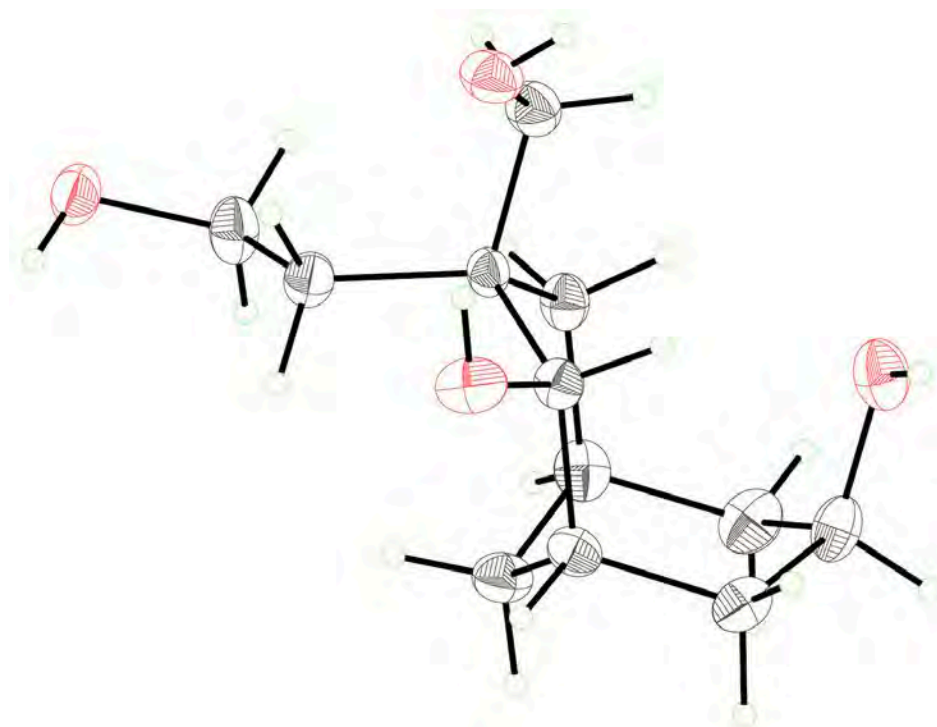


Crystal data for (+)-4b

Chemical formula	C ₁₂ H ₁₆ O ₃	
Formula weight	208.25 g/mol	
Temperature	100(2) K	
Wavelength	0.71076 Å	
Crystal size	0.080 x 0.100 x 0.220 mm	
Crystal habit	colorless block	
Crystal system	orthorhombic	
Space group	P 21 21 21	
Unit cell dimensions	a = 9.314(8) Å	α = 90°
	b = 10.597(9) Å	β = 90°
	c = 20.626(18) Å	γ = 90°
Volume	2036.(3) Å ³	2036.(3) Å ³
Z	8	
Density (calculated)	1.359 g/cm ³	
Absorption coefficient	0.096 mm ⁻¹	
F(000)	896	
Diffractometer	Bruker D8 QUEST ECO three-circle diffractometer	
Radiation source	Ceramic x-ray tube (Mo Kα, λ = 0.71076 Å)	
Theta range for data collection	2.91 to 41.13°	
Index ranges	-17 ≤ h ≤ 17, -19 ≤ k ≤ 19, -38 ≤ l ≤ 38	
Reflections collected	243361	
Independent reflections	13496 [R(int) = 0.0515]	
Coverage of independent reflections	99.7%	
Absorption correction	Multi-Scan	

Max. and min. transmission	0.9920 and 0.9790
Structure solution technique	direct methods
Structure solution program	SHELXT 2014/5 (Sheldrick, 2014)
Refinement method	Full-matrix least-squares on F^2
Refinement program	SHELXL-2017/1 (Sheldrick, 2017)
Function minimized	$\Sigma w(F_o^2 - F_c^2)^2$
Data / restraints / parameters	13496 / 0 / 399
Goodness-of-fit on F^2	1.116
Δ/σ_{\max}	0.001
Final R indices [$I > 2\sigma(I)$]	R1 = 0.0383, wR2 = 0.0917
Final R indices (all data)	R1 = 0.0497, wR2 = 0.0977
Weighting scheme	$w = 1/[\sigma^2(F_o^2) + (0.0488P)^2 + 0.2092P]$ where $P = (F_o^2 + 2F_c^2)/3$
Absolute structure parameter	0.08(10)
Largest diff. peak and hole	0.477 and -0.266 $e\text{\AA}^{-3}$
R.M.S. deviation from mean	0.055 $e\text{\AA}^{-3}$

IV. Single crystal structure of (+)-22:



Crystal data for (+)-22.

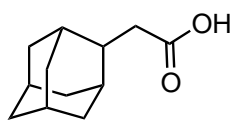
Chemical formula	$C_{12}H_{22}O_4$
Formula weight	230.29 g/mol
Temperature	293(2) K

Wavelength	0.71076 Å	
Crystal size	0.060 x 0.080 x 0.200 mm	
Crystal habit	colorless needle	
Crystal system	orthorhombic	
Space group	P 21 21 21	
Unit cell dimensions	a = 6.6389(10) Å	$\alpha = 90^\circ$
	b = 10.6291(19) Å	$\beta = 90^\circ$
	c = 16.794(3) Å	$\gamma = 90^\circ$
Volume	1185.1(4) Å ³	
Z	4	
Density (calculated)	1.291 g/cm ³	
Absorption coefficient	0.095 mm ⁻¹	
F(000)	504	
Diffractometer	Bruker D8 QUEST ECO three-circle diffractometer	
Radiation source	Ceramic x-ray tube (Mo K α , $\lambda = 0.71076$ Å)	
Theta range for data collection	3.30 to 25.33°	
Index ranges	-7 ≤ h ≤ 7, -12 ≤ k ≤ 11, -20 ≤ l ≤ 15	
Reflections collected	5500	
Independent reflections	2151 [R(int) = 0.0399]	
Coverage of independent reflections	99.6%	
Absorption correction	Multi-Scan	
Max. and min. transmission	0.9940 and 0.9810	
Structure solution technique	direct methods	
Structure solution program	SHELXT 2014/5 (Sheldrick, 2014)	
Refinement method	Full-matrix least-squares on F ²	
Refinement program	SHELXL-2017/1 (Sheldrick, 2017)	
Function minimized	$\Sigma w(F_o^2 - F_c^2)^2$	
Data / restraints / parameters	2151 / 0 / 149	
Goodness-of-fit on F²	1.017	
Final R indices	1602 data; I > 2 σ (I)	R1 = 0.0453, wR2 = 0.0784
	all data	R1 = 0.0700, wR2 = 0.0859
Weighting scheme	$w = 1 / [\sigma^2(F_o^2) + (0.0371P)^2]$ where $P = (F_o^2 + 2F_c^2) / 3$	
Absolute structure parameter	0.6(9)	
Largest diff. peak and hole	0.116 and -0.144 eÅ ⁻³	
R.M.S. deviation from mean	0.033 eÅ ⁻³	

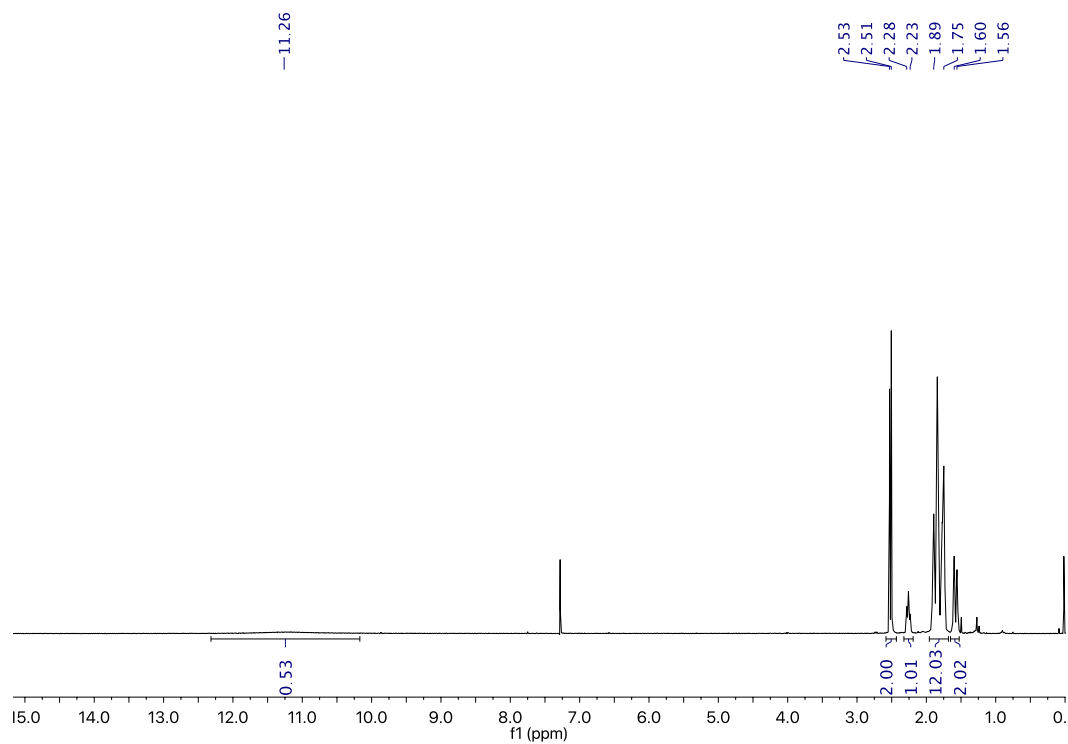
ANNEX CHAPTER V

NMR SPECTRA

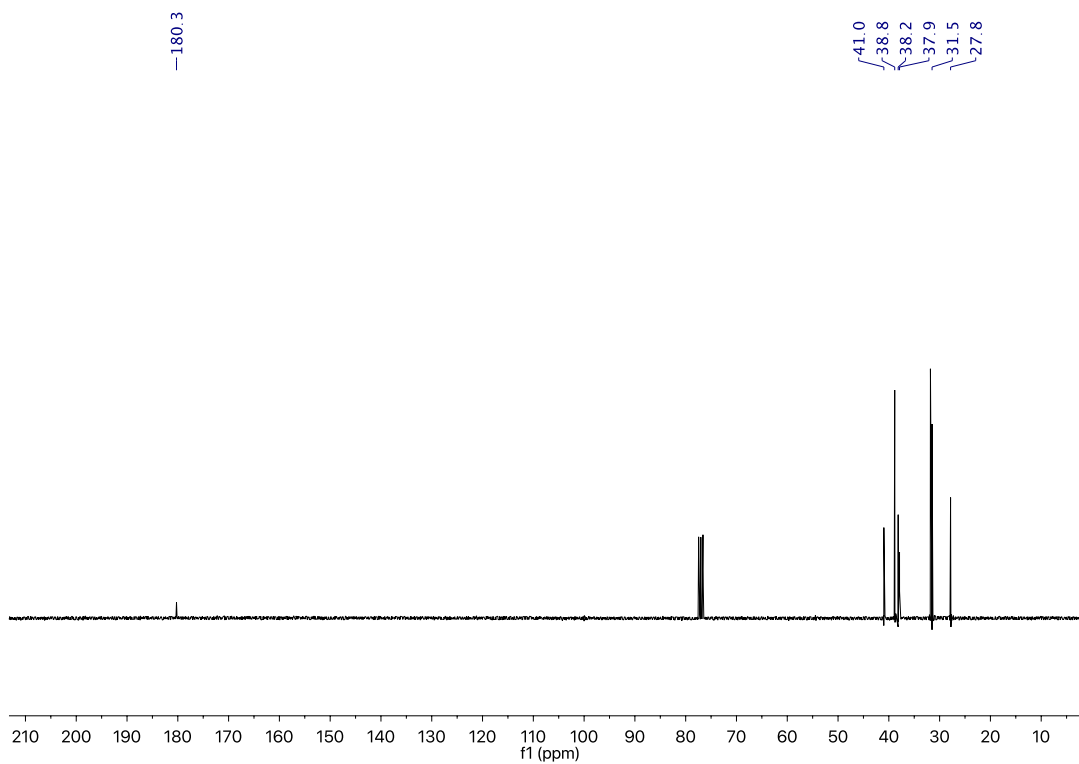
V. NMR characterization of 7



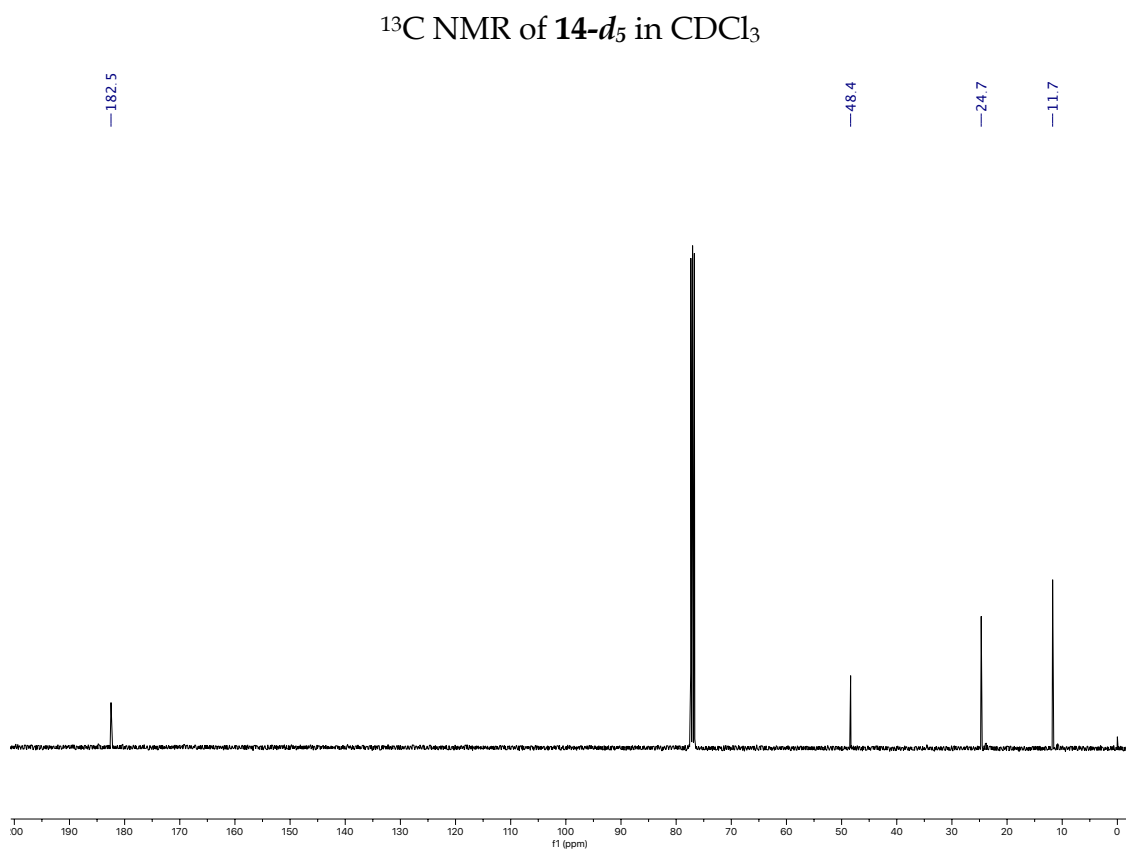
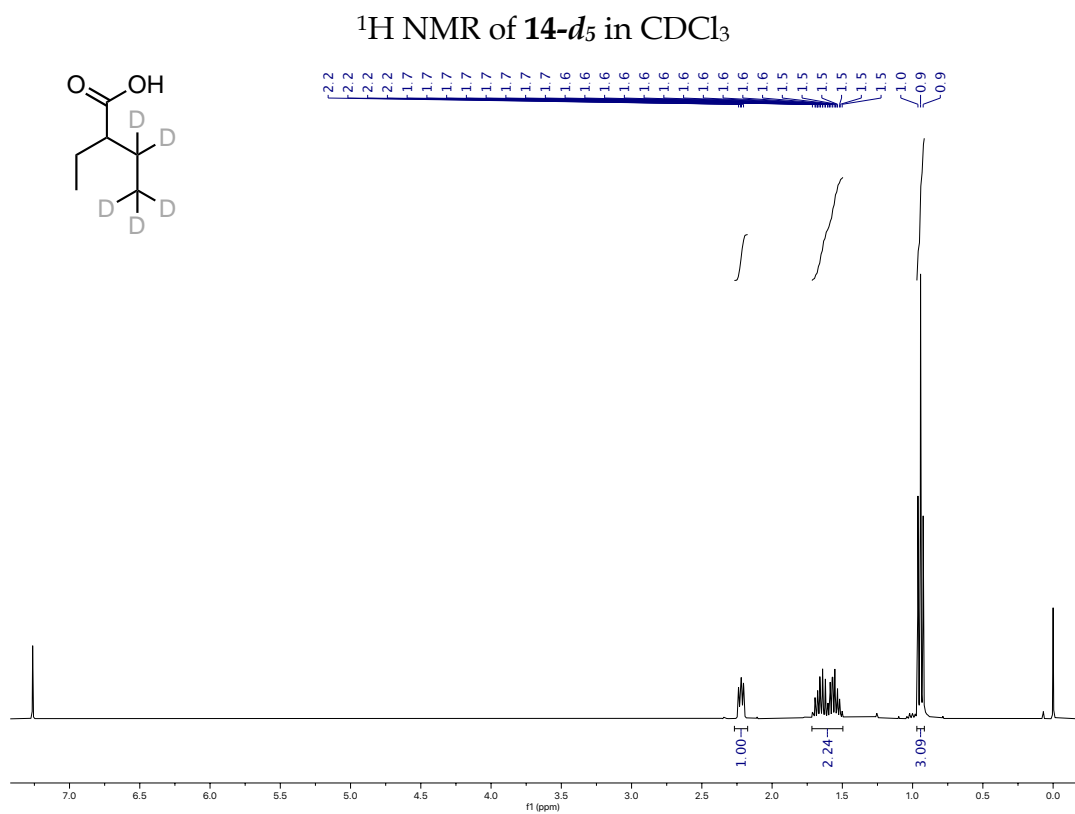
^1H -NMR of 7 in CDCl_3

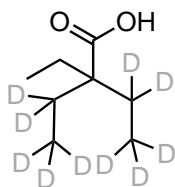


$^{13}\text{C}\{^1\text{H}\}$ -NMR of 7 in CDCl_3

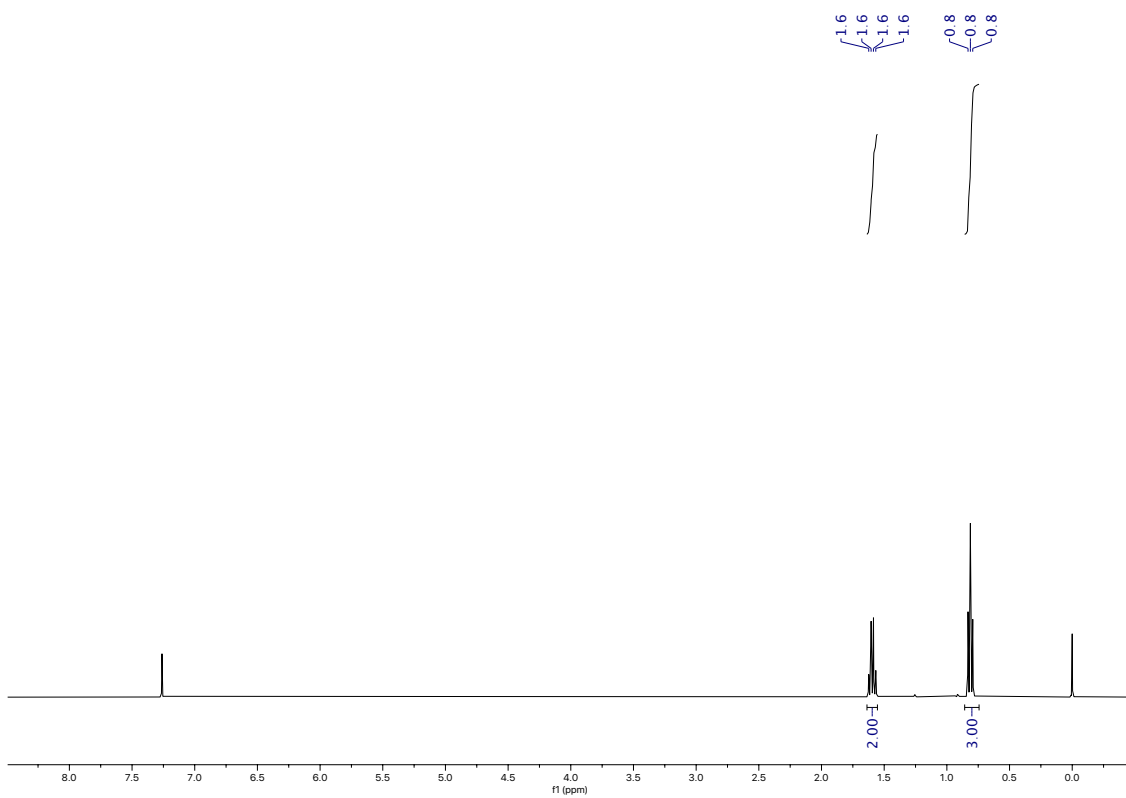


V. NMR characterization of the deuterated substrates

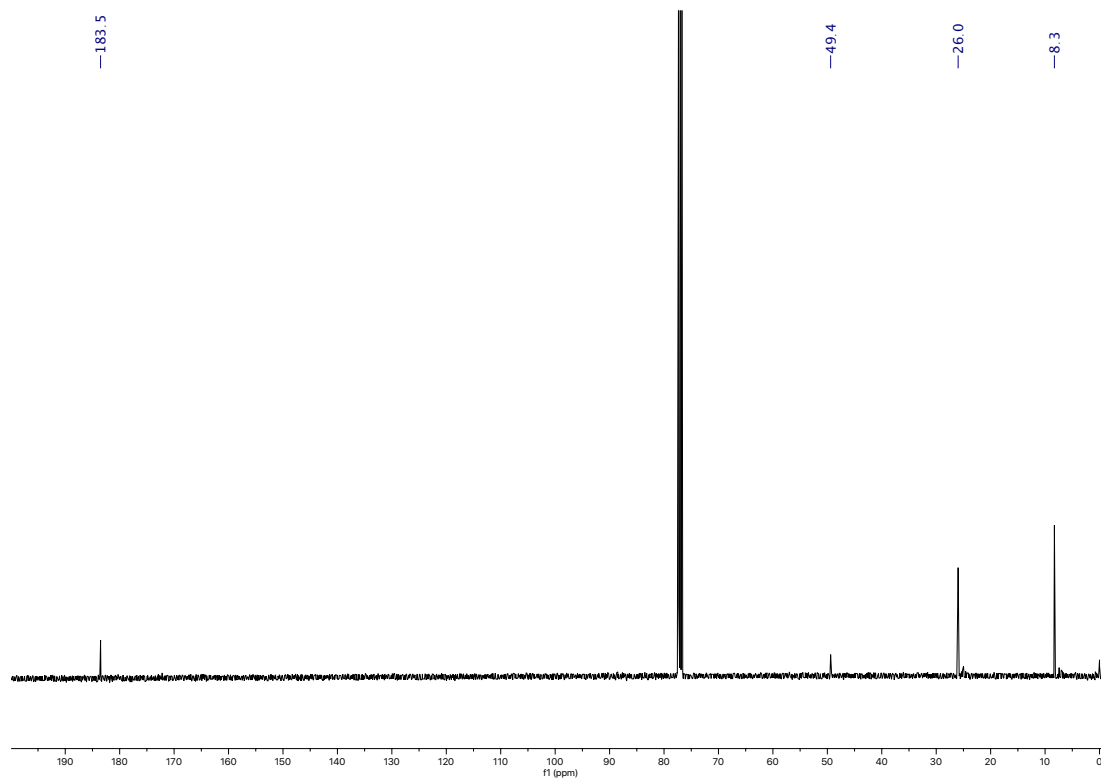


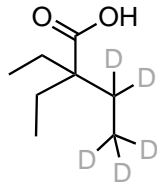


¹H NMR of 13-d₁₀ in CDCl₃

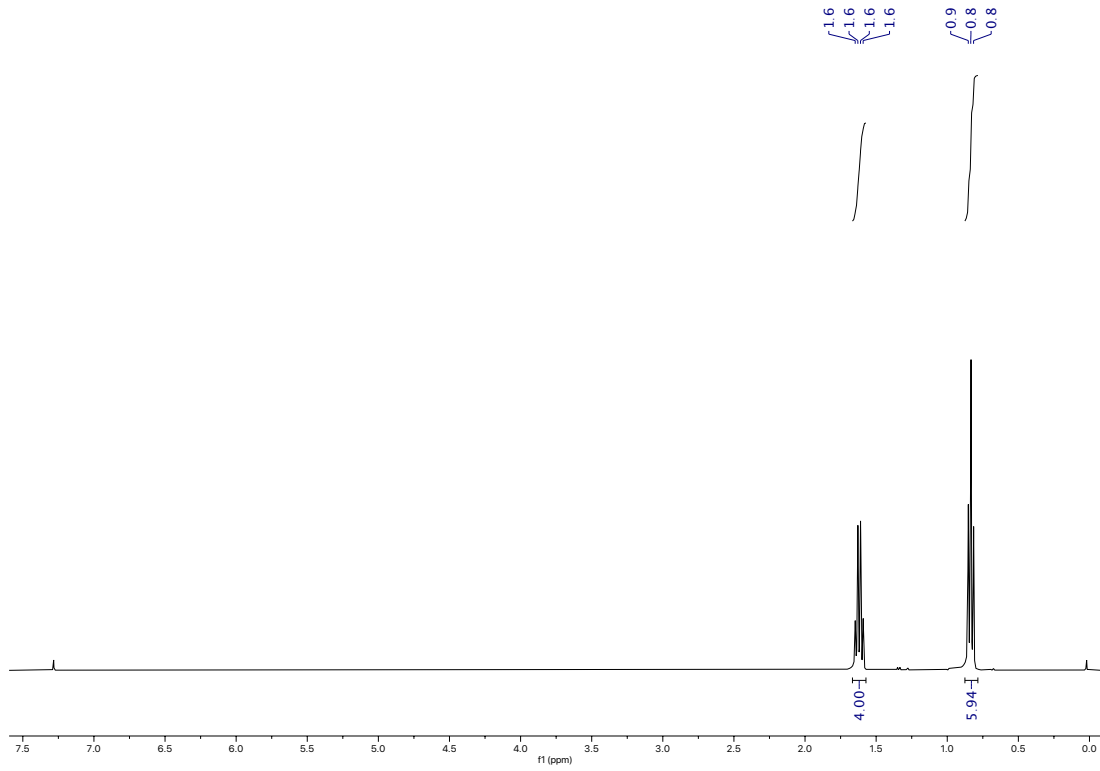


¹³C NMR of 13-d₁₀ in CDCl₃

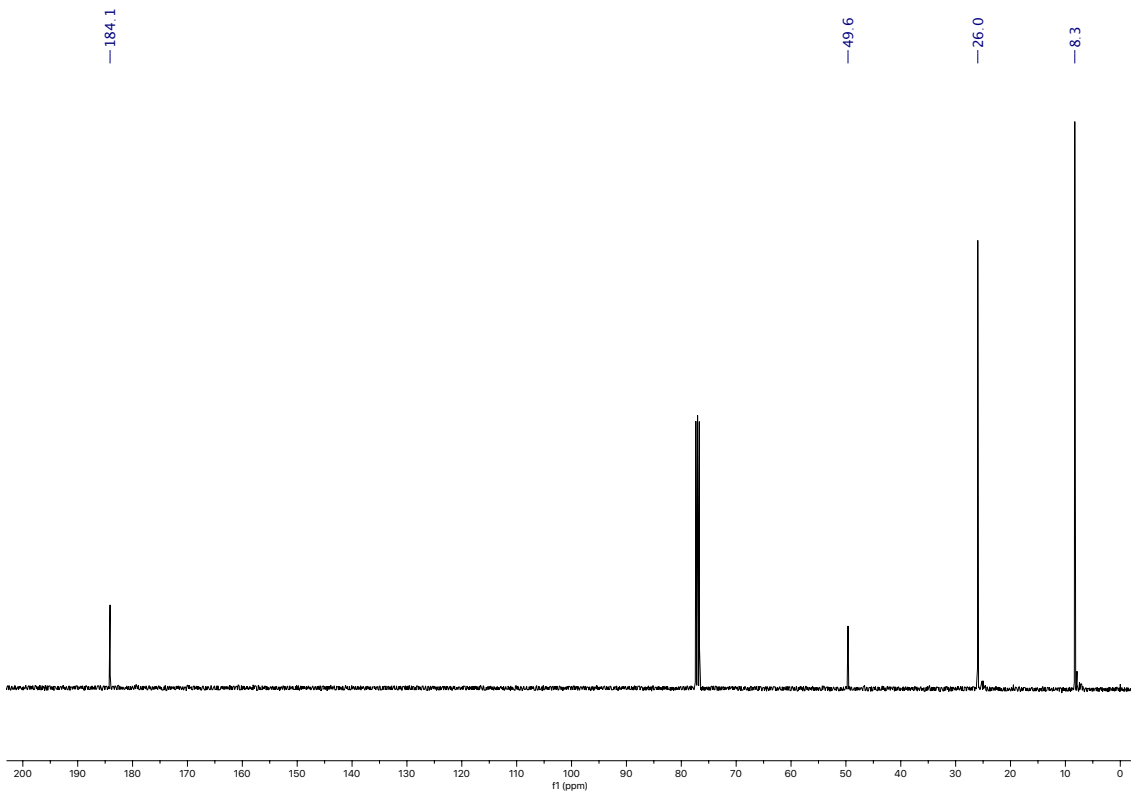




^1H NMR of **13-d₅** in CDCl_3

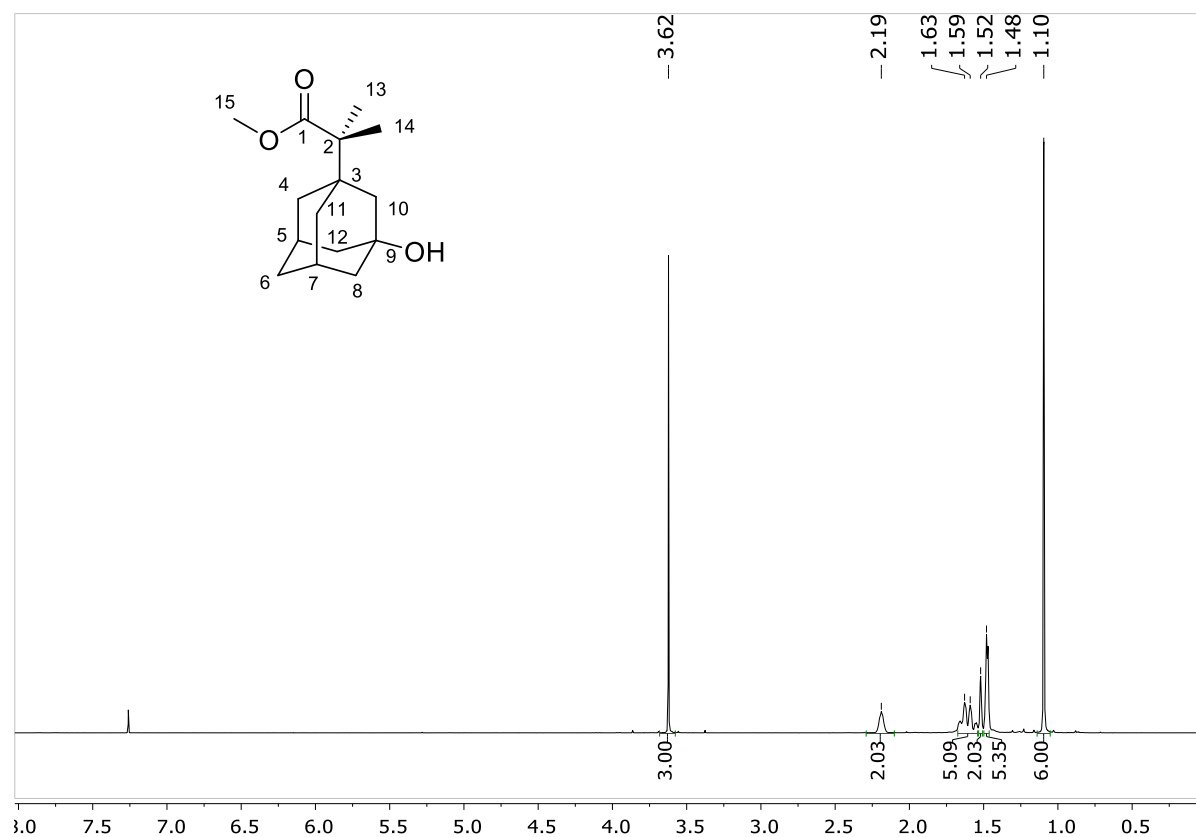


^{13}C NMR of **13-d₅** in CDCl_3



V. NMR characterization of the oxidized product **2a**

^1H NMR of **2a** in CDCl_3



^{13}C -NMR of **2a** in CDCl_3

